Genome mining and metabolic engineering for bioactive natural product production in Streptomyces

Yang, Zhijie

Publication date:
2024

Document Version
Publisher's PDF, also known as Version of record

DTU Bioengineering
Department of Biotechnology and Biomedicine

Genome mining and metabolic engineering for bioactive natural product production in *Streptomyces*

PhD Thesis

Zhijie Yang

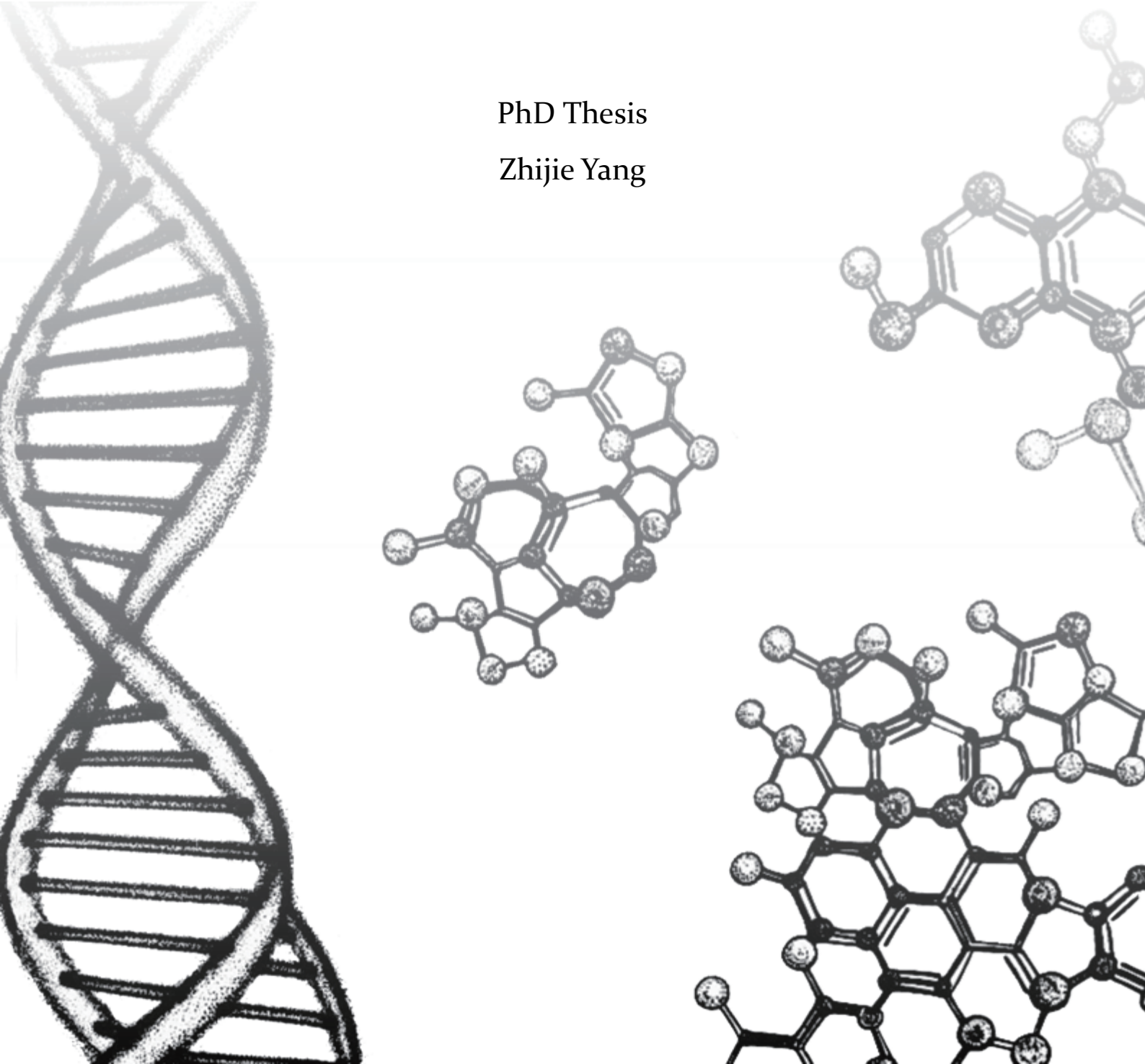

Genome-mining and metabolic engineering for bioactive natural product production in *Streptomyces*

PhD Thesis

Zhijie Yang

November 2023

Main Supervisor

Ling Ding, Associate Professor

Section for Microbial and Chemical Ecology

Department of Biotechnology and Biomedicine

Technical University of Denmark

Co-supervisor

Tilmann Weber, Professor

The Novo Nordisk Foundation Center for Biosustainability

Technical University of Denmark

Section for Microbial and Chemical Ecology
Department of Biotechnology and Biomedicine
Technical University of Denmark
Søltofts Plads, Building 221
DK-2800 Kgs. Lyngby
Denmark

Preface

This thesis was carried out in the Bioactive Microbial Small Molecules group at Department of Biotechnology and Biomedicine, Technical University of Denmark (DTU), in the period of December 2020 – December 2023. This thesis was supervised by Associate Prof. Ling Ding, and co-supervised by Prof. Tilmann Weber. The project was supported by grants from by China Scholarship Council (No. 202004910340) and DTU Bioengineering.

First, I would like to express my deepest gratitude to my supervisor, Associate Prof. Ling Ding, for giving me the opportunity to join your group. Your mentorship, expertise, and dedication have been the cornerstone of this thesis. I am also sincerely grateful to you for providing me with the freedom to explore and for fostering an exceptional research environment. I am very honored to be your first PhD student.

I extend my heartfelt appreciation to my co-supervisor, Prof. Tilmann Weber, for your insightful feedback and valuable suggestions during the past three years. Every conversation with you makes me feel warm and your views always hit the point and inspire me. Your dedication to excellence has also been an inspiration to me.

I would like to acknowledge the support of the faculty and staff from the Section for Microbial and Chemical Ecology in Department of Biotechnology and Biomedicine: Prof. Lone Gram, Prof. Thomas Ostenfeld Larsen, Prof. Jens Christian Frisvad, Dr. Yijun Qiao, Dr. Xinhui Wang, Dr. Kah Yean Lum, Dr. Scott Alexander Jarmusch, Dr. Rohitesh Kumar, Dr. Mario Wibowo, Dr. Thomas Isbrandt Petersen, Dr. Michael Scott Cowled, Dr. Johan Vormsborg Christiansen, Dr. Vincent Wiebach, Manar Magdy Mahmoud Mohamed, Manca Vertot, Emil Strøbech, and Daniel Jordan Otto; the Natural Products Genome Mining group in the Novo Nordisk Foundation Center for Biosustainability: Dr. Tetiana Gren, Dr. Kai Blin, Dr. Xinglin Jiang, Dr. Pep Charusanti, Dr. Tue Sparholt Jørgensen, Dr. Renata Sigrist, Dr. Christopher Martin Whitford, Dr. Agnieszka Litomska, Dr. Thomas Booth, Matiss Maleckis, Matin Nuhamunada, Eva Baggesgaard Sterndorff and Oliwia Vuksanovic. I would also like to acknowledge the support in plant assays provided by Prof. Erik Andreasson and Dr. Naga Charan Konakalla from Swedish University of Agricultural Sciences.

I am thankful to Prof. Charlotte Held Gotfredsen from DTU chemistry, Dr. Aaron John Christian Andersen, Urte Rubeziute and Mette Amfelt from DTU Metabolomics Core, and Dr. Marie Vestergaard

Lukassen from DTU Proteomics Core, whose technical expertise have facilitated the smooth progression of this research.

During my visit to the University of Warwick, I had the distinct pleasure of working with and learning from Prof. Greg Challis and Assistant Prof. Lona Alkhalaf. Your exceptional professionalism, expert guidance, and support during my stay were pivotal in improving my work. I also want to express my thanks to lab members in Challis group: Dr. James Duncan, Dr. Munro Passmore, Dr. Tianjie Yuan, Dr. Wei Li, Dr. Daniel Van, Dr. Fayrouz Elmaddah, Yu Zhang, Callum Bullock, Mabilly Cox, Emma Coker, Matt Pledge and Adam Hunt.

Finally, I want to acknowledge my family. Qian Li, my wife, you truly stand as the epitome of the finest partner in the world. Your love has been a constant source of inspiration, and I look forward to the new adventures we will embark on together. I am thankful for the support and unconditional love from my parents and grandparents, you always support my choices and encourage me when I feel depressed.

This thesis represents the culmination of the collective effort and support from these individuals and institutions, and I am profoundly grateful for their contributions to this work.

Kgs. Lyngby,
December 30, 2023

Zhijie Yang

Abstract

Streptomyces, a genus of Gram-positive bacteria widely distributed in natural environments, has garnered considerable attention due to its diverse metabolic pathways and the production of bioactive compounds. Among these, the secondary metabolites produced by *Streptomyces* exhibit substantial comprehensive pharmacological and industrial potential with significant applications in medical, agricultural, and biotechnological domains. To unravel the biosynthetic potential of *Streptomyces*, recent research efforts have shifted towards the elucidation and analysis of its genomic content. Employing high-throughput sequencing technologies and bioinformatics analysis, numerous putative biosynthetic gene clusters (BGCs) have been successfully unveiled within *Streptomyces* genomes, laying the foundation for a deeper understanding of the pathways responsible for the production of natural products. In addressing the gaps in our understanding of *Streptomyces* biosynthetic pathways, genome mining has emerged as a pivotal research approach. In-depth analysis of the *Streptomyces* genome enables the precise localization and identification of genes involved in biosynthesis, thereby providing crucial support for subsequent endeavors. Furthermore, the integration of metabolic engineering strategies, particularly the integration of CRISPR-based genome editing, offers a means to optimize metabolic pathways, enhance the production of target compounds, and establish effective technical platforms for the sustainable production of *Streptomyces*-derived natural products.

This thesis primarily unveils the discovery and biosynthesis mechanisms underlying two novel types of natural products: plant growth-promoting pteridic acids and antifungal spirolactone, derived from *Streptomyces iranensis*. We found that the culture broth of *S. iranensis* could significantly help plants relieve abiotic stresses such as salinity, osmotic, and drought stresses. Metabolomics, activity-guided chemical isolation, and structure elucidation led to the discovery of the bioactive ingredients, pteridic acids H and F. Pteridic acids also exhibited significant efficacy in enhancing plant stress resistance during *Arabidopsis* seedling experiments. Transcriptome analysis revealed that pteridic acids treatment not only upregulated the expression of plant photosynthesis and auxin biosynthesis-related genes but also activated various transcription factors associated with plant stress resistance under salt stress condition. The BGC and biosynthesis pathway of pteridic acids was determined by in silico analysis and in vivo CRISPR base editing. Phylogenetic and comparative genome mining indicated that the streptomycetes containing pteridic acids BGC were evolutionarily conserved and globally distributed (**Section 2.1** and **Paper 1**). Genome mining of *S. iranensis* revealed an unprecedented PKS-type BGC located in the terminal region of its linear chromosome. CRISPR-BEST mutation, combined with HR-LC-MS analysis, followed up by large-scale fermentation and purification led to the identification of a novel class of macrolide spirolactones A-C. Spirolactones showcased the structure of a rare β-lactone moiety, a [6,6]-

spiroketal ring, and an unusual extender unit in structure. Spirolactone A exhibits potent anti-*Aspergillus* activity and proteomic analysis shows it may act by affecting fungal cell wall integrity (**Section 2.2** and **Paper 2**). To further improve the production of pteridic acids and spirolactones, a comprehensive metabolic strategy was employed such as regulatory and transportation genes manipulation, precursors enhancement, promoter engineering, and side pathway elimination (**Section 2.3**). In addition to the application of the CRISPR-based gene editing toolbox in the aforementioned studies, we employed it in the other two non-model *Streptomyces* strains to elucidate the BGCs associated with diverse microbial natural products (**Section 2.4** and **Paper 3-4**).

In conclusion, this PhD study uncovered novel natural products, plant growth-promoting pteridic acids, and antifungal spirolactone, from *S. iranensis*. Pteridic acids exhibited significant efficacy in enhancing plant stress resistance, while spirolactone demonstrated potent anti-*Aspergillus* activity. Genomics, metabolomics, and CRISPR-based gene editing were employed to elucidate their biosynthetic pathways. This work also involved optimizing the production of pteridic acids and spirolactone through metabolic engineering. These findings significantly advance our understanding of ecological roles and therapeutic potential of *Streptomyces* secondary metabolites, presenting promising applications in the fields of sustainable agriculture and medicine.

Dansk Resumé

Streptomyces, en slægt af Gram-positive bakterier, der er vidt udbredt i naturlige miljøer, har fået stor opmærksomhed på grund af dens forskellige metaboliske veje og produktionen af bioaktive forbindelser. Blandt disse udviser de sekundære metabolitter produceret af *Streptomyces* et betydeligt omfattende farmakologisk og industrielt potentiale med betydelige anvendelser inden for medicinske, landbrugsmæssige og bioteknologiske domæner. For at afdække *Streptomyces*' biosyntetiske potentiale har den seneste forskningsindsats skiftet i retning af belysning og analyse af dets genetiske indhold. Ved at anvende high-throughput sekventeringsteknologier og bioinformatikanalyse er talrige formodede biosyntetiske genklynger (BGC'er) med succes blevet afsløret inden for *Streptomyces* genomer, hvilket lægger grundlaget for en dybere forståelse af de veje, der er ansvarlige for produktionen af naturlige produkter. Ved at adressere manglerne i vores forståelse af *Streptomyces* biosyntetiske veje, er genome mining opstået som en central forskningstilgang. Dybdegående analyse af *Streptomyces*-genomet muliggør den præcise lokalisering og identifikation af gener involveret i biosyntese og giver derved afgørende støtte til efterfølgende bestræbelser. Desuden tilbyder integrationen af metaboliske ingeniørmetoder, især integrationen af CRISPR-baseret genmodificering, et middel til at optimere metaboliske veje, forbedre produktionen af ønskede molekylære produkter og etablere effektive tekniske platforme for bæredygtig produktion af *Streptomyces*-afledte naturlige produkter.

Denne afhandling afslører primært opdagelsen og biosyntesemekanismerne bag to nye typer af naturlige produkter: plantevækstfremmende pteridic acids og svampedræbende spirolactone, afledt af *Streptomyces iranensis*. Vi fandt ud af, at tilføjelsen af *S. iranensis* signifikant kunne hjælpe planter med at lindre abiotiske belastninger såsom saltholdighed, osmotisk og tørkebelastning. Metabolomics, aktivitetsstyret kemisk isolering og strukturopklaring førte til opdagelsen af det bioaktive molekyler, pteridic acids H og F. Pteridic acids udviste også betydelig effektivitet til at øge plantestressresistens under *Arabidopsis* frøplanteeksperimenter. Transkriptomanalyse afslørede, at behandling med pteridic acids ikke kun opregulerede ekspressionen af plantefotosyntese og auxinbiosyntese-relaterede gener, men også aktiverede forskellige transkriptionsfaktorer forbundet med plantestressresistens. BGC- og biosynteseveien for pteridic acids blev bestemt ved in silico-analyse og in vivo CRISPR-baseret genmodificering. Fylogenetisk og komparativ genome mining indikerede, at streptomyceterne, der indeholder pteridic acids BGC, er evolutionært konserverede og globalt fordelt (**afsnit 2.1** og **papir 1**). Genom mining af *S. iranensis* afslørede en hidtil uset PKS-type BGC placeret i den terminale region af dets lineære kromosom. CRISPR-BEST mutation, kombineret med HR-LC-MS analyse, fulgt op af storskala fermentering og oprensning førte til identifikation af en ny klasse af makrolid spirolactoner A-

C. Spirolactone fremviste strukturen af en sjælden β-lactondel, en [6,6]-spiroketal og en usædvanlig forlængerenhed i strukturen. Spirolactone A udviser potent anti-*Aspergillus* aktivitet, og proteomisk analyse viser, at det kan virke ved at påvirke svampecellevæggens integritet (**afsnit 2.2** og **papir 2**). For yderligere at forbedre produktionen af pteridic acids og spirolactoner blev der anvendt en omfattende metabolisk strategi, såsom regulerings- og transportgenmanipulation, prækursor-forbedring, promotorteknologi og eliminering af irrelevante pathways (**afsnit 2.3**). Ud over anvendelsen af den CRISPR-baserede genredigeringsværktøjskasse i de førnævnte undersøgelser, brugte vi den i de to andre ikke-model *Streptomyces*-stammer for at belyse BGC'erne forbundet med forskellige mikrobielle naturlige produkter (**afsnit 2.4** og **papir 3-4**).

Afslutningsvis afslørede dette PhD-studie nye naturlige produkter, plantevækstfremmende pteridic acids og svampedræbende spirolactoner fra *S. iranensis*. Pteridic acids udviste betydelig effektivitet til at øge plantestressresistens, mens spirolactoner udviste potent anti-*Aspergillus* aktivitet. Denne undersøgelse brugte genomics, metabolomics og CRISPR-baseret genmodificering til at belyse biosyntetiske veje. Dette arbejde involverede også optimering af produktionen af pteridic acids og spirolacton gennem metabolisk manipulation. Disse resultater fremmer betydeligt vores forståelse af økologiske roller og terapeutiske potentiale af *Streptomyces* sekundære metabolitter, og præsenterer lovende anvendelser inden for bæredygtigt landbrug og medicin.

List of publication

Publications included in this thesis:

Paper 1: **Yang. Z.**, Qiao. Y., Konakalla. N. C., Strøbech. E., Harris. P., Peschel. G., Agler-Rosenbaum. M., Weber. T., Andreasson. E. & Ding. L.* *Streptomyces* alleviate abiotic stress in plant by producing pteridic acids. *Nat. Commun*. **14**, 7398 (2023)**.**

Paper 2: **Yang. Z.**, Qiao. Y., Strøbech. E., Morth. J. P., Weber. T. & Ding. L.* Spirolactone, an unprecedented antifungal β-lactone spiroketal polyketide from *Streptomyces iranensis*. *In preparation.*

Paper 3: Jarmusch. S. A.,* **Yang. Z.**, Wang. J, Anderson. J. A., Weber. T. & Ding. L.* Secondary metabolites shape *Streptomyces-Streptomyces* interactions: Mass Spectrometry Imaging reveals lydicamycins broadly induce sporulation. *In preparation.*

Paper 4: Mahmoud. M. M., **Yang. Z.**, Lum. K. Y., Peschel. G., Rosenbaum. M. A., Weber. T., Coriani. S., Gotfredsen. C. H. & Ding. L.* Genome-driven discovery of hygrocins in *Streptomyces rapamycinicus*. *Submitted*.

Table of contents

1. Introduction

1.1 *Streptomyces*

Streptomyces, Gram-positive filamentous bacteria, is the largest genus of *Actinomycetota*, and the typical genus of the family *Streptomycetaceae*. *Streptomyces* has a larger linear chromosome (6–12 MB) with high GC content (~ 72%). The core genes of *Streptomyces* are mostly located in the central region of the chromosome, while accessory genes are mostly located at both ends of the chromosome. In addition, terminal inverted repeats usually exist at both ends of linear chromosomes in *Streptomyces*. *Streptomyces* commonly survive in soil and decaying vegetation and are renowned for their distinctive "earthy" odor because of the production of the volatile secondary metabolite known as geosmin. Moreover, plenty of *Streptomyces* strains have also been isolated from various environments like oceans, mangroves, and different organisms like plants and animals. So far, there are over 700 species of *Streptomyces* bacteria that have been described.[1]

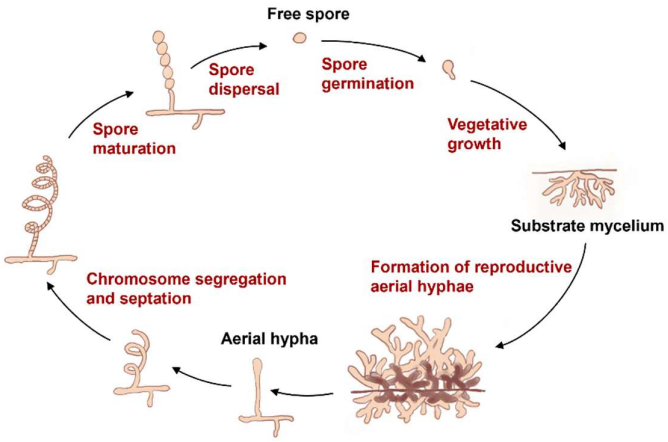

Fig. 1 The growth progress of *Streptomyces*.

The growth process of *Streptomyces* involves several distinct stages (Fig. 1).[2] Germination of spores is triggered by environmental cues, such as nutrient availability and pH levels. Germinated spores give rise to vegetative mycelium, which consists of a network of branching hyphae. These hyphae extend and grow through the substrate, exploring the environment and acquiring nutrients. During growth, *Streptomyces* cells produce a variety of secondary metabolites, including antibiotics and other bioactive compounds, which play important ecological and biotechnological roles. As the mycelium continues to grow and metabolize, it undergoes a process of morphological differentiation, characterized by the formation of aerial hyphae and the eventual development of spore chains. These aerial hyphae ultimately give rise to mature spores, called conidia, which are released into the surrounding environment. The life cycle of *Streptomyces* involves a complex regulatory network that controls the transition between different growth stages and the production of primary and secondary metabolites.

1.2 Secondary metabolites

The striking feature of *Streptomyces* is their great potential in the production of secondary metabolites with diverse structures like macrolides, polyenes, lipopeptides, and cyclopeptides, along with a wide range of various bioactivities including antibacterial, antifungal, antiviral, anticancer, and immunosuppressive (Fig. 2). Streptomycin, an aminoglycoside antibiotic initially isolated from *Streptomyces griseus* in 1943, was widely used to treat bacterial infections.[3] Oxytetracycline, a tetracycline antibiotic isolated from *Streptomyces rimosus* in 1950, is active against a wide variety of bacteria.[4] Amphotericin B, a polyene antibiotic isolated from *Streptomyces nodosus* in 1955, exhibits significant broad-spectrum antifungal activity via acting as sterol "sponges" and extracting ergosterol from the fungal membrane, causing cell death.[5-7] Actinomycin D, isolated from *Streptomyces* sp. in 1940, has been widely used in clinical practice as an anticancer drug for treating multiple tumors by inhibiting RNA synthesis.[8] Himastatin, isolated from *Streptomyces hygroscopicus*, exhibits *in vivo* antitumor activity against localized P388 leukemia and B16 melanoma in mice.[9] Chloropeptin I, a peptide antibiotic isolated from *Streptomyces* sp. WK-3419, has a potent anti-HIV activity as a gp120-CD4 binding inhibitor.[10] The immunosuppressive drug tacrolimus (FK-506), isolated from the fermentation broth of soil-derived *Streptomyces tsukubaenis* in 1978, has been widely used in organ transplantation and treatment of eczema.[11,12]

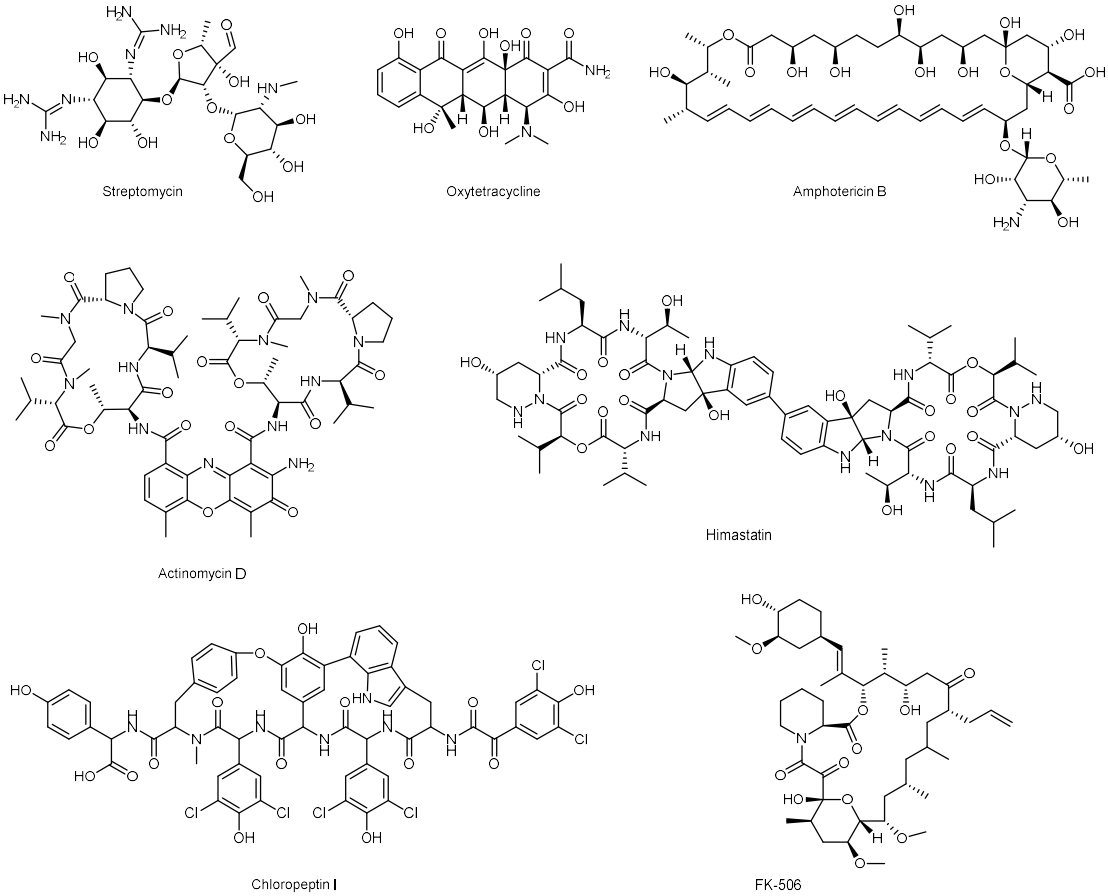

Fig. 2 Bioactive secondary metabolites produced by *Streptomyces*.

Biosynthetic genes encoding these bioactive secondary metabolites are usually clustered in *Streptomyces*, so-called biosynthetic gene cluster (BGC).[13] The variety of compositions within BGCs dictates the diversity of products. The complete genome of *Streptomyces coelicolor* A3(2) published in 2002 revealing that it harbors a total of 7,825 genes, including more than 20 BGCs coding for known or predicted secondary metabolites.[14] After that, with the application of high-throughput sequencing technology, it is becoming less difficult to obtain the genome information of a *Streptomyces* strain. To date (30-11-2023), there are a total of 3,341 genome assemblies of *Streptomyces* that have been released in the NCBI GenBank database. Meanwhile, the development of bioinformatics tools represented by antiSMASH has further revealed the excellent potential of *Streptomyces* to produce secondary metabolites from the DNA level.[15]

1.3 Biosynthesis mechanisms of secondary metabolites

1.3.1 PKS

Polyketides constitute a large and diverse group of *Streptomyces*-derived secondary metabolites with valuable pharmaceutical properties. Structurally, the carbon skeletons of polyketides comprise polyene, macrolides, polyphenols, enediynes, and polyethers.[16] Polyketides are assembled by multi-domain complex, polyketide synthase (PKS), using simple biosynthetic building blocks such as acetyl-CoA and malonyl-CoA.[17,18] Modular type I PKSs are the most common assembly line for polyketide biosynthesis in *Streptomyces*, their catalytic domains are physically grouped into modules that consist of a minimal set of domains for stepwise chain propagation. These include a ketosynthase (KS) that catalyzes the successive decarboxylative Clasien condensation with CoA-linked extender units, an acyltransferase (AT) that selects appropriate substrate and transfers acyl from CoA to the phosphopantetheine arm of acyl carrier protein (ACP), which tethers the growing chain to the enzyme. Additional domains may be present for keto group processing, such as ketoreductase (KR), dehydratase (DH), and enoyl reductase (ER). In general, the last PKS module terminates polyketide assembly with an additional thioesterase (TE). According to the molecular assembly line of modular PKSs, the order and architecture of the modules usually reflect the chain length as well as the degree of reduction of the resultant polyketide. The 6-deoxyerythronolide synthase (DEBS) required for archetypal erythromycin biosynthesis represents a well-studied example of modular type I PKS in bacteria (Fig. 2).[19] The biosynthesis model of iterative type I PKS, type II PKS, and type III PKS were also found in *Streptomyces*, which also confer the diversity of polyketides. In addition, several post-modification reactions such as oxidation, glycosylation, and methylation are often involved in the biosynthesis of polyketide products, which also shaped the structural diversity of polyketides.

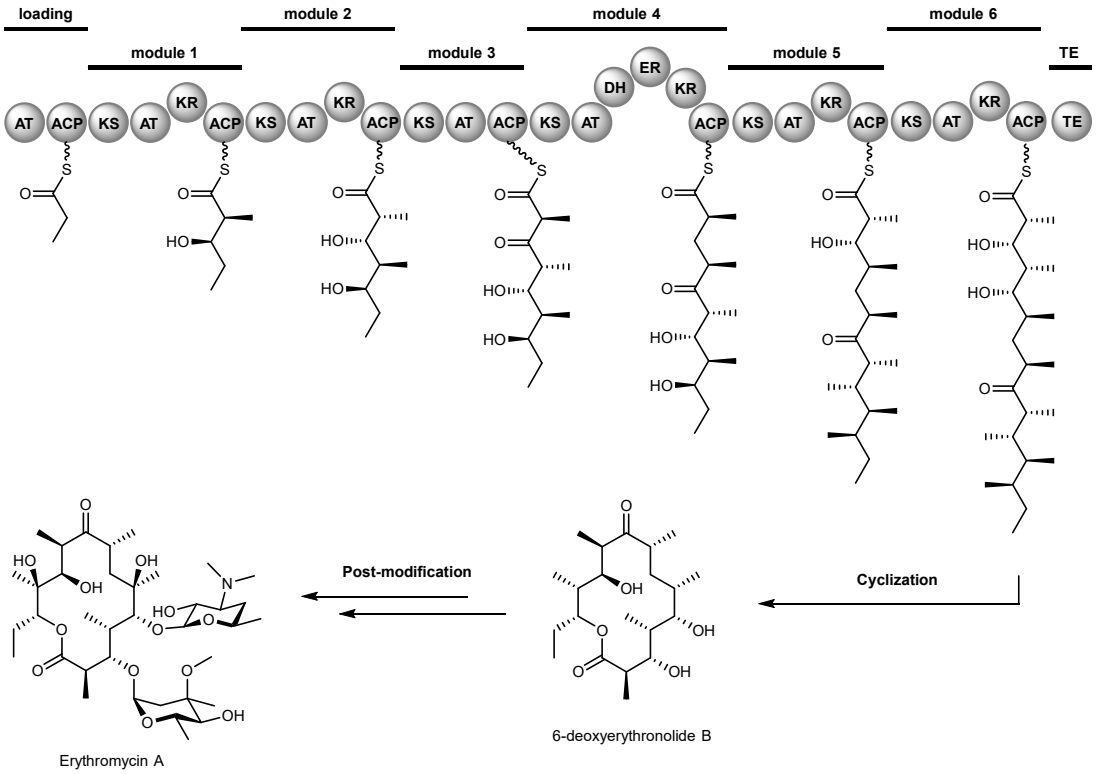

Fig. 2 The biosynthesis pathway of erythromycin A.

1.3.2 NRPS

Nonribosomal peptide-synthetase (NRPS) is composed of multiple modules, which are arranged in a specific spatial order. In general, each module includes multiple structural domains with different functions. A typical module includes 3 core structural domains, namely adenylation (A) domain, thiolation and peptide carrier protein with attached 4'-phosphopantetheine (T/PCP) domain, and condensation (C) domain.[20] The A domain is responsible for recognizing and activating amino acids as substrates, the T/PCP domain is responsible for transferring amino acids to the thiolation domain and growing peptide chains, while the C domain is responsible for catalyzing the formation of peptide bonds. Due to the A domain's key role in the specific recognition of substrates, it becomes possible to predict the structure of NRPS through sequence information.[21] In addition to A, T/PCP, and C domains, NRPS may also include some structural domains for peptide chain modification, such as epimerization (E) domain, oxidation (Ox) domain, formylation (F) domain, methylation (M) domain, heterocyclization (Cy) domain, and etc.[20] The last module of NRPS generally includes a thioesterase (TE) domain, which is responsible for terminating elongation and releasing the final product. Additionally, some TEs can also mediate the cyclization of the premature product. In addition, there are some terminal reductases or C domains that have similar activities to the TE domain and serve the function of releasing the final product.[22] The biosynthesis pathway of desotamide A represents a classical NRPS assembly line in

Streptomyces (Fig. 3).[23] In the past few years, the identification and elucidation of the biosynthetic mechanisms of NRPS incorporating non-natural amino acids, coupled with NRPS engineering, have presented significant potential for crafting NRPS with innovative structures and a wide range of bioactivities.[24,25]

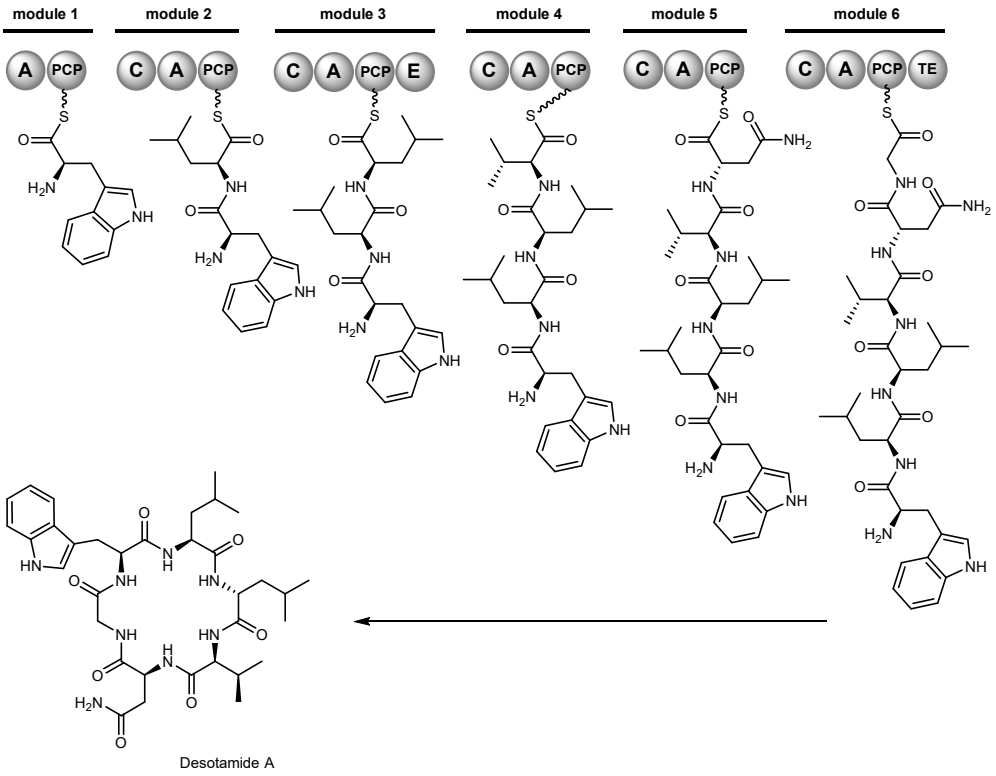

Fig. 3 The biosynthesis pathway of desotamide A.

1.3.3 RiPP

The biosynthesis of ribosomally synthesized and post-translationally modified peptides (RiPP) is based on precursor peptides (typically ~20–110 residues in length and encoded by a structural gene) synthesized by ribosome translation and structurally modified by a series of post-translational modifications.[26] In general, precursor peptides include an N-terminal leader peptide and a C-terminal core peptide. In some cases, C-terminal recognition sequence is required during the RiPPs biosynthesis. The biosynthetic machinery is initiated by the recognition of leader peptides and undergoing various post-translational modifications on core peptides, culminating in the removal of the leader peptide to yield the mature peptide. Complex and diverse post-translational modifications are an characteristic features of Ripps and play an extremely important role in the structural diversity and biological activity of RiPPs.[27] For instance, bottromycins are a class of antimicrobial RiPPs arising from an impressive series of modifications, which were originally isolated from *Streptomyces bottropensis* DSM 40262.[28] The biosynthesis studies of bottromycins showcase its precursor peptide does not contain an N-terminal leader peptide, but instead

a C-terminal extension of 35–37 amino acids.[29,30] Recently, An et. al. isolated and identified novel antibacterial RiPPs, cihunamides A-C, from volcanic-island-derived *Streptomyces* sp. GSM11.[31] The biosynthesis mechanism of cihunamides was elucidated via genome mining, comparative bioinformatics, and heterologous expression. The continuous emergence of RiPPs biosynthetic enzymes has greatly expanded our understanding of organic reactions in nature and the evolutionary adaptability of enzymes.

1.3.4 Terpenoid

Terpenoids are a large and highly diverse group of microbial natural products, which have valuable biological activities and are promising therapeutic agents.[32,33] Terpenoids are generally assembled by simple isoprene units including isopentenylallyl diphosphate (IPP) and dimethylallyl diphosphate (DMAPP). They are mainly biosynthesized through two pathways: mevalonate (MVA) pathway and methyl 2C-Methyl-D-erythritol-4-phosphate (MEP) pathway.[33,34] IPP and DMAPP are condensed under the action of polyisoprenyl diphpsphate synthase to form polyisoprenyl pyrophosphate chains of different lengths followed by cyclization and rearrangement to form a terpene skeleton under the catalysis of terpene cyclase. Typical bacterial terpene cyclase contains an Asp-rich domain and a downstream catalytic triad that binds to Mg^{2+}.[35] In addition, the cyclization reaction can also be initiated by epoxidation of linear isoprene chains.[36] Finally, these terpene products can be further diversified by subsequent modification reactions, such as methylation, hydroxylation, and glycosylation.[33,34] For example, teleocidin B is a unique indolactam-terpenoid isolated from *Streptomyces blastmyceticus* NBRC 12747, is a potent activator of protein kinase C. The biosynthesis studies of teleocidin B showed that there is a nonribosomal peptide synthetase (*tleA*), a cytochrome P450 monooxygenase (*tleB*), an indol prenyltransferase (*tleC*), and a C-methyltransferase (*tleD*) included in its BGC. Interestingly, the *tleD* is located outside the *tleABC* cluster and responsible for the catalyzation of the C-methylation of isoprene chain as well as the formation of indole-fused cyclic terpene structures.[37]

1.3.5 Hybrids

The hybrid biosynthesis of secondary metabolites in bacteria represents a sophisticated and versatile strategy employed by these bacteria in the production of complex bioactive molecules. So far, there are a variety of hybrid biosynthesis paradigms that have been reported. Hybrid assembly lines of PKS-NRPS construct intricately structured polyketide-amino acid/peptide hybrid molecules, incorporating both acyl and aminoacyl building blocks into their final products.[38] For example, bleomycin is an anticancer agent isolated from *Streptomyces verticillus* ATCC 15003, which is assembled by PKS-NRPS hybrid biosynthesis system.[39] The BGC of bleomycin consists of one PKS coding gene, seven NRPS coding genes, five sugar biosynthetic genes, as well as genes encoding other biosynthesis, resistance, and regulatory

proteins. The hybrid elongation chain is not conserved with gene order, and the *blmVII* (PKS gene) is responsible for malonyl-CoA insertion in the main peptide chain. Cinnamoyl-containing nonribosomal peptides (CCNPs), such as skyllamycin, atratumycin, anulamycin, is another class of PKS-NRPS molecules produced by different *Streptomyces* strains and exhibits various bioactivities.[40-42] The biosynthesis of CCNPs consists of two parts: a highly reduced Type II PKS moiety and a typical NRPS moiety. The cinnamoyl precursor biosynthesis begins with acetyl-CoA and progresses through multiple iterations, facilitated by the collaborative catalysis of ketosynthase/chain length factor, ketoreductase, dehydratase, and isomerase.[41] The mature cinnamoyl precursor is then introduced into the NRPS synthesis assembly line for loading of amino acids, followed by release and cyclization of premature products catalyzed by the TE domain in the last module. Furthermore, several studies have reported the biosynthesis of PKS-isoprenoid hybrids.[43,44] For example, Bringmann et al. discovered that the BGC of the polyketide-terpenoid hybrid compounds furanonaphthoquinone I and endophenazine A contains only a single gene for the MVA pathway synthesis gene.[44] Through isotope tracing experiments, the IPP precursor required for the assembly of furanonaphthoquinone I and endophenazine A was found to be provided by both the MVA (80%) and MEP (20%) pathways.[45]

1.4 CRISPR-based genome editing in *Streptomyces*

1.4.1 CRISPR-Cas9

The clustered regularly interspaced palindromic repeats (CRISPR)-Cas9 system is based on the natural immune process used by bacteria and archaea to defend themselves against invading viruses.[46] In the past decades, the CRISPR-Cas9 system was developed as a revolutionary tool in genome editing, operating on a sophisticated molecular mechanism rooted in the precise interplay of several key RNA molecules. CRISPR-Cas9 system requires two components: a Cas9 enzyme and a guide RNA (consists of crRNA and tracrRNA). To adapt this system for genome engineering, the fusion of crRNA and tracrRNA into a single synthetic guide RNA (sgRNA) transcript has been demonstrated.[47] Cellular repair mechanisms, such as non-homologous end joining (NHEJ) or homology-directed repair (HDR), facilitate the introduction of desired genetic modifications.[48] The precision and versatility of the CRISPR-Cas9 system make it a valuable tool for targeted genome editing, heralding a new era in genetic manipulation. The *Streptococcus pyogenes* CRISPR-Cas system (*spCas9*) has been successfully reconstructed in a variety of host organisms.[49,50] Targeting any site of interest merely requires the insertion of a short spacer into a CRISPR array/sgRNA construct, a process achievable rapidly and with high throughput DNA assembly techniques like Gibson assembly and Golden Gate assembly. The protospacer-adjacent motif (PAM) NGG responsible for specific recognition is very abundant in *Streptomyces*, which also facilitates the diversity of selectable targets.

Since 2015, several research groups have successively reported the application of CRISPR-Cas9 method for effective genome editing in *Streptomyces*.[51-53] Cobb et al. constructed the pSG5-based plasmid tool named *pCRISPomyces* including codon-optimized *spCas9*, sgRNA cassette, and apramycin resistance gene.[51] This plasmid could mediate the Type II CRISPR/Cas system of *S. pyogenes* to achieve targeted multiplex genome editing in various streptomycetes. Meanwhile, our group also developed a highly efficient CRISPR-Cas9-based toolkit to delete gene(s) and implement precise gene replacements in actinomycetes.[52] Moreover, a CRISPR interference (CRISPRi) method was constructed to control target genes' expression reversibly and efficiently by using a catalytically dead variant of Cas9 (dCas9). Compared with the classical PCR-targeting method based on cosmid libraries, the CRISPR-Cas9 tool greatly reduces the workload and time. In recent years, the CRISPR-Cas9 system for gene editing in *Streptomyces* has been continuously optimized to further optimize efficiency and reduce the off-target effect.[54,55]

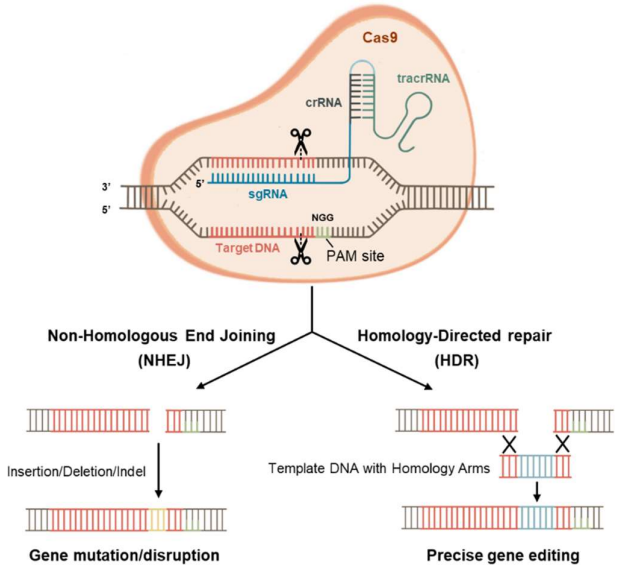

Fig. 4 CRISRP-Cas9 system in bacterial genome editing

1.4.2 CRISPR-Cas12a

Cas12a, also referred to as Cpf1, is a single RNA-guided endonuclease harnessed from class 2 type V-A CRISPR systems.[56] Upon binding to the target DNA, Cas12a undergoes a conformational change that activates its collateral, nonspecific endonucleolytic activity. This "trans-cleavage" activity of Cas12a not only induces cleavage at the intended target site but also results in indiscriminate cleavage of adjacent non-targeted single-stranded DNA. Importantly, the resultant DNA ends following Cas12a-mediated cleavage are predominantly sticky, which is distinguished from Cas9. CRISPR-Cas12a-based genome editing toolkit has been successfully used in different *Streptomyces* strains. For example, Li et al. developed a *Francisella novicida*-derived CRISPR-Cpf1 system for high-efficiency multiplex genome

editing and transcriptional repression in *Streptomyces*. In 2020, Zhang et al. developed CRISPR-FnCas12a system to conduct genetic manipulation in the industrial strain *Streptomyces hygroscopicus*, in which *SpCas9* does not work well.

1.4.3 CASCADE-Cas3

Type I CRISPR systems are widespread in bacteria and archaea and hold great potential for editing technologies.[59] The striking feature of Type I CRISPR systems are multi-effector CASCADE (CRISPR-associated complex for antiviral defense) needed for crRNA processing and target recognition, along with the 3'–5' single-strand DNA helicase-nuclease Cas3.[60] The endogenous CRISPR–Cas3 systems have been demonstrated as an effective genome editing tool in various native hosts such as *Sulfolobus islandicus* (Type I-A), *Clostridium species* (Type I-B), *Escherichia coli* (Type I-E), and *Pectobacterium atrosepticum* (Type I-F).[61-64] In 2020, Csörgő et al. optimized and used the Type I-C CRISPR system from *Pseudomonas aeruginosa* (*PaeCas3c*) to effectively generate genomic deletions in distinct bacteria including *E. coli*, *Pseudomonas syringae*, and *Klebsiella pneumoniae*.[65] Compared with helicase domain-absence *spyCas9*, Cas3 also showed advantages in knocking out large DNA fragments in bacteria. Recently, the CASCADE-Cas3 genome editing system was also successfully introduced into streptomycetes by our group.[66] The plasmid, called *pCRISRP-Cas3*, utilizes an optimized Type I-C CRISPR system to enable highly efficient deletions in *S. coelicolor* and *Streptomyces venezuelae*. These results highlight the promise of CASCADE-Cas3 as an important member of the CRISPR genome editing toolbox in *Streptomyces*.

1.4.4 CRISPR base editing

The expression of Cas9 in many *Streptomyces* strains has caused severe toxic effects and led to numerous unwanted off-target effects.[48,67] In addition, the linear chromosome of *Streptomyces* exhibits relatively high intrinsic instability with occasional large-scale chromosomal deletions and rearrangements.[68] DNA double-strand break (DSB) might act as the primary trigger of this instability and often occur concurrently with classical DSB-based genetic manipulation methods.[69] In 2019, our group developed a DSB-free CRISPR base editing method called CRISPR-BEST in *Streptomyces* to enable the effective conversion of C:G base pair to T:A base pair and A:T base pair to G:C base pair, which significantly accelerated the experiment process of gene inactivation and site-directed mutation.[70] The fusion of Cas9n(D10A)-cytidine deaminase (CRISPR-cBEST) and Cas9n(D10A)-adenosine deaminase (CRISPR-aBEST) exhibits great editing efficiency in the editing window. Meanwhile, the development of the online tool CRISPy-Web greatly facilitates the rapid selection of suitable sgRNA sites.[71] Another advantage of CRISPR base editing technology is that it can simultaneously conduct multiplex editing events. Recently, our group used Csy4-based sgRNA arrays to establish a multiplexed CRISPR base editing method in *S. coelicolor* that can edit up to 15 genes in one experiment, which significantly improves the throughput of

genetic manipulation.[72]

1.5 Metabolic engineering

1.5.1 Manipulation of regulator and transporter

The biosynthesis mechanism of secondary metabolites in *Streptomyces* is precisely regulated by multiple genes.[73] Tuning of regulatory and transportation mechanisms that control gene expression and product metabolism is an approach to increase the production of valuable fermentation bioactive secondary metabolites in *Streptomyces*.

The LuxR family regulator is one of the important pathway-specific regulators in *Streptomyces*. Its N-terminus has the conserved ATP/ADP binding domain with Walker A motif and Walker B motif, and its C terminus contains a helix-turn-helix (HTH) responsible for DNA binding.[74] The LuxR regulator PimM has been proven to positively regulate the biosynthesis of pimamycin in *Streptomyces natalensis*;[75] GdmRI and GdmRII can regulate the biosynthesis of geldanamycin in *Streptomyces hygroscopicus* 17997;[76] TmcN can regulate the biosynthesis of allosteric bacteria in *Streptomyces* sp. CK4412.[77] Li et al. demonstrated that the overexpression of a native LuxR regulatory gene led to 1.3-fold increased production of bafilomycins in marine-derived *Streptomyces lohii* ATCC BAA-1276. Recently, Park et al. discover lipoxiamycins A and B, which are new members of the xiamycin family and possessed a lipophilic chain linked to the indolosesquiterpenoid core structure by a N–O bond, through overexpression of LuxR regulator *orf2011* in a marine bacterium *Streptomyces* sp. HK18.[79]

SARP family regulator is another pathway-specific antibiotic regulatory gene, which is composed of an N-terminal DNA binding domain and a bacterial transcriptional activation domain.[73] ActII-ORF4, which regulates actinomycin biosynthesis, RedD, which regulates undecylprodigiosin biosynthesis, and CcaR, which regulates cephalosporin C biosynthesis, all belong to the SARP family regulators.[80-82] The manipulation of SARP family regulators also showed the potential to promote the production of secondary metabolites. Krause et al. reported that integration of heterologous SARP-type regulator gene *papR2* in *Streptomyces lividans* leads to the activation of the silent undecylprodigiosin gene cluster.[83] Li et al. identified a SARP family transcriptional regulator PieR in the BGC of piericidin A1, the overexpression of PieR in *Streptomyces piomogeues* resulted in 2.3-fold improvement of piericidin A1 production.[84]

ATP-binding cassette (ABC) transporter constitutes one of the largest families of membrane proteins in most organisms. Typically, an ABC transporter is composed of two components: hydrophilic nucleotide-binding domains (NBDs) and hydrophobic transmembrane domains (TMDs).[85] During performing the

transmembrane transport function, the transported substrates are first recognized and bound by the TMDs of the ABC transporter. Then the NBDs provide energy by catalyzing ATP to facilitate the TMDs pumping the substrates outside the cell through the membrane channel. ABC transporters were widely distributed in various BGCs and participated in multiple biological processes like antibiotic secretion, self-resistance, and feedback inhibition.[86,87] Overexpression of ABC transporter is one of the practical methods to improve the production of microbial secondary metabolites directionally. For example, overexpression of the ABC transporter AvtAB significantly increases avermectin production in *Streptomyces avermitilis*. The intracellular/extracellular accumulation ratio of avermectin B1a was also decreased from 6:1 to 4.5:1 in response to multiple copies of AvtAB.[87] Jin et al. used native temporal promoters to tune the expression of two ATP-binding cassette transporters TP2 and TP5, resulting in a maximal milbemycin A3/A4 titer increase by 36.9% to 3,321 mg/L in *Streptomyces bingchenggensis*.[88] In addition, TP2 and TP5 exhibit their important roles in other two macrolide biopesticide producers *Streptomyces avermitilis* and *Streptomyces cyaneogriseus*, introduction of TP2 and TP5 led to a maximal titer improvement of 34.1% and 52.6% for avermectin B1a and nemadectin, respectively.[88] In summary, overexpression of positive regulator genes and transporter genes is an effective strategy in metabolic engineering of specialized metabolites production in *Streptomyces*.

1.5.2 Promoter engineering

Promoters, serve as recognition sites for RNA polymerase, play a pivotal role in governing gene transcription in *Streptomyces* and exhibit a distinctive architecture characterized by conserved elements that contribute to their functionality.[89] The core promoter region typically encompasses the -10 and -35 conserved motifs, recognized by the RNA polymerase with associated sigma factor.[90] In addition to these conserved elements, promoters in *Streptomyces* often feature extended -10 motifs and an AT-rich spacer region between the -10 and -35 motifs, contributing to promoter strength and specificity.[91] The several natural constitutive promoters (like *ermE*p from *Saccharopolyspora erythraea*, SF14p from phage I19 isolated from *Streptomyces ghanaensis*, and *kasO*p from *S. coelicolor*) and inducible promoters (like *tipA*p from *Streptomyces lividans*, and *nitA*p from *Rhodococcus rhodochrous* J1) were previously identified and used to tune gene expression in *Streptomyces*.[90] Subsequently, researchers performed multiple site-directed mutagenesis on these natural promoters to obtain a series of robust artificial promoters, such as *ermE*p* and *kasO**p.[92,93] The availability of well-optimized promoters offers the possibility to use them for metabolic engineering in *Streptomyces*.[94] Promoter engineering has exhibited great potential in activating silent BGCs and improving the yield of secondary metabolites. In 2017, Zhang et al. developed a CRISPR-Cas9-based promoter knock-in strategy to rapidly introduce *kasO**p into *Streptomyces roseosporus* NRRL15998 and successfully activated two silent BGCs.[95] Through promoter engineering combined with fermentation optimization, Heng et al. activated a cryptic aromatic

polyketide BGC to obtain three new pentangular polyphenols lanthomicins A–C in *Streptomyces chattanoogensis* L10.[96] The yield of a potent bioherbicide thaxtomin A was also remarkably enhanced by refactoring the BGCs with strong constitutive synthetic promoters in *S. coelicolor* M1154.[97]

1.5.3 Precursors engineering

Secondary metabolites are usually composed of simple primary metabolites, and the availability of these foundational compounds can significantly constrain the synthesis of secondary metabolites. Precursor enhancement serves as a potent tool to augment the production yield of secondary metabolites. By bolstering the supply of essential precursors, the metabolic flux is directed toward the desired pathways, resulting in elevated production levels. This aspect is particularly crucial for industries involved in the production of pharmaceuticals and other valuable secondary metabolites. Taking polyketides as an example, common building blocks include acetyl-CoA, malonyl-CoA, methylmalonyl-CoA, and ethylmalonyl-CoA.[17,98] The accumulation and utilization of these substrates in *Streptomyces* largely affects the yield of polyketides. Wang et al. observed that the breakdown of intracellular triacylglycerols pool could redirect carbon flux towards polyketide biosynthesis based on multi-omics analysis. They enhanced this process by overexpressing specific acyl-CoA synthetases, leading to an improvement of polyketides production.[99] Acetyl-CoA carboxylase uses acetyl-CoA and bicarbonate as substrates to catalyze the formation of malonyl-CoA in an ATP-dependent manner. Liao et al. improved the titer of the antifungal polyene macrolide rimocidin up to 320.7 mg L^{-1} via overexpression of acetyl-CoA carboxylase to increase the supply of precursor malonyl-CoA in *Streptomyces rimosus* M527.[100] However, bicarbonate usually has low cell membrane permeability, and intracellular CO_2 conversion to bicarbonate is less efficient, limiting the use of malonyl-CoA and methylmalonyl-CoA during the production of polyketides.[101] Therefore, Hao et al. introduced heterologous genes *bicA* and *ecaA*, involved in cyanobacterial CO_2-concentrating mechanism, to improve intracellular CO2 concentration in *Streptomyces avermitilis*, leading to increased supply of malonyl-CoA and methylmalonyl-CoA precursors and increasement of avermectin B1a titer.[102] In addition, Lombó et al. successfully enhanced the production of 6-deoxyoerthronolide B in *S. coelicolor* through expressed malonyl-CoA synthetase MatB and dicarboxylate transport protein MatC from *Rhizobium trifolii*.[103] The crotonyl-CoA carboxylase/reductase (CCR) is responsible for the biosynthesis of diverse polyketide extender unit substrates, like ethylmalonyl-CoA and propylmalonyl-CoA.[98] The CCR homology SLNWT464 had been proved to be responsible for the formation of ethylmalonyl-CoA in *Streptomyces albus* DSM 41395.[104] Lu et al. demonstrated that the overexpression of SLNWT464 significantly increased the production of salinomycin.[104] In summary, the improvement of precursor supply is also an important means of metabolic engineering in *Streptomyces*.

1.5.4 Heterologous expression

Heterologous expression, the introduction of exogenous genetic elements into the genome of an organism, has emerged as a powerful strategy in the metabolic engineering of secondary metabolites in *Streptomyces* species. Native regulatory mechanisms may impose limitations on the expression of certain biosynthetic genes. Heterologous expression offers a solution by circumventing these regulatory constraints, allowing for the unhindered expression of foreign biosynthetic pathways, and consequently improving the overall titer of secondary metabolites.[105] The *attB* sequences are widespread existed in diverse *Streptomyces* genomes, facilitating the convenient use of ϕC31 integrase-based site-specific recombination for the rapid transformation of heterologous gene elements in engineered hosts.[106] In addition, the development of engineered *Streptomyces* chassis strains also provides the basis for efficient heterologous expression of BGCs.[107,108] Recently, the development of advanced CRISPR-assisted in vitro larger BGC capture also facilitated the application of heterologous expression in *Streptomyces*.[109,110] Therefore, heterologous expression has become an effective tool to activate silent BGC and improve the production of secondary metabolites. Yang et al. constructed a marine-derived Streptomyces chassis strain with a clean metabolic background by eliminating bypass metabolism. Based on this artificial host, site-specific recombination mediated by the ϕC31 integrase was successfully employed to achieve the heterologous expression of 19 secondary metabolites with notable efficiency.[106] Yin et al. transferred the BGC of oxytetracycline into a fast-growing heterologous host *Streptomyces venezuelae* WVR2006 and the production of oxytetracycline was significantly increased in this heterologous host from 75 to 431 mg L^{-1} only in 48 h.[111] Recently, Xu et al. reported the discovery of a novel β-lactone compound, globilactone A, through heterologous expression of a PKS-NRPS hybrid BGC in *Streptomyces albus* J1074.[112]

1.5.5 Genome-scale metabolic model

Genome-scale metabolic model (GEM), serving as a systemic biology tool, proficiently simulates and analyzes the intricate interactions among genes, proteins, and metabolites within the cellular milieu.[113] Through the amalgamation of extensive datasets stemming from genomics, transcriptomics, and metabolomics, these models intricately delineate the complex relationships governing myriad genes and metabolites.[114,115] With the development of DNA sequencing techniques and bioinformatics tools, the construction of a GEM for a new strain is rapid and less cumbersome.[116] Moreover, some algorithms aimed at increasing the production of specific metabolites have been developed, such as OptKnock, RobOKoD, IdealKnock, and GECKO.[117-120] GEM-based metabolic engineering was also widely used in *Streptomyces*.[121] In 2018, Wang et al. developed a versatile toolbox for metabolic network reconstruction namely RAVEN 2.0, which had been proved to effectively help optimize the production of actinorhodin, undecylprodigiosin, calcium-dependent antibiotic and geosmin in *S. coelicolor*.[122] Fondi et al. utilized an

integrated systems biology approach to characterize the metabolic landscape of *Streptomyces ambofaciens*, identifying potential metabolic engineering targets for enhanced spiramycin production.[123] Model predictions, experimentally validated through genetic manipulation, demonstrate the utility of in silico modeling for optimizing secondary metabolism in *S. ambofaciens*. As our understanding of microbial metabolic networks continues to deepen, the guiding role of GEMs in metabolic engineering will become increasingly prominent.[124]

1.6 Genome mining

Genome mining is a promising method of microbial bioprospecting, plays a crucial role in the exploration and exploitation of microbial secondary metabolites for pharmaceutical and industrial applications. By leveraging advanced genomic technologies, such as high-throughput sequencing and bioinformatics tools, genome mining enables the systematic identification, characterization, and prioritization of BGCs responsible for producing secondary metabolites in microorganisms.[125-127] This approach not only facilitates the discovery of novel bioactive compounds but also streamlines the optimization of microbial strains through targeted genetic manipulation, thereby unlocking the vast potential of microbial secondary metabolites for biotechnological development. Up to date, a variety of genome mining tools and methods have been proposed from different perspectives (Tab. 1).[128]

Tab. 1 The bioinformatics tools used in bacterial genome mining (Sources from ActinoBase).

Name	Functions
antiSMASH	Identification and annotation of secondary metabolite gene clusters
PRISM	Identification of nonribosomal peptides, type I and II polyketides and RiPPs
BAGEL	Identification of gene clusters for bacteriocins and RiPPs
CLUSEAN	Annotation and analysis of secondary metabolite gene clusters
ClusterFinder	Identification of secondary metabolite gene clusters
ARTS	Genome mining for secondary metabolites and potential antibiotics based on antibiotic resistance targets
2metDB	Genome mining for polyketides and nonribosomal peptides
PKMiner	Genome mining for type II polyketide synthases
SBSPKS	Sequence analysis of polyketide synthases
RiPPMINER	Genome mining and deciphering chemical structures of RiPPs
RODEO	Identification of BGCs and prediction of RiPP precursor peptides
RiPPER	Identification of RiPP precursor peptides and BGCs
BiG-SCAPE	Identification of gene cluster families and BGC similarity network construction through a collection of genomes
EvoMining	Identification of expansions of gene families from central metabolism that have been recruited into BGCs
BiG-SLiCE	Identification of cross-species BGC patterns from big data

1.6.1 Core biosynthetic genes-guided genome mining

As mentioned before, different types of microbial secondary metabolites are usually catalyzed using different types of biosynthetic enzymes, like PKS, NRPS, and ribosomally synthesized and post-translationally modified peptides (RiPPs). Based on structural conservation of these biosynthetic enzymes, BGC annotation tools including CLUSEAN and antiSMASH provide a fast and reliable way to understand the biosynthetic genes architecture within a given strain.[15,129] To date, many successful instances targeting to PKS and NRPS genes have been reported wherein genome mining methods have effectively targeted core biosynthetic genes, leading to the discovery of novel secondary metabolites from *Streptomyces*.[130] Wang et al. performed a bioinformatics analysis of sequenced bacterial genomes, unveiling a BGC with the potential to encode structurally diverse colistin homologs. The chemical synthesis of this structure yielded malacacin, exhibiting activity against Gram-negative pathogens expressing plasmid-borne mobilized colistin-resistance *mcr-1* and intrinsically resistant pathogens harboring a chromosomally encoded phosphoethanolamine transferase gene.[131] Using a similar methodology, they discovered a novel bifunctional lipopeptide antibiotic called cilagicin, which exhibits great antibacterial activity against multidrug-resistant clinical pathogens.[132] In 2022, Ueoka et al. conducted genome mining on the plant root-associated marine bacterium *Gynuella sunshinyii*, uncovering an atypical PKS-type gene cluster. They later isolated its corresponding products, janustatins, distinguished by a unique chemical structure and marked cytotoxic activity.[133] Recently, Hu et al. used terpene synthase as the target to explore the biosynthesis potential of terpenoids based on the massive bacterial genome database.[134] The sequence similarity network analysis of these detected terpene synthases suggested that there are many terpenoids that are still unknown. The heterologous expression of 16 novel terpene BGCs in engineered host *S. albus* J1074M resulted in the discovery of three new terpene skeletons.

1.6.2 Tailoring enzymes-guided genome mining

In addition to the core biosynthetic genes, specific tailoring enzymes responsible for the post-modification of certain microbial secondary metabolites also present viable targets for genome mining. For example, cytochrome P450 enzymes play a crucial guiding role in natural product biosynthesis by catalyzing a series of reactions, Malit et al. conducted a comprehensive global genome mining analysis of 162,672 bacterial genomes, uncovering 829 cyclodipeptide BGC with cytochrome P450 gene.[135] Through heterologous expression, two novel crownlike cyclodipeptides were isolated and identified. Moreover, two cytochrome P450s within the BGC were demonstrated to catalyze sequential reactions, leading to the cyclization of diketopiperazine dimers. Due to the importance of halogenation in terms of structural diversity, bioavailability, and biological activity, the search for new halogenated bioactive

compounds has become an interesting problem in the field of natural product discovery. Prado-Alonso et al. conducted a screening for halogenase coding genes in 12 *Streptomyces* strains isolated from fungus-growing ants of the *Attini* tribe. Through combing genome editing and metabolomics methods, a novel family of halogenated compounds, colibrimycins, were isolated and identified from *Streptomyces* sp. strain CS147.[136] In addition, targeted mining of BGC-specific regulatory genes (like LuxR family regulators and SARP family regulators) and transport genes (ABC transporters) has become an important method for genome mining.[137]

1.6.3 Resistance genes-guided genome mining

The resistance gene of microbial active natural products is a key gene present in microorganisms to protect the producing strains from toxic metabolites synthesized by themselves. By targeting resistance genes, BGCs with potentially important biological activities could be preferred from massive sequencing data.[138] An attractive example is the discovery of the natural herbicide aspterric acid with a new mode of action using the resistance-gene-directed method.[139] Dihydroxy-acid dehydratase, a key enzyme in the branched-chain amino acid biosynthetic pathway in plants, was used as a target to search for co-localized biosynthetic genes in filamentous fungi and revealed the BGC of aspterric acid. Vandova et al. applied the concept of genetically encoded self-resistance to identify and sequence PKS-type BGCs. This approach resulted in the creation of a catalog comprising 190 unique PKS clusters, with their products likely targeting known enzymes of antibacterial significance.[140] Additionally, this study identified a set of putative self-resistance genes, which could prove valuable in the identification of small molecules effective against novel microbial targets. Recently, Yuan et al. reported the development of a self-resistance gene-guided genome mining platform called FAST-NPS, which greatly increases the speed of *Streptomyces*-derived bioactive natural product development by incorporating laboratory automation.[141] Given the emergence of antibiotic-resistant pathogens and the pressing demand for novel antibiotics featuring innovative modes of action, the utilization of resistance-based genome mining technology is poised to evolve into a crucial toolset for the future exploration of distinct antibacterial compounds and the investigation of their mechanisms of action.[128]

1.6.4 Phylogeny-based genome mining

Phylogeny-based genome mining is a powerful approach that utilizes evolutionary relationships to uncover valuable genetic information within microbial genomes. By constructing phylogenetic trees based on the sequences of known and unknown marker genes, this method enables the rapid identification and prioritization of BGCs. These clusters often encode pathways responsible for the synthesis of secondary metabolites with diverse biological activities. Phylogeny-based genome mining has proven instrumental in efficiently navigating large datasets, aiding in the discovery of novel

biosynthetic pathways, and advancing our understanding of microbial secondary metabolism.[128] In 2012, Ziemert et al. developed a phylogeny-based bioinformatic tool NaPDoS to rapidly extract and classify KS and C domains from a wide range of sequence data.[142] In 2022, Klau et al. updated NaPDoS2 that integrated more KS sequences with the taxonomic and functional diversity represented in the webtool database.[143] NaPDoS2 provides a fast and high-resolution way to assess PKS biosynthetic potential using genomic, metagenomic, and PCR amplicon datasets. Another amazing example of phylogeny-based genome mining tool is EvoMining, which provides a powerful tool for uncovering new chemical scaffolds and providing guidance for the discovery of new antibiotics.[144]

1.6.5 Comparative genome mining

Comparative genome mining is essential for understanding the genetic diversity and functional potential across different microbial strains or species.[128] By systematically comparing genomes, researchers can identify conserved BGCs and discern variations that may lead to the discovery of novel bioactive compounds or metabolic pathways. In 2020, Navarro-Muñoz et al. established a computational framework to explore biosynthetic diversity based on the large-scale genome sequence dataset.[145] They designed a useful software namely BiG-SCAPE to enable interactive sequence similarity network analysis and clustering of microbial BGCs. The analysis of 3,080 actinomycete genomes using BiG-SCAPE revealed that BGCs of detoxin and rimosamide are taxonomically widespread and structurally diverse. Furthermore, Kautsar et al. developed a highly scalable BGCs analysis tool, BiG-SLiCE, to rapidly annotate and align the microbial BGCs by grouping them into gene cluster families (GCFs) in a non-pairwise, near-linear manner. Meanwhile, Kautsar et al. also established the BiG-FAM database consisting of 29,955 GCFs and an online interactive interface, which simplifies the use of computational workflow to analyze specific strain genomes or gene clusters in a user-friendly fashion.[147] In addition, the development of pangenome analysis tools, like Roary and PGAP, also effectively facilitate the progress of funding novel BGCs and biosynthetic genes by alignment and comparison of different genome sequences.[148-149] Recently, our group developed an automatic genome mining workflow called BGCFlow, which integrated multiple state-of-the-art genomic analysis tools for data selection, functional annotation, phylogenetic analysis, genome mining, and comparative analysis.[150] In the foreseeable future, data-driven genome mining methods will become the first choice for discovering bioactive microbial natural products.

1.6.6 Metagenome-based genome mining

With the development of DNA sequencing with long reads, high accuracy, and high throughput, we could more easily explore the biosynthetic information we need from metagenomic data.[151] Metagenome-based genome mining holds significant importance in microbial exploration by tapping into the collective genetic

material of entire microbial communities.[152] This approach allows researchers to analyze the genetic potential of diverse microorganisms without the need for individual isolates. By examining the collective metagenomic content, researchers can identify novel BGCs and unravel the metabolic capabilities of microbial communities in various environments. Metagenome-based genome mining is instrumental in expanding our understanding of microbial diversity, promoting the discovery of novel bioactive compounds, and facilitating the exploration of untapped genetic resources for potential biotechnological applications. In 2018, et al. used genome-resolved metagenomic methods to reconstruct draft genomes for hundreds of microorganisms from the soil ecosystem and found diverse PKS and BRPS BGCs that are divergent from well-studied clusters.[153] Recently, Lucas Paoli and his colleagues revealed the huge biosynthetic potential of the global ocean microbiome through the comprehensive analysis of 10,000 marine-derived microbial genomes obtained from both cultivated organisms and single cells, complemented by over 25,000 newly drafted genomes derived from over 1,000 seawater samples worldwide.[154] This breakthrough discovery reveals that there are still a large number of novel enzymes as well as microbial bioactive natural products waiting to be explored, especially in the marine environment.

1.6.7 AI-aided genome mining

Artificial Intelligence (AI) is a promising method in microbial natural product genome mining, streamlining the identification and analysis of BGCs, facilitating the discovery of novel compounds, and enhancing the efficiency of drug development from microbial sources.[155-157] Previously, the identification of natural product BGCs heavily relied on specific rules set artificially based on our knowledge of known biosynthetic information, which limited the prediction and analysis of novel gene clusters and non-clustered biosynthetic pathways. In recent years, various machine learning algorithms, such as DeepBGC, GECCO, and DeepRiPP, have gradually been integrated into genome mining and BGC prediction.[158-160] Moreover, the continuous reporting of AI's excellent performance in protein structure prediction, NMR and MS data processing, and multi-omics integration further promotes the development of AI-based genome mining method establishment.[155] With the ongoing accumulation of data and the iterative advancement of algorithms, AI-based genome mining methods are poised to proliferate in the future.

2. Results and discussion

2.1 Discovery and biosynthesis of plant growth-promoting pteridic acids

Increased water scarcity due to climate change poses a significant challenge for climate adaptation, and rising sea levels impact the salinity of coastal surface and groundwater. Climate-induced stress contributes to agricultural losses, jeopardizing global food security. [161] Drought, considered the most damaging environmental stress, directly affects the entire growth cycle of plants from germination to fruition.[162] Drought stress results in elevated osmotic regulators, inhibited photosynthesis, and altered endogenous hormone content.[163-165] Soil salinization, a growing threat to global agriculture, is particularly severe in coastal and arid regions. Factors such as irrigation with saline water, low precipitation, and high evapotranspiration contribute to rapid soil salinization.[168] These abiotic stresses, drought, and salinity pose unprecedented challenges to crop farming. In contrast to heavy chemical fertilizer use, the utilization of plant growth-promoting bacteria for enhancing plant growth under drought and salinity conditions is gaining attention for its sustainability. [169,170] Despite widespread claims regarding the efficacy of inoculating plant growth-promoting *Streptomyces*, the molecular mechanisms behind their growth-promoting effects and the specific role of secondary/specialized metabolites in this process remain largely unknown.

2.1.1 *S. iranensis* exhibits abiotic stress-mitigating activities in plant.

The impact of *S. iranensis* on barley growth was assessed amid various abiotic stresses, including osmotic, salinity, and drought. Osmotic stress was induced by adding 20% (w/v) PEG-6000 to soils, reducing water potential. *S. iranensis* notably mitigated osmotic stress, evident in treated seedlings exhibiting increased height, fresh weight, and dry weight compared to the untreated control group (Fig. 5a). The culture broth of *S. iranensis* exhibited significant activity in promoting barley growth under salinity stress induced by 100 mM NaCl (Fig. 5b), despite minimal enrichment of *S. iranensis* in the soil around barley roots. Moreover, *S. iranensis* treatment significantly enhanced barley growth recovery from drought stress, as observed in phenotypic analysis (Fig. 5c). Remarkably, *S. iranensis* stimulated barley seedling growth even under non-stress conditions, suggesting its potential as a biostimulant.

2.1.2 Genomic and metabolomic profiles of *S. iranensis*.

Genomic and metabolomic analyses were conducted on *S. iranensis* to identify potential bioactive components. Using antiSMASH 6.0, we annotated 47 putative secondary metabolite BGCs with diverse categories.[171] The clusters 3, 6, 7, 8, 23, 31, 35, and 40 exhibited over 80% similarity to BGCs responsible for coelichelin, azalomycin, nigericin, elaiophylin, desferrioxamin B, ectoine, rapamycin, and hygrocin

biosynthesis, respectively. High-resolution Liquid Chromatography-tandem Mass Spectrometry (HR-LC-MS/MS) and Global Natural Products Social (GNPS) molecular networking identified their corresponding products (Fig. 5d).[172] Despite these findings, numerous *S. iranensis* metabolites remain unknown. Given the absence of previously identified compounds associated with abiotic stress mitigation in plants, we upscaled the fermentation to 175 liters. The culture broth underwent separation through open-column chromatography on Amberchrom CG161Me resin, silica gel, and Sephadex LH-20. Bioactivity-guided fractionation resulted in the isolation of bioactive pteridic acid H along with its isomer pteridic acid F (Fig. 5e).

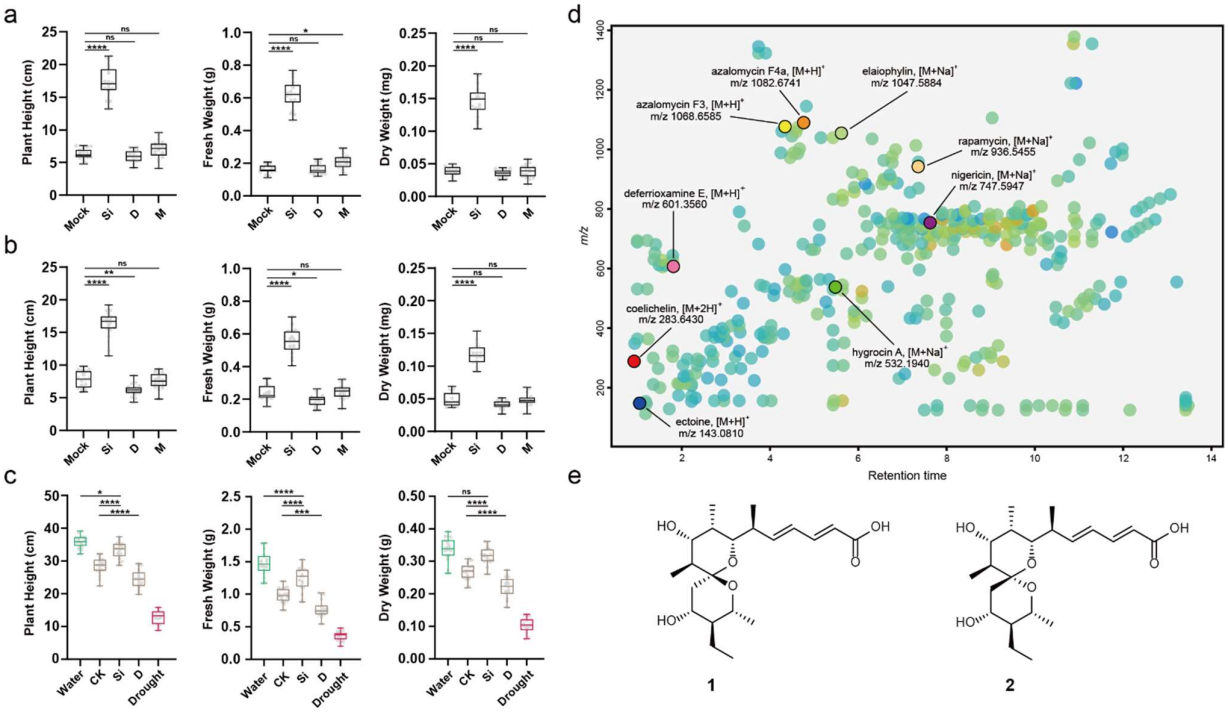

Fig. 5. The effect of *S. iranensis* on barley seedlings under the abiotic stress and the bioactive components produced by *S. iranensis*.

2.1.3 Pteridic acids alleviates abiotic stress in *Arabidopsis* seedlings.

Initially, different concentrations of pteridic acids H and F were tested on *Arabidopsis* growth without abiotic stress. A concentration of 0.5 ng ml^{-1} of both pteridic acids significantly promoted seedling growth. Under drought stress, pteridic acid H increased root length and fresh weight by 54.5% and 89%, surpassing the activity of IAA and ABA at the same molar concentration (Fig. 6a, 6c). Pteridic acid F also effectively alleviated drought stress, increasing root length and fresh weight by 30.5% and 56.7%, respectively (Fig. 6c). Pteridic acids demonstrated significant activity in mitigating NaCl-mediated salinity stress (Fig. 6b, 6d). Treatment with pteridic acids H and F increased root length by 74.0% and 61.8%, and fresh weight by 126.2% and 110.9%, respectively, compared to non-treated groups (Fig. 6d).

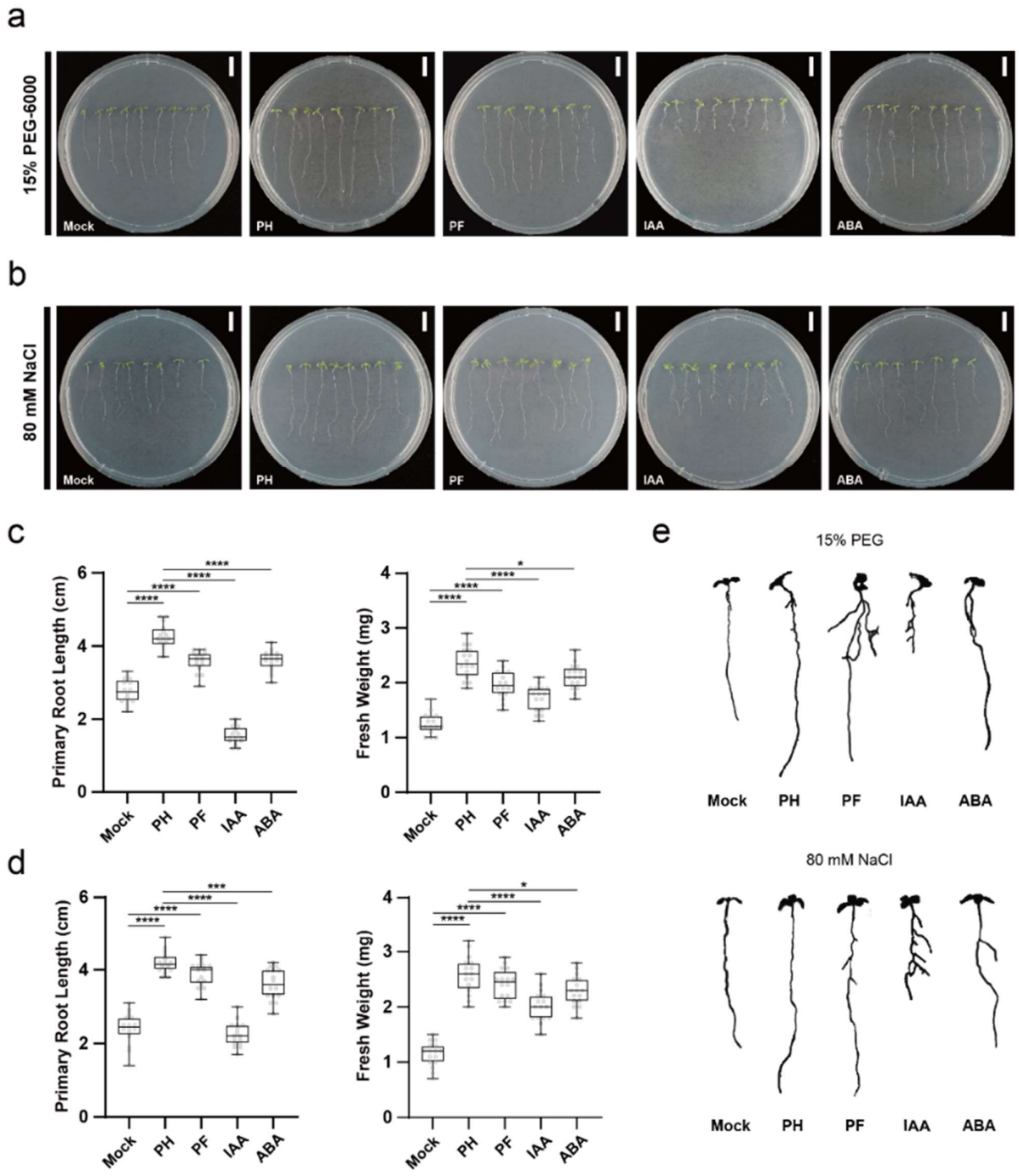

Fig. 6 The effect of pteridic acids H and F on *Arabidopsis* seedlings under abiotic stress.

2.1.4 Preliminary mode of action analysis of pteridic acids using RNA-seq.

To investigate the mechanism by which pteridic acids assist *Arabidopsis* in mitigating salinity stress, messenger RNA sequencing (mRNA-seq) was employed to profile the transcripts of *Arabidopsis* seedlings treated with pteridic acids F or H under NaCl-mediated salt stress (Fig. 7a). Significant differences in gene expression patterns were observed compared to the control (CK, treatment with an

equal amount of water under NaCl-mediated salt stress), as determined by Pearson correlation analysis. Differentially Expressed Genes (DEGs) analysis revealed 3,575 DEGs (1,405 upregulated and 2,170 downregulated) for pteridic acid H treatment versus control (PH vs. CK) and 3,727 DEGs (1,555 upregulated and 2,172 downregulated) for pteridic acid F treatment versus control (PF vs. CK). Additionally, 1,226 up-regulated genes and 1,860 down-regulated genes were shared between PH and PF treatments. Abiotic stress-related genes were significantly upregulated after pteridic acid treatment (Fig. 7b), including *SLAC1 HOMOLOGUE 1* (*SLAH1*, AT1G62280),[173] *PIN-FORMED* 6 (*PIN6*, AT1G77110),[174] *FERRIC REDUCTION OXIDASE* 6 (*FRO6*, AT5G49730),[175] and *TOO MANY MOUTHS* (*TMM*, AT1G80080).[176] Unique upregulation in PH treatment samples included *ALPHA CARBONIC ANHYDRASE* 8 (*ATACA8*, AT5G56330) and *IAA-LEUCINE RESISTANT* 2 (*ILR2*, AT3G18485),[177,178] while *ATP-BINDING CASSETTE* G17 (*ABCG17*, AT3G55100), *DIACYLGLYCEROL KINASE* 4 (*DGK4*, AT5G57690), and *MAP KINASE KINASE* 7 (*MKK7*, AT1G18350) were upregulated in the PF treatment samples.[179-181]

Among upregulated genes, enriched Gene Ontology (GO) terms such as "Photosynthesis (GO:0015979)," "Plastid organization (GO:0009657)," "Chloroplast organization (GO:0009658)," and "Response to light stimulus (GO:0009416)" suggested that pteridic acids enhance photosynthesis under abiotic stress. For DEGs with |log2FoldChange| ≥ 2, a total of 12 genes related to the "auxin-activated signaling pathway (GO:0009734)" were upregulated, indicating that pteridic acids trigger auxin-activated signaling transduction (Fig. 7c). Notably, downregulation of genes linked to "response to stimulus (GO:0050896)," "response to chemical (GO:0042221)," and "response to stress (GO:0006950)" suggested interference between different signaling pathways or a negative feedback mechanism for maintaining plant homeostasis (Fig. 7c).[182] Similar conclusions were supported by the Kyoto Encyclopedia of Genes and Genomes (KEGG) pathway analysis, highlighting activation of pathways like "Photosynthesis (ath00195)" and "Plant hormone signal transduction (ath04075)" in *Arabidopsis* seedlings. Additionally, pathways such as "Motor proteins (ath04814)," "Ribosome (ath03010)," "Glucosinolate biosynthesis (ath00966)," "Porphyrin metabolism (ath00860)," and "Flavonoid biosynthesis (ath00941)" were activated, known for their association with plant abiotic stress resistance.[183,184] Conversely, pteridic acids downregulated genes enriched in pathways like "Phenylpropanoid biosynthesis (ath00940)," "Cyanoamino acid metabolism (ath00460)," "Glutathione metabolism (ath00480)," "MAPK signaling pathway-plant (ath04016)," and "Starch and sucrose metabolism (ath00500)." Considering the established link between IAA signaling and salt stress in plants, we hypothesized that pteridic acids promote plant growth under salt stress by activating auxin signal transduction.[185,186]

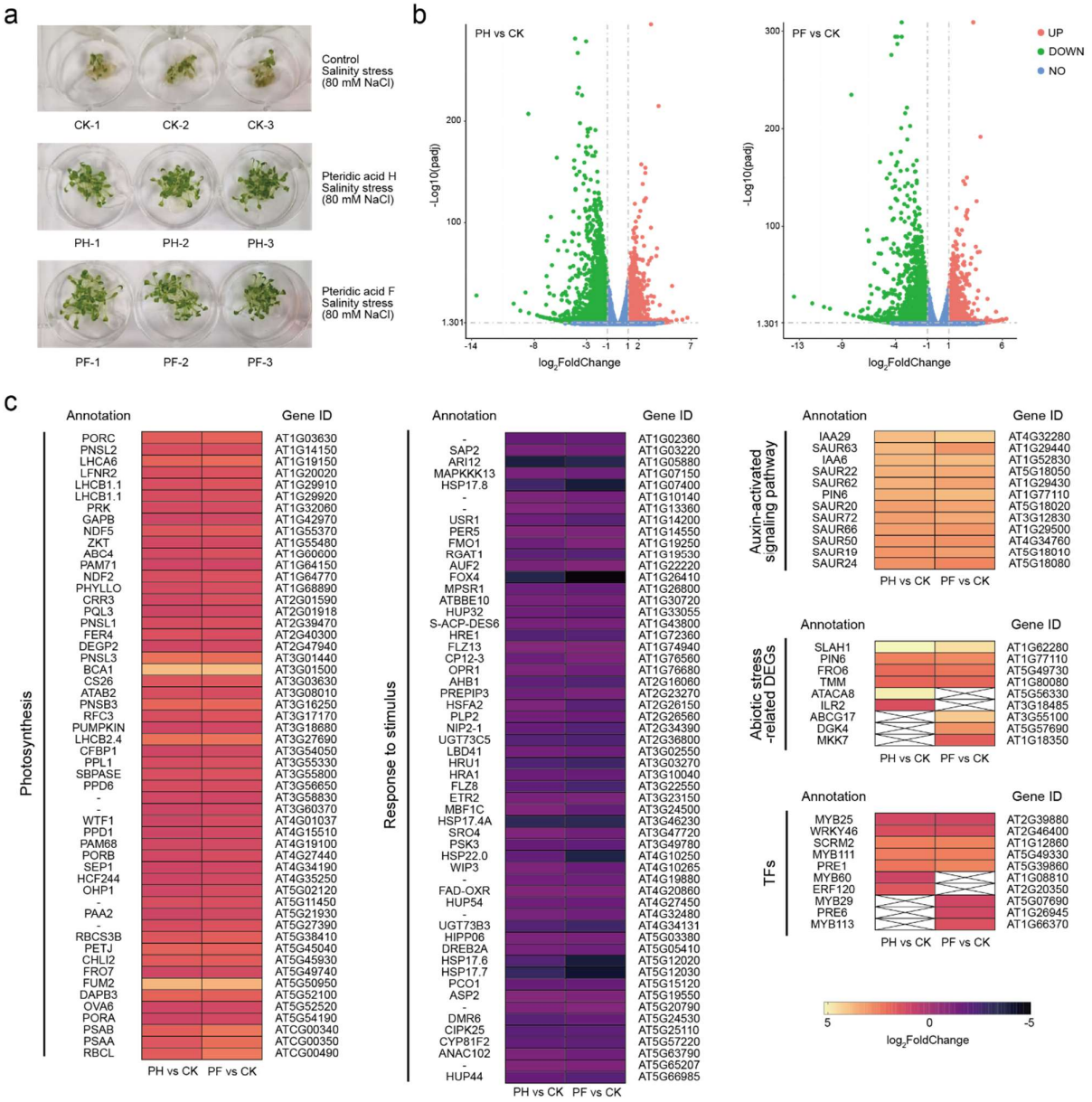

Fig. 7. Effect of exogenous pteridic acids on transcription in *Arabidopsis* seedlings under salt stress.

Transcription Factors (TFs) play a crucial role in enhancing abiotic stress tolerance in plants, with several TFs implicated in responses to salt stress, including AP2/ERF, bZIP, and MYB.[187-189] Among the Differentially Expressed Genes (DEGs), various TFs were identified within these DEGs, encompassing AP2/ERF (42 unigenes), MYB (35 unigenes), WRKY (27 unigenes), bHLH (31 unigenes), and bZIP families (6 unigenes). Noteworthy plant stress resistance-related TFs, such as MYB25, MYB111, WRKY46, PRE1, and SCRM2, were observed.[190-194] TFs associated with abiotic stress resistance, including MYB60 and ERF120, exhibited noticeable upregulation in PH treatment samples compared to the control.[195,196] Conversely, MYB29, MYB113, and PRE6 showed unique upregulation in the PF vs. CK group.[197,198] Among

these TFs, MYBs play diverse roles in plant biological processes, including growth, reproduction, secondary metabolism, and stress responses.[199] For instance, upregulated MYB25 reduces sensitivities to osmotic and salt stress in *Arabidopsis*, while upregulated MYB111 acts as a positive regulator of salt stress by binding to the promoter region of genes encoding flavonoid synthesis enzymes.[190,191] MYB60, upregulated in the PH vs. CK group, plays a dual role in abiotic stress responses through involvement in stomatal regulation and root growth for increased water uptake.[195] MYB29, uniquely upregulated in the PF vs. CK group, promotes lateral root growth under salinity stress.[197] MYB113 promotes anthocyanin biosynthesis for defense against abiotic and biotic stresses.[198] WRKY46, upregulated in pteridic acid-treated samples, enhances root development during salt stress through ABA signaling modulation, although other ABA-related DEGs were not observed.[192] Additionally, the upregulated bHLH family TFs PRE1 and SCRM2 experimentally promote plant growth and resistance to abiotic stress.[193,194]

2.1.5 Biosynthesis mechanism of pteridic acids.

Retro-biosynthesis analysis revealed that pteridic acids likely originate from a modular type I polyketide synthase. A putative pta BGC was identified in the whole genome of *S. iranensis*, sharing 87% antiSMASH similarity with the elaiophylin BGC (BGC0000053 in MiBiG database).[199] The *pta* BGC, spanning about 56 kb, comprises 20 biosynthetic genes responsible for core polyketide backbones, precursors, glycosylated substituents, transporters, and regulators. The five consecutive Type I polyketide synthase (PKS) genes in the *pta* BGC include a loading module and seven extender modules, sequentially extended to form a linear polyketide chain with ketosynthase (KS), acyltransferase (AT), acyl carrier protein (ACP), and additional ketoreductase (KR), dehydratase (DH), and enoyl reductase (ER) domains. Substrate specificity predictions for individual AT domains align with pteridic acids' structure. The KR domain in module 3 (PtaB) lacks the conserved "Asn" residue, indicating inactivity and consistent with the nonreduced carbonyl group on the α-carbon in module 3. The inactive first DH domain in module 1 lacks the conserved active motif, suggesting its inactivity. Thioesterase-mediated release of the polyketide chain is followed by spontaneous spiroketalization of the carbonyl group on C11 and the two hydroxyl groups on C17 and C25, forming the 6,6-spiroketal core structure of pteridic acids F and H (Fig. 8a). Notably, pteridic acid H exhibits molecular instability under extreme conditions, transforming into pteridic acid F in high-temperature (65°C) or acidic (pH = 3) water solutions. A similar spontaneous transformation from (*S*) to (*R*) chirality in the center of the spiroketal ring was observed, reminiscent of the process in 6,6-spiroketal avermectin.[200]

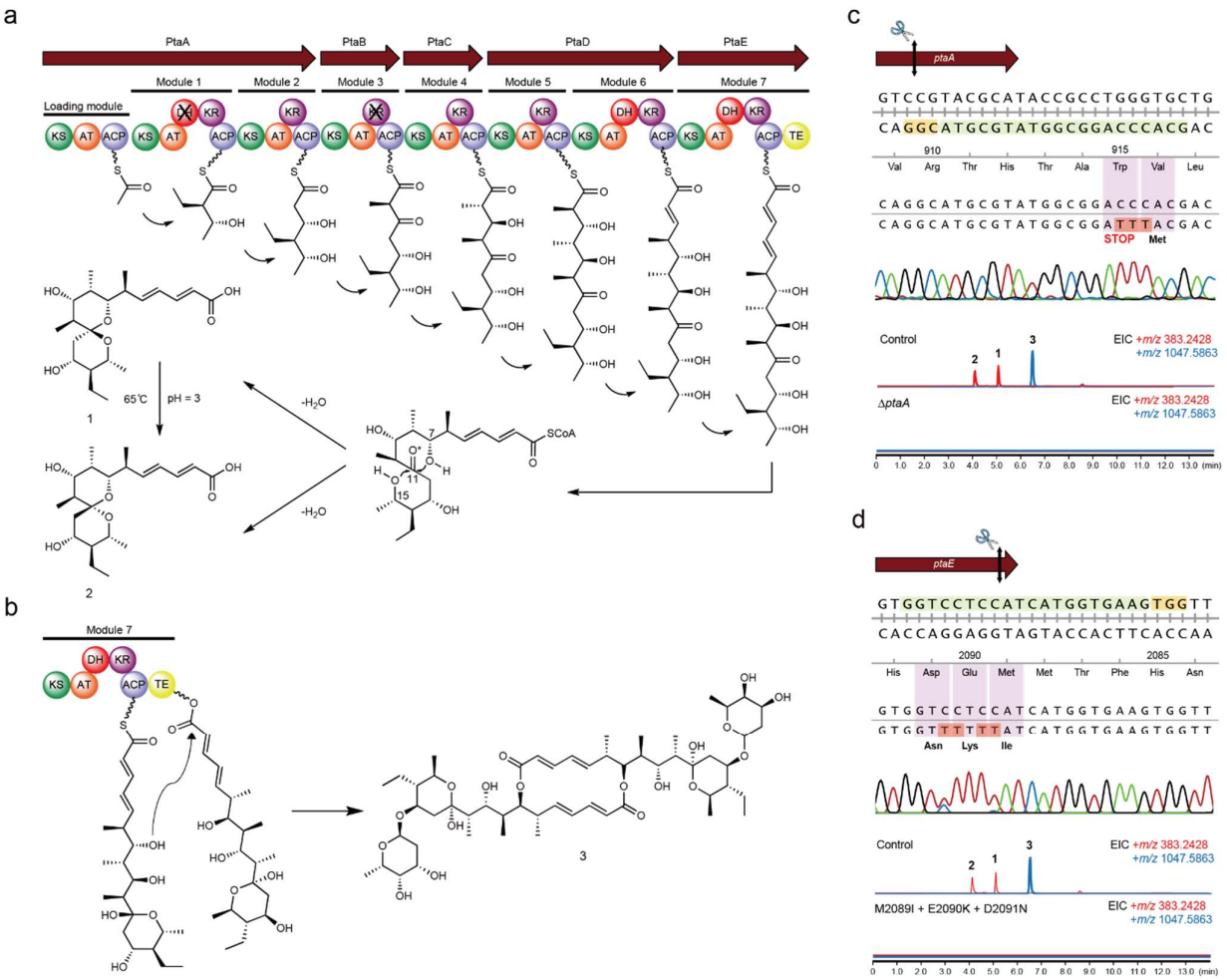

Fig. 8. Biosynthesis mechanism of pteridic acids and CRISPR base editing application in *S. iranensis*.

To validate the predicted *pta* BGC, CRISPR-cBEST was employed as an efficient base editing tool.[70] Given the genetic manipulation challenges of the non-model *Streptomyces*, the conjugation process was systematically optimized in *S. iranensis*.[201] The core polyketide synthase *ptaA* was targeted and inactivated by converting a TGG (Trp) codon at position 916 into the stop codon TAA using CRISPR base editing. The editing event was confirmed by PCR amplification and Sanger sequencing of the editing site (Fig. 8b). As anticipated, the production of pteridic acids was abolished in *S. iranensis*/Δ*ptaA*. Plant experiments revealed that the treatment with *S. iranensis*/Δ*ptaA* fermentation suspension eliminated the abiotic stress mitigating effects. Interestingly, the production of elaiophylin was also abolished because it shared the same assemble line with pteridic acids. Previous studies demonstrated that the thioesterase in the last module catalyzed the formation of symmetrical macrodiolide using two units of linear elaiophylin monomeric seco acid (Fig. 8c). To confirm whether biosynthesis of pteridic acids is also thioesterase-dependent, site-specific mutations were introduced into the active sites of the thioesterase domain in vivo. HR-LC-MS analysis confirmed that the mutant

strain (M2089I+E2090K+D2091M) no longer produced pteridic acids and elaiophylin (Fig. 8d). This in vivo inactivation and site-directed mutagenesis provide additional evidence. The co-production of plant growth-regulating pteridic acids and antimicrobial elaiophylin through a shared BGC suggests potential joint efforts in aiding plants against both biotic and abiotic stress.

2.1.6 Geographical distribution of pteridic acids producers.

We surveyed available gene cluster family (GCF) data for all bacteria in the BiG-FAM database.[60] We found that *pta* BGC (GCF_02696) is strictly restricted to the *Streptomyces* genus. In addition, a total of 55 BGCs with high similarity to the *pta* BGC were detected by BiG-SCAPE,[61] among a total of 9,386 type I polyketides BGCs in 1,965 *Streptomyces* from the NCBI assembly database. Through literature supplementation and data dereplication of other reported producers without sequence information, at least 81 *Streptomyces* are known to produce pteridic acids/elaiophylin or have specific *pta* BGC up to date. Based on the known sampling information, the *pta*-containing *Streptomyces* display a variety of geographic distribution and biological origins (Fig. 9a). We selected two available *Streptomyces* strains (*Streptomyces violaceusniger* Tu 4113 and *Streptomyces rapamycinicus* NRRL 5491) to test the potential plant growth-promoting activity of these potential pteridic acid producers. The HR-LC-MS analysis of both culture broths revealed that they shared similar metabolite profiles, and both produced pteridic acids H and F. Treatment with both culture broths on barley seedlings also exhibited significant plant growth-promoting activities under osmotic, salinity and drought stress. This evidence suggests that this class of *Streptomyces* and its specific secondary metabolite pteridic acids have unique ecological significance involved in plant abiotic stress resistance.

2.1.7 Phylogeny and evolution of *pta* BGC.

To explore the evolutionary clues of pteridic acid producers, 16S rRNA genes were initially used to assess the relatedness of the collected 34 potential producers of pteridic acids with other *Streptomyces* strains that do not contain *pta* BGC (Fig. 9b). Results showed clustering of *pta*-containing *Streptomyces* strains, except for *S. albus* DSM 41398 and *Streptomyces* sp. GMR22, indicating distinct lineages.[201] High-resolution housekeeping genes (*trpB* and *rpoB*) confirmed *S. albus* DSM 41398 in a unique phylogenetic lineage among pta-containing Streptomyces. Congruence in housekeeping gene clades suggested dominant vertical transmission and potential horizontal gene transfer of *pta* BGC in *Streptomyces*.

Comparative genomics involved 15 *pta*-containing *Streptomyces* with complete genome sequences. Genome similarity analysis revealed high similarity, except for *S. albus* DSM 41398 and *Streptomyces* sp. NA02950. Genome synteny analysis showed partial rearrangements despite high sequence similarities. The BGC of pteridic acids in *S. albus* DSM 41398 (*pta*-alb) was located at the chromosome end, a highly variable region,

suggesting acceptance of heterologous gene fragments. Nucleotide sequence alignment of *pta* BGC (Fig. 9c) indicated *pta*-alb completeness, proportional core gene similarity, and confirmed metabolite production (elaiophylin and pteridic acid H) in *S. albus* DSM 41398. Biosynthesis diversity assessment in related strains involved BGC similarity analysis, revealing similarities in vertically inherited *Streptomyces* strains (Fig. 10). Combining phylogenetic and comparative genomics, *S. albus* DSM 41398 is considered the most distinct member, obtaining *pta* BGC via horizontal gene transfer. However, most *pta*-containing *Streptomyces* strains inherit pta and other gene clusters vertically from ancient ancestors, potentially ecologically important but rarely studied.

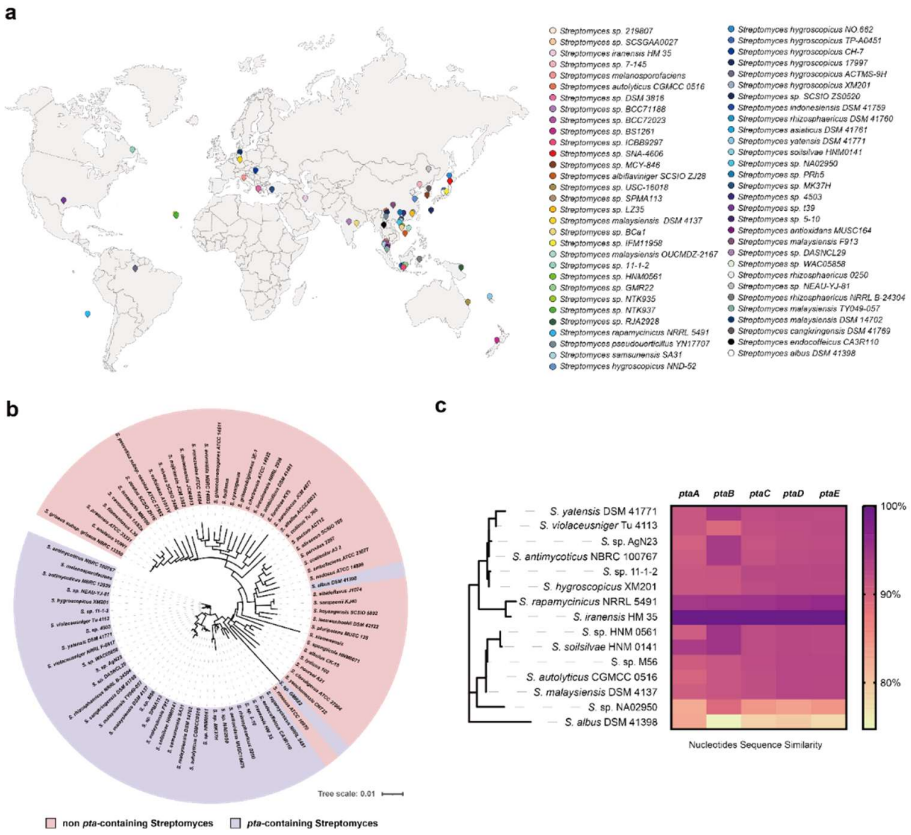

Fig. 9 Geographical distribution and phylogenetic analysis of *pta*-containing *Streptomyces* strains possessing pta BGC.

Horizontal gene transfer (HGT) is a key driver of BGC evolution, revealing independent processes in species phylogeny and BGC distribution.[202] Vertical inheritance also influences BGC evolutionary dynamics, as seen in the conservation of BGCs among closely related strains.[203] The *pta* BGC in *Streptomyces* is geographically dispersed and primarily inherited vertically, with some strains exhibiting notable biocontrol capabilities. For instance, *Streptomyces* sp. AgN23 activates *Arabidopsis* defense responses to fungal pathogens,[204] and *Streptomyces rhizosphaericus* 0250 and *Streptomyces* sp. 5-10 show significant biocontrol potential against fusarium wilt of bitter gourd.[205,206] The *pta*-containing *Streptomyces* family forms a distinct phylogenetic lineage with the highest BGC abundance and largest genome size among diverse *Streptomyces* strains.[207]

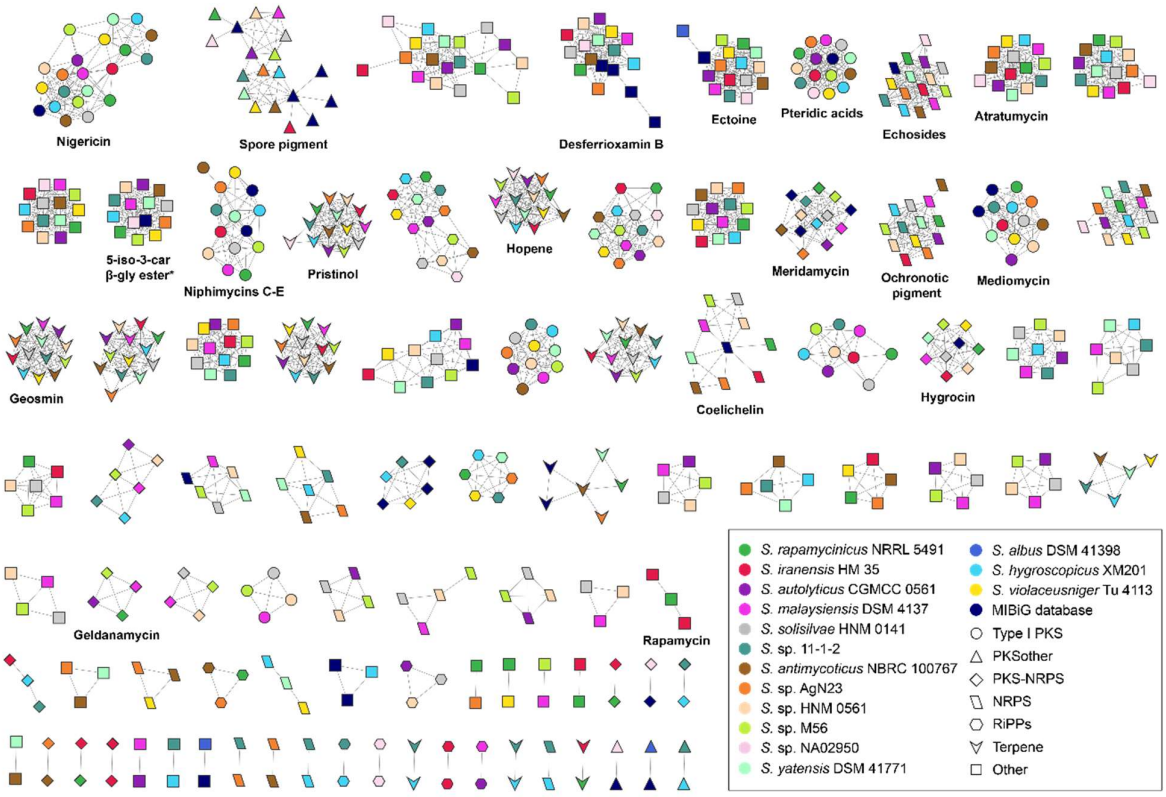

Fig. 10 The secondary metabolites BGCs similarity network of 15 *pta*-containing *Streptomyces* strains with complete genome information.

Despite biosynthetic diversity likely resulting from recent horizontal transfer events, rather than vertical BGC transfer, the multiple Type I polyketide synthases in these strains are highly conserved. Genetic similarity network analysis suggests potential complex cross-BGC regulation in this *Streptomyces* class. Jiang et al. demonstrated that the TetR family transcriptional regulator GdmRIII controls geldanamycin and elaiophylin biosynthesis in *Streptomyces autolyticus* CGMCC 0516.[208] He et al. recently found that the LAL family regulator RapH, situated in the rapamycin BGC, coordinates the biosynthesis of both rapamycin and elaiophylin in *S. rapamycinicus* NRRL 5491.[209] While these reports indicate cross-regulation between evolutionarily conserved BGCs, further investigation is needed to elucidate the details of these communications.

2.2 Discovery and biosynthesis of antifungal spirolactones

Fungal infections, posing a pervasive global threat, imperil both public health and food security.[210,211] The escalating prevalence and resistance of fungal pathogens contribute significantly to this crisis, with over 150 million individuals worldwide contending annually with severe fungal infections resulting in more than 1.5 million deaths.[213] The available therapeutic choices for fungal infections are restricted to a handful of antifungal medicines, such as azoles, polyenes, and echinocandins, with only a limited

number of candidates progressing through the clinical development pipeline.[214] Simultaneously, the agricultural sector confronts a substantial risk to global food security arising from fungal diseases, resulting in a loss of crops ranging from 10% to 23% during cultivation, with an additional 10% to 20% loss occurring post-harvest each year.[215] The widespread use of broad-spectrum fungicides further exacerbates the challenge of antifungal drug resistance in fungi.[216] Addressing these critical issues necessitates intensified research efforts directed toward the development of novel antifungal agents.

2.2.1 Genome mining of *S. iranensis* and identification of spirolactones

Due to the incompleteness of previously reported genomic data, we performed whole-genome resequencing of *S. iranensis* using the combination of the Oxford Nanopore Technologies MinION and Illumina MiSeq system. The high-resolution, full-genome sequencing of *S. iranensis* reveals a linear chromosome spanning 12,213,033 nucleotides, featuring inverted terminal repeats comprising 156,145 nucleotides. The BGC annotation of the acquired *S. iranensis* genome was carried out using antiSMASH version 7.0,[15] which resulted in the appearance of a cryptic BGC (*spl* gene cluster) situated at the terminal region of the linear chromosome (Fig. 11). The GCF annotation of *spl* gene cluster showed it belongs to GCF_00315 and a total of 11 hits were detected (distance ≤ 900.0) in the BiG-FAM database.[147] The distinctive biosynthetic gene architecture of *spl* gene cluster suggests its novelty as a modular Type-I PKS BGC, setting it apart from others. This finding spurred our interest in conducting a thorough investigation of this individual BGC. This cryptic *spl* gene cluster spanned 87.99 kb with 12 open reading frames (Fig. 11). The entire PKS contains five core polyketide synthases (*splA*, *splC*, *splD*, *splE*, and *splF*) within 16 separated biosynthetic modules. In addition, there is a crotonyl-CoA carboxylase/reductase (*splH*), an *O*-methyltransferase (*splG*), three cytochrome P450 (*splB*, *splK* and *splL*), and two hypothetical enzymes (*splI* and *splJ*) adjacent to the core PKS genes.

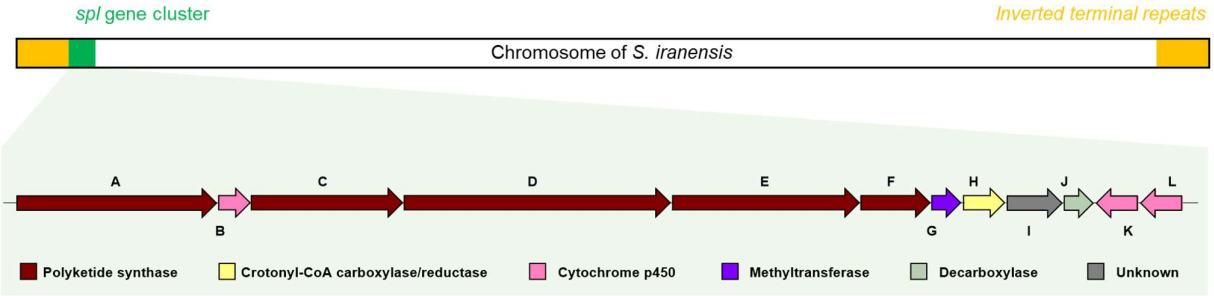

Fig. 11 The biosynthetic genes architecture of *spl* gene cluster.

To locate the products of the potential *spl* gene cluster, we were elucidating the products combining both genome editing and metabolomics. Initially, we constructed PKS knock-out mutant (Δ*splA*) and crotonyl-CoA carboxylase/reductase-inactivated mutant (Δ*splH*) using the DSB-based CRISPR-Cas9 and CRISPR base editing, respectively. Both mutants nearly abolished the antifungal activity against multiple

Aspergillus strains. Comparative metabolic profiling using LC-MS and LC-UV led to the identification of the potential bioactive principle as a major compound **1** with *m/z* 881.4656 ($[M+H]^+$) and other derivatives, which were specifically abolished in both mutants. The complementation of pGM1190-based *splH* in mutant *S. iranensis*/Δ*splH* led to the restoration of the production of **1**. Bioactivity-guided chemical isolation and structure elucidation led to the identification of spirolactones A-C (**1**-**3**).

2.2.2 Biosynthesis mechanism of spirolactones

Five PKS genes transcribed in the same direction encode one loading module and 15 chain extender modules and were suggested to assemble the polyketide backbone (Fig. 12). Based on multiple sequence alignment, most KS domains keep the conserved catalytic sites comprised of a cysteine (TACSSS motif) as well as two histidines (EA**H**GTG and KSNIG**H**T motifs).[18] Only the reactive cysteine in KS1 was replaced by glutamine. The conserved fingerprint residues for extender unit selectivity GHSIG and HAFH motifs are present in the nine AT domains (AT_1, AT_2, AT_5, AT_7, AT_8, AT_9, AT_{11}, AT_{12}, and AT_{14}) that are specifically binding to malonyl-CoA while GHSQG and YASH motifs are present in the six AT domains (AT_3, AT4, AT6, AT10, AT13, and AT15) that are specifically binding to for (2*S*)-methylmalonyl-CoA.[18] As previously discovered, AT_{16} from module 15, which was thought to be accountable for loading distinct extender units, exhibits an unusual IASH motif. KR domains have been previously classified into A1-, A2-, B1-, and B2-types, which reduce ketones to their $_L$-hydroxy or $_D$-hydroxy counterparts.[217] We determined that the KR_3, KR_4, and KR_{15} appear to belong to the B1-type: all have the fingerprint LDD motif but the absence of a P residue in the catalytic region. KR5 and KR_{12}, with the characteristic W residue but no LDD motif and H residue, were classified as A1-type KRs. The other KR domains couldn't be classified according to the sequence, but they should be functional according to the structure of spirolactone. Similarly, combined with structural information and conserved site analysis, the five DH domains (DH_6, DH_7, DH_8, DH_9 and DH_{10}) were considered inactive during spirolactone biosynthesis. ER11 is classified as $_L$-type due to the presence of a tyrosine residue that donates a proton to the enol intermediate in $_L$-type ER, whereas ER13 and ER14 belong to $_D$-type because it lacks tyrosine residue. The final release and cyclization of the linear product was probably accomplished by TE domain in the last module, which contains an α/β-hydrolase catalytic core and loop regions that form a substrate-binding lid.[218]

The above synthetic steps leading to PKS assembly are followed by a series of complex modifications including oxidation, carboxylation, and methylation (Fig. 12). The tailoring enzymes responsible for these transformations are scattered throughout the *spl* gene cluster. The multiple sequence alignments of three cytochromes P450 enzymes (SplB, SplK, and SplL) showed that they have conserved motifs of this family.[219] The cytochrome P450 enzyme BonL from *Burkholderia gladioli* was previously identified to confer the C-22 carboxyl group in the biosynthesis of bongkrekic acid via sequential six-electron-

oxidation.[220] In addition, there are some cytochromes P450 enzymes that catalyze the carboxyl group formation in microbial secondary metabolites, such as XiaM, PimG, AmphN, NysN, and FscP.[221-223] To identify the cytochromes P450s responsible for carboxylation, we built the Hidden Markov model (HMM) based on these sequences and the results showed that SplL exhibited the best match with these known P450s with an E-value of 4e-117. In addition, bioinformatic analysis of XiaM indicated that the P450s with carboxylation function harbor highly conserved segment AGHET, which was also presented in SplK. Therefore, SplK and SplL, were considered putative candidates for catalyzing the two-step oxidation to form carboxyl groups in postitions C-1 and C-5 during spirolactone biosynthesis. SplB, homologous cytochrome P450 monooxygenase CftA in clifednamide biosynthesis gene cluster with 45.6% similarity,[224] was likely to accomplish the oxidation at C-27 in spirolactone. We constructed mutant strains of *S. iranensis* inactivating the SplB, Splk and SplL enzymes (denoted as Δ*splB*, Δ*splk*, and Δ*splL*). Despite our efforts, no expected intermediates were observed in either mutant, likely due to their low yield. SplG, an *O*-methyltransferase homologous to AveD in avermectin biosynthesis (40% identity and 55% similarity),[225] was proposed to catalyze the methylation of a hydroxyl group in C-8 of spirolactone. The Δ*splG* mutant also showed no accumulation of spirolactone and other putative intermediates.

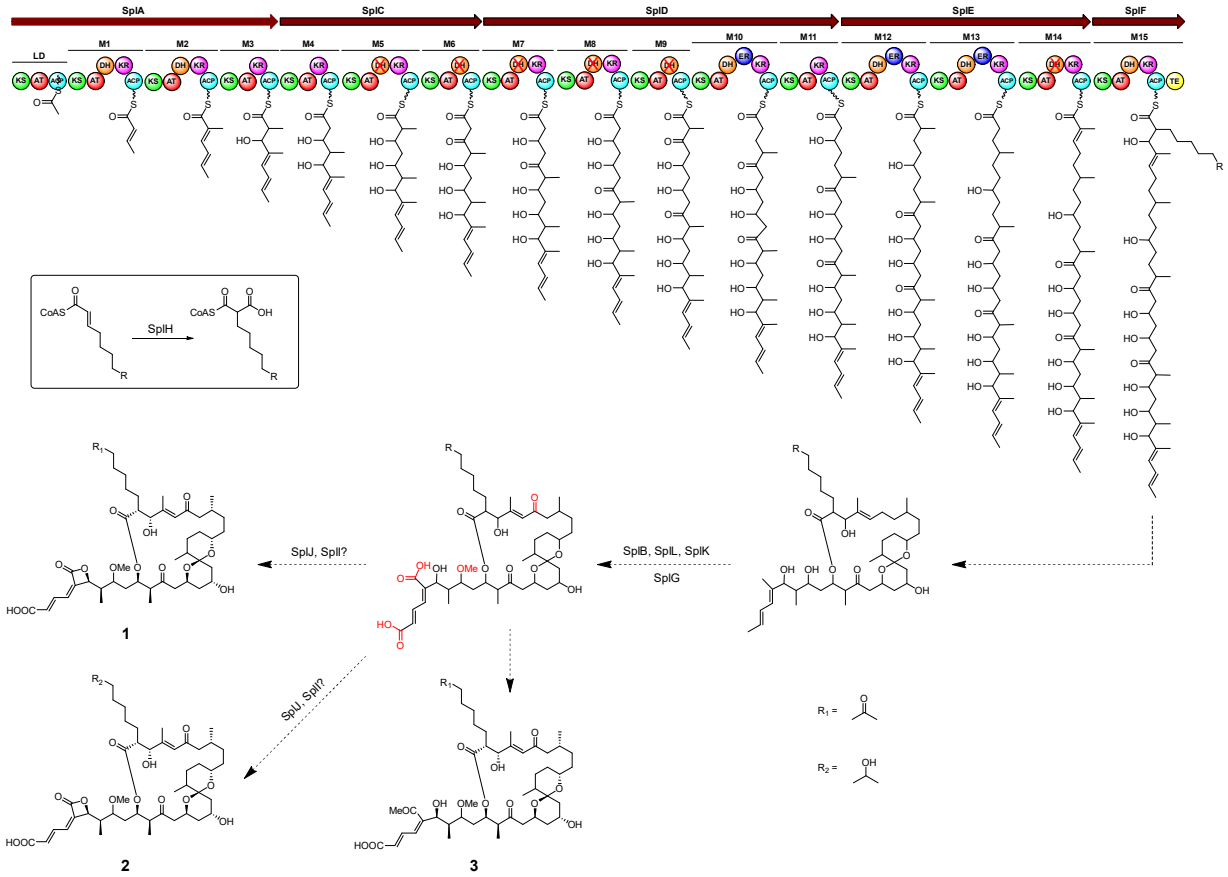

Fig. 12 Proposed biosynthesis pathway of spirolactones A-C (**1-3**).

Phylogenetic analysis indicated that SplH is a separate branch and clusters with other crotonyl-CoA reductase/carboxylases that catalyze long-chain precursors like butylmalonyl-CoA and hexylmalonyl-CoA.[226,227] The previous study showed that the large residue Phe380 in the crotonyl-CoA reductase/carboxylase from *S. coelicolor* may constrain the potential pocket to accept long-chain substrates, which were also found in most ethylmalonyl-CoA specific crotonyl-CoA reductase/carboxylases, while its corresponding residue in SplH is smaller cysteine.[228] Hence, we proposed that SplH catalyzes the conversion leading to the formation of 7-oxo-octylmalonyl-CoA in spirolactone A and B, and 7-hydroxyoctylmalonyl-CoA in spirolactone C. We also attempted to confirm the function of SplH in vitro, however, SplH with C-term His-tag or N-term His-tag couldn't be expressed in *E. coli* BL21(DE3).

Microbial β-lactone natural products are structurally diverse, nevertheless, there are only few enzymatic mechanisms corresponding to β-lactone ring formation that have been reported,[229] including: (1) the intramolecular cyclization from seven-membered ring, catalyzed by cyclase VibC in vibralactone biosynthesis;[230] (2) the tandem aldol-lactonization bicyclization reaction to generate the γ-lactam–β-lactone structure, catalyzed by standalone ketosynthase SalC in salinosporamide A biosynthesis;[231] (3) the β-lactone formation during the intramolecular attack of the β-hydroxyl group onto the thioester carbonyl, catalyzed by the C-terminal TE domain of ObiF in obafluorin biosynthesis or esterase GloD in globilactone A biosynthesis;[112,232] (4) the conversion of β-hydroxyl to β-lactone, catalyzed by β-lactone synthase OleC in olefin biosynthesis.[233,234] Due to the significant structural bias with reported molecules, we proposed that the beta-lactone formation in spirolactone involves two-step oxidation to form a carboxylic acid, followed by dehydration. It is likely that either the cytochrome P450 enzyme SplK or SplL is involved in the process, and we also identified several genes with unknown functions, such as *splJ* and *splI*. SplJ was annotated as a member of UbiD family decarboxylases,[235] but it exhibits very distinguished divergences from other proteins in this family based on sequence similarity network. In addition, NCBI Blastp results showed that proteins homologous to SplI have not been reported to have any clear biological functions. Inactivation of both genes *splJ* and *splI* also abolished spirolactone production.

2.2.3 Antifungal and cytotoxic activities of spirolactones

Spirolactones were inactive against Gram-positive bacteria *Staphylococcus aureus*. In the antifungal assay, spirolactone A exhibited greater inhibitory activity than amphotericin B against various fungal pathogens, including *Aspergillus niger*, *Aspergillus flavus*, and *Aspergillus tubingensis*, with minimum inhibitory concentrations (MIC) of 3.75, 15, and 3.75 ng mL^{-1}, respectively. Cell growth and toxicity effects of spirolactone on mammalian cells were assessed using the LNCaP and C4-2B prostate cancer cell lines, respectively. Exposure to spirolactones (10μM) increased the observed growth rate constant (k) in LNCaP

and C4-2B cells, from 0.5628 and 0.5632 to 2.659 and 1.889, respectively.

2.2.4 Proteomics analysis of antifungal spirolactone A

The preliminary mode-of-action studies of spirolactones were facilitated by the label-free quantitative proteomics analysis of model organism *A. niger* ATCC 1015. We initially cultured *A. niger* ATCC 1015 in PDB liquid medium for 16 hours followed by the 1-hour and 4-hour treatment with spirolactone A. The proteomics analysis showed that a total of 4,447 proteins (40.4% of the total encoded proteins) were detected, and 3,992 proteins (89.8% of the total detected proteins) didn't show significant differences between the treatment (1-hour or 4-hour treatment with spirolactone A) and the control (without spirolactone A treatment). Compared with the control, the abundance of 134 proteins significantly increased and 60 proteins significantly decreased after 1-hour spirolactone A treatment. In comparison, the abundance of 273 proteins significantly increased and 113 proteins significantly decreased after 4-hour spirolactone A treatment (Fig. 13). The Cluster of Orthologous Groups (COGs) functional classification of these differential proteins was performed by eggNOG-mapper v2.[236] Except for unknown function, these proteins were mainly clustered into a few biological processes including (Q) Secondary structure, (C) Energy production and conversion, (E) Amino acid metabolism and transport, and (O) Post-translational modifications, protein turnover, chaperone functions. The Gene Ontology (GO) annotations that these proteins were mainly involved in the metabolic process, cellular process, and single-organism process during the biological process. Cellular component analysis showed that these proteins were mainly localized intracellularly, especially in organelles. Meanwhile, most of these proteins participated in catalytic activity and binding in the category of molecular function. The Kyoto Encyclopedia of Genes and Genomes (KEGG) pathway analysis showed that these proteins mainly participate in amino acids metabolism and purine metabolism.

The fungal cell wall is an essential structure that maintains cell shape and protects fungi against environmental stress and plays roles in growth, invading ecological niches and counteracting the host immune response.[54] Fungal cell walls are composed mainly of glucans, chitin, and glycoproteins, synthesized by glycosyltransferases, glycoside hydrolases, and transglycosylases.[237] The fungal cell wall is a promising target as it contains polysaccharides absent in humans. Currently, four classes of antifungal drug classes including polyenes, allylamines, azoles, and echinocandins are used in clinical practice.[238,239] Their mechanisms are well-understood with most targeting the cell wall/membrane components or synthesis. Recent studies revealed that the mode of action of polyenes antibiotics involves acting as sterol "sponges" and extracting ergosterol from the fungal membrane, causing cell death.[240,241] Allylamine antibiotics (naftifin and terbinafine) inhibit squalene epoxidase, causing the accumulation of squalene, and thereby damaging the intracellular membranes of fungi.[242] Azoles inhibit ergosterol biosynthesis in

the lanosterol demethylation through the cytochrome P450 sterol-14α-demethylase (CYP51).[243] Echinocandins block the synthesis of cell wall component β-1,3-glucans through non-competitive inhibition of 1,3-β-D-glucan synthase.[242] Compared to the other antifungal drugs, spirolactone displayed a different antifungal spectrum, with selective activity against intrinsic resistant *Aspergillus* (*A. terreus*, *A. niger* and *A. calidoustus*) and no activity against *Candida* . This indicated that it has a new mode of action.

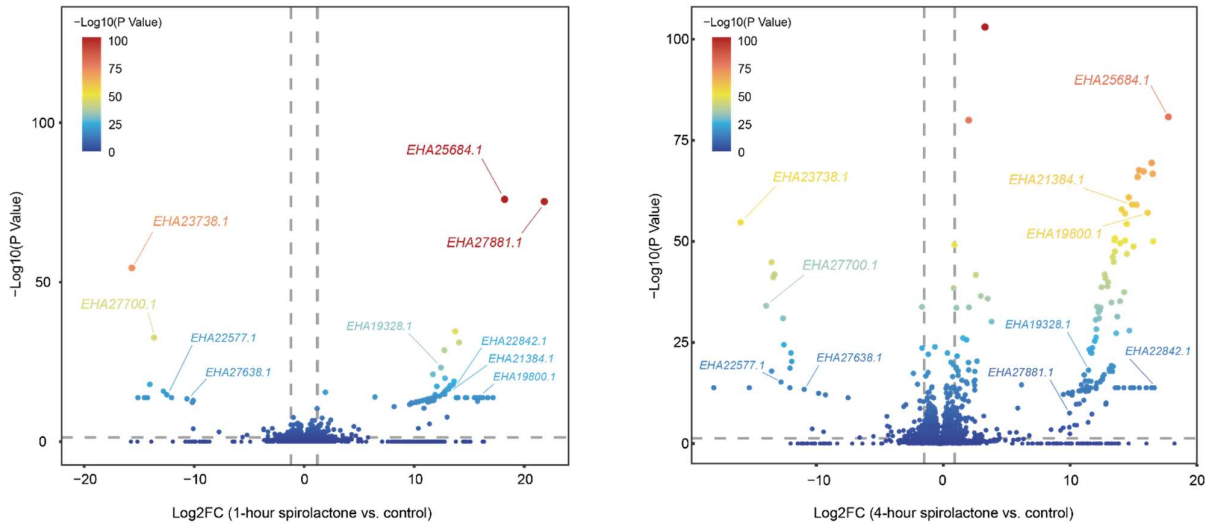

Fig. 13 Volcano plot of the abundance of protein after spirolactone A treatment based on proteomics analysis.

The abundance of Erg13 (EHA22977.1, involved in ergosterol biosynthesis) and manganese-superoxide dismutase (EHA27012.1, involved in oxidative stress response), which was regarded as polyene antibiotic (such as amphotericin B) responsive protein,[245] was not significantly altered in the presence of spirolactone A. Allylamine antibiotics (naftifin and terbinafine) inhibit squalene epoxidase, causing the accumulation of squalene, and thereby damaging the intracellular membranes of fungi.[246] However, spirolactone A is not belonging to the allylamine family and didn't induce any changes in the squalene epoxidase (EHA21184.1). Azoles are synthetic antifungal agents of non-natural origin that inhibit cytochrome P450 sterol-14α-demethylase (CYP51) to block the ergosterol biosynthesis in the fungi.[247] Similarly, spirolactone A lacked the azoles substructure and had no impact on the abundance of CYP51 (EHA19435.1). Natural echinocandins comprise cyclic hexapeptide and lipid residues, like caspofungin, anidulafungin and micafungin, preventing the biosynthesis of glucans of the fungal cell wall through non-competitive inhibition of 1,3-β-D-glucan synthase.[248] Previous proteomics analyses had proven that the level of chitinase ChiA1 in *Aspergillus fumigatus* was significantly decreased in response to caspofungin.[249] It may represent a common effect of self-resistance development due to caspofungin increased chitin content via induction of chitin synthases during cell wall remodeling.[250] We didn't observe the abundance of 1,3-β-D-glucan synthase (EHA18547.1) and ChiA1-like chitinase (EHA28582.1)

altered significantly after 1-hour and 4-hour treatment of spirolactone A in comparison to the control group.

Spirolactone A has a witness structural bias from known antifungal agents, which suggests that it may inhibit fungal growth through other targets. The fungal cell wall is an essential structure that maintains cell shape and protects fungi against environmental stress. Glycosyltransferases, glycoside hydrolases, and transglycosylases are involved in the biogenesis of the cell wall, required for growth, invading ecological niches, and counteracting the host immune response. The volcano plot of differential proteins indicated that a transglycosylase (EHA23738.1) was significantly inhibited, suggesting spirolactone A might interfere with the formation of the fungal cell wall. Trehalose-6-phosphate synthase/phosphatase is another important enzyme for cell wall integrity and fungal virulence in various *Aspergillus* species.[251] The relative abundance of trehalose 6-phosphate synthase (EHA27700.1) was also significantly decreased after spirolactone A treatment. The above data indicated that the mode of action of spirolactone A might be mediated by disrupting fungal cell wall biosynthesis and stability. Besides, we found two enzymes Erg24 (EHA26587.1) and Erg27 (EHA20711.1), which catalyze the biosynthesis of 4,4-dimethylcholesta-8,14,24-trienol to fecosterol,[252] were remarkably upregulated after spirolactone A treatment. Drug efflux and resistance in fungi could be mediated by ATP-binding cassette (ABC) transporters, such as CDR1 was induced to high expression in *A. fumigatus* AF293 in the presence of azole antibiotics.[253] The expression of an ABC transporter (EHA25684.1) was activated after spirolactone A treatment. The abundance of several putative spirolactone A-responsive proteins were significantly altered (Fig. 13). For example, KCS1 (EHA27881.1), ASI3 (EHA19328.1), PIC2 (EHA22842.1), pyridoxamine 5'-phosphate oxidase (EHA19800.1) and glucohydrolase (EHA21384.1) was significantly increased, but oxygen-dependent FAD-linked oxidoreductase (EHA22577.1) and dienelactone hydrolase (EHA27638.1) was significantly decreased in spirolactone-treated samples.

2.3 Metabolic engineering in *S. iranensis*

In Section 2.1 and Section 2.2, the discovery of plant growth-promoting pteridic acids and antifungal spirolactone A was reported, respectively. However, The restricted yield of these secondary metabolites in the wild-type strain poses constraints on their cost-effectiveness and commercial viability. To overcome these limitations, there is a growing need for metabolic engineering strategies to optimize and enhance the production of secondary metabolites. Moreover, advances in synthetic biology techniques and genetic engineering tools have provided researchers with powerful means to reprogram cellular metabolism for improved secondary metabolite production. Rational design and combinatorial approaches can be employed to fine-tune biosynthetic pathways and achieve higher yields of these valuable compounds. In this Section, comprehensive metabolic engineering in *S. iranensis* aimed at

improving the production of pteridic acids and spirolactone is described, including manipulation of regulators and transporters enzymes, branch metabolic pathways blocks, promoter engineering, and CASCADE-Cas3-based large BGC knock-out.

2.3.1 Manipulation of regulators and transporters

Based on biosynthetic gene annotation, there is a LuxR family transcriptional regulator (*pta3*) and a pair of ABC transporters (*pta4**, *pta5**) within the BGC of pteridic acids. The LuxR family transcriptional regulator functions as a positively regulated pathway-specific regulatory gene.[75-77] Additionally, the ABC transporter, acting as a carrier for the products of the cell efflux gene cluster, is recognized to play a positive regulatory role in the expression of BGCs.[87]

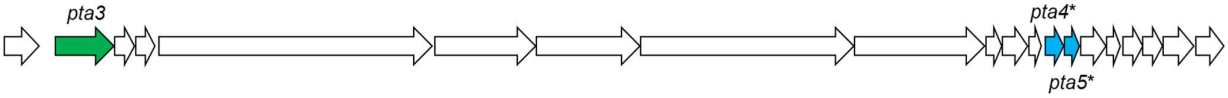

Fig. 14 The arrangement of regulatory and transporter genes in the *pta* gene cluster. Arrow in green: LuxR family transcriptional regulator; Arrow in blue: ABC transporter.

Hence, pGM1190-based overexpression vectors containing additional genes (*pta3*, *pta4**/*pta5**) were constructed and introduced into the wild-type strain to get double-copies mutants followed by confirmation via antibiotic selection and PCR verification. The relative quantification analysis showed that the production of pteridic acid H and F in *S. iranensis*::*pta3* were improved 2-fold compared to wild-type strain (Fig. 15). However, the overexpression of *pta4**/*pta5** (*S. iranensis*::*pta4**/*pta5**) didn't significantly affect the pteridic acids production (Fig. 15).

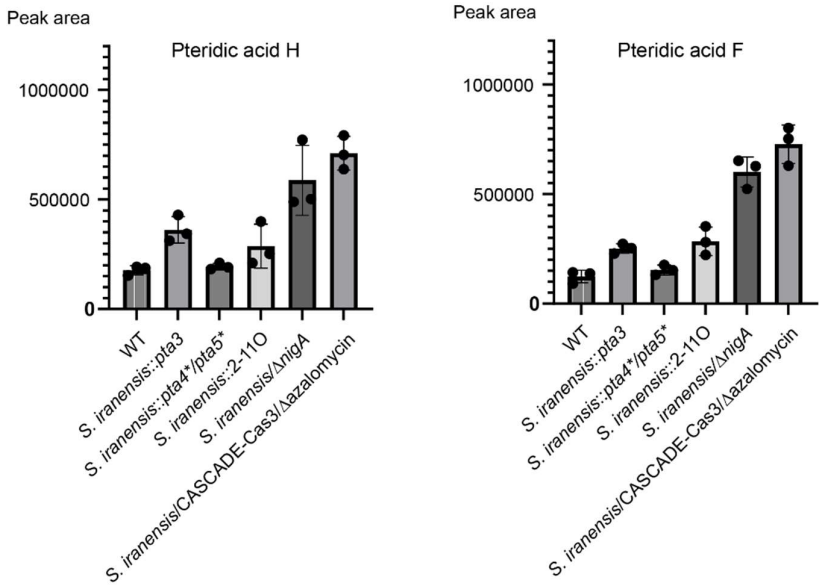

Fig. 15 The relative quantification analysis of pteridic acids production in different mutants.

2.3.2 BAC library construction and heterologous expression

To introduce multiple copies of the *pta* gene cluster into the wild-type strain and heterologous express it in other hosts, the pESAC13A-based bacterial artificial chromosome (BAC) library of *S. iranensis* HM35 was constructed by Bio S&T. The resulting library comprises 2,304 clones with an average insert size of 125 kb, and 20-fold coverage of the entire genome (Fig. 16a). Clone 2-11O, containing the entire *pta* BGC, was identified through the utilization of three primer pairs: ID-5989-F/R, ID-48680-F/R, and ID-6146-F/R. These primer sets were strategically designed to amplify regions situated both upstream and downstream of the left and right borders of the *pta* BGC, as well as the central regions within the gene cluster, as illustrated in Fig. 16b. Unfortunately, no clones with complete *spl* gene cluster were screened.

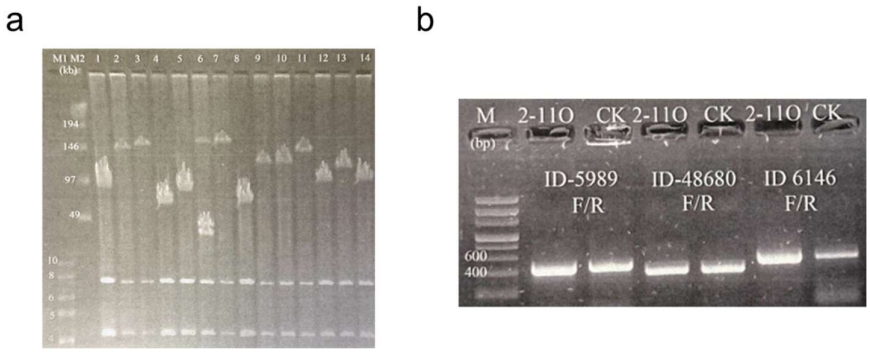

Fig. 16 Insert size determination of pESAC library and PCR confirmation of the triple-positive clone.

The clone 2-11O was also introduced into native host *S. iranensis* and heterologous hosts, including *S. colicolor* M1152 and *S. albus* J1074, using methylation deficient donor ET12567(pUB307)-mediated intergeneric conjugal transfer.[254] However, HR-LC-MS analysis revealed no significant alteration in the production of pteridic acids in *S. iranensis* with an additional *pta* BGC copy (Fig. 15). Moreover, the *pta* BGC did not exhibit expression in the heterologous host, which provided evidence of the conserved evolution relationship between *pta* BGC and it producers, and its expression may require the regulation of other genes outside the BGC.

2.3.3 Branch metabolic pathways blocking

The genome annotation indicated that there are many PKS-type BGC in the *S. iranensis* genome. As polyketides typically utilize common building blocks, hindering the regular synthesis of other polyketide synthases might promote the accumulation of substrates. This redirection of metabolic flow enhances the production of the desired target products. The metabolomics analysis suggested that two types of polyketides, azalomycins and nigericin, were the main products of *S. iranensis*. Firstly, the PKS genes responsible for the biosynthesis of azalomycin and nigericin, *azaA* and *nigA*, were inactivated through

the insertion of STOP codon in wild-type *S. iranensis* respectively (Fig. 17a, 17b). The HR-LC-MS analysis of mutants indicated that the production of azalomycin in mutant *S. iranensis*/Δ*azaA* and the production of nigericin in mutant *S. iranensis*/Δ*nigA* was totally abolished. Interestingly, the production of pteridic acids were also blocked in mutant *S. iranensis*/Δ*azaA*, which might be caused by off-target effect of CRISRP-BEST. The quantitative analysis shows the production of pteridic acid H, pteridic acid F and spirolactone A was increased 3.3-fold, 4.9-fold and 1.8-fold in *S. iranensis*/Δ*nigA*, respectively (Fig. 15, Fig. 18). The relative production of spirolactone A was increased 2.7-fold in double-genes inactivation mutant *S. iranensis*/Δ*azaA*/Δ*nigA* (Fig. 18).

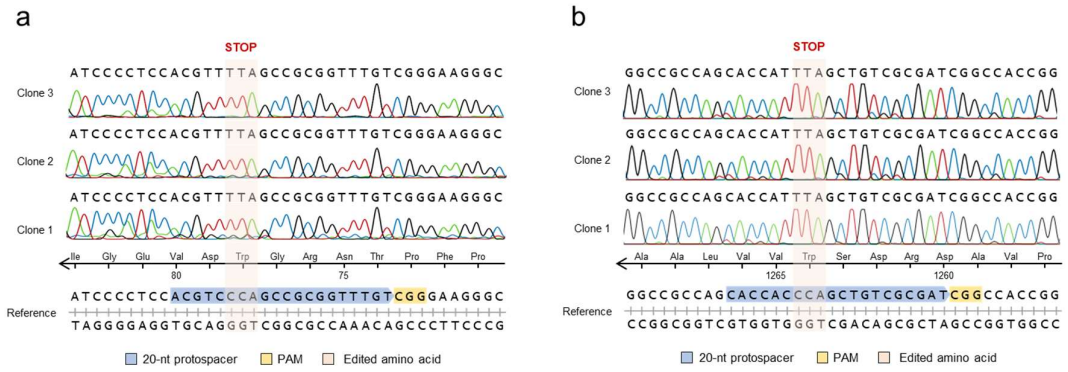

Fig. 17 Mapping of nanopore sequencing results to the genome.

The inactivation of *azaA* and *nigA* was further employed in *S. iranensis*/Δ*ptaA*, whose pSG5-based CRISPR plasmid was removed by high-temperature pressure. This process resulted in the generation of a triple-genes inactivation strain, denoted as *S. iranensis*/Δ*ptaA*/Δ*azaA*/Δ*nigA*. The production of spirolactone A was increased 4.5-fold in *S. iranensis*/Δ*ptaA*/Δ*azaA*/Δ*nigA* (Fig. 18).

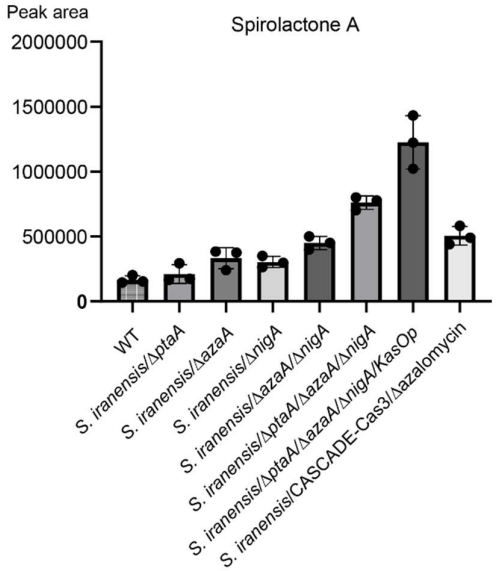

Fig. 18 The relative quantification analysis of spirolactone A production in different mutants.

2.3.4 Promoter engineering

To further improve the production of spirolactone, promoter engineering was employed in triple gene-inactivated mutant *S. iranensis*/Δ*ptaA*/Δ*azaA*/Δ*nigA*. The *KasOp* promoter was incorporated into the pCRISPR-Cas9 backbone, resulting in the creation of the modified vector named pCRISPR-Cas9-*KasOp*. Subsequently, flanking sequences necessary for homology recombination were inserted into the vector, following a method previously reported.[95] The experimental design was to insert the promoter in front of *splA*, the first PKS gene encoding spirolactone biosynthesis (Fig. 19), and the mutant strain was confirmed by sanger sequencing. The relative quantification analysis showed that the production of spirolactone A was improved 7.3-fold compared to wild-type strain (Fig. 18).

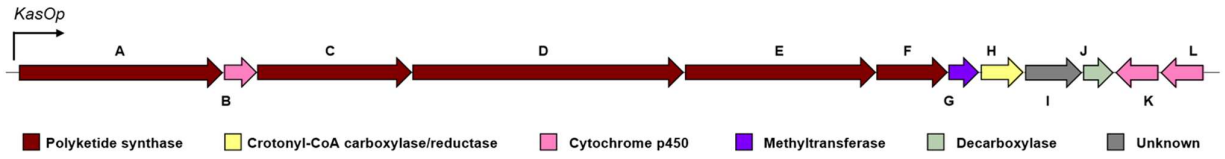

Fig. 19 Insertion of *KasOp* promoter in *spl* gene cluster.

2.3.5 Cascade-Cas3-based BGC knock-out

Metabolic pathway blocking based on CRISPR base editing only prevents the production of metabolites, but other biosynthetic genes are still transcribed and expressed. To further reduce competition for substrates from other PKS biosynthesis, the Cascade-Cas3 system was employed for large fragment deletion of the azalomycin gene cluster in *S. iranensis*. The assembly of pCRISPR-Cas3 followed established protocols,[66] and it was subsequently stepwise introduced into the wild-type *S. iranensis* to generate the mutant with lacking whole azalomycin BGC. The nanopore sequencing results indicated that the whole azalomycin gene cluster was successfully deleted (Fig. 20). The relative quantification analysis showed that the production of pteridic acid H, pteridic acid F and spirolactone A was improved 4-fold, 5.9-fold, and 3-fold, respectively, compared to wild-type strain (Fig. 18).

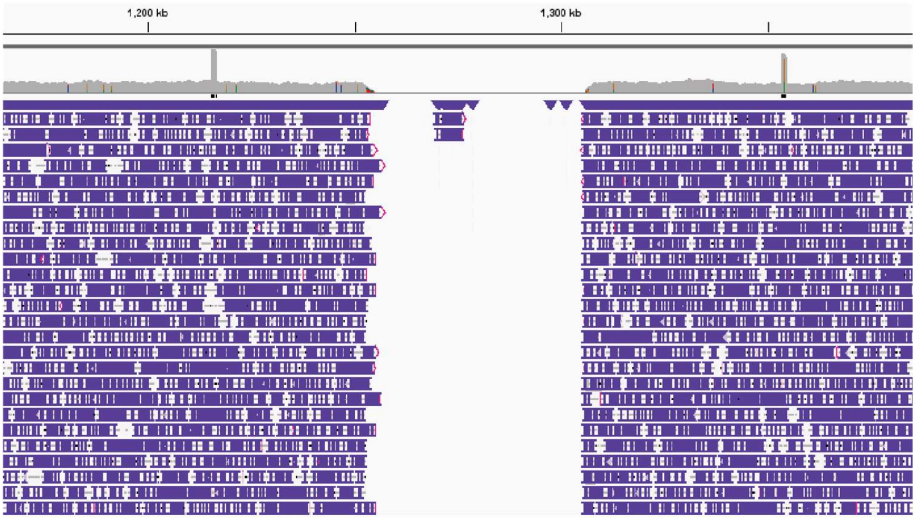

Fig. 20 Mapping of nanopore sequencing results to the genome

2.4 Genetic manipulation in non-model *Streptomyces* strains

Streptomyces have the characteristics of wide distribution, strong adaptability, and diverse metabolites. They are important biological resources for antibiotics and active substances such as anti-tumor and anti-plant diseases. Under conventional laboratory culture conditions, many natural product BGCs show no or low expression. Therefore, establishing a genetic manipulation system for environmental *Streptomyces* strains with the potential to mine secondary metabolites is helpful for the discovery of active natural products and the elucidation of the biosynthetic pathways of target active molecules. In this chapter, the CRIPSR/Cas9-based genetic manipulation methods were employed in three non-model *Streptomyces* strains including *Streptomyces* sp. P2-2B-1 and *Streptomyces rapamycinicus* IMET 43975. The successful establishment of genetic manipulation systems in these strains not only demonstrates the broad application potential of the current CRISPR toolbox but also solves practical problems in different scientific topics.

2.4.1 CRISPR base editing in *Streptomyces* sp. P9-2B-2

The *Streptomyces* life cycle encompasses three well-established developmental stages: vegetative growth, mycelium formation and sporulation. In response to nutrient depletion, *Streptomyces* start the transition from vegetative growth to aerial mycelium formation, and subsequently sporulation.[255] Interestingly, sporulation is a common phenotype change observed in dual *Streptomyces* interactions, yet tracing the responsible secondary metabolites is nearly non-existent.[256]

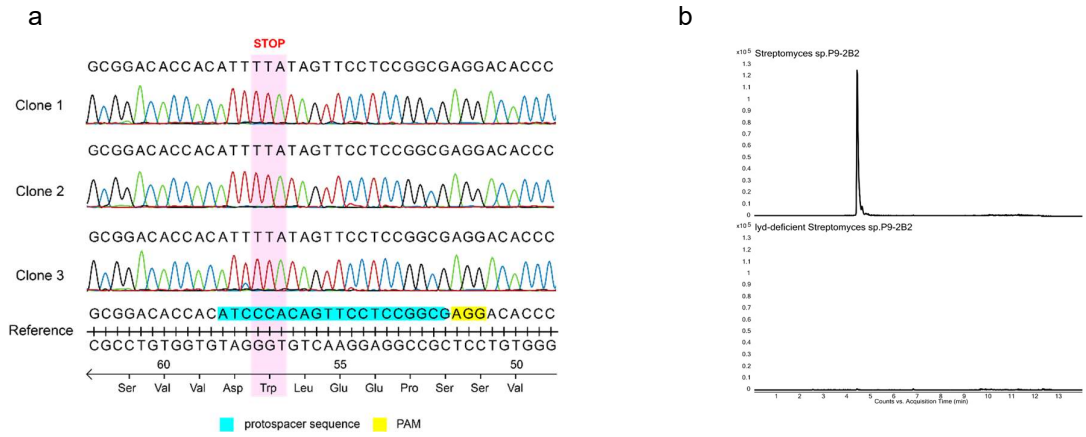

Fig. 21 Sanger sequencing and LC-MS analysis of mutant strain.

During a screening for *Streptomyces-Streptomyces* interaction, two environmental *Streptomyces* spp. were cocultured, with one strain (*Streptomyces* sp. P9-2B2) inducing a wave of sporulation in a receiver strain (*Streptomyces* sp. P9-2B1). Using a combination of MSI, molecular genetics and biological testing, a suite of antibiotic lydicamycins produced by *Streptomyces* sp. P9-2B2 was determined to induce the observed morphogenesis. The temporal production of lydicamycins was evaluated using LC-MS/MS and feature based molecular networking and we determined their production coincided with sporulation in the producer strain and aligned with the first observation of sporulation in receiver strain.

To confirm our lydicamycin-sporulation hypothesis, we generated a lyd-deficient mutant to test in coculture setups. The first core polyketide synthase *lyd6o* was targeted and inactivated by converting a TGG (Trp) codon at position 57 into the stop codon TAA using CRISPR-based base-editing tool CRISPR-BEST.[70] The deficient mutant (sgRNA:*lyd6o*) was confirmed by Sanger sequencing of the editing site (Fig. 21) and LC-MS analysis after 7 days of growth on PDA ensuring sporulation occurred. Subsequent timelapse images were taken over 10 days and no sporulation was observed in the receiver strain, *Streptomyces* sp. P9-2B1. The lydicamycin-deficient mutant observably had different growth in the first two days from the wild-type strain. The first indication of sporulation in WT P9-2B2 appears on Day 1 Hour 13 compared to Day 4 for the lydicamycin-deficient mutant, indicating the inactivation of the *lyd* BGC clearly delays sporulation in P9-2B2.

Lydicamycins and overall, the arginoketides, were shown to trigger the production of multiple secondary metabolites in *Aspergillus nidulans* and the pigment carviolin in a *Pencillium* sp., indicating as a chemical class, they have a wider ecological context.[257] The guanidine CoA-acyl carrier protein transacylase, which has been predicted to transfer the arginine-derived starting unit into the first steps of PKS machinery, is present in the surrounding region of known arginine-starting unit polyketides such as ECO-02301,[258]

azalomycin F3a,[259] linearmycin,[260] and lydicamycin. In addition, *Streptomyces* strains with arginine-containing metabolites are phylogenetically conserved (Fig. 22). The taxonomic distribution of 529 retrieved sequences showed the transacylases were mainly distributed in *Streptomyces* sp. As expected, the transacylases involved in desertomycin, azalomycin, linearmycin, and lydicamycin biosynthesis were clustered individually, indicating the high BGC-specificity of these proteins and most of the sequences retrieved and their corresponding BGCs remain vastly unexplored.

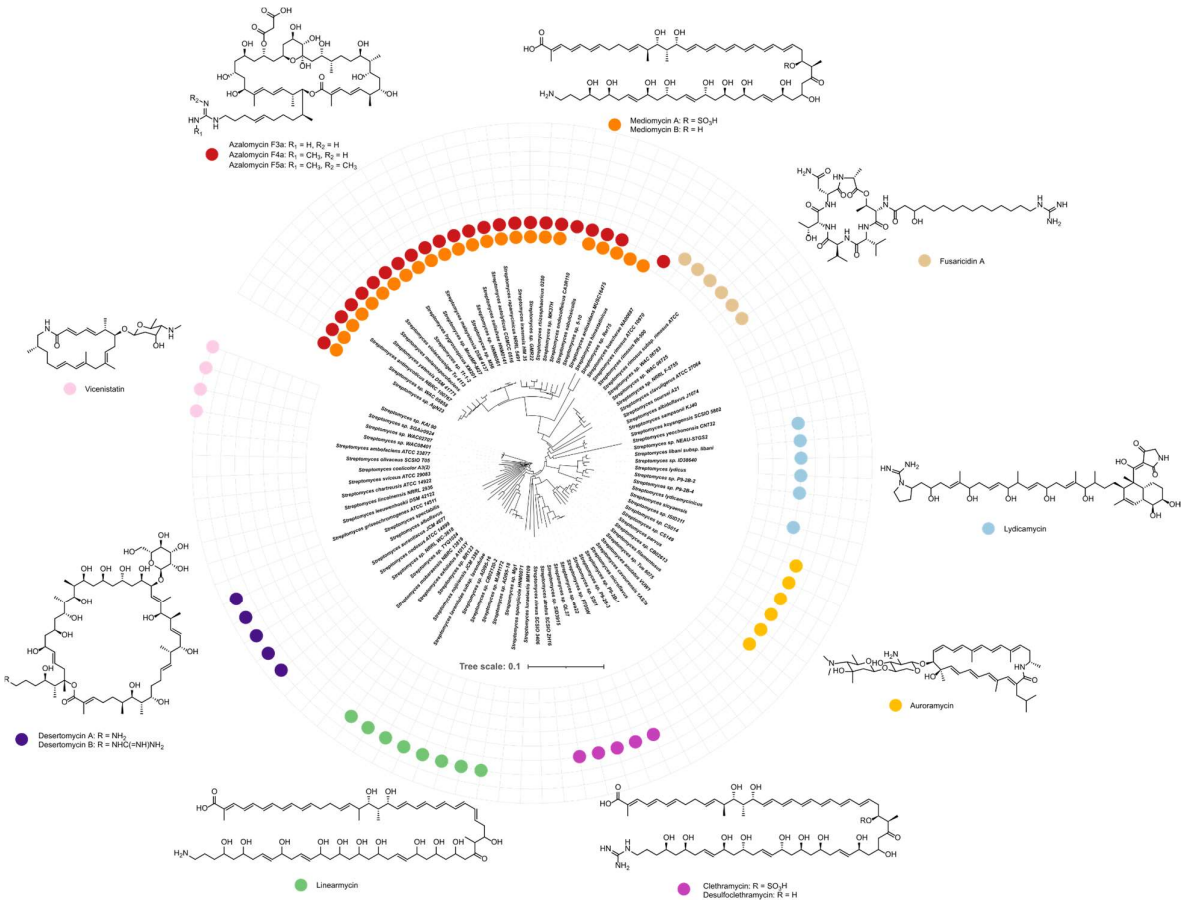

Fig. 22 Phylogenetic tree based on housekeeping gene *trpB* of *Streptomycetes* mapped with known arginine-containing metabolites.

2.4.2 CRISPR base editing in *Streptomyces rapamycinicus* IMET 43975

Ansamycins are a class of polyketide antibiotics with 3-amino-5-hydroxybenzoic acid (AHBA) as the starting unit and have various biological activities like antibacterial, anticancer and antiviral.[261] Up to date, there are more than 300 ansamycin compounds that have been characterized, such as the clinically used anti-tuberculosis drug rifamycin SV, the antibody conjugate drug maytansinoid and the first Hsp90 inhibitor geldanamycin.[262] Recently, the discovery of hygrocins and divergolides has further broadened the chemical diversity of ansamycins.

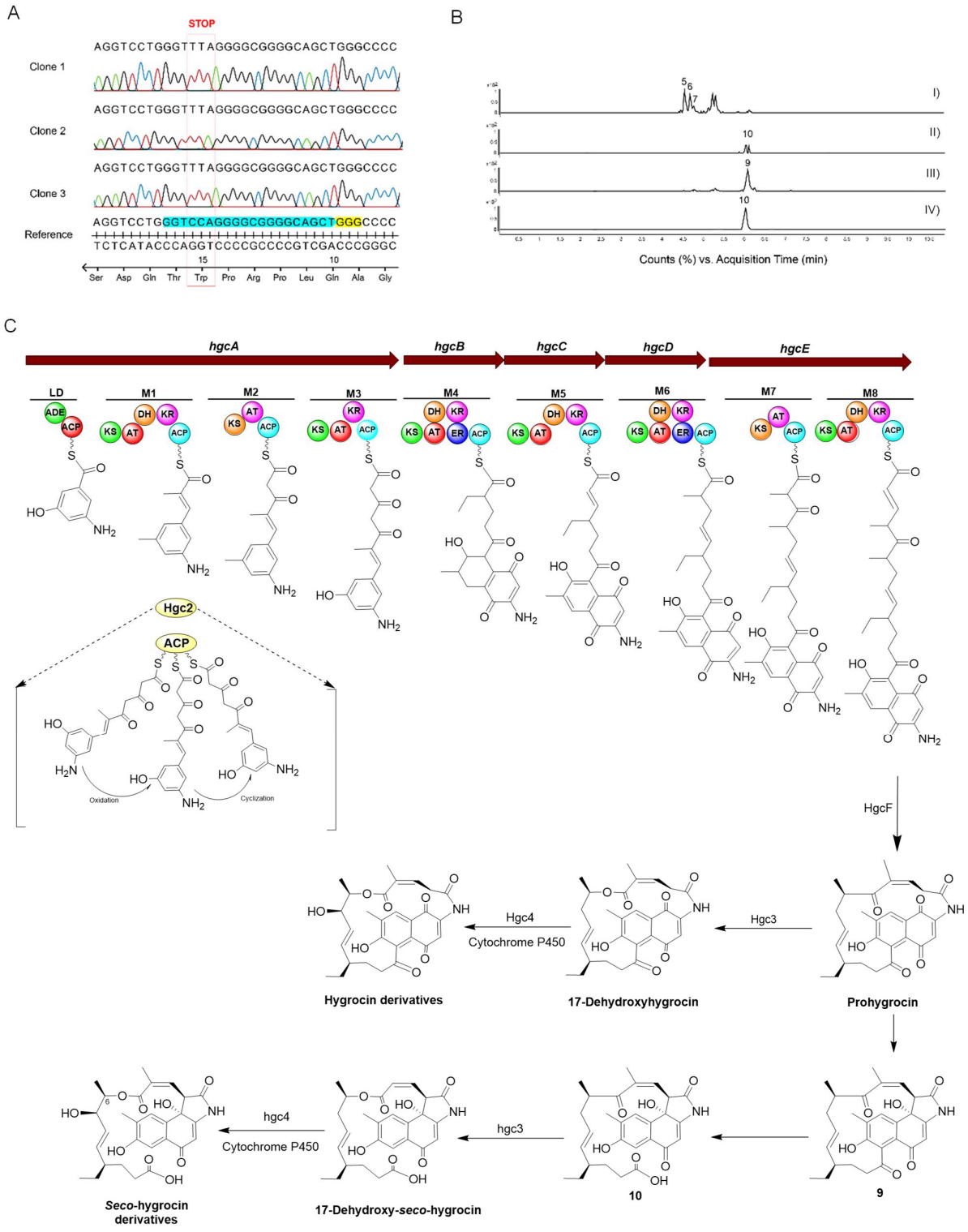

Fig. 23 Gene inactivation and proposed biosynthesis mechanism of hygrocins.

S. rapamycinicus IMET 43975 is a soil *Streptomyces* isolated from Easter Island, and it is a well-known rapamycin-producer.[263] Genome mining revealed that it is an abundant producer of secondary metabolites, with 48 BGCs including a putative hygrocin BGC. The metabolomics analysis of its culture broth suggested that some putative novel hygrocins were produced by *S. rapamycinicus*. Through the large-scale fermentation, chemical isolation and structure elucidation, four novel hygrocin derivatives and four known compounds were obtained and characterized.

The biosynthesis of hygrocin (*hgc*) has been well characterized, starting from AHBA as the building block derived from the shikimate pathway, and further elongated by eight PKS modules, using four malonyl-CoA, three methylmalonyl-CoA, and one (2*S*)-ethylmalonyl-CoA as chain extenders. The macrolide ester linkage in hygrocins and divergolides was proposed to be formed by a Baeyer-Villiger oxygenase, which catalyzes the oxidative cleavage of the carbon-carbon bond. Previous studies showed that the Baeyer–Villiger oxidation between C5 and C6/C7 in hygrocins was confirmed to be catalyzed by luciferase-like monooxygenase homologue Hgc3 after cyclization with amide synthase (HgcF) in *Streptomyces* sp. LZ35.[264] In this study, the CRISPR/Cas9-mediated base editing method was first applied in *S. rapamycinicus* to inactivate *hgc3*. According to sequencing results, the tryptophan (TGG) in position 15 of Hgc3 was successfully replaced by stop codon (TAA) in the mutant strains (Fig. 23a). The HR-ESI-MS analysis showed that the production of hygrocins I-J (**5**-**7**) was completely abolished (Fig. 23b). However, the production of hygrocin A (**9**, *m*/*z* 477.2151 $[M+H]^+$) and seco derivatives intermediates (**10**, *m*/*z* 495.2257 $[M+H]^+$) was still observed. Based on these intermediates, the ansa ring cleavage occurs prior to the Baeyer-Villiger oxidation was proposed, concluding that Hgc3 has no role in the cleavage of ansamycin seco-derivatives (Fig. 23c).

3. Conclusion and perspective

The overall aim of this PhD project is to focus on genome mining and metabolic engineering for bioactive natural product production in *Streptomyces*. Two novel polyketides derived from *S. iranensis*, plant growth-promoting pteridic acids, and antifungal spirolactone A, were discovered and their biosynthesis mechanisms were elucidated. The culture broth of *S. iranensis* was observed to significantly ameliorate abiotic stresses in plants, including salinity, osmotic, and drought stresses. Employing metabolomics, bioactivity-guided chemical isolation, and structure elucidation, the key ingredients were identified as pteridic acids H and F. Pteridic acids demonstrated noteworthy efficacy in enhancing plant stress resistance during *Arabidopsis* seedling experiments. Transcriptome analysis revealed that pteridic acids treatment not only upregulated the expression of plant photosynthesis and auxin biosynthesis-related genes but also activated various transcription factors associated with plant stress resistance. The biosynthesis pathway of pteridic acids were determined through in silico analysis and in vivo CRISPR base editing. Phylogenetic and comparative genome mining indicated the evolutionary conservation and global distribution of streptomycetes containing the pteridic acids BGC. Further genome mining of *S. iranensis* uncovered a cryptic BGC located in the terminal region of its linear chromosome. Through CRISPR-BEST mutation, HR-LC-MS analysis, and large-scale fermentation, a novel class of macrolide compounds spirolactones A-C were identified. Spirolactones featured a unique structure comprising a rare β-lactone moiety, a [6,6]-spiroketal, and an unusual extender unit. Notably, Spirolactone A exhibited potent anti-*Aspergillus* activity, and proteomic analysis suggested its potential mode of action by affecting fungal cell wall integrity. In addition, a comprehensive metabolic strategy was utilized to enhance the production of pteridic acids, resulting in a 2- to 5.9-fold increasement. The promoter engineering in *S. iranensis*/Δ*ptaA*/Δ*azaA*/Δ*nigA* resulted in the 7.3-fold increasement of spirolactone A. Meanwhile, the CRISPR-based gene editing toolbox was utilized in two non-model *Streptomyces* strains (*Streptomyces* sp. P9-2B-2, and *S. rapamycinicus* IMET 43975) to elucidate their BGCs associated with lydicamycin and hygrocins.

In the realm of bioactive natural product production in *Streptomyces*, the integration of genome-mining and metabolic engineering holds substantial promise for advancing our understanding and manipulation of biosynthetic pathways. The burgeoning availability of genomic data, coupled with sophisticated computational tools, facilitates comprehensive genome-mining endeavors, enabling the identification of cryptic BGCs that may encode novel bioactive compounds. As we look forward, continued advancements in high-throughput omics technologies will undoubtedly enhance our ability to predict and prioritize BGCs for targeted exploration.

The advent of CRISPR-based genome editing technologies has revolutionized the field, offering precise and efficient tools for targeted genetic modifications in *Streptomyces*. This capability opens avenues for the systematic manipulation of biosynthetic pathways, allowing researchers to fine-tune enzyme activities, optimize regulatory elements, and introduce heterologous genes with unparalleled precision. The application of CRISPR genome editing technologies in conjunction with genome-mining approaches not only expedites the identification of potential biosynthetic targets but also streamlines the subsequent engineering efforts, thereby accelerating the development of high-yield production strains. Furthermore, the synergy between genome mining and metabolic engineering offers unprecedented opportunities for the rational design and optimization of biosynthetic pathways. By leveraging insights gained from genomic analyses, tailored modifications to key enzymes and regulatory elements can be implemented to enhance the production of bioactive natural products. The prospect of employing synthetic biology principles to engineer *Streptomyces* strains with improved titers, as well as altered product profiles, represents a transformative avenue for the sustainable and scalable production of valuable compounds.

As we navigate the future landscape of natural product discovery and production in *Streptomyces*, interdisciplinary collaborations between genomics, bioinformatics, and synthetic biology will be pivotal. Integration of these approaches not only augments our capacity to unveil the hidden biosynthetic potential encoded within *Streptomyces* genomes but also propels the development of novel bioactive compounds with therapeutic and biotechnological applications. As challenges persist, including the elucidation of complex regulatory networks and the optimization of engineered strains at industrial scales, the holistic integration of diverse methodologies promises to illuminate new horizons in the field of natural product research and bioproduction.

4. Reference

1. Komaki, H. Recent progress of reclassification of the genus *Streptomyces*. *Microorganisms*, **11** 831 (2023).
2. Manteca, A. & Sanchez, J. *Streptomyces* development in colonies and soils. *Appl. Environ. Microbiol.* **75**, 2920-2924 (2009).
3. Schatz, A., Bugie, E. & Waksman, S. A. Streptomycin, a substance exhibiting antibiotic activity against gram positive and gram-negative bacteria. *Proc. Soc. Exp. Biol. Med.* **55**, 66-69 (1944).
4. Ory, E. M. The tetracyclines. *Med. Clin. N. Am.* **54**, 1173-1186 (1970).
5. Warnock, D. W. Amphotericin B: an introduction. *J. Antimicrob. Chemother.* **28**, 27-38 (1991).
6. Gray, K. C. et al. Amphotericin primarily kills yeast by simply binding ergosterol. *Proc. Natl Acad. Sci. USA* **109**, 2234–2239 (2012).
7. Anderson, T. M. et al. Amphotericin forms an extramembranous and fungicidal sterol sponge. *Nat. Chem. Biol.* **10**, 400–406 (2014).
8. Shiono, Y., Fujita, Y., Oka, S. & Yamazaki, Y. ATPase inhibitors suppress actinomycin D-induced apoptosis in leukemia cells. *Anticancer Res.* **22**, 2907-2911 (2002).
9. Lam, K. S., et al. Himastatin, a new antitumor antibiotic from *Streptomyces hygroscopicus*. *J. Antibiot.* **43**, 956-960 (1990).
10. Tanaka, H., et al. Chloropeptins, new anti-HIV antibiotics inhibiting gp120-CD4 binding from *Streptomyces* sp. *J. Antibiot.* **50**, 58-65 (1997)。
11. Assmann, T., Homey, B. & Ruzicka, T. Applications of tacrolimus for the treatment of skin disorders. *Immunopharmacology* **47**, 203-213 (2000).
12. Kehar, M., et al. Conversion from tacrolimus to sirolimus as a treatment modality in de novo allergies and immune-mediated disorders in pediatric liver transplant recipients. *Pediatr. Transplant.* **24**, e13737 (2020).
13. Rutledge, P. J. & Challis, G. L. Discovery of microbial natural products by activation of silent biosynthetic gene clusters. *Nat. Rev. Microbiol.* **13**, 509-523 (2015).
14. Bentley, S. D., et al. Complete genome sequence of the model actinomycete *Streptomyces coelicolor* A3(2). *Nature* **417**, 141-147 (2002).
15. Blin, K., et al. antiSMASH 7.0: new and improved predictions for detection, regulation, chemical structures and visualisation. *Nucleic Acids Res.* **51**, W46-W50 (2023).
16. Hertweck, C. The biosynthetic logic of polyketide diversity. *Angew. Chem. Int. Ed.* **48**, 4688-4716 (2009).
17. Risdian, C., Mozef, T. & Wink, J. Biosynthesis of polyketides in *Streptomyces*. *Microorganisms* **7**, 124

(2019).

18. Keatinge-Clay, A. T. The structures of type I polyketide synthases. *Nat. Prod. Rep.* **29**, 1050-1073 (2012).
19. Staunton, J. & Wilkinson, B. Biosynthesis of erythromycin and rapamycin. *Chem. Rev.* **97**, 2611-2629 (1997).
20. Süssmuth, R. D. & Mainz, A. Nonribosomal peptide synthesis-principles and prospects. *Angew. Chem. Int. Ed.* **56**, 3770-3821 (2017).
21. Röttig, M., et al. NRPSpredictor2-a web server for predicting NRPS adenylation domain specificity. *Nucleic Acids Res.* **39**, W362-W367 (2011).
22. Du, L. & Lou, LPKS and NRPS release mechanisms. *Nat. Prod. Rep.* **27**, 255-278 (2010).
23. Li, Q., et al. Identification of the biosynthetic gene cluster for the anti-infective desotamides and production of a new analogue in a heterologous host. *J. Nat. Prod.* **78**, 944-948 (2015).
24. Ma, J. Y., et al. Biosynthesis of ilamycins featuring unusual building blocks and engineered production of enhanced anti-tuberculosis agents. *Nat. Commun.* **8**, 391 (2017).
25. Beck, C., Garzón, J. F. G. & Weber, T. Recent advances in re-engineering modular PKS and NRPS assembly lines. *Biotechnol. Bioprocess Eng.* **25**, 886-894 (2020).
26. Arnison, P. G., et al. Ribosomally synthesized and post-translationally modified peptide natural products: overview and recommendations for a universal nomenclature. *Nat. Prod. Rep.* **30**, 108-160 (2013).
27. Ortega, M. A. & van der Donk, W. A. New insights into the biosynthetic logic of ribosomally synthesized and post-translationally modified peptide natural products. *Cell Chem. Biol.* **23**, 31-44 (2016).
28. Waisvisz, J. M., Vanderhoeven, M. G., Vanpeppen, J. & Zwennis, W. C. M. Bottromycin .1. a new sulfur-containing antibiotic. *J. Am. Chem. Soc.* **79**, 4520-4521 (1957).
29. Crone, W. J. K., Leeper, F. J. & Truman, A. W. Identification and characterisation of the gene cluster for the anti-MRSA antibiotic bottromycin: expanding the biosynthetic diversity of ribosomal peptides. *Chem. Sci.* **3**, 3516-3521 (2012).
30. Gomez-Escribano, J. P., Song, L. J., Bibb, M. J. & Challis, G. L. Posttranslational β-methylation and macrolactamidination in the biosynthesis of the bottromycin complex of ribosomal peptide antibiotics. *Chem. Sci.* **3**, 3522-3525 (2012).
31. An, J. S., et al. Discovery and biosynthesis of cihunamides, macrocyclic antibacterial ripps with a unique C-N linkage formed by CYP450 catalysis. *Angew. Chem. Int. Ed.* **62**, e202300998 (2023).
32. Walsh, C. T. & Fischbach, M. A. Natural products version 2.0: connecting genes to molecules. *J. Am. Chem. Soc.* **132**, 2469-2493 (2010).
33. Ajikumar, P. K., et al. Terpenoids: opportunities for biosynthesis of natural product drugs using

engineered microorganisms. *Mol. Pharm.* **5**, 167-190 (2008).

34. Kuzuyama, T. Biosynthetic studies on terpenoids produced by *Streptomyces*. *J. Antibiot.* **70**, 811-818 (2017).
35. Komatsu, M., Tsuda, M., Omura, S., Oikawa, H. & Ikeda, H. Identification and functional analysis of genes controlling biosynthesis of 2-methylisoborneol. *Proc. Natl. Acad. Sci. U. S. A.* **105**, 7422-7427 (2008).
36. Brown, G. D. The biosynthesis of steroids and triterpenoids. *Nat. Prod. Rep.* **15**, 653-696 (1998).
37. Abe, I. Biosynthetic studies on teleocidins in *Streptomyces*. *J. Antibiot.* **71**, 763-768 (2018).
38. Miyanaga, A., Kudo, F. & Eguchi, T. Protein-protein interactions in polyketide synthase-nonribosomal peptide synthetase hybrid assembly lines. *Nat. Prod. Rep.* **35**, 1185-1209 (2018).
39. Shen, B., et al. Cloning and characterization of the bleomycin biosynthetic gene cluster from *Streptomyces verticillus* ATCC15003. *J. Nat. Prod.* **65**, 422-431 (2002).
40. Pohle, S., Appelt, C., Roux, M., Fiedler, H. P. & Süssmuth, R. D. Biosynthetic gene cluster of the non-ribosomally synthesized cyclodepsipeptide skyllamycin: deciphering unprecedented ways of unusual hydroxylation reactions. *J. Am. Chem. Soc.* **133**, 6194-6205 (2011).
41. Sun, C., et al. Genome mining of *Streptomyces atratus* SCSIO ZH16: discovery of atratumycin and identification of its biosynthetic gene cluster. *Org. Lett.* **21**, 1453-1457 (2019).
42. Wang, H., et al. Anulamycins A-F, cinnamoyl-containing peptides from a lake sediment derived *Streptomyces*. *J. Nat. Prod.* **86**, 357-367 (2023).
43. Winter, J. M., et al. Molecular basis for chloronium-mediated meroterpene cyclization - Cloning, sequencing, and heterologous expression of the napyradiomycin biosynthetic gene cluster. *J. Biol. Chem.* **282**, 16362-16368 (2007).
44. Bringmann, G., Haagen, Y., Gulder, T. A. M., Gulder, T. & Heide, L. Biosynthesis of the isoprenoid moieties of furanonaphthoquinone I and endophenazine A in *Streptomyces cinnamonensis* DSM 1042. *J. Org. Chem.* **72**, 4198-4204 (2007).
45. Haagen, Y., et al. A gene cluster for prenylated naphthoquinone and prenylated phenazine biosynthesis in *Streptomyces cinnamonensis* DSM 1042. *ChemBioChem* **7**, 2016-2027 (2006).
46. Javed, M. R., et al. CRISPR-Cas system: history and prospects as a genome editing tool in microorganisms. *Curr. Microbiol.* **75**, 1675-1683 (2018).
47. Mali, P., et al. RNA-guided human genome engineering via Cas9. *Science* **339**, 823-826 (2013).
48. Tong, Y., Weber, T. & Lee, S. Y. CRISPR/Cas-based genome engineering in natural product discovery. *Nat. Prod. Rep.* **36**, 1262-1280 (2019).
49. Jiang, W., Bikard, D., Cox, D., Zhang, F. & Marraffini, L. A. RNA-guided editing of bacterial genomes using CRISPR-Cas systems. *Nat. Biotechnol.* **31**, 233-239 (2013).

50. Bao, Z. H., et al. Homology-integrated CRISPR-Cas (HI-CRISPR) system for one-step multigene disruption in *Saccharomyces cerevisiae*. *Acs Synth. Biol.* **4**, 585-594 (2015).
51. Cobb, R. E., Wang, Y. J. & Zhao, H. M. High-efficiency multiplex genome editing of *Streptomyces* species using an engineered CRISPR/Cas System. *Acs Synth. Biol.* **4**, 723-728 (2015).
52. Tong, Y., Charusanti, P., Zhang, L., Weber, T. & Lee, S. Y. CRISPR-Cas9 based engineering of actinomycetal genomes. *Acs Synth. Biol.* **4**, 1020-1029 (2015).
53. Huang, H., Zheng, G., Jiang, W., Hu, H. & Lu, Y. One-step high-efficiency CRISPR/Cas9-mediated genome editing in *Streptomyces*. *Acta Biochim. Biophys. Sin.* **47**, 231-243 (2015).
54. Zhang, Y., et al. Antisense RNA interference-enhanced CRISPR/Cas9 base editing method for improving base editing efficiency in *Streptomyces lividans* 66. *Acs Synth. Biol.* **10**, 1053-1063 (2021).
55. Jiang, Y., et al. Fine-tuning Cas9 activity with a cognate inhibitor AcrIIA4 to improve genome editing in *Streptomyces*. *Acs Synth. Biol.* **10**, 2833-2841 (2021).
56. Yao, R., et al. CRISPR-Cas9/Cas12a biotechnology and application in bacteria. *Synth. Syst. Biotechnol.* **3**, 135-149 (2018).
57. Li, L., et al. CRISPR-Cpf1-assisted multiplex genome editing and transcriptional repression in *Streptomyces*. *Appl. Environ. Microbiol.* **84**, e00827-18 (2018).
58. Zhang, J., et al. Efficient multiplex genome editing in *Streptomyces* via engineered CRISPR-Cas12a systems. *Front. bioeng. biotechnol.* **8**, 726 (2020).
59. Hidalgo-Cantabrana, C. & Barrangou, R. Characterization and applications of Type I CRISPR-Cas systems. *Biochem. Soc. Trans.* **48**, 15-23 (2020).
60. Sinkunas, T. et al. Cas3 is a single-stranded DNA nuclease and ATP-dependent helicase in the CRISPR/Cas immune system. *EMBO J.* **30**, 1335–1342 (2011).
61. Li, Y. et al. Harnessing Type I and Type III CRISPR-Cas systems for genome editing. *Nucleic Acids Res.* **44**, e34–e34 (2016).
62. Cheng, F. et al. Harnessing the native type I-B CRISPR-Cas for genome editing in a polyploid archaeon. *J. Genet. Genomics Yi Chuan Xue Bao* **44**, 541–548 (2017).
63. Hidalgo-Cantabrana, C., Goh, Y. J., Pan, M., Sanozky-Dawes, R. & Barrangou, R. Genome editing using the endogenous type I CRISPR-Cas system in *Lactobacillus crispatus*. *Proc. Natl Acad. Sci. USA* **116**, 15774–15783 (2019).
64. Hampton, H. G. et al. CRISPR-Cas gene-editing reveals RsmA and RsmC act through FlhDC to repress the SdhE flavinylation factor and control motility and prodigiosin production in *Serratia*. *Microbiology* **162**, 1047–1058 (2016).
65. Csörgo, B., et al. A compact Cascade-Cas3 system for targeted genome engineering. *Nat. Methods* **17**, 1183-1190 (2020).

66. Whitford, C. M., et al. CASCADE-Cas3 enables highly efficient genome engineering in *Streptomyces* species. *BioRxiv*, 2023.05.09.539971 (2023).
67. Alberti, F. & Corre, C. Editing streptomycete genomes in the CRISPR/Cas9 age. *Nat. Prod. Rep.* **36**, 1237-1248 (2019).
68. Dharmalingam, K. & Cullum, J. Genetic instability in *Streptomyces*. *J. Biosci.* **21**, 433-444 (1996).
69. Hoff, G., Bertrand, C., Piotrowski, E., Thibessard, A. & Leblond, P. Genome plasticity is governed by double strand break DNA repair in *Streptomyces*. *Sci. Rep.* **8**, 5272 (2018).
70. Tong, Y., et al. Highly efficient DSB-free base editing for streptomycetes with CRISPR-BEST. *Proc. Natl. Acad. Sci. U. S. A.* **116**, 20366-20375 (2019).
71. Blin, K., Shaw, S., Tong, Y. J. & Weber, T. Designing sgRNAs for CRISPR-BEST base editing applications with CRISPy-web 2.0. *Synth. Syst. Biotechnol.* **5**, 99-102 (2020).
72. Whitford, C. M., et al. Systems analysis of highly multiplexed CRISPR-base editing in streptomycetes. *Acs Synth. Biol.* **12**, 2353-2366 (2023).
73. Liu, G., Chater, K. F., Chandra, G., Niu, G. & Tan, H. Molecular regulation of antibiotic biosynthesis in *Streptomyces*. *Microbiol. Mol. Biol. Rev.* **77**, 112-143 (2013).
74. Walker, J. E., Saraste, M., Runswick, M. J. & Gay, N. J. Distantly related sequences in the alpha-subunits and beta-subunits of ATP synthase, myosin, kinases and other ATP-requiring enzymes and a common nucleotide binding fold. *EMBO J.* **1**, 945-951 (1982).
75. Antón, N., et al. PimM, a PAS domain positive regulator of pimaricin biosynthesis in *Streptomyces natalensis*. *Microbiology* **153**, 3174-3183 (2007).
76. He, W., Lei, J., Liu, Y. & Wang, Y. The LuxR family members GdmRI and GdmRII are positive regulators of geldanamycin biosynthesis in *Streptomyces hygroscopicus* 17997. *Arch. Microbiol.* **189**, 501-510 (2008).
77. Hur, Y. A., Choi, S. S., Sherman, D. H. & Kim, E. S. Identification of TmcN as a pathway-specific positive regulator of tautomycetin biosynthesis in *Streptomyces* sp. CK4412. *Microbiology* **154**, 2912-2919 (2008).
78. Li, Z., et al. Engineering bafilomycin high-producers by manipulating regulatory and biosynthetic genes in the marine bacterium *Streptomyces lohii*. *Mar. Drugs* **19**, 29 (2021).
79. Park, J., et al. Discovery of new indolosesquiterpenoids bearing a N-O linkage by overexpression of LuxR regulator in a marine bacterium *Streptomyces* sp. *Front. Mar. Sci.* **10**, 1140516 (2023).
80. Arias, P., Fernández-Moreno, M. A. & Malpartida, F. Characterization of the pathway-specific positive transcriptional regulator for actinorhodin biosynthesis in *Streptomyces coelicolor* A3(2) as a DNA-binding protein. *J. Bacteriol.* **181**, 6958-6968 (1999).
81. Narva, K. E. & Feitelson, J. S. Nucleotide-sequence and transcriptional analysis of the redD locus of

Streptomyces coelicolor A3(2). *J. Bacteriol.* **172**, 326-333 (1990).

82. PerezLlarena, F. J., Liras, P., RodriguezGarcia, A. & Martin, J. F. A regulatory gene (ccaR) required for cephamycin and clavulanic acid production in *Streptomyces clavuligerus*: Amplification results in overproduction of both beta-lactam compounds. *J. Bacteriol.* **179**, 2053-2059 (1997).
83. Krause, J., Handayani, I., Blin, K., Kulik, A. & Mast, Y. Disclosing the potential of the SARP-type regulator PapR2 for the activation of antibiotic gene clusters in streptomycetes. *Front. Microbiol.* **11**, 225 (2020).
84. Li, Y., et al. Characterization of the positive SARP family regulator PieR for improving piericidin A1 production in *Streptomyces piomogeues* var. Hangzhouwanensis. *Synth. Syst. Biotechnol.* **4**, 16-24 (2019).
85. Mendez, C. & Salas, J. A. ABC transporters in antibiotic-producing actinomycetes. *FEMS Microbiol. Lett.* **158**, 1-8 (1998).
86. Linton, K. J., Cooper, H. N., Hunter, I. S. & Leadlay, P. F. An ABC-transporter from *Streptomyces longisporoflavus* confers resistance to the polyether-ionophore antibiotic tetronasin. *Mol. Microbiol.* **11**, 777-785 (1994).
87. Qiu, J., et al. Overexpression of the ABC transporter AvtAB increases avermectin production in *Streptomyces avermitilis*. *Appl. Microbiol. Biotechnol.* **92**, 337-345 (2011).
88. Jin, P., et al. Mining and fine-tuning sugar uptake system for titer improvement of milbemycins in *Streptomyces bingchenggensis*. *Synth. Syst. Biotechnol.* **5**, 214-221 (2020).
89. Strohl, W. R. Compilation and analysis of DNA-sequences associated with apparent streptomycete promoters. *Nucleic Acids Res.* **20**, 961-974 (1992).
90. Myronovskyi, M. & Luzhetskyy, A. Native and engineered promoters in natural product discovery. *Nat. Prod. Rep.* **33**, 1006-1019 (2016).
91. Seghezzi, N., Amar, P., Koebmann, B., Jensen, P. R. & Virolle, M. J. The construction of a library of synthetic promoters revealed some specific features of strong *Streptomyces promoters*. *Appl. Microbiol. Biotechnol.* **90**, 615-623 (2011).
92. Siegl, T., Tokovenko, B., Myronovskyi, M. & Luzhetskyy, A. Design, construction and characterisation of a synthetic promoter library for fine-tuned gene expression in actinomycetes. *Metab. Eng.* **19**, 98-106 (2013).
93. Pédelacq, J. D., Cabantous, S., Tran, T., Terwilliger, T. C. & Waldo, G. S. Engineering and characterization of a superfolder green fluorescent protein. *Nat. Biotechnol.* **24**, 79-88 (2006).
94. Bai, C., et al. Exploiting a precise design of universal synthetic modular regulatory elements to unlock the microbial natural products in *Streptomyces*. *Proc. Natl. Acad. Sci. U. S. A.* **112**, 12181-12186 (2015).

95. Zhang, M. M., et al. CRISPR-Cas9 strategy for activation of silent *Streptomyces* biosynthetic gene clusters. *Nat. Chem. Biol.* **13**, 607-U173 (2017).
96. Liu, X., Wang, J. X., Chen, X. A., Liu, Y. & Li, Y. Q. Activation and characterization of Lanthomicins A-C by promoter engineering in *Streptomyces chattanoogensis* L10. *Front. Microbiol.* **13**, 902990 (2022).
97. Zhao, X., Zong, Y., Wei, W. & Lou, C. Multiplexed promoter engineering for improving Thaxtomin A production in heterologous *Streptomyces* hosts. *Life* **12**, 689 (2022).
98. Wilson, M. C. & Moore, B. S. Beyond ethylmalonyl-CoA: The functional role of crotonyl-CoA carboxylase/reductase homologs in expanding polyketide diversity. *Nat. Prod. Rep.* **29**, 72-86 (2012).
99. Wang, W., et al. Harnessing the intracellular triacylglycerols for titer improvement of polyketides in *Streptomyces*. *Nat. Biotechnol.* **38**, 76-83 (2020).
100. Liao, Z., et al. Improvement of rimocidin biosynthesis by increasing supply of precursor malonyl-CoA via over-expression of acetyl-Coa carboxylase in *Streptomyces rimosus* M527. *Curr. Microbiol.* **79**, 174 (2022).
101. Liu, B., et al. Efficient production of 3-hydroxypropionate from fatty acids feedstock in *Escherichia coli*. *Metab. Eng.* **51**, 121-130 (2019).
102. Hao, Y., et al. Avermectin B1a production in *Streptomyces avermitilis* is enhanced by engineering *aveC* and precursor supply genes. *Appl. Microbiol. Biotechnol.* **106**, 2191-2205 (2022).
103. Lombó, F., et al. Enhancing the atom economy of polyketide biosynthetic processes through metabolic engineering. *Biotechnol. Prog.* **17**, 612-617 (2001).
104. Lu, C., Zhang, X., Jiang, M. & Bai, L. Enhanced salinomycin production by adjusting the supply of polyketide extender units in *Streptomyces albus*. *Metab. Eng.* **35**, 129-137 (2016).
105. Huo, L., et al. Heterologous expression of bacterial natural product biosynthetic pathways. *Nat. Prod. Rep.* **36**, 1412-1436 (2019).
106. Yang, Z., et al. MGCEP 1.0: a genetic-engineered marine-derived chassis cell for a scaled heterologous expression platform of microbial bioactive metabolites. *Acs Synth. Biol.* **11**, 3772-3784 (2022).
107. Kang, H. & Kim, E. Recent advances in heterologous expression of natural product biosynthetic gene clusters in *Streptomyces* hosts. *Curr. Opin. Biotechnol.* **69**, 118-127 (2021).
108. Ke, J. & Yoshikuni, Y. Multi-chassis engineering for heterologous production of microbial natural products. *Curr. Opin. Biotechnol.* **62**, 88-97 (2020).
109. Jiang, W. & Zhu, T. Targeted isolation and cloning of 100-kb microbial genomic sequences by Cas9-assisted targeting of chromosome segments. *Nat. Protoc.* **11**, 960-975 (2016).
110. Enghiad, B., et al. Cas12a-assisted precise targeted cloning using in vivo Cre-*lox* recombination. *Nat. Commun.* **12**, 1171 (2021).

111. Yin, S., et al. Heterologous expression of oxytetracycline biosynthetic gene cluster in *Streptomyces venezuelae* WVR2006 to improve production level and to alter fermentation process. *Appl. Microbiol. Biotechnol.* **100**, 10563-10572 (2016).
112. Xu, Z., et al. Discovery and biosynthetic pathway analysis of cyclopentane–β-lactone globilactone A. *Nat. Synth.* (2023).
113. O'Brien, E. J., Monk, J. M. & Palsson, B. O. Using genome-scale models to predict biological capabilities. *Cell* **161**, 971-987 (2015).
114. King, Z. A., et al. BiGG Models: A platform for integrating, standardizing and sharing genome-scale models. *Nucleic Acids Res.* **44**, D515-D522 (2016).
115. Wang, X., Zhang, Y. & Wen, T. Progress on genome-scale metabolic models integrated with multi-omics data. *Chin. Sci. Bull.* **66**, 2393-2404 (2021).
116. Machado, D., Andrejev, S., Tramontano, M. & Patil, K. R. Fast automated reconstruction of genome-scale metabolic models for microbial species and communities. *Nucleic Acids Res.* **46**, 7542-7553 (2018).
117. Burgard, A. P., Pharkya, P. & Maranas, C. D. OptKnock: A bilevel programming framework for identifying gene knockout strategies for microbial strain optimization. *Biotechnol. Bioeng.* **84**, 647-657 (2003).
118. Gu, D., Zhang, C., Zhou, S., Wei, L. & Hua, Q. IdealKnock: A framework for efficiently identifying knockout strategies leading to targeted overproduction. *Comput. Biol. Chem.* **61**, 229-237 (2016).
119. Stanford, N. J., Millard, P. & Swainston, N. RobOKoD: microbial strain design for (over)production of target compounds. *Front. cell dev. biol.* **3**, 17 (2015).
120. Domenzain, I., et al. Reconstruction of a catalogue of genome-scale metabolic models with enzymatic constraints using GECKO 2.0. *Nat. Commun.* **13**, 3766 (2022).
121. Mohite, O. S., Weber, T., Kim, H. U. & Lee, S. Y. Genome-scale metabolic reconstruction of actinomycetes for antibiotics production. *Biotechnol. J.* **14**, 1800377 (2019)
122. Wang, H., et al. RAVEN 2.0: A versatile toolbox for metabolic network reconstruction and a case study on *Streptomyces coelicolor*. *PLoS Comp. Biol.* **14**, e1006541 (2018).
123. Fondi, M., et al. Time-resolved transcriptomics and constraint-based modeling identify system-level metabolic features and overexpression targets to increase spiramycin production in *Streptomyces ambofaciens*. *Front. Microbiol.* **8**, 835 (2017).
124. Lewis, J. E. & Kemp, M. L. Integration of machine learning and genome-scale metabolic modeling identifies multi-omics biomarkers for radiation resistance. *Nat. Commun.* **12**, 2700 (2021).
125. Challis, G. L. Genome mining for novel natural product discovery. *J. Med. Chem.* **51**, 2618-2628 (2008).
126. Albarano, L., Esposito, R., Ruocco, N. & Costantini, M. Genome mining as new challenge in natural

products discovery. *Mar. Drugs* **18**, 199 (2020).

127. Scherlach, K. & Hertweck, C. Mining and unearthing hidden biosynthetic potential. *Nat. Commun.* **12**, 3864 (2021).
128. Ziemert, N., Alanjary, M. & Weber, T. The evolution of genome mining in microbes - a review. *Nat. Prod. Rep.* **33**, 988-1005 (2016).
129. Weber, T., et al. *CLUSEAN*: A computer-based framework for the automated analysis of bacterial secondary metabolite biosynthetic gene clusters. *J. Biotechnol.* **140**, 13-17 (2009).
130. Lee, N., et al. Mini review: Genome mining approaches for the identification of secondary metabolite biosynthetic gene clusters in *Streptomyces*. *Comput. Struct. Biotechnol. J.* **18**, 1548-1556 (2020).
131. Wang, Z., et al. A naturally inspired antibiotic to target multidrug-resistant pathogens. *Nature* **601**, 606-611 (2022).
132. Wang, Z., Koirala, B., Hernandez, Y., Zimmerman, M. & Brady, S. F. Bioinformatic prospecting and synthesis of a bifunctional lipopeptide antibiotic that evades resistance. *Science* **376**, 991-996 (2022).
133. Ueoka, R., et al. Genome-based discovery and total synthesis of janustatins, potent cytotoxins from a plant-associated bacterium. *Nat. Chem.* **14**, 1193-1201 (2022).
134. Hu, Y., et al. Building *Streptomyces albus* as a chassis for synthesis of bacterial terpenoids. *Chem. Sci.* **14**, 3661-3667 (2023).
135. Malit, J. J. L., et al. Global genome mining reveals a cytochrome P450-catalyzed cyclization of crownlike cyclodipeptides with neuroprotective activity. *Org. Lett.* **23**, 6601-6605 (2021).
136. Prado-Alonso, L., et al. Colibrimycins, novel halogenated hybrid polyketide synthase-nonribosomal peptide synthetase (PKS-NRPS) compounds produced by *Streptomyces* sp. strain CS147. *Appl. Environ. Microbiol.* **88**, e01839-21 (2022).
137. Santos, C. L., Correia-Neves, M., Moradas-Ferreira, P. & Mendes, M. V. A walk into the LuxR regulators of actinobacteria: phylogenomic distribution and functional diversity. *PLoS ONE* **7**, e46758 (2012).
138. Sugiyama, M. Structural biological study of self-resistance determinants in antibiotic-producing actinomycetes. *J. Antibiot.* **68**, 543-550 (2015).
139. Yan, Y., et al. Resistance-gene-directed discovery of a natural-product herbicide with a new mode of action. *Nature* **559**, 416-418 (2018).
140. Vandova, G. A., et al. Identification of polyketide biosynthetic gene clusters that harbor self-resistance target genes. *BioRxiv*, 2020.06.01.128595 (2020).
141. Yuan, Y., et al. Automated, self-resistance gene-guided, and high-throughput genome mining of bioactive natural products from *Streptomyces*. *BioRxiv,* 2023.10.26.564101 (2023).
142. Ziemert, N., et al. The Natural Product Domain Seeker NaPDoS: a phylogeny based bioinformatic

tool to classify secondary metabolite gene diversity. *PLoS ONE* **7**, e34064 (2012).

143. Klau, L. J., et al. The Natural Product Domain Seeker version 2 (NaPDoS2) webtool relates ketosynthase phylogeny to biosynthetic function. *J. Biol. Chem.* **298**, 102480 (2022).
144. Sélem-Mojica, N., Aguilar, C., Gutiérrez-García, K., Martínez-Guerrero, C. E. & Barona-Gómez, F. EvoMining reveals the origin and fate of natural product biosynthetic enzymes. *Microb. Genom.* **5**, e000260 (2019).
145. Navarro-Muñoz, J. C., et al. A computational framework to explore large-scale biosynthetic diversity. *Nat. Chem. Biol.* **16**, 60-68 (2020).
146. Kautsar, S. A., van der Hooft, J. J. J., de Ridder, D. & Medema, M. H. BiG-SLiCE: A highly scalable tool maps the diversity of 1.2 million biosynthetic gene clusters. *Gigascience* **10**, 1-17 (2021).
147. Kautsar, S. A., Blin, K., Shaw, S., Weber, T. & Medema, M. H. BiG-FAM: the biosynthetic gene cluster families database. *Nucleic Acids Res.* **49**, D490-D497 (2021).
148. Zhao, Y., et al. PGAP: pan-genomes analysis pipeline. *Bioinformatics* **28**, 416-418 (2012).
149. Page, A. J., et al. Roary: rapid large-scale prokaryote pan genome analysis. *Bioinformatics* **31**, 3691-3693 (2015).
150. Nuhamunada, M., et al. BGCFlow: Systematic pangenome workflow for the analysis of biosynthetic gene clusters across large genomic datasets. *BioRxiv*, 2023.06.14.545018 (2023).
151. Sereika, M., et al. Oxford Nanopore R10.4 long-read sequencing enables the generation of near-finished bacterial genomes from pure cultures and metagenomes without short-read or reference polishing. *Nat. Methods* **19**, 823-826 (2022).
152. Zhu, J., Zhang, S., Wang, W. & Jiang, H. Strategies for discovering new antibiotics from bacteria in the post-genomic era. *Curr. Microbiol.* **77**, 3213-3223 (2020).
153. Crits-Christoph, A., Diamond, S., Butterfield, C. N., Thomas, B. C. & Banfield, J. F. Novel soil bacteria possess diverse genes for secondary metabolite biosynthesis. *Nature* **558**, 440-444 (2018).
154. Paoli, L., et al. Biosynthetic potential of the global ocean microbiome. *Nature* **607**, 111-118 (2022).
155. Mullowney, M. W., et al. Artificial intelligence for natural product drug discovery. *Nat. Rev. Drug Discovery* **22**, 895-916 (2023).
156. Saldívar-González, F. I., Aldas-Bulos, V. D., Medina-Franco, J. L. & Plisson, F. Natural product drug discovery in the artificial intelligence era. *Chem. Sci.* **13**, 1526-1546 (2022).
157. Sahayasheela, V. J., et al. Artificial intelligence in microbial natural product drug discovery: current and emerging role. *Nat. Prod. Rep.* **39**, 2215-2230 (2022).
158. Hannigan, G. D., et al. A deep learning genome-mining strategy for biosynthetic gene cluster prediction. *Nucleic Acids Res.* **47**, e110 (2019).
159. Carroll, L. M., et al. Accurate de novo identification of biosynthetic gene clusters with GECCO.

BioRxiv, 2021.05.03.442509 (2021).

160. Merwin, N. J., et al. DeepRiPP integrates multiomics data to automate discovery of novel ribosomally synthesized natural products. *Proc. Natl. Acad. Sci. U. S. A.* **117**, 371-380 (2020).
161. Wheeler, T. & von Braun, J. Climate change impacts on global food security. *Science* **341**, 508-513 (2013).
162. Zhang, H., Zhu, J., Gong, Z. & Zhu, J. Abiotic stress responses in plants. *Nat. Rev. Genet.* **23**, 104-119 (2022).
163. Kuromori, T., Fujita, M., Takahashi, F., Yamaguchi-Shinozaki, K. & Shinozaki, K. Inter-tissue and inter-organ signaling in drought stress response and phenotyping of drought tolerance. *Plant J.* **109**, 342-358 (2022).
164. Dos Santos, V., et al. Causes of reduced leaf-level photosynthesis during strong El Niño drought in a Central Amazon forest. *Global Change Biol.* **24**, 4266-4279 (2018).
165. Waadt, R., et al. Plant hormone regulation of abiotic stress responses. *Nat. Rev. Mol. Cell Biol.* **23**, 680-694 (2022).
167. Corwin, D. Climate change impacts on soil salinity in agricultural areas. *Eur. J. Soil Sci.* **72**, 842-862 (2021).
168. Ullah, A., Bano, A. & Khan. N. Climate change and salinity effects on crops and chemical communication between plants and plant growth-promoting microorganisms under stress. *Front. Sustain. Food Syst.* **5**, 618092 (2021).
169. Hong, Y., Zhou, Q., Hao, Y. & Huang, A. C. Crafting the plant root metabolome for improved microbe-assisted stress resilience. *New Phytol.* **234**, 1945-1950 (2022).
170. De Vries, F., Griffiths, R., Knight, C., Nicolitch, O. & Williams, A. Harnessing rhizosphere microbiomes for drought-resilient crop production. *Science* **368**, 270-274 (2020).
171. Blin, K., et al. antiSMASH 6.0: improving cluster detection and comparison capabilities. *Nucleic Acids Res.* **49**, W29-W35 (2021).
172. Wang, M., et al. Sharing and community curation of mass spectrometry data with Global Natural Products Social Molecular Networking. *Nat. Biotechnol.* **34**, 828-837 (2016).
173. Qiu, J., Henderson, S. W., Tester, M., Roy, S. J. & Gilliham, M. SLAH1, a homologue of the slow type anion channel SLAC1, modulates shoot Cl^- accumulation and salt tolerance in *Arabidopsis thaliana*. *J. Exp. Bot.* **67**, 4495-4505 (2016).
174. Krishnamurthy, P., et al. Transcriptomics analysis of salt stress tolerance in the roots of the mangrove *Avicennia officinalis*. *Sci. Rep.* **7**, 10031 (2017).
175. Li, L., Cai, Q., Yu, D. & Guo, C. Overexpression of AtFRO6 in transgenic tobacco enhances ferric chelate reductase activity in leaves and increases tolerance to iron-deficiency chlorosis. *Mol. Biol.*

Rep. **38**, 3605-3613 (2011).

176. Pillitteri, L. J. & Dong, J. Stomatal development in *Arabidopsis*. *Arabid. Book* **11**, e0162 (2013).
177. Zhang, J., Zhang, X., Wang, R. & Li, W. The plasma membrane-localised Ca^{2+}-ATPase ACA8 plays a role in sucrose signalling involved in early seedling development in *Arabidopsis*. *Plant Cell Rep.* **33**, 755-766 (2014).
178. Magidin, M., Pittman, J. K., Hirschi, K. D. & Bartel, B. ILR2, a novel gene regulating IAA conjugate sensitivity and metal transport in *Arabidopsis thaliana*. *Plant J.* **35**, 523-534 (2003).
179. Teng, Z., Lv, J., Chen, Y., Zhang, J. & Ye, N. Effects of stress-induced ABA on root architecture development: Positive and negative actions. *Crop J.* **11**, 1072-1079 (2023).
180. Foka, I. C. K., et al. The emerging roles of Diacylglycerol Kinase (DGK) in plant stress tolerance, growth, and development. *Agronomy-Basel* **10**, 1375 (2020).
181. Shen, L., et al. Phosphatidic acid promotes the activation and plasma membrane localization of *MKK7* and *MKK9* in response to salt stress. *Plant Sci.* **287**, 110190 (2019).
182. Wang, H., Zhao, X., Zhang, J., Lu. C., Feng, F. Arbuscular mycorrhizal fungus regulates cadmium accumulation, migration, transport, and tolerance in *Medicago sativa*. *J. Hazard. Mater.* **435**, 129077 (2022).
183. Nicolas-Espinosa, J., Garcia-Ibañez, P., Lopez-Zaplana, A., Yepes-Molina, L., Albaladejo-Marico, L., Carvajal, M. Confronting secondary metabolites with water uptake and transport in plants under abiotic stress. *Int. J. Mol. Sci.* **24**, 2826 (2023).
184. Zhang, Y., et al. Transcriptome and metabolome analyses of two contrasting sesame genotypes reveal the crucial biological pathways involved in rapid adaptive response to salt stress. *BMC Plant Biol* **19**, 66 (2019).
185. Ryu, H. & Cho, Y. G. Plant hormones in salt stress tolerance. *J. Plant Biol.* **58**, 147-155 (2015).
186. Jung, J. & Park, C. Auxin modulation of salt stress signaling in *Arabidopsis* seed germination. *Plant Signal. Behav.* **6**, 1198-1200 (2011).
187. Abogadallah, G. M., Nada, R. M., Malinowski, R. & Quick, P. Overexpression of *HARDY*, an AP2/ERF gene from *Arabidopsis*, improves drought and salt tolerance by reducing transpiration and sodium uptake in transgenic *Trifolium alexandrinum* L. *Planta* **233**, 1265-1276 (2011).
188. Bi, C., et al. The bZIP transcription factor TabZIP15 improves salt stress tolerance in wheat. *Plant Biotechnol. J.* **19**, 209-211 (2021).
189. Tang, Y., et al. Overexpression of a MYB family gene, *OsMYB6*, increases drought and salinity stress tolerance in transgenic rice. *Front. Plant Sci.* **10**, (2019).
190. Beathard, C., Mooney, S., Al-Saharin, R., Goyer, A. & Hellmann, H. Characterization of *Arabidopsis thaliana* R2R3 S23 MYB transcription factors as novel targets of the ubiquitin proteasome-pathway

and regulators of salt stress and abscisic acid response. *Front. Plant Sci.* **12**, 629208 (2021).

191. Li, B., et al. The *Arabidopsis* MYB transcription factor, MYB111 modulates salt responses by regulating flavonoid biosynthesis. *Environ. Exp. Bot.* **166**, 103807 (2019).
192. Ding, Z., et al. Transcription factor WRKY46 modulates the development of *Arabidopsis* lateral roots in osmotic/salt stress conditions via regulation of ABA signaling and auxin homeostasis. *Plant J.* **84**, 56-69 (2015).
193. Lee, S., et al. Overexpression of *PRE1* and its homologous genes activates gibberellin-dependent responses in *Arabidopsis thaliana*. *Plant Cell Physiol.* **47**, 591-600 (2006).
194. Gan, Y., et al. Stomatal clustering, a new marker for environmental perception and adaptation in terrestrial plants. *Bot. Stud.* **51**, 325-336 (2010).
195. Oh, J. E., et al. A dual role for *MYB60* in stomatal regulation and root growth of *Arabidopsis thaliana* under drought stress. *Plant Mol. Biol.* **77**, 91-103 (2011).
196. Najafi, S., Sorkheh, K. & Nasernakhaei, F. Characterization of the APETALA2/Ethylene-responsive factor (AP2/ERF) transcription factor family in sunflower. *Sci. Rep.* **8**, 11576 (2018).
197. Coleto, I., et al. *Arabidopsis thaliana* transcription factors *MYB28* and *MYB29* shape ammonium stress responses by regulating Fe homeostasis. *New Phytol.* **229**, 1021-1035 (2021).
198. Petroni, K. & Tonelli, C. Recent advances on the regulation of anthocyanin synthesis in reproductive organs. *Plant Sci.* **181**, 219-229 (2011).
199. Kautsar, S., et al. MIBiG 2.0: a repository for biosynthetic gene clusters of known function. *Nucleic Acids Res.* **48**, D454-D458 (2020).
200. Sun, P., et al. Spiroketal formation and modification in avermectin biosynthesis involves a dual activity of AveC. *J. Am. Chem. Soc.* **135**, 1540-1548 (2013).
201. Komaki, H. Resolution of housekeeping gene sequences used in MLSA for the genus *Streptomyces* and reclassification of *Streptomyces anthocyanicus* and *Streptomyces tricolor* as heterotypic synonyms of *Streptomyces violaceoruber*. *Int. J. Syst. Evol. Microbiol.* **72**, 005370 (2022).
202. McDonald, B. & Currie, C. Lateral gene transfer dynamics in the ancient bacterial genus *Streptomyces*. *Mbio* **8**, e00644-17 (2017).
203. Chase, A., Sweeney, D., Muskat, M., Guillen-Matus, D. & Jensen, P. Vertical inheritance facilitates interspecies diversification in biosynthetic gene clusters and specialized metabolites. *Mbio* **12**, e02700-21 (2021).
204. Vergnes, S., et al. Phyllosphere colonization by a soil *Streptomyces* sp. promotes plant defense responses against fungal infection. *Mol. Plant-Microbe Interact.* **33**, 223-234 (2020).
205. Li, X., Tian, Y., Peng, H., He, B. & Gao, K. Isolation, screening and identification of anantagonistic actinomycetes to control *Fusarium* wilt of *Momordica charantia*. *Ying Yong Sheng Tai Xue Bao* **31**,

3869-3879 (2020).

206. Yun, T., et al. Anti-Foc RT4 activity of a newly isolated *Streptomyces* sp. 5-10 from a medicinal plant (*Curculigo capitulate*). *Front. Microbiol.* **11**, 610698 (2021).

207. Chung, Y., et al. Comparative genomics reveals a remarkable biosynthetic potential of the *Streptomyces* phylogenetic lineage associated with rugose-ornamented spores. *Msystems* **6**, e00489-21 (2021).

208. Jiang, M., et al. GdmRIII, a TetR family transcriptional regulator, controls geldanamycin and elaiophylin biosynthesis in *Streptomyces autolyticus* CGMCC0516. *Sci. Rep.* **7**, 4803 (2017).

209. He, W., et al. Crossregulation of rapamycin and elaiophylin biosynthesis by RapH in *Streptomyces rapamycinicus*. *Appl. Microbiol. Biotechnol.* **106**, 2147-2159 (2022).

210. Lockhart, S. R., Chowdhary, A. & Gold, J. A. W. The rapid emergence of antifungal-resistant human-pathogenic fungi. *Nat. Rev. Microbiol.* **21**, 818-932 (2023).

211. Stukenbrock, E. & Gurr, S. Address the growing urgency of fungal disease in crops. *Nature* **617**, 31-34 (2023).

213. Bongomin, F., Gago, S., Oladele, R. O. & Denning, D. W. Global and multi-national prevalence of fungal diseases-estimate precision. *J. Fungi* **3**, 57 (2017).

214. Perfect, J. R. The antifungal pipeline: a reality check. *Nat. Rev. Drug Discovery* **16**, 603-616 (2017).

215. Fisher, M. C., et al. Emerging fungal threats to animal, plant and ecosystem health. *Nature* **484**, 186-194 (2012).

216. Fisher, M. C., Hawkins, N. J., Sanglard, D. & Gurr, S. J. Worldwide emergence of resistance to antifungal drugs challenges human health and food security. *Science* **360**, 739-742 (2018).

217. Keatinge-Clay, A. T. A tylosin ketoreductase reveals how chirality is determined in polyketides. *Chem. Biol.* **14**, 898-908 (2007).

218. Gehret, J. J., et al. Terminal alkene formation by the thioesterase of curacin a biosynthesis structure of a decarboxylating thioesterase. *J. Biol. Chem.* **286**, 14445-14454 (2011).

219. Rudolf, J. D., Chang, C. Y., Ma, M. & Shen, B. Cytochromes P450 for natural product biosynthesis in *Streptomyces*: sequence, structure, and function. *Nat. Prod. Rep.* **34**, 1141-1172 (2017).

220. Moebius, N., et al. Biosynthesis of the respiratory toxin bongkrekic acid in the pathogenic bacterium *Burkholderia gladioli*. *Chem. Biol.* **19**, 1164-1174 (2012).

221. Zhang, Q., et al. Carboxyl formation from methyl via triple hydroxylations by XiaM in xiamycin A biosynthesis. *Org. Lett*. **14**, 6142-6145 (2012).

222. Aparicio, J. F., Caffrey, P., Gil, J. A. & Zotchev, S. B. Polyene antibiotic biosynthesis gene clusters. *Appl. Microbiol. Biotechnol.* **61**, 179-188 (2003).

223. Chen, S., et al. Tailoring the P450 monooxygenase gene for FR-008/Candicidin biosynthesis. *Appl.*

Environ. Microbiol. **75**, 1778-1781 (2009).

224. Yang, J., Qi, Y., Blodgett, J. & Wencewicz, T. Multifunctional P450 monooxygenase CftA diversifies the clifednamide pool through tandem C-H bond activations. *J. Nat. Prod.* **85**, 47-55 (2022).
225. Ikeda, H. & Omura, S. Avermectin biosynthesis. *Chem. Rev.* **97**, 2591-2609 (1997).
226. Chan, Y. A., Podevels, A. M., Kevany, B. M. & Thomas, M. G. Biosynthesis of polyketide synthase extender units. *Nat. Prod. Rep.* **26**, 90-114 (2009).
227. Wilson, M. C. & Moore, B. S. Beyond ethylmalonyl-CoA: The functional role of crotonyl-CoA carboxylase/reductase homologs in expanding polyketide diversity. *Nat. Prod. Rep.* **29**, 72-86 (2012).
228. Quade, N., Huo, L. J., Rachid, S., Heinz, D. W. & Muller, R. Unusual carbon fixation gives rise to diverse polyketide extender units. *Nat. Chem. Biol.* **8**, 117-124 (2012).
229. Robinson, S. L., Christenson, J. K. & Wackett, L. P. Biosynthesis and chemical diversity of β-lactone natural products. *Nat. Prod. Rep.* **36**, 458-475 (2019).
230. Feng, K. N., et al. A hydrolase-catalyzed cyclization forms the fused bicyclic β-Lactone in vibralactone. *Angew. Chem. Int. Ed.* **59**, 7209-7213 (2020).
231. Bauman, K. D., et al. Enzymatic assembly of the salinosporamide γ-lactam-β-lactone anticancer warhead. *Nat. Chem. Biol.* **18**, 538-546 (2022).
232. Schaffer, J. E., Reck, M. R., Prasad, N. K. & Wencewicz, T. A. β-Lactone formation during product release from a nonribosomal peptide synthetase. *Nat. Chem. Biol.* **13**, 737-744 (2017).
233. Christenson, J. K., et al. β-Lactone synthetase found in the olefin biosynthesis pathway. *Biochemistry* **56**, 348-351 (2017).
234. Robinson, S. L., et al. Mechanism of a standalone β-lactone synthetase: new continuous assay for a widespread ANL superfamily enzyme. *ChemBioChem* **20**, 1701-1711 (2019).
235. Bailey, S. S., et al. Enzymatic control of cycloadduct conformation ensures reversible 1,3-dipolar cycloaddition in a prFMN-dependent decarboxylase. *Nat. Chem.* **11**, 1049-1057 (2019).
236. Cantalapiedra, C. P., Hernández-Plaza, A., Letunic, I., Bork, P. & Huerta-Cepas, J. eggNOG-mapper v2: functional annotation, orthology assignments, and domain prediction at the metagenomic scale. *Mol. Biol. Evol.* **38**, 5825-5829 (2021).
237. Fang, W., et al. Mechanisms of redundancy and specificity of the *Aspergillus fumigatus* Crh transglycosylases. *Nat. Commun.* **10**, 1669 (2019).
238. Maksimov, A. Y., Balandina, S. Y., Topanov, P. A., Mashevskaya, I. V. & Chaudhary, S. Organic antifungal drugs and targets of their action. *Curr. Top. Med. Chem.* **21**, 705-736 (2021).
239. Owens, R. A. & Doyle, S. Effects of antifungal agents on the fungal proteome: informing on mechanisms of sensitivity and resistance. *Expert Rev. Proteomics* **18**, 185-199 (2021).
240. Anderson, T. M. et al. Amphotericin forms an extramembranous and fungicidal sterol sponge. *Nat.*

Chem. Biol. **10**, 400–406 (2014).

241. Lewandowska, A. et al. Fungicidal amphotericin B sponges are assemblies of staggered asymmetric homodimers encasing large void volumes. *Nat. Struct. Mol. Biol.* **28**, 972–981 (2021).
242. Ghannoum, M., et al. *In vitro* antifungal activity of naftifine hydrochloride against dermatophytes. *Antimicrob. Agents Chemother.* **57**, 4369-4372 (2013).
243. Hitchcock, C. A. Cytochrome-P-450-dependent 14α-sterol demethylase of *Candida albicans* and its interaction with azole antifungals. *Biochem. Soc. Trans.* **19**, 782-787 (1991).
244. Sawistowskaschroder, E. T., Kerridge, D. & Perry, H. Echinocandin inhibition of 1,3-β-D-glucan synthase from *Candida albicans*. *FEBS Lett.* **173**, 134-138 (1984).
245. Gautam, P., et al. Proteomic and transcriptomic analysis of *Aspergillus fumigatus* on exposure to amphotericin B. *Antimicrob. Agents Chemother.* **52**, 4220-4227 (2008).
246. Ghannoum, M., et al. *In vitro* antifungal activity of naftifine hydrochloride against dermatophytes. *Antimicrob. Agents Chemother.* **57**, 4369-4372 (2013).
247. Hitchcock, C. A. Cytochrome-P-450-dependent 14α-sterol demethylase of *Candida albicans* and its interaction with azole antifungals. *Biochem. Soc. Trans.* **19**, 782-787 (1991).
248. Sawistowskaschroder, E. T., Kerridge, D. & Perry, H. Echinocandin inhibition of 1,3-β-D-glucan synthase from *Candida albicans*. *FEBS Lett.* **173**, 134-138 (1984).
249. Cagas, S. E., Jain, M. R., Li, H. & Perlin, D. S. Profiling the *Aspergillus fumigatus* proteome in response to caspofungin. *Antimicrob. Agents Chemother.* **55**, 146-154 (2011).
250. Walker, L. A., Gow, N. A. R. & Munro, C. A. Elevated chitin content reduces the susceptibility of *Candida* species to caspofungin. *Antimicrob. Agents Chemother.* **57**, 146-154 (2013).
251. Puttikamonkul, S., et al. Trehalose 6-phosphate phosphatase is required for cell wall integrity and fungal virulence but not trehalose biosynthesis in the human fungal pathogen *Aspergillus fumigatus*. *Mol. Microbiol.* **77**, 891-911 (2010).
252. Dhingra, S. & Cramer, R. Regulation of sterol biosynthesis in the human fungal pathogen *Aspergillus fumigatus*: opportunities for therapeutic development. *Front. Microbiol.* **8**, 92 (2017).
253. Fraczek, M. G., et al. The *cdr1B* efflux transporter is associated with non-*cyp51a*-mediated itraconazole resistance in *Aspergillus fumigatus*. *J. Antimicrob. Chemother.* **68**, 1486-1496 (2013).
254. Flett, F., Mersinias, V. & Smith, C. P. High efficiency intergeneric conjugal transfer of plasmid DNA from *Escherichia coli* to methyl DNA-restricting streptomycetes. *FEMS Microbiol. Lett.* **155**, 223-229 (1997).
255. Schlimpert, S. & Elliot, M. A. The best of both worlds-*Streptomyces coelicolor* and *Streptomyces venezuelae* as model species for studying antibiotic production and bacterial multicellular development. *J. Bacteriol.* **205**, e0015323 (2023).
256. Ueda, K. et al. Wide distribution of interspecific stimulatory events on antibiotic production and sporulation among *Streptomyces* species. *J. Antibiot.* **53**, 979–982 (2000).

257. Krespach, M. K. C. et al. Streptomyces polyketides mediate bacteria-fungi interactions across soil environments. *Nat. Microbiol.* **8**, 1348-1361 (2023).

258. McAlpine, J. B. et al. Microbial genomics as a guide to drug discovery and structural elucidation: ECO-02301, a novel antifungal agent, as an example. *J. Nat. Prod.* 68, 493–496 (2005).

259. Arai, M. & Hamano, K. Isolation of three main components. F3, F4 and F5, from azalomycin F-complex. *J. Antibiot.* **23**, 107–112 (1970).

260. Sakuda, S., Guce-Bigol, U., Itoh, M., Nishimura, T. & Yamada, Y. Linearmycin A, a novel linear polyene antibiotic. *Tetrahedron Lett.* **36**, 2777–2780 (1995).

261. Prelog, V. & Oppolzer, W. Ansamycins, new class of microbial metabolites. *Helv. Chim. Acta* **56**, 2279-2287 (1973).

262. Floss, H. G. & Yu, T. W. Rifamycin-mode of action, resistance, and biosynthesis. *Chem. Rev.* **105**, 621-632 (2005).

263. Kumar, Y. & Goodfellow, M. Five new members of the *Streptomyces violaceusniger* 16S rRNA gene clade: *Streptomyces castelarensis* sp nov., comb. nov., *Streptomyces himastatinicus* sp nov., *Streptomyces mordarskii* sp nov., *Streptomyces rapamycinicus* sp nov and *Streptomyces ruanii* sp nov. *Int. J. Syst. Evol. Microbiol.* **58**, 1369-1378 (2008).

264. Li, S. R., et al. Biosynthesis of hygrocins, antitumor naphthoquinone ansamycins produced by *Streptomyces* sp. LZ35. *ChemBioChem* **15**, 94-102 (2014).

Appendix 1

nature communications

Article

https://doi.org/10.1038/s41467-023-43177-3

Streptomyces alleviate abiotic stress in plant by producing pteridic acids

Received: 28 November 2022

Accepted: 31 October 2023

Published online: 15 November 2023

Check for updates

Zhijie Yang[1], Yijun Qiao[1], Naga Charan Konakalla[2], Emil Strøbech[1], Pernille Harris[3], Gundela Peschel[4], Miriam Agler-Rosenbaum[4], Tilmann Weber[5], Erik Andreasson[2] & Ling Ding[1]

Soil microbiota can confer fitness advantages to plants and increase crop resilience to drought and other abiotic stressors. However, there is little evidence on the mechanisms correlating a microbial trait with plant abiotic stress tolerance. Here, we report that *Streptomyces* effectively alleviate drought and salinity stress by producing spiroketal polyketide pteridic acid H (**1**) and its isomer F (**2**), both of which promote root growth in *Arabidopsis* at a concentration of 1.3 nM under abiotic stress. Transcriptomics profiles show increased expression of multiple stress responsive genes in *Arabidopsis* seedlings after pteridic acids treatment. We confirm in vivo a bifunctional biosynthetic gene cluster for pteridic acids and antimicrobial elaiophylin production. We propose it is mainly disseminated by vertical transmission and is geographically distributed in various environments. This discovery reveals a perspective for understanding plant-*Streptomyces* interactions and provides a promising approach for utilising beneficial *Streptomyces* and their secondary metabolites in agriculture to mitigate the detrimental effects of climate change.

According to the Food and Agriculture Organization of the United Nations, climate change generates considerable uncertainty about future water availability in many regions. Increased water scarcity under climate change will present a major challenge for climate adaptation, while sea-level rise will affect the salinity of surface and groundwater in coastal areas. Stress caused by climate change has led to increased agricultural losses and threatened global food security[1]. Drought is considered the most damaging environmental stress, which directly affects the entire growth period of plant seeds from germination to final fruiting[2]. Drought stress can lead to increased plant osmotic regulators, the inhibition of photosynthesis, and the change of plant endogenous hormone content[3–5]. Drought stress also induces reactive oxygen species, such as superoxide radicals, hydrogen peroxide, and hydroxyl radicals, leading to oxidative stress[6]. Crop loss due to soil salinisation is another increasing threat to agriculture worldwide, which is more severe in agricultural land in coastal and arid regions[7]. Irrigation with saline water, low precipitation, and high evapotranspiration are key factors of the rapid salinisation of agricultural land[8]. These abiotic stresses of drought and salinity have brought unprecedented challenges to the development of crop farming. Compared to the heavy use of chemical fertilisers, the use of plant growth-promoting bacteria to improve plant growth under drought and salinity environments is more sustainable and gaining more attention[9,10].

Soil microbial communities are critical to plant health and their resistance to both biotic and abiotic stressors, such as pathogens, drought, salinity, and heavy metal pollution[11]. A few studies have demonstrated that many beneficial soil bacteria harbour plant growth-

[1]Department of Biotechnology and Biomedicine, Technical University of Denmark, Søltofts Plads, Building 221, 2800 Kgs Lyngby, Denmark. [2]Department of Plant Protection Biology, Swedish University of Agricultural Sciences, Sundsvägen 14, SE-230 53 Alnarp, Sweden. [3]Department of Chemistry, Technical University of Denmark, Søltofts Plads, Building 206, 2800 Kgs Lyngby, Denmark. [4]Leibniz Institute for Natural Product Research and Infection Biology—Hans Knöll Institute (HKI), Beutenbergstr. 11a, 07745 Jena, Germany. [5]The Novo Nordisk Foundation Center for Biosustainability, Technical University of Denmark, Kemitorvet, Building 220, 2800 Kgs Lyngby, Denmark. e-mail: lidi@dtu.dk

promoting activities, *e.g.* by helping plants with disease suppression[12], nutrient acquisition[13], phosphorus uptake[14] and nitrogen fixations[15]. Beneficial root microbiota also regulate biosynthetic pathways in the plant itself, leading to differential alterations in the plant metabolome in response to stresses[16]. *Streptomyces* are Gram-positive filamentous bacteria, widely distributed in soil and marine environments. While they have long been considered the richest source of bioactive secondary metabolites[17], *Streptomyces* have recently drawn attention as a class of plant growth-promoting bacteria that help plants respond to adversity stress[18]. The growing evidence showed that *Streptomyces* can promote plant growth or tolerance to stressors in direct or indirect ways, by secreting plant growth regulator auxin (indole-3-acetic acid, IAA) and siderophores, inducing systemic resistance in plants, and regulating the rhizosphere microbiome via producing antibacterial compounds or signalling molecules[19–21]. Notably, the commercial product Actinovate® and Mycostop® are two *Streptomyces*-based formulations that have been widely used to suppress a wide range of diseases in a variety of crop groups as a biological fungicide/bactericide for the long term. Recently, the enrichment of *Streptomyces* has also been shown to play a subsequent role in the drought/salt tolerance of plants[22]. Despite the widespread claims of efficacy of inoculation of plant growth-promoting *Streptomyces*, the molecular basis of the growth-promoting effects and the key role of secondary/specialised metabolites in this process are largely unknown.

Here, we report that *Streptomyces iranensis* HM 35 has profound beneficial effects on helping barley alleviate osmotic, drought and salinity stress. The active components were identified as bioactive spiroketal polyketides pteridic acids H (**1**) and its isomer F (**2**) through large-scale fermentation and bioactivity-directed purification followed by NMR, MS, and X-ray crystallography. The abiotic stress mitigating effects of pteridic acids H and F have been confirmed on the model plant *Arabidopsis thaliana*, where it effectively reversed both drought and salinity stress as phytohormone-like small biomolecules at concentrations as low as 0.5 ng mL^{-1} (1.3 nM). RNA sequencing results suggested that pteridic acids may assist plants in stress resistance via activating photosynthesis and regulating multiple stress response genes. Moreover, the Biosynthetic Gene Cluster (BGC) of pteridic acids (*pta*) was identified and analysed in silico, and functionally confirmed by in vivo CRISPR-based genome editing. We have furthermore conducted a survey of 81 potential producers of pteridic acids, which are widely distributed around the world. Phylogenetic and comparative genomic analysis of *pta*-containing streptomycetes suggested that these strains have evolutionary convergence in disseminating *pta* BGC through main vertical transmission and occasional horizontal gene transfer. In summary, we reveal a strategy of *Streptomyces* to secret plant growth regulators that help plants cope with abiotic stresses, which is a promising alternative solution for plant development and crop yields under the current climate change-induced environmental stresses.

Results

Abiotic stress-mitigating activities exhibited by *S. iranensis*

The promotion of barley growth induced by *S. iranensis* was tested under multiple abiotic stresses including osmotic, salinity and drought. The osmotic stress experiment was simulated using soils supplemented with 20% (w/v) PEG-6000 by transiently reducing the water potential of the plant. We found that *S. iranensis* played a significant role in alleviating osmotic stress in barley seedlings. The treated seedlings showed a significant increase in height, fresh weight, and dry weight compared to the control group without any extra treatment (Fig. 1a). The culture broth of *S. iranensis* also showed considerable activity for the growth of barley in alleviating salinity stress mediated by 100 mM NaCl (Fig. 1b), while *S. iranensis* was not significantly enriched in the soil around the roots of barley seedlings (Supplementary Fig. 1). Additionally, based on the analysis of barley seedling phenotypes, the treatment with *S. iranensis* resulted in a significant improvement in plant growth recovery from drought stress (Fig. 1c). Surprisingly, *S. iranensis* promoted the growth of barley seedlings even in non-stress growth condition and thus indicate that *S. iranensis* may have potential for use as biostimulant (Supplementary Fig. 2).

Genomic and metabolomic profiles of *S. iranensis*

To reveal the potential bioactive components, we first annotated BGCs responsible for the biosynthesis of secondary metabolites in *S. iranensis* using antiSMASH 6.0[23]. Genome sequence analysis of *S. iranensis* revealed the presence of 47 putative secondary metabolites BGCs with a variety of biosynthetic categories (Supplementary Table 1). The clusters 3, 6, 7, 8, 23, 31, 35 and 40 were annotated to have greater than 80% similarity with BGCs responsible for the biosynthesis of coelichelin, azalomycin, nigericin, elaiophylin, desferrioxamin B, ectoine, rapamycin and hygrocin, respectively. Their corresponding products were also detected and identified through High-resolution Liquid Chromatography-tandem Mass Spectrometry (HR-LC-MS/MS) as well as Global Natural Products Social (GNPS) molecular networking (Fig. 1d, Supplementary Fig. 3)[24]. However, a large number of metabolites from *S. iranensis* are still unknown. Since none of the previously identified compounds have been associated with mitigating abiotic stress in plants, we were prompted to expand the fermentation process and identify the potential bioactive compounds.

Characterisation of the bioactive compound pteridic acid

To uncover the bioactive components, fermentation of *S. iranensis* was scaled up to 175 litres and the culture broth was subjected to separation through open-column chromatography on Amberchrom CG161Me resin, silica gel, and Sephadex LH-20. Bioactivity-guided fractionation led to the isolation of bioactive compound **1** (15.0 mg) together with its isomer compound **2** (4.0 mg) (Fig. 1e).

The bioactive component compound **1** was isolated as a white solid. Its formula of $C_{21}H_{34}O_6$ was deduced by *m/z* 383.2439 $[M+H]^+$ (calculated for 383.2428, Δ 2.84 ppm). The ^{1}H NMR spectrum exhibited signals for four olefinic protons (δ 7.33, 6.26, 6.13, 5.90) corresponding to two conjugated double bonds, four oxygen-bearing methines (δ 3.85, 3.69, 3.59, 3.43), five methyls, and other aliphatic protons. The ^{13}C NMR spectrum indicated the presence of one carbonyl group (δ 168.7) and one oxygen-bearing quaternary carbon (δ 103.2, C-11). The COSY spectrum established two partial substructures, which could be connected via a spiral function by analysing HSQC and HMBC correlations (Supplementary Figs. 4–11). Compound **1** was crystallised in methanol solution, and the structure was determined via X-ray crystallography (Supplementary Fig. 12). Therefore, compound **1** was identified as a new *Streptomyces*-derived natural product named pteridic acid H.

Compound **2**, a white solid, is an isomer of **1** deduced by MS with the same molecular formula of $C_{21}H_{34}O_6$. The ^{1}H NMR spectrum exhibited signals for four olefinic protons (δ 7.16, 6.25, 6.07, 5.97) corresponding to two conjugated double bonds, four oxygen-bearing methines (δ 3.88, 3.66, 3.56, 3.32), five methyls, and other aliphatic protons. The ^{13}C NMR spectrum indicated the presence of one carbonyl group (δ 170.2) and one oxygen-bearing quaternary carbon (δ 103.2, C-11). HSQC and HMBC correlations confirmed a spiroketal skeleton. NOESY spectrum confirmed its relative configurations, where correlations between H-21 and H-13 and H-15, H-7 and H-12a, and H6, H-10, and Me-18 were observed. The key NOESY correlations between H-7 and H-12a revealed a different spiroketal structure than **1** (Supplementary Fig. 11, 13-20). This can be reflected by the relative upfield NMR data for C-12 (δ 33.8 vs δ 37.4 in **1**). Compound **2** was identified as pteridic acid F, previously isolated from *Streptomyces pseudoverticillus* YN17707 and a marine-derived *Streptomyces* sp. SCSGAA 0027[25,26].

https://doi.org/10.1038/s41467-023-43177-3

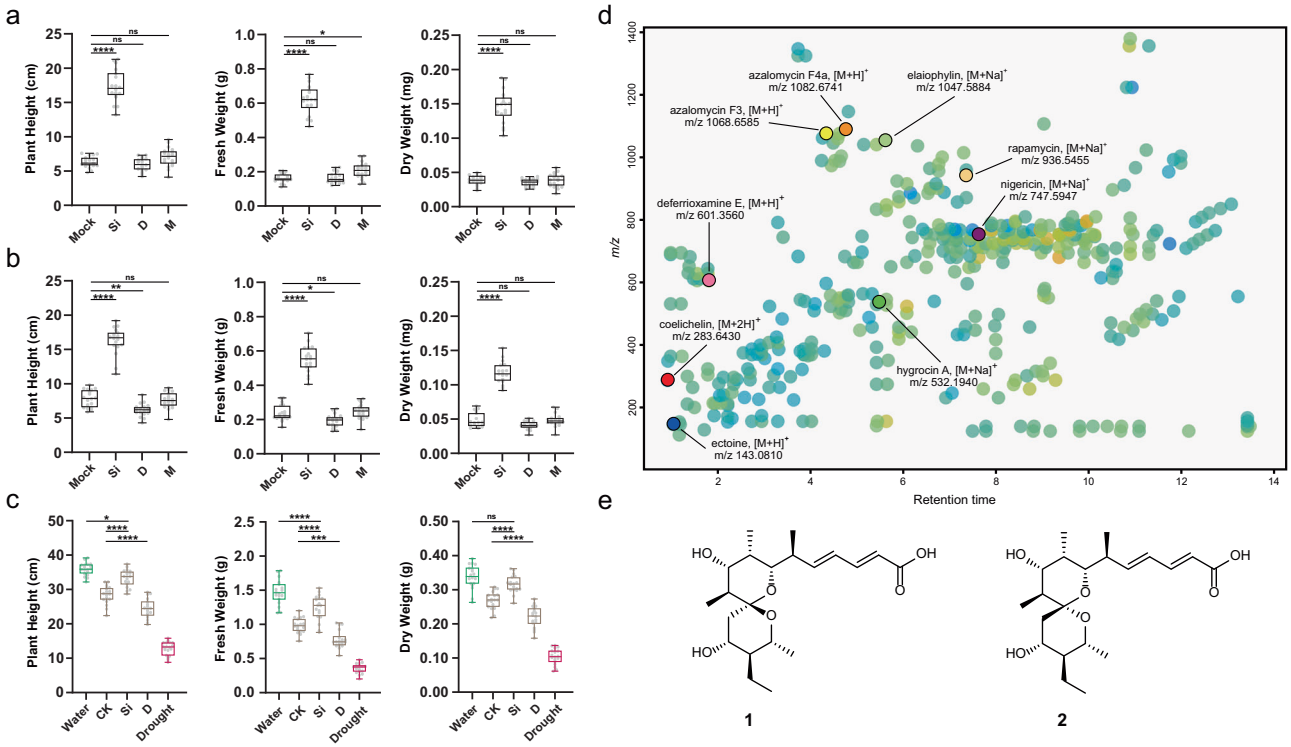

Fig. 1 | The effects of *S. iranensis* on barley seedlings under abiotic stress and the bioactive components produced by *S. iranensis*. **a** The box plots depict the plant height, fresh weight and dry weight of barley seedlings growing under osmotic stress mediated by 20% (w/v) PEG-6000 (mean ± SD, $n = 18$). **b** the box plots depict the plant height, fresh weight and dry weight of barley seedlings growing under salinity stress mediated by 100 mM NaCl (mean ± SD, $n = 18$). In **a** and **b**, statistical significance was assessed by one-way ANOVA with post hoc Dunnett's multiple comparisons test. Asterisks indicate the level of statistical significance: $^{*}p < 0.05$, $^{**}p < 0.01$, $^{***}p < 0.001$ and $^{****}p < 0.0001$. Abbreviation: Mock: control; Si: treatment of *S. iranensis* culture broth; D: treatment of *S. iranensis*/Δ*ptaA* culture broth; M: treatment of blank medium (ISP2). **c** The box plots depict the plant height, fresh weight and dry weight of barley seedlings growing under drought stress (mean ± SD, $n = 18$). Different colours of box plots indicate different growing conditions: green, 21 days water; brown, 7 days treatment after 7 days water followed by 7 days drought; red, 7 days water followed by 14 days drought. Statistical significance was assessed by one-way ANOVA with Tukey test. Asterisks indicate the level of statistical significance: $^{*}p < 0.05$, $^{**}p < 0.01$, $^{***}p < 0.001$ and $^{****}p < 0.0001$. Abbreviation: Water: well water for 21 days; CK, 7 days treatment of water after 7 days water + 7 days drought; Si: 7 days treatment of *S. iranensis* culture broth after 7 days water + 7 days drought; D: 7 days treatment of *S. iranensis*/Δ*ptaA* culture broth after 7 days water + 7 days drought; M: treatment of blank medium (ISP2); Drought: 14 days drought after 7 days water. Statistical significance was assessed by one-way ANOVA with Tukey test. **d** The metabolite profile of the native *S. iranensis* growing in liquid ISP2 medium, the known secondary metabolites were identified by HR-LC-MS and highlighted; **e** the bioactive components pteridic acid H (**1**) and pteridic acid F (**2**) isolated from *S. iranensis*. All box plots with centre lines showing the medians, boxes indicating the interquartile range, and whiskers indicating a range of minimum to maximum data beyond the box. Source data are provided as a Source Data file.

Abiotic stress mitigation of pteridic acids *in planta*

Initially, we tested the effects of different concentrations of pteridic acids H and F on *Arabidopsis* growth in the absence of abiotic stress. A concentration of 0.5 ng ml^{-1} of both pteridic acids H and F was found to significantly promote the growth of *Arabidopsis* seedlings (Supplementary Fig. 21). Under drought stress, pteridic acid H at a concentration of 0.5 ng mL^{-1} increased the root length and fresh weight of *Arabidopsis* seedlings by 54.5% and 89%, respectively, and its activity was significantly better than IAA and ABA at the same molar concentration (Fig. 2a, c). The treatment of pteridic acid F also showed great activity in alleviating drought stress, and the root length and fresh weight were increased by 30.5% and 56.7%, respectively (Fig. 2c). Pteridic acids H and F also showed significant activity in alleviating NaCl-mediated salinity stress (Fig. 2b, d). Compared to the non-treated groups, the treatment of 0.5 ng mL^{-1} pteridic acids H and F increased root length of *Arabidopsis* seedlings by 74.0% and 61.8%, as well as fresh weight by 126.2% and 110.9%, respectively (Fig. 2d).

To get a first understanding how pteridic acids help *Arabidopsis* mitigate salinity stress, we used messenger RNA sequencing (mRNA-seq) to profile the transcripts of *Arabidopsis* seedlings treated with pteridic acid F or H under NaCl-mediated salt stress (Fig. 3a). Compared to the control (CK, treatment with an equal amount of water under NaCl-mediated salt stress), we observed significant differences in the gene expression patterns upon treatment with pteridic acid (PH or PF) by Pearson correlation analysis (Supplementary Fig. 22). The Differentially Expressed Genes (DEGs) analysis revealed 3575 DEGs (1405 upregulated and 2170 downregulated), and 3727 DEGs (1555 upregulated and 2172 downregulated) in the pteridic acid H treatment versus control (PH vs. CK) and pteridic acid F treatment versus control (PF vs. CK), respectively (Supplementary Data 1). Meanwhile, 1226 up-regulated genes and 1860 down-regulated genes were shared between PH and PF treatments. Several abiotic stress-related genes were significantly upregulated after pteridic acids treatments (Fig. 3b), including *SLAC1 HOMOLOGUE 1* (*SLAH1*, AT1G62280)[27], *PIN-FORMED 6* (*PIN6*, AT1G77110)[28], *FERRIC REDUCTION OXIDASE 6* (*FRO6*, AT5G49730)[29] and *TOO MANY MOUTHS* (*TMM*, AT1G80080)[30]. Compared with the control, *ALPHA CARBONIC ANHYDRASE 8* (*ATACA8*, AT5G56330)[31], and *IAA-LEUCINE RESISTANT 2* (*ILR2*, AT3G18485)[32] were uniquely upregulated in the PH treatment samples, while *ATP-BINDING CASSETTE G17* (*ABCG17*, AT3G55100)[33], *DIACYLGLYCEROL KINASE 4* (*DGK4*, AT5G57690)[34] and *MAP KINASE KINASE 7* (*MKK7*, AT1G18350)[35] were upregulated in the PF treatment samples.

Next, we performed the Gene Ontology (GO) enrichment analysis of DEGs focusing primarily on the biological processes

https://doi.org/10.1038/s41467-023-43177-3

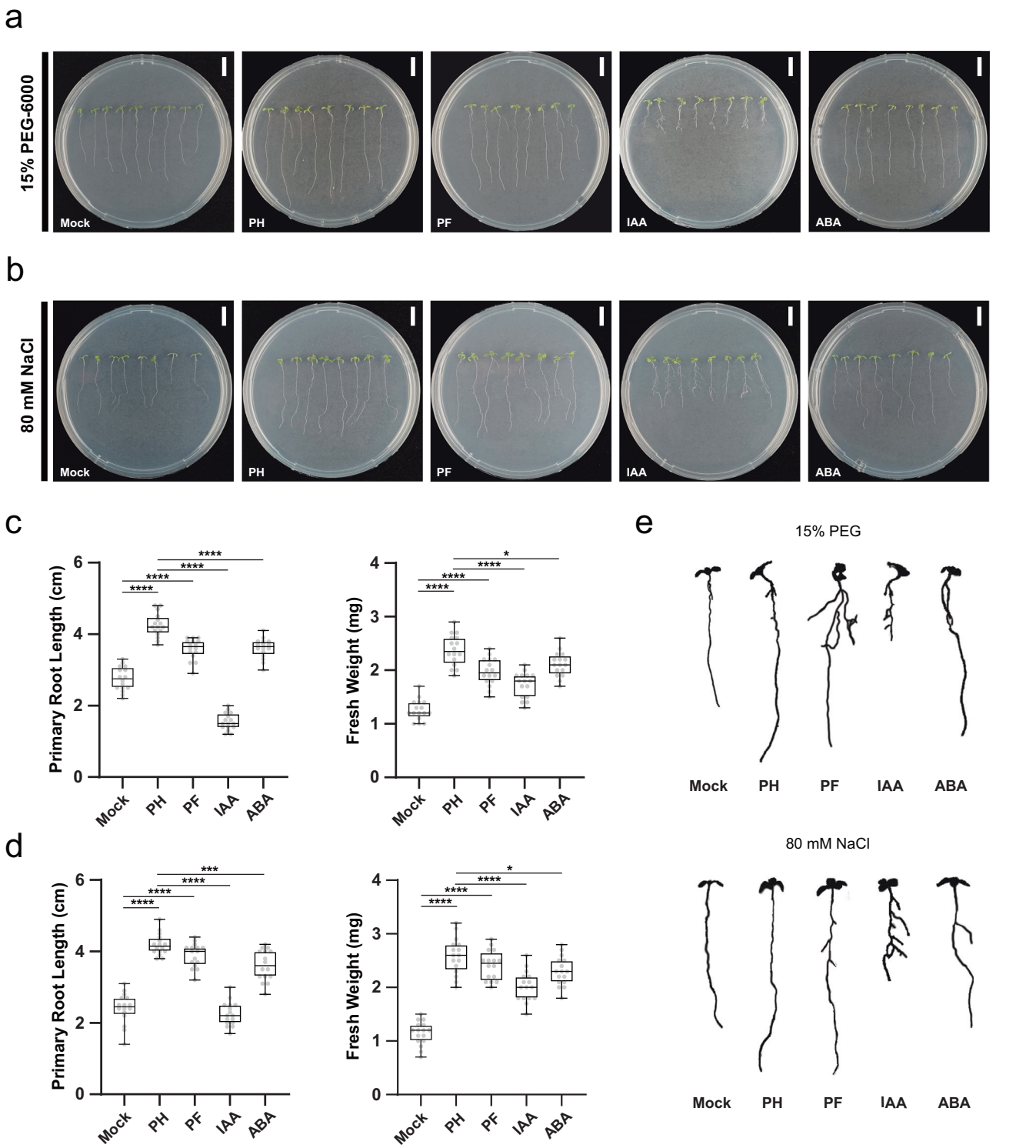

Fig. 2 | The effect of pteridic acids H and F on *Arabidopsis* seedlings under abiotic stress. a Phenotype of *Arabidopsis* seedlings growing under drought stress mediated by 15% (w/v) PEG-6000 using other treatments (bars = 1 cm); **b** Phenotype of *Arabidopsis* seedlings growing under salinity stress mediated by 80 mM NaCl using other treatments (bars = 1 cm); **c** The box plots depict the primary root length and fresh weight of *Arabidopsis* seedlings growing on non-stress condition (mean ± SD, $n = 16$); **d** The box plots depict the primary root length and fresh weight of *Arabidopsis* seedlings growing on drought stress condition (mean ± SD, $n = 16$). In **c** and **d**, statistical significance was assessed by one-way ANOVA with Tukey test. Asterisks indicate the level of statistical significance: $^{*}p < 0.05$, $^{**}p < 0.01$, $^{***}p < 0.001$ and $^{****}p < 0.0001$; **e** differences of lateral root growth of *Arabidopsis* seedlings growing in other conditions. Mock: control; PH: treatment of 0.5 ng mL^{-1} pteridic acid H; PF: treatment of 0.5 ng mL^{-1} pteridic acid F; IAA: treatment of 1.3 nM indole-3-acetic acid; ABA: treatment of 1.3 nM abscisic acid. All box plots with centre lines showing the medians, boxes indicating the interquartile range, and whiskers indicating a range of minimum to maximum data beyond the box. Source data are provided as a Source Data file.

https://doi.org/10.1038/s41467-023-43177-3

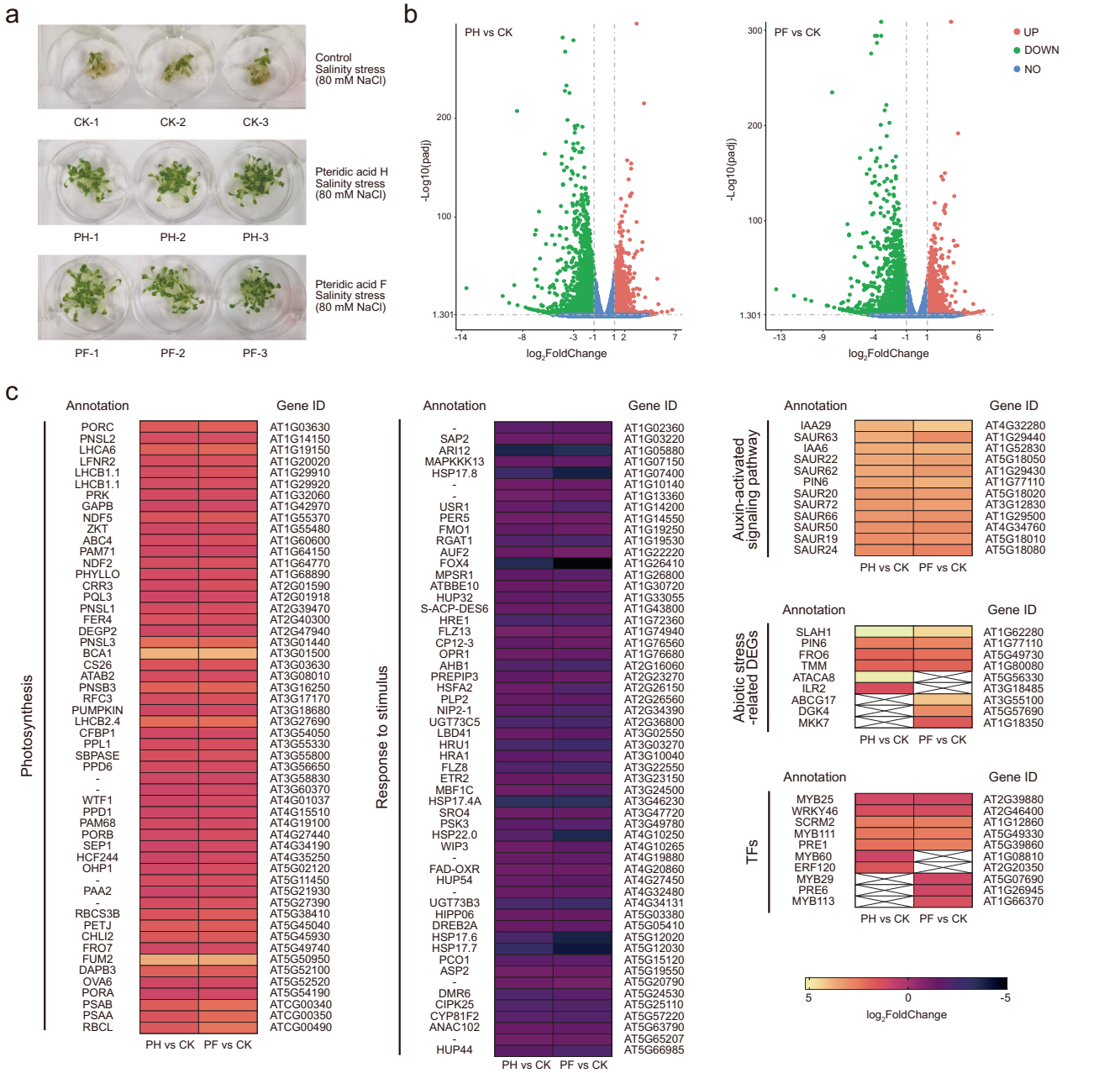

Fig. 3 | Effect of exogenous pteridic acids on transcription in *Arabidopsis* seedlings under salt stress. a The phenotype of *Arabidopsis* seedling samples in different treatments under salinity stress. CK: control; PF: pteridic acid F treatment; PH: pteridic acid H treatment. **b** The volcano plots of DEGs identified by mRNA-seq in *Arabidopsis* seedlings treated by pteridic acid H and F under salinity stress. **c** heat-maps of DEGs enriched in photosynthesis, response to stimulus, auxin-activated signalling pathway, abiotic stress defense and TFs.

(Supplementary Data 2). Among all upregulated genes, several highly enriched GO terms such as "Photosynthesis (GO:0015979)", "Plastid organization (GO:0009657)", "Chloroplast organization (GO:0009658)" and "Response to light stimulus (GO:0009416)" suggested pteridic acids could enhance photosynthesis under abiotic stress. For these DEGs with $\log_2$FoldChange ≥ 2, we observed upregulation of 12 genes belonging to the "auxin-activated signalling pathway (GO:0009734)" (Fig. 3c), suggesting that pteridic acids also trigger auxin-activated signalling transduction. Intriguingly, we observed the downregulations of genes related to "response to stimulus (GO:0050896)", "response to chemical (GO:0042221)" and "response to stress (GO:0006950)", which was speculated to be an interference between different signalling pathway or a negative feedback mechanism of plants to maintain homoeostasis (Fig. 3c)[36]. Moreover, similar conclusions were reached by the most enriched Kyoto Encyclopedia of Genes and Genomes (KEGG) pathway, pointing to the "Photosynthesis (ath00195)" and "Plant hormone signal transduction (ath04075)" pathways in the *Arabidopsis* seedlings. In addition, the pathway of "Motor proteins (ath04814)", "Ribosome (ath03010)", "Glucosinolate biosynthesis (ath00966)", "Porphyrin metabolism (ath00860)" and "Flavonoid biosynthesis (ath00941)" were also activated, which had been previously reported that these are closely associated with plant abiotic stress resistance[37,38]. On the contrary, pteridic acids downregulated several genes enriched in "Phenylpropanoid biosynthesis (ath00940)", "Cyanoamino acid metabolism (ath00460)", "Glutathione metabolism (ath00480)", "MAPK signalling pathway-plant (ath04016)" and "Starch and sucrose metabolism (ath00500)" pathways.

Transcription Factors (TFs) play an important function in coping with abiotic stress tolerance. Several TFs have been proved to participate in plant salt stress responses, such as AP2/ERF, bZIP and MYB[39–41]. Within these DEGs, we identified various TFs, comprising AP2/ERF (42 unigenes), MYB (35 unigenes), WRKY (27 unigenes), bHLH (31 unigenes) and bZIP families (6 unigenes) (Supplementary Data 3). A handful of plant stress resistance-related TFs were observed, such as *MYB25*, *MYB111*, *WRKY46*, *PRE1* and *SCRM2*[42–46]. TFs associated with resistance to abiotic stress, such as *MYB60* and *ERF120*, exhibited discernible upregulation in the PH treatment samples compared to the control[47,48]. Conversely, *MYB29*, *MYB113* and *PRE6* showed unique upregulation in the PF vs. CK group[49,50].

A previous study suggested that pteridic acids A and B might have a plant growth-promoting effect like IAA and could stimulate the formation of adventitious roots in kidney beans[25]. However, we observed that pteridic acids H and F displayed different IAA-induced phenotypes. Pteridic acids did not exhibit the function to significantly promote lateral root growth of *Arabidopsis* seedlings like IAA (Fig. 2e)[51]. They were also not capable of promoting the formation of adventitious roots in kidney beans, as shown in Supplementary Fig. 23. Except for drought and salinity stress, we also tested the $CuSO_4$-mediated heavy metal stress alleviation activity of pteridic acids on mung beans. The results showed that the 1 ng mL^{-1} pteridic acid H was as effective as ABA in helping mung beans to relieve heavy metal stress (Supplementary Fig. 24). In conclusion, pteridic acids H and F are widely applicable potent plant growth regulators produced by *Streptomyces* to assist plants in coping with different abiotic stress.

Biosynthesis of pteridic acids

The retro-biosynthesis analysis indicated that pteridic acids could derive from a modular type I polyketide synthase. A putative *pta* BGC was identified in the whole genome sequence of *S. iranensis*, which shows 87% antiSMASH similarity to the BGC of elaiophylin (BGC0000053 in MiBiG database)[52]. The *pta* BGC spans approximately 56 kb and encodes 20 individual biosynthetic genes responsible for the biosynthesis of core polyketide backbones, precursor, glycosylated substituents, transporters and regulators (Supplementary Table 2). The five consecutive Type I polyketide synthase (PKS) encoding genes within the *pta* BGC consist of one loading module and seven extender modules, which are sequentially extended to form a linear polyketide chain by ketosynthase (KS) domain, acyltransferase (AT) domain, acyl carrier protein (ACP), with additional ketoreductase (KR), dehydratase (DH), and enoyl reductase (ER) domains. The substrate specificity predictions for individual AT domains fit well with the structure of pteridic acids (Supplementary Table 3). The last "Asn" residue is absent in the conserved Lys-Ser-Tyr-Asn tetrad of the KR domain in module 3 (PtaB), which is predicted to be inactive (Supplementary Fig. 25). This is consistent with the nonreduced carbonyl group on the α-carbon in module 3. The first DH domain in module 1 is inactive since it does not have a conserved active motif LxxHxxGxxxxP (Supplementary Fig. 26). Following the thioesterase-mediated release of the polyketide chain, the 6,6-spiroketal core structure is likely formed by spontaneous spiroketalisation of the carbonyl group on C11 and the two hydroxyl groups on C17 and C25. Following a loss of H_2O, two differentially oriented spirocyclic rings were formed to yield pteridic acids F and H (Fig. 4a). Remarkably, pteridic acid H showed molecular instability under extreme conditions. In the water solution with high temperature (65°C) or acidity (pH = 3), pteridic acid H is transformed into pteridic acid F (Supplementary Fig. 27). A similar spontaneous transformation from (*S*) to (*R*) chirality at the centre of the spiroketal ring was also observed in 6,6-spiroketal avermectin[53].

CRISPR base editing in *S. iranensis*

To validate the in silico prediction, we utilised the efficient base editing tool CRISPR-cBEST to experimentally confirm the *pta* BGC[54]. As a non-model *Streptomyces* strain, *S. iranensis* is hard to genetically manipulate through intergeneric conjugation[55]. Therefore, the conjugation process was systematically optimised in this study (Supplementary Fig. 28). The core polyketide synthase *ptaA* was targeted and inactivated by converting a TGG (Trp) codon at position 916 into the stop codon TAA using CRISPR base editing. The editing event was confirmed by PCR amplification and Sanger sequencing of the editing site (Fig. 4c). As expected, the production of both pteridic acids and elaiophylin was abolished in *S. iranensis*/Δ*ptaA* (Fig. 4c). Plant experiments showed that the treatment of *S. iranensis*/Δ*ptaA* fermentation suspension led to the abolishment of the abiotic stress mitigating effects (Fig. 1a–c). To further confirm the *pta* gene cluster, a bacterial artificial chromosome (BAC) library of *S. iranensis* was constructed. BAC-based cross-complementation of *ptaA* in *S. iranensis*/Δ*ptaA* restored the production of pteridic acids and elaiophylin (Supplementary Fig. 29).

Interestingly, based on isotope-labelled precursor feeding and partial cosmid sequencing-based bioinformatics prediction, this BGC has long been inferred to be responsible for the biosynthesis of the antibacterial elaiophylin[56,57]. In 2015, Zhou et al. reported that the thioesterase in the last module catalysed the formation of symmetrical macrodiolide using two units of linear elaiophylin monomeric seco acid (Fig. 4b)[58]. To confirm whether the biosynthesis of pteridic acids is also thioesterase-dependent, site-specific mutations of residues Met-Glu-Asp to Ile-Lys-Asn were introduced into the active sites of the TE domain in vivo (Supplementary Fig. 30)[59]. HR-LC-MS analysis showed that the mutant strain (M2089I + E2090K + D2091N) no longer produced pteridic acids and elaiophylin (Fig. 4d). Hence, we provide additional evidence via in vivo inactivation and site-directed mutagenesis. Co-production of the plant growth-regulating pteridic acids and the antimicrobial elaiophylin through a shared BGC is intriguing and points to possible joint efforts in helping plants cope with both biotic and abiotic stress.

Geographical distribution of pteridic acid producers

We surveyed available gene cluster family (GCF) data for all bacteria in the BiG-FAM database[60]. We found that the *pta* BGC (GCF_02696) is strictly restricted to the *Streptomyces* genus. In addition, a total of 55 BGCs with high similarity to the *pta* BGC were detected by BiG-SCAPE[61], among a total of 9386 type I polyketides BGCs in 1965 *Streptomyces* from the NCBI assembly database. Through literature supplementation and data dereplication of other reported producers without sequence information, at least 81 *Streptomyces* are known to produce pteridic acids/elaiophylin or have specific *pta* BGC up to date (Supplementary Table 4). Based on the known sampling information, the *pta*-containing *Streptomyces* display a variety of geographic distribution and biological origins (Fig. 5a). We selected two available *Streptomyces* strains (*Streptomyces violaceusniger* Tu 4113 and *Streptomyces rapamycinicus* NRRL 5491) to test the potential plant growth-promoting activity of these potential pteridic acid producers. The HR-LC-MS analysis of both culture broths revealed that they shared similar metabolite profiles, and both produced pteridic acids H and F (Supplementary Fig. 31). Treatment with both culture broths on barley seedlings also exhibited significant plant growth-promoting activities under osmotic, salinity and drought stress (Supplementary Fig. 32). This evidence suggests that this class of *Streptomyces* and its specific secondary metabolite pteridic acids have unique ecological significance involved in plant abiotic stress resistance.

Phylogeny and evolution of *pta* BGC

To explore the evolutionary clues of pteridic acid producers, 16S rRNA genes were initially used to assess the relatedness of the collected 34 potential producers of pteridic acids with other streptomycetes that do not contain *pta* BGC (Fig. 5b). The results revealed that, except for *Streptomyces albus* DSM 41398 and *Streptomyces* sp. GMR22, and other

https://doi.org/10.1038/s41467-023-43177-3

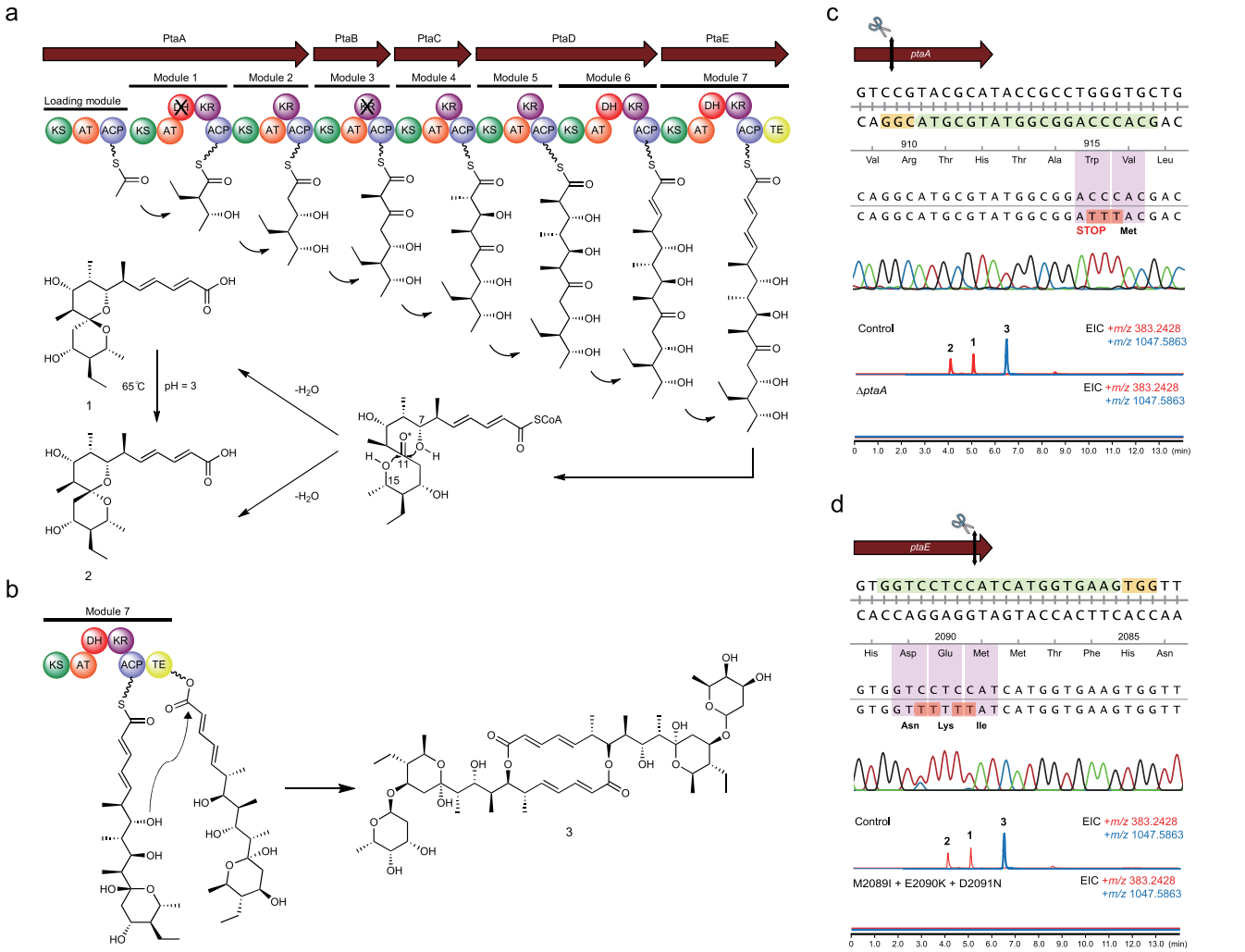

Fig. 4 | Biosynthesis mechanism of pteridic acids and CRISPR base editing application in *S. iranensis*. **a** the proposed biosynthetic pathway of pteridic acids H (**1**) and F (**2**); **b** the proposed biosynthesis mechanism of elaiophylin (**3**), and its macrodiolide formation is catalysed by thioesterase (TE) domain. **c** Sanger sequencing and HR-LC-MS output of CRISPR base editing application of STOP codon introduction targeting the *ptaA* of *S. iranensis*. The 20-nt protospacer sequence is highlighted in light green, whereas the 3-nt PAM sequence is shown in yellow. The codons and corresponding amino acids are indicated, and the black double-headed arrow represents the position of the editing window; Extracted Ion Chromatography (EIC) for **1** and **2** (*m/z* 383.2428 $[M+H]^+$) and **3** (*m/z* 1047.5863 $[M+Na]^+$) in the wild type *S. iranensis* (Control) and the mutant *S. iranensis*/Δ*ptaA*; **d** Sanger sequencing and HR-LC-MS output of CRISPR base editing application of site-directed mutagenesis targeting the TE domain of *pta* BGC. EIC for **1** and **2** (*m/z* 383.2428 $[M+H]^+$) and **3** (*m/z* 1047.5863 $[M+Na]^+$) in the wild type *S. iranensis* (Control) and the mutant *S. iranensis*/M2089I + E2090K + D2091N.

pta-containing streptomycetes cluster together and are distinct with divergent lineages. To further confirm this hypothesis, two high-resolution *Streptomyces* housekeeping genes, tryptophan synthase subunit beta (*trpB*) and RNA polymerase subunit beta (*rpoB*) were employed to analyse the phylogeny relationship among these strains (Supplementary Fig. 33)[62]. Consequently, only *S. albus* DSM 41398 was classified in a distinct phylogenetic lineage among the *Streptomyces* strains containing *pta* BGC. The strict congruence among the clades of the housekeeping genes indicated dominant vertical transmission and potential horizontal gene transfer of the *pta* BGC in *Streptomyces*.

A total of 15 *pta*-containing streptomycetes with complete genome sequence information were selected to conduct the comparative genomics investigation. The genetic diversity in these streptomycetes was initially revealed using genome sequence similarity analysis. Except for *S. albus* DSM 41398 and *Streptomyces* sp. NA02950, we observed a high degree of similarity in the aligned region, as indicated by both the average nucleotide identity (ANI) and the alignment percentage (AP) among these strains (Supplementary Fig. 34). Genome synteny analysis revealed that partial genome rearrangements happened among strains even with high sequence similarities (Supplementary Fig. 35). Notably, the *pta* BGC in *S. albus* DSM 41398 (*pta-alb*) is located at the end of the chromosome, a high variable region in *Streptomyces*, suggesting its existence by accepting heterologous biosynthetic gene fragments. The nucleotide sequence alignment of *pta* BGC results showed that *pta-alb* is relatively complete, and the similarity of core genes is proportional to evolutionary relatedness (Fig. 5c). The metabolite profile of *S. albus* DSM 41398 also confirmed the integrity of the *pta-alb* by detecting the production of elaiophylin and pteridic acid H (Supplementary Fig. 36). To further assess the biosynthesis diversity in remaining genetically related strains, we performed the similarity analysis of these BGCs (Supplementary Figs. 37 and 38). The connections between their secondary metabolites, BGCs, revealed that these vertically inherited *Streptomyces* strains also harbour striking similarities. Combining phylogenetic and comparative genomics analysis, we expect that *S. albus* DSM 41398 is evolutionarily the most distinct member from other *pta*-containing streptomycetes and obtained the *pta* BGC via horizontal gene transfer.

https://doi.org/10.1038/s41467-023-43177-3

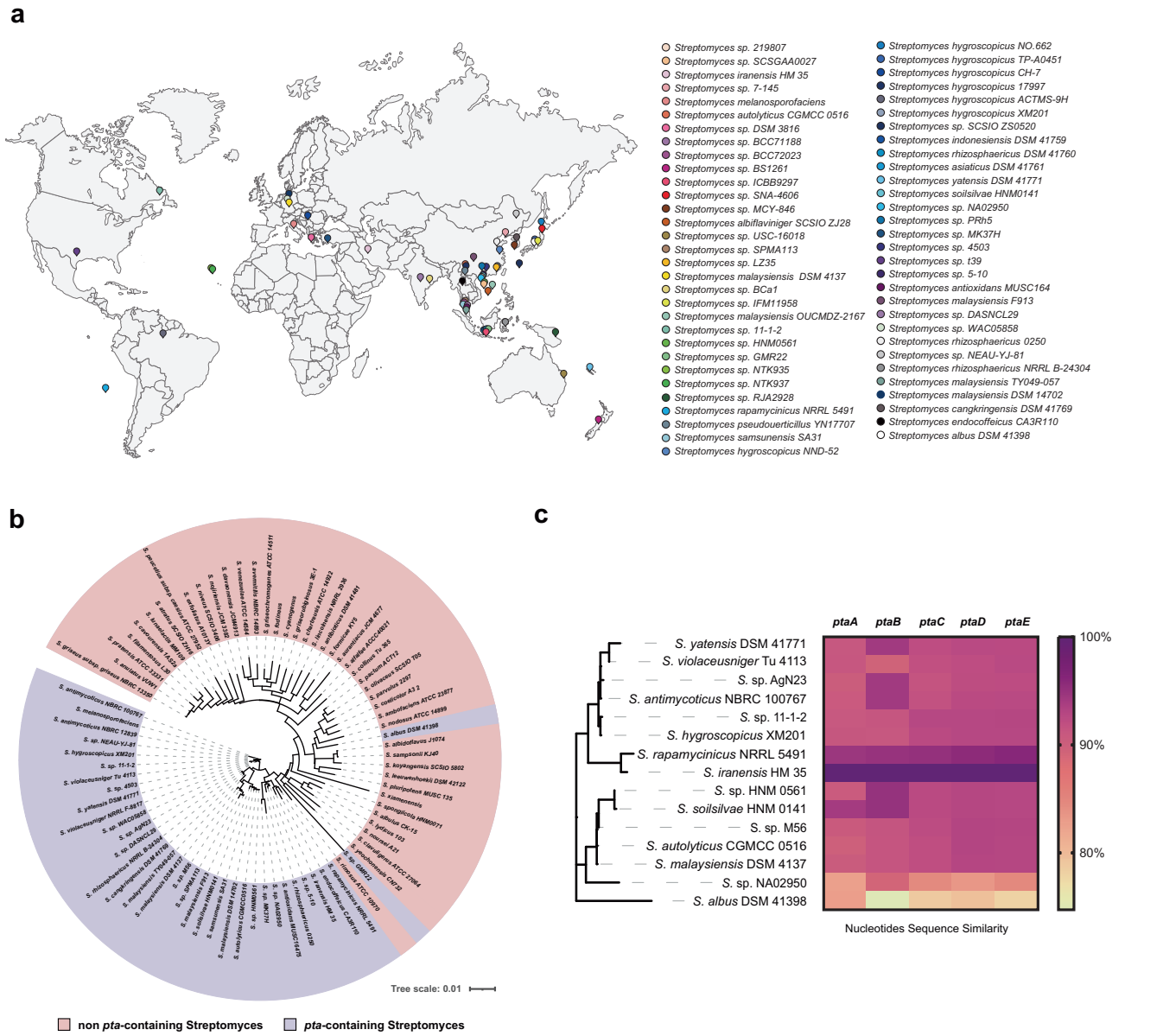

Fig. 5 | Geographical distribution and phylogenetic analysis of *pta*-containing streptomycetes possessing *pta* BGC. a A total of 61 streptomycetes were displayed on the map and distinguished by different colours. For detailed strain information, see (Supplementary Table 4). This figure was partly generated using Servier Medical Art (http://smart.servier.com/), licensed under a Creative Common Attribution 3.0 Generic License; **b** the phylogenetic tree of 16S rRNA nucleotides sequences of *pta*-containing streptomycetes and other streptomycetes; **c** the heatmap depicts similarity differences of core biosynthetic genes of *pta* BGC between *S. iranensis* and other 14 *pta*-containing streptomycetes.

However, most *pta*-containing streptomycetes have vertically inherited *pta* and other BGCs from their ancient ancestors that may be ecologically important and rarely studied.

Discussion

Drought and salinisation of soil are increasing globally, driving a reduction in crop yields that threatens food security. Plant growth-promoting bacteria is a class of beneficial microorganisms that positively interact with the plant to confer environmental stresses[63]. Although some *Streptomyces* species have been reported to have plant growth-promoting activity, the molecules mediating such positive effects are poorly understood. Deciphering the molecular mechanism is key to understanding the complex plant microbiota interaction. In this study, we present an example of *S. iranensis* secreting a family of secondary metabolites, pteridic acids, to assist plants to cope with abiotic stresses like osmotic, salinity and drought. Pteridic acids H and F were chemically isolated, structurally characterised and functional validated as plant-beneficial molecules.

Plants respond to harsh environments by changing their physiological processes for better survival[64]. Salt and drought stress signal transduction consists of ionic and osmotic homoeostasis signalling pathways, detoxification (i.e., damage control and repair) response pathways, and pathways for growth regulation[65,66]. Based on mRNA-seq analysis, we identified a total of 3086 DEGs, some of which are associated with diverse abiotic stress defenses in plants. For example, we observed that the upregulation of *SLAH1* is crucial for alleviating the toxicity of salt by root-to-shoot Cl^- transport in *Arabidopsis*[27]. *PIN6* was previously identified as the key salt tolerance-related gene in the roots of the mangrove *Avicennia officinalis*[28]. *AtACA8* is a plasma membrane localised Ca^{2+} pump and plays a role in sucrose signalling, ion homeostasis and root development during early seedling germination[31]. *MKK7* positively regulates plant salt tolerance and promotes primary

root growth in *Arabidopsis* seedlings[35]. The differentiation and development of Guard cells (GCs), which are in the epidermis of leaves and stems that regulate stomatal development, are regulated by *TMM*[30]. Under abiotic stress conditions, the upregulation of *ABCG17* expression facilitated the translocation of ABA from the shoot to the root, consequently stimulating lateral root growth[33]. Additionally, our study revealed an enhancement in the lateral root growth of *Arabidopsis* seedlings upon exposure to pteridic acid F, with the expression of the associated *ABCG17* gene observed exclusively in the PF vs. CK group.

Salt stress negatively affects photosynthesis in plants, prompting them to regulate the photosynthetic process, either through intrinsic mechanisms or in response to external stimuli, to enhance their salt tolerance[67]. Based on GO and KEGG pathway enrichment analysis, photosynthesis and its related physiological events of *Arabidopsis* seedlings treated with pteridic acids were immensely upregulated. Interestingly, previous studies also showed that small molecules, such as exogenously applied melatonin, can assist plants in resisting salt stress by improving photosynthesis in different plants[68,69]. Some studies have confirmed that IAA is involved in response to salt stress in plants and a link between IAA signalling and salt stress has been established[70,71]. Herein, we speculated that pteridic acids might also promote plant growth under salt stress via activating auxin signal transduction to promote plant growth under salt stress. B-ARR, as a positive regulator that regulated downstream activity in the cytokinin signalling pathway, was also uniquely upregulated in PF vs. CK group.

Among the various TFs, MYBs participate in various biological processes in plants such as growth, reproduction, secondary metabolism and stress responses[72]. For example, upregulated *MYB25* has been shown to reduce sensitivities toward osmotic and salt stress in *Arabidopsis* and upregulated *MYB111* is a positive regulator of salt stress in *Arabidopsis* by binding directly to the cis-acting element in the promoter region of genes encoding flavonoid synthesis enzymes[42,43]. *MYB60*, which was upregulated in the PH vs. CK group, was previously demonstrated to play a dual role in abiotic stress responses in *Arabidopsis* through its involvement in stomatal regulation and root growth for increased water uptake[47]. *MYB29*, which was uniquely upregulated in the PF vs. CK group, has been demonstrated to be an important factor in promoting *Arabidopsis* lateral root growth under salinity stress[49]. *MYB113* has also been reported to promote anthocyanin biosynthesis in *Arabidopsis* and pear for defense against abiotic and biotic stresses[50]. Previous studies have shown that overexpression of *WRKY46* enhanced root development during salt stress in *Arabidopsis* through modulation of ABA signalling[44]. We found that *WRKY46* was upregulated in pteridic acid-treated samples, which may also serve as a positive regulator in the ABA signalling pathway to confer abiotic stress resistance to plants, although we didn't observe other ABA-related DEGs. The two upregulated bHLH family TFs *PRE1* and *SCRM2* have also been experimentally proved to promote plant growth and resist abiotic stress[45,46].

Horizontal gene transfer is an integral driver of BGC evolution, revealing the independent processes of species phylogeny and BGCs distribution[73]. However, vertical inheritance also influences BGCs evolutionary dynamics, evident from BGCs conservation among closely related strains[74]. We found that the *pta* BGC in *Streptomyces* are widely dispersed geographically and mainly inherited through vertical gene transmission. Some of these strains have also been described to have remarkable biocontrol capabilities. For example, *Streptomyces* sp. AgN23 activates *Arabidopsis* defence responses to fungal pathogen infection by secreting plant elicitors[75], *Streptomyces rhizosphaericus* 0250 and *Streptomyces* sp. 5–10 displayed significant biocontrol potential to fusarium wilt of bitter gourd[76,77]. The family of *pta*-containing *Streptomyces* was also previously described as a specific phylogenetic lineage with the highest BGC abundance and largest genome size across diverse streptomycetes[78]. Although the biosynthetic diversity of these *Streptomyces* strains is likely due to horizontal transfer events that occurred relatively recently in their evolutionary history instead of genetic diversification through a vertical transfer of BGCs. The multiple Type I PKSs presenting among these strains are highly conserved based on genetic similarity network analysis. There is currently some evidence supporting potential complex cross-BGC regulation in this class of *Streptomyces* strains. Jiang et al. demonstrated that a TetR family transcriptional regulator, *GdmRIII*, controls the biosynthesis of geldanamycin and elaiophylin meanwhile, in *Streptomyces autolyticus* CGMCC 0516[79]. Recently, He et al. found that the rapamycin BGC-situated LAL family regulator RapH co-ordinately regulated the biosynthesis of both rapamycin and elaiophylin in *S. rapamycinicus* NRRL 5491[80]. Although these reports correspond to cross-regulation between evolutionarily conserved BGCs, more details of these communications need to be investigated.

In conclusion, pteridic acids are secondary metabolites produced by streptomycetes enhancing plant resistance to abiotic stress. Transcriptomics profile revealed a higher expression of a diverse set of genes, e.g., in photosynthesis and abiotic stress response genes after pteridic acids treatment. This is a useful illustration of the bacterial metabolite-mediated alteration of plants in response to environmental stress. It will open avenues for utilising *Streptomyces* to rewild plant microbiomes and improve plant abiotic stress resistance to tackle climate change[81].

Methods

Strains, plasmids, and cultivation

All strains and plasmids used in this study are listed in (Supplementary Table 5). All *Streptomyces* strains were obtained from the German Collection of Microorganisms and Cell Cultures GmbH (DSMZ, Germany). All *Escherichia coli* strains were grown in liquid/solid LB medium (5.0 g L^{-1} yeast extract, 10.0 g L^{-1} peptone, 10.0 g L^{-1} NaCl) at 37 °C. All *Streptomyces* strains were grown on SFM medium (20.0 g L^{-1} mannitol, 20.0 g L^{-1} soya flour, 20.0 g L^{-1} agar), and the SFM medium with the addition of 120 mM calcium chloride solution was used for the step of conjugation at 28 °C. The ISP2 medium (4.0 g L^{-1} yeast extract, 10.0 g L^{-1} malt extract, 4.0 g L^{-1} dextrose, and 1.0 L distilled water) was used for liquid fermentation of all *Streptomyces* strains used in plant assay and metabolomics analysis. Appropriate antibiotics were supplemented with the following working concentrations: apramycin (50 μg mL^{-1}), chloramphenicol (25 μg mL^{-1}), and kanamycin (50 μg mL^{-1}). All chemicals utilised in this study were from Sigma-Aldrich, USA.

Metabolomics analyses

High performance liquid chromatography was carried out on the Agilent Infinity 1290 UHPLC system (Agilent Technologies, USA). The 250 × 2.1 mm i.d., 2.7 μm, Poroshell 120 Phenyl Hexyl column (Agilent Technologies, USA) was used for separation. The 2-μL samples were eluted at a flow rate of 0.35 mL min^{-1} using a linear gradient from 10% acetonitrile in Milli-Q water buffered with 20 mM formic acid increasing to 100% in 15 min. Each starting condition was held for 3 min before the next run. Mass spectrometry detection was performed on an Agilent 6545 QTOF MS equipped with Agilent Dual Jet Stream electrospray ion source (ESI) with a drying gas temperature of 160 °C, a gas flow of 13 L min^{-1}, sheath gas temperature of 300 °C, and flow of 16 L min^{-1}. The capillary voltage was set to 4000 V and the nozzle voltage to 500 V in positive mode. MS spectra were recorded as centroid data at an m/z of 100–1700, and auto MS/HRMS fragmentation was performed at three collision energies (10, 20, and 40 eV) on the three most intense precursor peaks per programme. Data were analysed with MassHunter software (Agilent Technologies, USA) and compared with known compounds and crude extract spectral libraries stored in the GNPS platform[45]. The precursor and fragment ion mass tolerance were set as 0.1 Da and 0.02 Da, respectively. In addition, the minpairs cos was set as 0.65, and the minimum matched fragment ions were set as 6.0. The metabolites profile of wild-type *S. iranensis* was visualised by MS-Dial 4.9.2[82].

Large-scale fermentation and isolation

S. iranensis was cultivated in medium 2 (3.0 g L^{-1} $CaCl_2{\cdot}2H_2O$, 1.0 g L^{-1} citric acid/Fe III, 0.2 g L^{-1} $MnSO_4{\cdot}H_2O$, 0.1 g L^{-1} $ZnCl_2$, 0.025 g L^{-1} $CuSO_4{\cdot}5H_2O$, 0.02 g L^{-1} $Na_2B_4O_7{\cdot}10H_2O$, 0.01 g L^{-1} $Na_2MoO_4{\cdot}2H_2O$, and 20.0 g L^{-1} oatmeal in 1.0 L distilled water), at 175 L filling volume in a 300 L fermentation vessel (Sartorius, Germany). The fermentation was carried out for 6 days with aeration of 25-50 L min^{-1}, stirring at 200 rpm with a temperature of 28 °C and at a pH range of 5.4-6.4. The fermentation broth was separated, filtered, and loaded onto an Amberchrom CG161Me resin LC column (200 × 20 cm, 6 L). Elution with a linear gradient of H_2O-MeOH (from 30% to 100% v/v, flow rate 0.5 L min^{-1}, in 58 min) afforded seven fractions (A–G). Fraction G was firstly fractionated by silica gel chromatography with a CH_2Cl_2/CH_3OH gradient to yield 16 fractions, F01-F16. F07 was separated by a Sephadex LH-20 (MeOH) column and twelve sub-fractions F07a-l were obtained. From F07e, **1** (15.0 mg) and **2** (4.0 mg) were obtained by repeated HPLC RP-C_{18} (CH_3CN/H_2O as gradient).

Pteridic acid H (**1**): white solid; $[\alpha]_D^{20}$ 81 (0.32 mg mL^{-1}, CH_3OH), ^1H NMR (800 MHz, MeOD): 7.33 (dd, 15.4 Hz, 11.1 Hz, 1H), 6.26 (dd, 15.2 Hz, 10.8 Hz, 1H), 6.13 (dd, 15.3 Hz, 8.8 Hz, 1H), 5.90 (d, 15.4 Hz, 1H), 3.85 (dd, 10.2 Hz, 2.2 Hz, 1H), 3.69 (overlapping, 1H), 3.59 (m, 1H), 3.43 (m, 1H), 2.48 (m, 1H), 2.29 (dd, 14.9 Hz, 6.1 Hz, 1H), 2.01 (m, 1H), 1.64 (dd, 14.9 Hz, 1.9 Hz, 1H), 1.52 (m, 1H), 1.21 (d, 6.1 Hz, 3H), 1.49 (m), 1.01 (d, 6.8 Hz, 3H), 0.96 (d, 6.8 Hz, 3H), 0.93 (t, 7.3 Hz, 3H), 0.91 (d, 7.0 Hz, 3H); ^{13}C NMR (200 MHz, MeOD): 168.7, 151.0, 146.7, 129,6, 120.6, 103.2, 75.5, 72.8, 70.3, 70.1, 51.3, 42.2, 40.4, 37.5, 37.4, 24.8, 20.9, 16.0, 12.1, 10.1, 5.0; UV/vis (CH_3CN/H_2O) λ_{max} 262 nm; IR (ATR) υ_{max} 2967, 2934, 2879, 1712, 1642, 1600, 1458, 1410, 1383, 1300, 1266, 1223, 1187, 1142, 1109, 1058, 1002, 973 cm^{-1}; (+)-HR-ESI-MS (*m/z*) $[M+H]^+$ calcd for $C_{21}H_{35}O_6$, 383.2428; found, 383.2439. ^1H NMR and ^{13}C NMR see Supplementary Tables 6 and 7.

Pteridic acid F (**2**): white solid; $[\alpha]_D^{20}$ −18 (10 mg mL^{-1}, CH_3OH), ^1H NMR (800 MHz, MeOD): 5.97 (d, 15.1 Hz, 1H), 7.16 (dd, 15.1 Hz, 10.9 Hz, 1H), 6.25 (dd, 15.1 Hz, 10.9 Hz, 1H), 6.07 (dd, 15.1 Hz, 8.6 Hz, 1H), 3.88 (m, 1H), 3.66 (td, 10.8 Hz, 4.3 Hz, 1H), 3.56 (dd, 11.5 Hz, 4.7 Hz, 1H), 3.32 (m, 1H), 2.49 (m, 1H), 2.19 (dd, 13.1 Hz, 4.3 Hz, 1H), 2.02 (m, 1H), 1.69 (m, 1H), 1.32 (dd, 13.2 Hz, 11.2 Hz, 1H), 1.14 (d, 6.2 Hz, 3H), 1.02 (m, 1H), 1.02 (d, 6.8 Hz, 3H), 0.95 (d, 6.9 Hz, 3H), 0.98 (d, 6.8 Hz, 3H), 1.60 (m, 1H), 1.44 (m, 1H), 0.82 (t, 7.6 Hz, 3H); ^{13}C NMR (200 MHz, MeOD): 170.2, 148.1, 148.1, 129,6, 122.9, 103.2, 78.0, 74.7, 66.3, 66.3, 52.2, 42.1, 40.5, 38.0, 33.8, 20.4, 15.9, 12.7, 5.3; UV/vis (CH_3CN/H_2O) λ_{max} 264 nm; IR (ATR) υ_{max} 2968, 2931, 2877, 1692, 1643, 1618, 1458, 1410, 1380, 1299, 1270, 1188, 1138, 1106, 1059, 1002, 973, 850 cm^{-1}; (+)-HR-ESI-MS (*m/z*): $[M+H]^+$ calcd for $C_{21}H_{35}O_6$, 383.2428; found, 383.2433. ^1H NMR and ^{13}C NMR see Supplementary Tables 6 and 7.

Structure identification

NMR spectra were recorded on an 800 MHz Bruker Avance III spectrometer equipped with a TCI CryoProbe using standard pulse sequences. NMR data were processed using MestReNova 11.0. UHPLC-HRMS was performed on an Agilent Infinity 1290 UHPLC system equipped with a diode array detector. UV-Vis spectra were recorded from 190 to 640 nm. Specific rotations were acquired using Perkin-Elmer 241 polarimeter. IR data were acquired on Bruker Alpha FTIR spectrometer using OPUS version 7.2. TLC analysis was performed on silica gel plates (Sil G/UV_{254}, 0.20 mm, Macherey-Nagel). The Biotage Isolera One Flash Chromatography system was used for flash chromatography and performed on silica gel 60 (Merck, 0.04–0.063 mm, 230–400 mesh ASTM). Sephadex LH-20 was from Pharmacia.

Crystal structure determination

X-ray data collection of **1** was performed on an Agilent Supernova Diffractometer using CuKα radiation. Data were processed and scaled using the CrysAlisPro software (Agilent Technologies, USA). The structure was solved using SHELXS and refined using SHELXL. Hydrogen atoms were included in ideal positions using riding coordinates. The absolute configuration was determined based on the Flack parameter. Crystal Data for **1**: $C_{21}H_{34}O_6$, M = 382.50, monoclinic, a = 8.4619(1) Å, b = 15.6161(2) Å, c = 8.4994(1) Å, α = 90.00°, β = 107.768(1)°, γ = 90.00°, V = 1069.55(2)Å^3, T = 120.(2) K, space group $P21$, Z = 2, μ(Cu Kα) = 0.698 mm^{-1}, 17514 reflections collected, 4275 independent reflections (R_{int} = 0.0226, R_{sigma} = 0.0155). The final R_1 values were 0.0249 ($I > 2\sigma(I)$). The final wR_2 values were 0.0648 ($I > 2\sigma(I)$). The final R_1 values were 0.0252 (all data). The final wR_2 values were 0.0651 (all data). The goodness of fit on F^2 was 1.057. Flack parameter = 0.13(10).

Genetic manipulation

All primers used were synthesised by IDT (Integrated DNA Technologies, USA) and listed in (Supplementary Table 8). Plasmids and genomic DNA purification, PCR and cloning were conducted according to standard procedures using manufacturer protocols. PCR was performed using OneTaq Quick-Load 2X Master Mix with Standard Buffer (New England Biolabs, USA). DNA assembly was done by using NEBuilder HiFi DNA Assembly Master Mix (New England Biolabs, USA). DNA digestion was performed with FastDigest restriction enzymes (Thermo Fisher Scientific, USA). NucleoSpin Gel and PCR Clean-up Kits (Macherey-Nagel, Germany) were used for DNA clean-up from PCR products and agarose gel extracts. One Shot Mach1 T1 Phage-Resistant Chemically Competent *E. coli* (Thermo Fisher Scientific, USA) was used for cloning. NucleoSpin Plasmid EasyPure Kit (Macherey-Nagel, Germany) was used for plasmid preparation. Sanger sequencing was carried out using a Mix2Seq Kit (Eurofins Scientific, Luxembourg). All DNA manipulation experiments were conducted according to standard procedures using manufacturer protocols.

Gene inactivation and site-directed mutagenesis

To use the pCRISPR-cBEST for base editing applications, an oligo was designed as Del-ptaA by the online tool CRISPy-web, and the pCRISPR-cBEST plasmid was linearised by *Nco*I. Mixing the linearised pCRISPR-cBEST plasmid and Del-ptaA with the NEBuilder HiFi DNA Assembly Master Mix (New England Biolabs, USA). The linearised pCRISPR-cBEST plasmid was then bridged by Del-ptaA, ending with the desired pCRISPR-cBEST/Δ*ptaA*. Chemically competent *E. coli* were transformed with the recombinant plasmid and confirmed via PCR amplification (programme: 94 °C for 30 s, followed by 30 cycles consisting of 94 °C for 15 s; 54 °C for 15 s; 68 °C for 40 s, and 68 °C for 2 min) and Sanger sequencing. The experimental procedure for site-directed mutagenesis for the TE domain is the same as described above. The *E. coli-Streptomyces* conjugation experiment was conducted according to the modified protocol in this study, and the mutant *Streptomyces* strains were also confirmed by PCR and Sanger sequencing (Eurofins, France).

Construction of BAC and genetical complementation

The BAC library of *S. iranensis* was constructed using pESAC13-A from Bio S&T (Montreal, Canada). Based on a high-throughput screening method (unpublished), we selected two BACs 1J23 and 6M10 that cross-cover the *ptaA* gene (Supplementary Fig. 28). The selected BAC clones were further confirmed using four sets of primers, including ID-1J23-right-F/R, ID-1J23-left-F/R, ID-6M10-right-F/R, and ID-6M10-left-F/R (Supplementary Table 8). Subsequently, we introduced these two BAC clones 1J23 and 6M10 into *S. iranensis*/Δ*ptaA* (remove the pCRISPR-cBEST/Δ*ptaA* to obtain antibiotics resistance free strain) separately by conjugation. Exconjugants of mutants were further validated by apramycin resistance screening and PCR.

Enrichment evaluation of *S. iranensis* in rhizosphere soil

The *S. iranensis* (with the apramycin resistance gene) spore suspension was well mixed with fully sterilised soil and was transferred to a 250 mL

flask. The sterilised germinated barley seed was placed in the centre position of soil in flask and grown at 24 ± 2 °C, 8 h dark/16 h light in the growth chamber for 7 days. Samples were collected from soil within 0.1 cm and 3 cm distance from the barley root, with a specification of 0.1 g soil per sample. Then, these samples were transferred to sterilised 1.5 mL Eppendorf tubes and mixed with 500 µL sterilised H_2O. 200 µL of each sample was spread evenly over the solid MS medium with the addition of 50 µg mL^{-1} apramycin and grown at 28°C for 7 days. The number of *Streptomyces* colonies grown on each plate were counted and statistically analysed.

Arabidopsis growth assays

A. thaliana ecotype Columbia (Col-0) was used to test the effects of pteridic acids treatment under drought stress mediated by PEG-6000 (Duchefa Biochemie BV) and salinity stress mediated by NaCl (Duchefa Biochemie BV). The modified Murashige & Skoog medium (2.2 g L^{-1} Murashige & Skoog medium including B5 vitamins, 5.0 g L^{-1} of sucrose, 250 mg L^{-1} MES monohydrate, 7.0 g L^{-1} agar, and adjusted pH to 5.7 with KOH) was used in this study. PEG-6000 (15% w/v) was dissolved in water and filtered through 0.2-micron Sartorius Minisart™ Plus Syringe Filters (Fisher Scientific). 50 mL of the filtered solution was overlaid onto the surface of solidified Murashige & Skoog medium. The plates were left for 24 h to diffuse the PEG into the Murashige & Skoog medium. NaCl was added to the medium to a final concentration of 80 mM for the salinity stress alleviation test. The pure compound pteridic acids H and F (0.50 ng mL^{-1}), IAA (0.23 ng mL^{-1}), and ABA (0.34 ng mL^{-1}) were mixed with different media to a final concentration of approximately 1.3 nM and poured into the plates. Seeds were surface sterilised by washing with 70% ethanol for 2 min, then in sterilisation solution (10% bleach) for 1 min by inverting the tubes, and finally washed five times with sterilised water. The seeds were stratified for 2 days at 4 °C in the dark. Sterilised seeds were placed in Petri dishes (approx. 100 seeds per Petri dish) on Murashige & Skoog medium and grown for 3–4 days in the vertical position in a culture chamber at 22 °C under standard long-day conditions (16/8 h light/dark photoperiod). After three days of growth, seedlings with similar root lengths (7-10 mm) were transferred to square plates containing Murashige & Skoog medium (control) or Murashige & Skoog medium supplemented with 15% (w/v) PEG-6000 or 80 mM NaCl. 16 seedlings were used per replicate for each treatment. The initial position of the plant root tip was marked with a marker. The plants were grown in the vertical position under standard long day conditions (22 °C, 16/8 h light/dark) for 8 days, and then each plate was scanned using Image Scanner. Primary and lateral root lengths and the total plant weight were then scored. The primary and lateral root length measurements were performed by analysing pictures with the Image J software. Fresh weight measurements were estimated using a precision balance. Whole 8-day-old plants grown in the medium were removed using forceps, dried in tissue paper, and then weighed using a precision balance.

Barley and mung bean growth assays

The pteridic acid streptomycetes producers were tested for their effects on barley cultivars Guld grown in soil. *S. iranensis* HM 35, *S. rapamycinicus* NRRL 5491, and *S. violaceusniger* Tu 4113 were cultivated in ISP2 medium for 7 days at 28 °C. 500 µL culture broth (ca. 3×10^9 CFU/mL) was added to 100 g sand soil and well mixed. Treated soils were infiltrated with Milli-Q water, 20% PEG-6000 solutions to simulate osmotic stress, and 100 mM NaCl solutions to simulate salinity stress in soil environments. To simulate drought stress during barley growth, the plant was initially watered for 7 days, then subjected to 7 days of drought stress, and finally allowed to recover with various treatments for another 7 days. Barley seeds were rinsed in distilled water and sterilised with 1% sodium hypochlorite for 15 min. They were then washed with distilled water and germinated in distilled water at 24 °C for 2 days. Barley seeds were planted in each plastic pot (5 cm × 5 cm × 6 cm, six seedlings per pot) supplemented with different treated soil and grown at 24 ± 2 °C, 8 h dark/16 h light in the growth chamber for 7 days. Plant height (cm) was measured as the aerial part of the plant, and the fresh shoot weight (g) and fresh root weight (g) of each seedling were measured separately. Then, the seedlings were dried in the hot-air oven at 70 °C for 6 h to obtain the dry shoot and dry root weights (g). For heavy metal stress experiment, mung beans were pre-germinated and placed on top of the modified Murashige & Skoog medium agar, supplemented with 10 mM $CuSO_4$, with 1.0 ng mL^{-1} pure substances. All mung beans were grown in the dark at 24 ± 2 °C for 4 days.

Kidney beans growth assays

The seeds of kidney beans (appr. 2 cm in length, from organic farming) were firstly sterilised successively with ethanol (70% v/v) and sodium hypochlorite (5% v/v), each for 2 min and then rinsed with sterile Milli-Q water (three times). The sterilised seeds were cultivated on modified Murashige & Skoog agar plates for 3–4 days. After germination, the seedlings (with 1.5–2-cm-long roots) were soaked in 10 mL aliquots of testing compounds (pteridic acids H and F, 1.0 ng mL^{-1}, dissolved in sterile Milli-Q water) in ultra-clear polypropylene containers (ø 34 mm, vol. 20 mL) with polyethylene caps. The control group was treated with 10 mL sterile Milli-Q water. For each treatment, three repetitions (containers) were used, and each repetition included four seedlings. After 24 h, the seeds were transferred into a cut square petri dish, put on the top layer of sandy soil, and then incubated vertically in a growth chamber (24/22 °C, day/night cycle of 16/8 h, 50%, 60%, 70%, 100% of circulated wind velocity for 12 h, 2 h, 2 h, 8 h) for 7 days. Solutions of pteridic acids H and F (2 mL, 1.0 ng mL^{-1} for both) were added separately into corresponding containers, with sterile Milli-Q water as control, and an extra 8 mL of Milli-Q water was added to each petri dish every other day.

RNA extraction and mRNA-seq

Arabidopsis seeds were sterilised, and seven to ten seeds were cultured in each well of a 6-well plate in 2 mL medium containing modified Murashige & Skoog and 30 mM sucrose with 16 h light, at 24 °C in a controlled environment room. After 7 days, seedlings were washed in 20 mL modified Murashige & Skoog liquid medium and then moved to 20 mL of fresh liquid medium containing 80 mM NaCl and cultured in 50 ml E-flasks with 1 ng mL^{-1} of each pteridic acids H or F (or equal amount of water as control). Whole-seedling plant samples were collected after 72 h when significant phenotypic variation occurred between groups. Total RNA was extracted using RNeasy Plant Mini Kit (Qiagen, Germany). mRNA was purified from total RNA using poly-T oligo-attached magnetic beads. After fragmentation, the first strand cDNA was synthesised using random hexamer primers, followed by the second strand cDNA synthesis using dTTP for the non-directional library construction. The reads were generated using an Illumina NovaSeq 6000 (Novogene, UK) with a paired-end 150 bp configuration. DESeq2 was used to estimate DEGs between different treatments with the threshold of FDR-adjusted p values ≤ 0.05 and |log2(FoldChange)|≥1 if there is no additional statement[83]. The online software g:Profiler (http://biit.cs.ut.ee/gprofiler/gost) was used for GO enrichment and clusterProfiler R package was used to test the statistical enrichment of DEGs in KEGG pathways[84,85].

Bioinformatics analyses

The identification and annotation of all BGCs of *Streptomyces* secondary metabolites were carried out with antiSMASH 6.0[26]. The threshold for similar BGCs was selected as greater than 45% sequence similarity. The BiG-FAM database and BiG-SCAPE software were used to identify the distribution of *pta* gene clusters in different bacteria and generate the pta-gene cluster family similarity

network[60,61]. A cut-off of 0.3 was used as a raw index similarity metric for the BiG-SCAPE analysis. The alignment of 15 *pta*-containing *Streptomyces* genome sequences was performed using the whole-genome alignment plugin of the CLC Genomics Workbench version 22.0.2 (Qiagen). The minimum initial seed length was 15 bp, and the minimum alignment block length was 100 bp. The networks of Big-SCAPE and GNPS analysis were visualised using Cytoscape 3.9. The phylogenetic analysis was conducted by the online multiple sequence alignment tool MAFFT and visualised by iTOL v5[86,87].

Statistical analysis

Statistical significance was assessed by one-way ANOVA with post hoc Dunnett's multiple comparisons test, one-way ANOVA with Tukey test or t test (see each figure legend). All analyses were performed using GraphPad Prism version 9. p values < 0.05 were considered significant. Asterisks indicate the level of statistical significance: $^{*}p < 0.05$, $^{**}p < 0.01$, $^{***}p < 0.001$, and $^{****}p < 0.0001$. For all relevant figures, source data and exact p values are provided in the Source Data file.

Reporting summary

Further information on research design is available in the Nature Portfolio Reporting Summary linked to this article.

Data availability

The gene sequences used in this study were collected by searching National Center for Biotechnology Information (NCBI). The crystal structure data generated in this study have been deposited in the Cambridge Crystallographic Data Centre database under accession code 1984025. The metabolomics data generated in this study have been deposited in MassIVE under accession code MSV000090745 [https://massive.ucsd.edu/ProteoSAFe/dataset.jsp?task=f9aed10a976641d5b8e5e943b67a1953]. The mRNA-seq data were deposited at NCBI Sequence Read Archive (SRA) database with accession code PRJNA1020394. Source data are provided with this paper.

References

1. Wheeler, T. & von Braun, J. Climate change impacts on global food security. *Science* **341**, 508–513 (2013).
2. Zhang, H., Zhu, J., Gong, Z. & Zhu, J. Abiotic stress responses in plants. *Nat. Rev. Genet.* **23**, 104–119 (2022).
3. Kuromori, T., Fujita, M., Takahashi, F., Yamaguchi-Shinozaki, K. & Shinozaki, K. Inter-tissue and inter-organ signaling in drought stress response and phenotyping of drought tolerance. *Plant J.* **109**, 342–358 (2022).
4. Dos Santos, V. et al. Causes of reduced leaf-level photosynthesis during strong El Niño drought in a Central Amazon forest. *Global Change Biol.* **24**, 4266–4279 (2018).
5. Waadt, R. et al. Plant hormone regulation of abiotic stress responses. *Nat. Rev. Mol. Cell Biol.* **23**, 680–694 (2022).
6. Kerchev, P. & Van Breusegem, F. Improving oxidative stress resilience in plants. *Plant J.* **109**, 359–372 (2022).
7. Corwin, D. Climate change impacts on soil salinity in agricultural areas. *Eur. J. Soil Sci.* **72**, 842–862 (2021).
8. Ullah, A., Bano, A. & Khan, N. Climate change and salinity effects on crops and chemical communication between plants and plant growth-promoting microorganisms under stress. *Front. Sustain. Food Syst.* **5**, 618092 (2021).
9. Hong, Y., Zhou, Q., Hao, Y. & Huang, A. C. Crafting the plant root metabolome for improved microbe-assisted stress resilience. *New Phytol.* **234**, 1945–1950 (2022).
10. De Vries, F., Griffiths, R., Knight, C., Nicolitch, O. & Williams, A. Harnessing rhizosphere microbiomes for drought-resilient crop production. *Science* **368**, 270–274 (2020).
11. Arif, I., Batool, M. & Schenk, P. Plant microbiome engineering: expected benefits for improved crop growth and resilience. *Trends Biotechnol.* **38**, 1385–1396 (2020).
12. Berlanga-Clavero, M. et al. Bacillus subtilis biofilm matrix components target seed oil bodies to promote growth and anti-fungal resistance in melon. *Nat. Microbiol.* **7**, 1–15 (2022).
13. Das, P. et al. Plant-soil-microbes: a tripartite interaction for nutrient acquisition and better plant growth for sustainable agricultural practices. *Environ. Res.* **214**, 113821 (2022).
14. Hiruma, K. et al. Root endophyte *Colletotrichum tofieldiae* confers plant fitness benefits that are phosphate status dependent. *Cell* **165**, 464–474 (2016).
15. Henneron, L., Kardol, P., Wardle, D., Cros, C. & Fontaine, S. Rhizosphere control of soil nitrogen cycling: a key component of plant economic strategies. *New Phytol.* **228**, 1269–1282 (2020).
16. Etalo, D., Jeon, J. & Raaijmakers, J. Modulation of plant chemistry by beneficial root microbiota. *Nat. Prod. Rep.* **35**, 398–409 (2018).
17. Quinn, G., Banat, A., Abdelhameed, A. & Banat, I. *Streptomyces* from traditional medicine: sources of new innovations in antibiotic discovery. *J. Med. Microbiol.* **69**, 1040–1048 (2020).
18. Viaene, T., Langendries, S., Beirinckx, S., Maes, M. & Goormachtig, S. *Streptomyces* as a plant's best friend? *FEMS Microbiol. Ecol.* **92**, fiw119 (2016).
19. Myo, E. et al. Indole-3-acetic acid production by *Streptomyces fradiae* NKZ-259 and its formulation to enhance plant growth. *BMC Microbiol.* **19**, 1–14 (2019).
20. Sadeghi, A. et al. Plant growth promoting activity of an auxin and siderophore producing isolate of *Streptomyces* under saline soil conditions. *World J. Microbiol. Biotechnol.* **28**, 1503–1509 (2012).
21. Singh, S. & Gaur, R. Endophytic *Streptomyces* spp. underscore induction of defense regulatory genes and confers resistance against *Sclerotium rolfsii* in chickpea. *Biol. Control* **104**, 44–56 (2017).
22. Fitzpatrick, C. et al. Assembly and ecological function of the root microbiome across angiosperm plant species. *Proc. Natl. Acad. Sci. USA* **115**, E1157–E1165 (2018).
23. Blin, K. et al. antiSMASH 6.0: improving cluster detection and comparison capabilities. *Nucleic Acids Res.* **49**, W29–W35 (2021).
24. Wang, M. et al. Sharing and community curation of mass spectrometry data with Global Natural Products Social Molecular Networking. *Nat. Biotechnol.* **34**, 828–837 (2016).
25. Igarashi, Y., Iida, T., Yoshida, R. & Furumai, T. Pteridic acids A and B, novel plant growth promoters with auxin-like activity from *Streptomyces hygroscopicus* TP-A0451. *J. Antibiot.* **55**, 764–767 (2002).
26. Nong, X., Wei, X. & Qi, S. Pteridic acids C-G spirocyclic polyketides from the marine-derived *Streptomyces* sp. SCSGAA 0027. *J. Antibiot.* **70**, 1047–1052 (2017).
27. Qiu, J., Henderson, S. W., Tester, M., Roy, S. J. & Gilliham, M. SLAH1, a homologue of the slow type anion channel SLAC1, modulates shoot Cl^- accumulation and salt tolerance in *Arabidopsis thaliana*. *J. Exp. Bot.* **67**, 4495–4505 (2016).
28. Krishnamurthy, P. et al. Transcriptomics analysis of salt stress tolerance in the roots of the mangrove *Avicennia officinalis*. *Sci. Rep.* **7**, 10031 (2017).
29. Li, L., Cai, Q., Yu, D. & Guo, C. Overexpression of *AtFRO6* in transgenic tobacco enhances ferric chelate reductase activity in leaves and increases tolerance to iron-deficiency chlorosis. *Mol. Biol. Rep.* **38**, 3605–3613 (2011).
30. Pillitteri, L. J. & Dong, J. Stomatal development in *Arabidopsis*. *Arabid. Book* **11**, e0162 (2013).
31. Zhang, J., Zhang, X., Wang, R. & Li, W. The plasma membrane-localised Ca^{2+}-ATPase ACA8 plays a role in sucrose signalling involved in early seedling development in *Arabidopsis*. *Plant Cell Rep.* **33**, 755–766 (2014).

32. Magidin, M., Pittman, J. K., Hirschi, K. D. & Bartel, B. ILR2, a novel gene regulating IAA conjugate sensitivity and metal transport in *Arabidopsis thaliana*. *Plant J.* **35**, 523–534 (2003).
33. Teng, Z., Lv, J., Chen, Y., Zhang, J. & Ye, N. Effects of stress-induced ABA on root architecture development: Positive and negative actions. *Crop J.* **11**, 1072–1079 (2023).
34. Foka, I. C. K. et al. The emerging roles of Diacylglycerol Kinase (DGK) in plant stress tolerance. *growth, and development. Agronomy-Basel* **10**, 1375 (2020).
35. Shen, L. et al. Phosphatidic acid promotes the activation and plasma membrane localization of *MKK7* and *MKK9* in response to salt stress. *Plant Sci.* **287**, 110190 (2019).
36. Wang, H., Zhao, X., Zhang, J., Lu, C. & Feng, F. Arbuscular mycorrhizal fungus regulates cadmium accumulation, migration, transport, and tolerance in *Medicago sativa*. *J. Hazard. Mater.* **435**, 129077 (2022).
37. Nicolas-Espinosa, J. et al. Confronting secondary metabolites with water uptake and transport in plants under abiotic stress. *Int. J. Mol. Sci.* **24**, 2826 (2023).
38. Zhang, Y. et al. Transcriptome and metabolome analyses of two contrasting sesame genotypes reveal the crucial biological pathways involved in rapid adaptive response to salt stress. *BMC Plant Biol* **19**, 66 (2019).
39. Abogadallah, G. M., Nada, R. M., Malinowski, R. & Quick, P. Overexpression of *HARDY*, an AP2/ERF gene from *Arabidopsis*, improves drought and salt tolerance by reducing transpiration and sodium uptake in transgenic *Trifolium alexandrinum* L. *Planta* **233**, 1265–1276 (2011).
40. Bi, C. et al. The bZIP transcription factor TabZIP15 improves salt stress tolerance in wheat. *Plant Biotechnol. J.* **19**, 209–211 (2021).
41. Tang, Y. et al. Overexpression of a MYB family gene, *OsMYB6*, increases drought and salinity stress tolerance in transgenic rice. *Front. Plant Sci.* **10**, 168 (2019).
42. Beathard, C., Mooney, S., Al-Saharin, R., Goyer, A. & Hellmann, H. Characterization of *Arabidopsis thaliana* R2R3 S23 MYB transcription factors as novel targets of the ubiquitin proteasome-pathway and regulators of salt stress and abscisic acid response. *Front. Plant Sci.* **12**, 629208 (2021).
43. Li, B. et al. The *Arabidopsis* MYB transcription factor, MYB111 modulates salt responses by regulating flavonoid biosynthesis. *Environ. Exp. Bot.* **166**, 103807 (2019).
44. Ding, Z. et al. Transcription factor WRKY46 modulates the development of *Arabidopsis* lateral roots in osmotic/salt stress conditions via regulation of ABA signaling and auxin homeostasis. *Plant J.* **84**, 56–69 (2015).
45. Lee, S. et al. Overexpression of *PRE1* and its homologous genes activates gibberellin-dependent responses in *Arabidopsis thaliana*. *Plant Cell Physiol.* **47**, 591–600 (2006).
46. Gan, Y. et al. Stomatal clustering, a new marker for environmental perception and adaptation in terrestrial plants. *Bot. Stud.* **51**, 325–336 (2010).
47. Oh, J. E. et al. A dual role for *MYB60* in stomatal regulation and root growth of *Arabidopsis thaliana* under drought stress. *Plant Mol. Biol.* **77**, 91–103 (2011).
48. Najafi, S., Sorkheh, K. & Nasernakhaei, F. Characterization of the APETALA2/Ethylene-responsive factor (AP2/ERF) transcription factor family in sunflower. *Sci. Rep.* **8**, 11576 (2018).
49. Coleto, I. et al. *Arabidopsis thaliana* transcription factors *MYB28* and *MYB29* shape ammonium stress responses by regulating Fe homeostasis. *New Phytol.* **229**, 1021–1035 (2021).
50. Petroni, K. & Tonelli, C. Recent advances on the regulation of anthocyanin synthesis in reproductive organs. *Plant Sci.* **181**, 219–229 (2011).
51. Lavenus, J. et al. Lateral root development in *Arabidopsis*: fifty shades of auxin. *Trends Plant Sci.* **18**, 455–463 (2013).
52. Kautsar, S. et al. MIBiG 2.0: a repository for biosynthetic gene clusters of known function. *Nucleic Acids Res.* **48**, D454–D458 (2020).
53. Sun, P. et al. Spiroketal formation and modification in avermectin biosynthesis involves a dual activity of AveC. *J. Am. Chem. Soc.* **135**, 1540–1548 (2013).
54. Tong, Y. et al. Highly efficient DSB-free base editing for streptomycetes with CRISPR-BEST. *Proc. Natl. Acad. Sci. USA* **116**, 20366–20375 (2019).
55. Netzker, T. et al. An efficient method to generate gene deletion mutants of the rapamycin-producing bacterium *Streptomyces iranensis* HM 35. *Appl. Environ. Microbiol.* **82**, 3481–3492 (2016).
56. Gerlitz, M., Hammann, P., Thiericke, R. & Rohr, J. The biogenetic origin of the carbon skeleton and the oxygen atoms of elaiophylin, a symmetric macrodiolide antibiotic. *J. Org. Chem.* **57**, 4030–4033 (1992).
57. Haydock, S., Mironenko, T., Ghoorahoo, H. & Leadlay, P. The putative elaiophylin biosynthetic gene cluster in *Streptomyces* sp. DSM4137 is adjacent to genes encoding adenosylcobalamin-dependent methylmalonyl CoA mutase and to genes for synthesis of cobalamin. *J. Biotechnol.* **113**, 55–68 (2004).
58. Zhou, Y., Prediger, P., Dias, L., Murphy, A. & Leadlay, P. Macrodiolide formation by the thioesterase of a modular polyketide synthase. *Angew. Chem. Int. Ed.* **54**, 5232–5235 (2015).
59. Du, L. & Lou, L. PKS and NRPS release mechanisms. *Nat. Prod. Rep.* **27**, 255–278 (2009).
60. Kautsar, S., Blin, K., Shaw, S., Weber, T. & Medema, M. BiG-FAM: the biosynthetic gene cluster families database. *Nucleic Acids Res.* **49**, D490–D497 (2021).
61. Navarro-Munoz, J. et al. A computational framework to explore large-scale biosynthetic diversity. *Nat. Chem. Biol.* **16**, 60–68 (2020).
62. Komaki, H. Resolution of housekeeping gene sequences used in MLSA for the genus *Streptomyces* and reclassification of *Streptomyces anthocyanicus* and *Streptomyces tricolor* as heterotypic synonyms of *Streptomyces violaceoruber*. *Int. J. Syst. Evol. Microbiol.* **72**, 005370 (2022).
63. De Souza, R., Ambrosini, A. & Passaglia, L. M. P. Plant growth-promoting bacteria as inoculants in agricultural soils. *Genet. Mol. Biol.* **38**, 401–419 (2015).
64. Lopes, M., Dias, M. & Gurgel, E. Successful plant growth-promoting microbes: inoculation methods and abiotic factors. *Front. Sustain. Food Syst.* **5**, 606454 (2021).
65. Zhu, J. Salt and drought stress signal transduction in plants. *Annu. Rev. Plant Biol.* **53**, 247–273 (2002).
66. Van Zelm, E., Zhang, Y. & Testerink, C. Salt tolerance mechanisms of plants. *Annu. Rev. Plant Biol.* **71**, 403–433 (2020).
67. Muhammad, I. et al. Mechanisms regulating the dynamics of photosynthesis under abiotic stresses. *Front. Plant Sci.* **11**, 615942 (2021).
68. Yan, F. et al. Exogenous melatonin alleviates salt stress by improving leaf photosynthesis in rice seedlings. *Plant Physiol. Biochem.* **163**, 367–375 (2021).
69. Li, H. et al. Exogenous melatonin confers salt stress tolerance to watermelon by improving photosynthesis and redox homeostasis. *Front. Plant Sci.* **8**, 295 (2017).
70. Ryu, H. & Cho, Y. G. Plant hormones in salt stress tolerance. *J. Plant Biol.* **58**, 147–155 (2015).
71. Jung, J. & Park, C. Auxin modulation of salt stress signaling in *Arabidopsis* seed germination. *Plant Signal. Behav.* **6**, 1198–1200 (2011).
72. Ambawat, S., Sharma, P., Yadav, N. R. & Yadav, R. C. MYB transcription factor genes as regulators for plant responses: an overview. *Physiol. Mol. Biol. Plants* **19**, 307–321 (2013).
73. McDonald, B. & Currie, C. Lateral gene transfer dynamics in the ancient bacterial genus. *Streptomyces*. *Mbio* **8**, e00644–17 (2017).

74. Chase, A., Sweeney, D., Muskat, M., Guillen-Matus, D. & Jensen, P. Vertical inheritance facilitates interspecies diversification in biosynthetic gene clusters and specialized metabolites. *Mbio* **12**, e02700–e02721 (2021).
75. Vergnes, S. et al. Phyllosphere colonization by a soil *Streptomyces* sp. promotes plant defense responses against fungal infection. *Mol. Plant Microbe Interact.* **33**, 223–234 (2020).
76. Li, X., Tian, Y., Peng, H., He, B. & Gao, K. Isolation, screening and identification of anantagonistic actinomycetes to control *Fusarium* wilt of *Momordica charantia*. *Ying Yong Sheng Tai Xue Bao* **31**, 3869–3879 (2020).
77. Yun, T. et al. Anti-Foc RT4 activity of a newly isolated *Streptomyces* sp. 5-10 from a medicinal plant (*Curculigo capitulate*). *Front. Microbiol.* **11**, 610698 (2021).
78. Chung, Y. et al. Comparative genomics reveals a remarkable biosynthetic potential of the *Streptomyces* phylogenetic lineage associated with rugose-ornamented spores. *Msystems* **6**, e00489–21 (2021).
79. Jiang, M. et al. GdmRIII, a TetR family transcriptional regulator, controls geldanamycin and elaiophylin biosynthesis in *Streptomyces autolyticus* CGMCC0516. *Sci. Rep.* **7**, 4803 (2017).
80. He, W. et al. Crossregulation of rapamycin and elaiophylin biosynthesis by RapH in *Streptomyces rapamycinicus*. *Appl. Microbiol. Biotechnol.* **106**, 2147–2159 (2022).
81. Raaijmakers, J. & Kiers, E. Rewilding plant microbiomes. *Science* **378**, 599–600 (2022).
82. Tsugawa, H. et al. MS-DIAL: data-independent MS/MS deconvolution for comprehensive metabolome analysis. *Nat. Methods* **12**, 523–526 (2015).
83. Love, M. I., Huber, W. & Anders, S. J. Gb Moderated estimation of fold change and dispersion for RNA-seq data with DESeq2. *Genome Biol.* **15**, 1–21 (2014).
84. Raudvere, U. et al. g: Profiler: a web server for functional enrichment analysis and conversions of gene lists (2019 update). *Nucleic Acids Res.* **47**, W191–W198 (2019).
85. Yu, G., Wang, L., Han, Y. & He, Q. clusterProfiler: an R package for comparing biological themes among gene clusters. *OMICS* **16**, 284–287 (2012).
86. Madeira, F. et al. Search and sequence analysis tools services from EMBL-EBI in 2022. *Nucleic Acids Res.* **50**, W276–W279 (2022).
87. Letunic, I. & Bork, P. Interactive Tree Of Life (iTOL) v5: an online tool for phylogenetic tree display and annotation. *Nucleic Acids Res.* **49**, W293–W296 (2021).

Acknowledgements

We acknowledge Dr. Yaojun Tong for the discussions on CRISPR-BEST. We thank the support from Dr. Charlotte Held Gotfredsen (DTU NMR Centre) and Dr. Aaron John Christian Andersen (DTU Metabolomics Core). We acknowledge Dr. Ting Yang and Dr. Qing Liu for advice in the transcriptomics experiment. We acknowledge financial support from Carlsberg Infrastructure (CF20-0177), Novo Nordisk Foundation Proof of Concept (NNF20OC0062267), DTU Enable Program, InnoExplorer Grant, Innovation Fund Denmark, and Danish National Research Foundation (DNRF137) for support towards the Centre for Microbial Secondary Metabolites (CeMiSt). Z.Y. acknowledges funding from the China Scholarship Council (202004910340). T.W. acknowledges funding from the Novo Nordisk Foundation (NNF20CC0035580). Y.Q. thanks for Novo Nordisk Foundation (NNF22OC0079928).

Author contributions

Z.Y. and T.W. designed and carried out genetic experiments and bioinformatic analyses. E.S. isolated the metabolites and characterised the structures; L.D. did structure elucidation, compounds crystallisation, and preliminary plant assays; Z.Y., Y.Q., N.C.K. and E.A. performed the plant and mRNA-seq assays; G.P. and M. A. carried out large scale fermentation and downstream processing; P.H. carried out X-ray crystallography and data analysis. All the authors discussed the results and commented on the manuscript.

Competing interests

A patent related to this research was filed as a PCT application (PCT/EP2022/081635) by Ling Ding on behalf of Technical University of Denmark. All other authors declare no competing interests.

Additional information

Supplementary information The online version contains supplementary material available at https://doi.org/10.1038/s41467-023-43177-3.

Correspondence and requests for materials should be addressed to Ling Ding.

Peer review information *Nature Communications* thanks the anonymous reviewer(s) for their contribution to the peer review of this work. A peer review file is available.

Supplementary Information

Streptomyces alleviate abiotic stress in plant by producing pteridic acids

Zhijie Yang[1], Yijun Qiao[1], Naga Charan Konakalla[2], Emil Strøbech[1], Pernille Harris[3], Gundela Peschel[4], Miriam Agler-Rosenbaum[4], Tilmann Weber[5], Erik Andreasson[2], Ling Ding[1,*]

[1] Department of Biotechnology and Biomedicine, Technical University of Denmark, Søltofts Plads, Building 221, 2800 Kgs. Lyngby, Denmark.

[2] Department of Plant Protection Biology, Swedish University of Agricultural Sciences, Sundsvägen 14, SE-230 53, Alnarp, Sweden.

[3] Department of Chemistry, Technical University of Denmark, Søltofts Plads, Building 206, 2800 Kgs. Lyngby, Denmark.

[4] Leibniz Institute for Natural Product Research and Infection Biology - Hans Knöll Institute (HKI), Beutenbergstr. 11a, 07745 Jena, Germany.

[5] Novo Nordisk Foundation Center for Biosustainability, Technical University of Denmark, Kemitorvet, Building 220, 2800 Kgs. Lyngby, Denmark.

*Corresponding author: Ling Ding lidi@dtu.dk

Table of Contents

Tab. 1. The predicted biosynthetic gene clusters in *S. iranensis*.

Cluster	Type	Position	Most similar known cluster	Similarity
Cluster 1	T1PKS,transAT-PKS	49–114,601	sceliphrolactam	32%
Cluster 2	terpene,NRPS	161,367-220,243	carotenoid	63%
Cluster 3	NRPS	436,587-485,770	coelichelin	100%
Cluster 4	butyrolactone	773,681-782,636	cyphomycin	9%
Cluster 5	phosphonate,acyl_amino_acids, butyrolactone,NRPS-like, T1PKS,hserlactone	837,187-987,392	chlorothricin / deschlorothricin	13%
Cluster 6	T1PKS	1,074,827-1,216,558	azalomycin F3a	100%
Cluster 7	T1PKS	1,388,946-1,573,704	nigericin	100%
Cluster 8	T1PKS	1,677,611-1,756,225	elaiophylin	87%
Cluster 9	redox-cofactor	1,780,894-1,802,958		
Cluster 10	hserlactone	1,920,187-1,940,942	daptomycin	4%
Cluster 11	butyrolactone	1,951,656-1,962,588		
Cluster 12	T1PKS,NRPS	2,141,406-2,193,626	meilingmycin	4%
Cluster 13	NRPS,T3PKS,other	2,252,019-2,351,341	feglymycin	78%
Cluster 14	NRPS,T1PKS	2,405,901-2,618,214	pentamycin	46%
Cluster 15	terpene	2,865,078-2,887,266	hopene	76%
Cluster 16	T1PKS	3,033,413-3,115,318	geldanamycin	34%
Cluster 17	T2PKS	3,184,430-3,254,311	spore pigment	83%
Cluster 18	T1PKS	3,378,842-3,439,037	s56-p1	11%
Cluster 19	RiPP-like	3,492,148-3,502,022		
Cluster 20	siderophore	3,672,342-3,682,811		
Cluster 21	T2PKS	4,017,972-4,090,475	isoindolinomycin	61%
Cluster 22	NRPS-like	4,320,588-4,352,287	echoside A / echoside B / echoside C / echoside D / echoside E	100%
Cluster 23	siderophore	5,114,280-5,125,349	desferrioxamin B	100%
Cluster 24	terpene	6,324,614-6,344,943	geosmin	100%
Cluster 25	ladderane,arylpolyene,NRPS	6,588,275-6,690,850	RP-1776	48%
Cluster 26	NRPS	7,228,322-7,270,720	ochronotic pigment	75%
Cluster 27	Ladderane	7,332,623-7,372,653	atratumycin	34%
Cluster 28	RRE-containing	7,391,754-7,414,213	granaticin	10%
Cluster 29	T1PKS	7,547,548-7,732,661	mediomycin A	68%
Cluster 30	terpene	8,282,077-8,302,096		
Cluster 31	ectoine	8,948,675-8,959,079	ectoine	100%
Cluster 32	siderophore	9,122,543-9,136,295		
Cluster 33	terpene	9,187,376-9,204,614	BE-43547A1 / BE-43547A2 / BE-43547B1 / BE-43547B2 / BE-43547B3 / BE-43547C1 / BE-43547C2	25%
Cluster 34	nucleoside	9,422,403-9,459,458	toyocamycin	40%
Cluster 35	nucleoside,NRPS,T1PKS,NRPS-like	9,564,087-9,711,679	rapamycin	82%
Cluster 36	PKS-like	9,800,077-9,841,105	rustmicin	33%
Cluster 37	terpene	9,891,287-9,911,108	2-methylisoborneol	100%
Cluster 38	terpene	10,356,847-10,375,970	pristinol	100%
Cluster 39	T1PKS,ladderane,arylpolyene	10,470,251-10,521,311	atratumycin	28%

Cluster 40	NRPS-like,T1PKS,transAT-PKS	10,727,870-10,814,731	hygrocin A / hygrocin B	83%
Cluster 41	lanthipeptide-class-ii	10,908,405-10,931,776	reveromycin A	9%
Cluster 42	hglE-KS,T1PKS,RiPP-like	10,960,035-11,021,175		
Cluster 43	T1PKS,NRPS	11,024,823-11,167,452	ambruticin	17%
Cluster 44	terpene	11,218,988-11,239,914	brasilicardin A	30%
Cluster 45	terpene	11,368,510-11,389,418		
Cluster 46	NRPS-like,T1PKS	11,474,253-11,522,775	niphimycins C-E	9%
Cluster 47	betalactone	11,718,451-11,747,262	Sch-47554 / Sch-47555	7%

Tab. 2. The annotation of pteridic acids core biosynthetic genes in *S. iranensis*.

ORF	Size[a]	Proposed functions	SI/ID[b]	Protein homologue and origin
Pta5	1041	3-oxoacyl-ACP synthase III	98/97	WP_210951575.1, *Streptomyces* sp. MK37H
pta4	572	3-hydroxyacyl-CoA dehydrogenase	98/97	WP_020866330.1, *Streptomyces rapamycinicus*
pta3	958	LuxR family transcriptional regulator	99/99	WP_020866329.1, *Streptomyces rapamycinicus*
pta2	316	glucose-1-phosphate thymidylyltransferase	99/99	RLV74943.1, *Streptomyces rapamycinicus* NRRL 5491
pta1	324	TDP glucose 4,6 dehydratase	98/98	WP_214665150.1, *Streptomyces javensis*
ptaA	4535	Type I PKS	90/88	WP_214609358.1, *Streptomyces malaysiensis*
ptaB	1746	Type I PKS	91/89	WP_037957959.1, *Streptomyces* sp. PRh5
ptaC	1655	Type I PKS	95/94	WP_138910801.1, *Streptomyces* sp. DASNCL29
ptaD	3395	Type I PKS	96/95	WP_020866322.1, Streptomyces rapamycinicus
ptaE	2112	Type I PKS	95/95	WP_201848053.1, *Streptomyces* sp. 110
*pta1**	261	Thioesterase	97/95	GDY58888.1, *Streptomyces violaceusniger*
*pta2**	417	Glycosyltransferase	99/98	MBP8534388.1, *Streptomyces* sp. MK37H
*pta3**	196	dTDP-4-dehydrorhamnose 3,5-epimerase	97/97	WP_210946413.1, *Streptomyces* sp. MK37H
*pta4**	304	Exporter (membrane domain)	100/99	WP_138910796.1, *Streptomyces* sp. DASNCL29
*pta5**	245	Exporter (ATPase domain)	99/99	WP_020866316.1, *Streptomyces rapamycinicus*
*pta6**	420	Two-component regulator (sensor/kinase domain)	97/97	WP_199334865.1, *Streptomyces* sp. GMR22
*pta7**	223	Two-component regulator (effector domain)	98/98	WP_138910795.1, *Streptomyces* sp. DASNCL29
*pta8**	321	NAD(P)-dependent oxidoreductase	96/96	WP_164428021.1, *Streptomyces rhizosphaericus*
*pta9**	328	aldo/keto reductase	98/98	WP_191066610.1, *Streptomyces* sp. 5-10
*pta10**	469	NDP-hexose 2,3 dehydratase	97/95	GDY58900.1, *Streptomyces violaceusniger*
*pta11**	446	Crotonyl-CoA reductase	99/99	WP_020866310.1, *Streptomyces rapamycinicus*

a, The size of amino acids; b, similarity-identity ratio.

Tab. 3. Alignment of conserved motifs in the active site of AT domains.

domain name	specificity	198	199	200	201
ave_AT5	Malonyl-CoA	H	A	F	H
nid_AT3	Malonyl-CoA	H	A	F	H
epo_AT2	Malonyl-CoA	H	A	F	H
amp_AT18	Malonyl-CoA	H	A	F	H
rif_AT2	Malonyl-CoA	H	A	F	H
pta_LD	Malonyl-CoA	H	A	F	H
pta_AT2	Malonyl-CoA	H	A	F	H
pta_AT6	Malonyl-CoA	H	A	F	H
pta_AT7	Malonyl-CoA	I	A	A	H
ave_AT1	Methylmalony-CoA	Y	A	S	H
nid_AT4	Methylmalony-CoA	Y	A	S	H
ery_AT4	Methylmalony-CoA	Y	A	S	H
amp_AT2	Methylmalony-CoA	Y	A	S	H
rif_AT7	Methylmalony-CoA	Y	A	S	H
pta_AT3	Methylmalony-CoA	Y	A	S	H
pta_AT4	Methylmalony-CoA	Y	A	S	H
pta_AT5	Methylmalony-CoA	Y	A	S	H
nid_AT5	Ethylmalonyl-CoA	T	A	G	H
tyl_AT5	Ethylmalonyl-CoA	T	A	G	H
pta_AT1	Ethylmalonyl-CoA	T	A	G	H
ery_LD	Propionyl-CoA	M	A	A	H
meg_LD	Propionyl-CoA	M	A	A	H
epo_AT3	Flexible	H	A	S	H

* Abbreviations: LD, loading module; ave, avermectin; nid, niddamycin; epo, epothilone; amp, amphotericin; rif, rifamycin; ery, erythromycin; tyl, tylactone; meg, megalomicin; pta, pteridic acids.

Tab. 4. The *Streptomyces* strains that can produce elaiophylin, pteridic acids, or harbor *pta* BGC.

NO	Strain name	Geographic location	Source	Reference/Assembly
1	*Streptomyces iranensis* HM 35	Isfahan City, Iran	rhizosphere	GCA_000938975.1
2	*Streptomyces* sp. 219807	Sanya, Hainan, China	mangrove soil	1
3	*Streptomyces* sp. SCSGAA 0027	South China Sea, China	gorgonian-associated	2
4	*Streptomyces* sp. 7-145	Heishijiao Bay, Dalian, China	marine-sediment	3
5	*Streptomyces melanosporofaciens*	Italy	soil	4
6	*Streptomyces autolyticus* CGMCC 0516	Yunnan, China	soil	5
7	*Streptomyces* sp. DSM 3816	Kypcerissia, Greece	soil	6
8	*Streptomyces* sp. BCC 71188	Nakhon Si Thammarat Province, Thailand	soil	7
9	*Streptomyces* sp. BCC 72023	Chumphon province, Thailand	plant-associated	8
10	*Streptomyces* sp. BS 1261	New Zealand	soil	9
11	*Streptomyces* sp. ICBB 9297	Jatiroto, East Java, Indonesia	soil	10
12	*Streptomyces* sp. SNA-4606	Towada-shi, Aomori Prefecture, Japan	soil	11
13	*Streptomyces* sp. MCY-846	cheju-island, Korea	soil	12
14	*Streptomyees albiflaviniger* SCSIO ZJ28	South China Sea, China	marine-sediment	13
15	*Streptomyces* sp. USC-16018	Hastings Point, NSW, Australia	marine	14
16	*Streptomyces* sp. SPMA113	Prajinburi Province, Thailand	soil	15
17	*Streptomyces* sp. LZ35	Ji'mei, Xia'men, China	soil	16
18	*Streptomyces malaysiensis* DSM 4137	Germany	soil	17
19	*Streptomyces* sp. BCa1	Borra Caves, India	soil	18
20	*Streptomyces* sp. IFM11958	Sakuragi cemetery, Chiba city, Japan	soil	19
21	*Streptomyces malaysiensis* OUCMDZ-2167	South China Sea, China	marine	20
22	*Streptomyces* sp. 11-1-2	Newfoundland, Canada	plant-associated	21
23	*Streptomyces* sp. HNM0561	Hainan, China	marine-sediment	22
24	*Streptomyces* sp. GMR 22	Wanagama Forest, Indonesia	soil	23
25	*Streptomyces* sp. NTK 935	Canary Basin	marine sediment	24
26	*Streptomyces* sp. NTK 937	Canary Basin	marine sediment	24
27	*Streptomyces* sp. RJA 2928	Papua New Guinea	marine sediment	25
28	*Streptomyces rapamycinicus* NRRL 5491	Easter island, Fiji	soil	26
29	*Streptomyces pseudouerticillus* YN 17707	Xishuangbanna, Yunnan, China	soil	27
30	*Streptomyces* sp. SCSIO ZS0520	Okinawa, Japan	marine sediment	28
31	*Streptomyces hygroscopicus* NND-52	Suqian, Jiangsu, China	soil	29
32	*Streptomyces* hygroscopicus NO.662	Sapporo-city, Hokkaido, Japan	soil	30
33	*Streptomyces hygroscopicus* TP-A0451	Toyama, Japan	plant-associated	31
34	*Streptomyces hygroscopicus* CH-7	Vojvodina, Serbia	soil	32
35	*Streptomyces hygroscopicus* 17997	Yunnan, China	soil	33
36	*Streptomyces hygroscopicus* ACTMS-9H	Amazon, Brazil	rhizosphere	34
37	*Streptomyces hygroscopicus* XM 201	Xiamen, Fujian, China	soil	35
38	*Streptomyces yatensis* DSM 41771	New Caledonia	Ultramafic soil	36
39	*Streptomyces solisilvae* HNM0141	Bawangling, Hainan, China	soil	37
40	*Streptomyces* sp. NA02950	Hainan, China	marine-sediment	38

41	*Streptomyces* sp. PRh5	Dongxiang, China	plant-associated	39
42	*Streptomyces albus* DSM 41398	Fuji City, Shizuoka Pref, Japan	soil	GCA_000827005.1
43	*Streptomyces samsunensis* SA31	Songkhla, Thailand	soil	GCA_013345665.1
44	*Streptomyces* sp. MK37H	Antalya, Turkey	soil	GCA_018035285.1
45	*Streptomyces* sp. 4503	Guangxi, China	mangrove sediment	GCA_018883605.1
46	*Streptomyces* sp. t39	Austin, Texas, USA	soil	GCA_008042045.1
47	*Streptomyces* sp. 5-10	Hainan, China	plant-associated	GCA_014712245.1
48	*Streptomyces antioxidans* MUSC164	Malaysia	mangrove	GCA_000968685.2
49	*Streptomyces malaysiensis* F913	Chongqing, China	soil	GCA_002891865.1
50	*Streptomyces* sp. DASNCL29	Unkeshwar, India	soil	GCA_005938145.1
51	*Streptomyces* sp. WAC05858	Germeny	soil	GCA_003949695.1
52	*Streptomyces rhizosphaericus* 0250	Taian, China	soil	GCA_010892295.1
53	*Streptomyces* sp. NEAU-YJ-81	Harbin, China	soil	GCA_017592595.1
54	*Streptomyces rhizosphaericus* NRRL B-24304	Indonesia	rhizosphere	GCA_002155885.1
55	*Streptomyces malaysiensis* TY049-057	Bidor Perak, Malaysia	soil	GCA_008033485.1
56	*Streptomyces malaysiensis* DSM 14702	Germany	soil	GCA_011800555.1
57	*Streptomyces cangkringensis* DSM 41769	South Korea	-	GCA_019059395.1
58	*Streptomyces endocoffeicus* CA3R110	Lampang, Thailand	plant-associated	GCA_016741935.1
59	*Streptomyces indonesiensis* DSM 41759	Yogyakarta, Indonesia	rhizosphere	GCA_018138705.1
60	*Streptomyces rhizosphaericus* DSM 41760	Yogyakarta, Indonesia	rhizosphere	GCA_017942185.1
61	*Streptomyces asiaticus* DSM 41761	Yogyakarta, Indonesia	rhizosphere	GCA_018138715.1
62	*Streptomyces* sp. RCU064	Nong Jum Rung, Thailand	Peat swamp forest soil	GCA_024505145.1
63	*Streptomyces violaceusniger* Tu 4113	-	soil	GCA_000147815.3
64	*Streptomyces antimycoticus* NBRC 100767	-	soil	GCA_009936315.1
65	*Streptomyces antimycoticus* NBRC 12839	-	soil	GCA_005405925.1
66	*Streptomyces* sp. AgN23	-	rhizosphere	GCA_001598115.2
67	*Streptomyces* sp. NRRL 30748	-	soil	39
68	*Streptomyces* sp. M56	-	termite-associated	40
69	*Streptomyces* sp. CWJ-256	-	plant-associated	41
70	*Streptomyces* sp. 92JF-1	-	marine	42
71	*Streptomyces* sp. KIB-H869	-	plant-associated	43
72	*Streptomyces hygroscopicus* MSU-625	-	soil	44
73	*Streptomyces hygroscopicus* MSU-616	-	soil	45
74	*Streptomyces hygroscopicus* OUPS-N92	-	marine	46
75	*Streptomyces* sp. CBR53	-	-	47
76	*Streptomyces violaceusniger* NBRC 13459	-	-	GCA_005405945.1
77	*Streptomyces violaceusniger* NRRL F-8817	-	-	GCA_001509775.1
78	*Streptomyces* sp. HKI-0113	-	-	48
79	*Streptomyces* sp. HKI-0114	-	-	48
80	*Streptomyces* sp. 57-13	-	-	49
81	*Streptomyces javensis*	-	-	GCA_016103505.1

"-": information missing.

Tab. 5. Summary of strains and plasmids used in this study.

Strains	**Description**	**Source/[Ref]**
One Shot™ Mach1™ T1 Phage-Resistant Chemically Competent *E. coli*	For routine plasmids maintenance and cloning	Thermo Fisher Scientific
E. coli ET12567/pUZ8002	For conjugating plasmids into *Streptomyces*	[50]
S. iranensis	Wild-type strain	DSMZ
S. iranensis/Δ*ptaA*	Δ*ptaA* mutant strain	In this work
S. iranensis/Δ*ptaA*/1J23	Complementation strain of Δ*ptaA* mutant	In this work
S. iranensis/Δ*ptaA*/6M10	Complementation strain of Δ*ptaA* mutant	In this work
S. iranensis/M2089I + E2090K + D2091N	TE domain mutant strain	In this work
S. rapamycinicus NRRL 5491	Wild-type strain	DSMZ
S. violaceusniger Tu 4113	Wild-type strain	DSMZ
S. albus DSM 41398	Wild-type strain	DSMZ
Plasmids		
pCRISPR-cBEST	For C to T base editing	[51]
pCRISPR-cBEST/Δ*ptaA*	Modified plasmid for inactivation of *ptaA*	In this work
pCRISPR-cBEST/ M2089I + E2090K + D2091N	Modified plasmid for site-specific mutation of TE domain	In this work
pESCA13/1J23	BAC for complementation	In this work
pESCA13/6M10	BAC for complementation	In this work

Tab. 6. ^{1}H (800 MHz) NMR data for **1**–**2** (in MeOD).

position	Δ_H (J in Hz)	
	1	**2**
1	-	-
2	5.90 (d, 15.4)	5.97 (d, 15.1)
3	7.33 (dd, 15.4, 11.1)	7.16 (dd, 15.1, 10.9)
4	6.26 (dd, 15.2, 10.8)	6.25 (dd, 15.1, 10.9)
5	6.13 (dd, 15.3, 8.8)	6.07 (dd, 15.1, 8.6)
6	2.48 (m)	2.49 (m)
7	3.85 (dd, 10.2, 2.2)	3.32 (m)
8	2.01 (m)	2.02 (m)
9	3.69 (not determined)	3.56 (dd, 11.5, 4.7)
10	1.61 (m)	1.69 (m)
11	-	-
12	2.29 (dd, 14.9, 6.1), 1.64 (dd,	2.19 (dd, 13.1, 4.3)
	14.9, 1.9)	1.32 (dd, 13.2, 11.2)
13	3.59 (m)	3.66 (td, 10.8, 4.3)
14	1.49 (m)	1.02 (m)
15	3.43 (m)	3.88 (m)
16	1.21 (d, 6.1)	1.14 (d, 6.2)
17	1.01 (d, 6.8)	1.02 (d, 6.8)
18	0.91 (d, 7.0)	0.95 (d, 6.9)
19	0.96 (d, 6.8)	0.98 (d, 6.8)
20	1.52 (m), 1.21 (m)	1.60 (m), 1.44 (m)
21	0.93 (t, 7.3)	0.82 (t, 7.6)

Tab. 7. ^{13}C (200 MHz) NMR data for **1**–**2** (in MeOD).

position	Δ_C, type	
	1	**2**
1	168.7	170.2
2	120.6	122.9
3	146.7	148.1
4	129.6	129.6
5	151.0	148.1
6	40.4	40.5
7	75.5	78.0
8	37.5	38.0
9	70.3	74.7
10	42.2	42.1
11	103.2	103.2
12	37.4	33.8
13	70.1	66.3
14	51.3	52.2
15	72.8	66.3
16	20.9	20.4
17	16.0	15.9
18	5.0	5.3
19	12.1	12.7
20	24.8	19.7
21	10.1	10.5

Tab. 8. Summary of primers used in this study.

Primer name	Sequence (5' → 3')	Description
Del-*ptaA*	CGGTTGGTAGGATCGACGGCGCACCCAGGC GGTATGCGTAGTTTTAGAGCTAGAAATAGC	Inactivation of *ptaA*, the base marked in red is sgRNA sequence
Mut-*ptaE*	CCGGTTGGTAGGATCGACGGGGTCCTCCAT CATGGTGAAGGTTTTAGAGCTAGAAATAGC	Site-directed mutagenesis of TE domain in *ptaE*, the base marked in red is sgRNA sequence
ID-sgRNA-F	TGTGTGGAATTGTGAGCGGATA	Forward primer for screening plasmid
ID-sgRNA-R	CCCATTCAAGAACAGCAAGCA	Reverse primer for screening plasmid
ID-*ptaA*-F	TTGCACAGCTCGACGGACAT	Forward primer for screening *ptaA* mutants
ID-*ptaA*-R	GTGTCACCCGCTTTGTCGA	Reverse primer for screening *ptaA* mutants
ID-*ptaE*-F	CAACGCCATGATCGTCGTTC	Forward primer for screening TE domain mutants
ID-*ptaE*-R	CGTTCGAGACCGGGAAATG	Reverse primer for screening TE domain mutants
ID-1J23-right-F	GTCGACATGGCTTGCCTC	Forward primer for validating the right flank of *S. iranensis*/Δ*ptaA*/ 1J23
ID-1J23-right-R	ATCCGTCTCGACTCCGG	Reverse primer for validating the right flank of *S. iranensis*/Δ*ptaA*/ 1J23
ID-1J23-left-F	AGCAGAAGGTAGGGCAG	Forward primer for validating the left flank of *S. iranensis*/Δ*ptaA*/ 1J23
ID-1J23-left-R	GAGGAGACTTCTGCCATGTC	Reverse primer for validating the left flank of *S. iranensis*/Δ*ptaA*/ 1J23
ID-6M10-right-F	GATCTGCTGCTGTTCACGG	Forward primer for validating the right flank of *S. iranensis*/Δ*ptaA*/ 6M10
ID-6M10-right-R	CCGAGCAGATCCGAGATG	Reverse primer for validating the right flank of *S. iranensis*/Δ*ptaA*/ 6M10
ID-6M10-left-F	GAGCACCATCAGCAGGCG	Forward primer for validating the left flank of *S. iranensis*/Δ*ptaA*/ 6M10
ID-6M10-left-R	CATGATGTCCGTGTCGCTC	Reverse primer for validating the left flank of *S. iranensis*/Δ*ptaA*/ 6M10

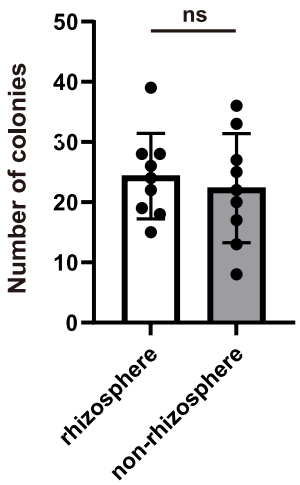

Fig. 1. Enrichment evaluation of *S. iranensis* in rhizosphere soil. Statistical significance was assessed by the unpaired T-test. Source data are provided as a Source Data file.

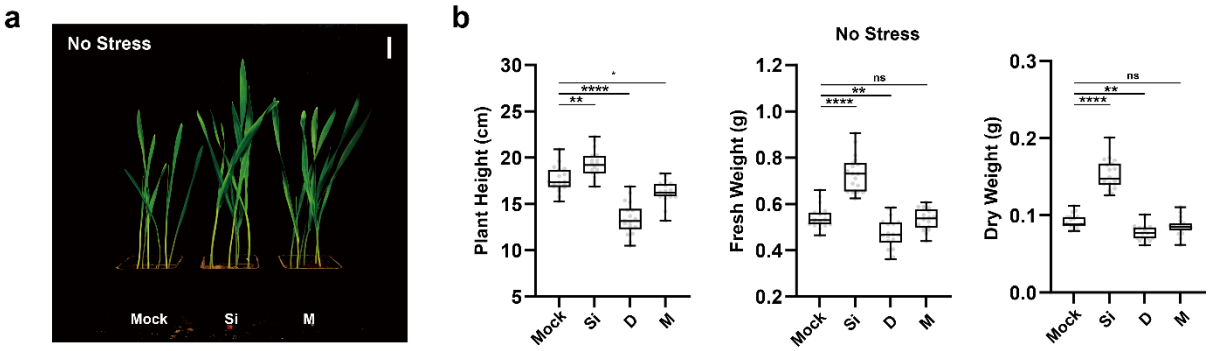

Fig. 2. Barley experiments of *S. iranensis* and *S. iranensis*/Δ*ptaA* treatment under non-stress condition. ***a***, *S. iranensis* and its plant growth-promoting activity on barley seedlings growth (bars=2 cm); ***b***, the box-plots depict the plant height, fresh weight and dry weight of barley seedlings growing on non-stress condition (data is mean ± SD, n =18); Abbreviation: *Mock*, control; *Si*, treatment of *S. iranensis* culture broth; *D*, treatment of *S. iranensis*/Δ*ptaA* culture broth; *M*, treatment of blank medium (ISP2). Statistical significance was assessed by one-way ANOVA with post hoc Dunnett's multiple comparisons test. Asterisks indicate the level of statistical significance: $^{*}p < 0.05$, $^{**}p < 0.01$, $^{***}p < 0.001$ and $^{****}p < 0.0001$. All box plots with center lines showing the medians, boxes indicating the interquartile range, and whiskers indicating a range of minimum to maximum data beyond the box. Source data are provided as a Source Data file.

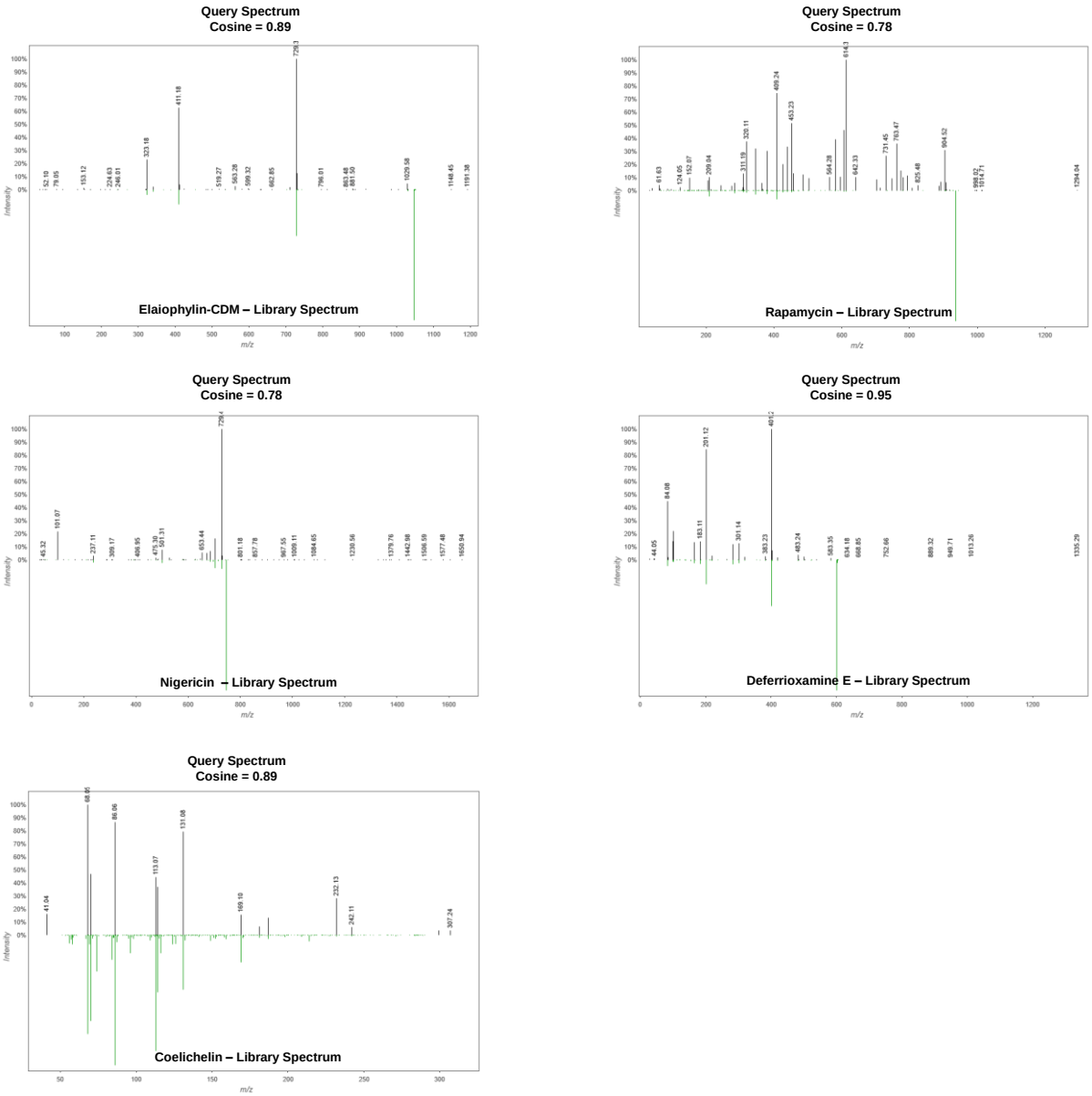

Fig. 3. Mirror plots comparing spectra from known metabolites from *S. iranensis* to standard spectra deposited in GNPS. In the upper part of the plot (black lines) is represented the MS spectra of the candidate feature and in the lower part (green lines) is the MS spectra of the standard compound. Mirror plots have been generated using https://metabolomics-usi.ucsd.edu/.

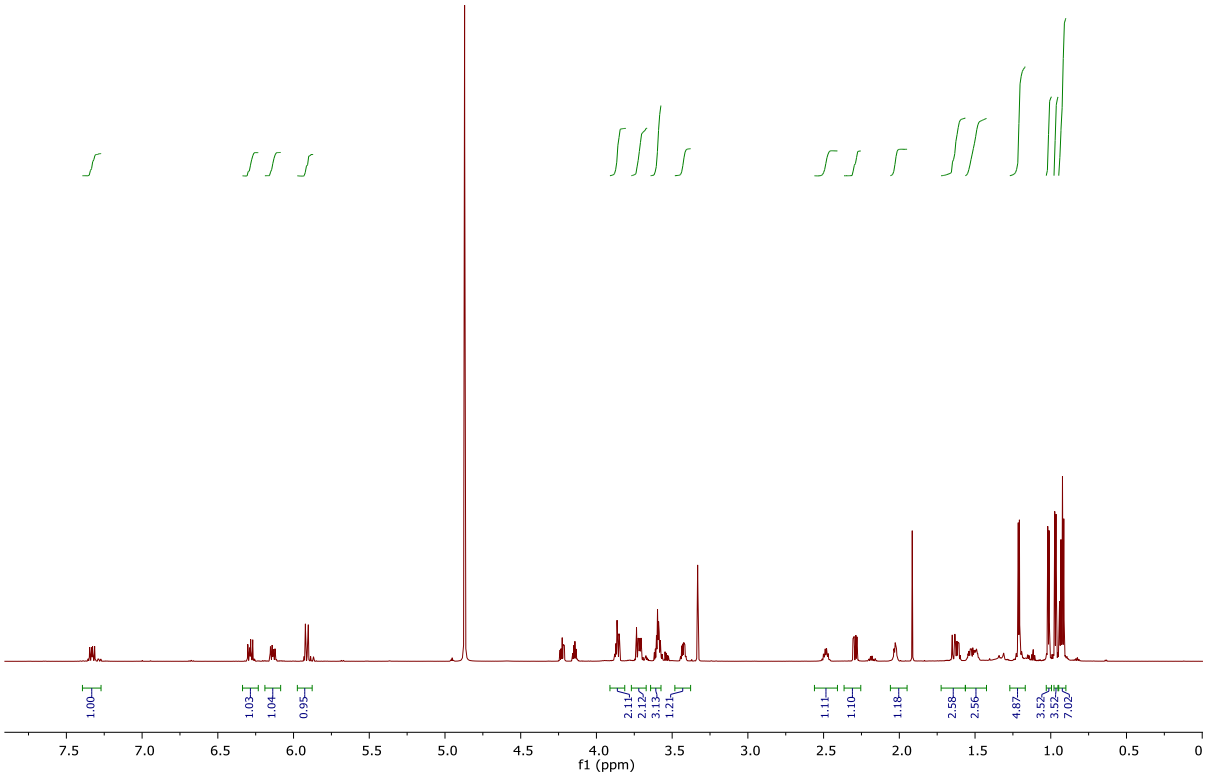

Fig. 4. ^{1}H NMR spectrum of **1.**

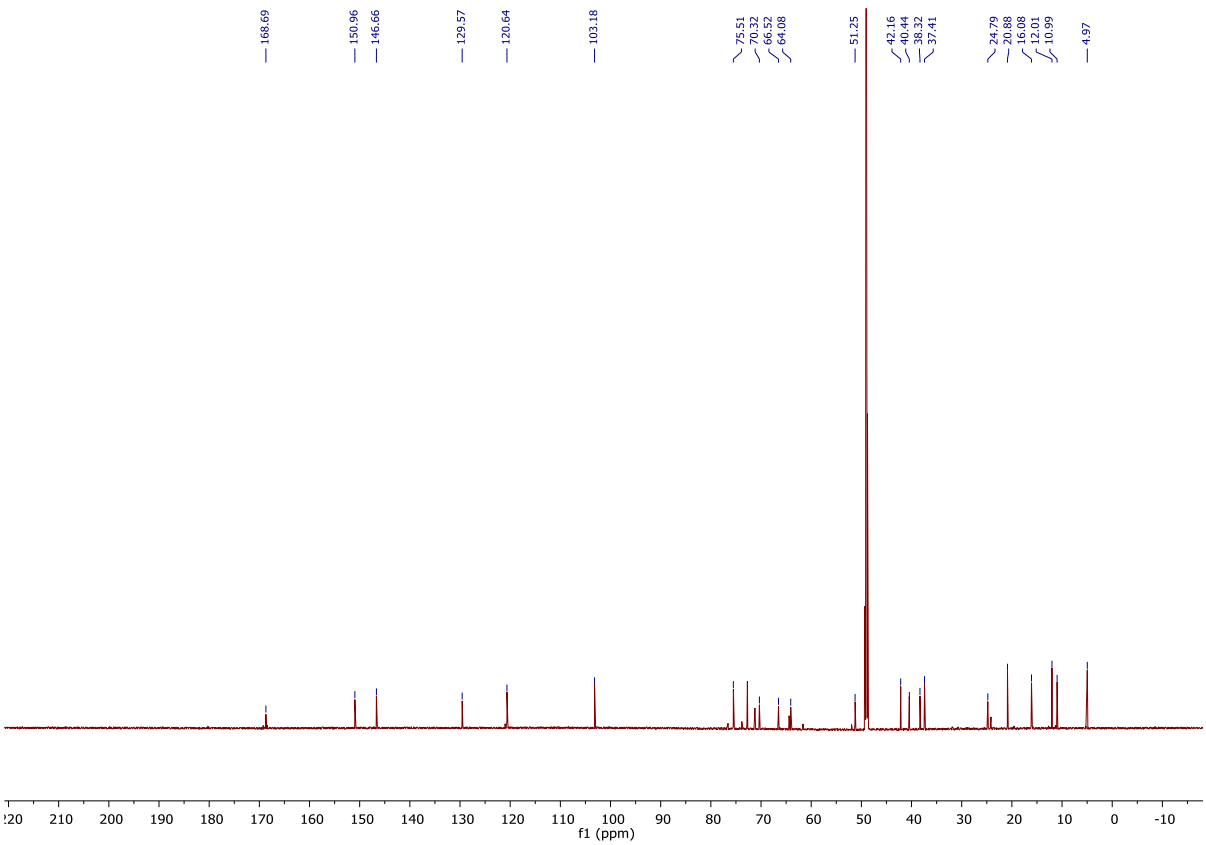

Fig. 5. ^{13}C NMR spectrum of **1.**

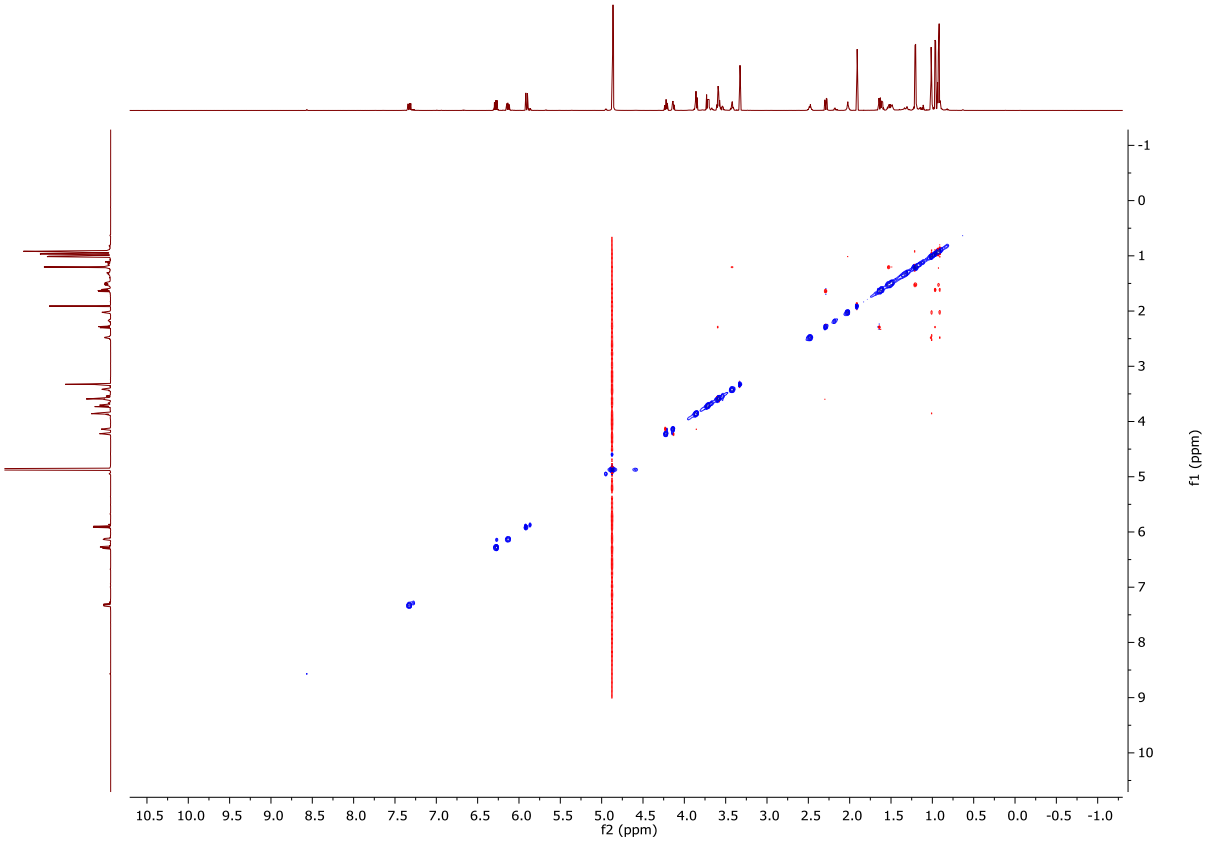

Fig. 6. NOESY spectrum of **1**.

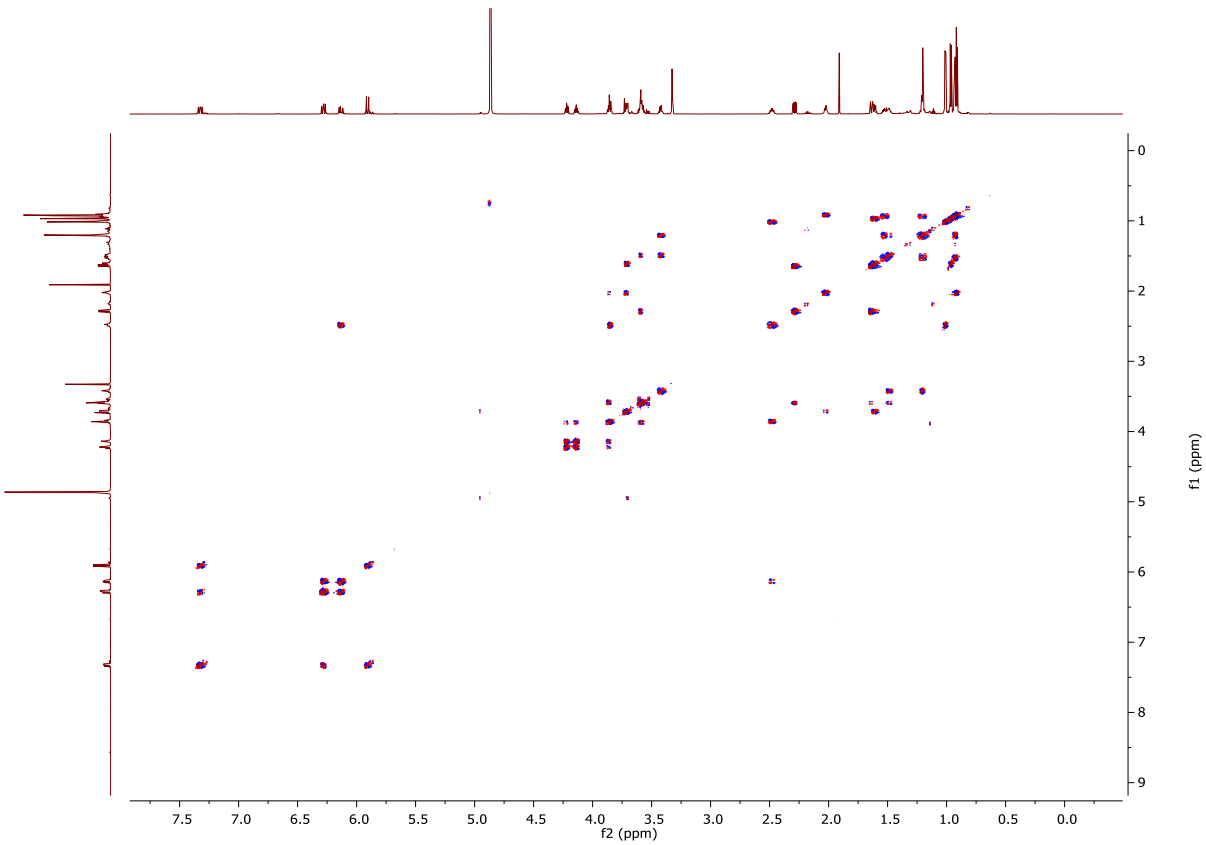

Fig. 7. COSY spectrum of **1**.

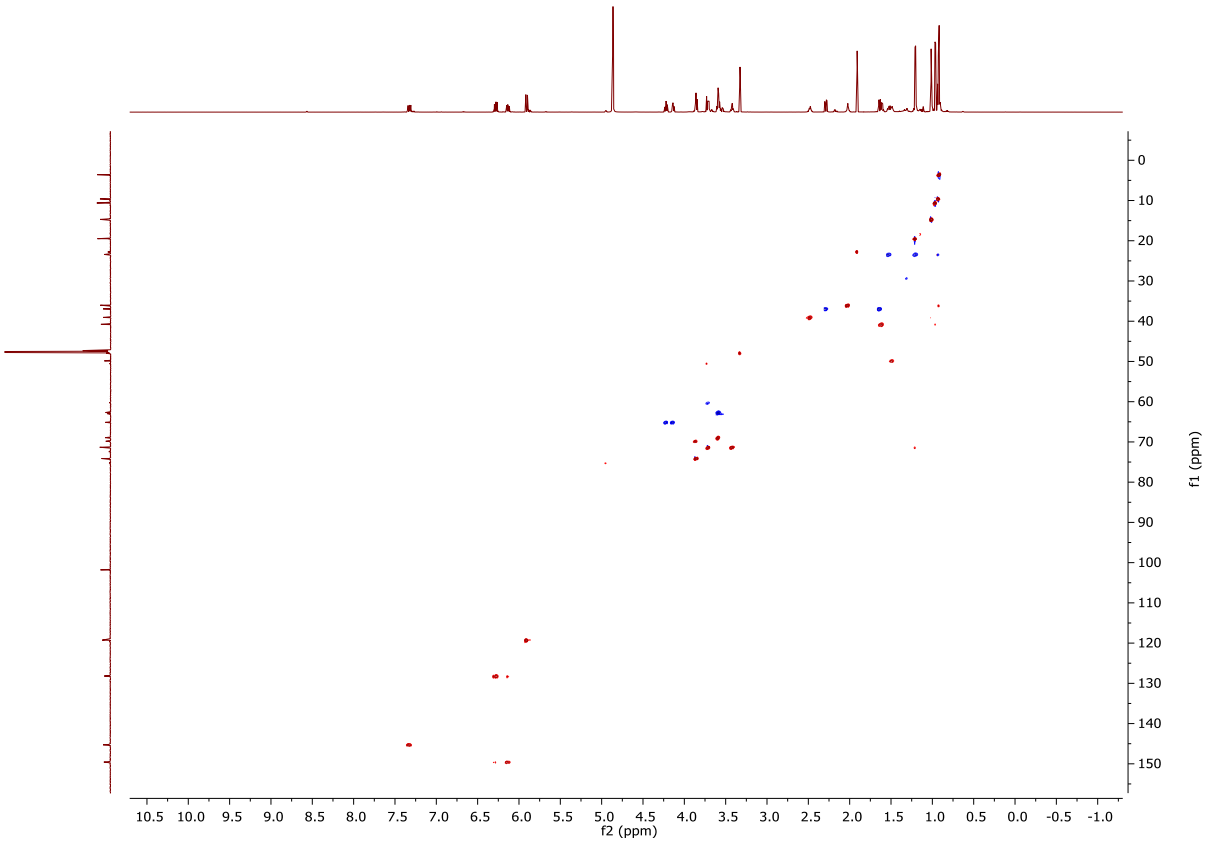

Fig. 8. HSQC spectrum of **1**.

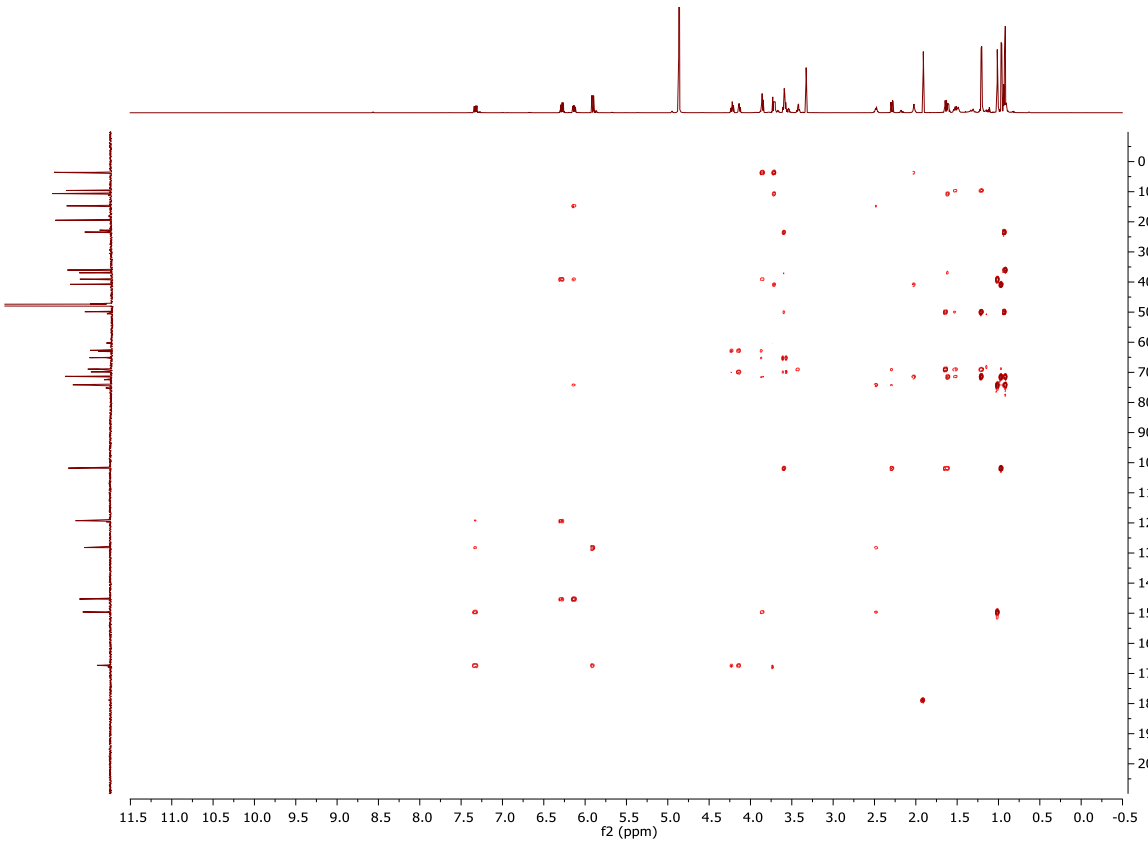

Fig. 9. HMBC spectrum of **1**.

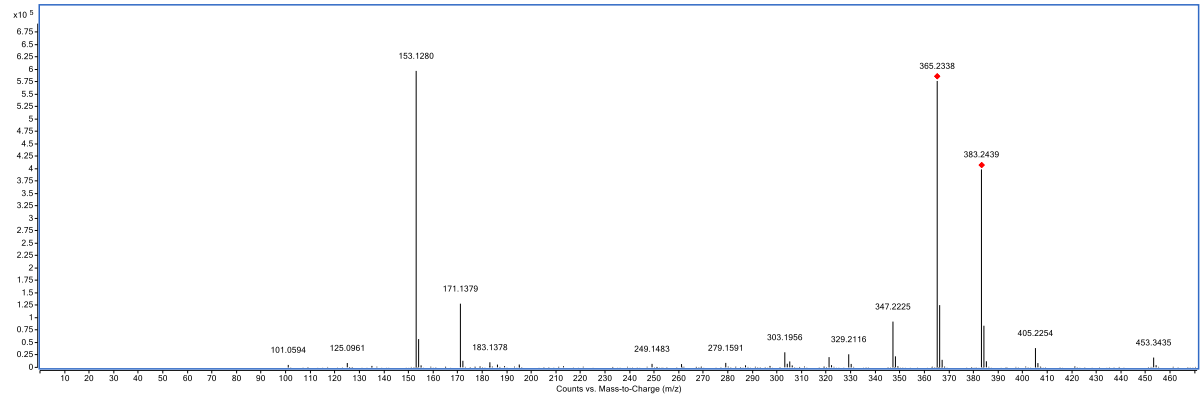

Fig. 10. Mass spectrum of **1**. Its formula of $C_{21}H_{34}O_6$ was deduced by *m/z* 383.2439 $[M+H]^+$ (calculated for 383.2428, Δ 2.84 ppm).

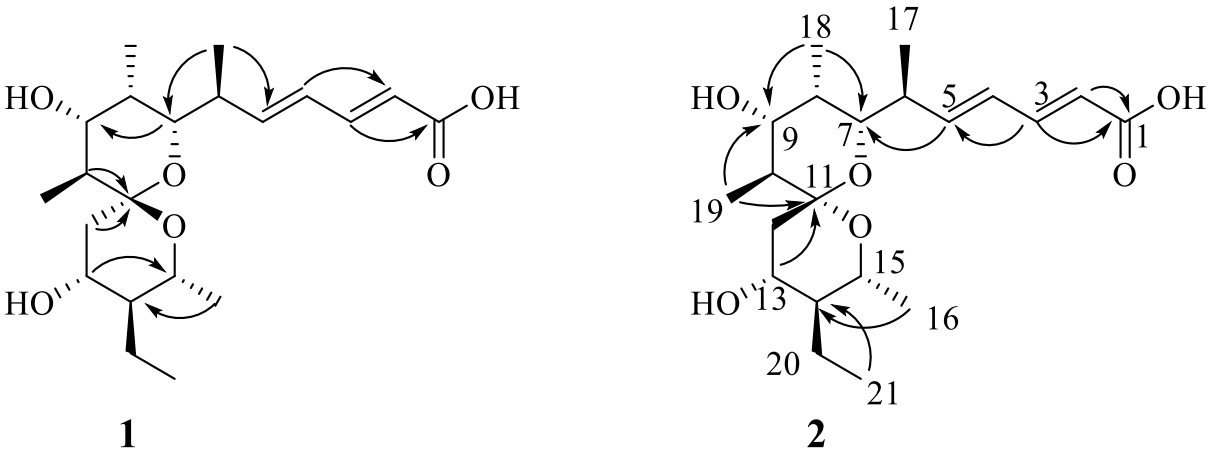

Fig. 11. Selected HMBC correlations for **1** and **2**.

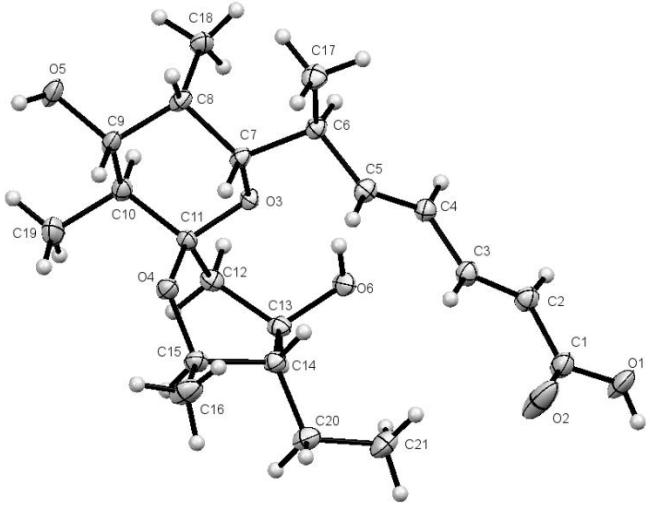

Fig. 12. Crystal structure of **1**. ORTEP diagram showing the atom-numbering scheme and solid-state conformation of **1**.

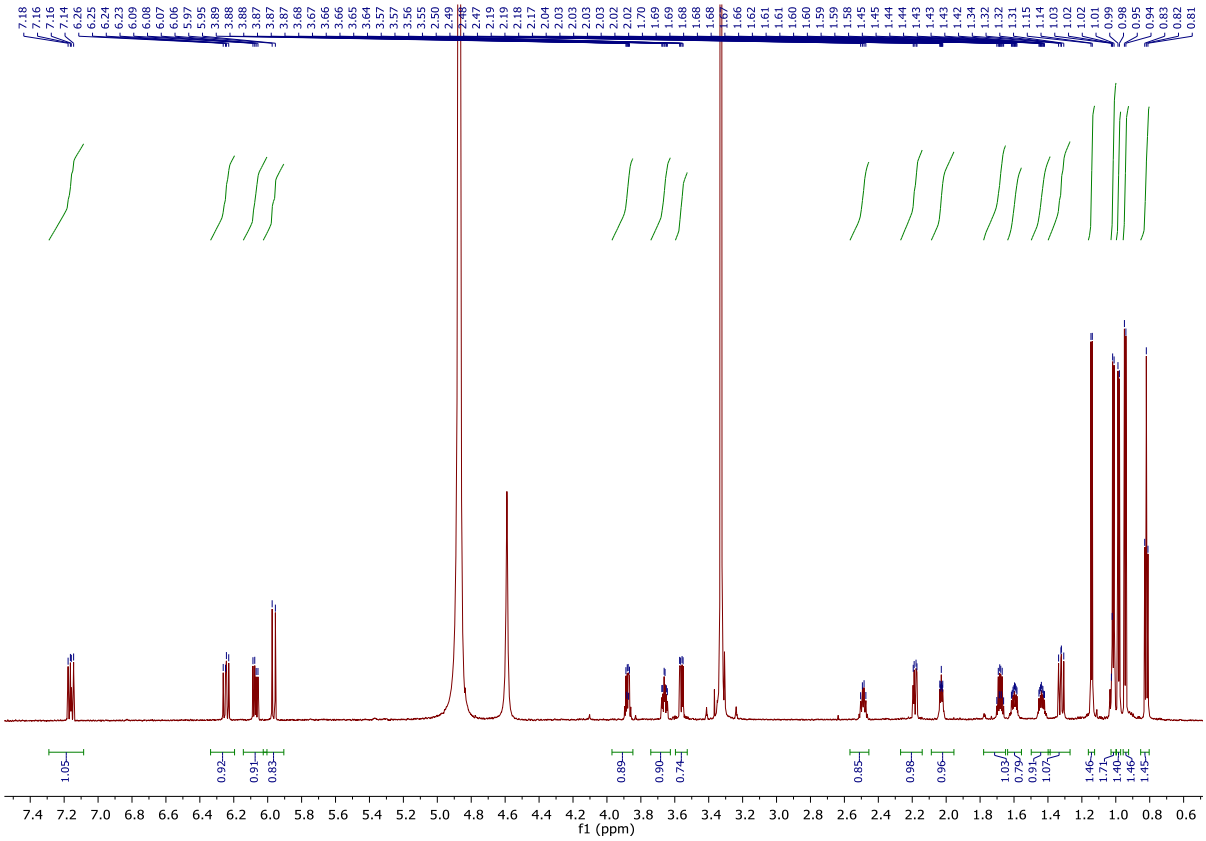

Fig. 13. ^{1}H NMR spectrum of **2**.

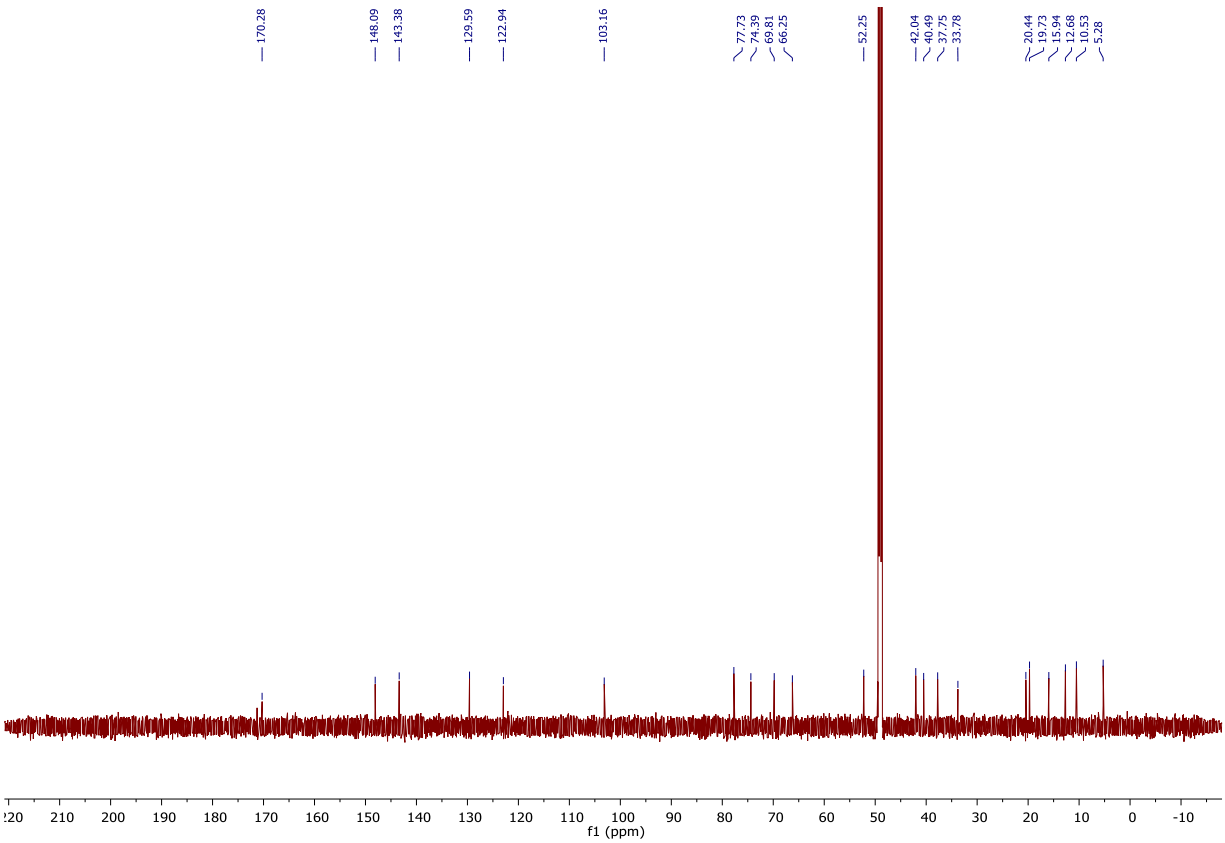

Fig. 14. ^{13}C NMR spectrum of **2**.

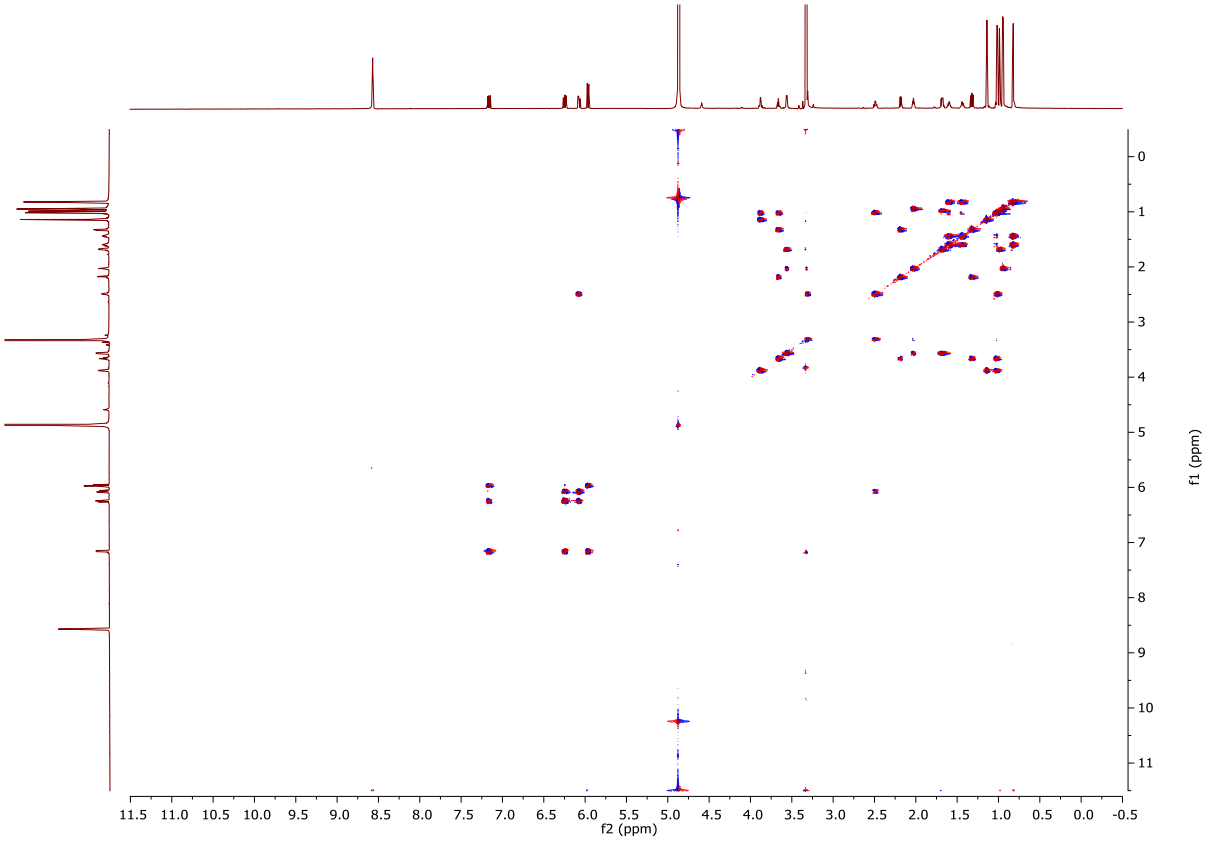

Fig. 15. COSY spectrum of **2**.

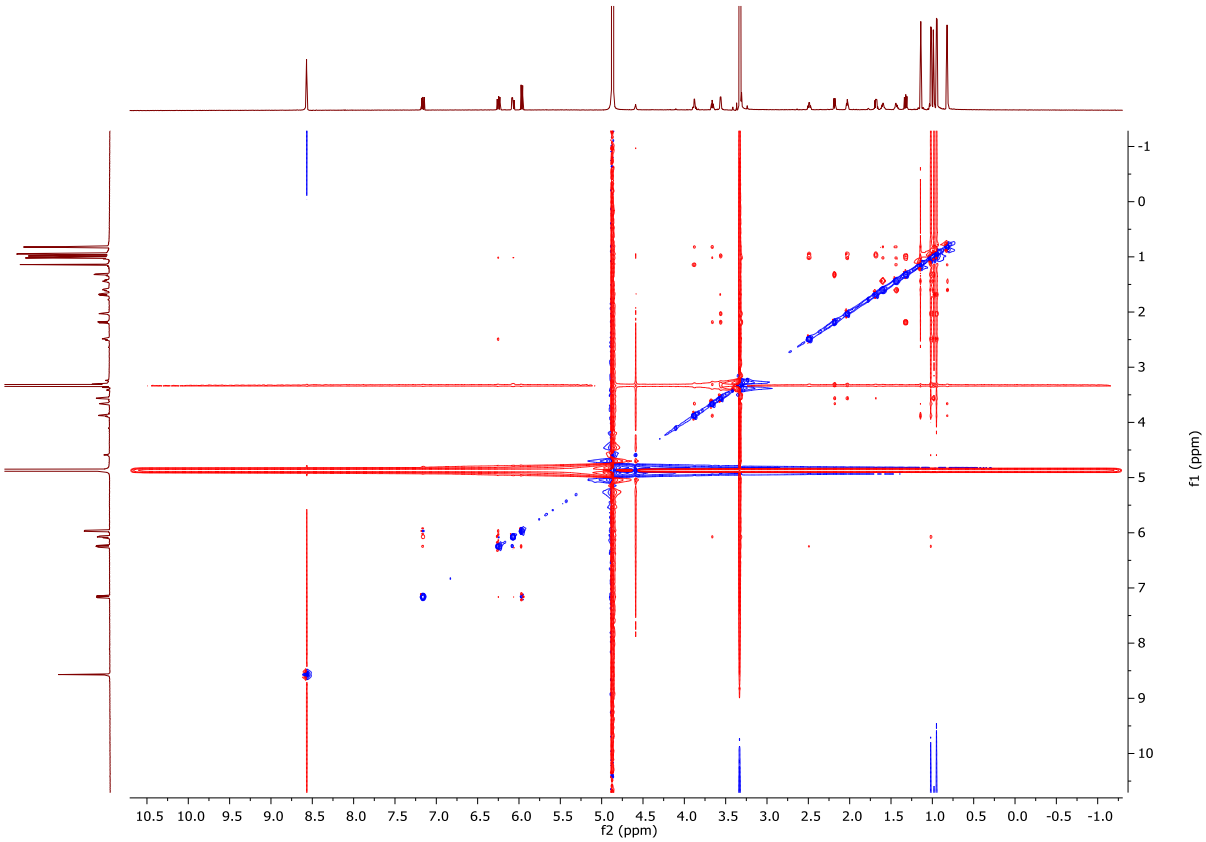

Fig. 16. NOESY spectrum of **2**.

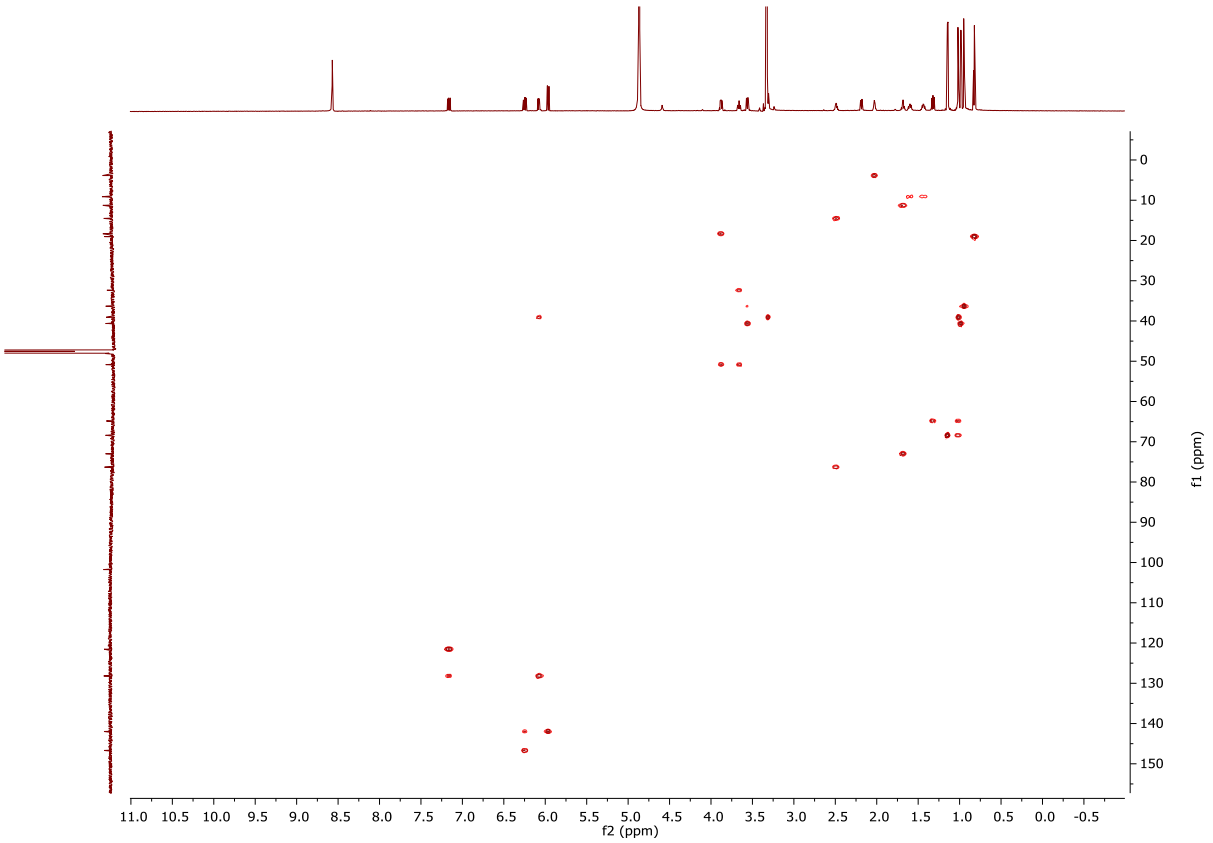

Fig. 17. H2BC spectrum of compound **2**.

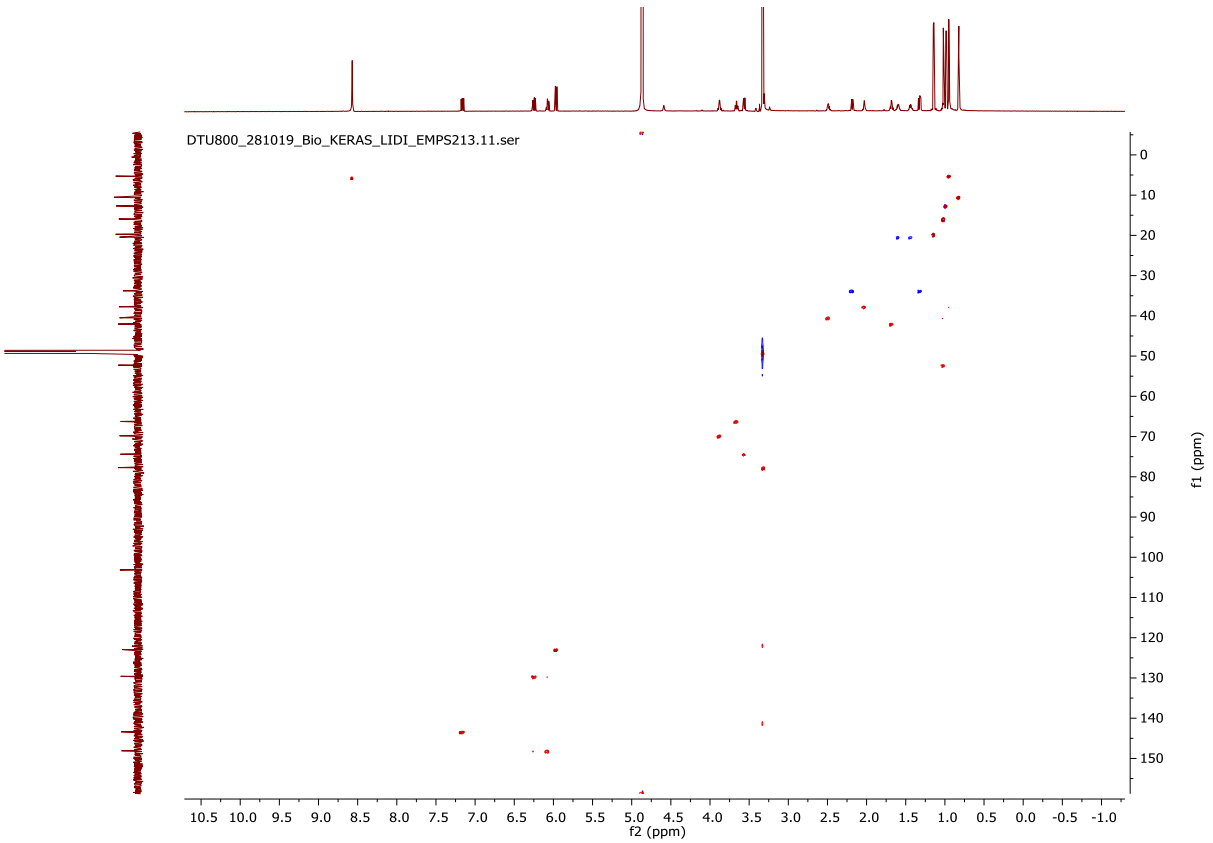

Fig. 18. HSQC spectrum of **2**.

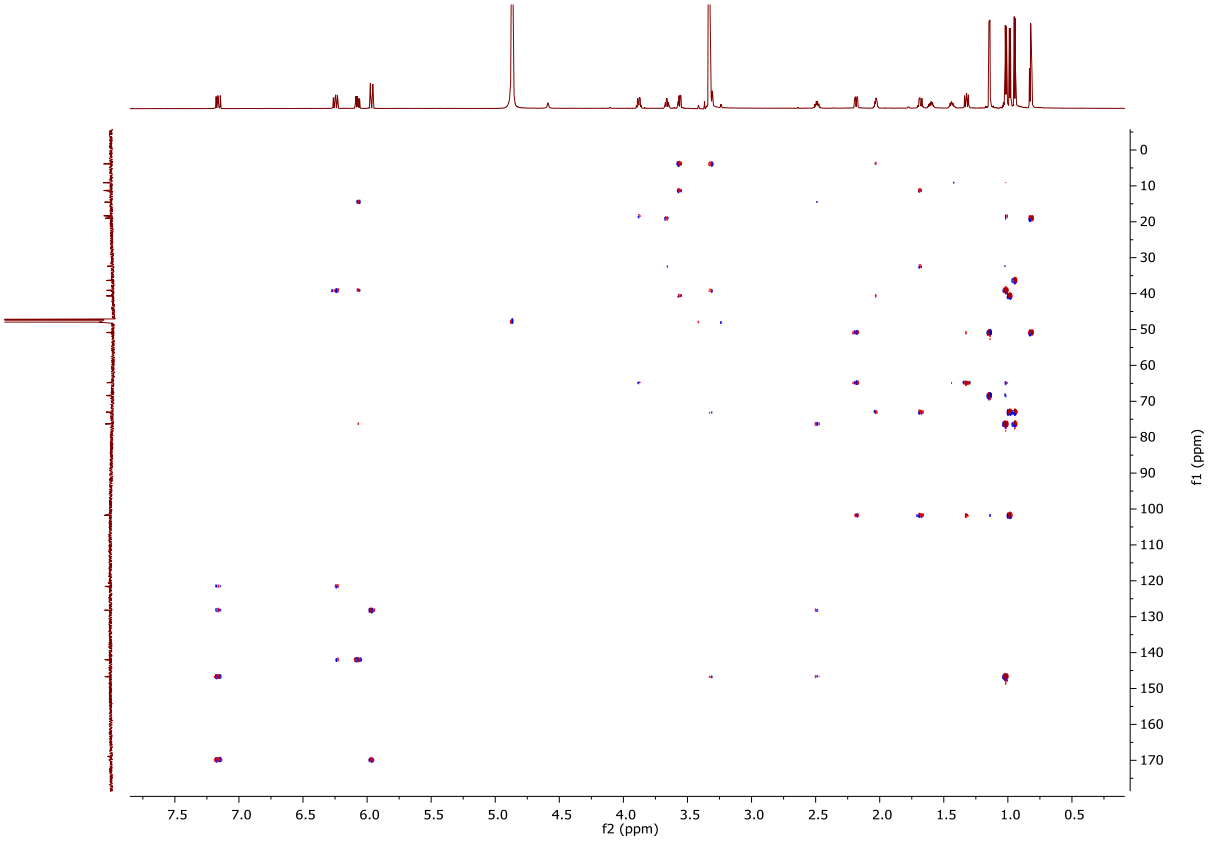

Fig. 19. HMBC spectrum of **2**.

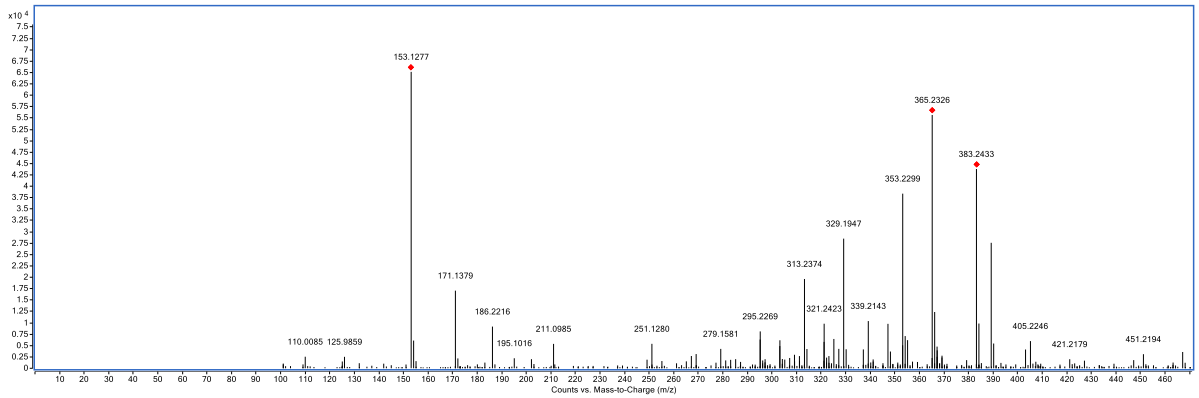

Fig. 20. Mass spectrum of **2**. Its formula of $C_{21}H_{34}O_6$ was deduced by *m/z* 383.2433 $[M+H]^+$ (calculated for 383.2428, Δ 1.27 ppm).

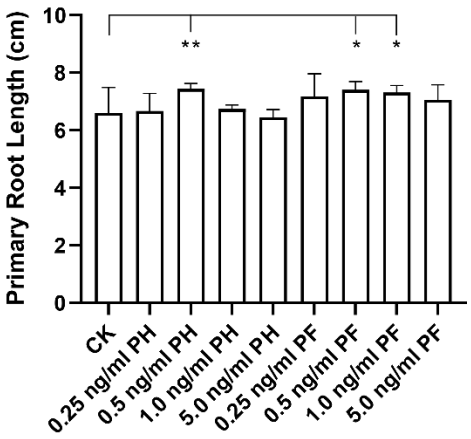

Fig. 21. Primary root length of *Arabidopsis* seedling treated with different concentrations of pteridic acids H and F. Abbreviation: *CK*, blank control treated by sterile Milli-Q water; *PH*, treatment of pteridic acid H; *PF*, treatment of pteridic acid F (mean ± SD, n=16). Statistical significance was assessed by T-test. Asterisks indicate the level of statistical significance: $^{*}p < 0.05$, $^{**}p < 0.01$. Source data are provided as a Source Data file.

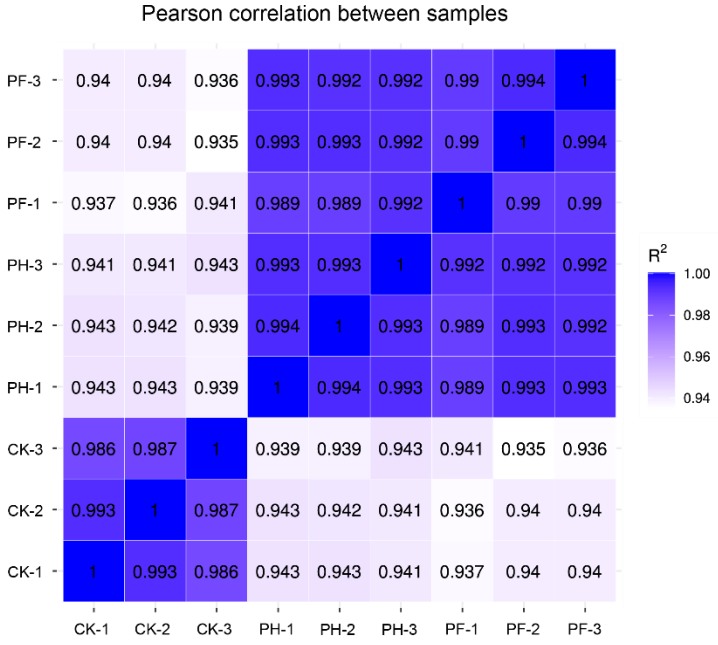

Fig. 22. Inter-sample correlation heat map. R^2: Square of Pearson correlation coefficient (R). Abbreviation: *PH*, treatment of pteridic acid H in *Arabidopsis* seedlings under NaCl-mediated salt stress; *PF*, treatment of pteridic acid F in *Arabidopsis* seedlings under NaCl-mediated salt stress; *CK*, treatment of equal water in *Arabidopsis* seedlings under NaCl-mediated salt stress as control.

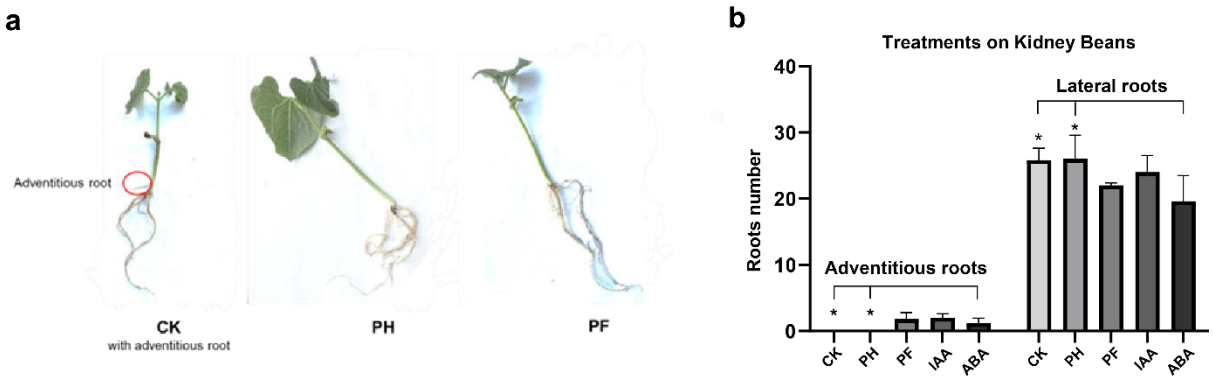

Fig. 23. Kidney beans growth experiment with pure pteridic acids. ***a***, the phenotypes of Kidney beans after treatments with pteridic acids H and F. ***b***, the numbers of adventitious roots and lateral roots of Kidney beans after different treatments (mean ± SD, n=5). Abbreviation: *CK*, control; *PH*, treatment of 1 ng mL^{-1} pteridic acid H; *PF*, treatment of 1 ng mL^{-1} pteridic acid F; *IAA*, treatment of 1 ng mL^{-1} IAA; *ABA*, treatment of 1 ng mL^{-1} ABA. Asterisks indicate the level of statistical significance: $^{*}p < 0.05$. Statistical significance was assessed by T-test. Source data are provided as a Source Data file.

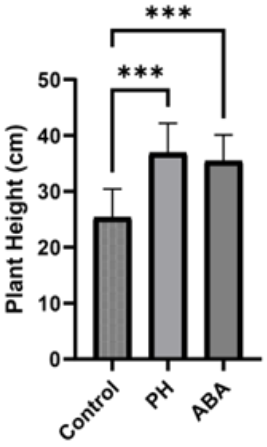

Fig. 24. Pteridic acid H and ABA at 1 ng mL^{-1} help Mung beans against heavy metal stress. The plant height of Mung beans after treatments with pteridic acids H and ABA. Abbreviation: *CK*, Control; *PH*, treatment of pure pteridic acid H; *ABA*, treatment of abscisic acid (mean ± SD, n=9). Statistical significance was assessed by one-way ANOVA with post hoc Dunnett's multiple comparisons test. Asterisks indicate the level of statistical significance: $^{***}p < 0.001$. Source data are provided as a Source Data file.

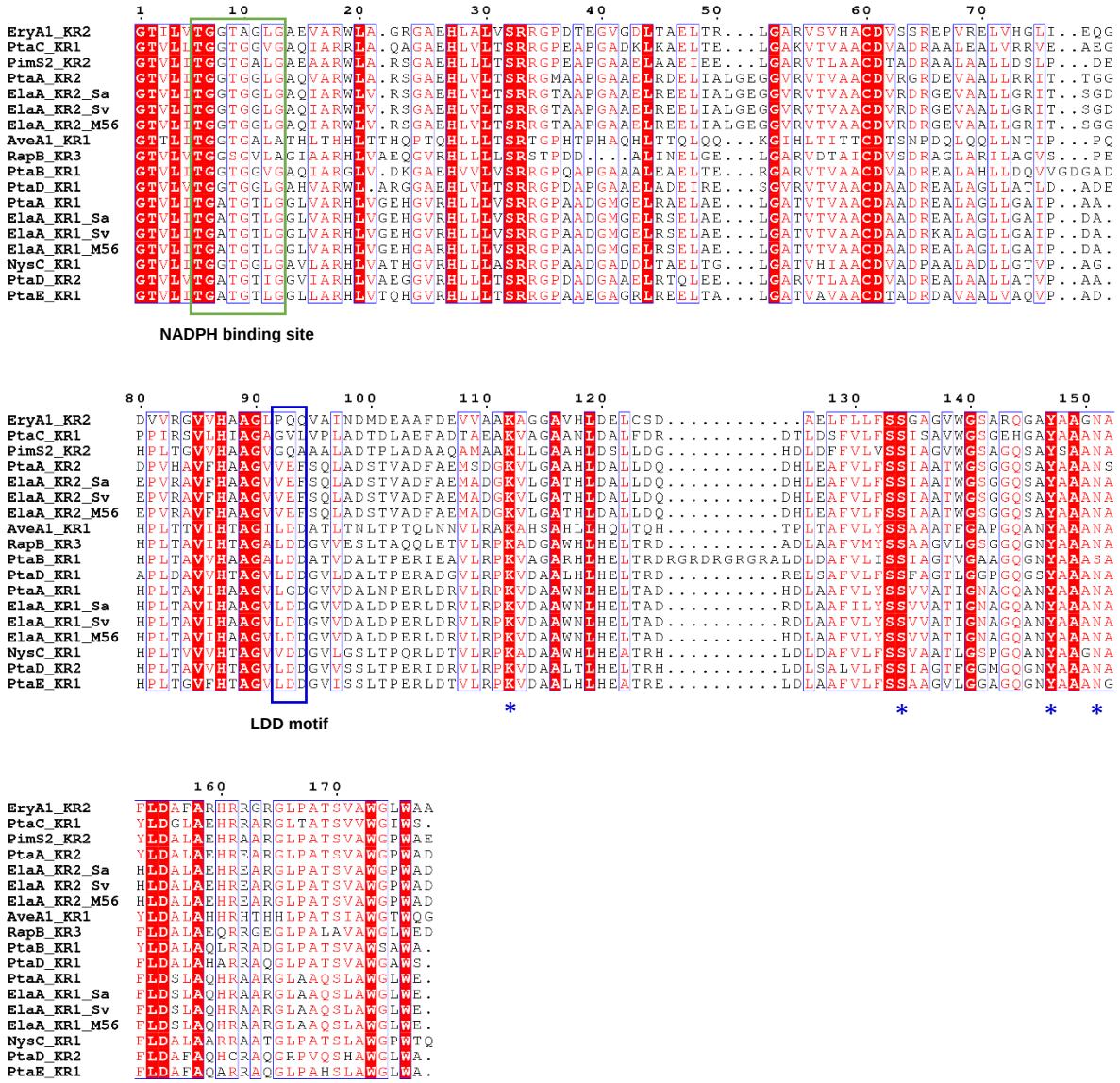

Fig. 25. Multiple sequence alignment of KR domains. The green box indicates NADPH binding site and blue box indicates the LDD motif. Abbreviation: Ery, erythromycin; Pta, pteridic acids; Pim, pimaricin; Ave, avermectin; Rap, rapamycin; Nys, nystatin.

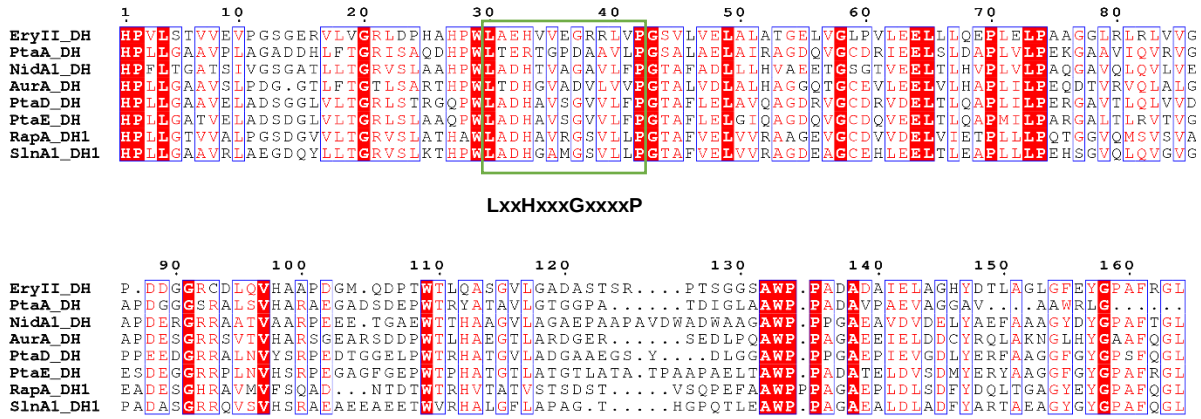

Fig. 26. Multiple sequence alignment of DH domains. The green box indicates the conserved LxxHxxGxxxxP motif. Abbreviation: Ery, erythromycin; Pta, pteridic acids; Nid, niddamycin; Aur, aureothin; Rap, rapamycin; Sln, salinomycin.

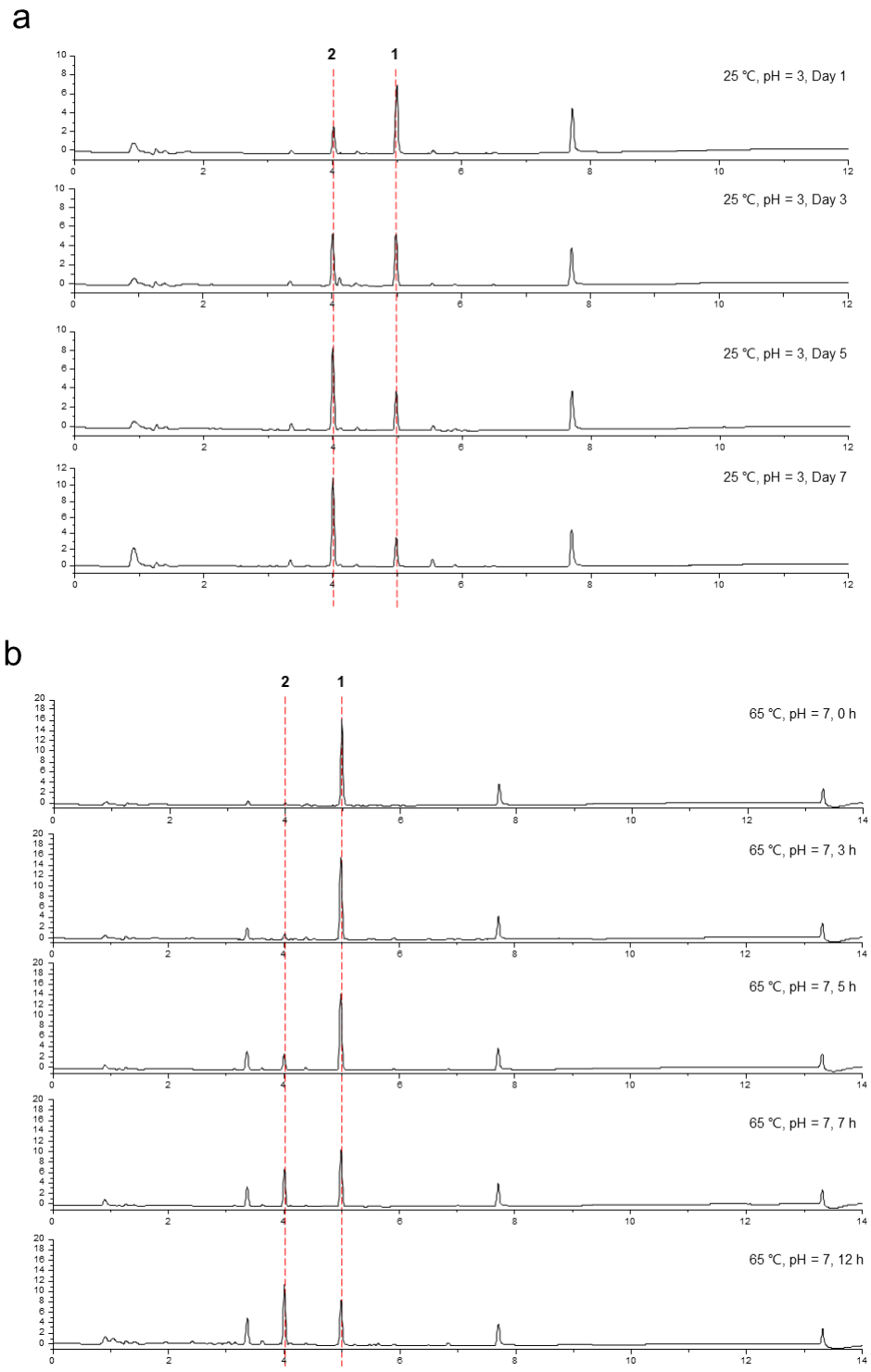

Fig. 27. Stability test of pteridic acids. Abbreviation: **1**, pteridic acid H; **2**, pteridic acid F. **1** was tested unstable in pH 3 buffer solution at 25 ˚C. ***a***, **1** was transformed to **2** fast, after 3 days the contents of them were as equal. The transformation rate is approximately 12.5%, 25%, 37.5%, 50% in 1 d, 3 d, 5 d and 7 d in pH 3 buffer solution at 25 ˚C. ***b***, **1** was unstable in water with 65 ˚C and transformed to **2** fast, after 12 hours, the content of **1** exceeded **2**. The transformation rate is approximately 7 %, 33 % and 47 % in 3 h, 7 h and 12 h, 65 ˚C.

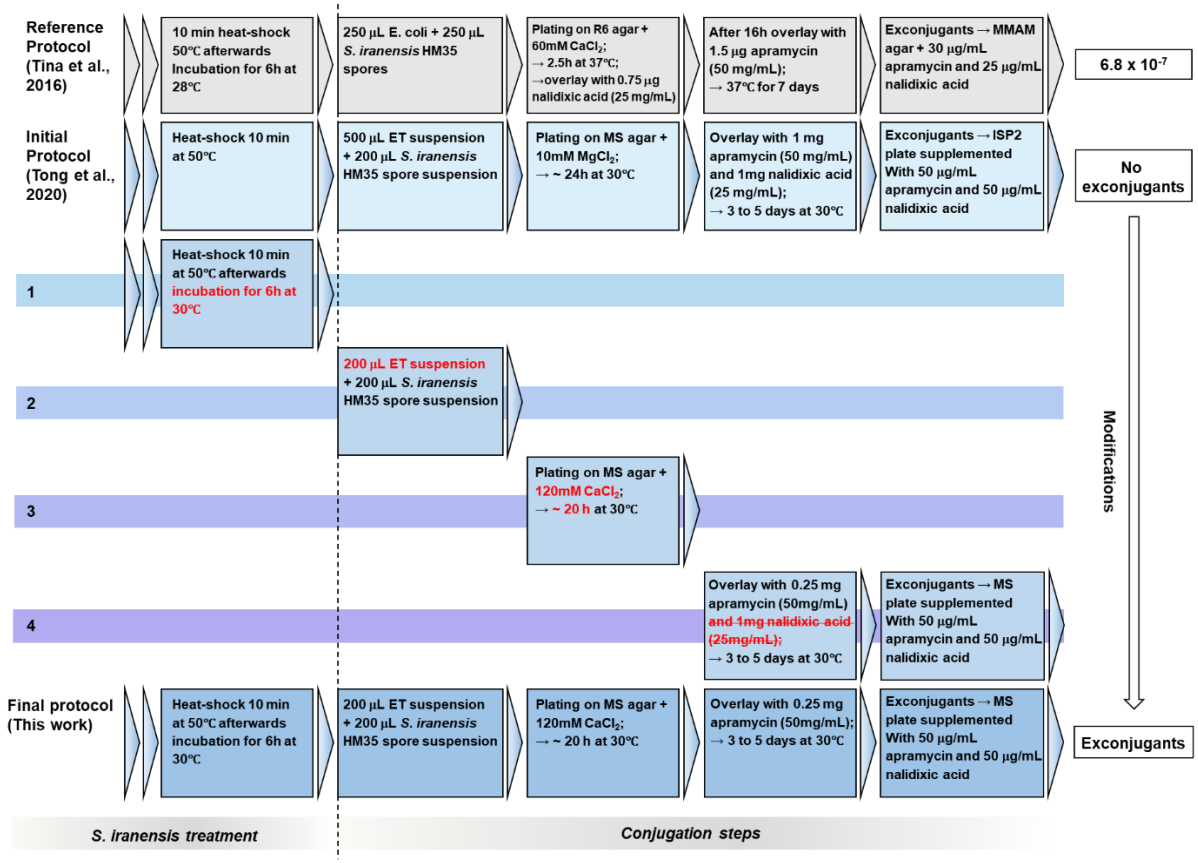

Fig. 28. The schematic of optimized genetic manipulation in *S. iranensis* by using CRISPR-cBEST system.

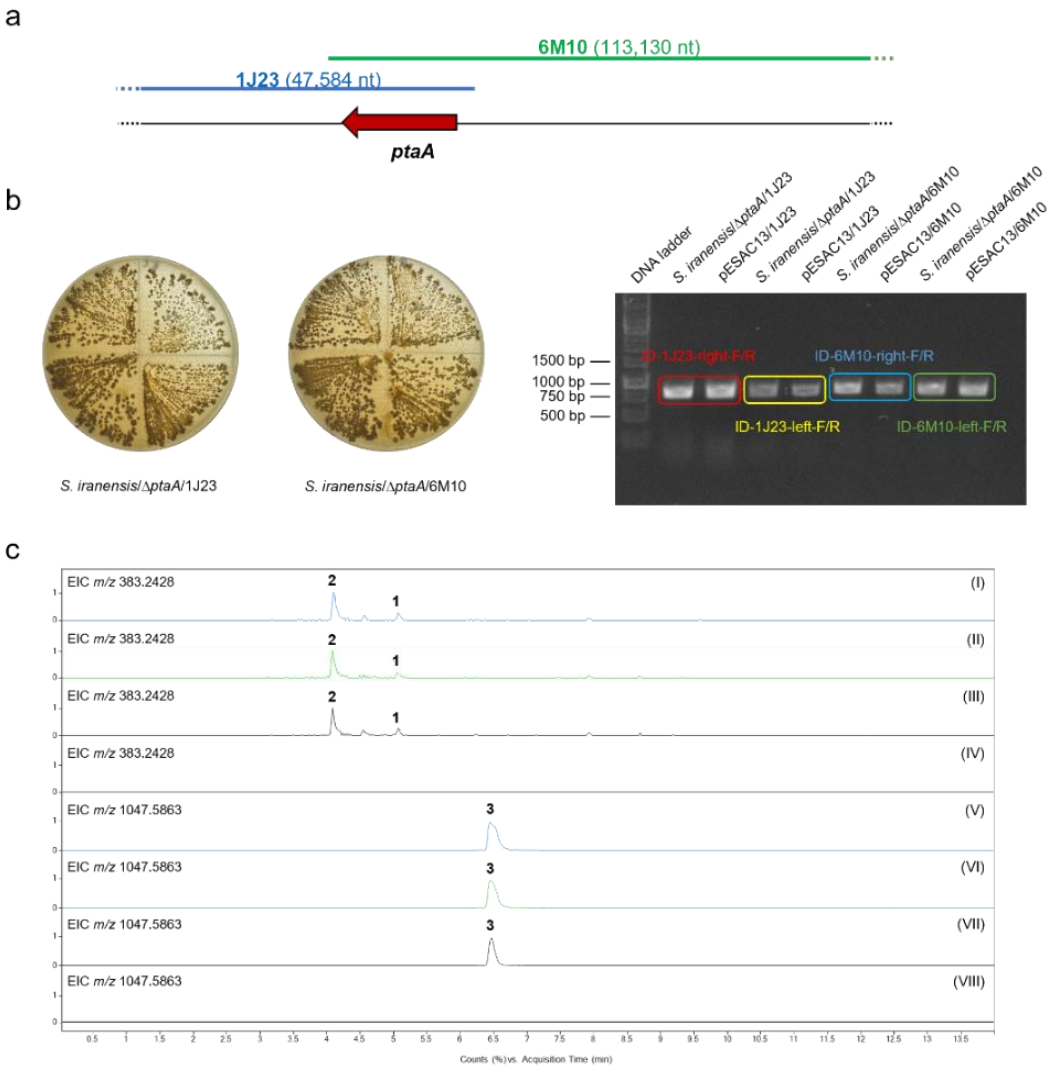

Fig. 29. Complementation experiment of *ptaA*-inactivation mutant of *S. iranensis*. ***a***, location of pESCA13/1J23 and pESCA13/6M10 in genome of *S.iranensis*. ***b***, apramycin-resistance screening and PCR verification of *S. iranensis*/Δ*ptaA*/1J23 and *S. iranensis*/Δ*ptaA*/6M10. ***c***, Extract Ion Chromatography (EIC) in positive mode was performed to detect pteridic acid H (1) and pteridic acid F (2) (*m/z* 383.2428 $[M+H]^+$ Δ ± 5 ppm) as well as elaiophylin (3) (*m/z* 1047.5863 $[M+Na]^+$ Δ ± 5 ppm) in the *S. iranensis*/Δ*ptaA*/1J23 (trace I and V), *S. iranensis*/Δ*ptaA*/6M10 (trace II and VI), wild-type *S. iranensis* (trace III and VII), and *S. iranensis*/Δ*ptaA* (trace IV and VIII).

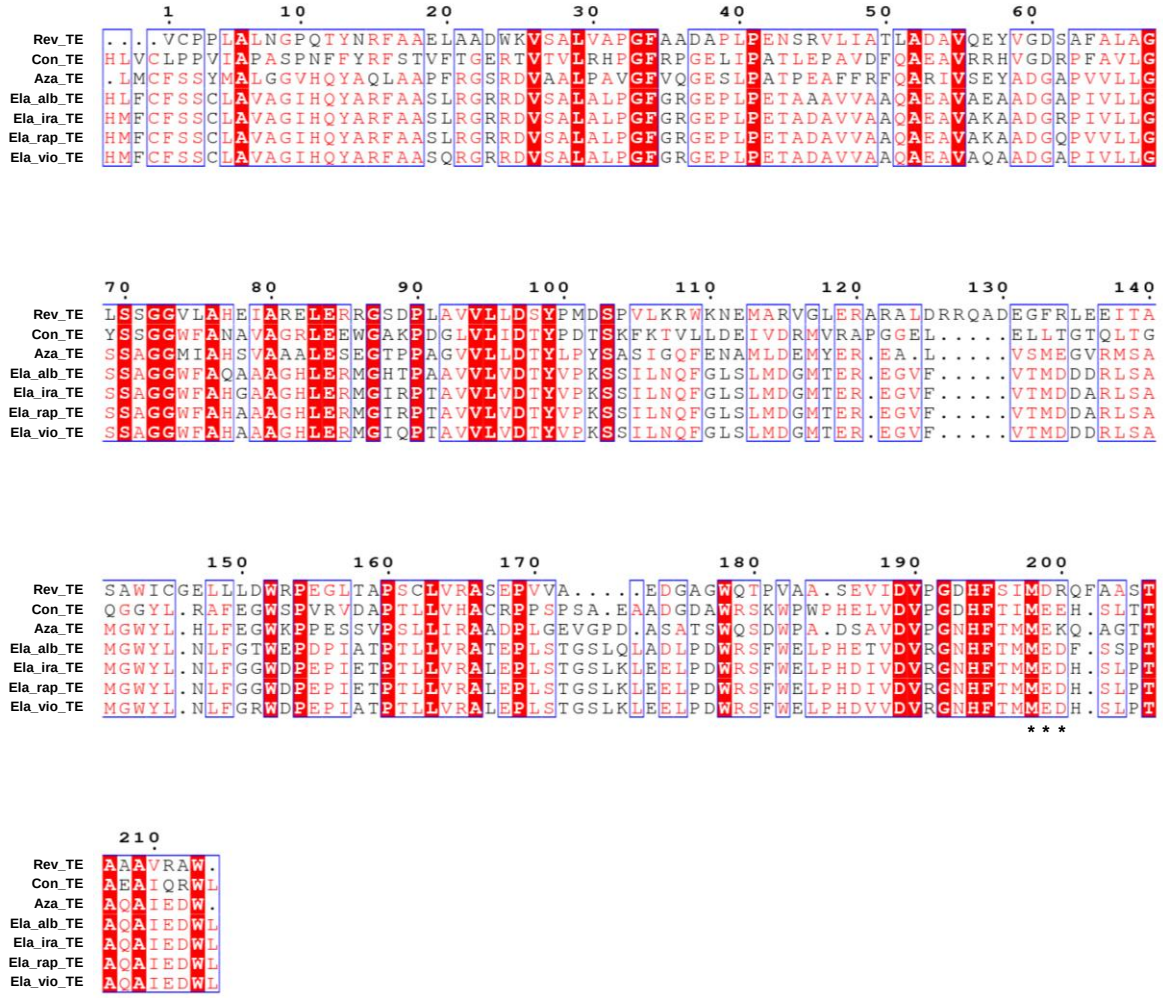

Fig. 30. Multiple sequence alignment of TE domains. The three amino acids marked with an asterisk were mutated in this study. Abbreviation: Rev_TE, the TE domain in reveromycin A biosynthesis from *Streptomyces* sp. SN-593; Con_TE, the TE domain in conglobatin biosynthesis from *Streptomyces conglobatus*; Aza_TE, the TE domain in azalomycin F3a biosynthesis from *Streptomyces* sp. 211726; Ela_alb_TE, the TE domain in elaiophylin biosynthesis from *S. albus* DSM 41398; Ela_ira_TE, the TE domain in elaiophylin biosynthesis from *S. iranensis* HM 35; Ela_rap_TE, the TE domain in elaiophylin biosynthesis from *S. rapamycinicus* NRRL 5491; Ela_vio_TE, the TE domain in elaiophylin biosynthesis from *S. violaceusniger* Tu 4113.

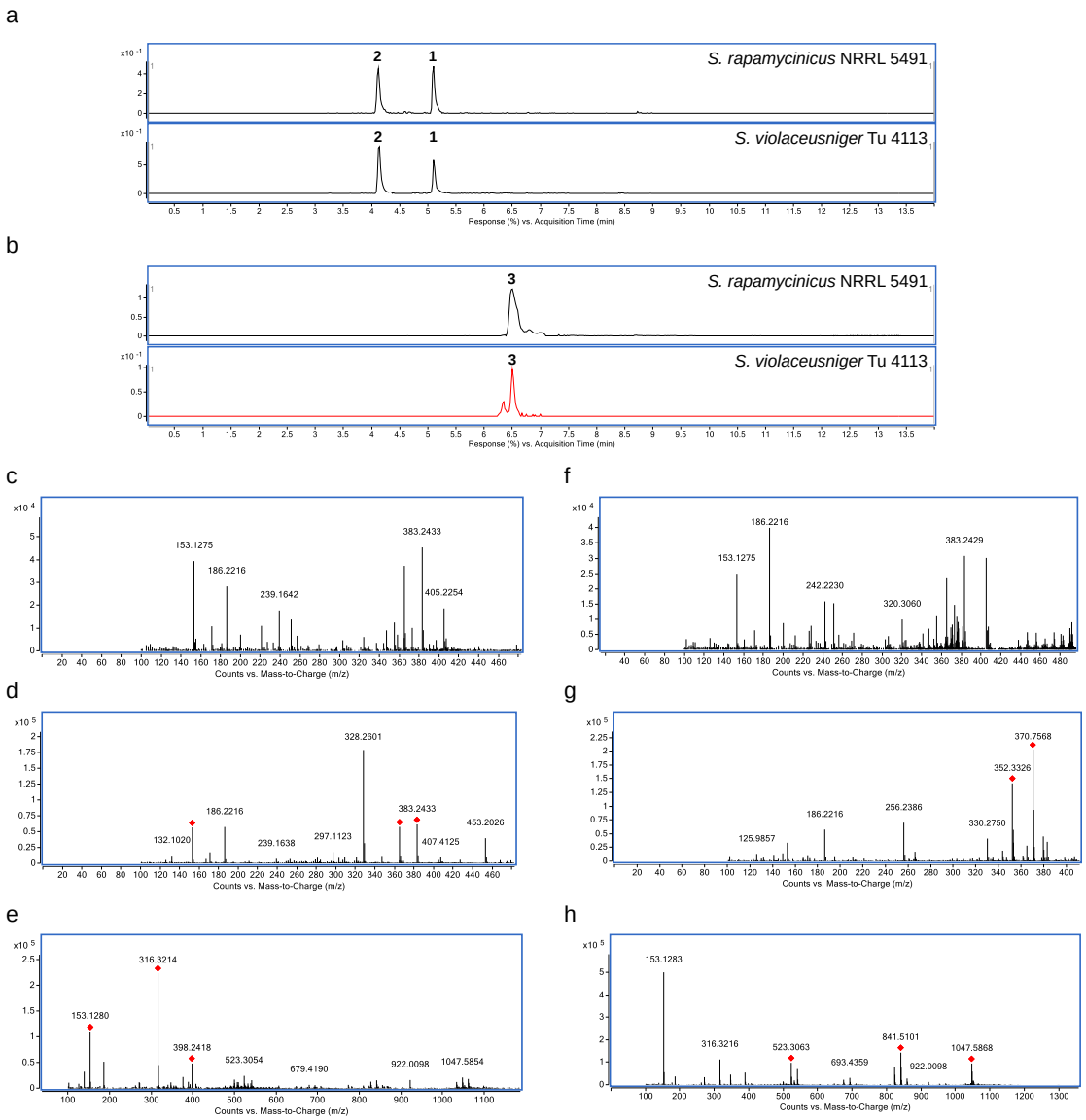

Fig. 31. The HR-LC-MS analysis of metabolites in *S. rapamycinicus* NRRL 5491 and *S. violaceusniger* Tu 4113. ***a***, the Extracted Ion Chromatography (EIC) of *m/z* 383.2428 $[M+H]^+$ in wild-type *S. rapamycinicus* NRRL 5491 and *S. violaceusniger* Tu 4113. The single *m/z* expansion for the chromatogram is ± 5 ppm. ***b***, the EIC of *m/z* 1047.5863 $[M+Na]^+$ in wild-type *S. rapamycinicus* NRRL 5491 and *S. violaceusniger* Tu 4113. The single *m/z* expansion for the chromatogram is ± 5 ppm. ***c***, the HR-LC-MS spectrum of **1** in wild-type *S. violaceusniger* Tu 4113. ***d***, the HR-LC-MS spectrum of **1** in wild-type *S. rapamycinicus* NRRL 5491. ***e***, the HR-LC-MS spectrum of **2** in wild-type *S. violaceusniger* Tu 4113. ***f***, the HR-LC-MS spectrum of **2** in wild-type *S. rapamycinicus* NRRL 5491. ***g***, the HR-LC-MS spectrum of **3** in wild-type *S. violaceusniger* Tu 4113. ***h***, the HR-LC-MS spectrum of **3** in wild-type *S. rapamycinicus* NRRL 5491.

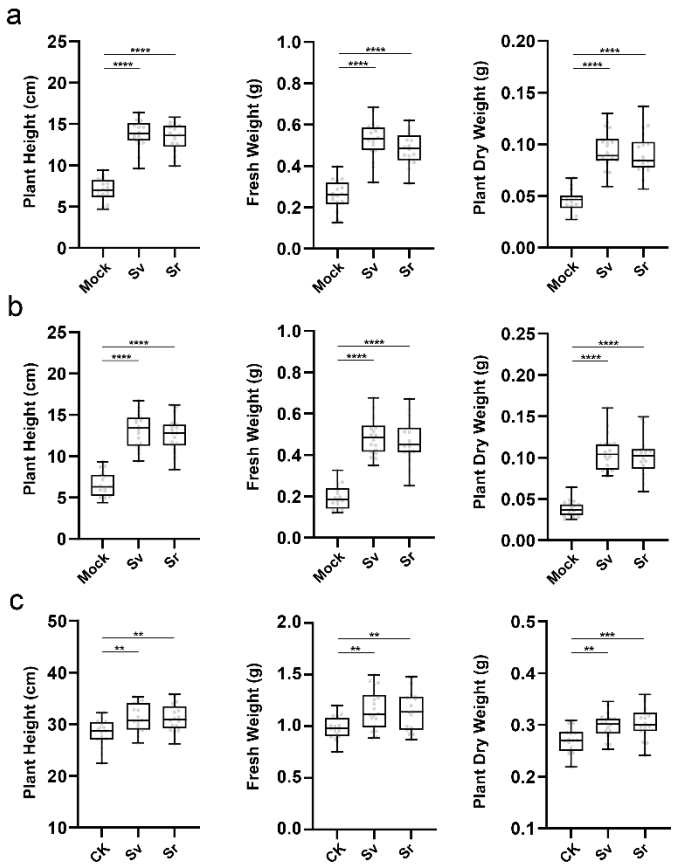

Fig. 32. Abiotic stresses alleviation led by *S. violaceusniger* Tu 4113 and *S. rapamycinicu*s NRRL 5491. ***a***, different growth of barley seedlings in osmotic stress mediated by 20% (w/v) PEG-6000 (data is mean ± SD, n=16). Abbreviation: *Mock*, control; *Sv*, treatment of *S. violaceusniger* Tu 4113 culture broth; *Sr*, treatment of *S. rapamycinicus* NRRL 5491 culture broth; *b*, different growth of barley seedlings in salinity stress mediated by 100 mM NaCl (mean ± SD, n=16). Abbreviation: *Mock*, control; *Sv*, treatment of *S. violaceusniger* Tu 4113 culture broth; *Sr*, treatment of *S. rapamycinicus* NRRL 5491 culture broth; *c*, different growth of barley seedlings in drought stress (mean ± SD, n=16). Abbreviation: *CK*, 7 days treatment of water after 7 days water + 7 days drought; *Sv*, 7 days treatment of *S. violaceusniger* Tu 4113 culture broth after 7 days water + 7 days drought; *Sr*, 7 days treatment of *S. rapamycinicus* NRRL 5491 culture broth after 7 days water + 7 days drought. Statistical significance was assessed by one-way ANOVA with post hoc Dunnett's multiple comparisons test. Asterisks indicate the level of statistical significance: $^{*}p < 0.05$, $^{**}p < 0.01$, $^{***}p < 0.001$ and $^{****}p < 0.0001$. All box plots with centre lines showing the medians, boxes indicating the interquartile range, and whiskers indicating a range of minimum to maximum data beyond the box. Source data are provided as a Source Data file.

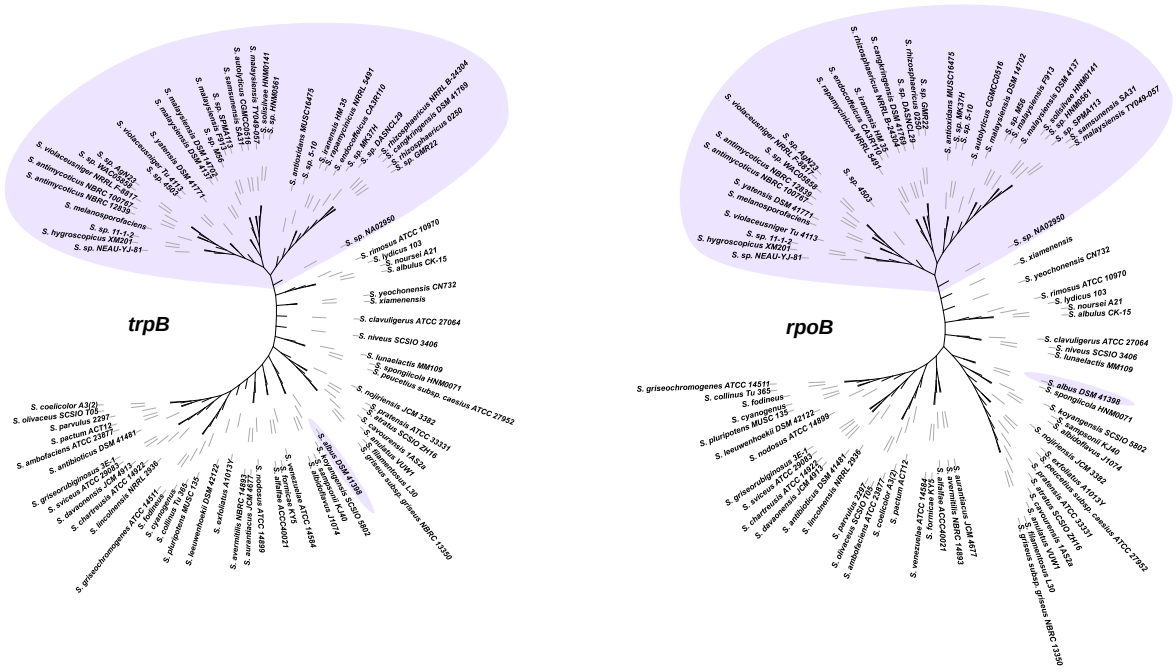

Fig. 33. The phylogenetic analysis of potential pteridic acids *Streptomyces* producers. The high-resolution *Streptomyces* sp. housekeeping genes: *trpB* (tryptophan synthase subunit beta) and *rpoB* (RNA polymerase subunit beta) were used in this analysis.

a

		1	2	3	4	5	6	7	8	9	10	11	12	13	14	15
S. rapamycinus NRRL 5491	1		95.78	83.53	91.79	91.64	91.73	91.65	91.60	91.75	91.72	91.61	91.59	86.13	91.59	91.50
S. iranensis HM 35	2	74.82		83.59	91.80	91.72	91.77	91.68	91.62	91.79	91.63	91.62	91.64	86.10	91.73	91.59
S. albus DSM 41398	3	10.75	10.61		83.56	83.60	83.52	83.57	83.60	83.54	83.54	83.61	83.63	83.70	83.47	83.56
S. antimycoticus NBRC 100767	4	70.38	68.49	11.36		91.65	95.60	91.63	91.58	95.58	97.58	91.58	91.58	86.14	95.59	96.12
S. autolyticus CGMCC0516	5	66.51	64.83	11.31	68.75		91.64	98.77	98.91	91.71	91.52	98.92	98.80	86.07	91.52	91.43
S. hygroscopicus XM201	6	66.63	65.41	11.15	73.49	69.52		91.65	91.61	98.90	95.18	91.61	91.59	86.15	96.12	95.16
S. malaysiensis DSM 4137	7	66.86	64.77	11.14	68.99	83.07	68.79		98.80	91.70	91.48	98.81	98.87	86.05	91.52	91.41
S. solisilvae HNM0141	8	65.56	62.94	10.79	67.61	87.21	67.84	89.60		91.63	91.44	99.99	98.80	86.06	91.46	91.38
S. sp. 11-1-2	9	67.91	66.17	11.21	74.30	70.01	87.13	70.25	69.05		95.17	91.64	91.63	86.14	96.11	95.18
S. sp. AgN23	10	68.18	64.40	11.33	78.86	67.16	70.61	67.94	66.24	72.65		91.44	91.47	86.09	95.22	95.78
S. sp. HNM0561	11	65.39	62.80	10.73	67.47	87.01	67.67	89.40	99.30	68.88	66.11		98.80	86.07	91.46	91.39
S. sp. M56	12	65.15	63.01	10.73	67.12	86.71	67.90	88.11	91.88	68.63	65.97	91.67		86.08	91.47	91.37
S. sp. NA02950	13	41.20	41.77	11.53	43.96	43.33	42.16	42.40	41.15	42.67	43.29	41.09	41.12		86.11	86.19
S. violaceusniger Tu 4113	14	67.65	67.66	11.52	76.23	68.53	73.87	68.27	66.21	75.44	72.44	66.08	66.28	43.88		95.25
S. yatensis DSM 41771	15	70.13	69.72	11.89	80.47	70.49	76.37	71.00	69.76	76.91	74.15	69.62	69.57	45.31	80.17	

Upper: average nucleotide identity **Lower:** alignment percentage

b

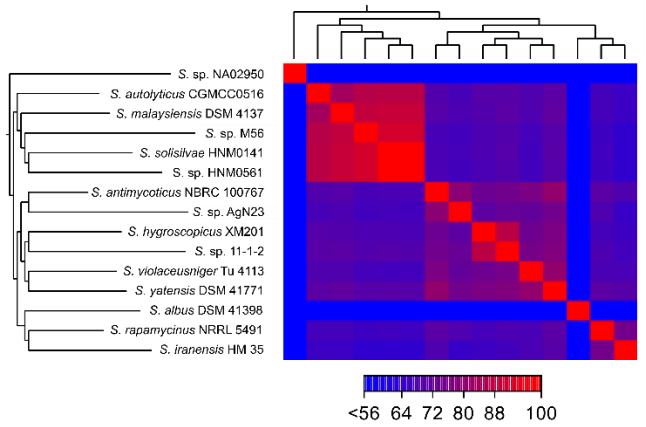

Fig. 34. Genome similarity analysis based on the alignment of 15 sequenced *pta*-containing *Streptomyces* genomes. ***a***, AP (alignment percentage) and ANI (average nucleotide identity) values between genomes. The AP value represents the average percentage of aligned genomic regions between two genomes, whereas the ANI value stands for the percentage of exactly matching nucleotides for these aligned regions. ***b***, Heat map showing genetic similarity between genomes based on AP values.

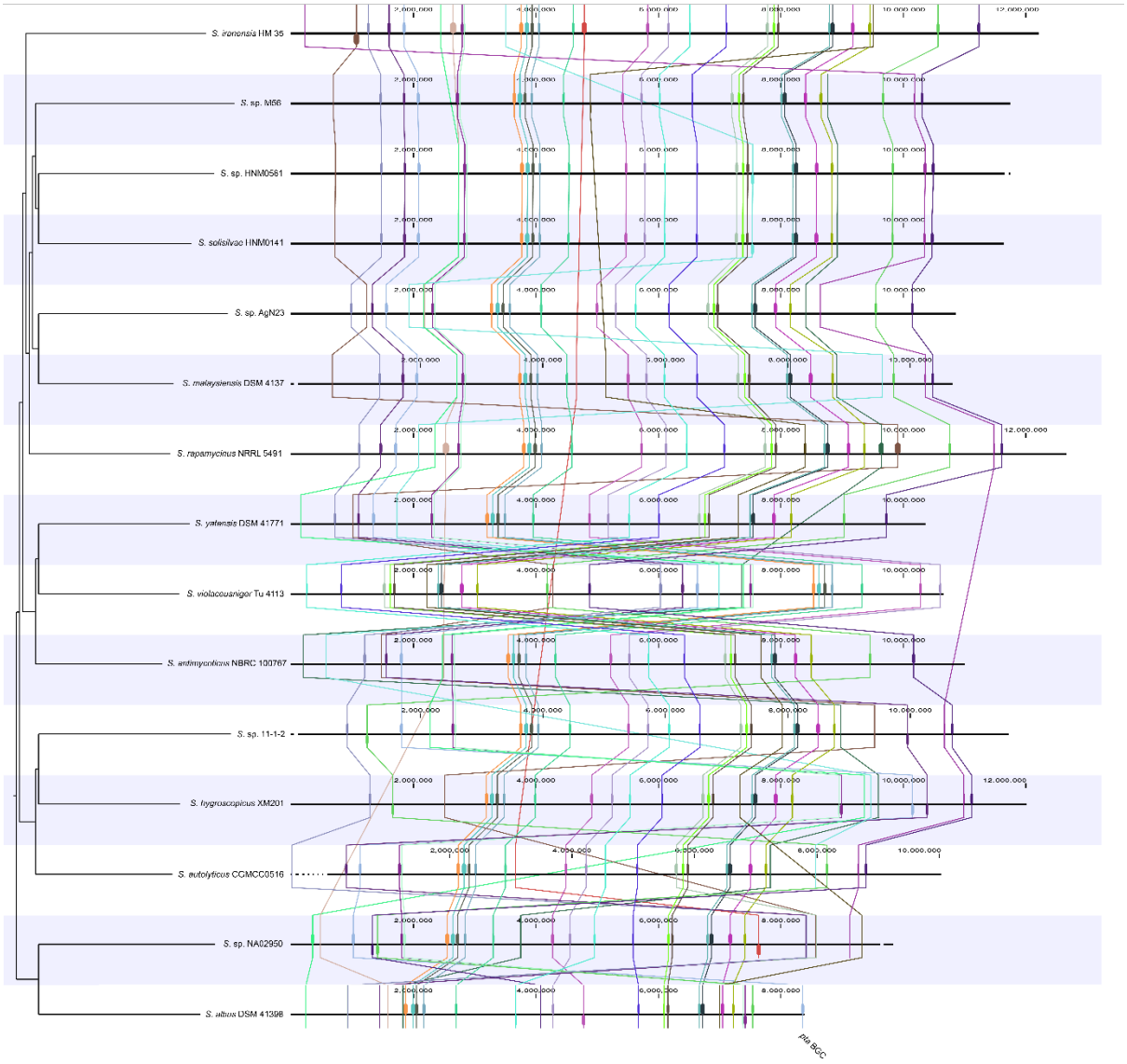

Fig. 35. The genome synteny analysis of selected 15 *pta*-containing *Streptomyces* strains. The colour squares each represent local alignment synteny blocks that are linked together among different genomes by lines with the same colours. The *pta* BGC is at the end of *S. albus* DSM 41398 chromosome.

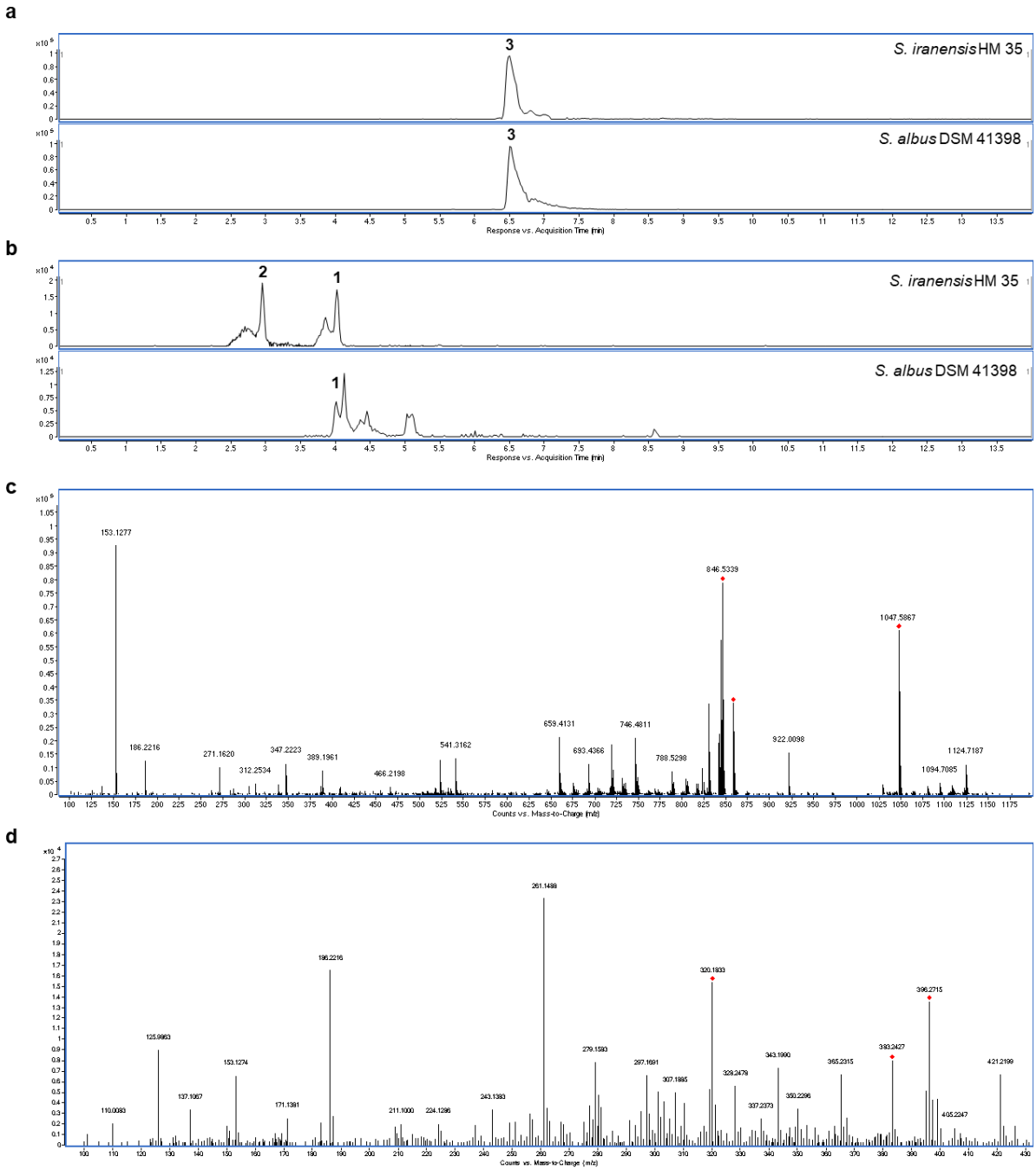

Fig. 36. The HR-LC-MS analysis of metabolites in *S. albus* DSM 41398. ***a***, the EIC of *m/z* 383.2428 $[M+H]^+$ in wild-type *S. iranensis* HM 35 and wild-type *S. albus* DSM 41398. The single *m/z* expansion for the chromatogram is ± 5 ppm. ***b***, the EIC of *m/z* 1047.5863 $[M+Na]^+$ in wild-type *S. iranensis* HM 35 and wild-type *S. albus* DSM 41398. The single *m/z* expansion for the chromatogram is ± 5 ppm. ***c***, the HR-LC-MS spectrum of **3** in wild-type *S. albus* DSM 41398. ***d***, the LC -MS spectrum of **1** in wild-type *S. albus* DSM 41398.

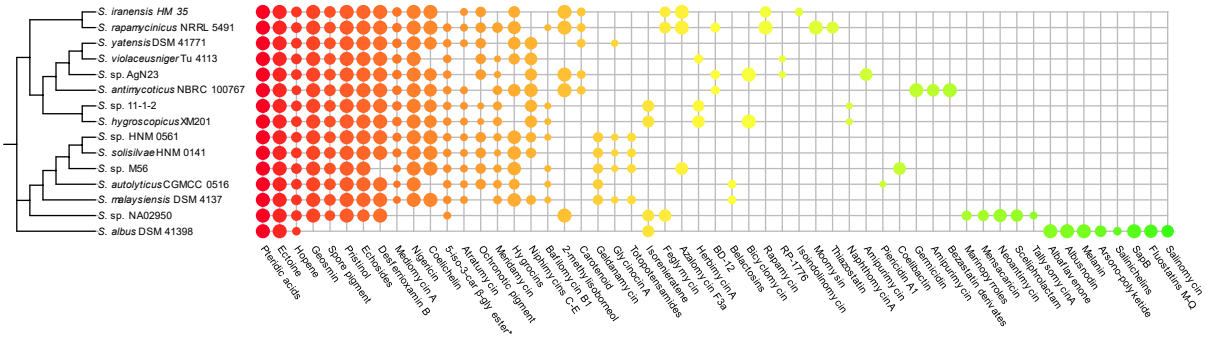

Fig. 37. The secondary metabolites biosynthetic gene clusters profiles of 15 *pta*-containing *Streptomyces* strains with complete genome information. BGCs with a similarity greater than 45% are displayed, and the size of the nodes represents the level of similarity *, 5-isoprenylindole-3-carboxylate β-glycosyl ester.

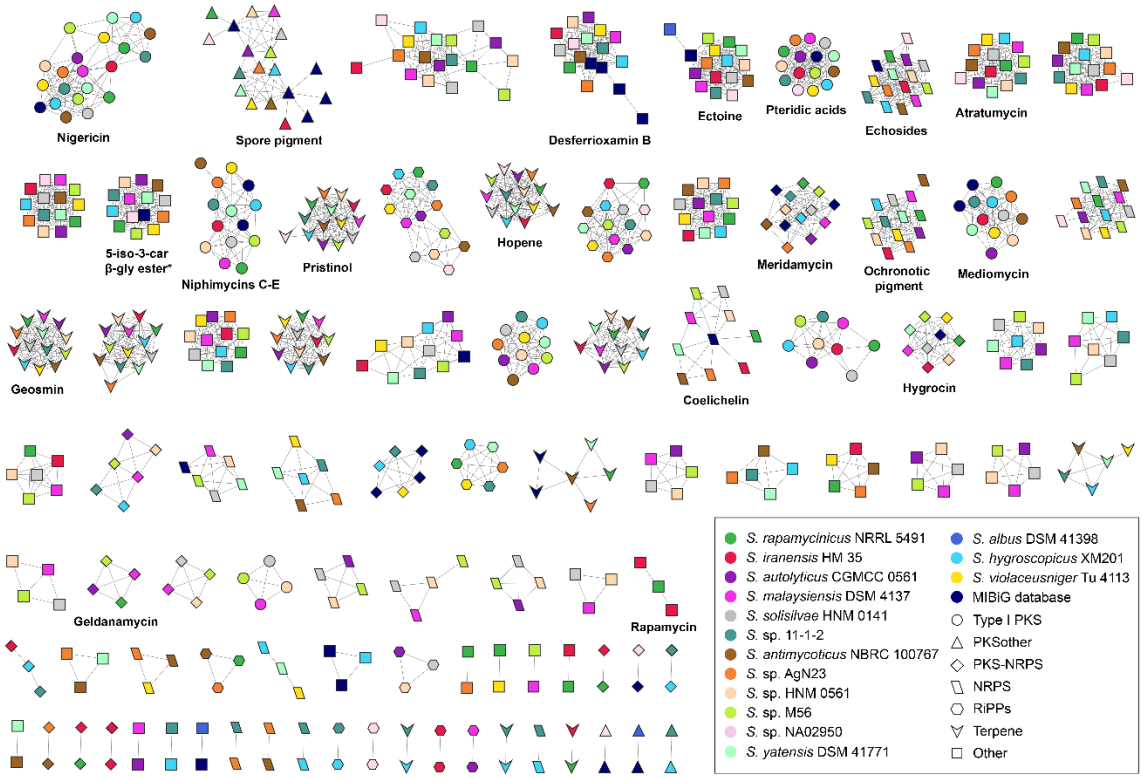

Fig. 38. The secondary metabolites BGCs similarity network of 15 *pta*-containing *Streptomyces* strains with complete genome information. Different strains and types of secondary metabolites are represented by different colours and shapes, respectively. *, 5-isoprenylindole-3-carboxylate β-glycosyl ester. Source data are provided as a Source Data file.

References:

1. Han, Y., et al. Halichoblelide D, a new elaiophylin derivative with potent cytotoxic activity from mangrove-derived *Streptomyces* sp. 219807. *Molecules* **21**, 970 (2016).
2. Nong, X., Wei, X. & Qi, S. Pteridic acids C-G spirocyclic polyketides from the marine-derived *Streptomyces* sp. SCSGAA 0027. *J. Antibiot.* **70**, 1047-1052 (2017).
3. Wu, C., et al. Identification of elaiophylin derivatives from the marine-derived actinomycete *Streptomyces* sp. 7-145 uing PCR-bsed screening. *J. Nat. Prod.* **76**, 2153-2157 (2013).
4. Cikosova, M., Blazsek, M., Kubis, M., Gajdosikova, J. & Borosova, G. Biotechnological preparation of the elaiophylin. *Folia Microbiol.* **49**, 731-736 (2004).
5. Yin, M., Jiang, M. X., Ren, Z., Dong, Y. & Lu, T. The complete genome sequence of *Streptomyces autolyticus* CGMCC 0516, the producer of geldanamycin, autolytimycin, reblastatin and elaiophylin. *J. Biotechnol.* **252**, 27-31 (2017).
6. Grabley, S., Hammann, P., Raether, W., Wink, J. & Zeeck, A. Secondary metabolites by chemical screening II. Amycins A and B, two novel niphimycin analogs isolated from a high producer strain of elaiophylin and nigericin. *J. Antibiot.* **43**, 639-647 (1990).
7. Supong, K., et al. Investigation on antimicrobial agents of the terrestrial *Streptomyces* sp. BCC71188. *Appl. Microbiol. Biotechnol.* **101**, 533-543 (2017).
8. Supong, K. & Tanasupawat, S. Secondary metabolites and biological activity of Actinomycetes. *Biotechnology of Microorganisms* 85-106 (2019).
9. Supong, K., et al. Antimicrobial compounds from endophytic *Streptomyces* sp. BCC72023 isolated from rice (*Oryza sativa* L.). *Res. Microbiol.* **167**, 290-298 (2016).
10. Sheng, Y., et al. Identification of elaiophylin skeletal variants from the Indonesian *Streptomyces* sp. ICBB 9297. *J. Nat. Prod.* **78**, 2768-2775 (2015).
11. Arai, M. Azalomycins B and F, two new antibiuotics. II. Properties of azalomycins B and F. *J. Antibiotics* **13**, 51-56 (1960).
12. Lee, S., Ha, S., Hong, Y., Hong, S. & Lee, J. Production of elaiophylin by the strain MCY-846 in a submerged culture. *J. Microbiol. Biotechnol.* **7**, 278-281 (1997).
13. Zhang, Y., et al. Elaiophylin from deep South China Sea-derived *Streptomyces albiflaviniger* SCSIO ZJ28. *Nat. Prod. Res. Dev.* **25**, 185-189 (2013).
14. Buedenbender, L., et al. HSQC-TOCSY fingerprinting-directed discovery of antiplasmodial polyketides from the marine ascidian-derived *Streptomyces* sp. (USC-16018). *Mar. Drugs* **16**, 189 (2018).
15. Komaki, H., Hosoyama, A., Ichikawa, N., Panbangred, W. & Igarashi, Y. Draft genome sequence of *Streptomyces* sp. SPMA113, a prajinamide producer. *Genome Announc.* **4**, e01126-16 (2016).
16. Zhao, G., et al. 16, 17-dihydroxycyclooctatin, a new diterpene from *Streptomyces* sp. LZ35. *Drug Discov. Ther.* **7**, 185-188 (2013).
17. Xu, J., Zhang, X., Huang, F., Li, G. & Leadlay, P. F. Efophylins A and B, two C2-asymmetric macrodiolide immunosuppressants from *Streptomyces malaysiensis*. *J. Nat. Prod.* **84**, 1579-1586 (2021).
18. Guo, Z., Liu, S., Ma, S. & Wang, R. Antibacterial metabolites from the mycelia of the cockchafer-derived *Streptomyces* sp. BCa1. *Chinese Journal of Tropical Crops* **36**, 1307-1311 (2015).
19. Ishibashi, M. Screening study of cancer-related cellular signals from microbial natural products. *J. Antibiot.* **74**, 629-638 (2021).
20. Wang, C., Wang, L., Fan, J., Sun, K. & Zhu, W. Cytotoxic compounds from the deep-sea sediment-derived *Streptomyces malaysiensis* OUCMDZ-2167. *Chinese J. Org. Chem.* **37**, 658-666 (2017).
21. Bown, L. & Bignell, D. R. D. Draft genome sequence of the plant pathogen *Streptomyces*

sp. strain 11-1-2. *Genome Announc.* **5**, (2017).
22. Zhu, J., et al. Complete genome sequence of *Streptomyces malaysiensis* HNM0561, a marine sponge-associated actinomycete producing malaymycin and mccrearamycin E. *Mar. Genom.* **63**, 100947 (2022).
23. Herdini, C., et al. Secondary bioactive metabolite gene clusters identification of anticandida-producing *Streptomyces* sp. GMR22 isolated from Wanagama forest as revealed by genome mining approach. *Indones. J. Pharm.* **28**, 26-33 (2017).
24. Nachtigall, J., et al. Benzoxacystol, a benzoxazine-type enzyme inhibitor from the deep-sea strain *Streptomyces* sp. NTK 935. *J. Antibiot.* **64**, 453-457 (2011).
25. Williams, D., et al. Structures of nahuoic acids B-E produced in culture by a *Streptomyces* sp. isolated from a marine sediment and evidence for the inhibition of the histone methyl transferase SETD8 in human cancer cells by nahuoic acid A. *J. Org. Chem.* **81**, 1324-1332 (2016).
26. He, W., et al. Crossregulation of rapamycin and elaiophylin biosynthesis by RapH in *Streptomyces rapamycinicus*. *Appl. Microbiol. Biotechnol.* **106**, 2147-2159 (2022).
27. Cui, C., Wang, H., Han, B. & Song, Y. Elaiophylins, new cell cycle inhibitors and apoptosis inducers, produced by *Streptomyces pseudoverticillus* (III) structural and NMR studies. *Chinese J. Org. Chem.* **11**, 25-31 (2001).
28. Zhang, H., et al. Secondary metabolites and biosynthetic gene clusters analysis of deep-sea hydrothermal vent-derived *Streptomyces* sp. SCSIO ZS0520. *Mar. Drugs* **20**, (2022).
29. Yang, S., Huang, W., Wang, S. & Wu, J. Extraction, purification and structure elucidation of antibiotic M1 in mycelia of *Streptomyces hygroscopicus* NND-52. *Zhongguo kang sheng su za zhi* **26**, 161-164 (2001).
30. Takesako, K. & Beppu, T. Studies on new antifungal antibiotics, guanidylfungins A and B I. Taxonomy, fermentation, isolation and characterization. *J. Antibiot.* **37**, 1161-1169 (1984).
31. Igarashi, Y., Iida, T., Yoshida, R. & Furumai, T. Pteridic acids A and B, novel plant growth promoters with auxin-like activity from *Streptomyces hygroscopicus* TP-A0451. *J. Antibiot.* **55**, 764-767 (2002).
32. Ilic, S., Konstantinovic, S., Cvijovic, G. & Veljkovic, V. Antibiotic production by *Streptomyces hygroscopicus* CH-7 in medium containing Schiff base complexes. *Hem. Ind.* **73**, 93-101 (2019).
33. Li, S., et al. Rapid identification of elaiophylin from *Streptomyces hygroscopicus* 17997, a geldanamycin producer. *Sheng wu Gong Cheng xue bao* **27**, 1109-1114 (2011).
34. Lima, S., et al. Characterization of the biochemical, physiological, and medicinal properties of *Streptomyces hygroscopicus* ACTMS-9H isolated from the Amazon (Brazil). *Appl. Microbiol. Biotechnol.* **101**, 711-723 (2017).
35. Martín, J., Ramos, A. & Liras, P. Regulation of geldanamycin biosynthesis by cluster-situated transcription factors and the master regulator PhoP. *J. Antibiot.* **8**, 87 (2019).
36. Chung, Y., et al. Comparative genomics reveals a remarkable biosynthetic potential of the *Streptomyces* phylogenetic lineage associated with rugose-ornamented spores. *Msystems* **6**, e00489-21 (2021).
37. Zhou, Y., Li, C., Xu, Y., Wu, W., Xia, W., Huang, X., Huang, D. & Zhou, S. Analysis of complete genome sequence of *Streptomyces solisilvae* HNM0141 of the Streptomyces violaceusniger clade. *Chinese Journal of Tropical Crops* **43**, 455-462 (2022).
38. Yang, H., Zhang, Z., Yan, R., Wang, Y. & Zhu, D. Draft genome sequence of *Streptomyces* sp. strain PRh5, a novel endophytic actinomycete isolated from Dongxiang wild rice root. *Genome Announc.* **2**, e00012-14 (2014).
39. Haltli, B. Elaiophylin Biosynthetic Gene Cluster. *U.S. Patent* 7,595,187 (2009).
40. Klassen, J., Lee, S., Poulsen, M., Beemelmanns, C. & Kim, K. Efomycins K and L from a termite-associated *Streptomyces* sp. M56 and their putative biosynthetic origin. *Front.*

Microbiol. **10**, 1739 (2019).
41. Xin, W., et al. Studies on secondary metabolites of *Acanthopanax senticosus* endophyte *Streptomyces* sp. CWJ-256. *Zhongguo Kang Sheng Su Za Zhi* **42**, 891-895 (2018).
42. Qi, S. Screening of marine actinomycetes producing antimicrobial sustances and study on their secondary metabolites and activities. *Nanchang University* (2020).
43. She, Z., et al. Investigation on the secondary metabolites and activities of four Actinomycetes strains related medicinal plants. *Xinjiang Medical University* (2017).
44. Muller, H., et al. Efomycins a, e and g as Antiinflammatory Agents. *U.S. Patent* 5,185,326A (1993).
45. Nair, M., et al. Gopalamicin, an antifungal macrodiolide produced by soil Actinomycetes. *J. Agric. Food Chem.* **42**, 2308-2310 (1994).
46. Yamada, T., Minoura, K. & Numata, A. Halichoblelide, a potent cytotoxic macrolide from a *Streptomyces* species separated from a marine fish. *Tetrahedron Lett.* **43**, 1721-1724 (2002).
47. Boya P, C., et al. Imaging mass spectrometry and MS/MS molecular networking reveals chemical interactions among cuticular bacteria and pathogenic fungi associated with fungus-growing ants. *Sci. Rep.* **7**, 5604 (2017).
48. Ritzau, M., Heinze, S., Fleck, W., Dahse, H. & Grafe, U. New macrodiolide antibiotics, 11-O-monomethyl- and 11,11 '-O-dimethylelaiophylins, from *Streptomyces* sp. HKI-0113 and HKI-0114. *J. Nat. Prod.* **61**, 1337-1339 (1998).
49. Ivanova, V., Schlegel, R. & Dornberger, K. N '-methylniphimycin, a novel minor congener of niphimycin from *Streptomyces* spec. 57-13. *J. Basic Microbiol.* **38**, 415-419 (1998).
50. Hamedi, J., et al. *Streptomyces iranensis* sp. nov., isolated from soil. *Int. J. Syst. Evol. Microbiol.* **60**, 1504-1509 (2010).
51. Tong, Y., et al. Highly efficient DSB-free base editing for streptomycetes with CRISPR-BEST. *Proc. Natl. Acad. Sci. U. S. A.* **116**, 20366-20375 (2019).

Appendix 2

Spirolactone, an unprecedented antifungal β-lactone spiroketal polyketide from *Streptomyces iranensis*

Zhijie Yang,[a] Yijun Qiao,[a] Emil Strøbech,[a] Jens Preben Morth,[a] Tilmann Weber,[b] Ling Ding[a,*]

[a] Department of Biotechnology and Biomedicine, Technical University of Denmark, Søltofts Plads, Building 221, 2800 Kgs Lyngby, Denmark.

[e] The Novo Nordisk Foundation Center for Biosustainability, Technical University of Denmark, Kemitorvet, Building 220, 2800 Kgs. Lyngby, Denmark.

*Corresponding author: Ling Ding lidi@dtu.dk

Abstract

Fungal infections pose a great threat to public health and there are only a few classes of antifungals that have limitations due to their high toxicity, drug-drug interactions, and drug-resistance. *Streptomyces* represent an important source of antifungal antibiotics, represented by amphotericin B. The rapamycin-producer *Streptomyces iranensis* displayed strong antifungal activities against *Aspergillus*. Revisiting its genome revealed several intriguing biosynthetic gene clusters, including one unparalleled Type-I polyketide synthase, which codes for uncharacterized metabolites. The identification of a novel class of macrolide spirolactones A-C was facilitated through CRISPR gene editing, HR-ESI-MS analysis, and subsequent large-scale fermentation and purification. Spirolactone A possesses an undescribed carbon skeleton with 13 chiral centers, featuring a rare β-lactone moiety, a [6,6]-spiroketal ring, and an unusual 7-oxo-octylmalonyl-CoA extender unit. Spirolactone A exhibited profound anti-*Aspergillus* activity. Proteomic analysis revealed spirolactone A potentially disrupted the integrity of fungal cell walls and induced the expression of stress-response proteins.

Introduction

About 1.2 billion people worldwide are estimated to suffer from a fungal disease.[1] Among those, invasive fungal diseases (IFDs) are hidden killers, causing at least 1.5 million deaths every year, and supposing malaria or tuberculosis.[1] It is rising overall and particularly among immunocompromised populations, such as HIV/AIDS, chronic lung diseases, prior tuberculosis, cancer, diabetes, and patients receiving immunosuppressant treatment and invasive medical procedures.[2] Yet, invasive diseases are of greater concern because they are associated with unacceptably high mortality rates. For example, *Aspergillus* has emerged as one of the most common causes of infectious death in severely immunocompromised patients, with mortality rates up to 40% to 50% in patients with acute leukemia and recipients of hematopoietic stem cell transplantation (HSCTs).[1] Despite posing a growing threat to human health, fungal infections receive very little attention and resources globally.[2] Currently, only four classes of systemic antifungal medicines (azoles, echinocandins, pyrimidines, and polyenes) are used in clinical practice, and only a limited number of candidates are under the clinical development pipeline.[3-6] Although existing antifungal medicines are effective, they are toxic and have drawbacks due to drug-drug interactions.[7] Moreover, the emergence of resistance made the existing medicines ineffective and this is partly driven by inappropriate antifungal use.[8] For example, agricultural use is responsible for rising rates of azole-resistant *Aspergillus fumigatus* infections, with azole-resistance rates of 15–20% reported in parts of Europe and over 80% in environmental samples in Asia.[8-10]

Streptomyces are producers of small bioactive molecules exhibiting a broad range of structural and functional diversity called secondary metabolites (SMs). These compounds are relevant to human health, as many demonstrate pharmaceutical properties such as antibacterial, antifungal, anticancer, and immunosuppressive activities. Nearly two-thirds of antibiotics approved for clinical use originate from *Streptomyces*, and of all new drugs from 1981-2019 over 60 % of the 1394 approved small molecule drugs were SMs or derivatives thereof.[11-13] Polyketides represent a large and diverse group of *Streptomyces*-derived SMs, and many of them possess valuable antifungal properties. Amphotericin B, first isolated from *Streptomyces nodosus* in 1955, stands as a crucial component in the therapeutic arsenal for combating invasive fungal diseases.[14] However, the toxicity of amphotericin B to human renal cells was revealed, which substantially

hampers its safe dosage range and, consequently, therapeutic efficacy.[15,16] A sustained interest persists in the exploration of novel antifungal leads from *Streptomyces*. Notable examples include turonicin A, hygrobafilomycin, iseolides, cyphomycin, azalomycins, niphimycins, and resistomycin.[17-23] Nonetheless, the majority of these compounds lack selectivity and exhibit toxicity toward human cells. Therefore, the development of clinically significant antifungal drug candidates, with a new mode of action and low cytotoxicity.

Considering *Streptomyces* harbors a large number of biosynthetic gene clusters (BGCs), their metabolites are yet to be discovered.[24] Access to modern analytical chemistry techniques in combination with genetics and bioinformatics tools enabled us to revisit the "talented" microbes discovered decades ago.[25] *Streptomyces iranensis*, initially identified as a rapamycin producer, was isolated from the soil in Isfahan City, Iran.[26] Subsequent investigations revealed its great capability to produce elaiophylin, azalomycins, nigericin, and other new metabolites yet to be discovered.[27] In our recent research, we found that *S. iranensis* produced pteridic acids H and F to help plants cope with abiotic stress.[27] During our pipeline search for antifungal polyketides, *S. iranensis* exhibited profound antifungal activity in co-cultivation with *Aspergillus tubingensis*, indicating the production of antifungal metabolites. Genome mining of *S. iranensis* indicated there is an uncharacterized type-I modular polyketides BGC featuring sixteen modules, capturing our particular interest. The products of this BGC, namely spirolactones A-C, were identified through a combination of CRISPR-BEST mutation, combined with metabolomic analysis, and large-scale fermentation and isolation. The structures and absolute configuration of spirolactones A-C were elucidated using nuclear magnetic resonance (NMR), mass spectrometry (MS), and X-ray crystallography. The striking structural features of spirolactone include a spiroketal ring, a rare β-lactone moiety, and a distinctive PKS extender unit. The BGC of spirolactones (*spl* gene cluster) was further identified through genomic DNA resequencing, in silico analyses, and in vivo genome editing. Spirolactone A exhibits potent antifungal activity against *Aspergillus* species with a narrow spectrum, which might be caused by disrupting fungal cell wall integrity based on the label-free quantitative proteomics analysis. This study provides a paradigm for mining novel molecules from extensive natural microorganisms, with the potential to lead to the discovery of innovative antifungal agents to combat antimicrobial resistance.

Results and Discussion

Genome mining of *S. iranensis*. Due to the incompleteness of previously reported genomic data, we performed whole-genome resequencing of S. iranensis using the combination of the Oxford Nanopore Technologies MinION and Illumina MiSeq system. The high-resolution, full-genome sequencing of S. iranensis reveals a linear chromosome spanning 12,213,033 nucleotides, featuring inverted terminal repeats comprising 156,145 nucleotides. The BGC annotation of the acquired *S. iranensis* genome was carried out using antiSMASH version 7.0,[28] which resulted in the appearance of a cryptic BGC (*spl* gene cluster) situated at the terminal region of the linear chromosome (Fig. 1 and *Supplementary information* Fig. 1). The gene cluster family (GCF) annotation of *spl* gene cluster showed it belongs to GCF_00315 and a total of 11 hits were detected (distance ≤ 900.0) in the BiG-FAM database (*Supplementary information* Tab. 2). [26] The distinctive biosynthetic gene architecture of *spl* gene cluster suggests its novelty as a modular Type-I PKS BGC, setting it apart from others (*Supplementary information* Fig. 2). This finding spurred our interest in conducting a thorough investigation of this individual BGC. This cryptic *spl* gene cluster spanned 87.99 kb with 12 open reading frames (Fig. 1). The entire PKS contains five core polyketide synthases (*splA*, *splC*, *splD*, *splE*, and *splF*) within 16 separated biosynthetic modules. In addition, there is a crotonyl-CoA carboxylase/reductase (*splH*), an *O*-methyltransferase (*splG*), three cytochrome P450 (*splB*, *splK* and *splL*), and two hypothetical enzymes (*splI* and *splJ*) adjacent to the core PKS genes (*Supplementary information* Tab. 3).

To locate the products of the potential *spl* gene cluster, we were elucidating the products combining both genome editing and metabolomics. Initially, we constructed PKS knock-out mutant (Δ*splA*) and crotonyl-CoA carboxylase/reductase-inactivated mutant (Δ*splH*) using the CRISPR-Cas9 method and CRISPR base editing, respectively (*Supplementary information* Fig. 3). Both mutants nearly abolished the antifungal activity against multiple *Aspergillus* strains. Comparative metabolic profiling using LC-MS and LC-UV led to the identification of the potential bioactive principle as a major compound **1** with *m/z* 881.4656 ($[M+H]^+$) and other derivatives, which were specifically abolished in both mutants (*Supplementary information* Fig. 3). The complementation of pGM1190-based *splH* in mutant *S. iranensis*/Δ*splH* led to the restoration of the production of **1** (*Supplementary information* Fig. 3).

Isolation and structure elucidation of spirolactone. We have previously accumulated the crude extracts of *S. iranensis* from 175 L fermentation.[24] To obtain the products of *spl* gene cluster, the open-column chromatography on Amberchrom 161c resin, silica gel, and Sephadex LH-20 was employed in sub-fractions of organic extract to yield pure compounds spirolactones A-C (**1**-**3**). Their structures were elucidated by HR-ECI-MS, NMR, and X-ray crystallography.

Spirolactone A (**1**) was obtained as a white solid and a molecular formula of $C_{47}H_{70}O_{14}$ by a sodium adduct ion (calcd *m*/*z* 881.4658 $[M+Na]^+$) was determined by HR-ESI-MS. It was assigned to the molecular formula on HR-ESI-MS combined with the NMR data. ^{1}H NMR spectrum revealed signals for six methyl groups H3-39 (δ 2.15), H3-41 (δ 0.94), H3-43 (δ 0.98), H3-44 (δ 0.93), H3-45 (δ 2.10), and OCH_3-8 (δ 3.37). Additionally, four olefinic protons were observed for H-2 (δ 6.19), H-3 (δ 7.91), H-4 (δ 6.47) and H-28 (δ 6.48). The coupling constant between H-2 and H-3 (*J* 15.4 Hz) confirmed a trans-orientation of a double bond. Besides the presence of several oxygen-bearing methines (H-6, H-8, H-10, H-14, H-16, and H-22), various other aliphatic proton signals were also observed (*Supplementary information* Fig. 4-10).

The ^{13}C NMR spectrum showed signals for an ester carbonyl C-1 (δ 168.6), three keto- groups C-12 (δ 207.3), C-27 (δ 201.3) and C-38 (δ 209.6) and two ester groups C-40 (δ 161.8) and C-47 (δ 174.9). Furthermore, signals were observed for six olefinic methines C-2 (δ 128.5), C-3 (δ 137.8), C-4 (δ 129.1), C-5 (δ 143.2), C-28 (δ 123.0), and C-29 (δ 156.4). Finally, signals for the methyl groups C-39 (δ 29.9), C-41 (δ 8.4), C-42 (δ 9.2), C-43 (δ 14.3), C-44 (δ 19.5), C-45 (δ 17.4) and the oxygenated methyl group C-42 (δ 59.6) were also observed. The chemical shift of C-18 (δ 101.0) indicated the presence of an acetal moiety. The ^{1}H and ^{13}C NMR data of **1** is shown in *Supplementary information*, Tab. 4.

COSY correlations further established six fragments including one saturated aliphatic chain. HMBC correlations (Fig. 2a) further established a beta-lactone moiety as HMBC correlations between H-4, H-6, and C-40 (16) were observed. A further connection of this beta-lactone to a polyene moiety was established by HMBC correlations between H-6 and C-4, and H-6 and C-40. A macrolactone bridge between H-10 and C-46 was established by HMBC correlation between them. The key HMBC correlation between H-13 and C-18 indicated the presence of an oxane ring. Moreover, H-16 and Me-43 showed HMBC correlations with C-18. Considering the double bond equivalence and the number of oxygen atoms inferred from HR-ESI-MS, a spiroketal structure was proposed. Finally, a planar structure with a novel carbon skeleton was proposed and named Spirolactone. The complex structure exhibited no similarities

to reported natural products. Meanwhile, the dispersion of the thirteen chiral centers made it challenging to elucidate the absolute configuration. Interestingly, the compound could form crystals in dichloromethane/methanol solution. One crystal was subjected to X-ray crystallography analysis, which successfully elucidated the configurations (*Supplementary information* Fig. 11).

Spirolactone B (**2**) was isolated as a derivative of spirolactone A. A molecular formula of $C_{47}H_{72}O_{14}$ was confirmed by HR-ESI-MS (*m/z* 859.4857 $[M-H]^-$ with one DBE less than spirolactone A. Its NMR spectra exhibited high similarity to A, except for the absence of the carbonyl carbon signal at C-38. Instead, a new secondary alcohol group was indicated by the presence of δ 3.85 (H-38) in the ^1H NMR spectrum, which correlated with the methyl group at H-39. 2D NMR data confirmed its structure as spirolactone B (*Supplementary information* Fig. 12-16). The ^1H and ^{13}C NMR data of **2** is shown in *Supplementary information*, Tab. 3.

Spirolactone C (**3**) was isolated as a second derivative of spirolactone A. A molecular formula of $C_{48}H_{74}O_{15}$ was confirmed by HR-ESI-MS (*m/z* 889.4966 $[M-H]^-$). Its NMR spectra exhibited some similarity to A. However, an opened beta-lactone ring compared to A was indicated by the higher chemical shift of δ 166.9 at C-40. Meanwhile, an OMe group was indicated to be connected to C-40 through HMBC correlations. 2D NMR data further confirmed its structure as spirolactone C (*Supplementary information* Fig. 17-22). The ^1H and ^{13}C NMR data of **3** is shown in *Supplementary information*, Tab. 3.

Proposed biosynthesis of spirolactone. Five PKS genes transcribed in the same direction encode one loading module and 15 chain extender modules and were suggested to assemble the polyketide backbone. Based on multiple sequence alignment, most KS domains keep the conserved catalytic sites comprised of a cysteine (TA**C**SSS motif) as well as two histidines (EA**H**GTG and KSNIG**H**T motifs).[29] Only the reactive cysteine in KS_1 was replaced by glutamine (*Supplementary information* Fig. 23), which was observed in the platensimycin/FabF (the type II FAS homology of KS) complex.[30] The conserved fingerprint residues for extender unit selectivity GHSIG and HAFH motifs are present in the nine AT domains (AT_1, AT_2, AT_5, AT_7, AT_8, AT_9, AT_{11}, AT_{12}, and AT_{14}) that are specifically binding to malonyl-CoA while GHSQG and YASH motifs are present in the six AT domains (AT_3, AT_4, AT_6, AT_{10}, AT_{13}, and AT_{15}) that are specifically binding to for (2*S*)-methylmalonyl-CoA (*Supplementary information* Tab. 5 and Fig. 24).[29] As previously discovered, AT_{16} from module 15, which was thought to be accountable for loading distinct

extender units, exhibits an unusual IASH motif. KR domains have been previously classified into A1-, A2-, B1-, and B2-types, which reduce ketones to their L-hydroxy or D-hydroxy counterparts.[31] We determined that the KR_3, KR_4, and KR_{15} appear to belong to the B1-type: all have the fingerprint LDD motif but the absence of a P residue in the catalytic region. KR_5 and KR_{12}, with the characteristic W residue but no LDD motif and H residue, were classified as A1-type KRs (*Supplementary information* Fig. 25). The other KR domains couldn't be classified according to the sequence, but they should be functional according to the structure of spirolactone. Similarly, combined with structural information and conserved site analysis, the five DH domains (DH_6, DH_7, DH_8, DH_9 and DH_{10}) were considered inactive during spirolactone biosynthesis (*Supplementary information* Fig. 26). ER_{11} is classified as L-type due to the presence of a tyrosine residue that donates a proton to the enol intermediate in L-type ER, whereas ER_{13} and ER_{14} belong to D-type because it lacks tyrosine residue (*Supplementary information* Fig. 27). The final release and cyclization of the linear product was probably accomplished by TE domain in the last module, which contains an α/β-hydrolase catalytic core and loop regions that form a substrate-binding lid.[32]

The above synthetic steps leading to PKS assembly are followed by a series of complex modifications including oxidation, carboxylation, and methylation. The tailoring enzymes responsible for these transformations are scattered throughout the *spl* gene cluster. The multiple sequence alignments of three cytochromes P450 enzymes (SplB, SplK, and SplL) showed that they have conserved motifs of this family (*Supplementary information* Fig. 28).[33] The cytochrome P450 enzyme BonL from *Burkholderia gladioli* was previously identified to confer the C-22 carboxyl group in the biosynthesis of bongkrekic acid via sequential six-electron-oxidation.[34] In addition, there are some cytochromes P450 enzymes that catalyze the carboxyl group formation in microbial SMs, such as XiaM, PimG, AmphN, NysN, and FscP.[35-37] To identify the cytochromes P450s responsible for carboxylation, we built the Hidden Markov model (HMM) based on these sequences and the results showed that SplL exhibited the best match with these known P450s with an E-value of 4e-117. In addition, bioinformatic analysis of XiaM indicated that the P450s with carboxylation function harbor highly conserved segment AGHET, which was also presented in SplK (*Supplementary information* Fig. 28). Therefore, SplK and SplL, were considered putative candidates for catalyzing the two-step oxidation to form carboxyl groups in postitions C-1 and C-

5 during spirolactone biosynthesis. SplB, homologous cytochrome P450 monooxygenase CftA in clifednamide biosynthesis gene cluster with 45.6 % similarity,[38] was likely to accomplish the oxidation at C-27 in spirolactone. We constructed mutant strains of *S. iranensis* inactivating the SplB, Splk and SplL enzymes (denoted as Δ*splB*, Δ*splk*, and Δ*splL*) (*Supplementary information* Fig. 29). Despite our efforts, no expected intermediates were observed in either mutant, likely due to their low yield. SplG, an *O*-methyltransferase homologous to AveD in avermectin biosynthesis (40% identity and 55% similarity),[39] was proposed to catalyze the methylation of a hydroxyl group in C-8 of spirolactone. The Δ*splG* mutant also showed no accumulation of spirolactone and other putative intermediates (*Supplementary information* Fig. 29).

Phylogenetic analysis indicated that SplH is a separate branch and clusters with other crotonyl-CoA reductase/carboxylases that catalyze long-chain precursors like butylmalonyl-CoA and hexylmalonyl-CoA.[40,41] The previous study showed that the large residue Phe380 in the CCR from *S. coelicolr* may constrain the potential pocket to accept long-chain substrates, which were also found in most ethylmalonyl-CoA specific crotonyl-CoA reductase/carboxylases, while its corresponding residue in SplH is smaller cysteine (*Supplementary information* Fig. 30).[42] Hence, we proposed that SplH catalyzes the conversion leading to the formation of 7-oxo-octylmalonyl-CoA in spirolactone A and B, and 7-hydroxyoctylmalonyl-CoA in spirolactone C. We attempted to confirm the function of SplH in vitro, however, SplH with C-term His-tag or N-term His-tag couldn't be expressed in *Escherichia coli* BL21 (DE3).

Microbial β-lactone natural products are structurally diverse, nevertheless, there are only few enzymatic mechanisms corresponding to β-lactone ring formation that have been reported,[43] including: (1) the intramolecular cyclization from seven-membered ring, catalyzed by cyclase VibC in vibralactone biosynthesis;[44] (2) the tandem aldol-lactonization bicyclization reaction to generate the γ-lactam–β-lactone structure, catalyzed by standalone ketosynthase SalC in salinosporamide A biosynthesis;[45] (3) the β-lactone formation during the intramolecular attack of the β-hydroxyl group onto the thioester carbonyl, catalyzed by the C-terminal TE domain of ObiF in obafluorin biosynthesis or esterase GloD in globilactone A biosynthesis;[46,47] (4) the conversion of β-hydroxyl to β-lactone, catalyzed by β-lactone synthase OleC in olefin biosynthesis.[48,49] Due to the significant structural bias with reported molecules, we proposed that the beta-lactone formation in spirolactone involves two-step oxidation to form a carboxylic acid,

followed by dehydration. It is likely that either the cytochrome P450 enzyme SplK or SplL is involved in the process, and we also identified several genes with unknown functions, such as *splJ* and *splI*. SplJ was annotated as a member of UbiD family decarboxylases, but it exhibits very distinguished divergences from other proteins in this family based on sequence similarity network (Supplementary information Fig. 31). In addition, NCBI Blastp results showed that proteins homologous to SplI have not been reported to have any clear biological functions. Inactivation of both genes *splJ* and *splI* also abolished spirolactone production (Supplementary information Fig. 29).

Antifungal and cytotoxic assays of spirolactones. Natural products containing β-lactones have been found to exhibit significant biological activities. For instance, obaflurin, an antibiotic derived from *Pseudomonas fluorescens*, demonstrated antibacterial effects against *Staphylococcus aureus*, *Escherichia coli*, *Enterobacter cloacae*, *Providencia rettgeri*, and *Pseudomonas aeruginosa*.[50] This highlights its potential as a versatile antimicrobial agent. Salinosporamide, obtained from the marine bacterium *Salinospora tropica*, acts as a cytotoxic proteasome inhibitor. Notably, it successfully completed a phase 2 clinical trial for multiple myeloma cancer therapy.[51] Lipstatin, isolated from *Streptomyces toxytricini*, serves as a potent and selective inhibitor of human pancreatic lipase.[52] Several β-lactones like F-244 and ebelactone A were revealed to inhibit activity the activity of homoserine transacetylase, an attractive target for new antimicrobial agents, catalyzes the biosynthesis of methionine from aspartic acid in many fungi.[53] These examples underscore the diverse therapeutic applications of natural products containing the β-lactones moiety. Spirolactones were inactive against Gram-positive bacteria Staphylococcus aureus. In the antifungal assay, spirolactone A exhibited greater inhibitory activity than amphotericin B against various fungal pathogens, including *Aspergillus niger*, *Aspergillus tubingensis*, and *Aspergillus flavus*, with minimum inhibitory concentrations (MIC) of 4, 4, and 15 ng mL^{-1}, respectively (Supplementary information Tab. 6). Cell growth and toxicity effects of spirolactone on mammalian cells were assessed using the LNCaP and C4-2B prostate cancer cell lines, respectively (Supplementary information Fig. 32). Exposure to spirolactones (10μM) increased the observed growth rate constant (k) in LNCaP and C4-2B cells, from 0.5628 and 0.5632 to 2.659 and 1.889, respectively.

Studies of the mechanism of action of spirolactone. The fungal cell wall is an essential structure that maintains cell shape and protects fungi against environmental stress and plays roles in growth, invading ecological niches and counteracting the host immune response.[54] Fungal cell walls are composed mainly of glucans, chitin, and glycoproteins, synthesized by glycosyltransferases, glycoside hydrolases, and transglycosylases.[55] The fungal cell wall is a promising target as it contains polysaccharides absent in humans. Currently, four classes of antifungal drug classes including polyenes, allylamines, azoles, and echinocandins are used in clinical practice.[56,57] Their mechanisms are well-understood with most targeting the cell wall/membrane components or synthesis. Recent studies revealed that the mode of action of polyenes antibiotics involves acting as sterol "sponges" and extracting ergosterol from the fungal membrane, causing cell death.[58,59] Allylamine antibiotics (naftifin and terbinafine) inhibit squalene epoxidase, causing the accumulation of squalene, and thereby damaging the intracellular membranes of fungi.[60] Azoles inhibit ergosterol biosynthesis in the lanosterol demethylation through the cytochrome P450 sterol-14α-demethylase (CYP51).[61] Echinocandins block the synthesis of cell wall component β-1,3-glucans through non-competitive inhibition of 1,3-β-D-glucan synthase.[62] Compared to the other antifungal drugs, spirolactone displayed a different antifungal spectrum, with selective activity against intrinsic resistant *Aspergillus* and no activity against *Candida* (Supplementary information Tab. 6).

To get a clue on how spirolactone A functions and how it impacts *Aspergillus*, we carried out a label-free quantitative proteomics analysis of model organism *A. niger* ATCC 1015. We initially cultured *A. niger* ATCC 1015 in PDB liquid medium for 16 hours followed by the 1-hour and 4-hour treatment with spirolactone A. The proteomics analysis showed that a total of 4,447 proteins (40.4% of the total encoded proteins) were detected, and 3,992 proteins (89.8% of the total detected proteins) didn't show significant differences between the treatment (1-hour or 4-hour treatment with spirolactone A) and the control (without spirolactone A treatment). Compared with the control, the abundance of 134 proteins significantly increased and 60 proteins significantly decreased after 1-hour spirolactone A treatment. In comparison, the abundance of 273 proteins significantly increased and 113 proteins significantly decreased after 4-hour spirolactone A treatment (Fig. 5). The Cluster of Orthologous Groups (COGs) functional classification of these differential proteins was performed by eggNOG-mapper v2.[63] Except for (S)

function unknown, these proteins were mainly clustered into a few biological processes including (Q) Secondary structure, (C) Energy production and conversion, (E) Amino acid metabolism and transport, and (O) Post-translational modifications, protein turnover, chaperone functions (*Supplementary information* Fig. 33). The Gene Ontology (GO) annotation of these proteins was mainly involved in the metabolic process, cellular process, and single-organism process during the biological process (*Supplementary information* Fig. 34). Cellular component analysis showed that these proteins were mainly localized intracellularly, especially in organelles. Meanwhile, most of these proteins participated in catalytic activity and binding in the category of molecular function. The Kyoto Encyclopedia of Genes and Genomes (KEGG) pathway analysis showed that these proteins mainly participate in amino acids metabolism and purine metabolism (*Supplementary information* Fig. 35).

The abundance of Erg13 (EHA22977.1, involved in ergosterol biosynthesis) and manganese-superoxide dismutase (EHA27012.1, involved in oxidative stress response), which was regarded as polyene antibiotic (such as amphotericin B) responsive protein,[64] was not significantly altered in the presence of spirolactone A. Allylamine antibiotics (naftifin and terbinafine) inhibit squalene epoxidase, causing the accumulation of squalene, and thereby damaging the intracellular membranes of fungi.[65] However, spirolactone A is not belonging to the allylamine family and didn't induce any changes in the squalene epoxidase (EHA21184.1). Azoles are synthetic antifungal agents of non-natural origin that inhibit cytochrome P450 sterol-14α-demethylase (CYP51) to block the ergosterol biosynthesis in the fungi.[66] Similarly, spirolactone A lacked the azoles substructure and had no impact on the abundance of CYP51 (EHA19435.1). Natural echinocandins comprise cyclic hexapeptide and lipid residues, like caspofungin, anidulafungin and micafungin, preventing the biosynthesis of glucans of the fungal cell wall through non-competitive inhibition of 1,3-β-D-glucan synthase.[67] Previous proteomics analyses had proven that the level of chitinase ChiA1 in *Aspergillus fumigatus* was significantly decreased in response to caspofungin.[68] It may represent a common effect of self-resistance development due to caspofungin increased chitin content via induction of chitin synthases during cell wall remodeling.[69] We didn't observe the abundance of 1,3-β-D-glucan synthase (EHA18547.1) and ChiA1-like chitinase (EHA28582.1) altered significantly after 1-hour and 4-hour treatment of spirolactone A in comparison to the control group.

Spirolactone A has a witness structural bias from known antifungal agents, which suggests that it may inhibit fungal growth through other targets. The fungal cell wall is an essential structure that maintains cell shape and protects fungi against environmental stress. Glycosyltransferases, glycoside hydrolases, and transglycosylases are involved in the biogenesis of the cell wall, required for growth, invading ecological niches, and counteracting the host immune response. Congo Red Hypersensitivity (CRH) family transglycosylases are usually highly expressed in multiple stages during the conidial germination of fungi and may be involved in cell wall synthesis and stability. The volcano plot of differential proteins indicated that a CRH family transglycosylase (EHA23738.1) was significantly inhibited, suggesting spirolactone A might interfere with the formation of the fungal cell wall. Trehalose-6-phosphate synthase/ phosphatase is another important enzyme for cell wall integrity and fungal virulence in various *Aspergillus* species.[70] The relative abundance of trehalose 6-phosphate synthase (EHA27700.1) was also significantly decreased after spirolactone A treatment. The above data indicated that the mode of action of spirolactone A might be mediated by disrupting fungal cell wall biosynthesis and stability (Fig. 4). Besides, we found two enzymes Erg24 (EHA26587.1) and Erg27 (EHA20711.1), which catalyze the biosynthesis of 4,4-dimethylcholesta-8,14,24-trienol to fecosterol,[71] was remarkably upregulated after spirolactone A treatment (Fig. 4). Drug efflux and resistance in fungi could be mediated by ATP-binding cassette (ABC) transporters, such as CDR1 was induced to high expression in *A. fumigatus* AF293 in the presence of azole antibiotics.[72] The expression of an ABC transporter (EHA25684.1) was activated after spirolactone A treatment. We observed the abundance of several putative spirolactone A-responsive proteins were significantly altered (Fig. 4). For example, the relative abundance of several proteins including inositol hexaphosphate kinase KCS1 (EHA27881.1), ubiquitin-protein ligase ASI3 (EHA19328.1), mitochondrial phosphate carrier protein PIC2 (EHA22842.1), pyridoxamine 5'-phosphate oxidase (EHA19800.1), and glucohydrolase (EHA21384.1) was significantly increased, but oxygen-dependent FAD-linked oxidoreductase (EHA22577.1) and dienelactone hydrolase (EHA27638.1) was significantly decreased in spirolactone-treated samples. Interestingly, an amount of unknown function proteins was found to increase or decrease in abundance affected by spirolactone and their functions still need to be further explored.

Conclusion

Herein, we report the discovery of a novel class of antifungal compound spirolactones A-C, featuring an unexpected carbon skeleton. We unravel the biosynthesis machinery of spirolactone through a variety of in silico and in vivo analyses. Spirolactone A exhibited selective antifungal activities against several Aspergillus. Proteomics analysis showed a significant inhibition of CRH transglycosylase in A. niger, along with several responsive proteins activation after spirolactone A treatment.

Methods and Materials

Strains, plasmids, and culture conditions. All strains and plasmids used in this study were summarized in *Supplementary information* Tab. 5. All primers used in this study were summarized in *Supplementary information* Tab. 6. All constructed *E. coli* strains were growing on lysogeny broth (LB) liquid or agar medium at 37 °C. Wild-type *Streptomyces* strains and its mutants were cultivated on Mannitol Soya Flour (MS) agar medium (20.0 g mannitol, 20.0 g soya flour, 20.0 g agar, 1.0 L tap water, pH=7.0-7.5) at 30 °C. The small-scale fermentation of *Streptomyces* strains was using 50 mL MS liquid medium in 250 mL flask at 30 °C with shaking at 200 rpm for 7 days. The large-scale fermentation of *Streptomyces* strains were carried out in medium 2 ($CaCl_2{\cdot}2H_2O$, 3.0 g; citric acid/Fe III, 1.0 g; $MnSO_4{\cdot}H_2O$, 0.2 g; $ZnCl_2$, 0.1 g; $CuSO_4{\cdot}5H_2O$, 0.025 g; $Na_2B_4O_7{\cdot}10H_2O$, 0.02 g; $Na_2MoO_4{\cdot}2H_2O$, 0.01 g; and oatmeal, 20.0 g, in 1.0 L distilled water), at 200 L scale in a 300 L fermentation vessel, for 6 days with aeration of 25-50 L min^{-1}, stirring at 200 rpm with a temperature of 28 °C, and at a pH range of 5.4-6.4. Antibiotics such as apramycin (50 mg mL^{-1}), kanamycin (50 mg mL^{-1}) or chloramphenicol (25 mg mL^{-1}) were appropriately used for resistance selection.

Genomic DNA extraction, sequencing, and assembly. The *S. iranensis* culture was growing in 50 mL sterilized liquid ISP2 medium (yeast extract 4.0 g; malt extract 10.0 g; and dextrose 4.0 g in 1.0 L distilled water, pH = 7.2) in 250 mL flask at 30 °C and 160 rpm for 5 days to generate sufficient biomass. The genomic DNA of *S. iranensis* was isolated using the QIAGEN Genomic-tip G100 kit according to manufacturer's instructions. The procedure of genomic DNA sequencing was combining Oxford Nanopore Technologies MinION and Illumina MiSeq system.

The *de novo* assembly of genome using Flye (v2.9-b1768) and Unicycler (v0.4.8) polishing module.

Genetic manipulation. To verify the BGC of spirolactone and its individual biosynthetic genes, the classical CRISPR-Cas9 method, and advanced CRISPR-cBEST base editing toolkit were used to construct gene-inactive mutants.[73] The function-specific plasmids (Supplementary information Tab. 3) were constructed according to the respective protocol followed by introducing into wild-type *S. iranensis* HM 35 by conjugation with donor strain ET12567/pUZ8002 on SFM solid medium (soya flour 20.0 g; mannitol 20.0 g; and bacteria agar 20.0 g, in 1.0 L distilled water, pH = 7.2) according to modified protocol. The exconjugants after resistance screening (50 mg mL^{-1} apramycin and 25 mg mL^{-1} nalidixic acid) were further verified by DNA extraction, PCR reaction, and Sanger sequencing.

DNA polymerases (Q5® High-Fidelity 2X Master Mix with Standard Buffer and OneTaq® 2X Master Mix with Standard Buffer) and restriction enzymes (NcoI, EcoRI) were purchased from New England Biolabs. PCR amplifications and restriction enzyme digestions were carried out on Bio-Rad's thermal cyclers according to the manufacturer's instructions. Plasmid DNA extraction was performed using NucleoSpin Plasmid EasyPure Kit (Macherey-Nagel, Germany). DNA purification was conducted on 1 % Tris-acetate-EDTA (TAE) agarose gel followed by using NucleoSpin Gel and PCR Clean-up Kits (Macherey-Nagel, Germany). One Shot™ Mach1™ T1 Phage-Resistant Chemically Competent E. coli from Invitrogen™ was used for transformation. All oligonucleotides were ordered from Integrated DNA Technologies and Sanger sequencing was offered by Eurofins Genomics. All solvents used for chromatography and HR-MS were purchased from VWR Chemicals with LC-MS grade, while for metabolites extraction, the solvents were of HPLC grade.

HR-ESI-MS analysis. HR-ESI-MS analysis was carried out via ultra-high-performance liquid chromatography–diode array detection–quadrupole time-of-flight mass spectrometry (UHPLC–DAD–QTOFMS) depending on an Agilent Infinity 1290 UHPLC system equipped with a diode array detector. Separation was achieved on a 250 × 2.1 mm i.d., 2.7 µm, Poroshell 120 Phenyl Hexyl column (Agilent Technologies) held at 60°C. The sample, 1 µL, was eluted at a flow rate of 0.35 mL min^{-1} using a linear gradient from 10% acetonitrile in Milli-Q water buffered with 20 mM

formic acid increasing to 100% in 15 min, staying there for 2 min before returning to 10% in 0.1 min. Starting conditions were held for 3 min before the following run. MS detection was performed on an Agilent 6545 QTOF MS equipped with Agilent Dual Jet Stream ESI with a drying gas temperature of 160°C, a gas flow of 13 L min^{-1}, sheath gas temperature of 300°C and flow of 16 L min^{-1}. Capillary voltage was set to 4000 V and nozzle voltage to 500 V in positive mode. All data were processed using Agilent MassHunter Qualitative Analysis software (Agilent Technologies, USA).

Isolation and purification. The culture broth was filtered and loaded onto an Amberchrom 161c resin LC column (200 × 20 cm, 6 L) as described before. Elution with a linear gradient of H_2O-MeOH (from 30% to 100% v/v, flow rate 0.5 L min^{-1}, in 58 min) afforded seven fractions (Fr.A-Fr.G). Fr.G was first fractionated by silica gel chromatography with a CH_2Cl_2-CH_3OH gradient to yield 16 fractions, Fr.1-Fr.16. Fr.7 was further separated by a Sephadex LH-20 (MeOH) column, and twelve sub-fractions were obtained. The fourth sub-fraction was separated by semipreparative high performance liquid chromatography (HPLC) RP-C18 (MeCN-H_2O as gradient) to afford compound **1-3.**

NMR spectroscopy. NMR spectra were recorded on 800 MHz Bruker Avance III spectrometer equipped with a TCI CryoProbe using standard pulse sequences. Measurements were carried out using ^{1}H and ^{13}C NMR, ^{1}H-^{13}C heteronuclear single quantum coherence (HSQC), ^{1}H-^{13}C heteronuclear multiple bond correlation (HMBC), ^{1}H-^{1}H correlation spectroscopy (COSY), ^{1}H-^{1}H nuclear overhauser effect spectroscopy (NOESY). Chemical shifts (δ) were reported in parts per million (ppm) and referenced to the solvent signals. Data are described as follows: chemical shift, multiplicity (*br* = broad, *s* = singlet, *d* = doublet, *t* = triplet, *dd* = doublet of doublet, *m* = multiplet and *ov* = overlapped) and coupling constants (in hertz). All NMR data were processed using MestReNova 14.0.

X-ray crystal structure determination. X-ray data collection of spirolactone was performed on an Agilent Supernova Diffractometer using CuKα radiation. Data was processed and scaled using the *CrysAlisPro* software (Agilent Technologies). The structure was solved using SHELXS and

refined using SHELXL. Hydrogen atoms were included in ideal positions using riding coordinates. The absolute configuration was determined based on the Flack parameter.

Sample preparation for proteomics analysis. Approximately 1.0 x 10^7 conidia mL^{-1} of *A. niger* ATCC 1015 strain were used to inoculate 100 mL (three biological replicates) of liquid cultures (PDB) in 1 L flask that were incubated in a reciprocal shaker at 28 °C in 180 rpm for 16 hours. Afterwards, samples in the treatment group were treated with 0.2 ug (concentration of 2 ng/mL) of spirolactone for 1-hour and 4-hour. Mycelia were then harvested by filtering, washed thoroughly with sterile water and quickly frozen in liquid nitrogen. Pellets were lysed in 100 µl lysis buffer (6 M Guanidium Hydrochloride, 10 mM TCEP, 40 mM CAA, 50 mM HEPES, pH 8.5) by boiling the samples at 95 °C for 5 mins, sonicating on high for 5 x 60 sec on/30sec off using the bioruptor pico sonication water bath (Diagenode) and finally disrupting twice with the tissuelyser (Qiagen) going from 3 to 30 hz in 1 min. Lysed samples were centrifuged at 18,000 g for 10 mins, and supernatants were transferred to clean LoBind Eppendorf tubes. Protein concentration was determined by BCA rapid gold (Thermo) and 10 µg of protein was taken forward for digestion. Samples were diluted 1:3 with digestion buffer (10% acetonitrile in 50mM HEPES pH 8.5) and incubated with 1:100 enzyme to protein ratio of LysC (MS Grade, Wako) at 37 °C for 4 hours. Samples were further diluted to a final 1:10 with more digestion buffer and digested with 1:100 trypsin for 18 hours at 37 °C. After digestion, samples were acidified with TFA and desalted using the SOLAµ SPE plate (HRP, Thermo).[74] Between each application, the solvents were spun through by centrifugation at 1,500 rpm. For each sample, the filters were activated with 200 ul of 100% Methanol, then 200 ul of 80% Acetonitrile, 0.1% formic acid. The filters were subsequently equilibrated 2x with 200 ul of 1% TFA, 3% acetonitrile, after which the sample was loaded. After washing the tips twice with 200 ul of 0.1% formic acid, the peptides were eluted into clean 0.5 ml Eppendorf tubes using 40% acetonitrile, 0.1% formic acid. The eluted peptides were concentrated in an Eppendorf Speedvac. Samples were reconstituted in 12 µL A* buffer with iRT peptides (Biognosys).

MS analysis for proteomics analysis. Peptides were loaded onto a 2cm C18 trap column (ThermoFisher 164946), connected in-line to a 15cm C18 reverse-phase analytical column

(Thermo EasySpray ES904) using 100% Buffer A (0.1% Formic acid in water) at 750 bar, using the Thermo EasyLC 1200 HPLC system, and the column oven operating at 30°C. Peptides were eluted over a 70 minute gradient ranging from 10% to 60% of Buffer B (80% acetonitrile, 0.1% formic acid) at 250 nl/min, and the Orbitrap Exploris instrument (Thermo Fisher Scientific) was run in DIA mode with FAIMS ProTM Interface (ThermoFisher Scientific) with CV of -45 V. Full MS spectra were collected at a resolution of 120,000, with an AGC target of 300 % or maximum injection time set to 'auto' and a scan range of 400–1000 m/z. The MS2 spectra were obtained in DIA mode in the orbitrap operating at a resolution of 60.000, with an AGC target 1000% or maximum injection time set to 'auto', a normalised HCD collision energy of 32. The isolation window was set to 6 m/z with a 1 m/z overlap and window placement on. Each DIA experiment covered a range of 200 m/z resulting in three DIA experiments (400-600 m/z, 600-800 m/z and 800-1000 *m/z*). Between the DIA experiments a full MS scan is performed. MS performance was verified for consistency by running complex cell lysate quality control standards, and chromatography was monitored to check for reproducibility.

Data process for proteomics analysis. The raw files were analyzed using Spectronaut™ (version 17.4) spectra were matched against the reviewed *A. niger* ATCC 1015 NCBI database. Dynamic modifications were set as Oxidation (M) and Acetyl on protein N-termini. Cysteine carbamidomethyl was set as a static modification. All results were filtered to a 1% FDR, and protein quantitation done on the MS1 level. Only proteotypic peptides were used for quantification and protein groups were inferred by IDPicker.

Antimicrobial assays. For the MIC assay, the solution of spirolactone A at 1.6 mg mL^{-1} was prepared in MeOH, DMSO (for Amphotericin B), and 50% EtOH (for Tetracycline), with 8 mL required per replicate for each strain. Fungal and bacterial cultures were maintained in Potato Dextrose Broth (PDB) and Luria-Bertani (LB) broth, respectively. Spore suspensions were collected from fungal cultures on PDB agar plates, adjusted to 1.04×10^4 CFU mL^{-1}, and bacterial cultures were diluted to 1.06×10^6 CFU mL^{-1}. In the assay, 92 mL of blank medium and 8 mL of compound solution/solvent/blank medium were added to the first column of a 96-well plate, while the second column received 50 mL of blank medium. After mixing the contents of the first

column and transferring 50 mL to the second, this process was repeated across the plate. An additional 50 mL of spore suspension or blank medium was added to different wells. The plate was then incubated at 37 °C overnight, followed by MIC determination for each tested compound.

Cytotoxic activities of Spirolactone. The LNCaP and C4-2B prostate cancer cell lines, as well as two derivative drug-resistant sublines ($C4\text{-}2B^R$ and $LNCaP^R$, respectively) were used (ref is PMID: 33799432). All cell lines were cultured and maintained in RPMI-1640 medium + glutaMAX™-I (Gibco, Invitrogen, Carlsbad, CA, United States) supplemented with 10% fetal bovine serum (FBS). One day prior to drug exposure measurements, cells were seeded into 6-well plates at a density of $0.3x10^6$ cells/well. On the next day, the medium in each well was supplemented with 1mL of fresh warm medium containing two-fold concentrations of the analytes. Cell proliferation dynamics were monitored in real-time for up to 72h using a lens-free Cellwatcher microscopy device (PHIO, Germany). The cell growth curves were generated with the analysis module available from PHIO to determine the total area covered by cells.

Cytotoxicity was measured as an endpoint assay at 48h drug-exposure using the CellTox Green Cytotoxicity Assay kit according to manufacturer's instructions. Briefly, CellTox green cytotoxicity reagent was added to the media at a final concentration of 1X, and the relative cytotoxicity was calculated relative to the control well treated with vehicle. The drug concentrations that caused inhibition of 50% cell viability (IC_{50}) were determined from the dose-response curves.

Bioinformatics analysis. All annotated CCR/AT containing BGCs were compared to reference known BGCs from MIBiG repository 3.0 using BiG-SCAPE 1.0.0 with Pfam database 32.0. The analysis was conducted using default settings with the mode "auto", mixing all lassess and retaining singletons. Networks were computed for a raw distance cutoff of 0.3. Results were visualized as a network using Cytoscape 3.9.

Reference

1. Brown, G. D., et al. Hidden Killers: Human Fungal Infections. *Sci. Transl. Med.* **4**, 165rv13-165rv13 (2012).
2. Bongomin, F., Gago, S., Oladele, R. O. & Denning, D. W. Global and multi-national prevalence of fungal diseases-estimate precision. *J. Fungi.* 3, **57** (2017).
3. Osherov, N. & Kontoyiannis, D. P. The anti-*Aspergillus* drug pipeline: Is the glass half full or empty? *Med. Mycol.* **55**, 118-124 (2017).
4. Hoenigl, M., et al. The antifungal pipeline: fosmanogepix, ibrexafungerp, olorofim, opelconazole, and rezafungin. *Drugs* **81**, 1703-1729 (2021).
5. Perfect, J. R. The antifungal pipeline: a reality check. *Nat. Rev. Drug Discovery* **16**, 603-616 (2017).
6. Denning, D. W. & Bromley, M. J. How to bolster the antifungal pipeline. *Science* **347**, 1414-1416 (2015).
7. Gubbins, P. O. & Amsden, J. R. Drug-drug interactions of antifungal agents and implications for patient care. *Expert Opin. Pharmacother.* **6**, 2231-2243 (2005).
8. Rhodes, J., et al. Population genomics confirms acquisition of drug-resistant *Aspergillus fumigatus* infection by humans from the environment. *Nat. Microbiol.* 7, 663- 674 (2022).
9. Vermeulen, E., Lagrou, K. & Verweij, P. E. Azole resistance in *Aspergillus fumigatus*: a growing public health concern. *Curr. Opin. Infect. Dis.* 26, 493-500 (2013).
10. Zhou, D., et al. Extensive genetic diversity and widespread azole resistance in greenhouse populations of *Aspergillus fumigatus* in Yunnan, China. *mSphere* 6, e00066-21 (2021).
11. Newman, D. J. & Cragg, G. M. Natural products as sources of new drugs over the nearly four decades from 01/1981 to 09/2019. *J. Nat. Prod.* **83**, 770-803 (2020).
12. Jiang, T., Pu, H., Duan, Y., Yan, X. & Huang, Y. New natural products of *Streptomyces* sourced from deep-sea, desert, volcanic, and polar regions from 2009 to 2020. *Chin. J. Org. Chem.* **41**, 1804-1820 (2021).
13. Alam, K., et al. *Streptomyces*: The biofactory of secondary metabolites. *Front. Microbiol.* **13**, 968053 (2022).
14. Oura, M., Sternberg, T. H. & Wright, E. T. A New antifungal antibiotic, amphotericin B. *Antibiot. Annu.* **3**, 566–573 (1955).

15. Hamill, R. Amphotericin B formulations: a comparative review of efficacy and toxicity. *Drugs* **73**, 919-934 (2013).
16. Fanos, V. & Cataldi, L. Amphotericin B-induced nephrotoxicity: A review. *J. Chemother.* **12**, 463-470 (2000).
17. Chen, R., et al. Turonicin A, an antifungal linear polyene polyketide from an Australian *Streptomyces* sp. *J. Nat. Prod.* **86**, 2054-2058 (2023).
18. Ndejouong, B., et al. Hygrobafilomycin, a cytotoxic and antifungal macrolide bearing a unique monoalkylmaleic anhydride moiety, from *Streptomyces varsoviensis*. *J. Antibiot.* **63**, 359-363 (2010).
19. Zhang, Z. W., Zhou, T., Harunari, E., Oku, N. & Igarashi, Y. Iseolides A-C, antifungal macrolides from a coral-derived actinomycete of the genus *Streptomyces*. *J. Antibiot.* **73**, 534-541 (2020).
20. Chevrette, M. G., et al. The antimicrobial potential of *Streptomyces* from insect microbiomes. *Nat. Commun.* **10**, 516 (2019).
21. Arai, M. Isolation of three main components. F3, F4 and F5, from azalomycin F-complex. *J. Antibiot.* **23**, 107-112 (1970).
22. Chen, Y., et al. Discovery of niphimycin C from *Streptomyces yongxingensis* sp. nov. as a promising agrochemical fungicide for controlling banana *Fusarium* Wilt by destroying the mitochondrial structure and function. *J. Agric. Food Chem.* **70**, 12874-12795 (2022).
23. Zhang, Y., et al. Antifungal activities of metabolites produced by a termite-associated *Streptomyces canus* BYB02. *J. Agric. Food Chem.* **61**, 1521-1524 (2013).
24. Nguyen, C. T., Dhakal, D., Pham, V. T., Nguyen, H. T. & Sohng, J. K. Recent advances in strategies for activation and discovery/characterization of cryptic biosynthetic gene clusters in *Streptomyces*. *Microorganisms* 8, 616 (2020).
25. Ziemert, N., Alanjary, M. & Weber, T. The evolution of genome mining in microbes - a review. *Nat. Prod. Rep.* **33**, 988-1005 (2016).
26. Hamedi, J., et al. *Streptomyces iranensis* sp nov., isolated from soil. *Int. J. Syst. Evol. Microbiol.* **60**, 1504-1509 (2010).
27. Yang, Z., et al. *Streptomyces* alleviate abiotic stress in plant by producing pteridic acids. *Nat. Commun.* **14**, 7398 (2023).

28. Blin, K., et al. antiSMASH 7.0: new and improved predictions for detection, regulation, chemical structures and visualisation. *Nucleic Acids Res.* **51**, W46-W50 (2023).

29. Keatinge-Clay, A. T. The structures of type I polyketide synthases. *Nat. Prod. Rep.* **29**, 1050-1073 (2012).

30. Wang, J., et al. Platensimycin is a selective FabF inhibitor with potent antibiotic properties. *Nature* **441**, 358-361 (2006).

31. Keatinge-Clay, A. T. A tylosin ketoreductase reveals how chirality is determined in polyketides. *Chem. Biol.* **14**, 898-908 (2007).

32. Gehret, J. J., et al. Terminal alkene formation by the thioesterase of curacin a biosynthesis structure of a decarboxylating thioesterase. *J. Biol. Chem.* **286**, 14445-14454 (2011).

33. Rudolf, J. D., Chang, C. Y., Ma, M. & Shen, B. Cytochromes P450 for natural product biosynthesis in *Streptomyces*: sequence, structure, and function. *Nat. Prod. Rep.* **34**, 1141-1172 (2017).

34. Moebius, N., et al. Biosynthesis of the respiratory toxin bongkrekic acid in the pathogenic bacterium *Burkholderia gladioli*. *Chem. Biol.* **19**, 1164-1174 (2012).

35. Zhang, Q., et al. Carboxyl formation from methyl via triple hydroxylations by XiaM in xiamycin A biosynthesis. *Org. Lett.* **14**, 6142-6145 (2012).

36. Aparicio, J. F., Caffrey, P., Gil, J. A. & Zotchev, S. B. Polyene antibiotic biosynthesis gene clusters. *Appl. Microbiol. Biotechnol.* **61**, 179-188 (2003).

37. Chen, S., et al. Tailoring the P450 monooxygenase gene for FR-008/Candicidin biosynthesis. *Appl. Environ. Microbiol.* **75**, 1778-1781 (2009).

38. Yang, J., Qi, Y., Blodgett, J. & Wencewicz, T. Multifunctional P450 monooxygenase CftA diversifies the clifednamide pool through tandem C-H bond activations. *J. Nat. Prod.* **85**, 47-55 (2022).

39. Ikeda, H. & Omura, S. Avermectin biosynthesis. *Chem. Rev.* **97**, 2591-2609 (1997).

40. Chan, Y. A., Podevels, A. M., Kevany, B. M. & Thomas, M. G. Biosynthesis of polyketide synthase extender units. *Nat. Prod. Rep.* **26**, 90-114 (2009).

41. Wilson, M. C. & Moore, B. S. Beyond ethylmalonyl-CoA: The functional role of crotonyl-CoA carboxylase/reductase homologs in expanding polyketide diversity. *Nat. Prod. Rep.* **29**, 72-86 (2012).

42. Quade, N., Huo, L. J., Rachid, S., Heinz, D. W. & Muller, R. Unusual carbon fixation gives rise to diverse polyketide extender units. *Nat. Chem. Biol.* **8**, 117-124 (2012).

43. Robinson, S. L., Christenson, J. K. & Wackett, L. P. Biosynthesis and chemical diversity of β-lactone natural products. *Nat. Prod. Rep.* **36**, 458-475 (2019).

44. Feng, K. N., et al. A hydrolase-catalyzed cyclization forms the fused bicyclic β-Lactone in vibralactone. *Angew. Chem. Int. Ed.* **59**, 7209-7213 (2020).

45. Bauman, K. D., et al. Enzymatic assembly of the salinosporamide γ-lactam-β-lactone anticancer warhead. *Nat. Chem. Biol.* **18**, 538-546 (2022).

46. Schaffer, J. E., Reck, M. R., Prasad, N. K. & Wencewicz, T. A. β-Lactone formation during product release from a nonribosomal peptide synthetase. *Nat. Chem. Biol.* **13**, 737-744 (2017).

47. Xu, Z., et al. Discovery and biosynthetic pathway analysis of cyclopentane–β-lactone globilactone A. *Nat. Synth.* (2023).

48. Christenson, J. K., et al. β-Lactone synthetase found in the olefin biosynthesis pathway. *Biochemistry* **56**, 348-351 (2017).

49. Robinson, S. L., et al. Mechanism of a standalone β-lactone synthetase: new continuous assay for a widespread ANL superfamily enzyme. *ChemBioChem* **20**, 1701-1711 (2019).

50. Wells, J. S., Trejo, W. H., Principe, P. A. & Sykes, R. B. Obafluorin, a novel beta-lactone produced by *Pseudomonas fluorescens* - taxonomy, fermentation and biological properties. *J. Antibiot.* **37**, 802-803 (1984).

51. Feling, R. H., et al. Salinosporamide A: a highly cytotoxic proteasome inhibitor from a novel microbial source, a marine bacterium of the new genus *Salinospora*. *Angew. Chem. Int. Ed.* **42**, 355-357 (2003).

52. Hochuli, E., et al. Lipstatin, an inhibitor of pancreatic lipase, produced by *Streptomyces toxytricini*. *J. Antibiot.* **40**, 1086-1091 (1987).

53. De Pascale, G., Nazi, I., Harrison, P. H. M. & Wright, G. D. β-Lactone natural products and derivatives inactivate homoserine transacetylase, a target for antimicrobial agents. *J. Antibiot.* **64**, 483-487 (2011).

54. Garcia-Rubio, R., de Oliveira, H. C., Rivera, J. & Trevijano-Contador, N. The fungal cell wall: *Candida*, *Cryptococcus*, and *Aspergillus* species. *Front. Microbiol.* 10, 2993 (2020).

55. Fang, W., et al. Mechanisms of redundancy and specificity of the *Aspergillus fumigatus* Crh

transglycosylases. *Nat. Commun.* **10**, 1669 (2019).

56. Maksimov, A. Y., Balandina, S. Y., Topanov, P. A., Mashevskaya, I. V. & Chaudhary, S. Organic antifungal drugs and targets of their action. *Curr. Top. Med. Chem.* **21**, 705-736 (2021).
57. Owens, R. A. & Doyle, S. Effects of antifungal agents on the fungal proteome: informing on mechanisms of sensitivity and resistance. *Expert Rev. Proteomics* **18**, 185-199 (2021).
58. Anderson, T. M. et al. Amphotericin forms an extramembranous and fungicidal sterol sponge. *Nat. Chem. Biol.* **10**, 400–406 (2014).
59. Lewandowska, A. et al. Fungicidal amphotericin B sponges are assemblies of staggered asymmetric homodimers encasing large void volumes. *Nat. Struct. Mol. Biol.* **28**, 972–981 (2021).
60. Ghannoum, M., et al. *In vitro* antifungal activity of naftifine hydrochloride against dermatophytes. *Antimicrob. Agents Chemother.* **57**, 4369-4372 (2013).
61. Hitchcock, C. A. Cytochrome-P-450-dependent 14α-sterol demethylase of *Candida albicans* and its interaction with azole antifungals. *Biochem. Soc. Trans.* **19**, 782-787 (1991).
62. Sawistowskaschroder, E. T., Kerridge, D. & Perry, H. Echinocandin inhibition of 1,3-β-D-glucan synthase from *Candida albicans*. *FEBS Lett.* **173**, 134-138 (1984).
63. Cantalapiedra, C. P., Hernández-Plaza, A., Letunic, I., Bork, P. & Huerta-Cepas, J. eggNOG-mapper v2: functional annotation, orthology assignments, and domain prediction at the metagenomic scale. *Mol. Biol. Evol.* **38**, 5825-5829 (2021).
64. Gautam, P., et al. Proteomic and transcriptomic analysis of *Aspergillus fumigatus* on exposure to amphotericin B. *Antimicrob. Agents Chemother.* **52**, 4220-4227 (2008).
65. Ghannoum, M., et al. *In vitro* antifungal activity of naftifine hydrochloride against dermatophytes. *Antimicrob. Agents Chemother.* **57**, 4369-4372 (2013).
66. Hitchcock, C. A. Cytochrome-P-450-dependent 14α-sterol demethylase of *Candida albicans* and its interaction with azole antifungals. *Biochem. Soc. Trans.* **19**, 782-787 (1991).
67. Sawistowskaschroder, E. T., Kerridge, D. & Perry, H. Echinocandin inhibition of 1,3-β-D-glucan synthase from *Candida albicans*. *FEBS Lett.* **173**, 134-138 (1984).
68. Cagas, S. E., Jain, M. R., Li, H. & Perlin, D. S. Profiling the *Aspergillus fumigatus* proteome in response to caspofungin. *Antimicrob. Agents Chemother.* **55**, 146-154 (2011).
69. Walker, L. A., Gow, N. A. R. & Munro, C. A. Elevated chitin content reduces the susceptibility

of *Candida* species to caspofungin. *Antimicrob. Agents Chemother.* **57**, 146-154 (2013).

70. Puttikamonkul, S., et al. Trehalose 6-phosphate phosphatase is required for cell wall integrity and fungal virulence but not trehalose biosynthesis in the human fungal pathogen *Aspergillus fumigatus*. *Mol. Microbiol.* **77**, 891-911 (2010).
71. Dhingra, S. & Cramer, R. Regulation of sterol biosynthesis in the human fungal pathogen *Aspergillus fumigatus*: opportunities for therapeutic development. *Front. Microbiol.* **8**, 92 (2017).
72. Fraczek, M. G., et al. The *cdr1B* efflux transporter is associated with non-*cyp51a*-mediated itraconazole resistance in *Aspergillus fumigatus*. *J. Antimicrob. Chemother.* **68**, 1486-1496 (2013).
73. Tong, Y., et al. CRISPR-Cas9, CRISPRi and CRISPR-BEST-mediated genetic manipulation in streptomycetes. *Nat. Protoc.* **15**, 2470-2502 (2020).
74. Rappsilber, J., Mann, M. & Ishihama, Y. Protocol for micro-purification, enrichment, pre-fractionation and storage of peptides for proteomics using StageTips. *Nat. Protoc.* **2**, 1896-1906 (2007).

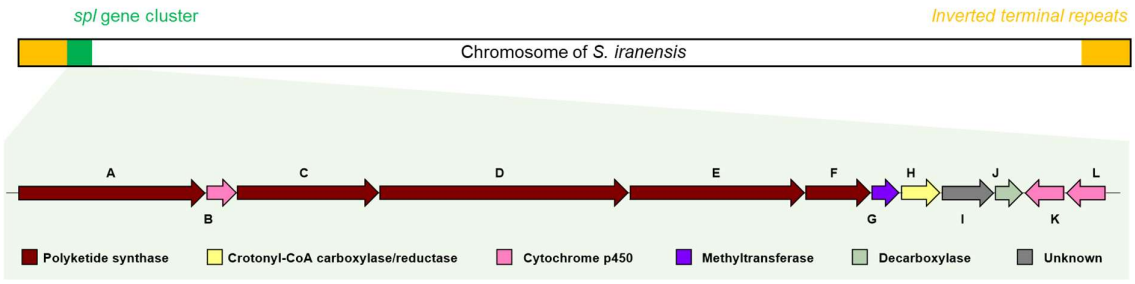

Fig. 1 The biosynthetic genes architecture of *spl* gene cluster.

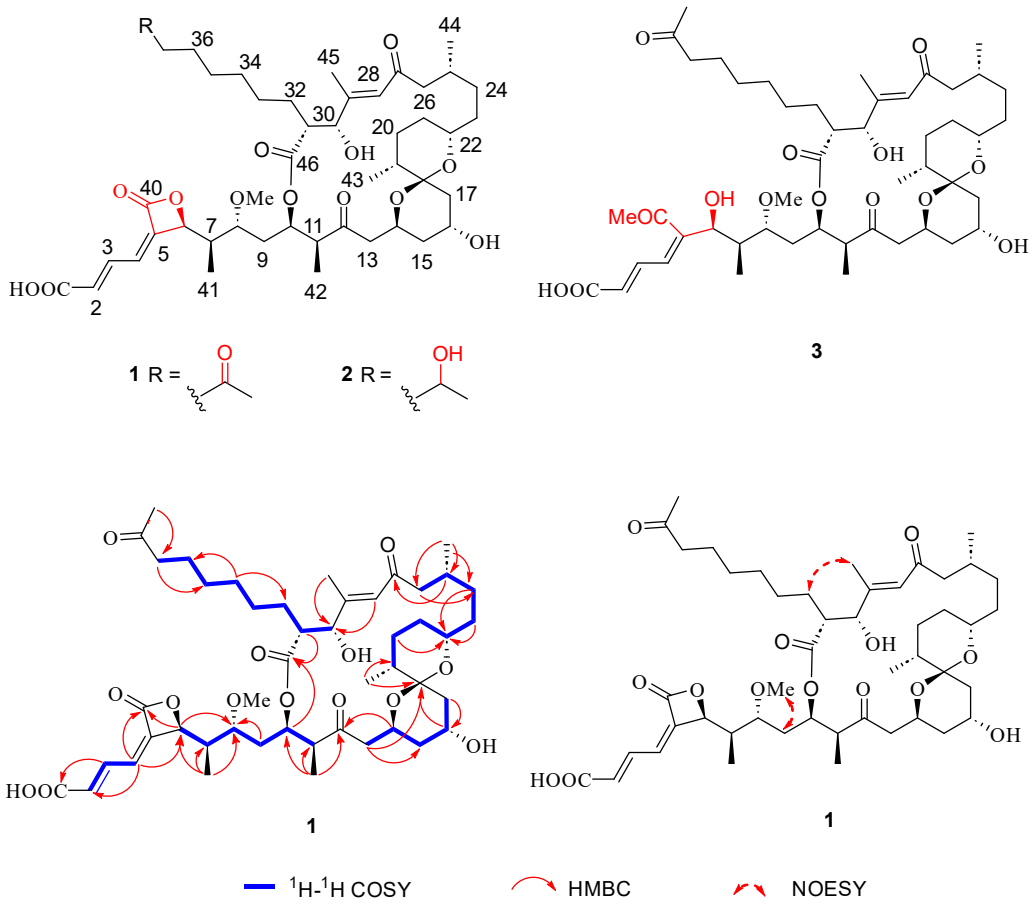

Fig. 2 Chemical structures of spirolactone and key ^{1}H-^{1}H COSY, HMBC and NOESY correlations of spirolactones A-C (**1-3**).

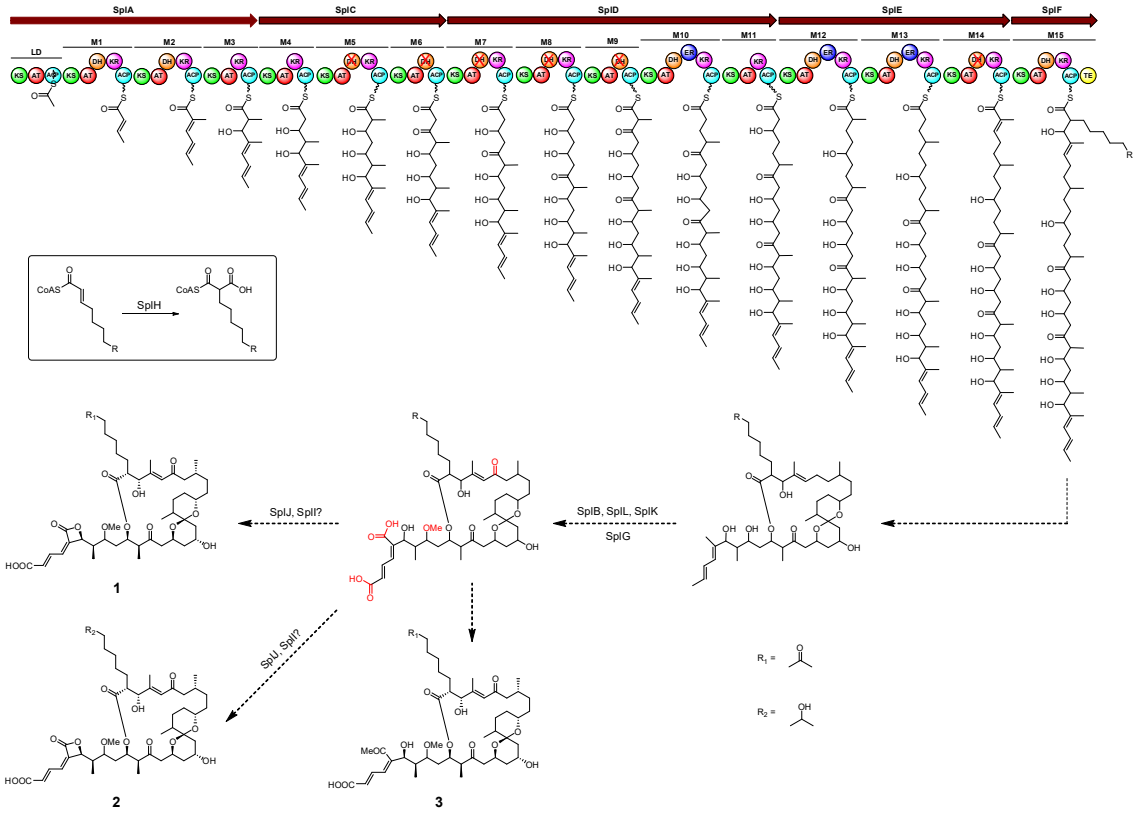

Fig. 3 Proposed biosynthesis pathway of spirolactones.

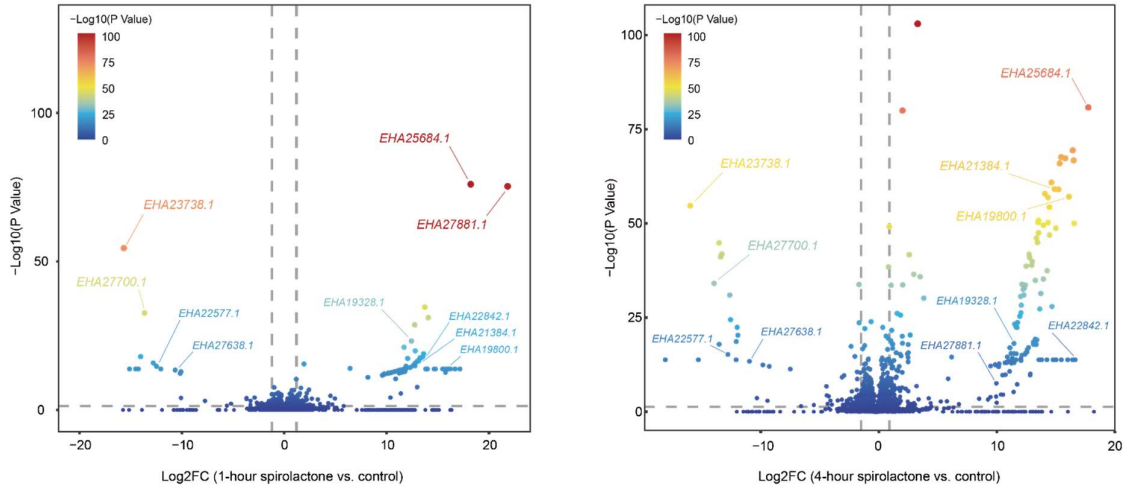

Fig. 4 Volcano plot of the abundance of protein after spirolactone A treatment based on proteomics analysis.

Supplementary Information

Spirolactone, an unprecedented antifungal β-lactone spiroketal polyketide from *Streptomyces iranensis*

Zhijie Yang,[a] Yijun Qiao,[a] Emil Strøbech,[a] Jens Preben Morth,[a] Tilmann Weber,[b] Ling Ding[a,*]

[a] Department of Biotechnology and Biomedicine, Technical University of Denmark, Søltofts Plads, Building 221, 2800 Kgs Lyngby, Denmark.

[e] The Novo Nordisk Foundation Center for Biosustainability, Technical University of Denmark, Kemitorvet, Building 220, 2800 Kgs. Lyngby, Denmark.

*Corresponding author: Ling Ding lidi@dtu.dk

Table of Contents

Tab. 1. All detected BGCs belonging to the GCF_00315 in BiG-FAM database.

Dataset	BGC	Distance to model	Length (kb)	Taxon
MIBiG	BGC0001670.1	640	88.86	*Streptomyces cinnamonensis*
MIBiG	BGC0000058.1	712	74.32	*Streptomyces graminofaciens*
Isolated bacterial draft	GCF_001941325.1/NZ_LYDV01000578.region001	742	28.08	*Streptomyces acidiscabies*
Isolated bacterial draft	GCF_001941265.1/NZ_LYDT01000970.region001	760	19.82	*Bacteria* (Kingdom)
MIBiG	BGC0000114.1	760	95.7	*Streptomyces violaceusniger*
Isolated bacterial draft	GCF_010548575.1/c00095_NZ_JAAG...region001	794	44.15	*Streptomyces* (Genus)
Isolated bacterial draft	GCF_001949645.1/NZ_BCML01000004.region001	819	63.06	*Streptomyces acidiscabies*
Isolated bacterial draft	GCF_001485105.1/NZ_BCMK01000018.region001	826	63.14	*Streptomyces acidiscabies*
MIBiG	BGC0000109.1	835	80.36	*Streptomyces cyaneogriseus*
MIBiG	BGC0000100.1	844	103.45	*Streptomyces cinnamonensis*

Tab. 2. The biosynthetic gene clusters in *S. iranensis* based on genome resequencing.

Region	Type	Position		Most similar known cluster	Similarity
Region 1	lassopeptide	47,826	67,848	SSV-2083	18%
Region 2	NRPS-like, T1PKS, NRPS	89,243	264,517	meridamycin	10%
Region 3	terpene, NRPS	310,755	369,526	carotenoid	63%
Region 4	NRPS	584,615	633,798	coelichelin	100%
Region 5	butyrolactone	920,071	929,026	cyphomycin	9%
Region 6	phosphonate, acyl_amino_acids, butyrolactone, NRPS-like, T1PKS, hserlactone	983,576	1,129,298	cyphomycin	5%
Region 7	T1PKS	1,216,733	1,353,478	azalomycin F3a	100%
Region 8	T1PKS	1,525,866	1,708,371	nigericin	70%
Region 9	T1PKS	1,812,276	1,890,013	efomycin K/F	95%
Region 10	redox-cofactor	1,914,682	1,936,746		
Region 11	hserlactone	2,054,025	2,074,780	heronamides	8%
Region 12	butyrolactone	2,085,494	2,096,426		
Region 13	T1PKS, NRPS	2,274,879	2,327,099	meilingmycin	4%
Region 14	NRPS, T3PKS, other	2,383,216	2,482,446	feglymycin	78%
Region 15	NRPS, T1PKS	2,535,309	2,739,409	kitacinnamycin	16%
Region 16	terpene	2,985,464	3,007,479	hopene	76%
Region 17	T1PKS	3,153,626	3,235,531	bafilomycin B1	55%
Region 18	T2PKS	3,304,807	3,374,688	spore pigment	83%
Region 19	T1PKS	3,499,162	3,559,357	notonesomycin A	11%
Region 20	RiPP-like	3,612,469	3,622,637		
Region 21	siderophore	3,792,665	3,803,134		
Region 22	T2PKS	4,140,701	4,213,204	isoindolinomycin	61%
Region 23	NRPS-like	4,442,739	4,484,596	echosides	100%
Region 24	siderophore	5,229,788	5,240,857	legonoxamines/ desferrioxamin B	83%
Region 25	terpene	6,441,503	6,461,832	TVA-YJ-2	9%
Region 26	ladderane, arylpolyene, NRPS	6,705,172	6,807,080	kitacinnamycins	50%
Region 27	NRPS	7,345,535	7,387,933	ochronotic pigment	75%
Region 28	ladderane	7,449,836	7,489,866	cinnapeptin	53%
Region 29	RRE-containing	7,510,172	7,530,691	granaticin	10%
Region 30	T1PKS	7,664,407	7,848,116	desulfoclethramycin /clethramycin	59%
Region 31	terpene	8,396,931	8,416,950		
Region 32	ectoine	9,062,415	9,072,819	ectoine	100%
Region 33	siderophore	9,237,702	9,251,453	peucechelin	20%
Region 34	terpene	9,301,372	9,319,391	BE-43547s	25%
Region 35	nucleoside	9,535,814	9,572,869	huimycin	100%
Region 36	nucleoside, NRPS, T1PKS, NRPS-like	9,677,504	9,821,457	rapamycin	82%
Region 37	PKS-like	9,909,290	9,950,318	rustmicin	33%
Region 38	terpene	10,000,500	10,020,321	2-methylisoborneol	100%
Region 39	terpene	10,464,893	10,484,016	pristinol	100%
Region 40	T1PKS, ladderane,arylpolyene	10,578,295	10,629,355	cinnapeptin	46%
Region 41	T1PKS, NRPS-like	10,835,982	10,918,034	hygrocins	83%

Region 42	lanthipeptide-class-ii	11,011,708	11,035,079	reveromycin A	9%
Region 43	hglE-KS, T1PKS, RiPP-like	11,062,970	11,124,110	Hexacosalactone A	68%
Region 44	T1PKS, NRPS	11,127,758	11,269,230	neomediomycin B	32%
Region 45	terpene	11,320,894	11,341,820	brasilicardin A	30%
Region 46	terpene	11,470,415	11,491,323		
Region 47	T1PKS, NRPS-like	11,577,719	11,624,306	niphimycins C-E	12%
Region 48	betalactone	11,818,784	11,847,595	Sch-47554 / Sch-47555	7%
Region 49	NRPS, NRPS-like, T1PKS	12,040,448	12,123,871	notonesomycin A	3%
Region 50	lassopeptide	12,143,153	12,165,683	SSV-2083	18%

Tab. 3. The function annotation of biosynthetic genes of *spl* gene cluster.

ORF	Size[a]	Proposed functions	SI/ID[b]	Protein homologue and origin
orf(-3)	99	Transposase	95/98	KQV94169.1, *Streptomyces* sp. Root369
orf(-2)	139	Transposase	93/95	GHA09393.1, *Strepotmyces tauricus*
orf(-1)	543	IS701 family transposase	96/96	WP_210609107.1, *Streptomyces rhizosphaericus*
splA	5764	Type I polyketide synthase	70/77	WP_069850026.1, *Actinoalloteichus hymeniacidonis*
splB	416	Cytochrome P450	68/79	WP_028677909.1, *Salinispora arenicola*
splC	4443	Type I polyketide synthase	54/65	WP_098246318.1, *Streptomyces formicae*
splD	8121	Type I polyketide synthase	55/67	WP_100583907.1, *Streptomyces* sp. CB02120-2
splE	5720	Type I polyketide synthase	49/60	BAE93731.1, *Streptomyces* sp. NRRL 11266
splF	1969	Type I polyketide synthase	56/66	WP_116210512.1, *Streptomyces olivoreticuli*
splG	269	Methyltransferase domain-containing protein	65/75	WP_198270846.1, *Streptomyces sabulosicollis*
splH	411	Crotonyl-CoA carboxylase/reductase	74/85	WP_042181611.1, *Kibdelosporangium* sp. MJ126-NF4
splI	654	Hypothetical protein	42/54	WP_089101481.1, *Streptomyces hyaluromycini*
splJ	338	UbiD family decarboxylase	60/75	WP_106196453.1, *Umezawaea tangerina*
splK	394	Cytochrome P450	58/72	MBR7672783.1, *Streptomyces daliensis*
splL	403	Cytochrome P450	52/68	WP_227725975.1, *Streptomyces* sp. ET3-23
orf(1)	115	Glycoside hydrolase family 3 C-terminal domain-containing protein	81/83	WP_164421869.1, *Streptomyces* sp. SID13726
orf(2)	183	TIGR03086 family meta-binding protein	93/96	WP_228053099.1, *Streptomyces antimycoticus*
*orf(3)**	119	GNAT family N-acetyltransferase	88/93	WP_043236267.1, *Streptomyces violaceusniger*
*orf(4)**	420	ATP-grasp domain-containing protein	82/89	WP_014057722.1, *Streptomyces violaceusniger*

[a], The size of amino acids; [b], similarity-identity ratio; *, located in the inverted terminal repeat region.

Tab. 4. ^{1}H and ^{13}C NMR data of compounds **1**, **2**, and **3** ($CDCl_3$).

pos.	**1**		**2**		**3**	
	δ_C, type	δ_H, (*J* in Hz)	δ_C, type	δ_H, (*J* in Hz)	δ_C, type	δ_H, (*J* in Hz)
1	168.6, C	-	167.3, C	-	168.3, C	-
2	128.5, CH	6.19 (d, 15.4)	128.3, CH	6.19 (d, 15.5)	125.9, CH	6.11 (d, 15.7)
3	137.8, CH	7.91 (dd, 15.4, 11.8)	137.8, CH	7.92 (dd, 15.5, 11.5)	141.0, CH	7.94 (dd, 15.7,11.7)
4	129.1, CH	6.47 (d, 10.7)	129.0, CH	6.47 (d, 11.5)	133.6, CH	6.74 (d, 11.6)
5	143.2, C		143.2, C	-	144.2, C	-
6	79.4, CH	4.88 (d, 8.9)	79.4, CH	4.90 (d, 9.0)	75.8, CH	4.35 (d, 8.4)
7	41.5, CH	1.93 (overlapping)	41.3, CH	1.89 (overlapping)	40.7, CH	1.98 (overlapping)
8	76.5, CH	3.37 (overlapping)	76.3, CH	3.36 (m)	79.6, CH	3.45 (m)
9	32.0, CH_2	1.51 (d, 4.7), 1.46 (d, 4.10)	31.6, CH_2	1.51 (m)	33.6, CH_2	1.58 (m)
10	71.2, CH	5.15 (dq, 3.4, 2.1)	71.8, CH	5.12 (d, 11.4)	72.0, CH	5.14 (dq, 3.4, 2.1)
11	48.4, CH	3.03 (m)	48.2, CH	3.04 (m)	48.7, CH	2.97 (m)
12	207.3, C		207.2, C	-	207.3, C	-
13	47.8, CH_2	2.81 (dd, 12.4, 2.9), 2.50 (dd, 12.4, 10.1)	47.6, CH_2	2.79 (dd, 12.4, 2.9), 2.49 (dd, 12.4, 10.1)	47.9, CH_2	2.73 (dd, 13.2, 3.9), 2.53 (dd, 13.2, 9.2)
14	60.7, CH	4.12 (overlapping)	60.5, CH	4.10 (overlapping)	60.7, CH	4.13 (overlapping)
15	38.2, CH_2	1.93 (overlapping), 1.51 (overlapping)	38.1, CH_2	1.91 (overlapping), 1.50 (overlapping)	37.1, CH_2	1.93 (overlapping), 1.51 (overlapping)
16	65.0, CH	4.15 (overlapping)	64.7, CH	4.13 (m)	64.9, CH	4.14 (overlapping)
17	37.0, CH_2	1.97 (d, 14.1), 1.45 (dd, 14.2, 3.5)	36.8, CH_2	1.96 (d, 14.1), 1.43(dd, 14.2, 3.5)	37.0, CH_2	1.97 (d, 14.1), 1.45 (dd, 14.2, 3.5)
18	101.0, C	-	101.0, C	-	101.0, C	-
19	34.8, CH	1.66 (m)	34.5, CH	1.65 (m)	34.8, CH	1.66 (m)
20	25.4, CH_2	2.10 (overlapping)	25.2, CH_2	2.09 (overlapping)	25.4, CH_2	2.10 (overlapping)
21	25.4, CH_2	1.40 (overlapping), 1.28 (overlapping)	25.2, CH_2	1.41 (overlapping), 1.27 (overlapping)	25.4, CH_2	1.40 (overlapping), 1.25 (overlapping)
22	72.0, CH	3.23 (dt, 11,5, 9.6)	72.0, CH	3.22 (m)	72.0, CH	3.23 (dt, 11,5, 9.6)
23	33.6, CH_2	1.58 (m), 1.26 (overlapping)	33.6, CH_2	1.58 (m), 1.24 (overlapping)	33.6, CH_2	1.58 (m), 1.26 (overlapping)
24	33.9, CH_2	1.14 (m)	34.0, CH_2	1.15 (m)	34.0, CH_2	1.15 (m)
25	30.0, CH	2.15 (overlapping)	29.8, CH	2.14 (m)	30.0, CH	2.15 (overlapping)
26	51.8, CH_2	2.61 (dd, 16.3, 10.7), 2.24 (dd, 16.3, 7.8)	51.5, CH_2	2.60 (dd, 16.3, 10.8), 2.24 (16.3, 7.8)	51.8, CH_2	2.61 (dd, 16.0, 10.5), 2.24 (dd, 16.3, 7.8)
27	201.3, C	-	201.3, C	-	201.6, C	-
28	123.0, CH	6.48 (s)	123.0, CH	6.49 (s)	123.2, CH	6.52 (s)
29	156.4, C	-	156.4, C	-	156.4, C	-
30	75.8, CH	4.14 (overlapping)	75.7, CH	4.13 (overlapping)	75.5, CH	4.14 (overlapping)
31	47.2, CH	2.83 (dd, 8.8, 2.4)	46.8, CH	2.82 (dd, 8.8, 2.4)	47.2, CH	2.83 (dt, 8.8, 2.4)
32	30.7, CH_2	1.93 (overlapping), 1.81 (m)	30.4, CH_2	1.84 (m)	30.7, CH_2	1.93 (overlapping), 1.81 (m)
33	27.4, CH_2	1.48 (overlapping), 1.34 (overlapping)	27.3, CH_2	1.47 (overlapping), 1.30 (overlapping)	27.4, CH_2	1.48 (overlapping), 1.34 (overlapping)
34	29.2, CH_2	1.38 (overlapping)	29.1, CH_2	1.36 (overlapping)	29.2, CH_2	1.38 (overlapping)
35	28.8, CH_2	1.33 (overlapping)	30.0, CH_2	1.28 (m)	28.8, CH_2	1.33 (overlapping)
36	23.6, CH_2	1.58 (m)	25.6, CH_2	1.45, 1.35	23.6, CH_2	1.58 (m)

37	43.6, CH_2	2.46 (t,7.4)	39.1, CH_2	1.46 (m)	43.6, CH_2	2.46 (t, 7.4)
38	209.6, C	-	68.0, CH	3.84 (m)	209.6, C	-
39	29.9, CH_3	2.15 (s)	23.6, CH_3	1.22 (dd, 6.2, 2.7)	30.0, CH_3	2.13 (s)
40	161.8, C	-	161.8, C	-	166.9, C	
41	8.4, CH_3	0.94 (d, 7.2)	8.4, CH_3	0.93 (d, 7.2)	11.6, CH_3	0.77 (d, 7.2)
42	9.2, CH_3	0.95 (d,6.8)	9.2, CH_3	0.93 (d,6.8)	9.6, CH_3	0.96 (d,7.2)
43	14.3, CH_3	0.98 (d, 7.2)	14.0, CH_3	0.97 (d,7.2)	14.3, CH_3	0.87 (d,7.2)
44	19.5, CH_3	0.93 (d, 6.8)	19.5, CH_3	0.92 (d, 6.8)	19.5, CH_3	0.92 (d, 6.8)
45	17.4, CH_3	2.10 (s)	17.0, CH_3	2.09 (s)	17.3, CH_3	2.07 (s)
46	174.9, C	-			175.0, C	-
8-OMe	59.6, CH_3	3.37 (s)	59.1	3.34 (s)	58.7, CH3	3.36 (s)
40-OMe					52.1, CH3	3.85 (s)

Tab. 5. Alignment of conserved motifs in the active site of AT domains.

domain name	specificity	198	199	200	201
ave_AT5	Malonyl-CoA	H	A	F	H
nid_AT3	Malonyl-CoA	H	A	F	H
epo_AT2	Malonyl-CoA	H	A	F	H
amp_AT18	Malonyl-CoA	H	A	F	H
rif_AT2	Malonyl-CoA	H	A	F	H
spl_AT1	Malonyl-CoA	H	A	F	H
spl_AT2	Malonyl-CoA	H	A	F	H
spl_AT5	Malonyl-CoA	H	A	F	H
spl_AT7	Malonyl-CoA	H	A	F	H
spl_AT8	Malonyl-CoA	H	A	F	H
spl_AT9	Malonyl-CoA	H	A	F	H
spl_AT11	Malonyl-CoA	H	A	F	H
spl_AT12	Malonyl-CoA	H	A	F	H
spl_AT14	Malonyl-CoA	H	A	F	H
ave_AT1	Methylmalony-CoA	Y	A	S	H
ery_AT4	Methylmalony-CoA	Y	A	S	H
amp_AT2	Methylmalony-CoA	Y	A	S	H
rif_AT7	Methylmalony-CoA	Y	A	S	H
spl_AT3	Methylmalony-CoA	Y	A	S	H
spl_AT4	Methylmalony-CoA	Y	A	S	H
spl_AT5	Methylmalony-CoA	Y	A	S	H
spl_AT10	Methylmalony-CoA	Y	A	S	H
spl_AT13	Methylmalony-CoA	Y	A	S	H
spl_AT15	Methylmalony-CoA	Y	A	S	H
nid_AT5	Ethylmalonyl-CoA	T	A	G	H
tyl_AT5	Ethylmalonyl-CoA	T	A	G	H
spl_AT16	-CoA	I	A	S	H

Abbreviations: ave, avermectin; nid, niddamycin; epo, epothilone; amp, amphotericin; rif, rifamycin; ery, erythromycin; tyl, tylactone; meg, megalomicin; pta, pteridic acids.

Tab. 6. Bioactivity assays of spirolactone A.

Species	Tetracycline MIC in mg L^{-1}	Amphotericin B MIC in mg L^{-1}	Spirolactone A MIC in mg L^{-1}
Staphylococcus aureus	1	-	>64
Aspergillus niger	-	0.5	0.004
Aspergillus tubingensis	-	0.125	0.004
Aspergillus flavus	-	4	0.015
Candida auris	-	1	>8
Candida albicans (Echinocandin resistant)	-	0.125	>8
Candida albicans (Echinocandin sensitive)	-	0.06	>8
Candida glabrata (Echinocandin resistant)	-	0.5	>8
Candida glabrata (Echinocandin sensitive)	-	0.5	>8
Candida parapsilosis (Azol resistant)	-	0.25	>8
Candida parapsilosis (Azol sensitive)	-	0.25	>8
Fusarium musae	-	4	>8
Fusarium proliferatum	-	4	>8
Lomentospora prolificans	-	>8	>8
Mucor circinelloides	-	0.06	>8
Purpureocilium lilacinum	-	>16	>8
Rhizopus arrhizus	-	0.125	>8
Trichoderma longibrachiatum	-	2	>8

Tab. 7. The strains and plasmids used in this study.

Strains	**Description**	**Source/[Ref]**
One Shot™ Mach1™ T1 Phage-Resistant Chemically Competent *E. coli*	For routine plasmids maintenance and cloning	Thermo Fisher Scientific
E. coli ET12567/pUZ8002	For conjugating plasmids into *Streptomyces*	[1]
S. iranensis	Wild-type strain	DSMZ
S. iranensis/Δ*splA*	Knock-out of *splA* in *S. iranensis*	In this work
S. iranensis/Δ*splB*	Inactivation of *splB* in *S. iranensis*	In this work
S. iranensis/Δ*splG*	Inactivation of *splG* in *S. iranensis*	In this work
S. iranensis/Δ*splH*	Inactivation of *splH* in *S. iranensis*	In this work
S. iranensis/Δ*splI*	Inactivation of *splI* in *S. iranensis*	In this work
S. iranensis/Δ*splJ*	Knock-out of *splJ* in *S. iranensis*	In this work
S. iranensis/Δ*splK*	Inactivation of *splK* in *S. iranensis*	In this work
S. iranensis/Δ*splL*	Inactivation of *splL* in *S. iranensis*	In this work
S. iranensis/Δ*splH::splH*	Complementation strain of Δ*splH* mutant	In this work
Plasmids		
pCRISPR-Cas9	Gene knockout/in for actinomycetes	[2]
pCRISPR-cBEST	For C to T base editing	[3]
pGM1190	Plasmid for gene complementation	[4]
pCRISPR-Cas9/Δ*splA*	Modified plasmid for knock-out of *splA*	In this work
pCRISPR-Cas9/Δ*splJ*	Modified plasmid for knock-out of *splJ*	In this work
pCRISPR-cBEST/Δ*splB*	Modified plasmid for inactivation of *splB*	In this work
pCRISPR-cBEST/Δ*splG*	Modified plasmid for inactivation of *splG*	In this work
pCRISPR-cBEST/Δ*splH*	Modified plasmid for inactivation of *splH*	In this work
pCRISPR-cBEST/Δ*splI*	Modified plasmid for inactivation of *splI*	In this work
pCRISPR-cBEST/Δ*splK*	Modified plasmid for inactivation of *splK*	In this work
pCRISPR-cBEST/Δ*splL*	Modified plasmid for inactivation of *splL*	In this work
pGM1190-*splH*	Modified plasmid for complementation	In this work

Tab. 8. The primers used in this study.

Primer name	Sequence (5' → 3')	Description
Del-*splA*-sgRNA	CCGGTTGGTAGGATCGACGGGgaccagtggcctccgcgtaGTTTTAGAGCTAGAAATAGC	Knock-out of *splA,* the base marked in red is sgRNA sequence
Del-*splA*-uparm-F	tcgtcgaaggcactagaaggatctggttgcagtcgtcgta	Forward primer for amplification of upstream homologous flank of *splA*
Del-*splA*-uparm-R	actcacctgttccagtgatccacttgcacgaactgaccag	Reverse primer for amplification of upstream homologous flank of *splA*
Del-*splA*-downarm-F	ctggtcagttcgtgcaagtggatcactggaacaggtgagt	Forward primer for amplification of downstream homologous flank of *splA*
Del-*splA*-downarm-R	ggtcgatccccgcatatagggtacatgatcgacggacaag	Reverse primer for amplification of downstream homologous flank of *splA*
ID-*splA*-F1	atgaagaagatcgagctgatg	Forward primer for screening *splA* mutants
ID-*splA*-R1	ctcaacgcgttccagatc	Reverse primer for screening *splA* mutants
ID-*splA*-F2	cttcgaggagctcgtcgtac	Forward primer for screening *splA* mutants
ID-*splA*-R2	catctgttaacggcacacc	Reverse primer for screening *splA* mutants
Del-*splJ*-sgRNA	CCGGTTGGTAGGATCGACGGtcgagaagtccccgatcatgGTTTTAGAGCTAGAAATAGC	Knock-out of *splJ*, the base marked in red is sgRNA sequence
Del-*splJ*-uparm-F	tcgtcgaaggcactagaagggcgcaaactggtcaacatggc	Forward primer for amplification of upstream homologous flank of *splJ*
Del-*splJ*-uparm-R	gagagatcgacggcgacatggagcatccacgtgctgaccgacaacc	Reverse primer for amplification of upstream homologous flank of *splJ*
Del-*splJ*-downarm-F	ggttgtcggtcagcacgtggatgctccatgtcgccgtcgatctctc	Forward primer for amplification of downstream homologous flank of *splJ*
Del-*splJ*-downarm-R	ggtcgatccccgcatataggctgaccgactacctgagcacgg	Reverse primer for amplification of downstream homologous flank of *splJ*
ID-*splJ*-F1	gacctcgaagacggactcg	Forward primer for screening *splJ* mutants
ID-*splJ*-R1	gaagagtccgatcaggaag	Reverse primer for screening *splJ* mutants
ID-*splJ*-F2	ctccctgatcttcaacaagctc	Forward primer for screening *splJ* mutants
ID-*splJ*-R2	ttcccgctggccttcaac	Reverse primer for screening *splJ* mutants
Inact-*splB*	CCGGTTGGTAGGATCGACGGcaaccagatcctgcgccacaGTTTTAGAGCTAGAAATAGC	Inactivation of *splB*, the base marked in red is sgRNA sequence
Inact-*splG*	CCGGTTGGTAGGATCGACGGcggtccagtagccgaggtgcGTTTTAGAGCTAGAAATAGC	Inactivation of *splG*, the base marked in red is sgRNA sequence
Inact-*splH*	CCGGTTGGTAGGATCGACGGgctcccagccacacaactgcGTTTTAGAGCTAGAAATAGC	Inactivation of *splH*, the base marked in red is sgRNA sequence
Inact-*splI*	CCGGTTGGTAGGATCGACGGgaaccagaccttcagcgtacGTTTTAGAGCTAGAAATAGC	Inactivation of *splI*, the base marked in red is sgRNA sequence
Inact-*splK*	CCGGTTGGTAGGATCGACGGctgatccaggcccgtgacgaGTTTTAGAGCTAGAAATAGC	Inactivation of *splK*, the base marked in red is sgRNA sequence
Inact-*splL*	CCGGTTGGTAGGATCGACGGaactcccagagtccgtagaaGTTTTAGAGCTAGAAATAGC	Inactivation of *splL*, the base marked in red is sgRNA sequence
ID-*splB*-F	cagcatcgtgcggaagatc	Forward primer for screening *splB* mutants
ID-*splB*-R	ctgctcgctctgctgga	Reverse primer for screening *splB* mutants
ID-*splG*-F	cttgtctagttcctggatcc	Forward primer for screening *splG* mutants
ID-*splG*-R	gtcttcgactatcccacg	Reverse primer for screening *splG* mutants
ID-*splH*-F	gacgatctggatggccatc	Forward primer for screening *splH* mutants
ID-*splH*-R	catatgacacggaccgtgtac	Reverse primer for screening *splH* mutants
ID-*splI*-F	actcccttgacgttcttcttg	Forward primer for screening *splI* mutants
ID-*splI*-R	ctacgtctggctcatgaacac	Reverse primer for screening *splI* mutants
ID-*splK*-F	tggtcaagaactcgccgaac	Forward primer for screening *splK* mutants
ID-*splK*-R	aagcggagtacctcctcgac	Reverse primer for screening *splK* mutants
ID-*splL*-F	catccaggagatcgtcgac	Forward primer for screening *splL* mutants
ID-*splL*-R	cgtgccgttcaccaataac	Reverse primer for screening *splL* mutants
pGM1190-*splH*-F	agaagggagcggacatatgaatgacacggaccgtgtacga	Forward primer for amplification of *splH*
pGM1190-*splH*-R	acaaaactttagatctggggctagttcctggatccgggtt	Reverse primer for amplification of *splH*
ID-pGM1190-*splH*-F	gaggtcattactggaccgg	Forward primer for verification of *splH* complementation
ID-pGM1190-*splH*-R	cactccgctgaaactgttg	Reverse primer for verification of *splH* complementation

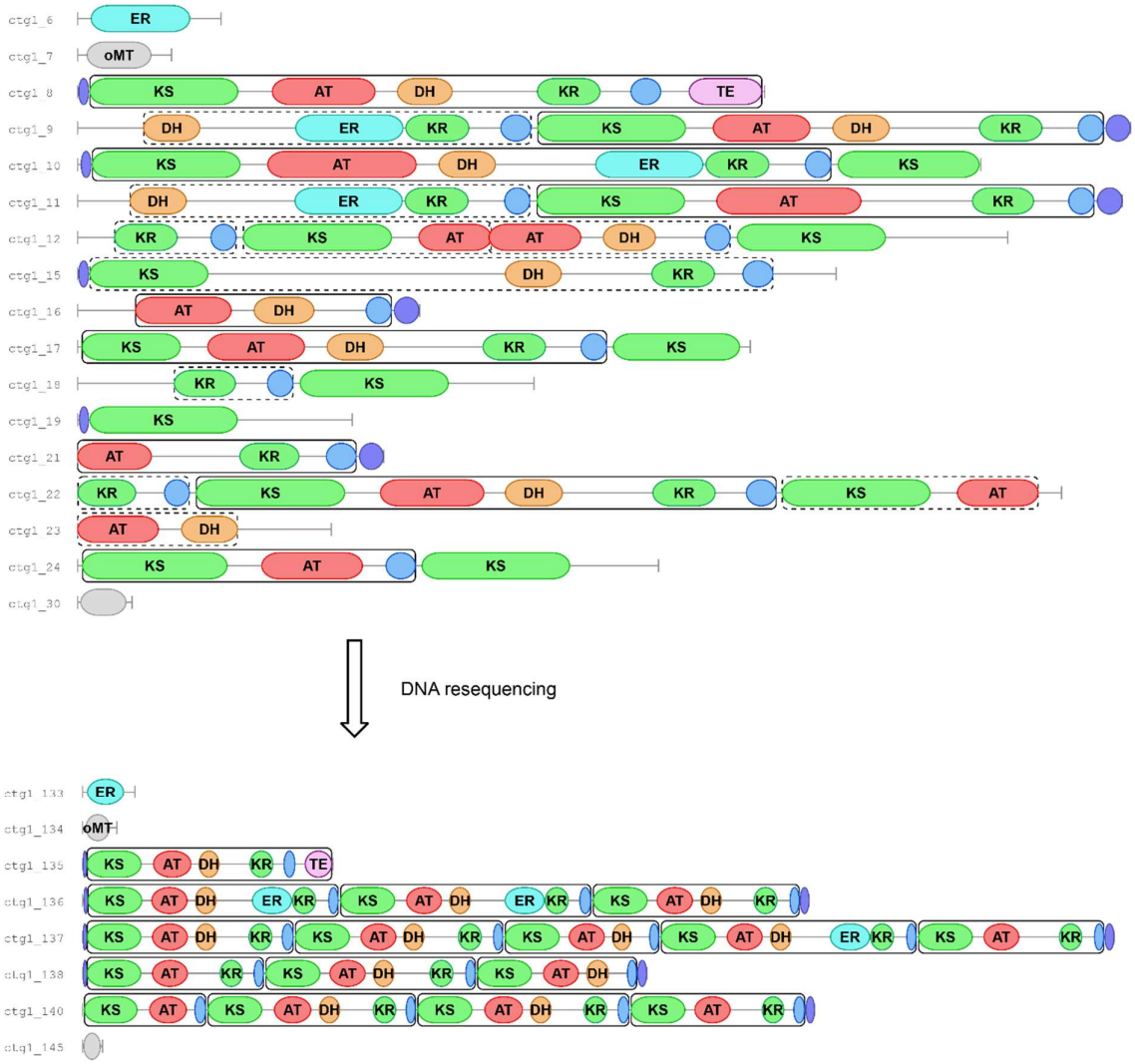

Fig. 1. Domain annotation of *spl* gene cluster in *S. iranensis* before and after whole-genome resequencing.

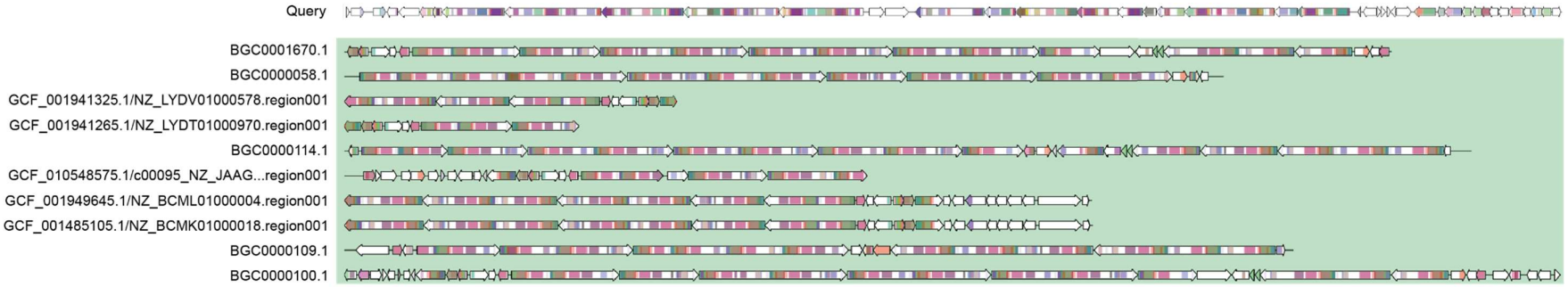

Fig. 2. The biosynthetic gene architecture of spirolactone from *S. iranensis* and other BGCs from GCF_00315.

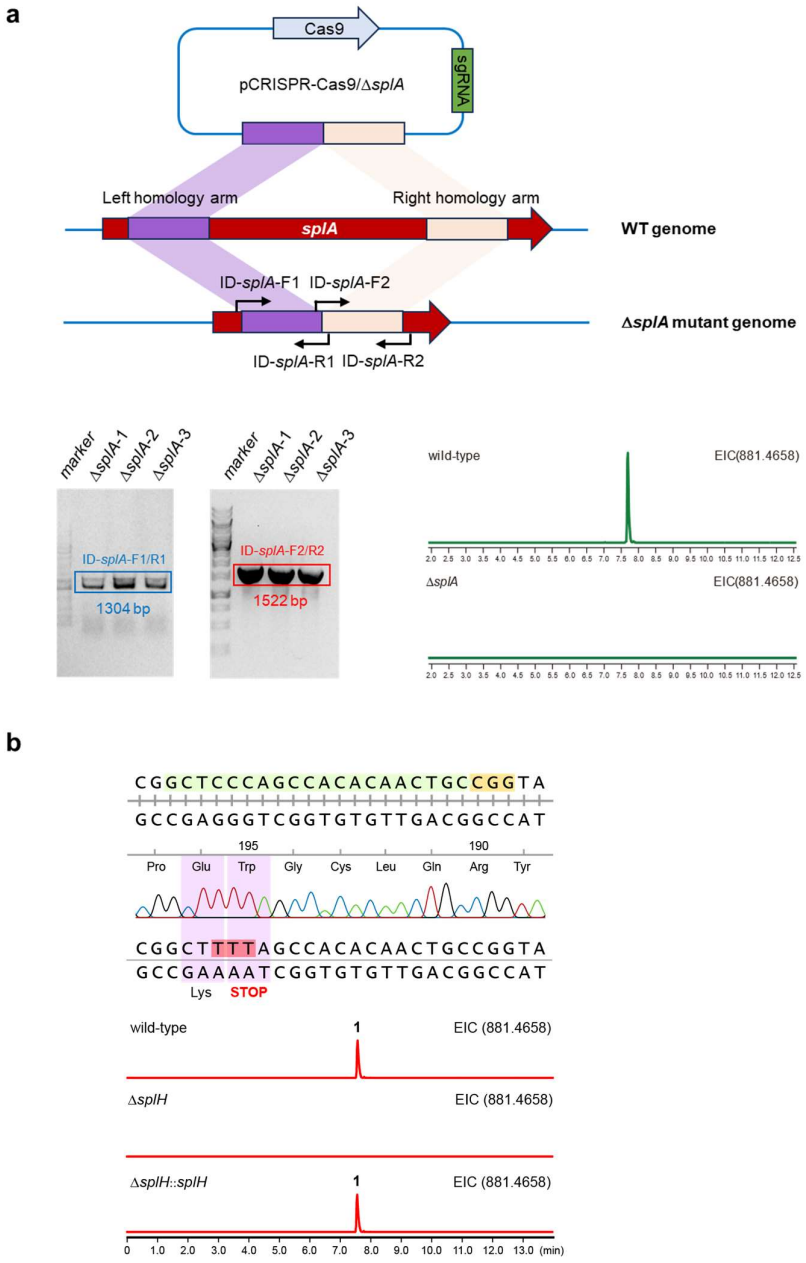

Fig. 3. Knock-out of *splA* and inactivation of *splH* in wild-type *S. iranensis*.

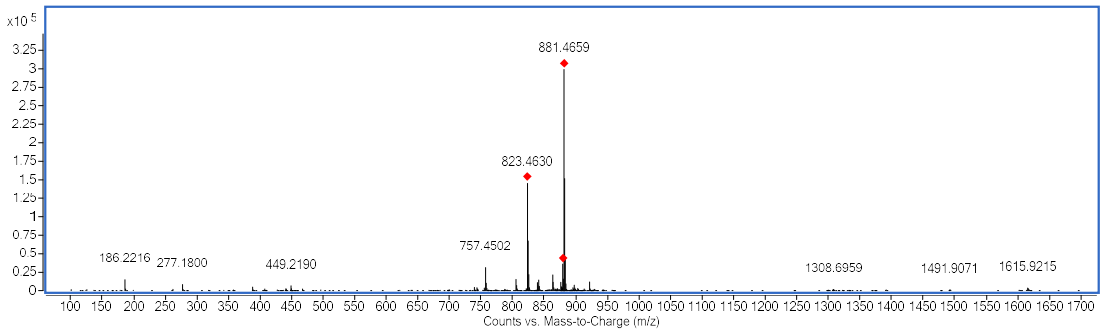

Fig. 4. HR-ESI-MS spectrum of **1**.

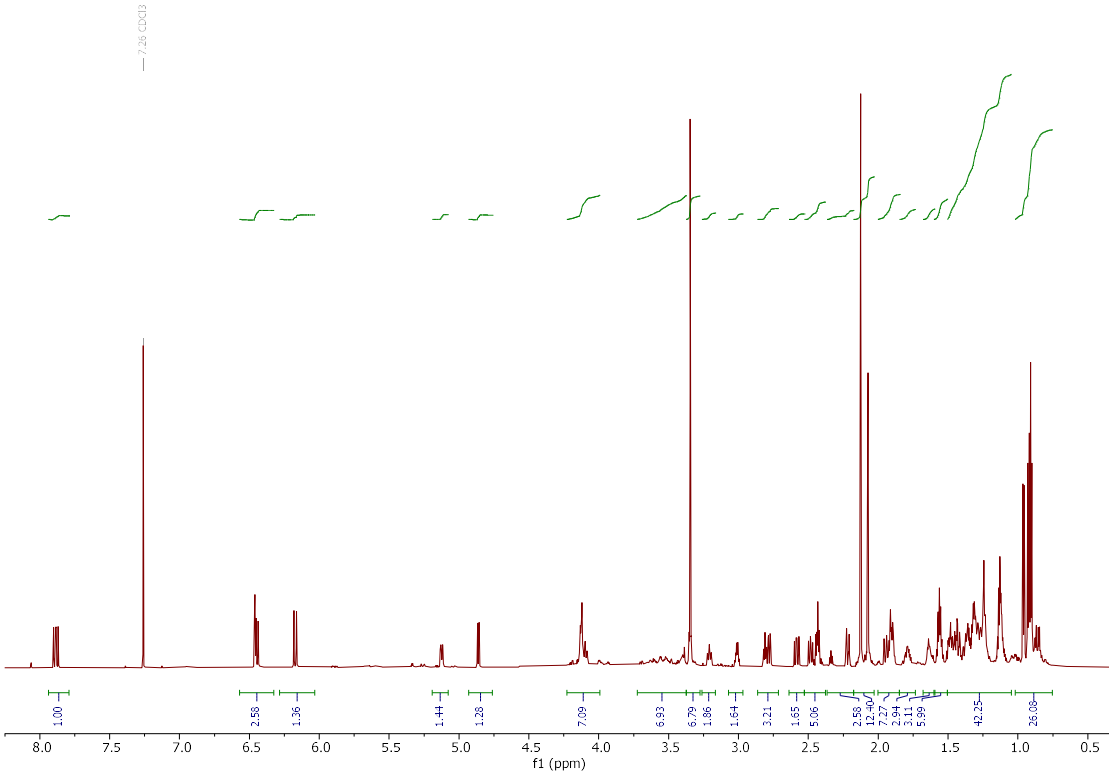

Fig. 5. ^{1}H NMR (800 MHz) spectrum of **1** in CD_3Cl_3.

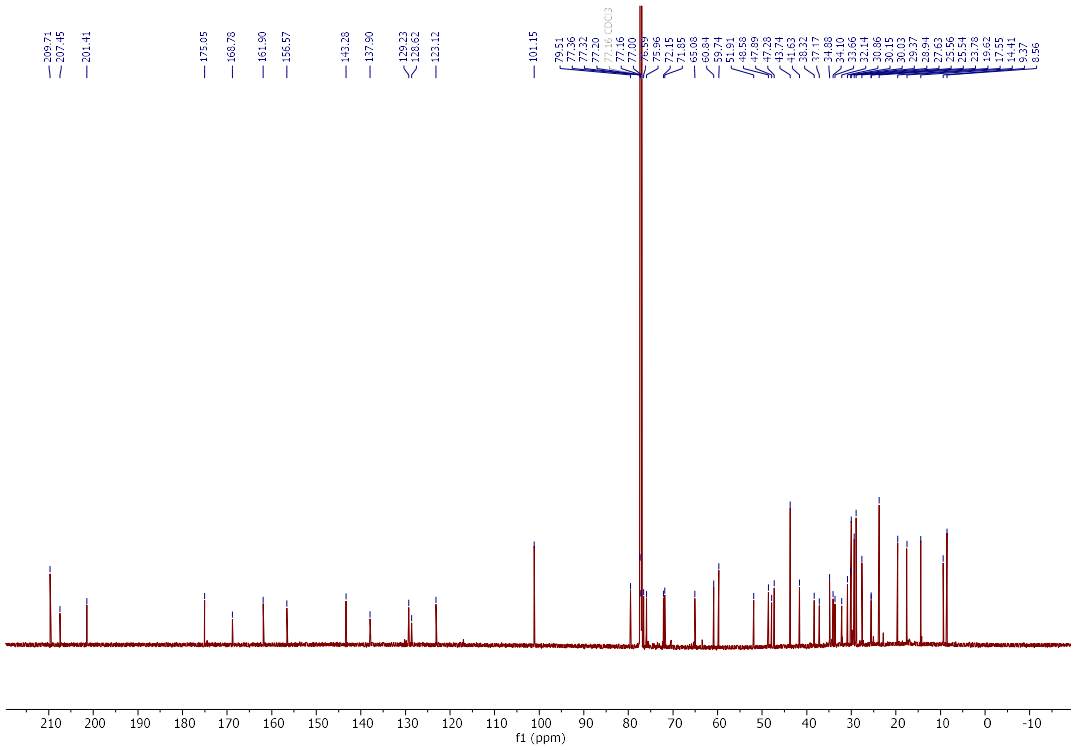

Fig. 6. ^{13}C NMR (200 MHz) spectrum of **1** in CD_3Cl_3.

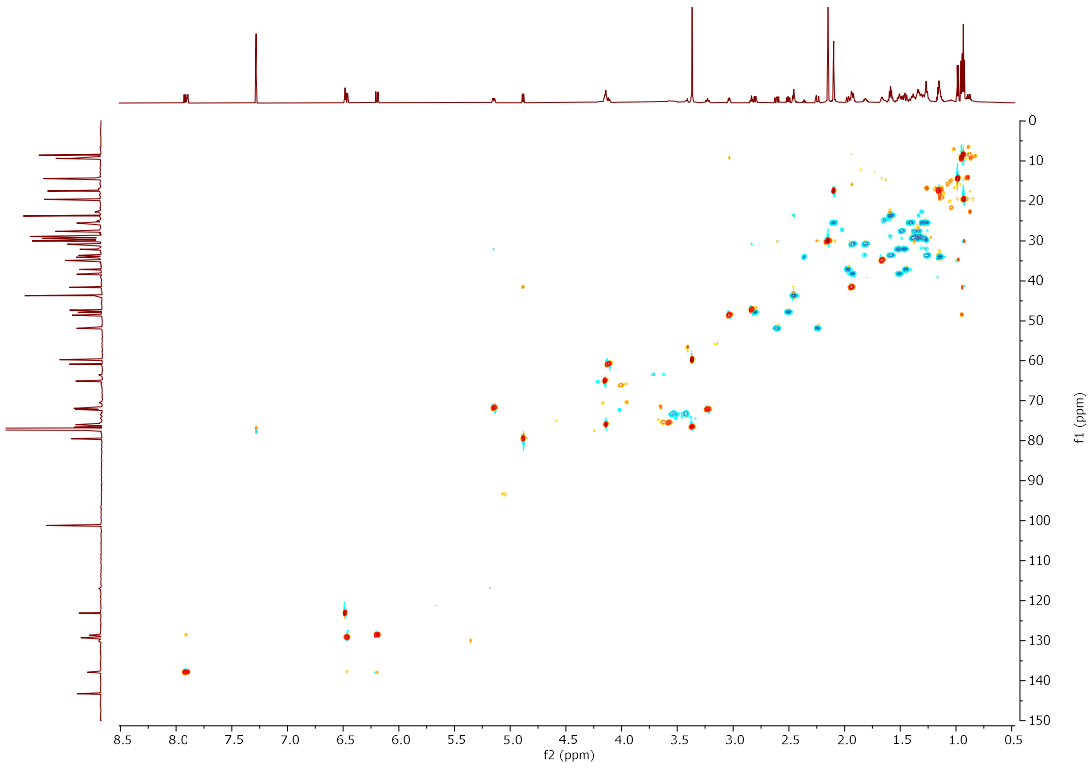

Fig. 7. HSQC (800 MHz) spectrum of **1** in CD_3Cl_3.

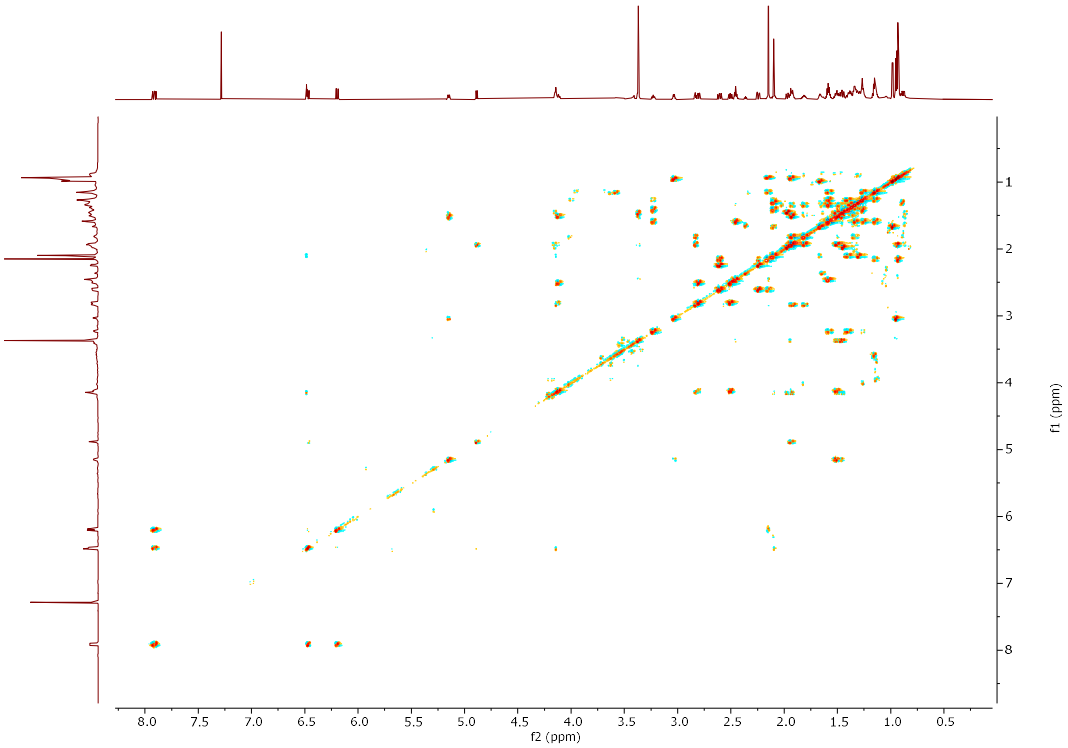

Fig. 8. ^{1}H-^{1}H COSY (800 MHz) spectrum of **1** in CD_3Cl_3.

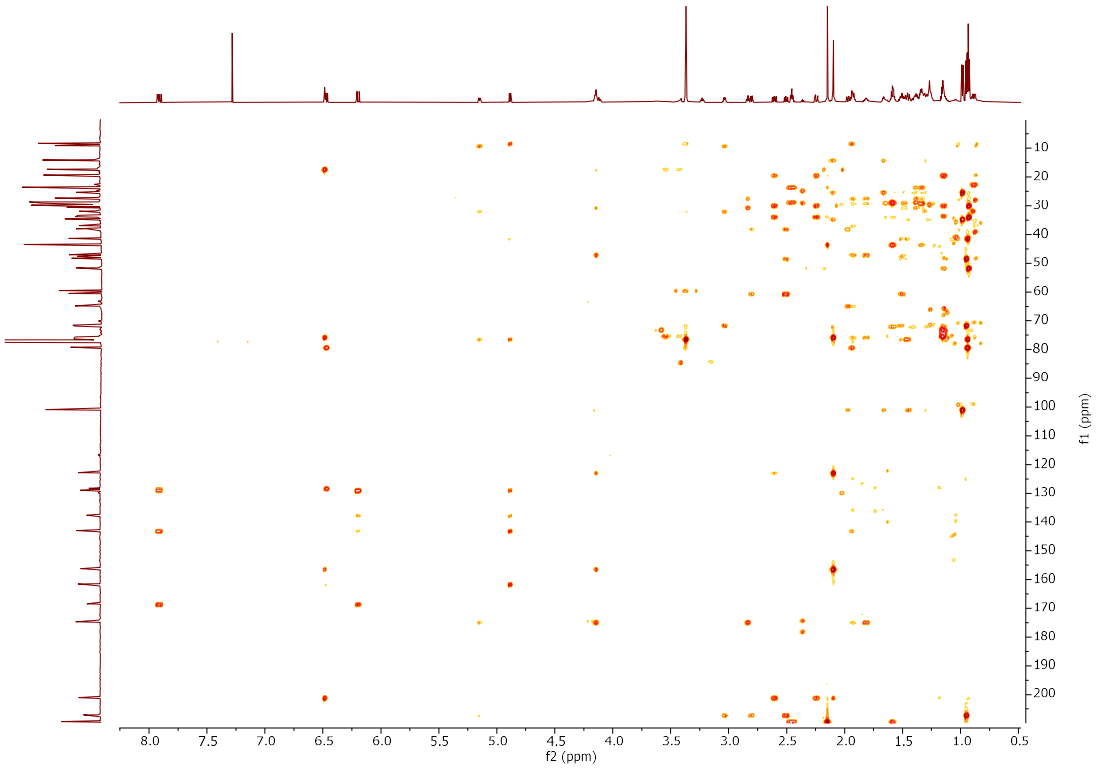

Fig. 9. HMBC (800 MHz) spectrum of **1** in CD_3Cl_3.

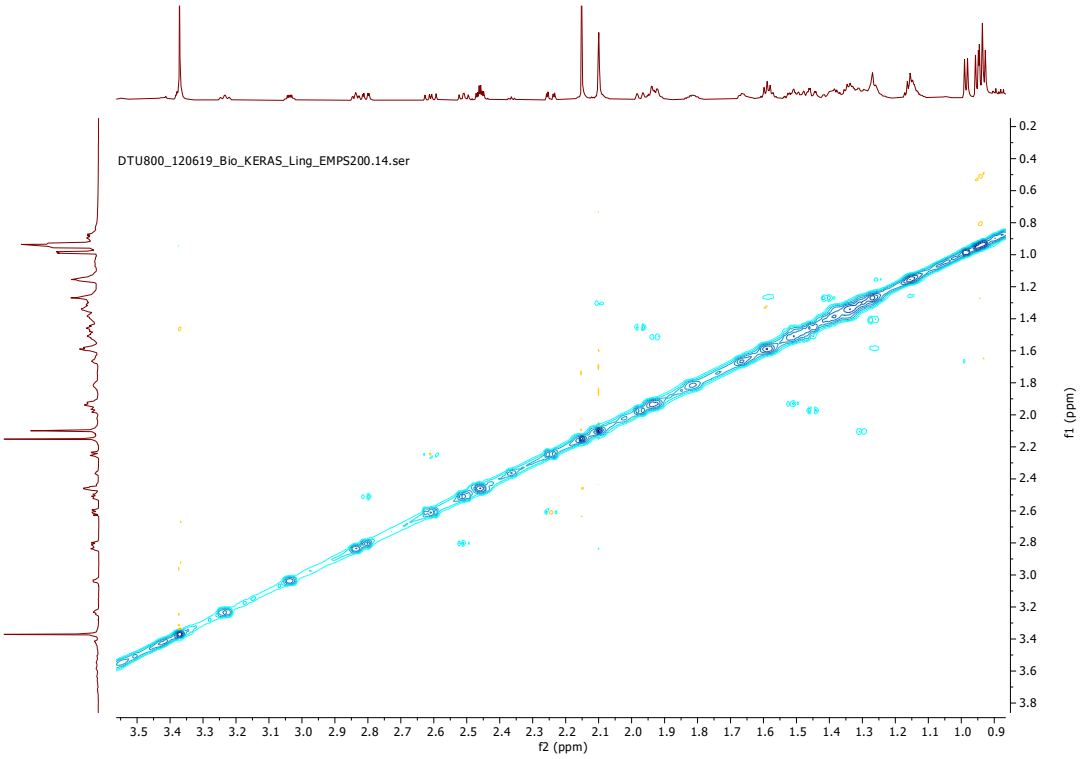

Fig. 10. ROESY (800 MHz) spectrum of **1** in CD_3Cl_3.

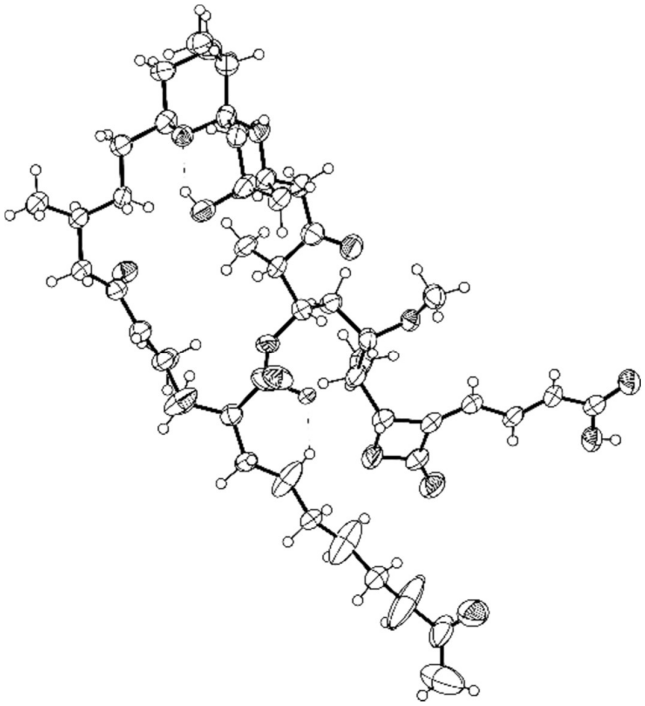

Fig. 11. X-ray crystallographic structure of compound **1**.

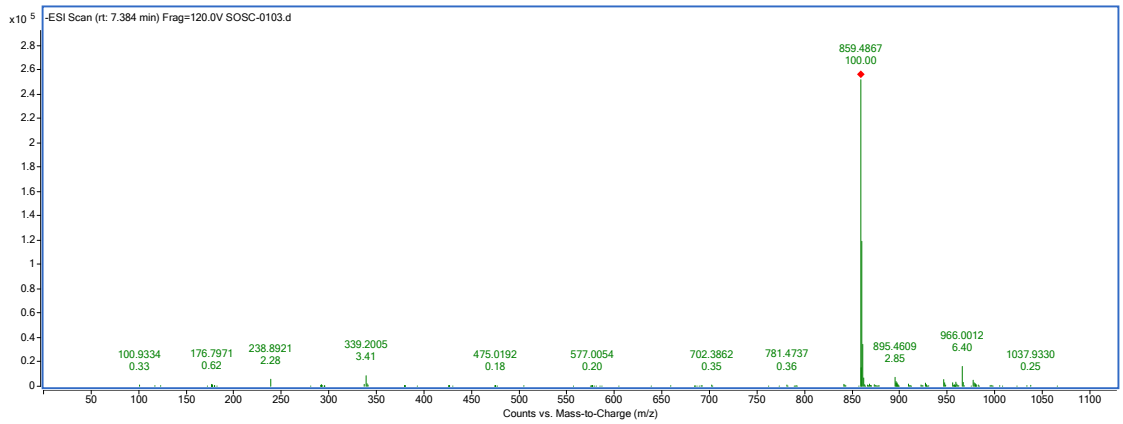

Fig. 12. HR-ESI-MS spectrum of **2**.

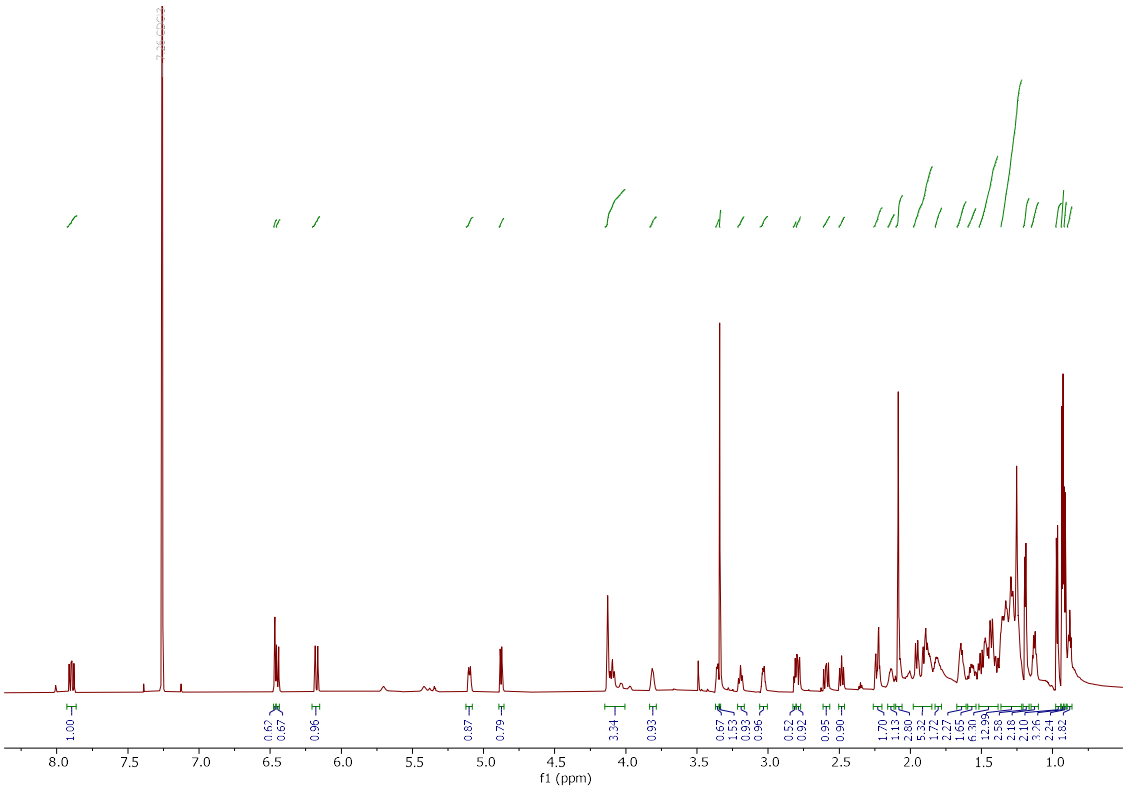

Fig. 13. ^{1}H NMR (800 MHz) spectrum of **2** in CD_3Cl_3.

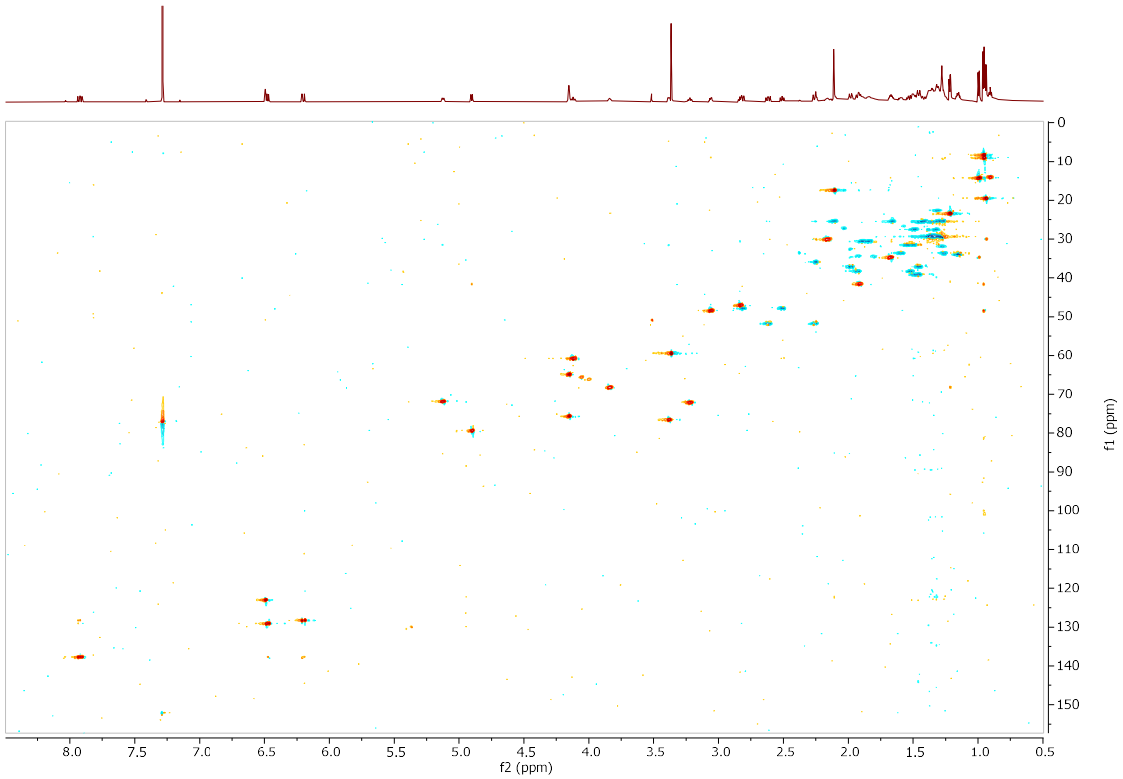

Fig. 14. HSQC (800 MHz) spectrum of **2** in CD_3Cl_3.

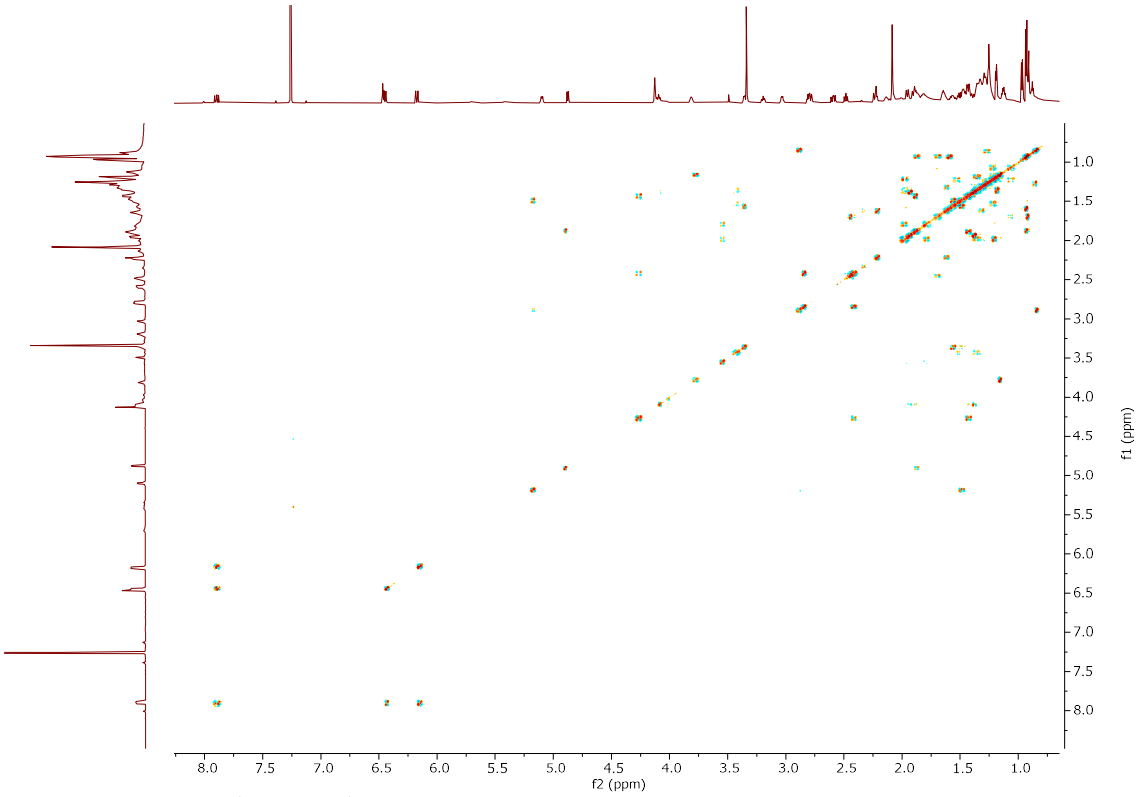

Fig. 15. ^1H-^1H COSY (800 MHz) spectrum of **2** in CD_3Cl_3.

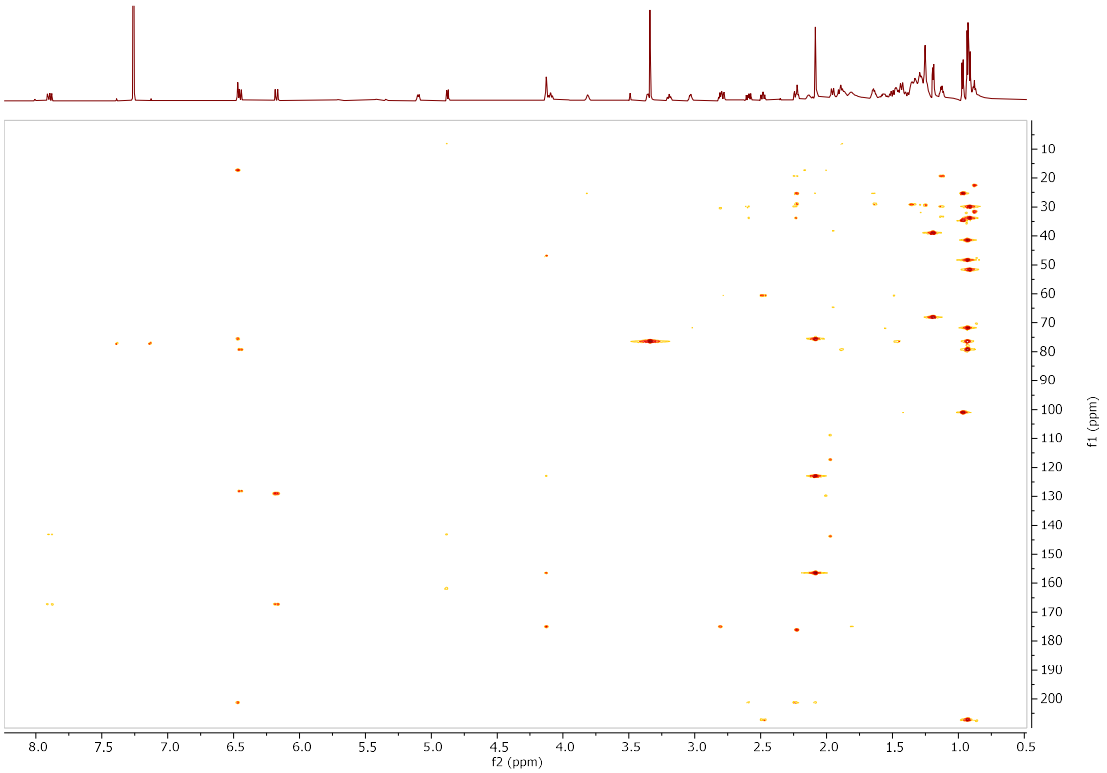

Fig. 16. HMBC (800 MHz) spectrum of **2** in CD_3Cl_3.

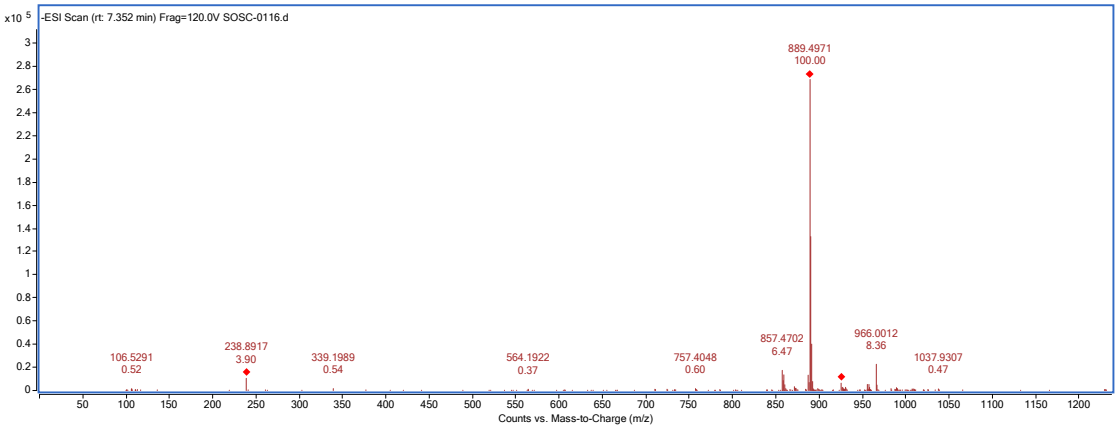

Fig. 17. HR-ESI-MS spectrum of **3**.

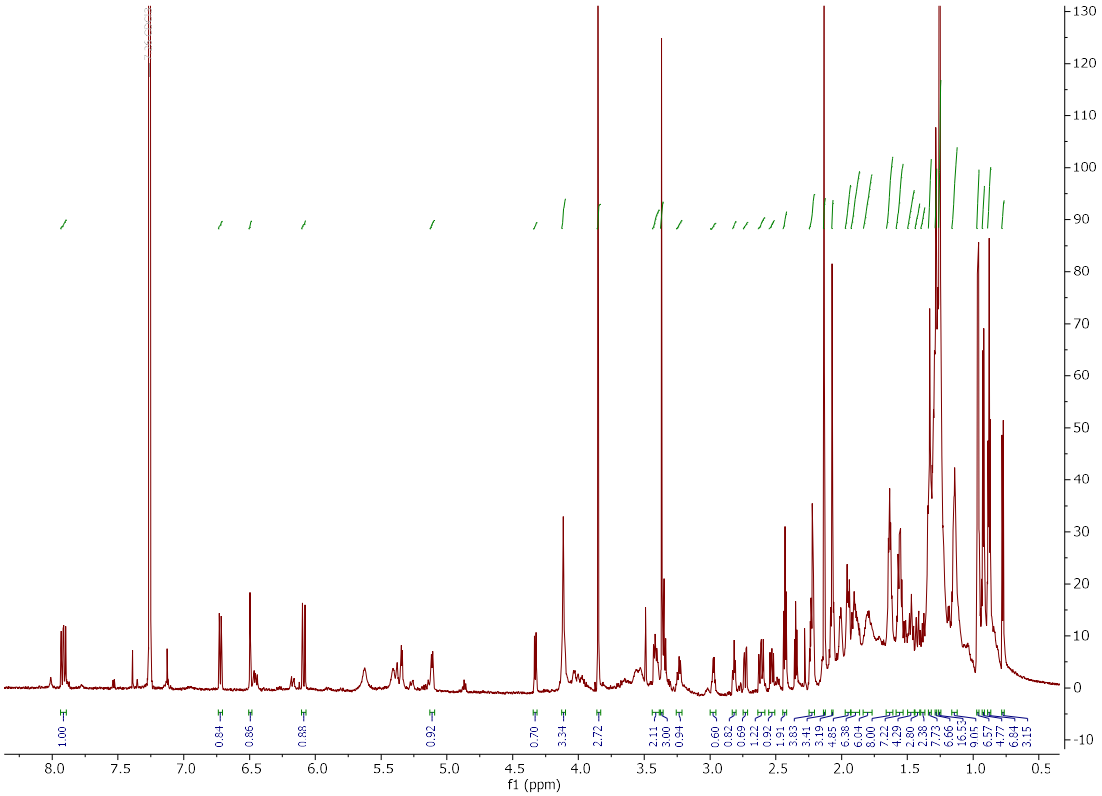

Fig. 18. ^{1}H NMR (800 MHz) spectrum of **3** in CD_3Cl_3.

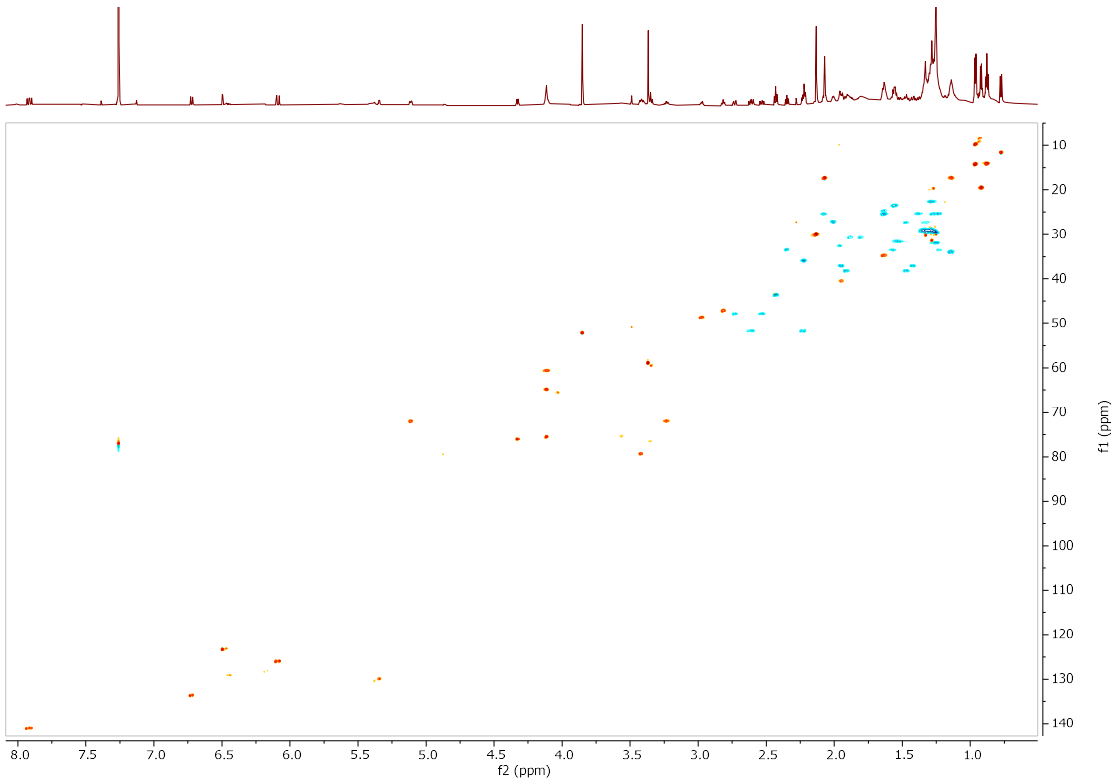

Fig. 19. HSQC (800 MHz) spectrum of **3** in CD_3Cl_3.

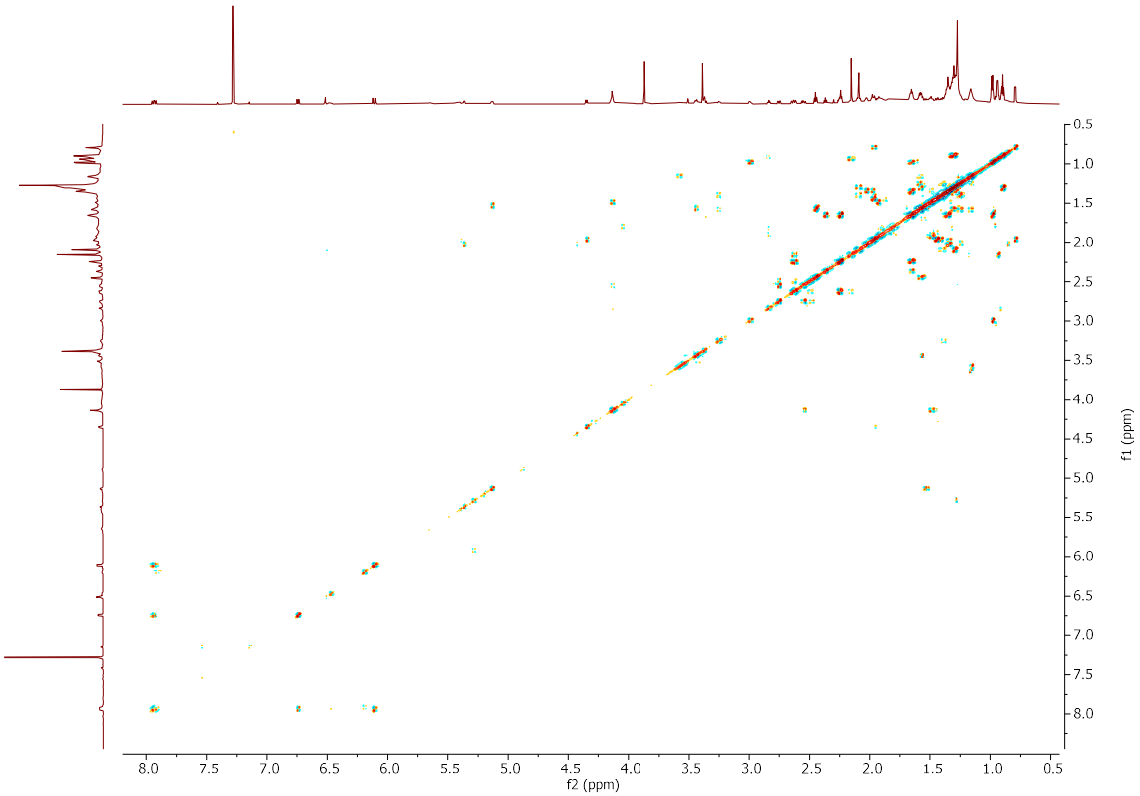

Fig. 20. ^{1}H-^{1}H COSY (800 MHz) spectrum of **3** in CD_3Cl_3.

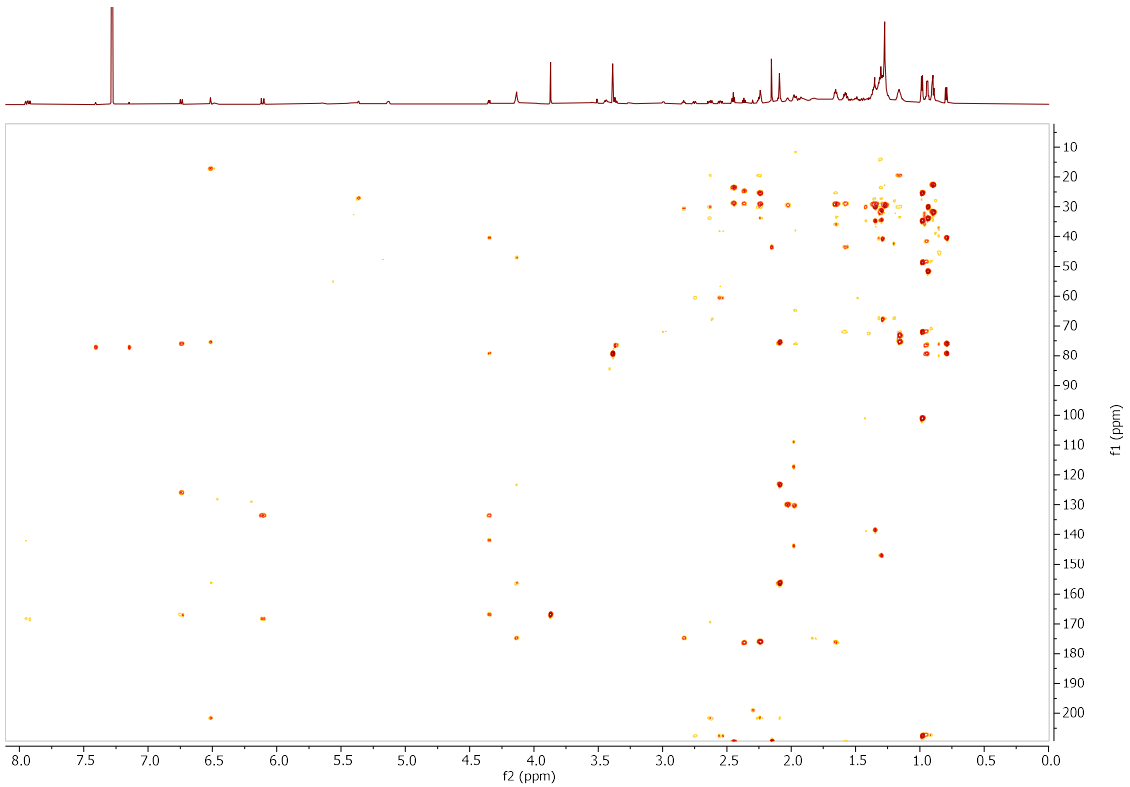

Fig. 21. HMBC (800 MHz) spectrum of **3** in CD_3Cl_3.

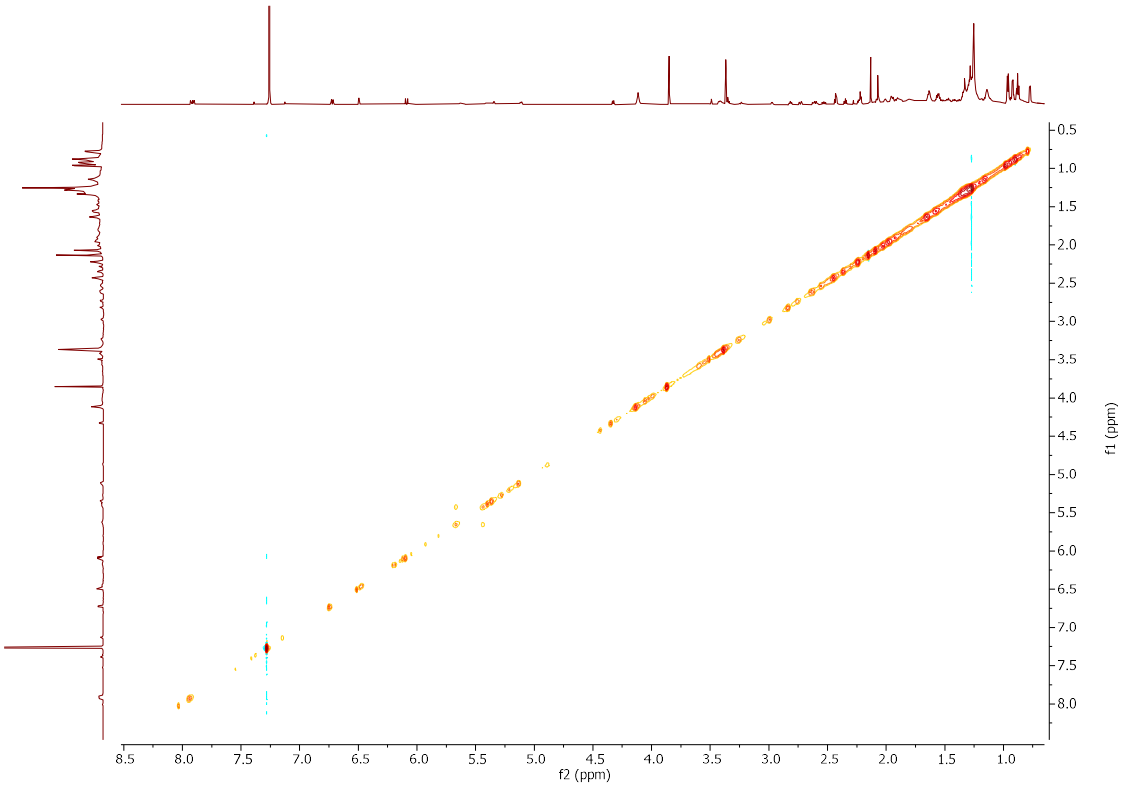

Fig. 22. ROESY (800 MHz) spectrum of **3** in CD_3Cl_3.

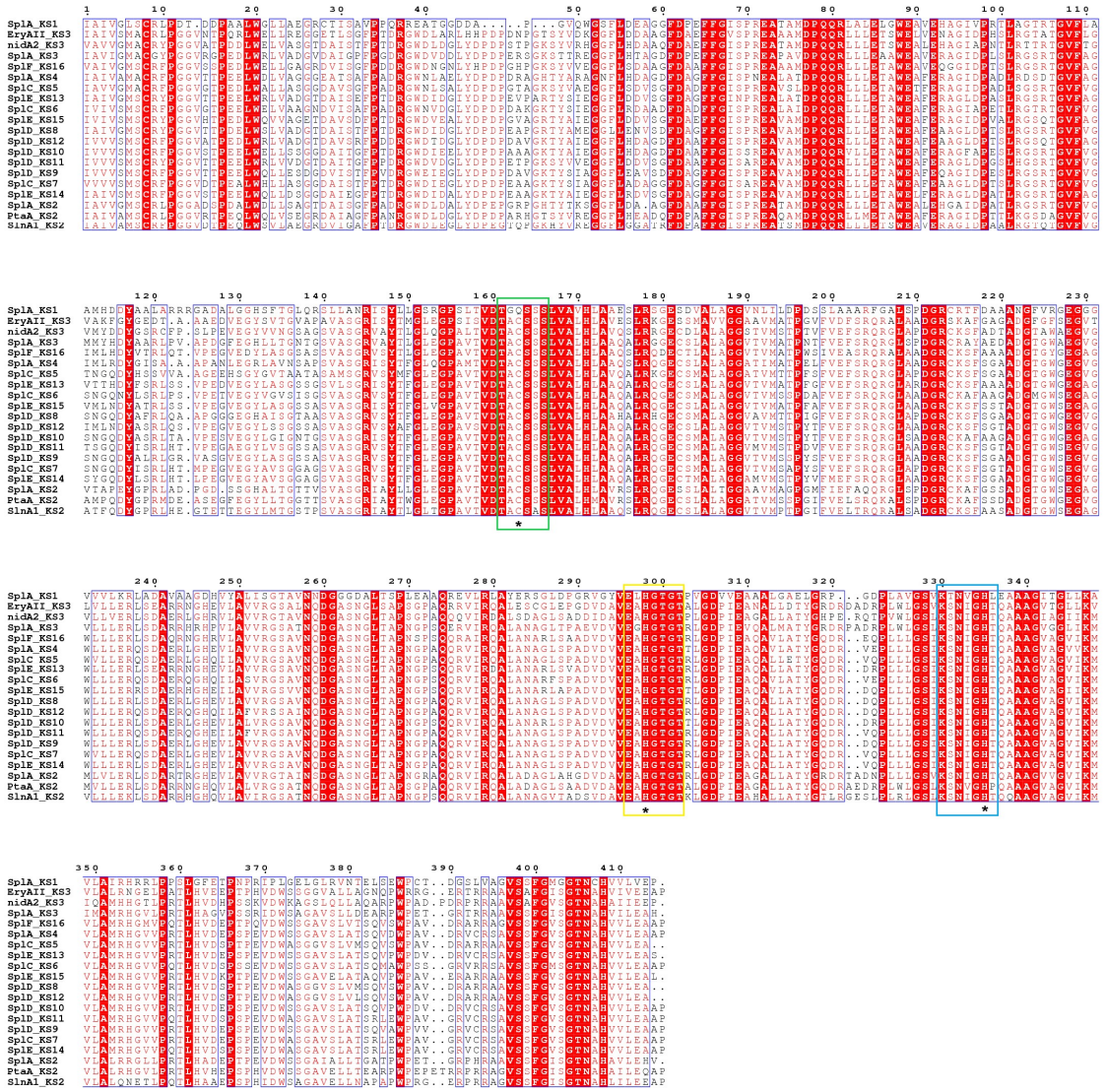

Fig. 23. Multiple sequence alignment of KS domains. The catalytic machinery including a cysteine (TACSSS motif in green box) as well as two histidines (EAHGTG motif in pink box and KSNIGHT motif in blue box) was marked with an asterisk. Abbreviation: Spl, spirolactone; Ery, erythromycin; Nid, niddamycin; Pta, pteridic acid; Sln, salinomycin.

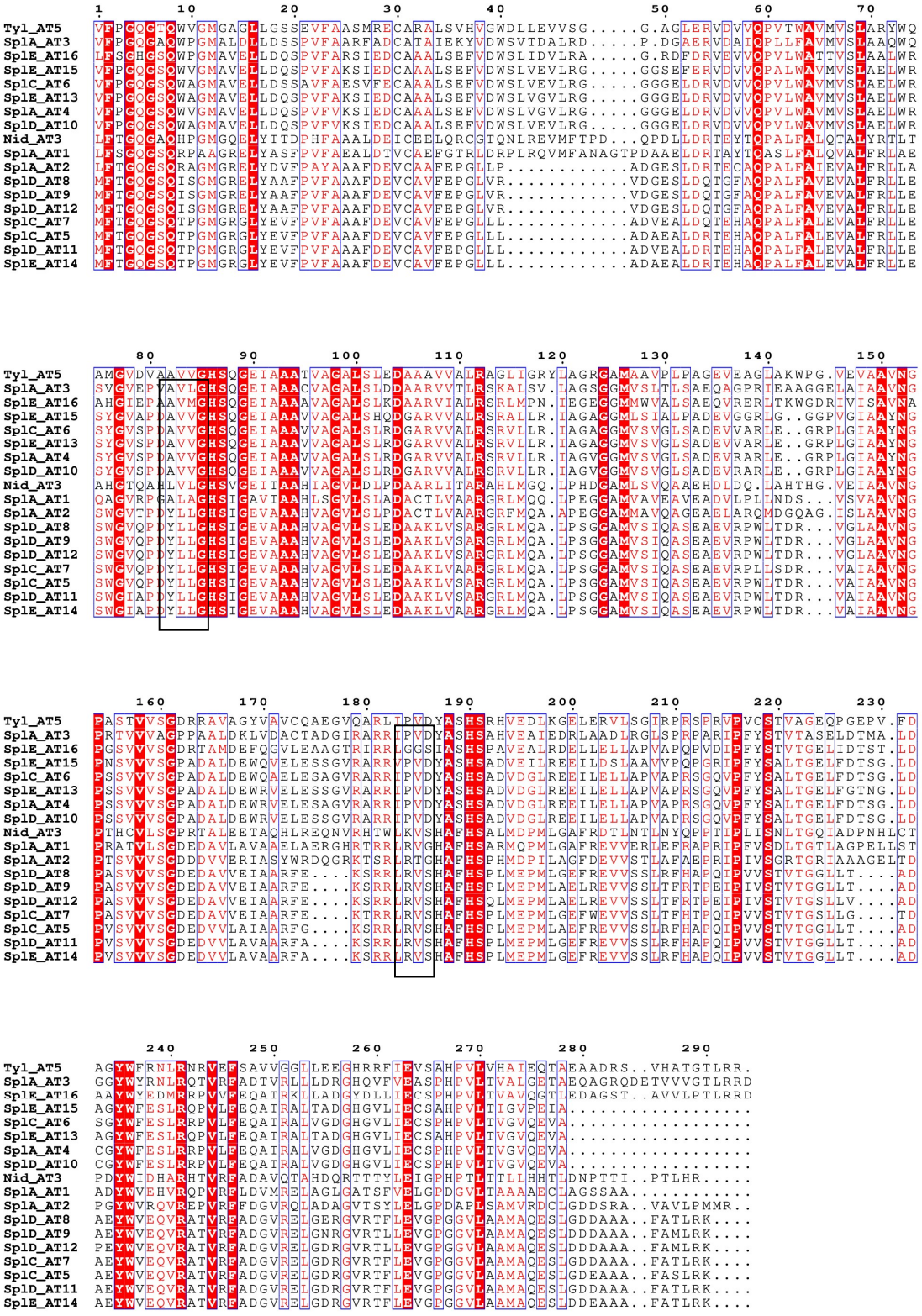

Fig. 24. Multiple sequence alignment of AT domains. The black boxes indicate the conserved motifs. Abbreviation: Spl, spirolactone; Nid, niddamycin; tyl, tylactone.

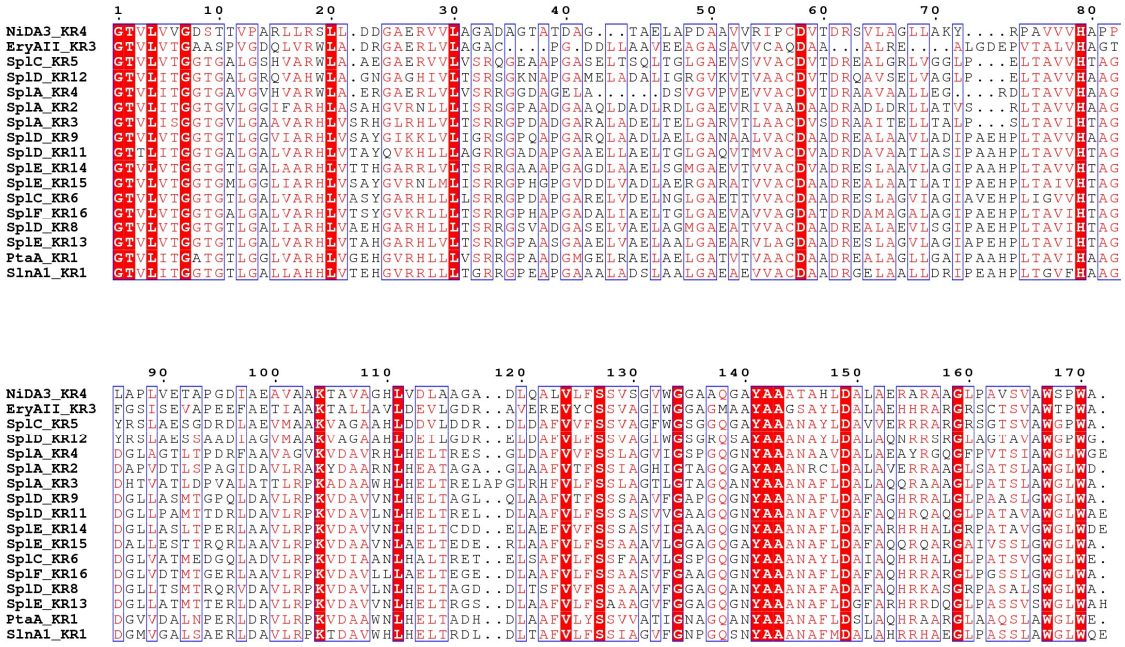

Fig. 25. Multiple sequence alignment of KR domains. Abbreviation: Spl, spirolactone; Ery, erythromycin; Nid, niddamycin; Pta, pteridic acid; Sln, salinomycin.

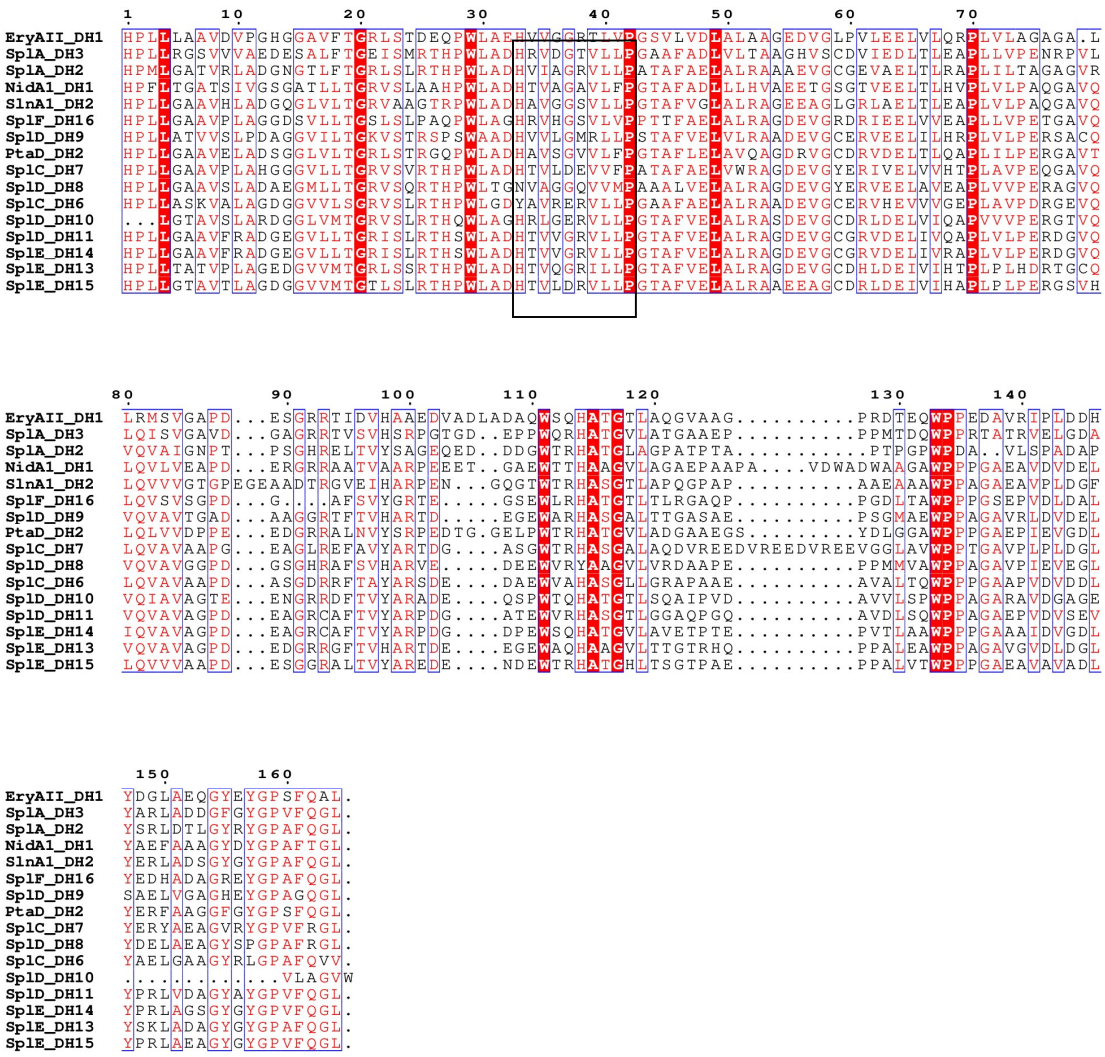

Fig. 26. Multiple sequence alignment of DH domains. The black box indicates the conserved HxxxGxxxxP motif. Abbreviation: Spl, spirolactone; Ery, erythromycin; Nid, niddamycin; Pta, pteridic acid; Sln, salinomycin.

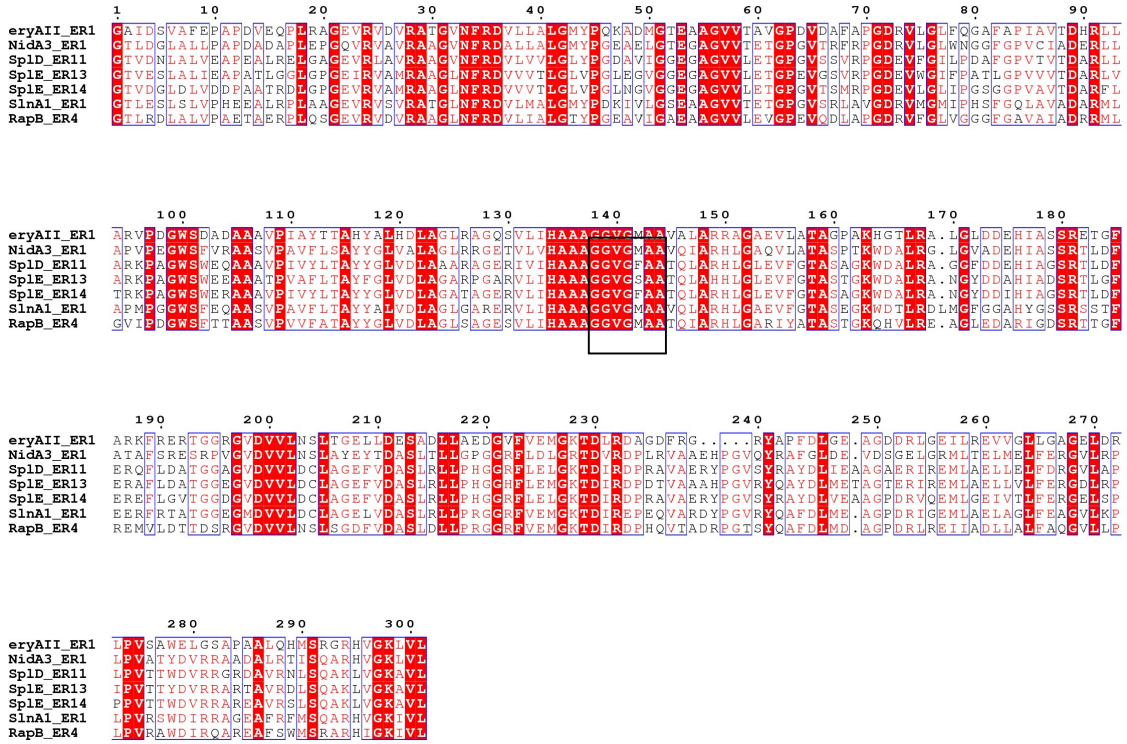

Fig. 27. Multiple sequence alignment of ER domains. The unique residue correlated with (2*S*/2*R*)-configuration in the polyketide product is marked with blacked triangles. The position of the NADPH binding site is marked with a black box. Abbreviation: Spl, spirolactone; Ery, erythromycin; Nid, niddamycin; Rap, rapamycin; Sln, salinomycin.

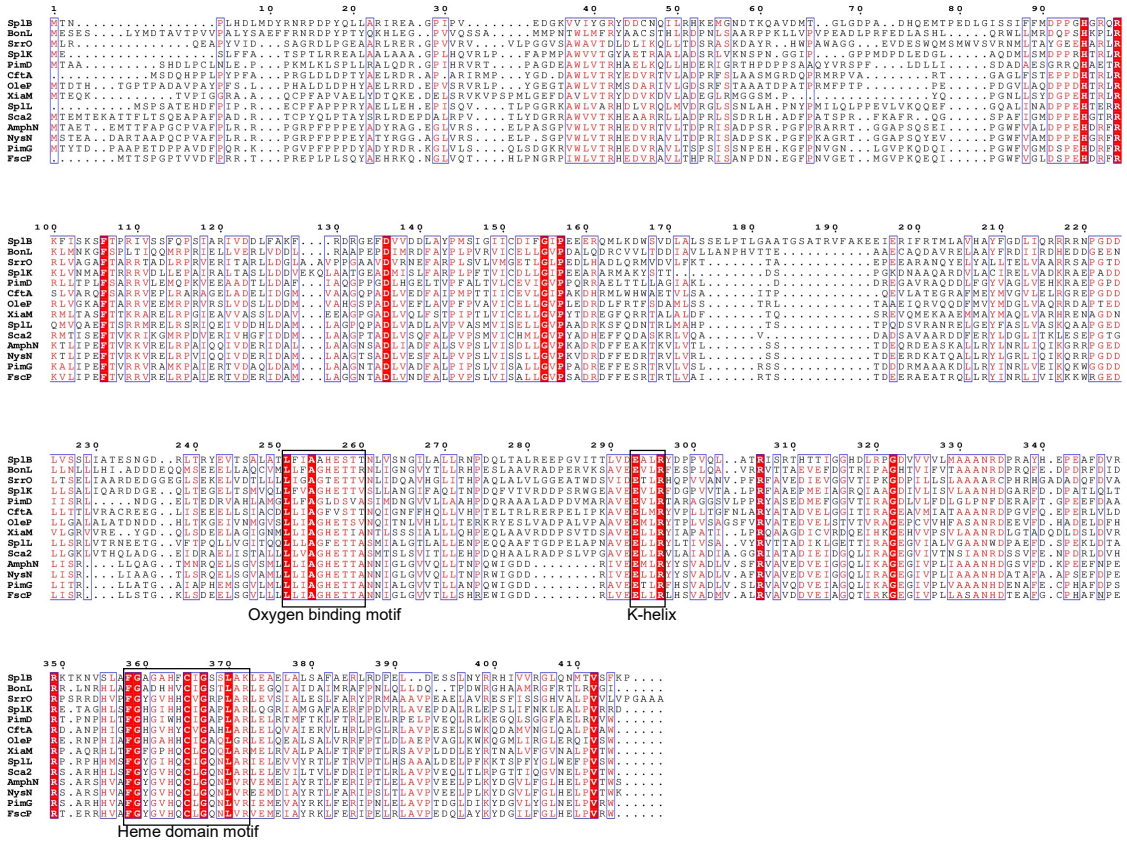

Fig. 28. Sequence alignment of SplB, SplK, SplL and other cytochrome P450s. These sequences used in this study: BonL (AFN27475, *Burkholderia gladioli*); SrrO (WP_259329015.1, *Streptomyces rochei*); PimD (CAC20928, *Streptomyces natalensis*); CftA (WP_099966040.1, *Streptomyces* sp. JV178); OleP (AAA92553, *Streptomyces antibioticus*); XiaM (AFK78079, *Streptomyces* sp. SCSIO 02999); Sca2 (BAA06492, *Streptomyces carbophilus*); AmphN (AAK73509, *Streptomyces nodosus*); NysN (AAF71771, *Streptomyces noursei* ATCC 11455); PimG (CAC20928, *Streptomyces natalensis*); FscP (AAQ82557, *Streptomyces* sp. FR-008).

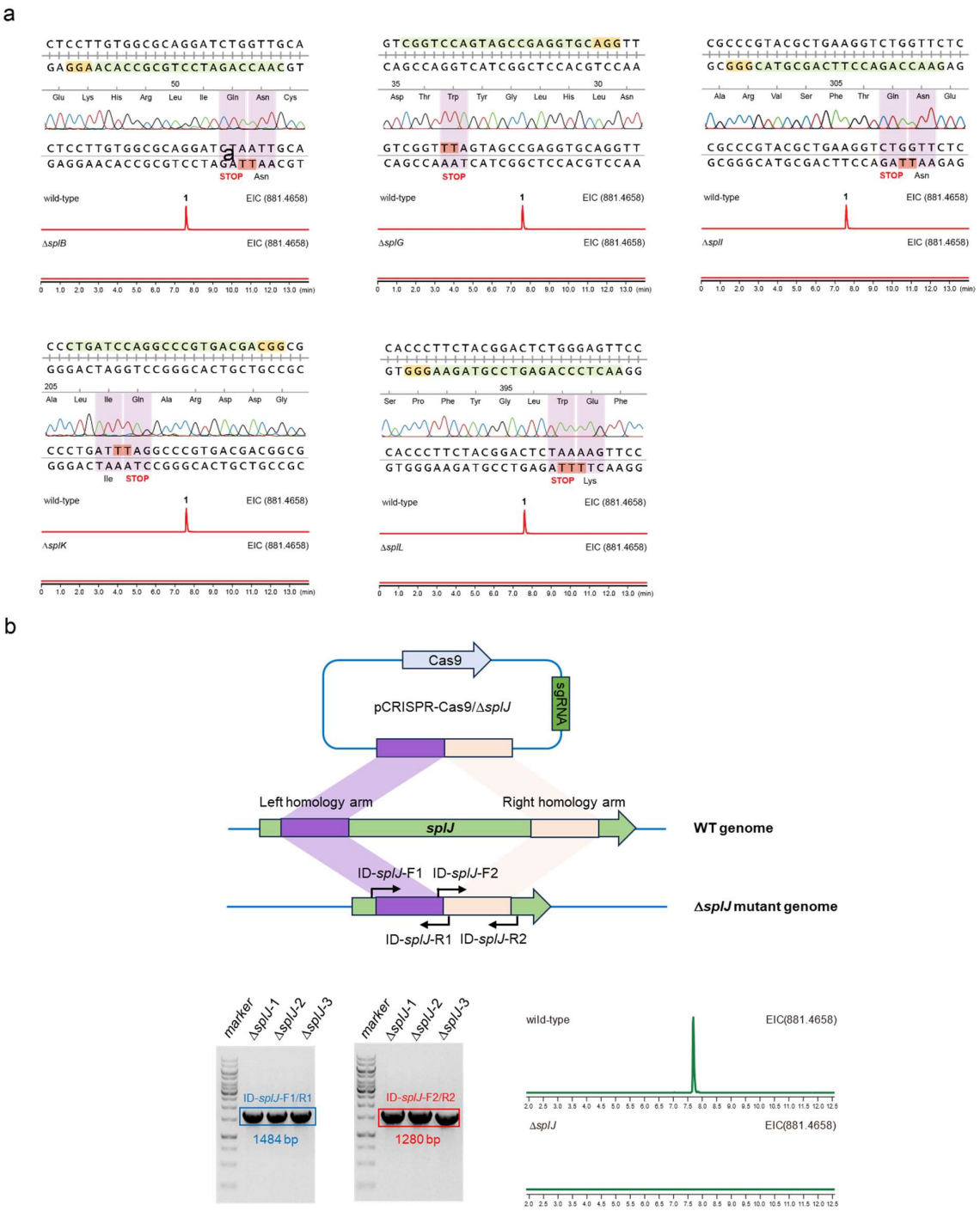

Fig. 29. The genome editing of tailoring enzymes in spirolactone biosynthesis. **a**, CRISPR base editing of *splB*, *splG*, *splH*, *splK*, and *splL*. **b**, homology directed repair-based CRISRP-Cas9 genome editing.

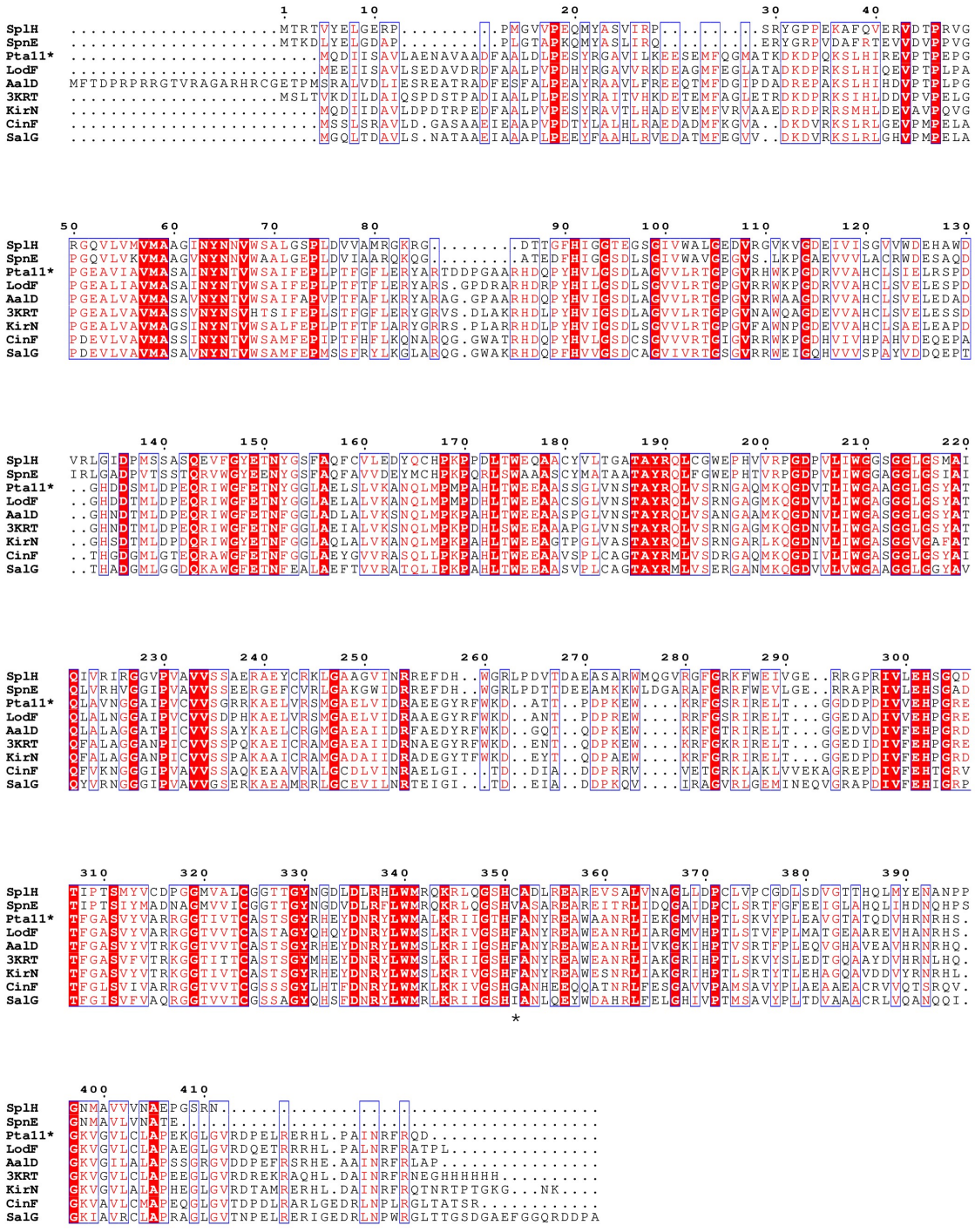

Fig. 30. Multiple sequence alignment of SplH and other crotonyl-CoA carboxylase/reductases. These sequences used in this study: SpnE (AKA54628.1, *Streptomyces* sp. CNQ431), Pta11* (WP_044567907.1, *S. iranensis* HM 35), LodF (ANR02547.1, *Streptomyces lasaliensis*), AalD (BBA66510.1, *Streptomyces spiroverticillatus*), 3KRT (*Streptomyces coelicolor*), KirN (CAN89653.1, *Streptomyces collinus* Tu 365), CinF (CBW54676.1, *Streptomyces cinnabarigriseus*), SalG (ABP73651.1, *Salinispora pacifica*).

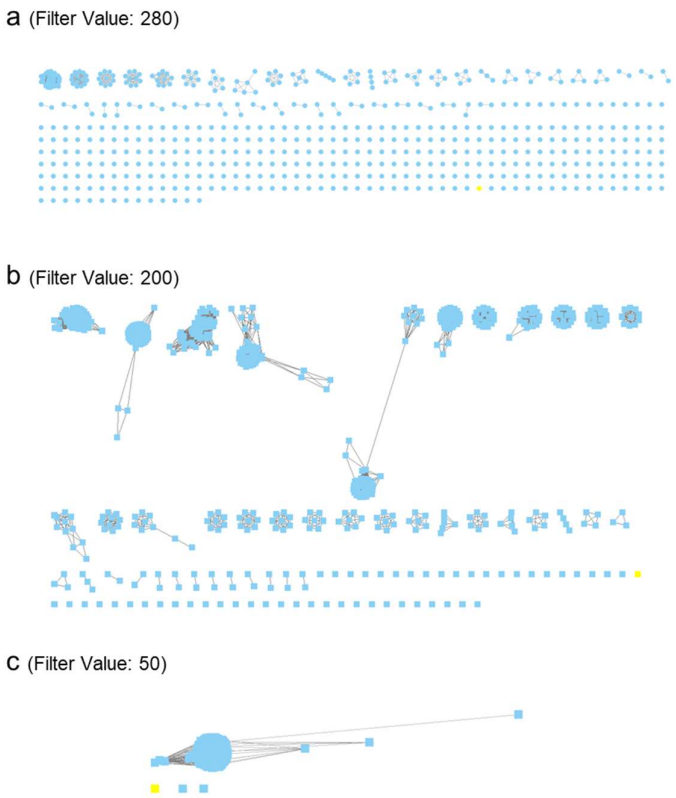

Fig. 31. Sequence similarity network of SplJ (colored in yellow). The network was constructed using EFI - enzyme similarity tool (https://efi.igb.illinois.edu/efi-est/).

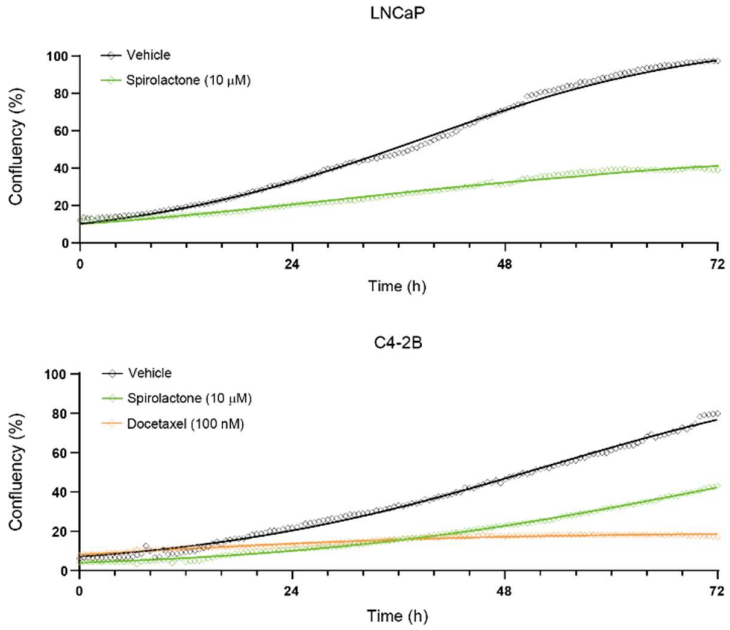

Fig. 32. Cell growth and toxicity effects of spirolactone A on mammalian cells.

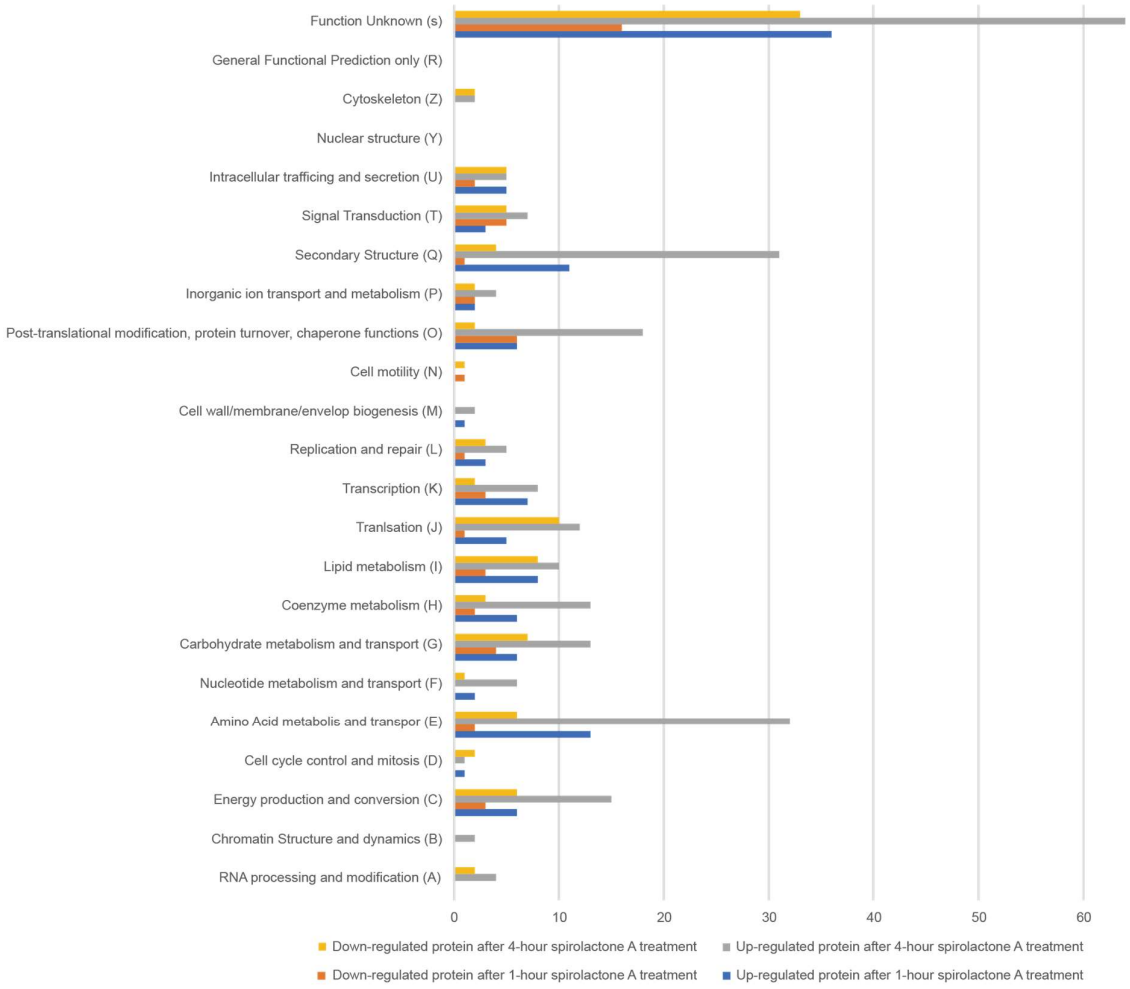

Fig. 33. The COGs functional classification of differential proteins.

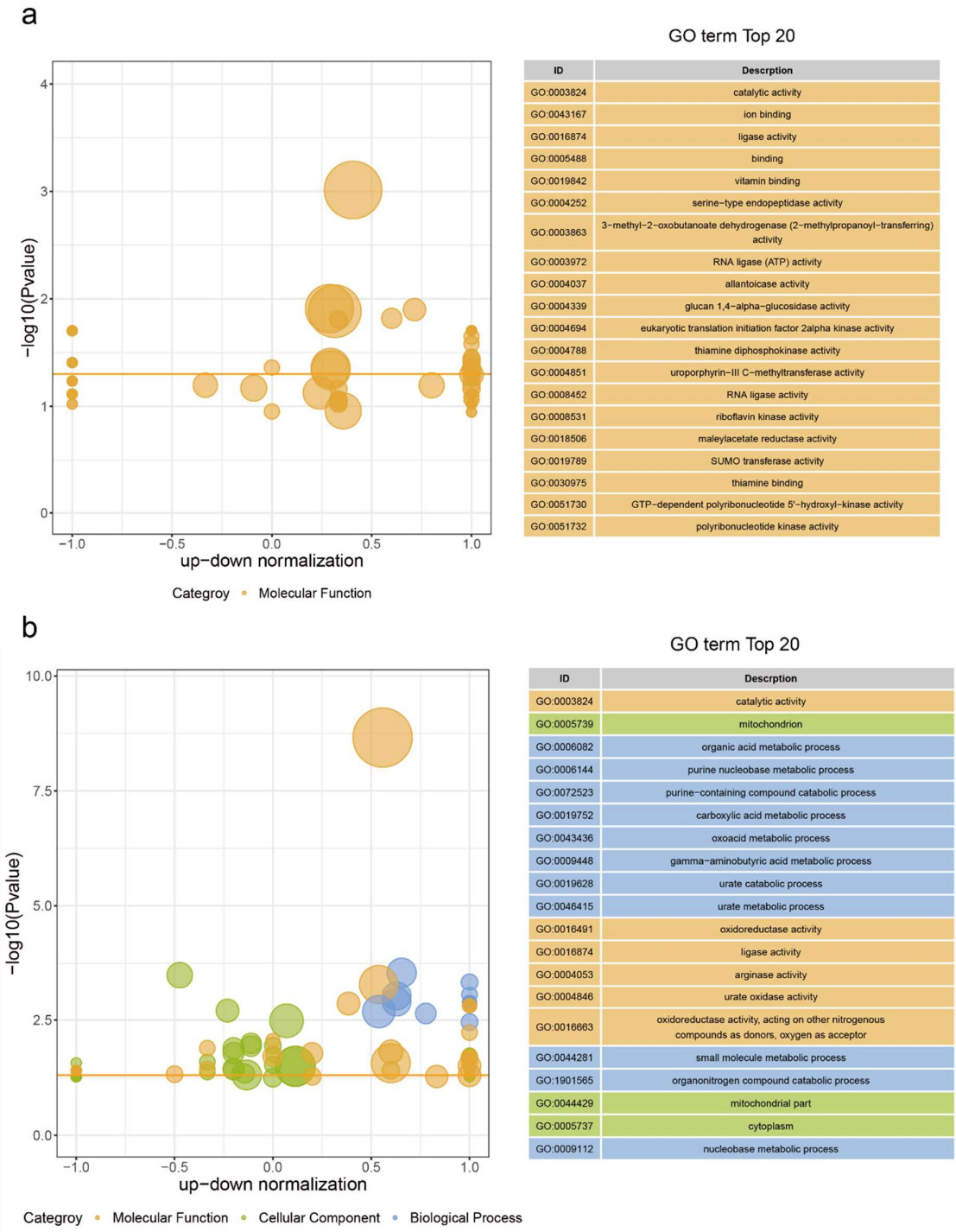

Fig. 34. The GO annotation of differential proteins. ***a***, treatment of 1-hour spirolactone A in *A. niger*. ***b***, treatment of 4-hour spirolactone A in *A. niger*.

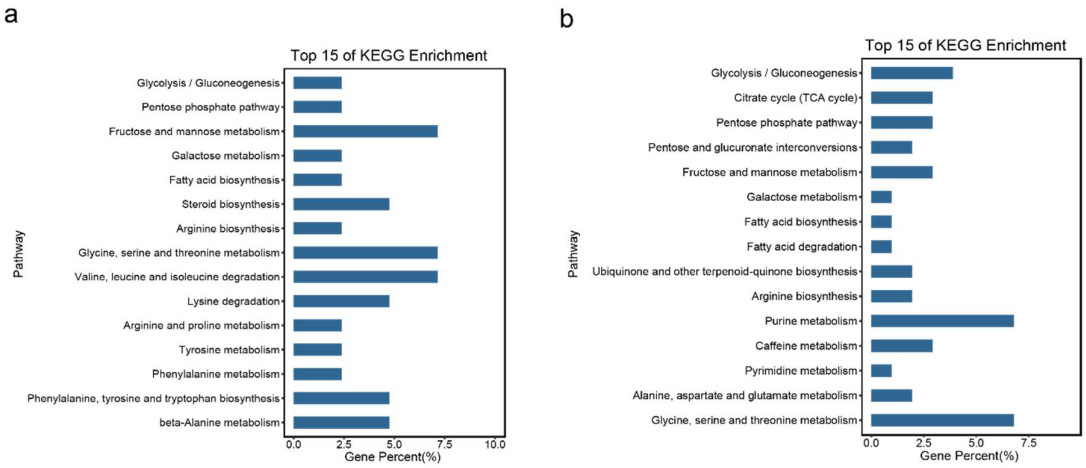

Fig. 35. The KEGG pathway enrichment analysis of differential proteins. ***a***, treatment of 1-hour spirolactone A in *A. niger*. ***b***, treatment of 4-hour spirolactone A in *A. niger*.

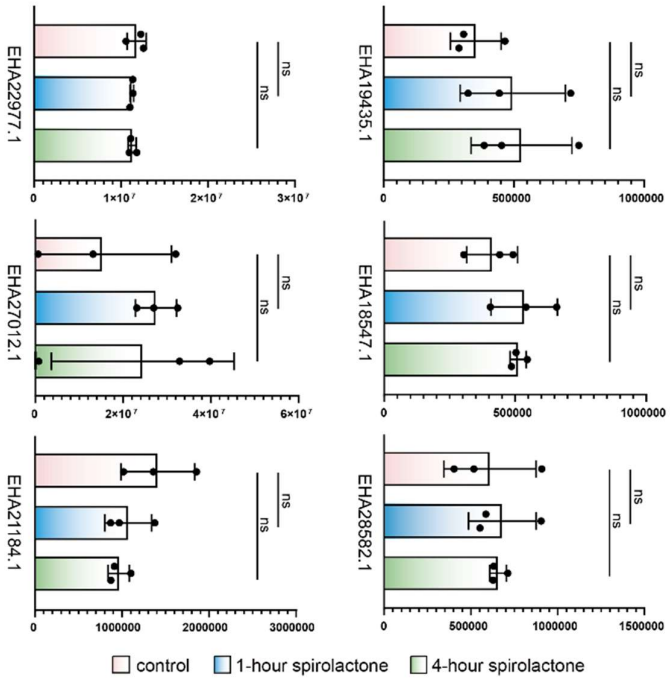

Fig. 36. The abundance of responsive protein of known antifungal drugs in spirolactone treatment. EHA22977.1, Erg13; EHA27012.1, manganese-superoxide dismutase; EHA21184.1, squalene epoxidase; EHA19435.1, CYP51; EHA18547.1, 1,3-β-D-glucan synthase (EHA18547.1); EHA28582.1, ChiA1-like chitinase.

Reference:

1. Paget, M. S. B., Chamberlin, L., Atrih, A., Foster, S. J. & Buttner, M. J. Evidence that the extracytoplasmic function sigma factor σ^E is required for normal cell wall structure in *Streptomyces coelicolor* A3(2). *J. Bacteriol.* **181**, 204-211 (1999).
2. Tong, Y., Charusanti, P., Zhang, L., Weber, T. & Lee, S. Y. CRISPR-Cas9 based engineering of actinomycetal genomes. *Acs Synth. Biol.* **4**, 1020-1029 (2015).
3. Tong, Y., et al. Highly efficient DSB-free base editing for streptomycetes with CRISPR-BEST. *Proc. Natl. Acad. Sci. U. S. A.* **116**, 20366-20375 (2019).
4. Muth, G. The pSG5-based thermosensitive vector family for genome editing and gene expression in actinomycetes. *Appl. Microbiol. Biotechnol.* **102**, 9067-9080 (2018).

Appendix 3

Secondary metabolites shape *Streptomyces-Streptomyces* interactions: Mass Spectrometry Imaging reveals lydicamycins broadly induce sporulation

Scott A. Jarmusch*[1], Zhijie Yang[1], Jinglin Wang[1], Aaron JC Anderson[1], Tilmann Weber[2], Ling Ding*[1]

[1] Department of Biotechnology and Biomedicine, Technical University of Denmark, DK 2800 Kgs, Lyngby, Denmark

[2] The Novo Nordisk Foundation Center for Biosustainability, Technical University of Denmark, Kemitorvet, building 220, 2800 Kgs. Lyngby, Denmark

Abstract

Pairwise interactions involving *Streptomyces-Streptomyces* are rarely described, yet these major players in the soil microbiome are interacting with one another, utilizing their secondary metabolism to shape their environment. This study resulted from the observation of induced sporulation between two environmental isolates, *Streptomyces* sp. P9-2B1 and *Streptomyces* sp. P9-2B2. When co-cultivated on PDA, P9-2B2 induced a wave-like sporulation in strain P9-2B1. Using Mass Spectrometry Imaging, we revealed that a suite of lydicamycins, antibacterial NRPS-PKS hybrid metabolites, were present in this induced sporulation zone. Lydicamycin deficient mutants were generated using CRISPR-base editing and the inducible sporulation ceased, confirming their role in triggering morphological differentiation. In agar diffusion assays, pure lydicamycin was inhibitory when added concurrently with bacterial inoculation and induced sporulation when delayed addition occurred. Subsequent testing of additional environmental isolates resulted in the same inducible sporulation wave phenomenon, including in the model strain *Streptomyces coelicolor* M145. We further evaluated the temporal production of the lydicamycins in monoculture over a 10-day time scale. On PDA, production was detectable upon sporulation at day 4 on PDA and peaked at day 9. On ISP2, lydicamycin production was minimal and stable over the 10 days, coinciding with a lack of sporulation. Lastly, we mapped the biosynthetic gene responsible for the addition of the arginine-derived starter unit from various known secondary metabolites onto publicly available strains to locate putative novel biosynthetic gene clusters.

Introduction

Streptomyces are one of the most widely utilized natural sources, principally for their prolific production of ~70% of clinical antibiotics.[1,2] The attention to this veritable 'arms race' has diverted resources towards drug discovery, whereas in contrast, the wider ecological influence of *Streptomyces* secondary metabolites (SMs) has severely lagged behind, despite of few reported signaling molecules, *e.g.* γ-butyrolactones[3], governing the production of other SMs or transition of life stage. *Streptomyces* serve vital roles in soil microbiomes, evidenced by their diverse ecological distribution and their SMs are the 'language' they communicate with

friends and foes.[4,5] While interesting observations have been found for interkingdom interactions, such as *Streptomyces*-fungi[6] and *Streptomyces-Bacillus subtilis* interactions[7], a large gap exists in understanding the role SMs play in *Streptomyces-Streptomyces* interactions.

The *Streptomyces* life cycle encompasses three well-established developmental stages: vegetative growth, mycelium formation and sporulation. In response to nutrient depletion, *Streptomyces* start the transition from vegetative growth to aerial mycelium formation, and subsequently sporulation.[8] Interestingly, sporulation is a common phenotype change observed in dual *Streptomyces* interactions[9], yet tracing the responsible SMs is nearly non-existent. Goadsporin was the first SM described to cause sporulation in *Streptomyces* (and potentially target *Streptomyces* specifically), most likely through antibiotic stress-induced sporulation.[10] A major challenge is the difficulty in directly linking the phenotype change to the SMs. Traditionally, extracts of cocultivations (either the entire plate or plug extractions) have been employed with varying success.[11] Beyond issues like scaling up production and characterization, identifying the metabolite from the earliest stages of analysis is the bottleneck allowing for efficient linkage of SM and ecology. Mass Spectrometry Imaging offers attractive solutions to resolving this spatial problem[12,13] through direct visualization of metabolites on cocultivations.[11] In *Streptomyces*-focused studies, Traxler et al. set the primer for evaluating actinobacterial-actinobacterial cocultivations, leading to the discovery of new acylated desferrioxamines[14], and many studies have followed thereafter proving Mass Spectrometry Imaging (MSI) on cocultures is a faster route to discovery of novel compounds with cocultures.

During a screening for *Streptomyces-Streptomyces* antibiosis, two environmental *Streptomyces* spp. were cocultured, with one strain (P9-2B2) inducing a wave of sporulation in a receiver strain (P9-2B1). Using a combination of MSI, molecular genetics and biological testing, we determined a suite of antibiotic lydicamycins produced by strain P9-2B2 induced the observed morphogenesis. The temporal production of lydicamycins was evaluated using LC-MS/MS and feature based molecular networking and we determined their production coincided with sporulation in the producer strain and aligned with the first observation of sporulation in receiver strain. Furthermore, we evaluated the range of the lydicamycin-induced morphogenesis on relevant environmental strains. Along with the model strain *Streptomyces coelicolor* M145, we determined all but one strain tested, a phylogenetically related isolate which sporulated prior to lydicamycin production, had inducible sporulation waves at variable times. Pure lydicamycin further induced morphogenesis, although at a slower rate, whereas the related arginoketide, azalomycin F, did not produce the same effect. Finally, due to the growing interest in the arginoketides, we wanted to map the biosynthetic potential of this metabolite class. We found the guanidine-CoA transacylases linked to multiple arginoketide biosynthetic gene clusters (BGCs) were highly conserved and therefore used *lyd62* (malonyl-CoA ACP transacylase) as a marker for polyketide BGCs and found this class remains vastly underexplored. Our study further suggests MSI is the most powerful technique for mapping these interactions studies and we suggest there are further roles for *Streptomyces*-produced SMs against *Streptomyces*.

Materials and methods

Isolates and phylogenetic analysis. All environmental isolates used in this study were isolated from soil collected in 2020 from the UNESCO World Heritage Site, Jægorsborg Deer Park (Dyrehaven), Denmark. Selective isolation using standard techniques were carried out to isolate actinobacteria and specifically *Streptomycetes*.[15,16] *S. coelicolor* M145 was obtained from Tilmann Weber's lab at DTU Biosustain. The genome sequencing of *Streptomyces* sp. P9-2B1 (CP129125) and Streptomyces sp. P9-2B2 (CP129126 and CP129127) was deposited into BioProject PRJNA985726. The phylogenetic tree of *Streptomyces* sp. was constructed using multiple sequence alignment tool Clustal Omega (https://www.ebi.ac.uk/Tools/msa/clustalo/) and visualized by iTOL: Interactive Tree Of Life (https://itol.embl.de).[17]

***Streptomyces*-*Streptomyces* cocultivation and monocultures.** All spore stocks used in this study were standardized to 1.0E5 CFU/mL, 10 µL of inoculum was added for each isolate, and all cocultivations were carried out on BD Difco Potato Dextrose Agar (PDA). Environmental isolates cocultures and cocultivation with *S. coelicolor* M145 were inoculated on the same day, approximately 1.5 cm distance apart. Inocula used for MSI were incubated at 30 °C for 7 days and then prepared for imaging. Inocula used for timelapse imaging were placed in a 30 °C incubator room with a Reshape Timelapse Imager and one image was taken every 60 minutes for 7-10 days depending on experiment length. Experiments involving pure lydicamycin (Santa Cruz Biotechnology Inc.) and azalomycin F: bacterial spore stocks were plated and pre-incubated for 4 days and then pure metabolites were added to an agar well 1.5 cm away. Pre-incubation was carried out to (1) mimic the time point lydicamycin production is seen in P9-2B2 monocultures and (2) to prevent inhibitory effects of the metabolite. P9-2B2 monocultures for temporal SM production: 10 PDA plates with three 10 µL spots were incubated, where every day one plate was removed, one colony was imaged using a Leica S9i digital microscope and extracted as described below. The exact same procedure was carried out with ISP2 plates but only sampling on days 1, 2, 3, 4, 7 and 10.

Inactivation of the lydicamycin BGC by inactivating *lyd6o*. In order to inactivate the core biosynthetic gene *lyd6o (NCBI Genbank accession:* WP_290354452.1*),* coding for the first modules of the lydicamycin PKS, a STOP codon via base editing (sgRNA:*lyd6o*) was designed using the online tool CRISPy-web[18]. pCRISPR-cBEST plasmid was linearized by NcoI and NEBuilder HiFi DNA Assembly Master Mix was used to insert the sgRNA:*lyd6o* deactivation, resulting in pCRISPR-cBEST/*lyd6o*. Subsequently, Mach1 T1 Phage-Resistant Chemically Competent *E. coli* was transformed with the plasmid. The plasmid was re-isolated and transferred into chemically competent *E. coli* ET12567/pUZ8002. The *E. coli*-*Streptomyces* conjugation experiment was conducted according to the standard protocol and mutant *Streptomyces* strains were confirmed by Sanger sequencing.[1]

All primers used were synthesized by IDT (Integrated DNA Technologies, USA) and are listed in Supplementary Table S1. Plasmids and genomic DNA purification, polymerase chain reaction (PCR), and

cloning were conducted according to standard procedures using manufacturer protocols. PCR was performed using Q5® High-Fidelity 2X Master Mix (New England Biolabs, USA). DNA assembly was done by using NEBuilder HiFi DNA Assembly Master Mix (New England Biolabs, USA). DNA digestion was performed with FastDigest restriction enzymes (Thermo Fisher Scientific, USA). NucleoSpin Gel and PCR Clean-up Kits (Macherey-Nagel, Germany) were used for DNA clean-up from PCR products and agarose gel extracts. One Shot Mach1 T1 Phage-Resistant Chemically Competent *E. coli* (Thermo Fisher Scientific, USA) was used for cloning. NucleoSpin Plasmid EasyPure Kit (Macherey-Nagel, Germany) was used for plasmid preparation. Sanger sequencing was carried out using a Mix2Seq Kit (Eurofins Scientific, Luxembourg). All DNA manipulation experiments were conducted according to standard procedures using manufacturer protocols.

Sample preparation and Mass Spectrometry Imaging. 10 µL glycerol spore stocks of each microbe were plated onto 4 mm thick PDA agar for all MSI experiments. Sample preparation was adapted from Yang et al.[19] Typical agar height is 1-2 mm but early indications showed the time required for sporulation to be observed required more nutrients for the *Streptomyces* spp. To grow. Upon observation of induced sporulation in the receiver strain, colonies were excised using a scalpel and placed on a Bruker IntelliSlide, coated with a layer of glue applied with a glue pen. Samples were subsequently dried for 2-4 hours at 35°C followed by matrix application (40 mg/mL DHB, 50:50:0.1% H_2O:MeOH:TFA) for 15 passes using HTX-Sprayer (Chapel Hill, NC, USA). Samples were further dried at 35°C for 1 hour prior to MSI. The samples were then subjected to timsTOF flex (Bruker Daltonik GmbH) mass spectrometer for Matrix-assisted laser desorption/ionization (MALDI)-MSI acquisition in positive MS scan mode with 20 µm raster width and a mass range of 100-2000 Da. Calibration was done using red phosphorus. The settings in the timsControl were as follow: Laser: imaging 20 µm, Power Boost 3.0%, scan range 16 µm in the XY interval, and laser power 70%; Tune: Funnel 1 RF 300 Vpp, Funnel 2 RF 300 Vpp, Multipole RF 300 Vpp, isCID 0 eV, Deflection Delta 70 V, MALDI plate offset 100 V, quadrupole ion energy 5 eV, quadrupole loss mass 100 m/z, collision energy 10 eV, focus pre TOF transfer time 75 µs, pre-pulse storage 8 µs. All data was analyzed using Bruker SciLS (2021b Pro) and data was normalized to the root mean squared.

MS-based Metabolomics. All extracts for LC-MS were generated using an agar plug method.[20] Liquid chromatography was performed on an Agilent Infinity 1290 UHPLC system. 20 µL extract was injected onto an Agilent Poroshell 120 phenyl-C6 column (2.1 × 150 mm, 1.9 µm) at 40°C using CH_3CN and H_2O, both containing 20 mM formic acid. Initially, a linear gradient of 10% CH_3CN/H_2O to 100% CH_3CN over 10 min was employed, followed by isocratic elution of 100% CH_3CN for 2 min. Then, the gradient was returned to 10% CH_3CN/H_2O in 0.1 min and finally isocratic condition of 10% CH_3CN/H_2O for 1.9 min, all at a flow rate of 0.35 min ml^{-1}. HRMS data was recorded in positive ionization on an Agilent 6545 QTOF MS equipped with an Agilent Dual Jet Stream electrospray ion (ESI) source with a drying gas temperature of 250°C, drying gas flow of 8 min l^{-1}, sheath gas temperature of 300°C and sheath gas flow of 12 min l^{-1}. The capillary voltage was 4000

V and nozzle voltage was set to 500 V. The HRMS data were processed and analyzed using Agilent MassHunter Qualitative Analysis B.07.00. HPLC grade solvents (VWR Chemicals) were used for extractions while LCMS grade solvents (VWR Chemicals) were used for LCMS. Raw data was converted to .mzML using MSConvert (ProteoWizard) and preprocessed using Mzmine 3.[21] Molecular networking was all completed within the GNPS platform,[22] which includes: Feature Based Molecular Networking.[23] Visualization of the molecular networks was completed using Cytoscape 3.8.2.[24]

Sequence Similarity Network of guanidine CoA-acyl carrier protein transacylase. The Sequence Similarity Network (SSN) was generated utilizing EFI-EST[25] (https://efi.igb.illinois.edu/efi-est/) using the resultant sequence BLAST of potential guanidine CoA-acyl carrier protein transacylase (NCBI Accession: AVV61977.1, *Streptomyces* sp. ID38640) found in the lydicamycin biosynthetic gene cluster (MIBiG Accession: BGC0001477).[26] The UniProt BLAST query *E* value was set as 10^{-5} and the alignment score threshold for figure generation was assigned as 10^{-130}. Cytoscape 3.8.2[24] was used for network visualization and both self-loops and duplicate loops were deleted.

Data Availability. LC-MS data can be found in GNPS-MassIVE at MSV000092216 and MSI data can be found at Metaspace at https://metaspace2020.eu/project/jarmusch-2023. Isolate sequencing data have been deposited at the NCBI BioProject database with accession number PRJNA985726. FBMN workflow can be found here: https://gnps.ucsd.edu/ProteoSAFe/status.jsp?task=a3dd5a7a459e475d8ca492ef7d- 05f3b7.

Results

Diffusible metabolites induce sporulation of *Streptomyces* sp. P9-2B1. While searching for *Streptomyces-Streptomyces* interactions, *Streptomyces* sp. P9-2B2 was cocultured with a relevant environmental isolate, *Streptomyces* sp. P9-2B1. After 7 days of growth, it was observed that P9-2B1 had a zone of sporulation emanating from P9-2B2, indicating the potential of a diffused metabolite causing morphogenesis. The observed morphogenesis of P9-2B1 occurred in three distinct phases starting from the edge closest to P9-2B2 (Figure 1A): (1) substrate hyphae first changed in pigmentation, from pale to bright yellow; (2) production of aerial hyphae (white); (3) production of spores (greenish grey). Although the mechanism behind sporulation and the transcriptional effects of sporulation are well understood, metabolites that cause sporulation are essentially unknown, thus peaking our excitement.

Due to the 'wave-like' nature of the morphogenesis, we proposed an agar diffusible metabolite produced by P9-2B2 that was causing the phenotype change in P9-2B1. To initially confirm the hypothesis, a distance-based assay was carried out where P9-2B1 was incrementally (0.5 cm) moved away from the producer, P9-2B2. As P9-2B1 is distanced farther away, the inducible morphogenesis disappears (Figure 1B). This indicates that diffusible metabolites are indeed responsible for the phenotype change, like previously reported observations of *Streptomyces-Streptomyces* induced sporulation.[9] Furthermore, when the P9-2B1 macro-colonies are in

very close proximity (5-10 mm), their growth is visibly affected at the nearest point to P9-2B2. In contrast, the colony at 15 mm distance is more comparable to those at 20-25 mm in overall shape, yet aerial hyphae production has begun.

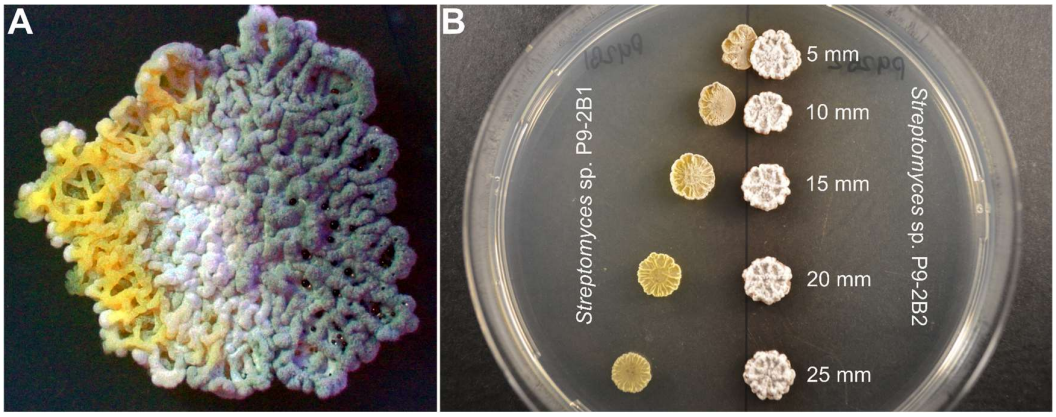

Figure 1. (A) observed differentiation of *Streptomyces* sp. P9-2B1 on PDA in cocultivation with *Streptomyces* sp. P9-2B2. (B) Distance based assay showing the diffusible zone of sporulation induced by secondary metabolite production by *Streptomyces* sp. P9-2B2.

Mass Spectrometry Imaging illuminates lydicamycin production causes sporulation. Traditionally, researchers have attempted to characterize chemistry derived from cocultures using standard extraction techniques.[11,20] Therefore, our first attempt to identify the responsible metabolites was via agar plug extracts taken from three distinct locations and analyzed using LC-MS: (1) P9-2B2, P9-2B1 (non-sporulating area) and P9-2B1 (sporulated area). No candidate metabolites were differentially observed when comparing the base peak chromatograms nor did the chemistry of P9-2B1 change in these sporulated areas (Figure S1). The lack of identifying any viable SMs with agar plugs and LC-MS led us to use MSI to directly visualize the spatial metabolome.

Using an adapted method based on previous studies focusing on imaging microbial interactions on agar,[19,27,28] *Streptomyces-Streptomyces* interactions were carried out on PDA, excised and prepared for MSI. Original methods call for culturing on steel plate (ultra-thin agar) or onto thin agar (1-2 mm), to minimize topological interference of ion transmission. These were not feasible due to the combined effects of the long growth time required to observe sporulation (6-9 days) and substrate mycelium 'digging' into the agar caused severe agar splitting and subsequent flaking. Therefore, we adapted the

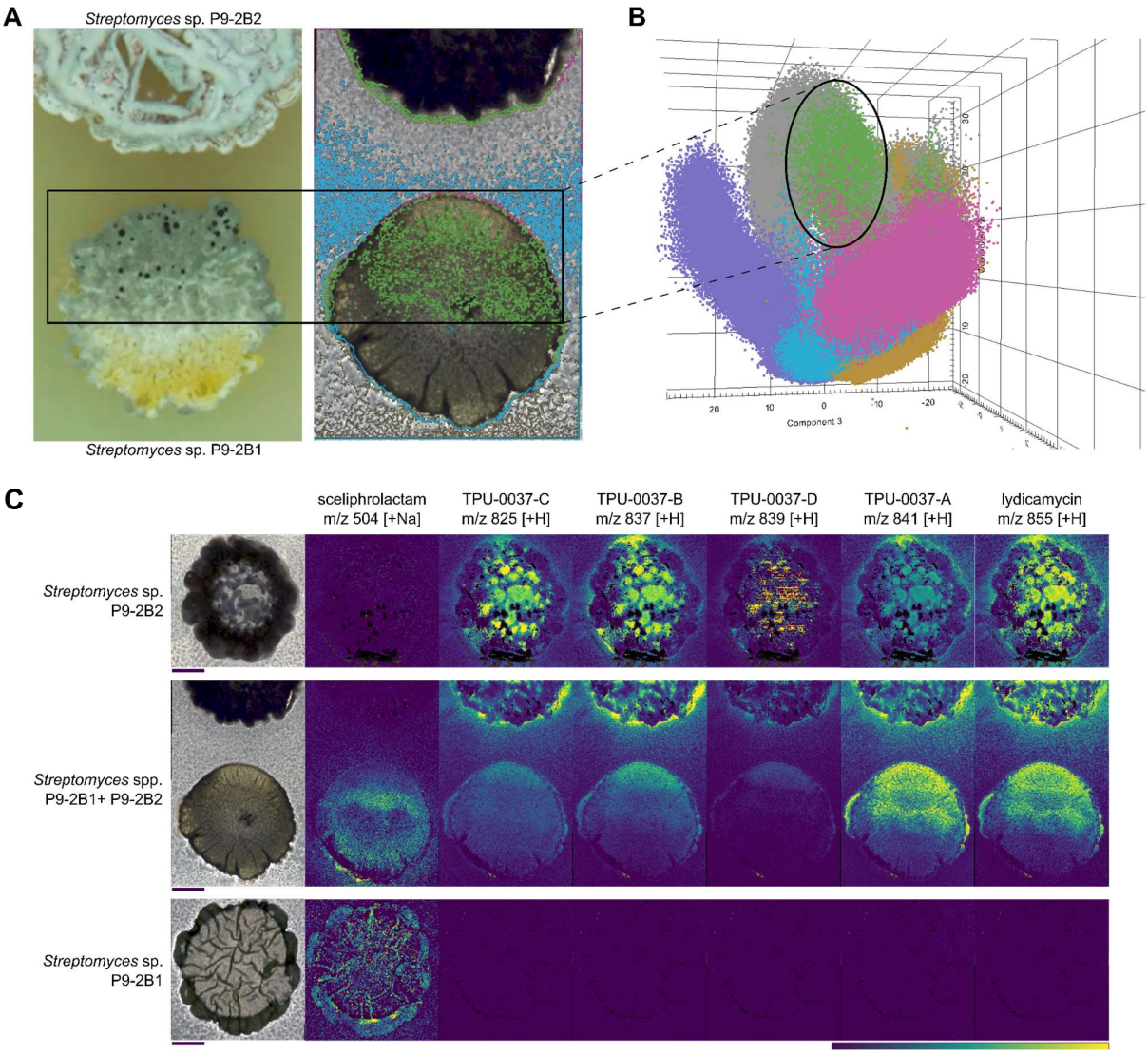

Figure 2. MALDI-MSI of *Streptomyces* sp. P9-2B1 and *Streptomyces* sp. P9-2B2. (A) Digital microscope image of sporulation and interaction zone between the *Streptomyces* (left) and MSI sampling region with segmentation differentiating P9-2B1 (blue), sporulation zone of P9-2B1 (green) and P9-2B2 (magenta). (B) 3D PCA plot of MSI spectra with two additional segments of the P9-2B1 monoculture (lavender) and P9-2B2 monoculture (orange). (C) Ion images (viridis color scheme) of sceliphrolactam and the various lydicamycins produced (TPU-0037-A through D are congeners of lydicamycin). Scale bars: 4 mm. Colored scale bar indicates relative ion abundance with hotspot removal activated.

methodology to work on thicker agar plates (2-4 mm), allowing for proper sample adherence to glass slides as well as minimal air bubbles and flaking. The half-sporulated sample of P9-2B1 (Figure 2A) as well as two monocultures were analyzed using MALDI-MSI. Using Bruker SciLS, co-localized features from the sporulation zone of P9-2B1 were parsed from the dataset, leaving a group of ions ranging from 800-950. Upon further examination, there were two distinct spatial patterns from this mass range: m/z 800-860 originating from P9-2B2 and m/z 861-950 being produced by P9-2B1, with the former of more interest. Focusing on the features from m/z 800-860, MSI of the monocultures show these features are present in and around P9-2B2,

the strain causing sporulation. These features were present in the sporulation area of P9-2B1, giving a strong indication these are the responsible features for the observed sporulation. Furthermore, Principal Component Analysis revealed the sporulation zone of P9-2B1 (Figure 2B) was more similar to the surrounding agar and colony of P9-2B2 than of the surrounding agar and non-sporulated colony of P9-2B1. Additionally, the P9-2B1 monoculture was distinctly separated from the sporulation zone, indicating they share no metabolic overlap. Upon dereplication using BGC predictions via antiSMASH[29] and NPAtlas[30], we hypothesized the responsible metabolites to be lydicamycins.

Lydicamycins are NRPS-PKS hybrids, recently named arginoketides,[31] that have a proposed biosynthesis starting from an enzymatically converted arginine26 or a separate enzymatic process.[32] Five known derivatives were originally described (lydicamycin and TPU-0037-A, B, C, D) and MSI was able to observe all known derivatives (Figure 2C).[33,34] P9-2B2 produces the lydicamycins, which are diffused across the agar and then taken up by P9-2B1, principally in the sporulation zone. There are very few known metabolites produced by P9-2B1 yet we can observe sceliphrolactam (m/z 504.2299 $[M+Na]^+$), which is produced throughout the P9-2B1 monoculture, however in coculture, it lacks production corresponding to the region nearest to P9-2B2, possibly due to the effects of the lydicamycins.

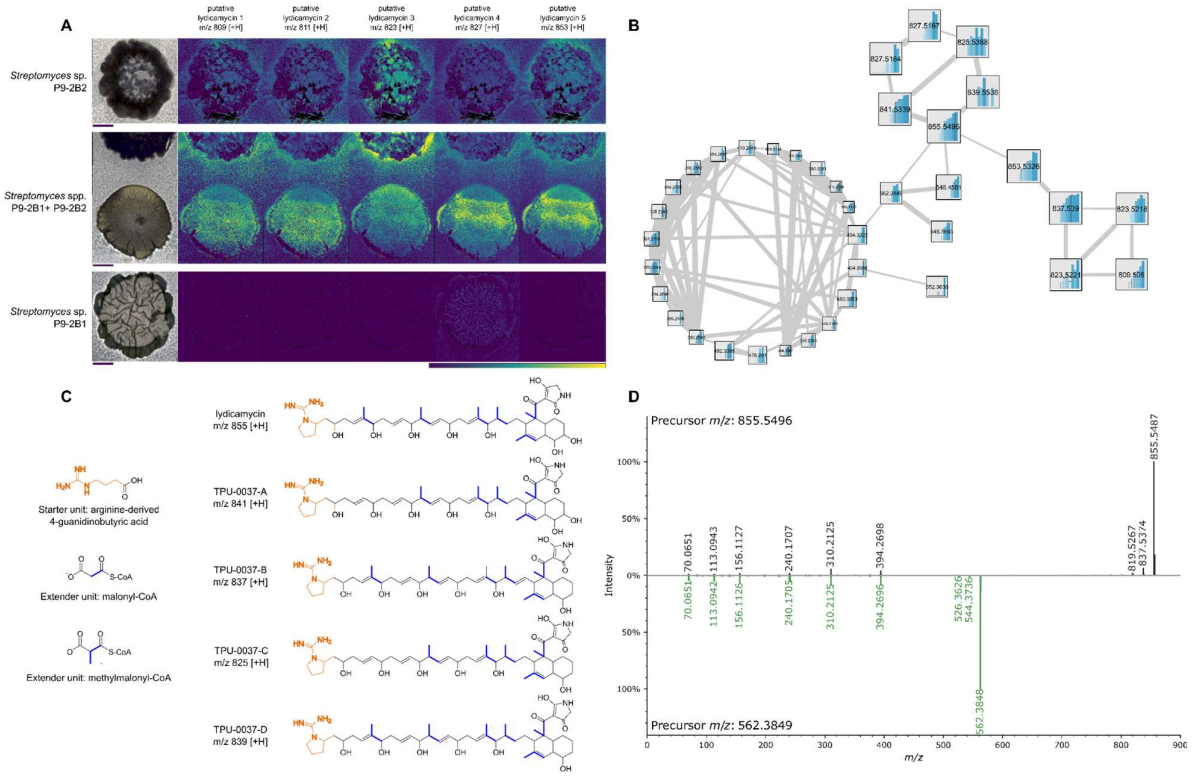

Figure 3. (A) Ion images (viridis color scheme) of putative lydicamycins produced. Scale bars: 4mm. Colored scale bar indicates relative ion abundance with hotspot removal activated. (B) Lydicamycin molecular family where increased edge width indicates higher fragmentation similarity. Internal bar graphs indicate peak area over each day from Day 1-10 (C) Structures and biosynthetic origin of lydicamycins. (D) Fragmentation mirror plot of lydicamycin (*m/z* 855.5496) and the putative shunt product *m/z* 562.3849. Green highlights indicate a cosine score-based match.

On top of the five known lydicamycins detected via MSI, additional lydicamycins were also detected that linked to the known lydicamycins via GNPS molecular networking (Figure 3A). *m/z* 809.5084 $[M+H]^+$, 823.5110 $[M+H]^+$, and 853.5326 $[M+H]^+$, are structurally related to TPU-0037-B based on molecular networking analysis (Figure 3B), which contains an additional degree of unsaturation from a seemingly flexible dehydratase domain (Figure 3C). *m/z* 827.5167 $[M+H]^+$ is structurally related to TPU-0037-A and C. A recent study that also utilized molecular networking to identify new derivatives of lydicamycins also proposed these new congeners which we detect, including *m/z* 811.511 $[M+H]^+$, which links in their study to TPU-0037-A.[32] They further identify several other features which we also observe (*m/z* 843.5352, 857.5474, 869.53 and 871.54; $[M+H]^+$) and additionally, we observe putative analogs (*m/z* 809.5084, 829.5238; $[M+H]^+$) which they do not, pointing to the fact there are further products in the biosynthetic pathway to uncover (raw data available). Type 1 PKS architecture in some cases allows for substrate flexibility. For instance, putative lydicamycins *m/z* 809.5084 $[M+H]^+$, *m/z* 823.511 $[M+H]^+$ and TPU-0037-B may be explained by different extender units (4, 5 and 6 methylmalonyl, respectively) but where they are located needs full confirmation via NMR (Figure 3C). All confirmed and putative lydicamycin MS/MS spectra were deposited into the GNPS Spectral Library (Table S2).

Lastly, an additional set of features was connected in the Feature Based Molecular Networking (FBMN) via lydicamycin (*m/z* 855) yet were significantly smaller in *m/z* (Figure 3B). Zhang et al. also observed these smaller features in their molecular network yet provided no explanation for their presence.[32] Due to their connectivity, we knew their fragmentation was similar, pointing to their structural similarity as well (Figure 3D). Upon further investigation, the fragments at *m/z* 394.2696, 310.2125, 240.1707, and 156.1126 can all be traced to the polyketide backbone and to the previously reported fragmentation,[33] on the C-C bond adjacent to hydroxyls. Due to this fragmentation similarity, we hypothesize these remaining features are shunt products or byproducts of the biosynthesis of lydicamycins that are 'incomplete'. Polyketide shunt products have been studied in type II PKS systems,[35] most extensively involving actinorhodin production.[36,37] The study by Deng et al.[37] shows a similar metabolic flux to shunt production as we observe here; upon production of lydicamycins at day 4, we see immediate detection of potential shunts and an increase towards days 9 and 10. Predicting shunt products of PKS biosynthesis is implausible due to rearrangements and therefore, future studies should focus on generating mutant libraries to study the biosynthesis more thoroughly.

Temporal dynamics of lydicamycin production. The temporal nature of secondary metabolite production in *Streptomyces* has so far been scantly investigated,[38] similar to the regulatory control.[39] Due to this gap of knowledge and the role time plays in our coculture system, we sought to investigate when lydicamycins are produced and attempt to link that to morphogenesis. We conducted an untargeted metabolomics analysis over 10 days, where each day a new plate containing three separate macro-colonies was imaged and extracted using plug extraction. Principal Coordinate Analysis (PCoA) in Qiime2 View allowed us to observe a shift in metabolism over this 10-day time scale (Figure 4A).[40] Furthermore, Pearson r correlation distinguishes three sample groupings: days 1-3, 4-5 and 6-10 (Supplementary Figure S2). Nodes from the FBMN (Figure 4A)

indicate all the lydicamycins and the putative shunt products increased in production up to day 9 (saturation of the LC-MS). When comparing this data to the microscopy images taken on each of these days, we observe morphogenesis and the onset of sporulation strongly correlates with the three metabolomics-based sample groupings: Day 1-3 are defined by substrate mycelium growth and no detectable lydicamycin production, days 4-5 are the onset of aerial mycelium production and the beginning of production and days 6-10 are defined by full sporulation and maturation along with the highest level of production (Figure 4B and C).

Figure 4. (A) PCoA showing the difference in metabolome over the cultivation time of P9-2B2. Molecular networking nodes show the production of lydicamycins (*m/z* 855.5496 and 841.5339) and the putative shunt product, *m/z* 562.3849. (B) Microscopy of P9-2B2 colonies on PDA and ISP2 from 1, 4, and 7 days of growth on solid agar. (C) Extracted ion chromatograms of *m/z* 855.5496 corresponding to the timed images in B for P9-2B2 grown on PDA (top) and ISP2 (bottom).

In early experiments, we also observed when the two *Streptomyces* isolates were cocultivated on ISP2 agar, neither the receiver strain P9-2B1 had sporulation induced nor did P9-2B2 sporulate itself. Therefore, we hypothesized that lydicamycin production must be lacking due to both observations. The same untargeted time-based experimental setup as described above (with fewer timepoints) was carried out on ISP2 and the results showed no sporulation in P9-2B2 over 7 days (Figure 4B). Surprisingly, lydicamycin production began on Day 1 when cultured on ISP2 and was stagnant through Day 7, but overall, the relative quantities were 10x lower than that on PDA. Based on the timing of lydicamycin production of PDA compared to that of ISP2 and their corresponding phenotypes, we concluded that the onset of sporulation kickstarts lydicamycin production, a typical phenomenon of secondary metabolite production in *Streptomyces*.

Additional metabolites (Figure S3) observed in the dataset were three diketopiperazines (cyclo Val-Pro, cyclo Phe-Pro and cyclo Leu-Pro) were all detected maximally at day 1 and then trailing off to no detection at day 9, indicating they may play an early role in substrate growth. The biosynthesis of the protease inhibitor antipain (*m/z* 605.3597) was also predicted by antiSMASH and the metabolite was found in our data at its highest on Day 1 and trailed off to no detection beyond Day 6, indicating it must also play a more vital role during substrate growth. Riboflavin was matched against the GNPS spectral library (and riBA_1 was also found in the genome); it showed an increase beginning at day 5 and peaking at day 9, indicating its production must

also be sporulation dependent. Riboflavin is an important micronutrient for biochemical reactions[41] and some *Streptomyces* spp. further convert it into antimicrobial analogs like roseoflavin.[42] Roseoflavin production has been tied to the stationary growth phase,[43] yet our strain cannot produce it, therefore ruling it out as inducing sporulation. Lastly, using DEREPLICATOR+[44] we observed the production of the extended hopanoid, bacteriohopanetetrol (*m/z* 546.4882). Production of bacteriohopanetetrol and other hopanoids occurs from the transition from substrate mycelium and aerial mycelium,[45] exactly like we observe in our data.

Lydicamycins are broad inducers of morphogenesis. Lydicamycins have known antimicrobial activity against Gram positive bacteria like *Bacillus subtilis*, *Staphylococcus aureus* and *Micrococcus luteus* and lack any antimicrobial effect against Gram negative bacteria tested.[34,46] Having shown the effect of P9-2B2 and lydicamycin production on P9-2B1 in this study, we set out to explore if sporulation is also triggered in other environmentally relevant *Streptomyces* from our collection site. Four additional environmental *Streptomyces* isolates (P9-2B3, P9-2B4, P9-2B5, P9-2B6) and *Streptomyces coelicolor* M145 were cocultured with P9-2B2 and timelapse images for each were taken. Results showed that 3/4 environmental strains and M145 exhibited the same phenotype change as P9-2B1 (Figure S4). Sporulation waves began to appear on M145, P9-2B3, 2B5, starting on Day 7 and progressing towards full sporulation on Day 10 (Figure 5), similar to P9-2B1. The remaining two isolates not pictured in Figure 5 were *Streptomyces* sp. P9-2B6, which sporulated on Day 11 (outside of the timelapse), and *Streptomyces* sp. P9-2B4, which sporulated prior to the lydicamycin producer (Figure S4). Digging deeper into genomics, 2B2 and 2B4 are in fact related to isolates of the same species (Figure S5) which may explain why they sporulate similarly on PDA. However, strain 2B4 lacks the *lyd* BGC. Timelapse videos of each interaction can be found in the supplementary data (Videos S1-6).

To confirm our lydicamycin-sporulation hypothesis based on imaging, metabolomics, and genomics, we generated a *lyd*-deficient mutant to test in coculture setups. The first core polyketide synthase lyd60 was targeted and inactivated by converting a TGG (Trp) codon at position 57 into the stop codon TAA using CRISPR-based base-editing tool CRISPR-BEST.[47] The deficient mutant (sgRNA:*lyd60*) was confirmed by Sanger sequencing of the editing site and LC-MS analysis after 7 days of growth on PDA ensuring sporulation occurred (Figure S6). Subsequent timelapse images were taken over 10 days and no sporulation was observed in the receiver strain, P9-2B1 (Video S7). The lydicamycin-deficient mutant observably had different growth in the first two days from the wild type (WT). The first indication of sporulation in WT P9-2B2 appears on Day 1 Hour 13 compared to Day 4 for the *lyd*-deficient mutant (Videos S8-9), indicating the inactivation of the *lyd* BGC clearly delays sporulation in P9-2B2. To further confirm lydicamycin's role in sporulation, pure lydicamycin (*m/z* 855) was added into an agar well and induced sporulation in P9-2B1 but only at a high concentration (100 µg) and a distinctively longer interval (9 days) than when cocultured (6-7 days) (Video S10). Sporulation assays were conducted on pregrown cultures of 3 days, otherwise, P9-2B1 was inhibited by pure lydicamycin when cultured simultaneously, indicating its overall antimicrobial effect towards the *Streptomyces* isolate. We wanted to test an additional bioactive member of the arginoketides, to see if we

observed induced morphogensis and due to ease of purified material, azalomycin F (100 µg) was tested was tested in the identical manner as pure lydicamycin and no sporulation was observed over 10 days (Video S11). The study by Krespach et al. showed that the presence of an amino-guanidyl was necessary to observe the effect in various fungi, indicating a specific mechanism of action tied to the moiety. Unlike their result, our tests indicate the amino-guanidyl moiety likely plays no factor in the sporulation-inducing effects of lydicamycins and these results indicate differentiation is not inducible simply by the presence of antibacterial SMs.

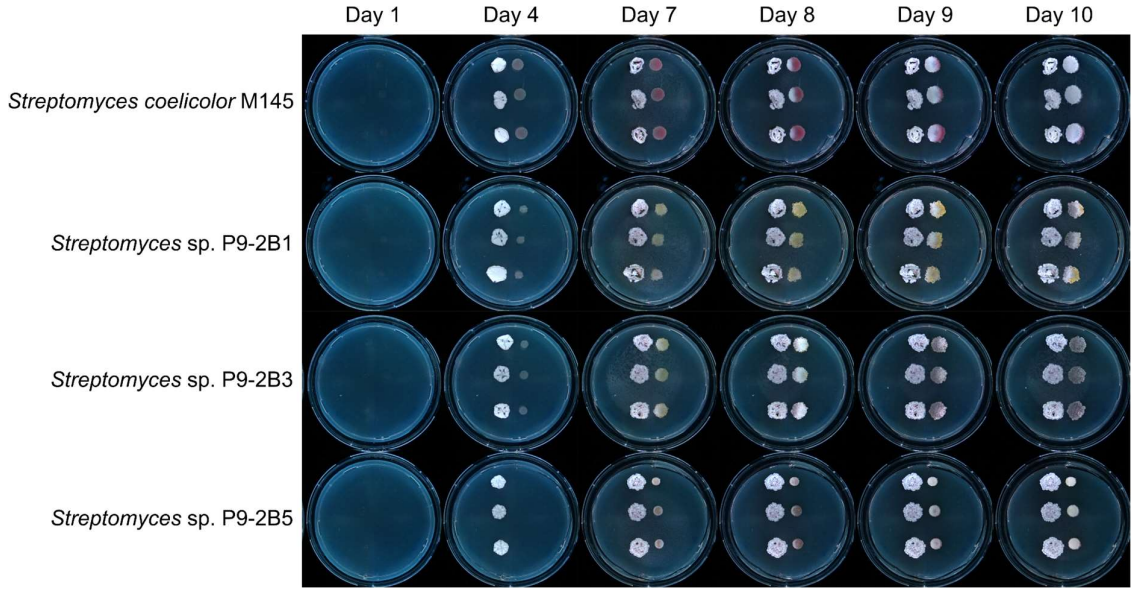

Figure 5. Time series of *Streptomyces-Streptomyces* interactions between environmental isolates (right colony) and *Streptomyces* sp. P9-2B2 (left colony).

The biosynthetic potential of arginoketides is expansive. Lydicamycins and overall, the arginoketides, were shown to trigger the production of multiple SMs in *Aspergillus nidulans* and the pigment carviolin in a *Pencillium* sp., indicating as a chemical class, they have a wider ecological context.[31] Therefore, we wanted to evaluate the biosynthetic potential of this metabolite class in publicly available genomes. The guanidine CoA-acyl carrier protein transacylase, which has been predicted to transfer the arginine-derived starting unit into the first steps of PKS machinery, is present in the surrounding region of known arginine-starting unit polyketides such as ECO-02301,[48] azalomycin F3a,[49] linearmycin,[50] and lydicamycin (Figure S7). Known BGCs containing the transacylase were aligned using clinker[51] and anchored via the protein. The linear polyketides mediomycin[52], ECO-02301, linearmycin and desulfoclethramycin[53] share a more similar biosynthetic architecture to each other than to the other BGCs (Figure S8).

To gain further insight into the distribution of these BGCs in bacteria and the uniqueness of their transacylases, we generated a Sequence Similarity Network (SSN) based on the guanidine CoA-acyl carrier protein transacylases. The taxonomic distribution of 529 retrieved sequences showed the transacylases were

mainly distributed in *Streptomyces* spp. (Figure S9). As expected, the transacylases involved in desertomycin,[54] azalomycin, linearmycin, and lydicamycin biosynthesis were clustered individually, indicating the high BGC-specificity of these proteins (Figure S10), and most of the sequences retrieved and their corresponding BGCs remain vastly unexplored. Furthermore, we mapped these producers as well as additional metabolites encoded from transacylase-containing BGCs onto the wider phylogenetic context of *Streptomyces* sp. using the housekeeping gene *trpB* (tryptophan synthase subunit beta)(Figure 6).[55] We further hypothesized these transacylases were highly associated to BGCs, therefore we mined a subset of genomes: *Salinispora tropica*, *Amycolotopsis orientalis* and *Saccharothrix australiensis*. The three actinobacteria all contained Type I Polyketide Synthase BGCs. *Salinispora tropica* returned the known metabolite BGC, salinilactam,[56] while *Amycolotopsis orientalis* contained a BGC with no similarity to a known cluster and *Saccharothrix australiensis* contained a highly similar (77%) BGC to mediomycin (Figure S11). Therefore, we believe it is possible to mine for arginoketides and other aminated polyketides involving the transacylase in their biosynthesis.

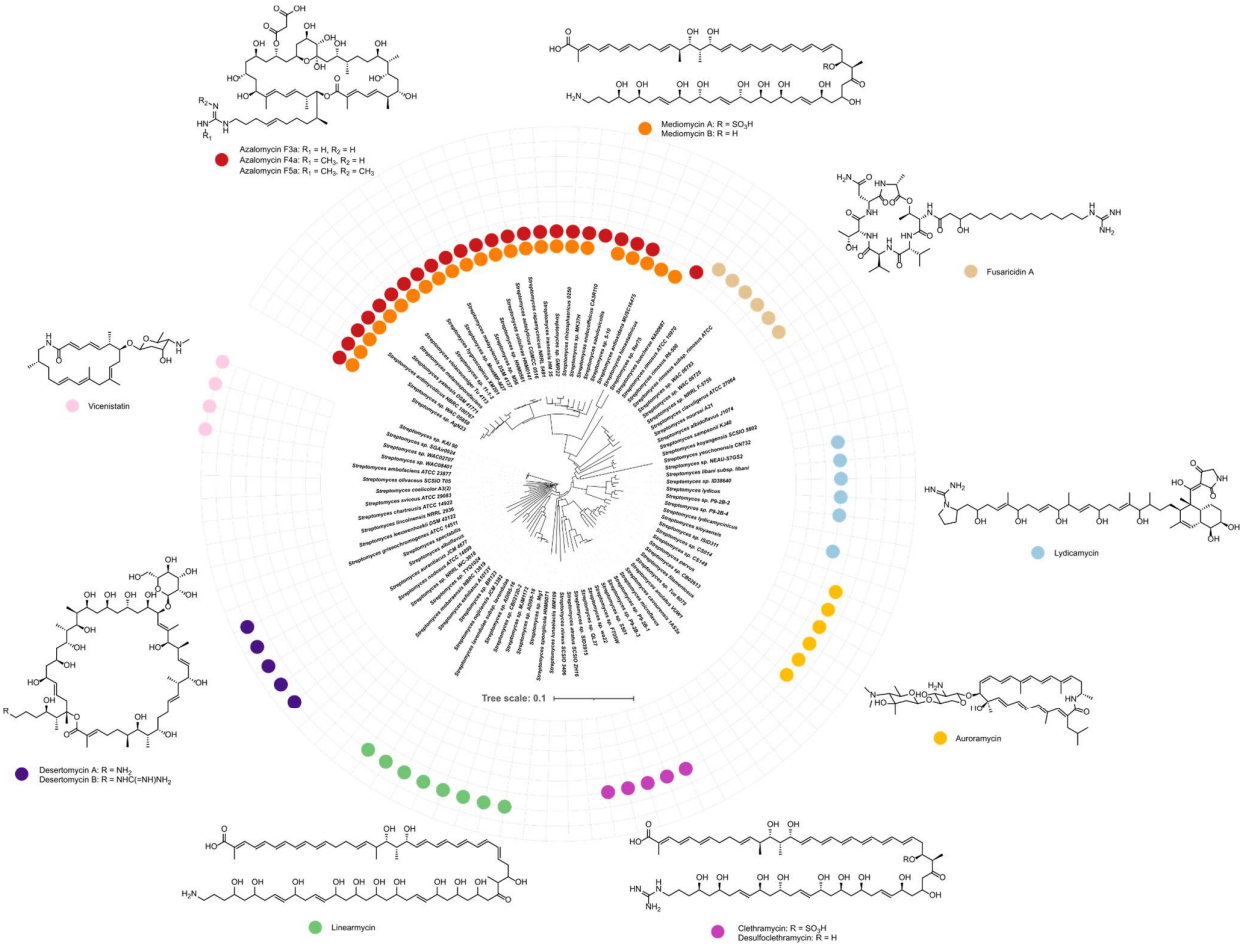

Figure 6. Phylogenetic tree based on housekeeping gene *trpB* of *Streptomyces* sp. mapped with known arginine-containing metabolites.

Discussion

The induction of sporulation by lydicamycin makes this one of a handful of described SMs with the same ecology. The two other SMs described with sporulation inducing effects are goadsporin and desferrioxamine E, with our results more similarly mirroring goadsporin as both are antibiotic and sporulation inducing. Yamanaka et al. reported the sporulation-inducing activity of desferrioxamine E and confirmed the observation via BGC knockout studies.[57] They showed their susceptible strain, *S. tanashiensis*, lacked the des BGC and the siderophore transporter, therefore making it prone to iron starvation. However, this is most likely a very rare case amongst *Streptomycetes* as the vast majority of *Streptomycete* genomes code for a highly conserved desferrioxamine BGC. Additionally, there are several metabolites further responsible for differentiation, specifically germination, which are described,[58] pointing to the fact that *Streptomyces* SMs may play larger roles in its life cycle than previously anticipated.

There are two main factors leading to the underreported number of sporulation inducing SMs: (1) the low number of pathogenic *Streptomycetes* discourages biological testing in traditional drug discovery efforts and (2) low compound yields make it difficult to test against a broad enough range of bacteria. The induction of morphological differentiation, *i.e.* sporulation, is a viable strategy for increasing the production of antibiotics[59,60] and may be a route for eliciting cryptic biosynthetic pathways through subinhibitory concentrations, yet the latter requires further investigation. Nevertheless, we require ecological studies to identify metabolites capable of inducing sporulation to begin investigating the potential downstream effects. Furthermore, as we reveal further ecological functions of SMs, the ability to utilize microbes as biocontrol agents will also gain further attention, beyond their high interest already garnered.

Traditional analytical techniques like HPLC or LC-MS lack the ability to quickly discern metabolites which may be involved in cocultures (unless they are produced in high titres), either lacking noticeable differences in UV chromatograms or difficulty deconvoluting many features, respectively. On the other hand, MSI is a burgeoning technique equipped uniquely to handle these types of samples, as seen through this study and others.[12,61,62] Through the use of MSI, we were able to quickly define potential candidate features based on their spatial distribution and through dereplication via MS and genome mining, propose and confirm the sporulation-inducing nature of lydicamycins. MSI suffers from topological challenges and actinobacteria and other filamentous microbes can be difficult to chemically image, therefore, modified strategies like what we have demonstrated, or new techniques may be required to increase the utility of MSI. Furthermore, MS-based metabolomics like molecular networking and multivariate statistics continue to be able to differentiate microbial metabolomes, as we have demonstrated with a temporal study of SM production. While transcriptomics and proteomics have traditionally been utilized to track changes over time, metabolomics offers visibility towards the end of these processes, providing a picture of what and potentially how much is produced by microbes. Ultimately, all three -omics provide separate details in the life of a microbe and integration of these data will begin to reveal the larger picture of SM production.

We herein show that via MSI, the characterization of lydicamycins as the responsible metabolites in a

dual *Streptomyces* coculture is the optimal technique for these agar-based setups. Not only were the standard congeners detected but several additional newly discovered and putative derivatives were also visible in the data. Temporal production of the lydicamycins nicely correlated with self-induced sporulation of the producing strain and the generation of a deficient mutant significantly delayed the onset of sporulation when compared to the wild type. Furthermore, beyond testing a single isolate, lydicamycins induced sporulation in other environmental *Streptomyces* as well as the model strain *S. coelicolor* M145, indicating their broad-spectrum activity. Lastly, by mapping the presence of guanidino-CoA transacylases on *Streptomyces* phylogeny, we observed the highly specific nature of this chemical class, indicating they may have specialized ecologies that require further investigation. We hope this study provides an important primer for tracking down the responsible metabolites in microbial interactions but also begins to illuminate the ecological role and temporal nature of lydicamycins.

References

1. Kieser, T., Bibb, M. J., Buttner, M. J., Chater, K. F. & Hopwood, D. A. Practical *Streptomyces* genetics. *The John Innes Foundation*, (2000).
2. Bibb, M. J. Understanding and manipulating antibiotic production in actinomycetes. *Biochem. Soc. Trans.* **41**, 1355–1364 (2013).
3. Takano, E. Gamma-butyrolactones: *Streptomyces* signalling molecules regulating antibiotic production and differentiation. *Curr. Opin. Microbiol.* **9**, 287–294 (2006).
4. Mithöfer, A. & Boland, W. Do you speak chemistry? Small chemical compounds represent the evolutionary oldest form of communication between organisms. *EMBO Rep.* **17**, 626–629 (2016).
5. Traxler, M. F. & Kolter, R. Natural products in soil microbe interactions and evolution. *Nat. Prod. Rep.* **32**, 956–970 (2015).
6. van Bergeijk, D. A., Terlouw, B. R., Medema, M. H. & van Wezel, G. P. Ecology and genomics of Actinobacteria: new concepts for natural product discovery. *Nat. Rev. Microbiol.* **18**, 546-558 (2020).
7. Yang, Y.-L., Xu, Y., Straight, P. & Dorrestein, P. C. Translating metabolic exchange with imaging mass spectrometry. *Nat. Chem. Biol.* **5**, 885–887 (2009).
8. Schlimpert, S. & Elliot, M. A. The best of both worlds-*Streptomyces coelicolor* and *Streptomyces venezuelae* as model species for studying antibiotic production and bacterial multicellular development. *J. Bacteriol.* **205**, e0015323 (2023).
9. Ueda, K. et al. Wide distribution of interspecific stimulatory events on antibiotic production and sporulation among *Streptomyces* species. *J. Antibiot.* **53**, 979–982 (2000).
10. Onaka, H., Tabata, H., Igarashi, Y., Sato, Y. & Furumai, T. Goadsporin, a chemical substance which promotes secondary metabolism and morphogenesis in *Streptomycetes*. I. Purification and characterization. *J. Antibiot.* **54**, 1036–1044 (2001).
11. Knowles, S. L., Raja, H. A., Roberts, C. D. & Oberlies, N. H. Fungal–fungal co-culture: a primer for generating chemical diversity. *Nat. Prod. Rep.* **39**, 1557-1573 (2022).
12. Dong, Y. & Aharoni, A. Image to insight: exploring natural products through mass spectrometry imaging. *Nat. Prod. Rep.* **39**, 1510–1530 (2022).
13. Jarmusch, A. K. & Cooks, R. G. Emerging capabilities of mass spectrometry for natural products. *Nat. Prod. Rep.* **31**, 730-738 (2014).
14. Traxler, M. F., Watrous, J. D., Alexandrov, T., Dorrestein, P. C. & Kolter, R. Interspecies interactions stimulate diversification of the *Streptomyces coelicolor* secreted metabolome. *MBio* 4, 10-1128 (2013).
15. Feeney, M. A. et al. ActinoBase: tools and protocols for researchers working on and other filamentous actinobacteria. *Microb. Genom.* **8**, mgen000824 (2022).
16. Wibowo, M. et al. Azodyrecins A–C: azoxides from a soil-derived *Streptomyces* species. *J. Nat. Prod.* 83, 3519–3525 (2020).

17. Letunic, I. & Bork, P. Interactive Tree Of Life (iTOL) v5: an online tool for phylogenetic tree display and annotation. *Nucleic Acids Res.* 49, W293–W296 (2021).
18. Blin, K., Shaw, S., Tong, Y. & Weber, T. Designing sgRNAs for CRISPR-BEST base editing applications with CRISPy-web 2.0. *Synth. Syst. Biotechnol.* **5**, 99–102 (2020).
19. Yang, J. Y. et al. Primer on agar-based microbial imaging mass spectrometry. *J. Bacteriol.* **194**, 6023–6028 (2012).
20. Smedsgaard, J. Micro-scale extraction procedure for standardized screening of fungal metabolite production in cultures. *J. Chromatogr. A* **760**, 264–270 (1997).
21. Schmid, R. et al. Integrative analysis of multimodal mass spectrometry data in MZmine 3. *Nat. Biotechnol.* **41**, 447-449 (2023).
22. Wang, M. et al. Sharing and community curation of mass spectrometry data with Global Natural Products Social Molecular Networking. *Nat. Biotechnol.* **34**, 828–837 (2016).
23. Nothias, L. F. et al. Feature-based molecular networking in the GNPS analysis environment. *Nat. Methods* **17**, 905–908 (2020).
24. Shannon, P. et al. Cytoscape: a software environment for integrated models of biomolecular interaction networks. *Genome Res.* **13**, 2498–2504 (2003).
25. Zallot, R., Oberg, N. & Gerlt, J. A. The EFI Web resource for genomic enzymology tools: leveraging protein, genome, and metagenome databases to discover novel enzymes and metabolic pathways. *Biochemistry* **58**, 4169–4182 (2019).
26. Komaki, H., Ichikawa, N., Hosoyama, A., Fujita, N. & Igarashi, Y. Draft genome sequence of marine-derived *Streptomyces* sp. TP-A0598, a producer of anti-MRSA antibiotic lydicamycins. *Stand. Genomic Sci.* **10**, 58 (2015).
27. Watrous, J. D. & Dorrestein, P. C. Imaging mass spectrometry in microbiology. *Nat. Rev. Microbiol.* **9**, 683–694 (2011).
28. Dunham, S. J. B., Ellis, J. F., Li, B. & Sweedler, J. V. Mass spectrometry imaging of complex microbial communities. *Acc. Chem. Res.* **50**, 96–104 (2016).
29. Blin, K. et al. antiSMASH 7.0: new and improved predictions for detection, regulation, chemical structures and visualisation. *Nucleic Acids Res.* **51**, W46-W50 (2023)
30. van Santen, J. A. et al. The Natural Products Atlas 2.0: a database of microbially-derived natural products. *Nucleic Acids Res.* **50**, D1317–D1323 (2022).
31. Krespach, M. K. C. et al. *Streptomyces* polyketides mediate bacteria-fungi interactions across soil environments. *Nat. Microbiol.* **8**, 1348-1361 (2023).
32. Zhang, H., Li, X., Pan, S., Huang, J. & Qin, Z. Dissecting the biosynthesis of the polyketide alkaloid lydicamycin using a complex metabolic network. *New J. Chem.* **47**, 12093-12100 (2023).
33. Hayakawa, Y., Kanamaru, N., Morisaki, N., Furihata, K. & Seto, H. Lydicamycin, a new antibiotic of a novel skeletal type. II. Physico-chemical properties and structure elucidation. *J. Antibiot.* **44**, 288–292

(1991).

34. Furumai, T. et al. TPU-0037-A, B, C and D, Novel lydicamycin congeners with anti-MRSA activity from S*treptomyces platensis* TP-A0598. *J. Antibiot.* **55**, 873-80 (2002).
35. Hertweck, C. The biosynthetic logic of polyketide diversity. *Angew. Chem. Int. Ed.* **48**, 4688–4716 (2009).
36. Hopwood, D. A. Genetic contributions to understanding polyketide synthases. *Chem. Rev.* **97**, 2465–2498 (1997).
37. Deng, M.-R. et al. An aberrant metabolic flow toward early shunt products in the granaticin biosynthetic machinery of *Streptomyces vietnamensis* GIMV4.0001. *J. Antibiot.* **73**, 260–264 (2020).
38. Čihák, M. et al. Secondary metabolites produced during the germination of *Streptomyces coelicolor*. *Front. Microbiol.* **8**, 2495 (2017).
39. van Wezel, G. P. & McDowall, K. J. The regulation of the secondary metabolism of *Streptomyces*: new links and experimental advances. *Nat. Prod. Rep.* **28**, 1311–1333 (2011).
40. Bolyen, E. et al. Reproducible, interactive, scalable and extensible microbiome data science using QIIME 2. *Nat. Biotechnol.* **37**, 852–857 (2019).
41. Averianova, L. A., Balabanova, L. A., Son, O. M., Podvolotskaya, A. B. & Tekutyeva, L. A. Production of vitamin B2 (riboflavin) by microorganisms: an overview. *Front. Bioeng. Biotechnol.* **8**, 570828 (2020).
42. Schwarz, J., Konjik, V., Jankowitsch, F., Sandhoff, R. & Mack, M. Identification of the key enzyme of roseoflavin biosynthesis. *Angew. Chem. Int. Ed*. **55**, 6103–6106 (2016).
43. Kißling, L. et al. The roseoflavin producer *Streptomyces* davaonensis has a high catalytic capacity and specific genetic adaptations with regard to the biosynthesis of riboflavin. *Environ. Microbiol.* **22**, 3248–3265 (2020).
44. Mohimani, H. et al. Dereplication of microbial metabolites through database search of mass spectra. *Nat. Commun.* **9**, 4035 (2018).
45. Poralla, K., Muth, G. & Härtner, T. Hopanoids are formed during transition from substrate to aerial hyphae in *Streptomyces coelicolor* A3(2). *FEMS Microbiol. Lett*. **189**, 93–95 (2000).
46. Hayakawa, Y., Kanamaru, N., Shimazu, A. & Seto, H. Lydicamycin, a new antibiotic of a novel skeletal type. I. Taxonomy, fermentation, isolation and biological activity. *J. Antibiot.* **44**, 282–287 (1991).
47. Tong, Y. et al. Highly efficient DSB-free base editing for streptomycetes with CRISPR-BEST. *Proc. Natl. Acad. Sci. U. S. A.* **116**, 20366–20375 (2019).
48. McAlpine, J. B. et al. Microbial genomics as a guide to drug discovery and structural elucidation: ECO-02301, a novel antifungal agent, as an example. *J. Nat. Prod.* **68**, 493–496 (2005).
49. Arai, M. & Hamano, K. Isolation of three main components. F3, F4 and F5, from azalomycin F-complex. *J. Antibiot.* **23**, 107–112 (1970).
50. Sakuda, S., Guce-Bigol, U., Itoh, M., Nishimura, T. & Yamada, Y. Linearmycin A, a novel linear polyene antibiotic. *Tetrahedron Lett.* **36**, 2777–2780 (1995).
51. Gilchrist, C. L. M. & Chooi, Y. H. clinker & clustermap.js: automatic generation of gene cluster comparison

figures. *Bioinformatics* **37**, 2473–2475 (2021).

52. Sun, F., Xu, S., Jiang, F. & Liu, W. Genomic-driven discovery of an amidinohydrolase involved in the biosynthesis of mediomycin A. *Appl. Microbiol. Biotechnol.* **102**, 2225–2234 (2018).
53. Igarashi, Y. et al. Clethramycin, a new inhibitor of pollen tube growth with antifungal activity from *Streptomyces hygroscopicus* TP-A0623. II. Physico-chemical properties and structure determination. *J. Antibiot.* **56**, 705–708 (2003).
54. Mohamed, O. G. et al. Identification of a new antimicrobial, desertomycin H, utilizing a modified crowded plate technique. *Mar. Drugs* **19**, 424 (2021).
55. Komaki, H. Resolution of housekeeping gene sequences used in MLSA for the genus *Streptomyces* and reclassification of *Streptomyces anthocyanicus* and *Streptomyces tricolor* as heterotypic synonyms of *Streptomyces violaceoruber*. *Int. J. Syst. Evol. Microbiol.* **72**, 005370 (2022).
56. Udwary, D. W. et al. Genome sequencing reveals complex secondary metabolome in the marine actinomycete *Salinispora tropica*. *Proc. Natl. Acad. Sci. U. S. A.* **104**, 10376–10381 (2007).
57. Yamanaka, K. et al. Desferrioxamine E produced by *Streptomyces griseus* stimulates growth and development of *Streptomyces tanashiensis*. *Microbiology* **151**, 2899–2905 (2005).
58. Bobek, J., Šmídová, K. & Čihák, M. A waking review: old and novel insights into the spore germination in *Streptomyces*. *Front. Microbiol.* **8**, 2205 (2017).
59. Barabás, G. & Szabó, G. Role of streptomycin in the life of *Streptomyces griseus*: streptidine-containing fractions in the cell walls of *Streptomyces griseus* strains. *Can. J. Microbiol.* **14**, 1325–1331 (1968).
60. Lu, T. et al. Sulfane sulfur-activated actinorhodin production and sporulation is maintained by a natural gene circuit in *Streptomyces coelicolor*. *Microb. Biotechnol.* **13**, 1917–1932 (2020).
61. Spraker, J. E., Luu, G. T. & Sanchez, L. M. Imaging mass spectrometry for natural products discovery: a review of ionization methods. *Nat. Prod. Rep.* **37**, 150–162 (2020).
62. Zink, K. E. et al. A small molecule coordinates symbiotic behaviors in a host organ. *MBio* **12**, e03637-20 (2021).

Supplementary information

Table of contents

Table S1. All bacteria, plasmid and primers were used in this study.

Strains	**Description**	**Source/[ref]**
One Shot™ Mach1™ T1 Phage-Resistant Chemically CAompetent *E. coli*	For routine plasmids maintenance and cloning	Thermo Fisher Scientific
E. coli ET12567/pUZ8002	For conjugating plasmids into *Streptomyces*	Kieser et al. 2000[1]
Streptomyces sp. P9-2B1	Wild-type strain	In this work
Streptomyces sp. P9-2B2	Wild-type strain	In this work
Streptomyces sp. P9-2B2/*lyd60*	*lyd60* inactivation mutant strain	In this work
Streptomyces sp. P9-2B4	Wild-type strain	In this work
Plasmids	**Sequence**	**Description**
pCRISRP-cBEST-*lyd60*	CCGGTTGGTAGGATCGACGGatcccacaggttcctccggcgGTTTTAGAGCTAGAAATAGC	Oligo for protospacer sequence construction
ID-lyd60-F	ccgtagtcgtggtacatcac	Identification primer for mutant
ID-lyd60-R	gaaagagtccgagccgatc	Identification primer for mutant

Table S2. GNPS library annotations of lydicamycins.

CCMS library ID	**Metabolite name**	**Adduct**	***m/z***
CCMSLIB00011430331	lydicamycin	M+H	855.55
CCMSLIB00011430332	lydicamycin derivative: TPU-0037A	M+H	841.53
CCMSLIB00011430333	lydicamycin derivative: TPU-0037D	M+H	839.55
CCMSLIB00011430334	lydicamycin derivative: TPU-0037B	M+H	837.54
CCMSLIB00011430335	lydicamycin derivative: TPU-0037C	M+H	825.54
CCMSLIB00011430336	putative lydicamycin 1	M+H	809.51
CCMSLIB00011430337	putative lydicamycin 2	M+H	811.52
CCMSLIB00011430338	putative lydicamycin 3	M+H	823.52
CCMSLIB00011430339	putative lydicamycin 4	M+H	853.53
CCMSLIB00011430340	putative lydicamycin 5	M+H	869.53
CCMSLIB00011430341	putative lydicamycin 6	M+H	871.54

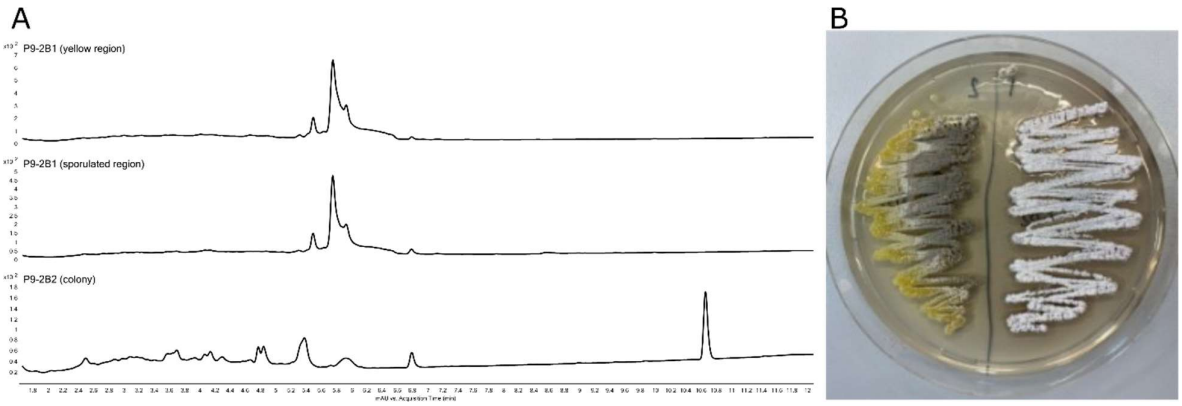

Figure S1. LC-MS analysis of metabolites of *Streptomyces*. (A) Base peack chromatograms of agar plugs extracted from the rergions identifed in (B). Not discernible difference in metabolome is present in the sporulated region.

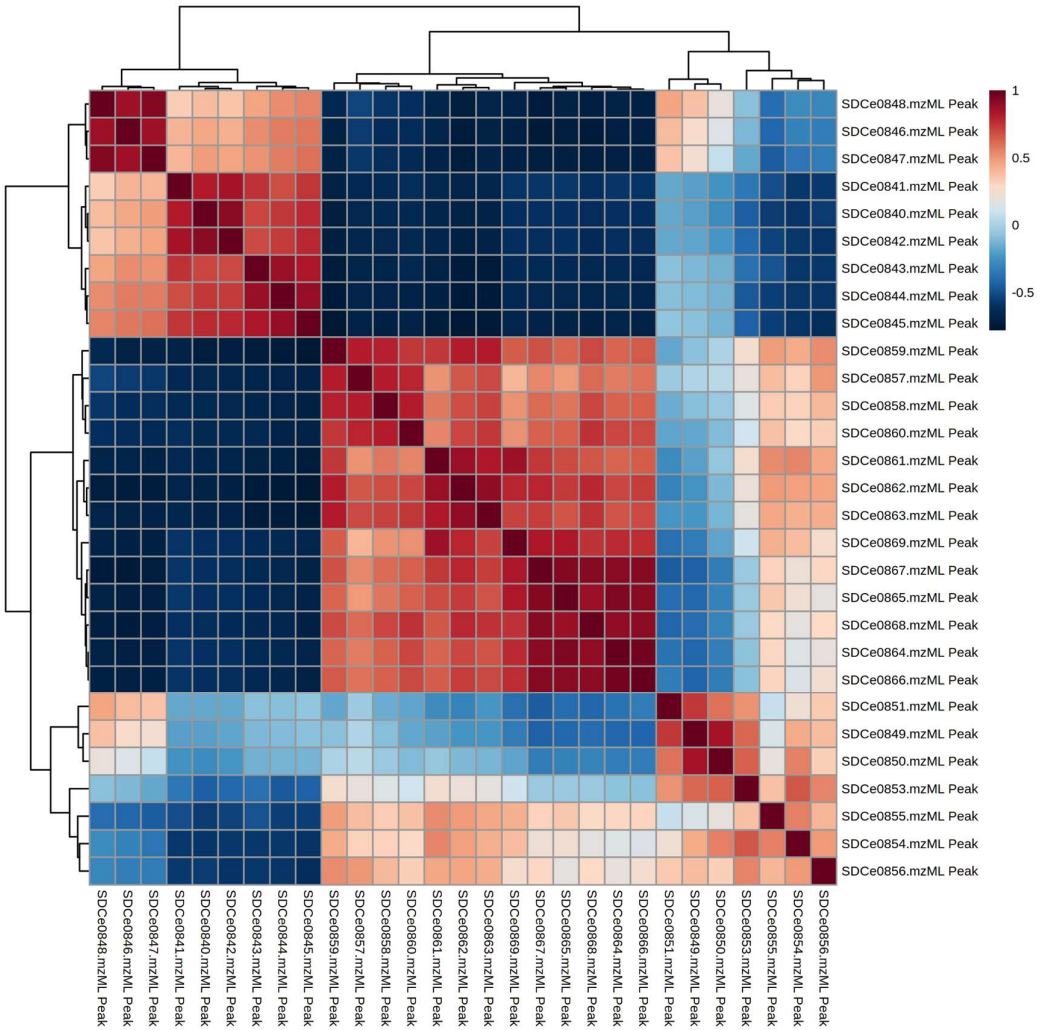

Figure S2. Pearson correlation of temporal metabolomics samples over 10 days grown on PDA. Sample IDs range from SDCe0840 (Day 1) – SDCe0869 (Day 10), with biological triplicates represented every three sequential samples (*i.e.* 0840-0842 correspond to Day 1 extracts).

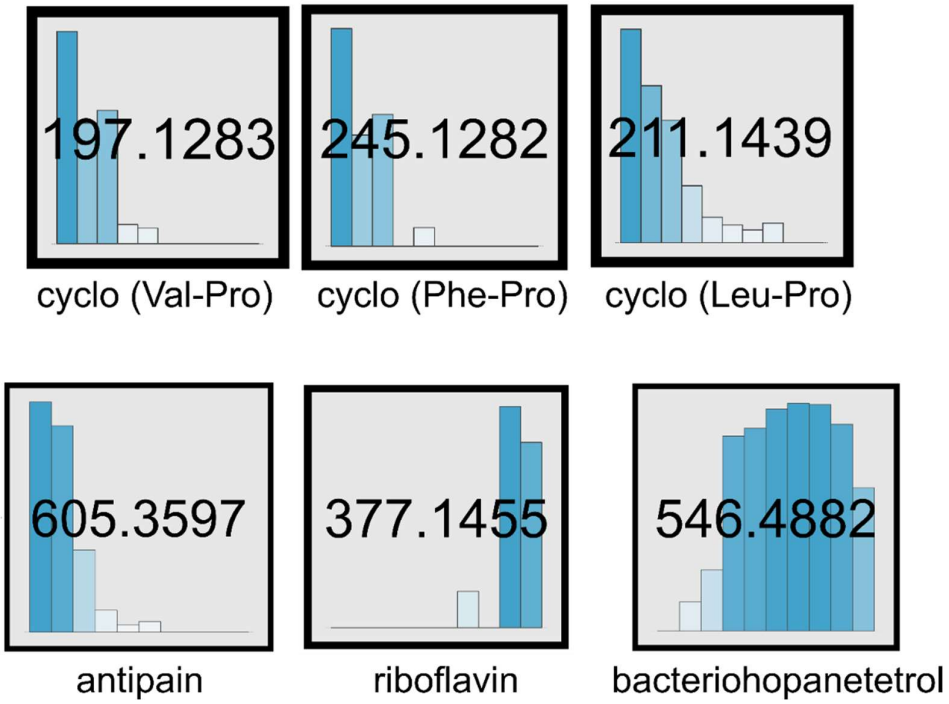

Figure S3. Additional known metabolites identified via feature based molecular networking. Bar graphs within each node are representative of the 10-day time scale which *Streptomyces* sp. P9-2B2 was grown on PDA plates. Coloration of the bar graphs are representative of the peak area (darker = more area).

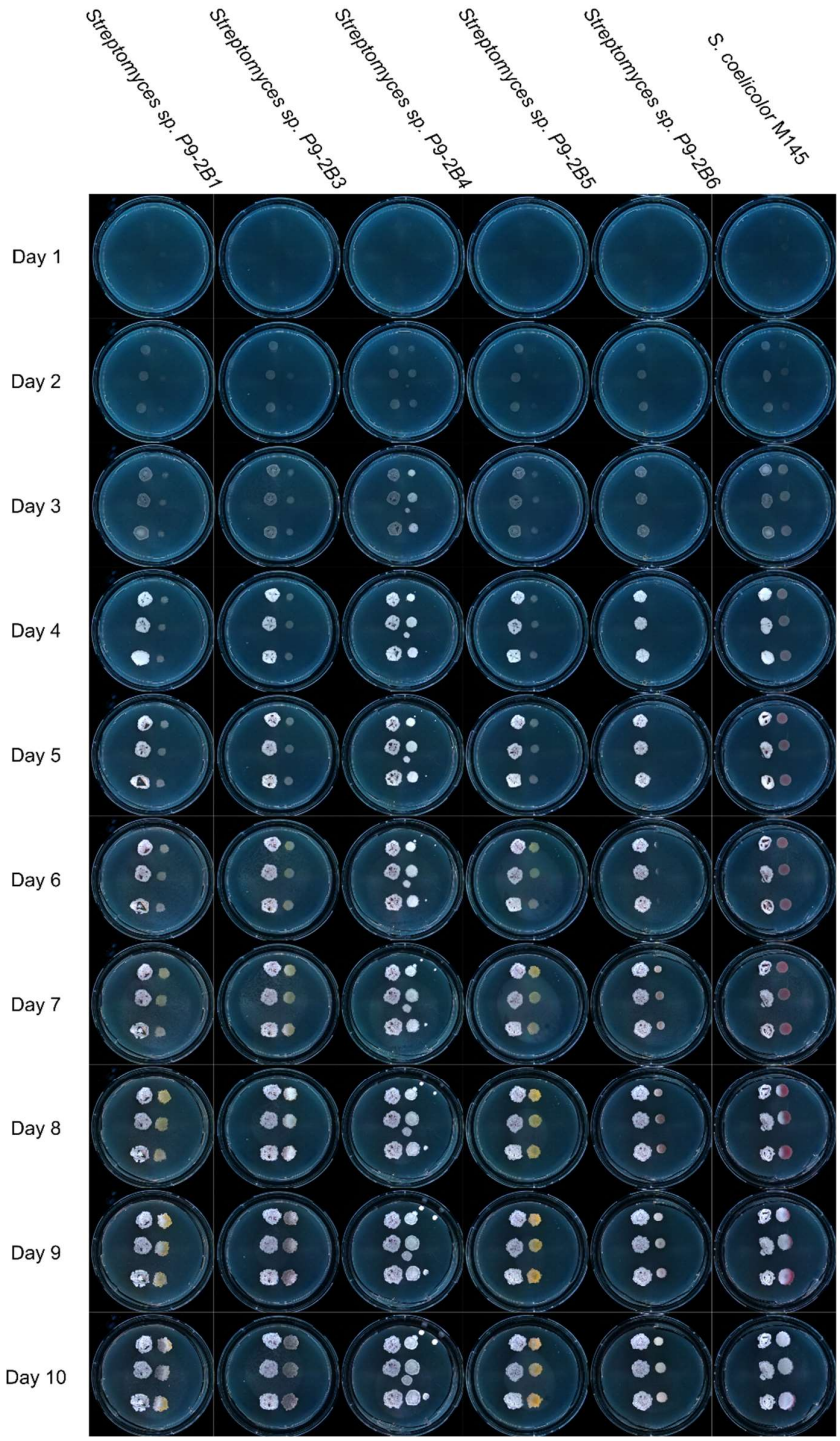

Figure S4. imelapse microscopy images taken every 24 hours showing the cocultivation of *Streptomyces* sp. P9-2B2 alongside additional environmental isolates and model strain *S. coelicolor* M145.

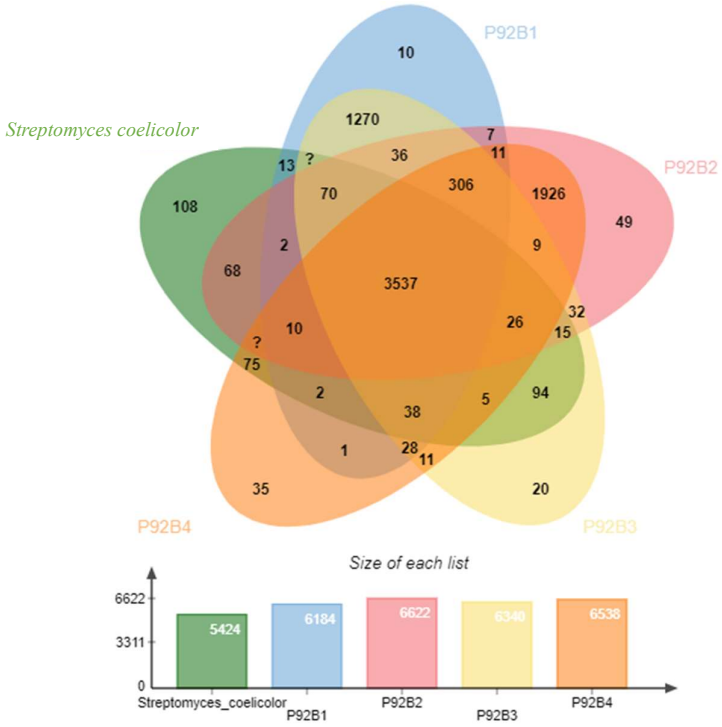

Figure S5. Protein similaritry venn diagram showing the overlap in protein similarity between strains. Importantly, P9-2B2 and P9-2B4 share a high number of homologs, indicating they are closely related.

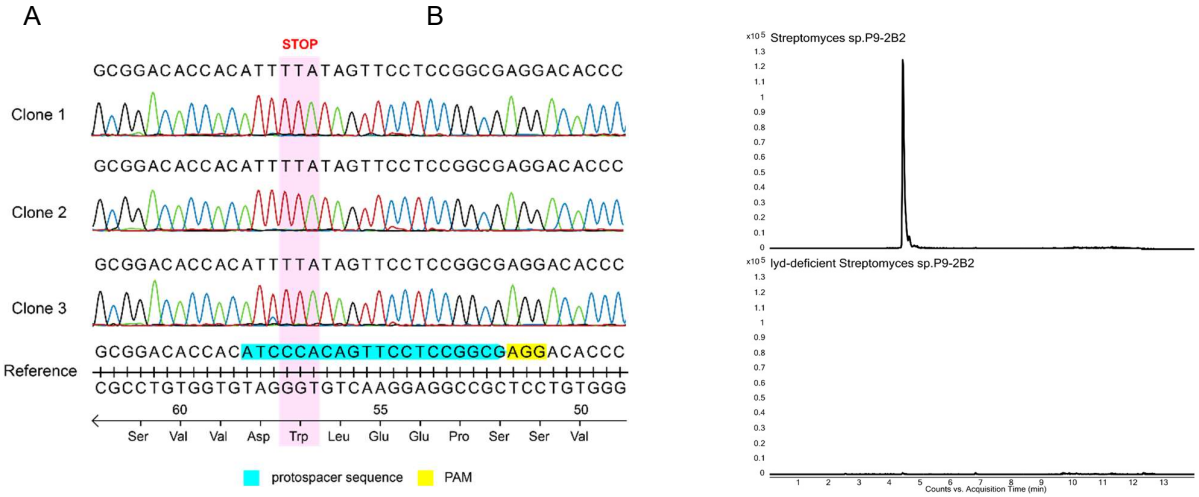

Figure S6. Sanger sequence results and LC-MS analysis of mutant strain. (A) Sanger sequencing of CRISPR base editing application of STOP codon introduction targeting the *lyd6o* of *Streptomyces* sp. P9-2B2 strain. The 20-nt protospacer sequence (light green) and the 3-nt PAM sequence (yellow) are shown. (B) Lydicamycin (*m/z* 855.5) Extract Ion Chromatograms of WT P9-2B2 (top) and lyd-deficient P9-2B2 (bottom).

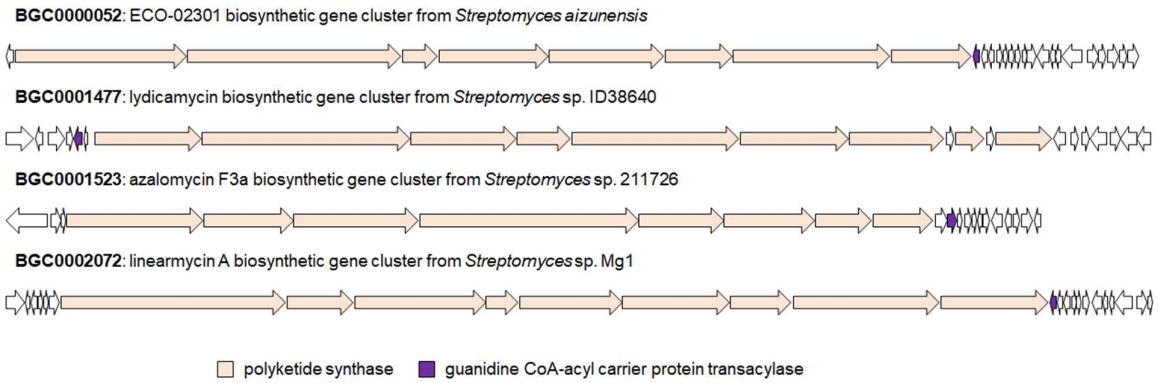

Figure S7. Representative arginine-derived polyketide biosynthetic gene clusters for ECO-02301, lydicamycin, azalomycin F3a and linearmycin. The potential guanidine CoA-acyl carrier protein transacylases is highlighted blue.

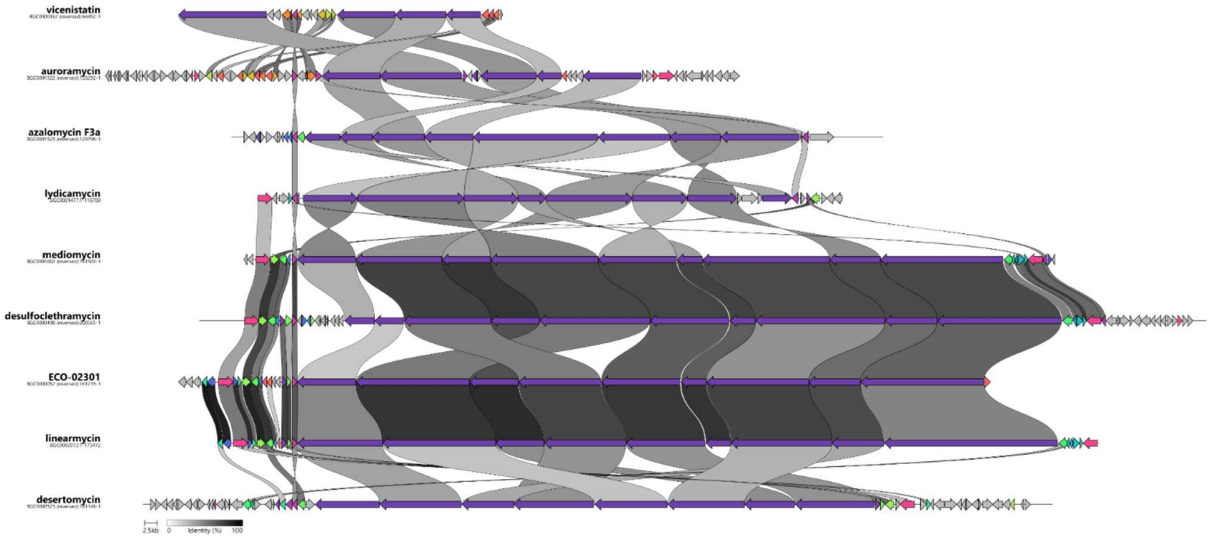

Figure S8. CLinker of arginine-starting unit BGCs. Alignment is anchored upon the guanidine-CoA transacylase in each BGC and the BGCs are organized based on their correlation matching to each other.

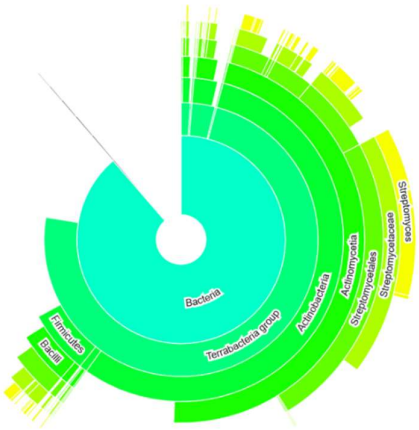

Figure S9. The taxonomy sunburst of 526 retrieved guanidine-CoA acyl carrier protein transacylase sequences.

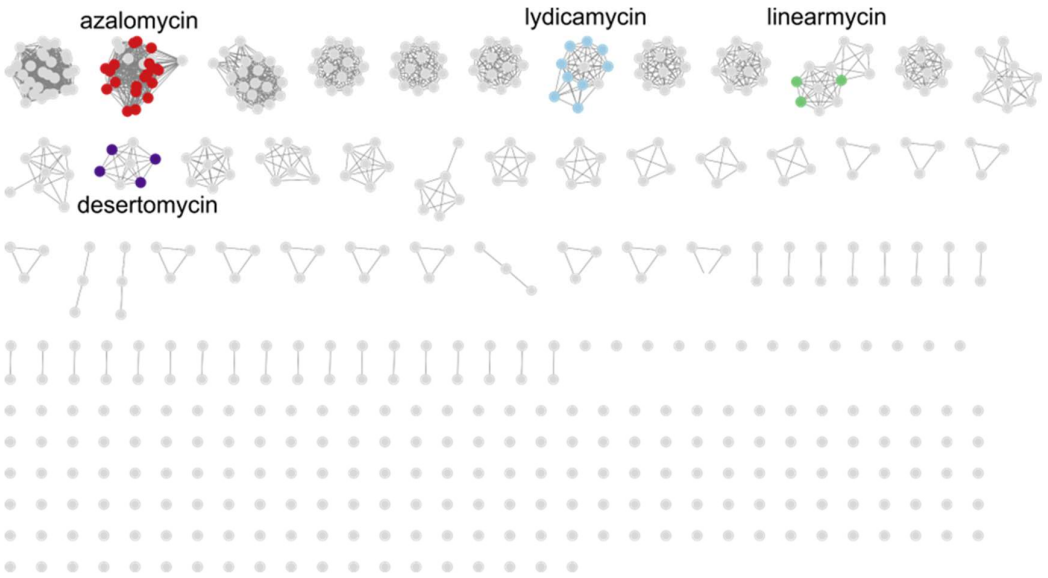

Figure S10. Sequence similarity network generated using guanidine CoA-acyl carrier protein transacylases. Four known BGCs are highlighted above, showing their distinct specificity.

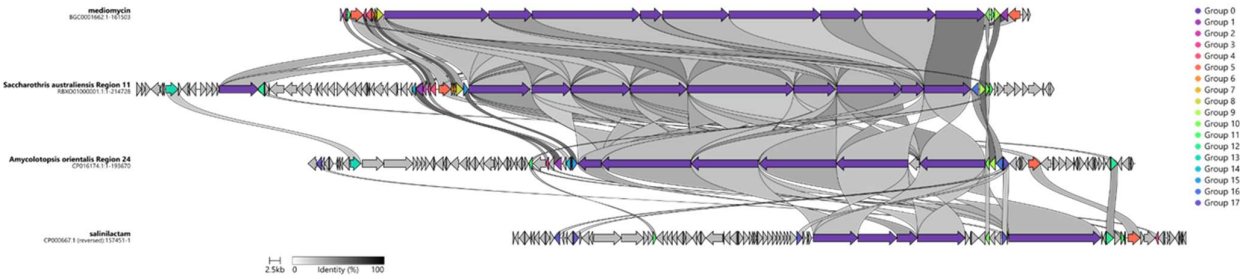

Figure S11. Clinker analysis of mediomycin and BGCs retrieved based on their transacylases in the SSN. Anchoring was done on the transacylase. antiSMASH results pointed to the Saccharothrix BGC being closely related to mediomycin, as seen here.

Appendix 4

Genome-driven Discovery of Hygrocins in *Streptomyces rapamycinicus*

Manar M. Mahmoud,[1] Zhijie Yang,[1] Kah Yean Lum,[1] Gundela Peschel,[2] Miriam A. Rosenbaum,[2] Tilmann Weber,[3] Sonia Coriani,[4] Charlotte H. Gotfredsen,[4] Ling Ding[1,*]

[1] Department of Biotechnology and Biomedicine, Technical University of Denmark, Søltofts Plads 221, 2800 Kgs. Lyngby, Denmark.

[2] Leibniz Institute for Natural Product Research and Infection Biology - Hans-Knöll-Institute (HKI), Beutenbergstr. 11a, 07745 Jena, Germany.

[3] The Novo Nordisk Foundation Center for Biosustainability, Technical University of Denmark, Kemitorvet, Building 220, 2800 Kgs. Lyngby, Denmark.

[4] Department of Chemistry, Technical University of Denmark, Kemitorvet Building 207, 2800 Kgs. Lyngby, Denmark.

Abstract

Ansamycins, represented by an antituberculosis drug rifamycin are an important family of natural products. To obtain new members of ansamycins, *Streptomyces rapamycinicus* IMET 43975 harboring an ansamycin biosynthetic gene cluster was fermented in a 50 L scale, and subsequent purification work led to the isolation of four new analogues, where hygrolansamycin E (**2**) belongs to benzoquinonoid ansamycins, and the other three hygrocins, W–Y (**5–7**), are new seco-hygrocins. The structures of ansamycins (**1–8**) were determined by analysis of spectroscopic (1D/2D NMR and ECD) and MS spectrometric data. The Baeyer-Villiger enzyme which catalyzed the ester formation in the ansa-ring was confirmed through in vivo CRISPR base editing. The discovery of these compounds further enriched the structural diversity of ansamycins.

Introduction

Ansamycins have been defined as cyclic molecules with long aliphatic chains that connect two opposite points of an aromatic ring, like a handle (the Latin word ansa).[1] They have proven to be very potent molecules, displaying anticancer, antibacterial, and antiviral activities.[2-4] Based on the different aromatic moieties, ansamycins can be divided into two classes: benzenoid and naphthalenoid.[5] The best-known benzenoid ansamycins are Hsp90 inhibiting geldanamycins[3] and antiproliferative maytansinoids.[6] A well-known example for naphthalenoid ansamycin is rifamycin, an anti-tuberculosis drug that acts as RNA polymerase inhibitor,[2] isolated from the actinobacterium *Amycolatopsis mediterranei*.[7,8] Recently, the discovery of hygrocins and divergolides has further broadened the chemical diversity of ansamycins.[7–10] They represent another novel type of ansa-macrolide featuring unprecedented nucleus, such as benzopyran/chromene in divergolide B.[10] They feature different cyclic scaffolds and showed different antibacterial and cytotoxic activities.[10] However, seco-form of hygrocins are rare, represented by some recently reported seco-hygrocins

and divergolides, such as divergolides M–N.[11]

Despite the structural variations of all ansamycins, they share a common aromatic starter unit, 3-amino-5-hydroxy-benzoic acid (AHBA),[12] and biosynthesis involving a modular type I polyketide synthase (PKS).[13] For example, the biosynthesis of hygrocin (*hgc*) has been well characterized, starting from 3-amino-5-hydroxy-benzoic acid (AHBA) as the building block derived from the shikimate pathway, and further elongated by eight PKS modules, using four malonyl-CoA, three methylmalonyl-CoA, and one (2*S*)-ethylmalonyl-CoA as chain extenders.[13] The macrolide ester linkage in hygrocins and divergolides was proposed to be formed by a Baeyer-Villiger oxygenase, which catalyzes the oxidative cleavage of the carbon-carbon bond.[14]

S. rapamycinicus IMET 43975 is a soil *Streptomyces* isolated from Easter Island,[15] and it is a well-known rapamycin-producer. Genome mining revealed that it is an abundant producer of secondary metabolites, with 48 BGCs predicted by antiSMASH.[16] We observed that it harbors a putative hygrocin biosynthetic gene cluster including a Baeyer-Villiger-type oxygenase (Figure S2). Metabolomic analysis using Global Natural Product Social Molecular Networking (GNPS) revealed several nodes representing new hygrocins (Figure S1). We hereby report the isolation, purification, structural identification, and biological activities of four new ansa macrolides, where **2** belongs to benzoquinonoid ansamycin and the other three, **5–7**, are seco-hygrocins. We successfully established an in vivo CRISPR base editing system in the producer and confirmed the Baeyer-Villiger enzyme which catalyzed the ester formation in the ansa-ring.

Results and discussion

Genome-mining on *S. rapamycinicus* using antiSMASH revealed a putative hygrocin biosynthetic gene cluster (BGC) with a homology of 93% with the *hgc* biosynthetic gene cluster of *Streptomyces* sp. LZ35 (Figure S2). The strain was cultivated on a small scale and the MeOH extract was analyzed by high-resolution electrospray ionization mass spectrometry (HR-ESI-MS). Metabolomic analysis using GNPS molecular networking revealed some putative new hygrocins with formulas of $C_{28}H_{33}NO_8$ and $C_{28}H_{31}NO_8$. Dereplication through SciFinder and Reaxys indicated the production of new hygrocins. To elucidate the structures of these hygrocins, the strain was large-scale fermented in a 50 L fermentation and the supernatant was fractionated by an Amberchrom 161c resin column. Following various isolation and purification steps with the hygrocins-containing fractions, four new hygrocins (**2**, **5–7**), as well as four known compounds (**1**, **3**, **4**, **8**), were obtained and characterized by detailed NMR, MS, and ECD data analysis.

Compounds **1** was isolated as colorless crystals with a molecular formula of $C_{28}H_{35}NO_8$ deduced by HR-ESI-MS ion at *m/z* 514.2448 $[M+H]^+$. The ^1H NMR revealed signals for five sp^2 protons (δ_H 7.81, 6.28, 6.12, 5.53, 5.02), three sp^3 methine protons next to an oxygen (δ_H 5.08, 5.07, 3.89), one methyl doublet (δ_H 2.06), two methyl doublets (δ_H 1.22, 1.01), and one methyl triplet (δ_H 0.89). The ^{13}C NMR data revealed resonances for one ketone carbonyl (δ_C 208.6), two amide/ester carbonyls (δ_C 170.7, 168.0), ten methines including three sp^2 olefinic methines (δ_C 137.6, 136.8, 125.4), two aromatic methines (δ_C 108.6, 108.4) three oxygenated methines

(δ_C 79.8, 77.3, 69.4) and two aliphatic (δ_C 50.4, 45.4), five methylenes (δ_C 53.1, 40.7, 39.3, 29.6, 28.4), and four methyls (δ_C 20.6, 18.8, 12.5, 10.1) and six other quartenary sp^2 carbon resonances. The COSY spectrum showed the presence of two spin systems starting from H-6 to H-13 plus H15-H16 and H-2", H-3" to H-6". The HMBC correlations from δ_H 5.08 (H-11) to δ_C 168.0 (C-5") confirmed the connection of the aliphatic bridge to the α,β unsaturated ester moiety via a C-11/5" ester bond (Figure 3). A relatively downfield chemical shift at δ_C 20.6 indicated a *Z* configuration at C-4". Additionally, the six aromatic carbon signals (δ_C 150.9, 133.6, 128.3, 120.1, 108.6 and 108.4), as well as HMBC correlations suggest the presence of the 2, 4, 5, 6 substitute benzene moiety connected to a six-membered *O*-heterocyclic ring. Compound **1** is a stereoisomer of divergolide O and was recently identified as hygrolansamycin C.[17]

Compound **2** was isolated as a yellow powder. According to HR-ESI-MS, the molecular formula of **2** was determined to be $C_{28}H_{35}NO_8$ (*m/z* 514.2446 $[M+H]^+$), and it was predicted to be an isomer of compound **1**. This was supported by a similar ^{1}H NMR spectrum which revealed signals for five sp^2 protons (δ_H 7.52, 6.27, 6.15, 5.61, 5.36), three sp^3 methine protons (δ_H 5.07, 5.0, 4.17), a doublet methyl (δ_H 2.1) which appears as a broad singlet in ^{1}H NMR spectrum as in the DQF-COSY it can be seen that it couples to both H2" and H3" with small *J*-coupling constant. Two methyl doublet (δ_H 1.34, 1.02), and one methyl triplet (δ_H 0.92). The ^{13}C NMR data also showed comparable data revealed resonances for one ketone carbonyl (δ_c 208.7), two amide/ester carbonyls (δ_H 170.0, 168.4), ten methines including five sp^2 alkene methines and three oxymethines, five methylene and four methyl groups. Further investigation showed a similar *Z* configuration at C-6" as well as a syn orientation between H-1 and H-2. However, HMBC correlations from the alkene proton H-9 (δ_H 5.36) to C-11 with a relative upfield shift of the isopropanol proton δ_H 4.17, and another correlation between H-10 (δ_H 5.61) to C-12 (δ_c 77.3), and H-12 (δ_H 5.00) to C-5" (δc 168.4), indicating the formation of a C-12/5" ester linkage, instead of C-11/5" in compound **1**. Analysis of the cross-peaks at H-10/H-11/H-12/H-13 in DQF-COSY spectrum further confirmed the assignment, and hence compound **2** is reported here as a new hygrocin, named hygrolansamycin E. Both compounds **1–2** belong to the recently reported *O*-heterocyclic macrolides isolated from *Streptomyces* sp. KCB17JA11.[17] To confirm the structure configuration and the chirality of **1** and **2**, ECD data were acquired. The ECD spectrum of **1** (Figure S48) exhibited positive Cotton effect at 216 (Δε = +1.3) nm, 275 (Δε = +1.6) nm, 316 (Δε = +2.0) nm and negative one at 243 (Δε = -6.4) nm, resembling the ECD reported for divergolide A, which was structurally confirmed by X-ray crystallography.[17] Meanwhile, the ECD spectrum of **2** (Figure S48) exhibited a mirror imaged ECD spectrum of **1**. Thus compounds 1–2 exhibited an opposite configuration at C-1 and C-2, while both shared the same relative configurations at C-1 and C-2 (Table 1). Compound **2** exhibited very similar ECD spectrum to divergolide O, which further confirmed the configurations.[18] Besides the two ansamycins, another two known (**3–4**) and three new (**5–7**) seco-form hygrocins were isolated. Compound **3** and **4** were obtained both as red amorphous powder and were assigned a molecular formula of $C_{28}H_{31}NO_8$ (*m/z* 510.2123 $[M+H]^+$) deduced by the HR-ESI-MS data. Following 1D/2D NMR data analysis and comparison with the literature data, the presence of an additional aromatic signal at δ_H 7.46 (H–14) and a carboxyl carbon resonated at δ_C 177.6 (C-13) indicated the

breakage of the aromatic bonding between C-13/C-14, and hence compounds **3** and **4** were determined to be hygrocin I and J, respectively.[19]

Compounds **5** and **6** were assigned the molecular formula of $C_{28}H_{33}NO_9$ deduced by HR-ESI-MS ion at *m/z* 528.2237 $[M+H]^+$. For compound **5**, the ^1H NMR spectrum showed the presence of two aromatic protons at δ_H 7.40, 7.24, four alkene protons observed (δ_H 6.50, 5.74, 5.37, and 5.33). Two sp^3 protons; a secondary alcohol and an ether respectively (δ_H 5.09, 3.78), two sp^3 methine protons (δ_H 4.60, 1.78), one methyl singlet (δ_H 2.20), two methyl doublet (δ_H 2.20, 1.08), one methyl triplet (δ_H 0.66), and three methylene proton pairs were also observed. The ^{13}C NMR data revealed resonances for 11 quaternary carbons, including one ketone carbonyl (δ_c 186.6), two amide/ester carbonyls (δ_c 177.1, 168.4), an acid functional group (δ_c 177.4). The COSY spectrum, combined with HMBC correlation analysis, established the presence of two spin systems: C-6a/C-6/C-7/C-8/C-9/C-10/C-10a/C-10-b/C-11/C-12 and C-2/C-3/C-4a. The presence of an aromatic methine on C-14 indicated the same breaking at the original C-13/C-14 and a seco-form of hygrocin. In comparison with hygrocins C-G, compound **5** has one double bond equivalent less, confirming the breakage of the ansa-ring. The large *J*-coupling constants ($J > 15.0$ Hz) between H-8 and H-9 led to assignment of the *E* configuration for **5**. The relative downfield shift C-4a (δ_c 21.3) suggests the *Z* configuration of the double bonds at C-3 and C-4. Furthermore, HMBC correlations of H-7 with C-5 established the linkage of C5 and C7 through an ester linkage. The NMR data of **6** were very similar to those of **5**. **6** was proposed to be a stereoisomer of **5** which showed a mirror imaged ECD spectrum (Figure 1) compared to **5**. The aromatic chromophore shows the characteristic UV absorption for naphthoquinones (316, 278 and 202 nm). The ECD spectrum of **5** (Figure S50) exhibited a positive Cotton effect at 219 nm ($\Delta\varepsilon$ =+13), 272 nm ($\Delta\varepsilon$ = +3.1) and a negative Cotton effect at 248 nm ($\Delta\varepsilon$ =-2) and 298 nm ($\Delta\varepsilon$ = -3.6). This indicated that **5** is an isomer of **6**. Additionally, compound **7** was isolated as an isomer of **5-6**. Following HMBC data analysis, the correlations from H-6 (δ_H 4.92) to C-5 (δ_C 168.3) and C-8 (δ_C 131.0), and H-7 (δ_H 4.92) to both C-8 and C-9 (δ_C 138.0) indicated the formation ester linkage at C-5 and C-6. This assignment was further confirmed by the difference in the COSY correlations of the fragment H-6a/H-6/H-7 compared to compounds **5–6**, and thus compound **7** was named hygrocin Y.

Compounds **5–7** are closely related to previously reported hygrocins C, D and E with closed ansa rings, while hygrocin C was confirmed by an X-ray crystal structure. All **5–7** showed similar downfield chemical shift at H-2 comparable to hygrocin C with 2*R*, 19*S* configuration instead of 2*S*, 19*S* in hygrocin D, indicating a same relative configuration for **5–7** as hygrocin C. To establish the absolute configuration, quantum chemical calculations of ECD spectra for **5–7** were carried out (Figure 1, S58 and S59). Conformational searches for 3D structures of (2*S*, 6*S*, 7*S*, 10*S*, 19*S*), (2*R*, 6*S*, 7*S*, 10*S*, 19*R*) and (2*S*, 6*S*, 7*S*, 10*S*, 19*R*) and (2*R*, 6*S*, 7*S*, 10*S*, 19*S*) gave between 74–110 possible conformers, among them, 8, 11, 9, and 19 conformers bearing Boltzmann populations higher than 0.9%, respectively were selected for subsequent calculations. The geometric optimization and calculation of ECD spectra were shown in Tables S60. The experimental ECD spectrum of **5** was in good agreement with the calculated spectrum for (2*R*, 6*S*, 7*S*, 10*S*, 19*R*) and the experimental ECD spectrum of **6** and **7** best aligned with the calculated spectrum for (2*S*, 6*S*, 7*S*, 10*S*, 19*S*) with enantiomeric similarity index

(Δ_{ESI}) of 0.7958. Compound **3–7** belong to the seco-formed ansamycins, with a carboxylic acidic moiety. The other three seco-divergolides L, M and N were reported as shunt products of the biosynthetic pathway of other divergolides;[11] moreover, seco-hygrocin congeners showed the same exact ring cleavage of the C-C bond at the aromatic site, which is hypothesized of being formed by decarboxylation after spontaneous hydrolysis of the macrolide.[11]

The Baeyer–Villiger oxidation between C5 and C6/C7 was confirmed to be catalyzed by luciferase-like monooxygenase homologue Hgc3 after cyclization with amide synthase (HgcF) in *Streptomyces* sp. LZ35.[14] Here, we applied the CRISPR/Cas9-mediated base editing tool to inactivate *hgc3* in *S. rapamycinicus*. According to sequencing results, the tryptophan (TGG) in position 15 of Hgc3 was successfully replaced by stop codon (TAA) in the mutant strains (Figure S2). The HR-ESI-MS analysis showed that the production of hygrocins I-J (**3-8**) was completely abolished (Figure S2). However, we observed that the production of hygrocin A and seco derivatives intermediates, **9** (*m/z* 477.2151 $[M+H]^+$) and **10** (*m/z* 495.2257 $[M+H]^+$), respectively (Figure S2). Based on these intermediates, we hypothesized that the ansa ring cleavage occurs prior to the Baeyer-Villiger oxidation, concluding that *hgc3* has no role in the cleavage of ansamycin seco-derivatives (Figure S2).

Hygrocins were reported to have antitumor, antiproliferative, and biofilm inhibition activity.[14,19,20] We have tested the antimicrobial activities of compounds **1–8** against a series of bacteria and fungi, including *Staphylococcus aureus* strain 8325, *Bacillus subtilis*, *Pseudomonas aeruginosa* PAO1, and *Candida albicans* IBT 656. However, none of them exhibited considerable activities (MIC >50 μg/mL).

Methods and materials

General Experimental Procedures. Optical rotations were recorded on an AUTOPOL III - S2 Dual Wavelength (589/546nm) Automatic Polarimeter (Rudolph Research Analytical). ECD spectra were obtained in MeOH using a 10 mm path cuvette on a JASCO J-1500 CD spectrometer. IR data were acquired on Bruker Alpha FTIR spectrometer using OPUS version 7.2. The NMR spectra were recorded on a Bruker AVANCE III 800 MHz spectrometer equipped with a 5 mm TCI CryoProbe using standard pulse sequences. The ^1H and ^{13}C NMR chemical shifts were referenced to the residual solvent signals at δ_H 7.26, δ_C 77.16 ppm for $CDCl_3$ and δ 3.31, δ 49.0 ppm for CD_3OD. UHPLC-HRMS was performed on an Agilent Infinity 1290 UHPLC system equipped with a diode array detector. UV–vis spectra were recorded from 190 to 640 nm. All solvents and chemicals used for HR-ESI-MS, and chromatography were LC-MS grade, while the solvents for metabolite extraction were of HPLC grade. Water was purified using a Milli-Q system.

Strains, primers and plasmids. All strains, primers and plasmids were listed in Table S3. All primers used were synthesized by IDT (Integrated DNA Technologies, USA). *S. rapamycinicus* was obtained from DSMZ (German Collection of Microorganisms and Cell Cultures GmbH). All *Escherichia coli* strains were grown in liquid/solid LB medium (5.0 g/L yeast extract, 10.0 g/L peptone, 10.0 g/L NaCl) at 37 °C. All *Streptomyces*

strains were grown on ISP2 medium (4.0 g/L yeast extract, 10.0 g/L malt extract, 4.0 g/L dextrose, and 1.0 L distilled water) at 28 °C. Appropriate antibiotics were supplemented with the following working concentrations: apramycin (50 μg/mL), chloramphenicol (25 μg/mL), and kanamycin (50 μg/mL).

The antiSMASH and GNPS workflow. The genome sequence information was retrieved from NCBI (Assembly NO: GCA_024298965.1) and was annotated by online tool antiSMASH 7 (https://antismash.secondarymetabolites.org) with default setting.[16] The acquired MS/MS data from analysis by liquid chromatography–diode array detection–quadrupole time-of flight mass spectrometry (LC-DAD-TOFMS) were pre-processed by MZmine 2.53 and analyzed using the feature-based molecular networking workflow on the Global Natural Product Social Molecular Networking platform.[21,22] The generated molecular networks were visualized in Cytoscape.

Fermentation, extraction, and isolation. Liquid organic medium 79 (10 g/L dextrose, 10 g/L bactopeptone, 1 g/L casamino acids, 2 g/L yeast extract, 6 g/L NaCl in 1 L H2O; 2 × 100 mL/flask) was inoculated with a suspension of mycelium of *S. rapamycinicus*. After incubation for 48 h on a rotary shaker at 28 °C, the culture was transferred to 3200 mL of ISP2 and incubated at 28 °C under shaking conditions for 48 h to yield pre-fermentation culture, which was poured into a 75 L-scale stirred-tank bioreactor filled with 50 L of medium ISP2 and fermented for 6 days. The fermentation parameters were 200 rpm stirring speed, aeration 0.5 ppm reduced after 24 h to 0.1 ppm. The initial pH of the process was 6.7. It was not controlled during fermentation. After fermentation, the mycelia were extracted twice with methanol, then twice with butanol for the second round of extraction. The supernatant was separated by an Amberchrom 161M resin LC column (15 × 10 cm, 1 L), eluted with a linear gradient of H_2O–MeOH (from 30% to 100% v/v, flow rate 0.13 L min^{-1}, in 58 min) to afford seven fractions (F1–F7), which were subsequently lyophilized.

The lyophilized fraction 6 (F6, 8 g) was loaded on normal phase silica gel SNAP 100 g Biotage Flash Cartridge Isolera, the gradient used was 50% Hexane/50% DCM to 100% DCM for 10 minutes, a gradient to 10% DCM/90% MeOH over 30 minutes (25 mL min^{-1}). The 70% DCM/MeOH subfraction (1g) was further fractionated using a linear gradient from 10% MeOH/90%H_2O to 100 % MeOH on a semipreparative C18 HPLC column to get four subfractions (F6A–6D). Hygrolansamycin C (**1**, 3.0 mg), hygrolansamycin E (**2**, 2.5 mg) and hygrocin G (**8**, 4.0 mg) were purified from 6B on a phenyl-hexyl column (Luna, 100 Å, 250×10 mm i.d., 5 μm, Phenomenex) held at 40 °C by linear gradient elution 50-80% to MeCN in Milli-Q water over 20 min.

Purification of subfraction 4 (5 g) was performed on a SNAP 100 g column packed with C18 (Grace, 15 μm/100 Å) silica using the Biotage Isolera One automated flash system. A linear gradient from 10% CH_3OH/90% H_2O to 100% CH_3OH was employed over 45 minutes, at a flow rate of 45 mL min^{-1}. Fractions were automatically collected based on UV signals (254 and 320 nm) 5 fractions were afforded. Fractin 1 was purified by Sephadex LH-20 eluted with MeOH to obtain seven fractions (F4-1A to F4-1G) in accordance with the TLC results. Fraction 4-1B was fractionated using a semipreparative phenyl-hexyl column (Luna, 100 Å, 250×10 mm i.d., 5

μm, Phenomenex) HPLC column, with a linear gradient from 40% MeCN/60% H_2O to 50% MeCN/50% H_2O over 20 min, a flow rate of 4 mL min^{-1}. Fractions containing targeted compounds were further purified using the same conditions to afford hygrocin I (**3**, 1.5 mg), hygrocin J (**4**, 1.5 mg), hygrocin W (**5**, 3.0 mg), hygrocin X (**6**, 3.0 mg), hygrocin Y (**7**, 3.0 mg).

Gene inactivation. pCRISPR-cBEST was used to inactivate *hgc3* by inserting a premature STOP codon.[23] The oligo Del-*hgc3* was designed with online tool CRISPy-web.[24] To clone the gene base editing construct, pCRISPR-cBEST plasmid was initially linearized by NcoI. DNA digestion was performed with FastDigest restriction enzymes (Thermo Fisher Scientific, USA). NucleoSpin Gel and PCR Clean-up Kits (Macherey-Nagel, Germany) were used for DNA clean-up from PCR products and agarose gel extracts. Del-hgc3 was inserted into the linearized pCRISPR-cBEST plasmid using the NEBuilder HiFi DNA Assembly Master Mix (New England Biolabs, USA) resulting in the desired pCRISPR-cBEST/D*hgc3* plasmid. NucleoSpin Plasmid EasyPure Kit (Macherey-Nagel, Germany) was used for plasmid preparation. The *E. coli-Streptomyces* conjugation experiment was conducted according to the standard protocol,[25] and the mutant S. rapamycinicus/D*hgc3* were also confirmed by PCR and Sanger sequencing (Mix2Seq Kit, Eurofins Scientific, Luxembourg).

Antimicrobial activity test. The antimicrobial activity of compounds **1–8** was assessed against bacteria *S. aureus* 8325, *B. subtilis* and *P. aeruginosa* PAO1 using Mueller–Hinton agar (10 g/L peptone, 5 g/L yeast extract, 5 g/L NaCl) and yeast *C. albicans* IBT 656 using a standard broth microdilution method using RPMI 1640 growth medium. Chloramphenicol was used as a positive control against bacteria. Amphotericin B was used as a positive control against *Candida*. Data were recorded after incubation at 37°C for 24 hours. For agar diffusion assay, sterile filter paper disks (d = 9 mm) were impregnated with 50 μg of the samples using methanol as the carrier solvent.[26] The impregnated disks were then placed on agar plates previously inoculated with *S. aureus* 8325, *B. subtilis* or *P. aeruginosa* PAO1. The test sample was considered active when the zone of inhibition was greater than 9 mm. The minimal inhibition concentration values were recorded after incubation at 37°C for 12 hours and 24 hours, for bacteria and fungi, respectively. Protocols for agar diffusion and minimal inhibition concentration were followed by The MIC assay using test strains *C. albicans* IBT 656 was done by the broth dilution method according to the NCCLS.[27] The test sample was considered active when the MIC values was less than 50 μg/mL.

ECD calculation and ECD spectra acquisition. The absolute configurations of compounds **5–7** were tentatively assigned by comparing experimental and calculated ECD spectra. To this end, we followed the recommendations of Good Computational Practice in the Assignment of Absolute Configurations[28] and carried out an initial molecular-mechanics-based conformational search in gas phase with the Molecular Merck force field (MMFF) using MacroModel, which is part of Schrödinger Maestro 13.3_ref. All conformers

contributing to more than 0.9 % of the Boltzmann population were then selected and optimized using density functional theory (DFT), adopting the B3LYP functional and the 6-31G(d,p) basis set. For each optimized structure, the excitation energies, oscillator strengths and ECD rotatory strengths of the first 50 excited states were then calculated using time-dependent density functional theory, employing the CAM-B3LYP functional and the 6-31+G(d,p) basis set. The effect of methanol as solvent on both the geometry and the spectra was included via the polarizable continuum model in the integral equation formalism (IEF-PCM).[29] The Gaussian 16 program package was used for the DFT/TDDFT calculations.[30]

The ECD spectra were calculated by Boltzmann averaging (based on the computed DFT Gibbs energies) the spectra of each conformer and exported using the SpecDis software with different half-bandwidth broadening values for each molecule.[31] Experimental ECD spectra were obtained on a JASCO J-1500 CD Spectrometer and processed using the software SDAR, after solvation in methanol and transfer into a quartz cuvette, with specific parameters for the measurement. The enantiomeric similarity index (ΔESI) as implemented in SpecDis was used to assess the reliability of the absolute configuration assignment by comparison of the calculated and experimental ECD spectra. All computed spectra are reported in the supporting information (Table S1).

Hygrolansamycin C (**1**): Colorless crystal; molecular formula $C_{28}H_{35}NO_8$; $[\alpha]_D^{25}$ +133 (c 1.5, CH_3OH); UV (CH_3CN/H_2O) λ_{max} 250, 310 nm; ECD λ_{ext} (Δε) (CH_3OH) 216 (-1.0), 243 (+3.9) nm; IR ν_{max} 3384, 2956, 2872, 2856, 1712, 1665, 1644, 1541, 1455, 1377, 1356, 1234 and 1189 cm^{-1}; ^1H and ^{13}C NMR data (CD_3OD, 800 MHz), see Table 1; HR-ESI-MS *m/z* 514.2448 $[M+H]^+$ (calcd 514.2435 for $C_{28}H_{35}NO_8^+$).

Hygrolansamycin F (**2**): Colorless solid; molecular formula $C_{28}H_{35}NO_8$; $[\alpha]_D^{25}$ -16 (c 0.9, CH_3OH); UV (CH_3CN/H_2O) λ_{max} 250, 310 nm; ECD λ_{ext} (Δε) (CH_3OH) 209 (-4.0) nm, 221 (+1.3) nm, 253 (+7.7) nm, 313.1 (+0.8) nm; IR ν_{max} 3384, 2958, 2928, 2874, 2857, 1708, 1637, 1543, 1456, 1374, 1239, 1156, 1132 and 976 cm^{-1}; ^1H and ^{13}C NMR (CD_3OD, 800 MHz) see Table 1; HR-ESI-MS *m/z* 514.2442 $[M+H]^+$ (calcd 514.2435 for $C_{28}H_{35}NO_8^+$).

Hygrocin I (**3**): Red powder; molecular formula $C_{28}H_{31}NO_8$; $[\alpha]_D^{25}$ +4 (c 0.6, CH_3OH); UV (CH_3CN/H_2O) λ_{max} 285, 335, 380 nm; ECD λ_{ext} (Δε) (CH_3OH) 217 (+10.0) nm, 272 (+2.5) nm, 323 (+1.6) nm; IR ν_{max} 3393, 2926, 1654 and 1189 cm^{-1}; ^1H and ^{13}C NMR data (CD_3OD, 800 MHz), see Table 1 ; HR-ESI-MS *m/z* 510.2123 $[M+H]^+$ (calcd 510.2122 for $C_{28}H_{31}NO_8^+$).

Hygrocin J (**4**): Red powder; molecular formula $C_{28}H_{31}NO_8$; $[\alpha]_D^{25}$ -1 (c 0.5, CH_3OH); UV (CH_3CN/H_2O) λ_{max} 220, 285, 335, 380 nm; ECD λ_{ext} (Δε) (CH_3OH) 227 (+1.48), 257 (–3.38) nm; ^1H and ^{13}C NMR data (CD_3OD, 800 MHz), see Table 1; HR-ESI-MS m/z 510.2118 $[M+H]^+$ (calcd 510.2122 for $C_{28}H_{31}NO_8^+$).

Hygrocin W (**5**): Reddish white powder; molecular formula $C_{28}H_{33}NO_9$; $[\alpha]_D^{25}$ -71 (c 1.0, CH_3OH); UV (CH_3CN/H_2O) λ_{max} 230, 275, 305 nm; ECD λ_{ext} (Δε) (CH_3OH) 219 (+13) nm, 272 (+3.1) nm, 248 (-2) nm, 298 (-3.6) nm; IR ν_{max} 3373, 2923, 1702, 1646, 1604, 1578, 1195, 1155 and 1045 cm^{-1}; ^1H and ^{13}C NMR data (CD_3OD, 800

MHz), see Table 1-3; HR-ESI-MS m/z 528.2237 $[M+H]^+$ (calcd 528.2228 for $C_{28}H_{33}NO_9^+$).

Hygrocin X (**6**): Reddish white crystal; molecular formula $C_{28}H_{33}NO_9$; $[\alpha]_D^{25}$ +72 (c 1.6, CH_3OH); UV (CH_3CN/H_2O) λ_{max} 230, 275, 305 nm; ECD λ_{ext} ($\Delta\varepsilon$) (CH_3OH) 219 (+13) nm, 248 (-2), 272 (+3.1) nm, 298 (–3.6) nm; IR ν_{max} 3122, 3060, 2958, 2928, 1702, 1647, 1633, 1603, 1578, 1455, 1434, 1378,13330, 1194, 1155 and 1044 cm^{-1}; ^1H and ^{13}C NMR data (CD_3OD, 800 MHz), see Table 1-3; HR-ESI-MS m/z 528.2235 $[M+H]^+$ (calcd 528.2228 for $C_{28}H_{33}NO_9^+$).

Hygrocin Y (**7**): Reddish white powder; molecular formula $C_{28}H_{33}NO_9$; $[\alpha]_D^{25}$ +115 (c 1.2, CH_3OH); UV (CH_3CN/H_2O) λ_{max} 230, 275, 305 nm; ECD λ_{ext} ($\Delta\varepsilon$) (CH_3OH) 219 (–14.4) nm, 248 (+8.0) nm, 272 (–4.7) nm, 298 (+16.6) nm; IR ν_{max} 3385, 2926, 1636, 1191, 1047 cm^{-1}; ^1H and ^{13}C NMR data (CD_3OD, 800 MHz), see Table 1-3; HR-ESI-MS *m/z* 528.2233 $[M+H]^+$ (calcd 528.2228 for $C_{28}H_{33}NO_9^+$).

Hygrocin G (**8**): Yellow powder; molecular formula $C_{28}H_{29}NO_8$; $[\alpha]_D^{25}$ -17.2 (c 1.0, CH_3OH); UV (CH_3CN/H_2O) λ_{max} 220, 275, 320 nm. ECD λ_{ext} ($\Delta\varepsilon$) (CH_3OH); 216 (+7.2) nm, 256 (3.2) nm, 305 (-0.6) nm, 336 (-4.9) nm, 372 (-2,2) nm; IR ν_{max} 3432, 2927, 1735, 1690, 1660, 1573, 1476,1451, 1367, 1342, 1256 and 1225 cm^{-1}; HR-ESI-MS *m/z* 508.1971 $[M+H]^+$ (calcd 508.1966 for $C_{28}H_{29}NO_8^+$).

Reference

1. Cimino, G.; Coates, R. M.; de Stefano, S.; Fontana, A.; Hemmerich, P.; Minale, L.; Rinehart, K. L.; Shield, L. S.; Sodano, G.; Toniolo, C. *Prog. Chem. Org. Nat. Prod.* **1976**, 33.
2. Floss, H. G.; Yu, T. W. *Chem. Rev.* **2005**, 105, 621–632.
3. Fukuyo, Y.; Hunt, C. R.; Horikoshi, N. *Cancer Lett.* **2010**, 290, 24–35.
4. Hamel, E. Pharmacol. Ther. **1992**, 55, 31–51.
5. Fan, Y.; Wang, C.; Wang, L.; Chairoungdua, A.; Piyachaturawat, P.; Fu, P.; Zhu, W. *Mar. Drugs* **2018**, 16, 282.
6. Cassady, J.M.; Chan, K.K.; Floss, H.G.; Leistner, E. *Chem. Pharm. Bull.* **2004**, 52, 1-26.
7. Cai, P.; Kong, F.; Ruppen, M.E.; Glasier, G.; and Carter, G.T. *J. Nat. Prod.* **2005**, 68, 1736–1742.
8. Lu, C.; Li, Y.; Deng, J.; Li, S.; Shen, Y.; Wang, H.; Shen, Y. *J. Nat. Prod.* **2013**, 76, 2175–2179.
9. Ding, L.; Maier, A.; Fiebig, H. H.; Görls, H.; Lin, W. H.; Peschel, G.; Hertweck, C. *Angew. Chem. Int. ed.* **2011**, 50, 1630–1634.
10. Xu, Z.; Baunach, M.; Ding, L.; Peng, H.; Franke, J.; Hertweck, C. ChemBioChem 2014, 15, 1274–1279.
11. Ding, L.; Franke, J.; Hertweck, C. *Org. Biomol. Chem.* **2015**, 13, 1618–1623.
12. Kang, Q.; Shen, Y.; Bai, L. *Nat. Prod. Rep.* **2012**, 30, 243–263.
13. Kim, C. G.; Yu, T. W.; Fryhle, C. B.; Handa, S.; Floss, H. G. *J. Biol. Chem.* **1998**, 273, 6030–6040.
14. Li, S.; Wang, H.; Li, Y.; Deng, J.; Lu, C.; Shen, Y. *ChemBioChem* **2014**, 15, 94–102.
15. Kumar, Y.; Goodfellow, M. *Int. J. Syst. Evol. Microbiol.* **2008**, 58, 1369–1378.
16. Blin, K., Shaw, S., Augustijn, H. E., Reitz, Z. L., Biermann, F., Alanjary, M., Fetter, A., Terlouw, B. R., Metcalf, W. W., Helfrich, E. J. N., van Wezel, G. P., Medema, M. H. & Weber, T. *Nucleic Acids Res.* **2023**, 51, W46-W50.
17. Jang, J. P.; Lee, B.; Heo, K. T.; Oh, T. H.; Lee, H. W.; Ko, S. K.; Hwang, B. Y.; Jang, J. H.; Hong, Y. S. *J. Microbiol. Biotechnol.* **2022**, 32, 1299–1306.
18. Nong, X. H.; Tu, Z. C.; Qi, S. H. *Bioorg. Med. Chem. Lett.* **2020**, 30, 7168.
19. Li, S.; Lu, C.; Ou, J.; Deng, J.; Shen, Y. *RSC Adv.* **2015**, 5, 83843–83846.
20. Wang, J.; Nong, X.; Amin, M.; Qi, S. *Appl. Microbiol. Biotechnol.* **2018**, 102, 1417–1427.
21. Pluskal, T.; Castillo, S.; Villar-Briones, A.; Orešič, M. *BMC Bioinform.* **2010**, 11, 1-11.
22. Aron, A. T.; Gentry, E. C.; McPhail, K. L.; Felix Nothias, L.; Nothias-Esposito, M.; Bouslimani, A.; Petras, D.; Gauglitz, J. M.; Vargas, F.; J van der Hooft, J. J.; Ernst, M.; bin Kang, K.; Aceves, C. M.; Mauricio Caraballo-Rodríguez, A.; Koester, I.; Bertrand, S.; Roullier, C.; Sun, K.; Tehan, R. M.; Boya, C. A.; Martin, C. H.; Gutiérrez, M.; Moreno Ulloa, A.; Andres Tejeda Mora, J.; Mojica-Flores, R.; Lakey-Beitia, J.; Zhang, Y.; Calderon, A. I.; Tayler, N.; Tugizimana, F.; Ndlovu, N.; Aksenov, A. A.; Schmid, R.; Truman, A. W.; Bandeira, N.; Wang, M.; Dorrestein, P. C. *Nat. Protoc.* **2020**, 15, 1954-1991.
23. Tong, Y.; Whitford, C. M.; Robertsen, H. L.; Blin, K.; Jørgensen, T. S.; Klitgaard, A. K.; Gren, T.; Jiang, X.;

Weber, T.; Lee, S. Y. *Proc. Natl. Acad. Sci. U. S. A.* **2019**, 116, 20366–20375.

24. Blin, K.; Shaw, S.; Tong, Y.; Weber, T. *Synth. Syst. Biotechnol.* **2020**, 5, 99–102.
25. Tong, Y.; Whitford, C. M.; Blin, K.; Jørgensen, T. S.; Weber, T.; Lee, S. Y. *Nat. Protoc.* **2020**, 15, 2470-2502.
26. Bauer, A. W.; Kirby, W. M.; Sherris, J. C.; Turck, M. *Am. J. Clin. Pathol.* **1966**, 45, 493-496.
27. Cantón, E.; Espinel-Ingroff, A.; Pemán, J. *Expert Rev. Anti. Infect. Ther.* **2014**, 7, 107-119.
28. Pescitelli, G.; Bruhn, T. *Chirality* **2016**, 28, 466–474
29. Tomasi, J.; Mennucci, B.; Cammi, R. *Chem. Rev.* **2005**, 105, 2999-3094.
30. Gaussian 16, Revision A. 03, Frisch, M. J.; Trucks, G. W.; Schlegel, H. B.; Scuseria, G. E.; Robb, M. A.; Cheeseman, J. R.; Montgomery, Jr., J. A.; Vreven, T.; Kudin, K. N.; Burant, J. C.; Millam, J. M.; Iyengar, S. S.; Tomasi, J.; Barone, V.; Mennucci, B.; Cossi, M.; Scalmani, G.; Rega, N.; Petersson, G. A.; Nakatsuji, H.; Hada, M.; Ehara, M.; Toyota, K.; Fukuda, R.; Hasegawa, J.; Ishida, M.; Nakajima, T.; Honda, Y.; Kitao, O.; Nakai, H.; Klene, M.; Li, X.; Knox, J. E.; Hratchian, H. P.; Cross, J. B.; Bakken, V.; Adamo, C.; Jaramillo, J.; Gomperts, R.; Stratmann, R. E.; Yazyev, O.; Austin, A. J.; Cammi, R.; Pomelli, C.; Ochterski, J. W.; Ayala, P. Y.; Morokuma, K.; Voth, G. A.; Salvador, P.; Dannenberg, J. J.; Zakrzewski, V. G.; Dapprich, S.; Daniels, A. D.; Strain, M. C.; Farkas, O.; Malick, D. K.; Rabuck, A. D.; Raghavachari, K.; Foresman, J. B.; Ortiz, J. V.; Cui, Q.; Baboul, A. G.; Clifford, S.; Cioslowski, J.; Stefanov, B. B.; Liu, G.; Liashenko, A.; Piskorz, P.; Komaromi, I.; Martin, R. L.; Fox, D. J.; Keith, T.; Al-Laham, M. A.; Peng, C. Y.; Nanayakkara, A.; Challacombe, M.; Gill, P. M. W.; Johnson, B.; Chen, W.; Wong, M. W.; Gonzalez, C.; and Pople, J. A.; Gaussian, Inc., Wallingford CT, **2016**.
31. Bruhn, T.; Schaumlöffel, A.N.; Hemberger, Y.; Bringmann, G. *Chirality*, **2013**, 25, 243-249.

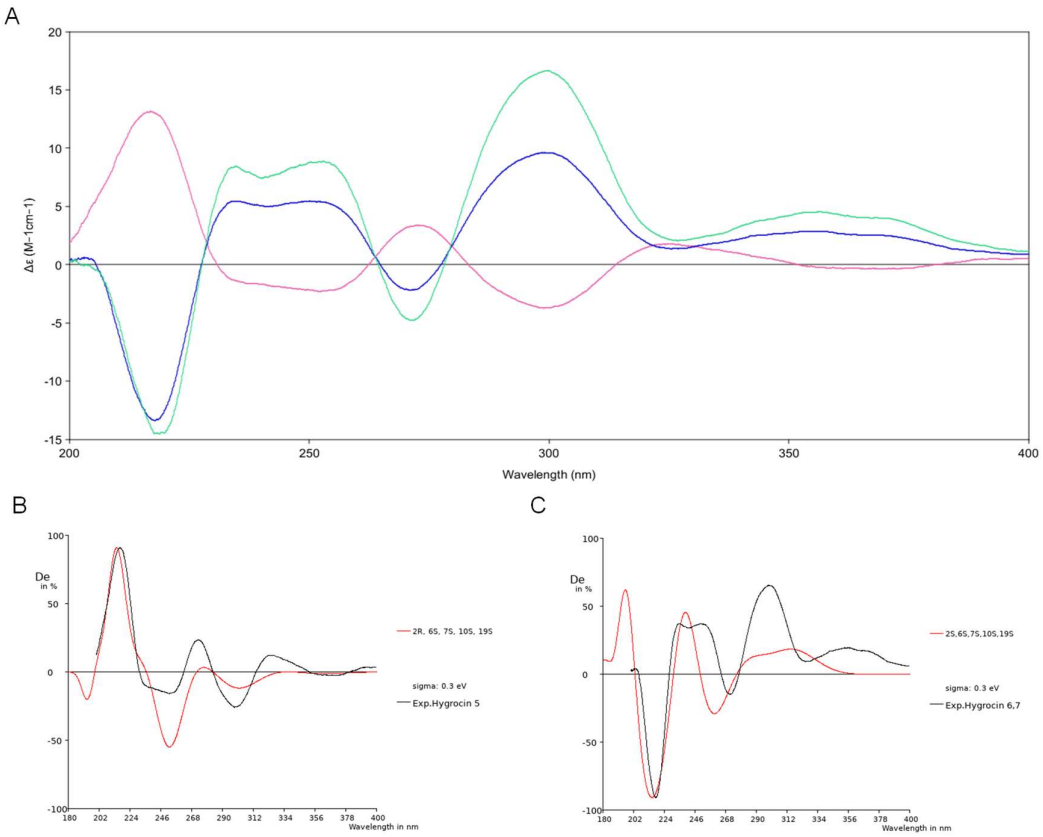

Figure 1. ECD analysis. (A) Experimental ECD curves of **5-7**. (B) Calculated and experimental ECD spectra of **5** of the highest similarity index 2R,6S,7S,10S,19R (Δ_{ESI}) 0.82722S, (C) Calculated and experimental ECD spectra of **6** & **7** in MeOH of the highest similarity index 6S,7S,10S,19S (Δ_{ESI}) 0.7958.

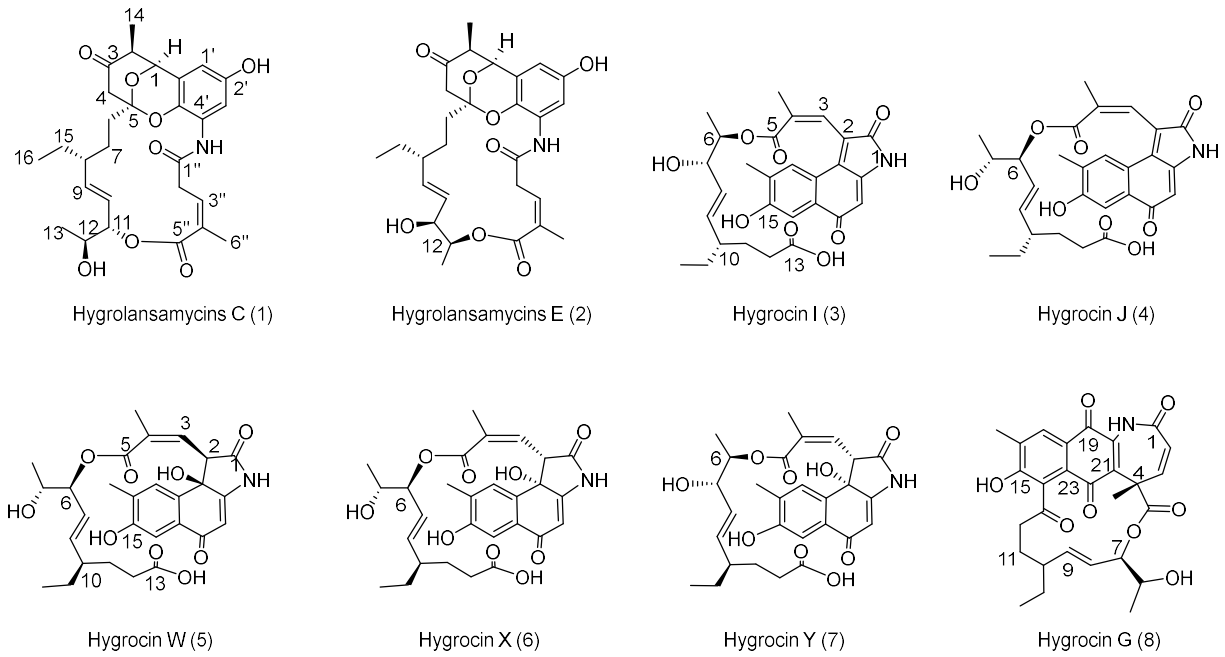

Figure 2. Structures of hygrocins (**1–8**), isolated from *S. rapamycinicus*. **2**, **5-7** are new hygrocins.

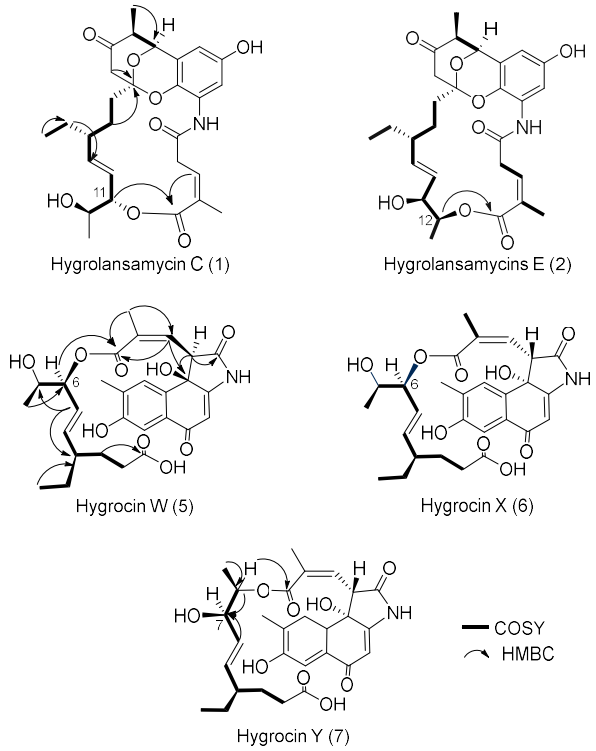

Figure 3. COSY, HMBC correlations of hygrocins (**1–2** and **5–7**).

Table 1. ^{1}H (800 MHz) and ^{13}C (200 MHz) NMR Data for Hygrolansamycins C (1) and E (2) in CD_3OD.

	1		2	
Pos.	**δ_C, type**	**δ_H (mult., *J* in Hz)**	**δ_C, type**	**δ_H (mult., *J* in Hz)**
1	77.3, CH	5.07 (1H, d, 5.3)	77.5, CH	5.07 (1H, d, 5.3)
2	50.4, CH	3.17 (1H, qd, 6.8, 5.3)	49.9, CH	3.16 (1H, qd, 6.8, 5.3)
3	208.6, C		208.7, C	
4	53.1, CH_2	2.61 (1H, d, 15.5), 2.86 (1H, d, 15.5)	50.4, CH_2	2.33 (1H, d, 15.5), 3.00 (1H, d, 15.5)
5	104.9, C		105.3, C	
6	39.3, CH_2	1.85 (1H, dt, 13.3, 1.7), 2.13 (1H, dt, 13.3, 2.2)	40.6, CH_2	1.84 (1H, dt, 13.6, 6.3), 1.56 (1H, dt, 31.0, 3.2),
7	28.4, CH_2	1.07 (1H, m), 1.78 (1H, m)	28.4, CH_2	1.45 (1H, m), 1.65 (1H, m)
8	45.4, CH	1.79 (1H, m)	47.1, CH	1.88 (1H, m)
9	136.8, CH	5.02 (1H, ddd, 15,7, 9. 3, 1.3)	135.91, CH	5.36 (1H, dd, 15.8, 9.1)
10	125.4, CH	5.53 (1H, dd, 15.7, 3.7)	133.7, CH	5.61 (1H, dd, 15.8, 7.4)
11	79.8, CH	5.08 (1H, ddd, 6.0, 3.7, 1.7)	75.2, CH	4.17 (1H, m)
12	69.4, CH	3.89 (1H, dq, 6.6, 6.4)	77.3, CH	5.0 (1H, qd. 6.7, 2.0)
13	18.8, CH_3	1.22 (3H, d, 6.4)	16.7, CH_3	1.34 (3H, d, 6.7)
14	10.1, CH_3	1.01 (3H, d, 6.8)	10.0, CH_3	1.02 (3H, d, 6.8)
15	29.6, CH_2	1.41 (1H, m), 1.33 (1H, m)	29.6, CH_2	1.37 (1H, m), 1.51 (1H, m)
16	12.5, CH_3	0.89 (3H, t, 7.4)	12.2, CH_3	0.92 (3H, t, 7.4)
1'	108.6, CH	6.12 (1H, d, 2.8)	109.1, CH	6.15 (1H, d, 2.8)
2'	150.9, C		151.0, C	
3'	108.4, CH	7.81 (1H, d, 2.8)	109.1, CH	7.52 (1H, d, 2.8)
4'	128.3, C		127.3, C	
5'	133.6, C		134.0, C	
6'	120.1, C		120.4, C	
1``	170.7, C		170.0, C	
2``	40.7, CH_2	2.85 (1H, dd, 11.5, 7.2) 4.24 (1H, t, 11.5)	40.1, CH_2	3.00 (1H, m, overlap) 3.92 (1H, dd, 14.5, 9.9)
3``	137.6, CH	6.28 (1H, ddd, 11.2, 7.2, 1.2)	135.93, CH	6.27 (1H, m, overlap)
4``	132.0, C		134.1, C	
5``	168.0, C		168.4, C	
6``	20.6, CH_3	2.06 (3H, br.s)*	20.7, CH_3	2.11 (3H, br. s)*

*br.s (Broad singlet)

Table 2. ^{1}H (800 MHz) and ^{13}C (200 MHz) NMR data for Hygrocin I (**3**) and J (**4**) in CD_3OD.

	3		**4**	
Pos.	**δc, type***	**δ_H (mult., *J* in Hz)**	**δC, type***	**δ_H (mult., *J* in Hz)**
1	171.5, C		171.6, C	
2	126.7, C		126.7, C	
3	129.6, CH	7.54 (1H, brq, 1.4)	129.6, CH	7.56 (1H, brq, 1.5)
4	137.5, C		137.4, C	
4a	16.2, CH_3	1.93 (3H, d, 1.4)	16.2, CH_3	1.93 (3H, d, 1.5)
5	168.0, C		167.7, C	
6	75.4, CH	5.07 (1H, dq, 6.6, 6.5)	69.7, CH	3.94 (1H, dq, 6.4)
6a	16.2, CH_3	1.34 (3H, d, 6.5)	19.5, CH_3	1.24 (3H, d, 6.4)
7	75.2, CH	4.20 (1H, t, 6.0)	81.2, CH	5.24 (1H, t, 6.4)
8	131.3, CH	5.55 (1H, dd, 15.5, 6.6)	127.7, CH	5.56 (1H, dd, 15.5, 6.9)
9	138.1, CH	5.50 (1H, dd, 15.5, 8.8)	141.1, CH	5.57 (1H, dd, 15.5, 8.3)
10	45.4, CH	1.96 (1H, m)	45.6, CH	1.98 (1H, m)
10a	29.1, CH_2	1.44 (1H, m), 1.31 (1H, m)	28.9, CH_2	1.32 (1H, m), 1.49 (1H, m)
10b	12.1, CH_3	0.89 (3H, t, 7.5)	12.2, CH_3	0.88 (3H, t, 7.4)
11	31.0, CH_2	1.74 (1H, m), 1.46 (1H, m)	31.0, CH_2	1.77 (1H, m), 1.53 (1H, m)
12	32.9, CH_2	2.29 (1H, ddd, 16.0, 8.9, 5.7), 2.22 (1H, ddd, 16.0, 8.9, 7.6)	32.9, CH_2	2.25 (1H, ddd, 16.0, 8.8, 7.4), 2.31 (1H, ddd, 16.0, 8.8, 5.8)
13	177.6, C		177.5, C	
14	113.8, CH	7.46 (1H, s)	113.7, CH	7.46 (1H, s)
15	159.8, C		159.7, C	
16	131.8, C		131.8, C	
16a	16.7, CH_3	2.25 (3H, s)	16.6, CH_3	2.22 (3H, s)
17	131.5, CH	7.45 (1H, s)	131.5, CH	7.44 (1H, s)
18	122.7, C		122.7, C	
19	137.3, C		137.3, C	
20	154.0, C		153.9, C	
21	106.1, CH	5.90 (1H, s)	106.2, CH	5.91 (1H, s)
22	186.4, C		186.3, C	
23	131.8, C		131.8, C	

*Estimated from HSQC & HMBC

Table 3. ^{1}H (800 MHz) and ^{13}C (200 MHz) NMR data for Hygrocins W (**5**), X (**6**) and Y (**7**) in CD_3OD.

	5		**6**		**7**	
Pos.	**δ_C, type**	**δ_H (mult., *J* in Hz)**	**δ_C, type**	**δ_H (mult., *J* in Hz)**	**δ_C, type**	**δ_H (mult., *J* in Hz)**
1	177.1, C		177.2, C		177.2, C	
2	53.4, CH	4.60 (1H, d, 9.8)	53.5, CH	4.70 (1H, d, 9.8)	53.3, CH	4.82 (1H, d, 9.6)
3	131.4, CH	6.50 (1H, dq, 9.8, 1.6)	131.8, CH	6.55 (1H, dq, 9.8, 1.5)	132.5, CH	6.56 (1H, dq, 9.6, 1.6)
4	136.4, C		135.9, C		135.7, C	
4a	21.3, CH_3	2.20 (3H, d, 1.6)	21.5, CH_3	2.20 d (3H, d, 1.5)	21.5, CH_3	2.18 (3H, d, 1.6)
5	168.4, C		168.2, C		168.3, C	
6	69.5, CH	3.78 (1H, dq, 6.4)	69.4, CH	3.71, (1H, dq, 6.4)	75.04, CH	4.92 (1H, qd, 6.4, 5.6)
6a	19.1, CH_3	1.08 (3H, d, 6.5)	19.1, CH_3	1.09 (3H, d, 6.5)	16.0, CH_3	1.12 (3H, d, 6.4)
7	80.5, CH	5.09 (1H, t, 6.6)	80.2, CH	5.14 (1H, t, 6.3)	75.0, CH	3.94 (1H, t, 5.6)
8	127.2, CH	5.33 (1H, dd, 15.5, 7.0)	127.2, CH	5.36 (1H, dd, 15.5, 6.3)	131.0, CH	5.34 (1H, dd, 15.4, 6.0)
9	140.8, CH	5.37 (1H, dd, 15.5, 8.7)	140.4, CH	5.33 (1H, dd, 15.5, 8.4)	138.0, CH	5.36 (1H, dd, 15.4, 7.6)
10	45.5, CH	1.78 (1H, m)	45.5, CH	1.81 (1H, m)	45.3, CH	1.76 (1H, m)
10a	28.7, CH_2	1.09 (1H, m), 1.29 (1H, m)	28.7, CH_2	1.29 (1H, m), 1.04 (1H, m)	28.9, CH_2	1.24 (1H, m), 1.38 (1H, m)
10b	12.1, CH_3	0.66 (3H, t, 7.4)	12.1, CH_3	0.69 (3H, t, 7.4)	12.1, CH_3	0.83 (3H, t, 7.4)
11	30.8, CH_2	1.33 (1H, m), 1.64 (1H, m)	30.8, CH_2	1.64 (1H, m), 1.34 (1H, m)	31.1, CH_2	1.65 (1H, m), 1.39 (1H, m)
12	32.8, CH_2	2.12 (1H, ddd, 16.0, 8.6, 7.4), 2.17 (1H, ddd, 16.0, 8.8, 5.8)	32.8, CH_2	2.12 (1H, ddd, 16.0, 8.6, 7.4), 2.17 (1H, ddd, 16.0, 8.6, 5.8)	33.2, CH_2	2.04 (1H, ddd, 15.7, 9.3, 6.9), 2.17 (1H, ddd, 15.7, 9.3, 5.6)
13	177.4, C		177.5, C		178.1, C	
14	112.6, CH	7.40 (1H, s)	112.6, CH	7.41 (1H, s)	112.5, CH	7.41 (1H, s)
15	157.3, C		157.3, C		157.3, C	
16	131.5, C		131.5, C		131.4, C	
16a	16.8, CH_3	2.20 (3H, s)	16.7, CH_3	2.20 (3H, s)	16.7, CH_3	2.21 (3H, s)
17	130.0, CH	7.24 (1H, s)	129.9, CH	7.24 (1H, s)	130.1, CH	7.25 (1H, s)
18	133.7, C		133.8, C		133.8, C	
19	73.1, C		73.2, C		73.2, C	
20	165.2, C		165.2, C		165.3, C	
21	103.2, CH	5.74 (1H, s)	103.2, CH	5.74 (1H, s)	103.2, CH	5.75 (1H, s)
22	186.6, C		186.6, C		186.6, C	
23	131.8, C		131.9, C		131.9, C	

Supplementary information

Table of contents

Table S1. ECD calculations of four possible structures of hygrocins (**5-7**) by B3LYP functional and 6-31G(d,p) basis set.

Absolute configurations	Conformer no.	Heat of formation (kJ mol–1)	Weighting factor
2S, 6S, 7S, 10S, 19S	C1	-1818.215916	1.35
	C2	-1818.217478	7.05
	C3	-1818.217479	7.06
	C4	-1818.219813	83.82
	C5	-1818.214277	0.24
	C6	-1818.214293	0.24
	C7	-1818.212798	0.05
	C8	-1818.214099	0.2
2R, 6S, 7S, 10S, 19S	C1	-1818.217517	26.82
	C2	-1818.215662	3.75
	C3	-1818.215565	3.39
	C4	-1818.217345	22.35
	C5	-1818.213663	0.45
	C6	-1818.216494	9.07
	C7	-1818.213462	0.36
	C8	-1818.215332	2.65
	C9	-1818.214376	0.96
	C10	-1818.213053	0.24
	C11	-1818.213431	0.35
	C12	-1818.212647	0.15
	C13	-1818.212426	0.12
	C14	-1818.217458	25.19
	C15	-1818.214465	1.06
	C16	-1818.211447	0.04
	C17	-1818.215286	2.52
	C18	-1818.212724	0.17
	C19	-1818.213462	0.36
2S, 6S, 7S, 10S, 19R	C1	-1818.212065	0
	C2	-1818.220642	30.43
	C3	-1818.218844	4.52
	C4	-1818.218053	1.96
	C5	-1818.220665	31.18
	C6	-1818.217366	0.94
	C7	-1818.216169	0.27
	C8	-1818.220608	29.36
	C9	-1818.217690	1.33
2R, 6S, 7S, 10S, 19R	C1	-1818.221177	0.00
	C2	-1818.218620	0.00
	C3	-1818.218852	0.00
	C4	-1818.220309	0.00
	C5	-1818.220285	0.00
	C6	-1818.216040	0.00
	C7	-1818.290989	49.07
	C8	-1818.216336	0.00
	C9	-1818.211269	0.00

Figure S2. The BGC annotation of *S. rapamycinicus* using antiSMASH.

Region	From	To	Known BGCs	Similarity
Region 1	1	106876	lobophorin A	36%
Region 2	490714	549079	coelichelin	100%
Region 3	859144	868463	cyphomycin	9%
Region 4	1024465	1112648	azalomycin F3a	100%
Region 5	1298486	1437158	nigericin	66%
Region 6	1439806	1483779	salinomycin	8%
Region 7	1585031	1663130	efomycin K/efomycin L	95%
Region 8	1690280	1712398	lankacidin C	13%
Region 9	1836607	1857362	heronamide A/heronamide B/heronamide C/heronamide D/heronamide E/heronamide F	8%
Region 10	1867930	1878862		
Region 11	2083936	2136122	meilingmycin	4%
Region 12	2194053	2294639	feglymycin	84%
Region 13	2376523	2596226	thiazostatin/watasemycin A/watasemycin B/2-hydroxyphenylthiazoline enantiopyochelin/isopyochelin	86%
Region 14	2599171	2623572	steffimycin D	16%
Region 15	2763243	2785685		
Region 16	2825088	2847488	hopene	76%
Region 17	3223797	3296312	spore pigment	83%
Region 18	3440208	3501621	notonesomycin A	10%
Region 19	3744643	3755156		
Region 20	4330901	4372987	echoside A/echoside B/echoside C/echoside D/echoside E	100%
Region 21	4931246	4942037	legonoxamine A/desferrioxamine B/legonoxamine B	83%
Region 22	5234705	5353578	alchivemycin A/alchivemycin B	88%
Region 23	6279853	6301507	TVA-YJ-2	9%
Region 24	6595547	6698033	kitacinnamycin A/kitacinnamycin B/kitacinnamycin C/kitacinnamycin D/kitacinnamycin E/kitacinnamycin F	54%
Region 25	6995321	7016463	5-isoprenylindole-3-carboxylate β-D-glycosyl ester	61%
Region 26	7233050	7275286	ochronotic pigment	75%
Region 27	7325972	7367065	cinnapeptin	50%
Region 28	7384936	7396042	granaticin	10%
Region 29	7536753	7718885	desulfoclethramycin/clethramycin	69%
Region 30	8222414	8242984		
Region 31	8900244	8910648	ectoine	100%
Region 32	9081916	9139461	peucechelin	20%
Region 33	9152238	9168506	aurachin C/aurachin D/aurachin SS	20%
Region 34	9476760	9606190	akaeolide	20%
Region 35	9680021	9720124	BD-12	71%
Region 36	9758976	10004255	rapamycin	100%
Region 37	10085595	10126623	rustmicin	20%
Region 38	10130161	10149631	2-methylisoborneol	100%
Region 39	10565677	10585422	pristinol	100%
Region 40	10679301	10730137	cinnapeptin	46%
Region 41	10976611	11092238	meridamycin	76%
Region 42	11099441	11181894	hygrocin A/hygrocin B	93%
Region 43	11336115	11459137	hexacosalactone A	79%
Region 44	11461501	11471719	hexacosalactone A	9%
Region 45	11477449	11554061	cyclofaulknamycin	8%
Region 46	11606908	11627280	brasilicardin A	38%
Region 47	11765022	11785930	clipibycyclene	4%
Region 48	11835848	11877612	echoside A/echoside B/echoside C/echoside D/echoside E	11%
Region 49	11969269	11998132	Sch-47554/Sch-47555	7%
Region 50	12035215	12100906	linearmycin A/linearmycin B/linearmycin C/linearmycin C	37%
Region 51	12222724	12274150	desulfoclethramycin/clethramycin	4%
Region 52	12289607	12332156	geldanamycin	39%

Table S3. Summary of strains and plasmids were used in this study.

Strains	Description
One Shot™ Mach1™ T1 Phage-Resistant Chemically Competent *E. coli*	For routine plasmids maintenance and cloning
E. coli ET12567/pUZ8002	For conjugating plasmids into *Streptomyces*
S. rapamycinicus	wild-type strain
S. rapamycinicus/D*hgc3*	Mutant strain with *hgc3*-inactivation
Plasmids	
pCRISPR-cBEST	For C to T base editing
pCRISPR-cBEST/D*hgc3*	Modified plasmid for inactivation of *hgc3*

Table S4. Primers were used in this study.

Primer name	Sequence (5' → 3')	Description
Del-*hgc3*	GCTACAATCAATACTCGATTggtccaggggcggggcagctGTTTTAGAGCTAGAAATAGC	Inactivation of *hgc3*, the base marked in red is sgRNA sequence
ID-sgRNA-F	TGTGTGGAATTGTGAGCGGATA	Forward primer for screening plasmid
ID-sgRNA-R	CCCATTCAAGAACAGCAAGCA	Reverse primer for screening plasmid
ID-*hgc3*-F	CGAAGTTGAAGAACTGGACG	Forward primer for screening *hgc3* mutants
ID-*hgc3*-R	CTCACCAACAACATGTTCAC	Reverse primer for screening *hgc3* mutants

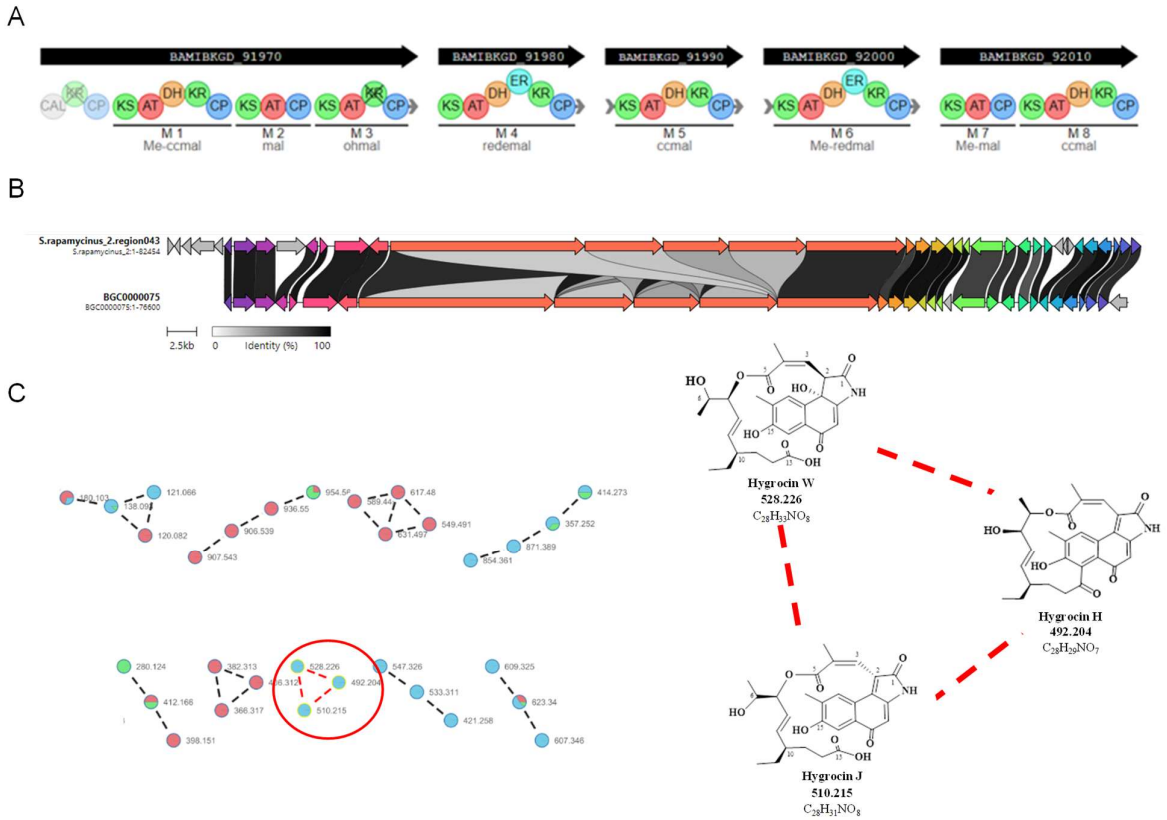

Figure S1. Bioinformatics and metabolomics analysis of *S. rapamycinicus*. (A) PKS module precursor-prediction for *S. rapamycinicus* using antiSMASH. (B) BGC homology analysis of hygrocins in *S. rapamycinicus* and *Streptomyces* sp. LZ35. (C) Molecular networking of the MeOH fractions of *S. rapamycinicus* with the clusters correlating to hygrocins including compounds **5–7**.

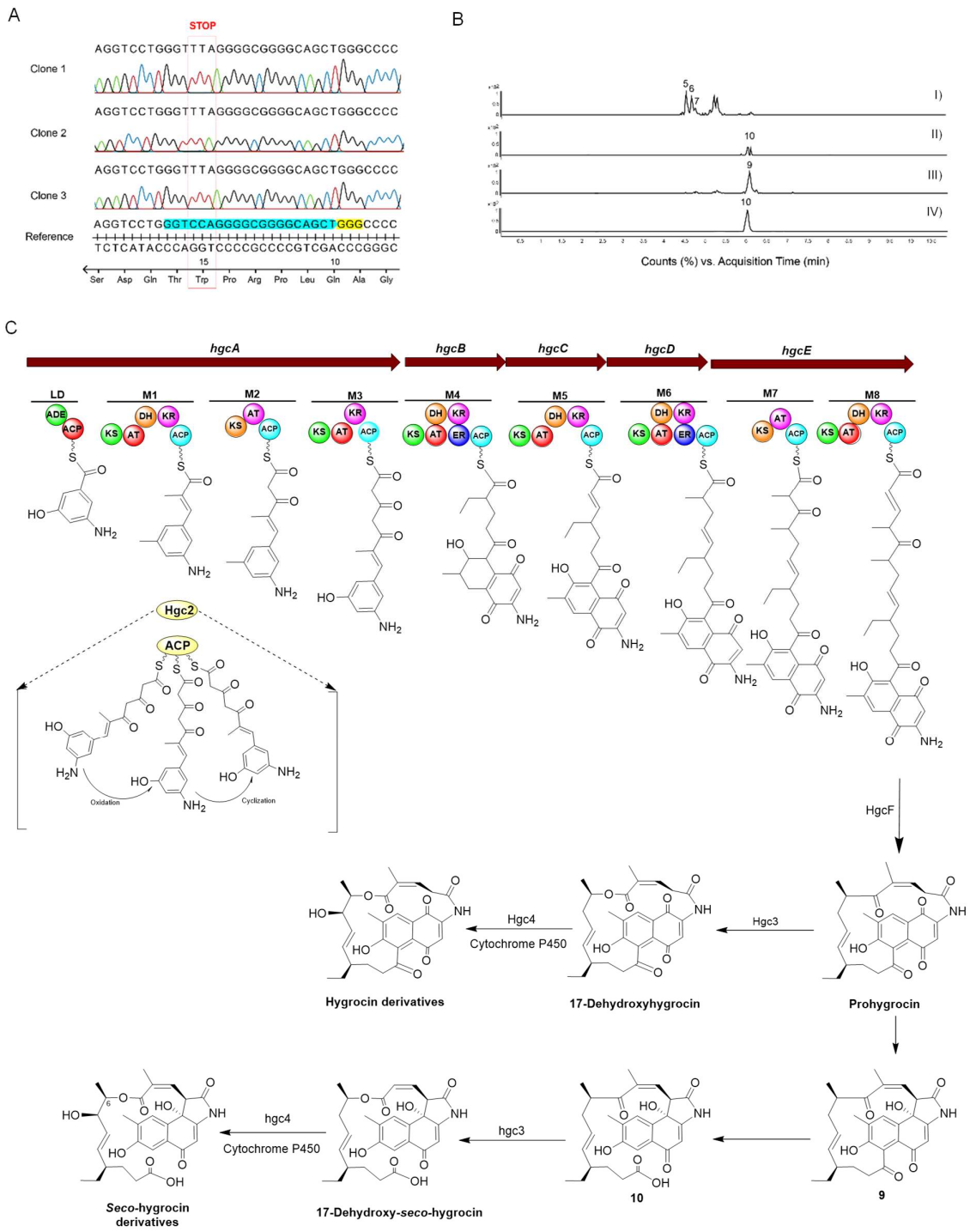

Figure S2. Gene inactivation and proposed biosynthesis mechanism. (A) Inactivation of Hgc3 in *S. rapamycinicus*. (B) HR-ESI-MS-based metabolomic analysis of *S. rapamycinicus* wild type (trace I), Δ*hgc3* gene disruption mutant showing the production of hygrocin intermediate in mutant strain (trace II-IV). Extracted ion chromatogram extraction for **9** (*m/z* 477.2151 $[M+H]^+$) and **10** (*m/z* 495.2257 $[M+H]^+$).

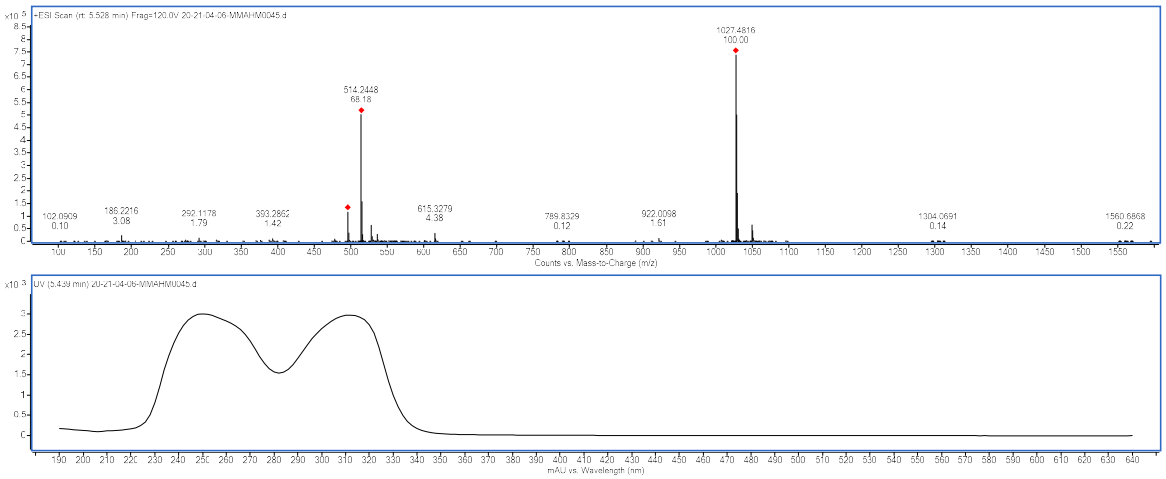

Figure S3. Base peak chromatogram (BPC) and UV spectrum of **1** with m/z 514.2448 $[M+H]^+$.

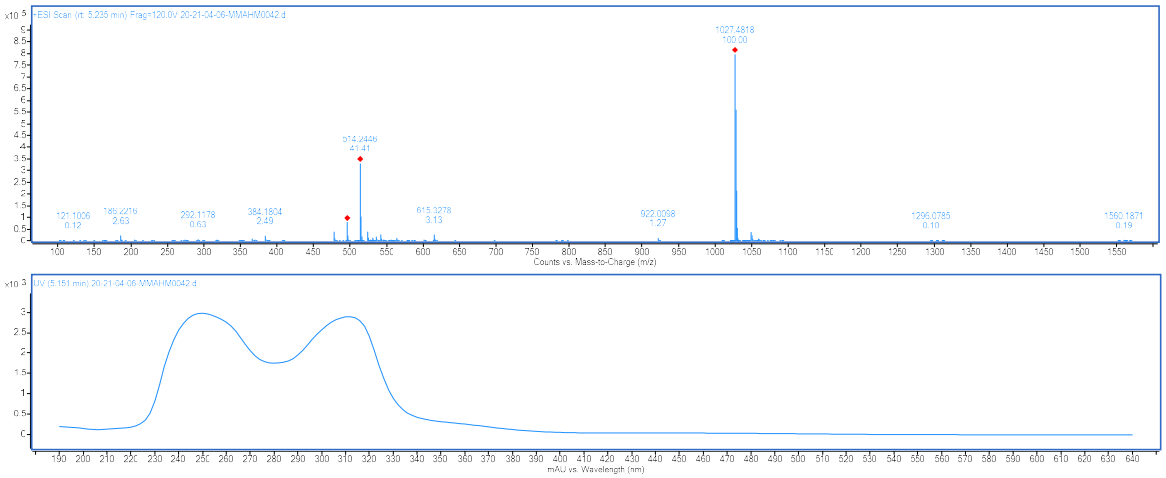

Figure S4. BPC and UV spectrum of **2** with m/z 514.2446 $[M+H]^+$.

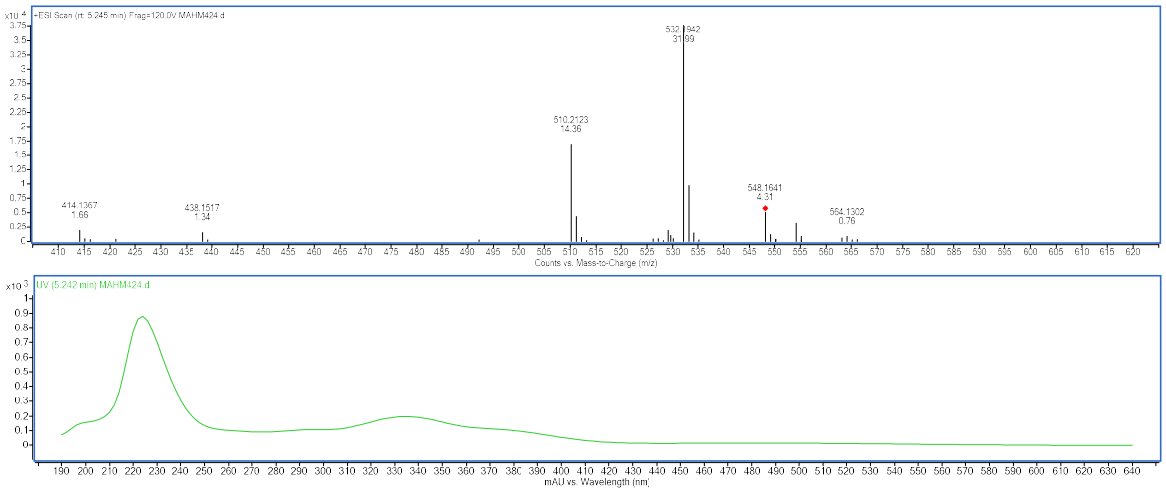

Figure S5. BPC and UV spectrum of **3** with m/z 510.2123 $[M+H]^+$.

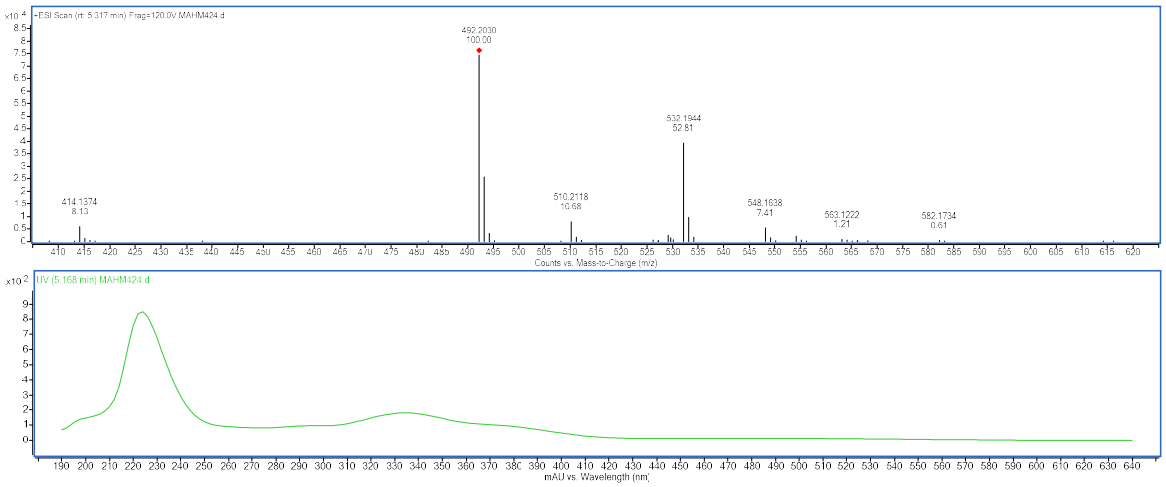

Figure S6. BPC and UV spectrum of **4** with m/z 510.2118 $[M+H]^+$.

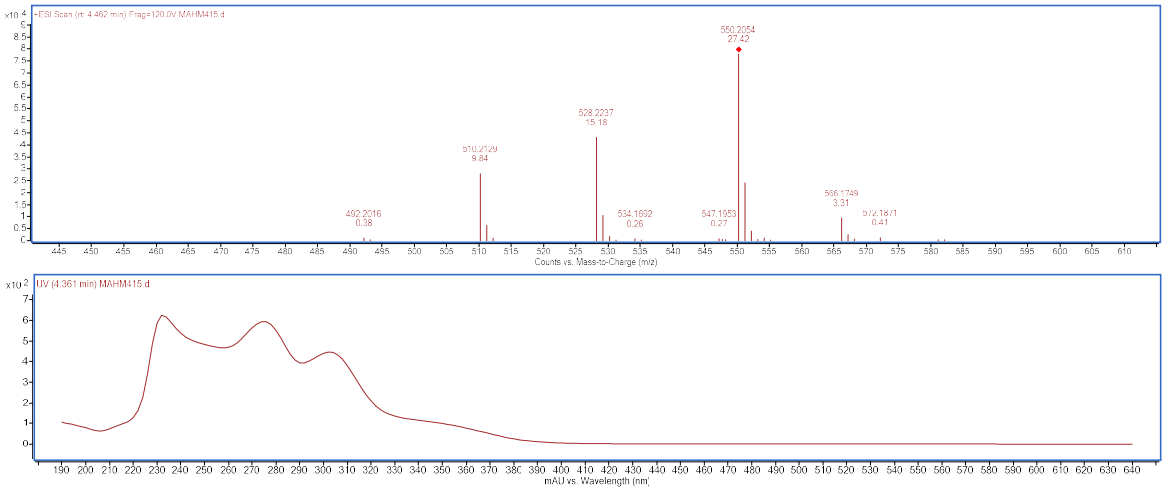

Figure S7. BPC and UV spectrum of **5** with m/z 528.2237 $[M+H]^+$.

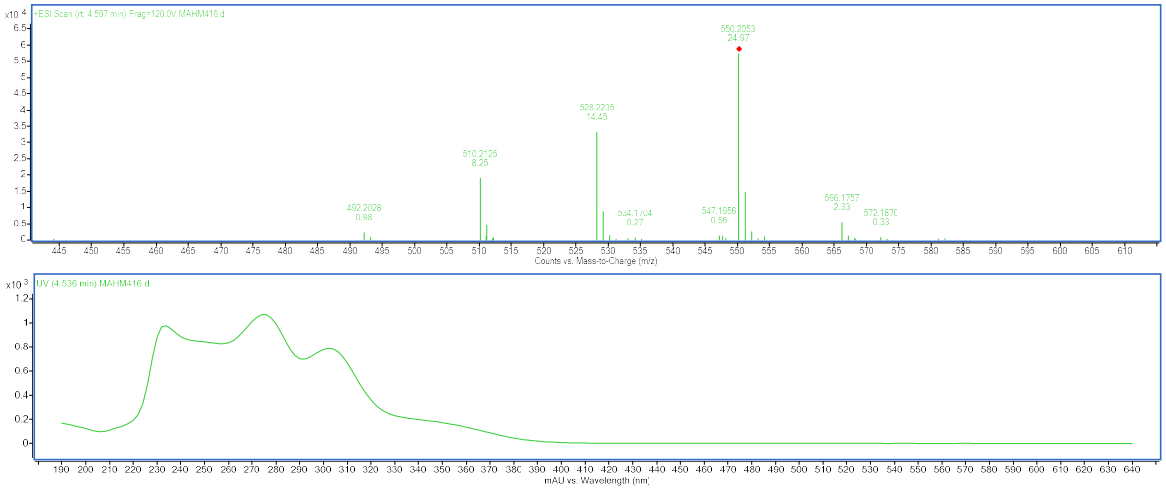

Figure S8. BPC and UV spectrum of **6** with m/z 528.2235 $[M+H]^+$.

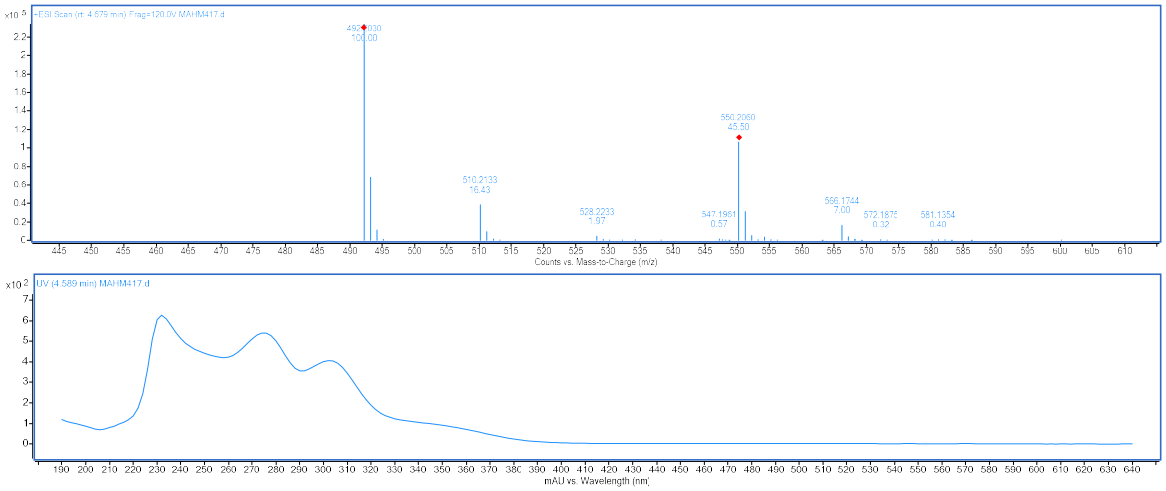

Figure S9. BPC and UV spectrum of **7** with *m/z* 528.2233 $[M+H]^+$.

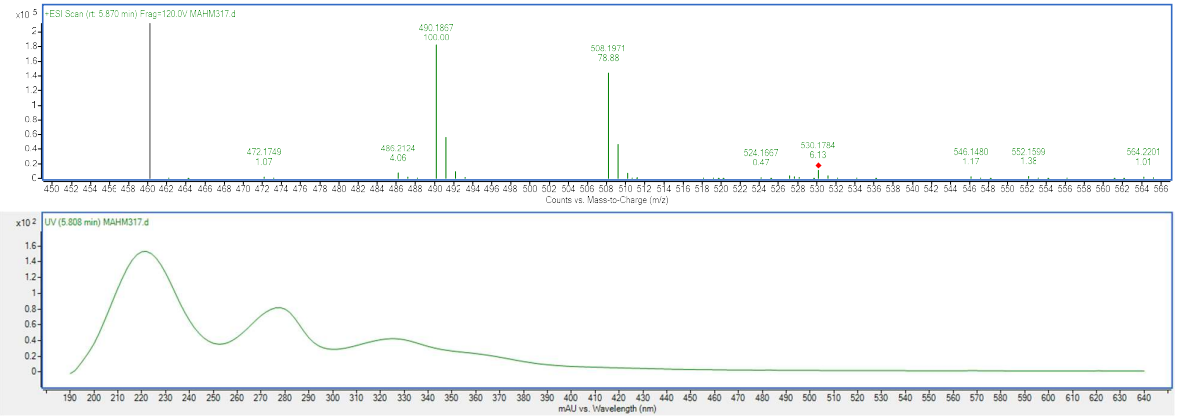

Figure S10. BPC and UV spectrum of **8** with *m/z* 508.1971 $[M+H]^+$.

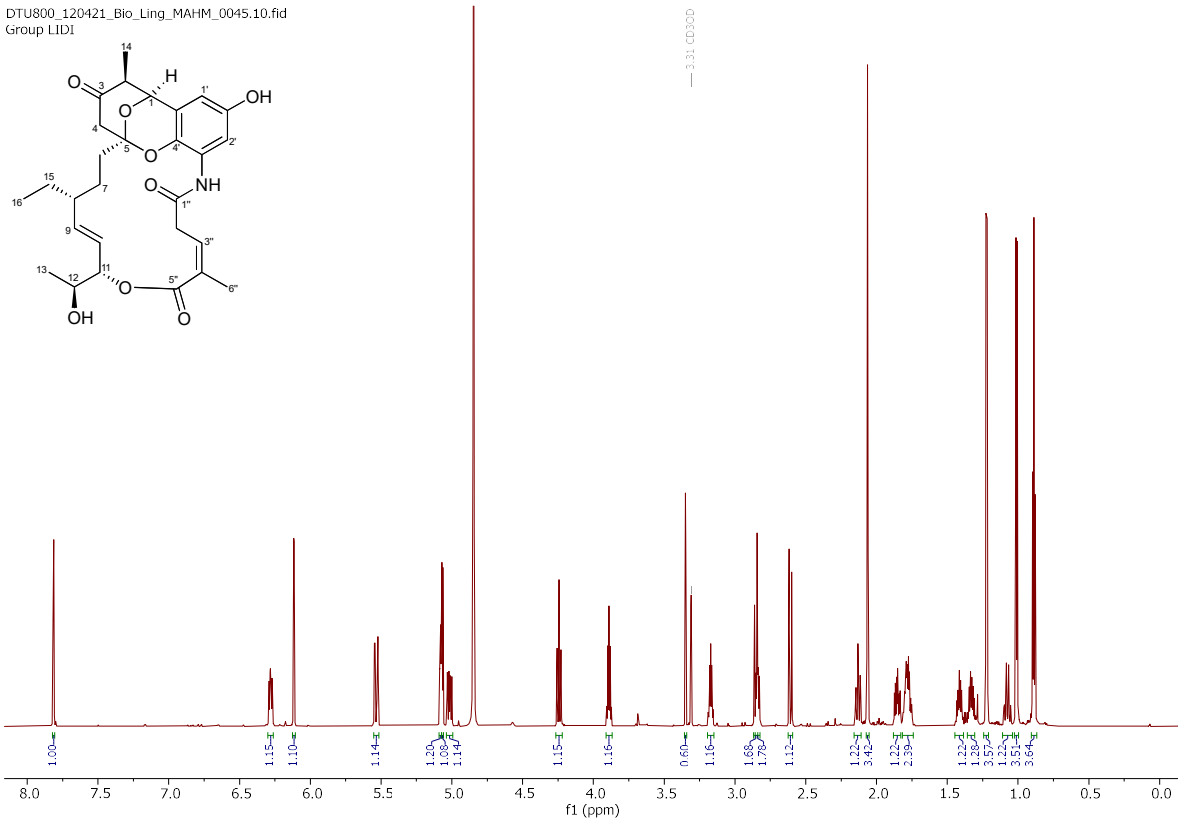

Figure S11. ^{1}H NMR (800 MHz) spectrum of **1** in CD_3OD.

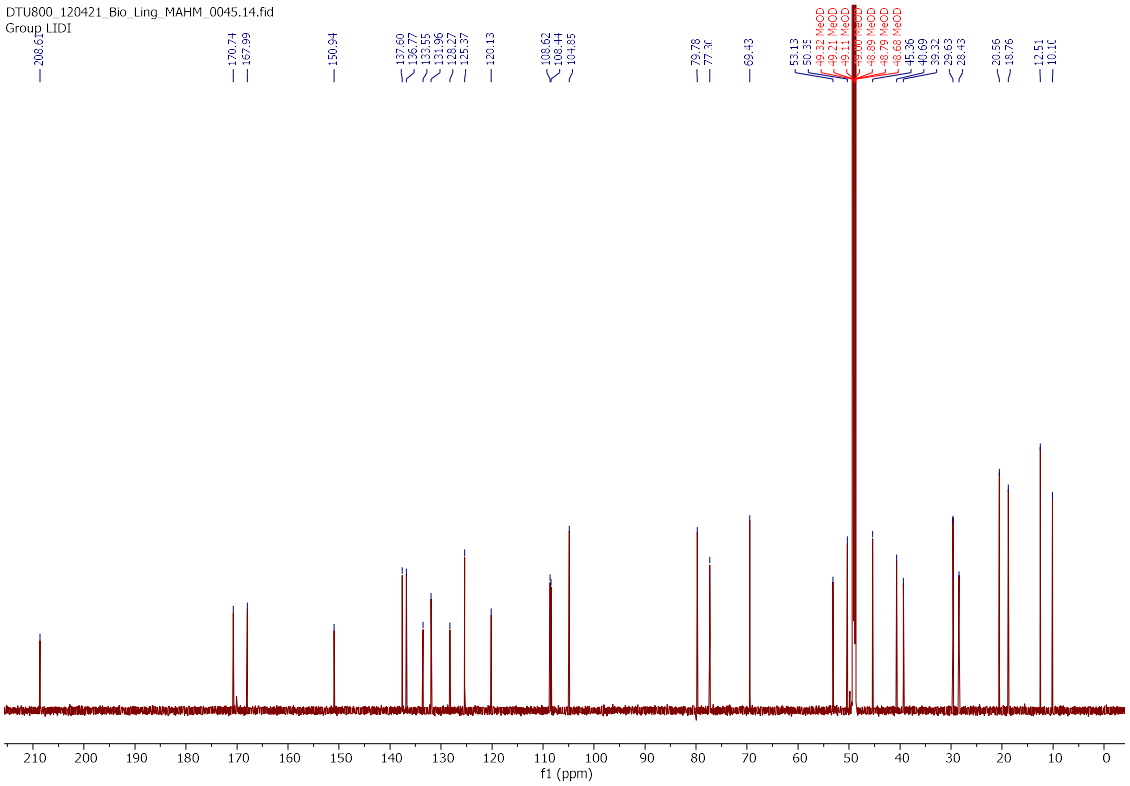

Figure S12. ^{13}C NMR (200 MHz) spectrum of **1** in CD_3OD.

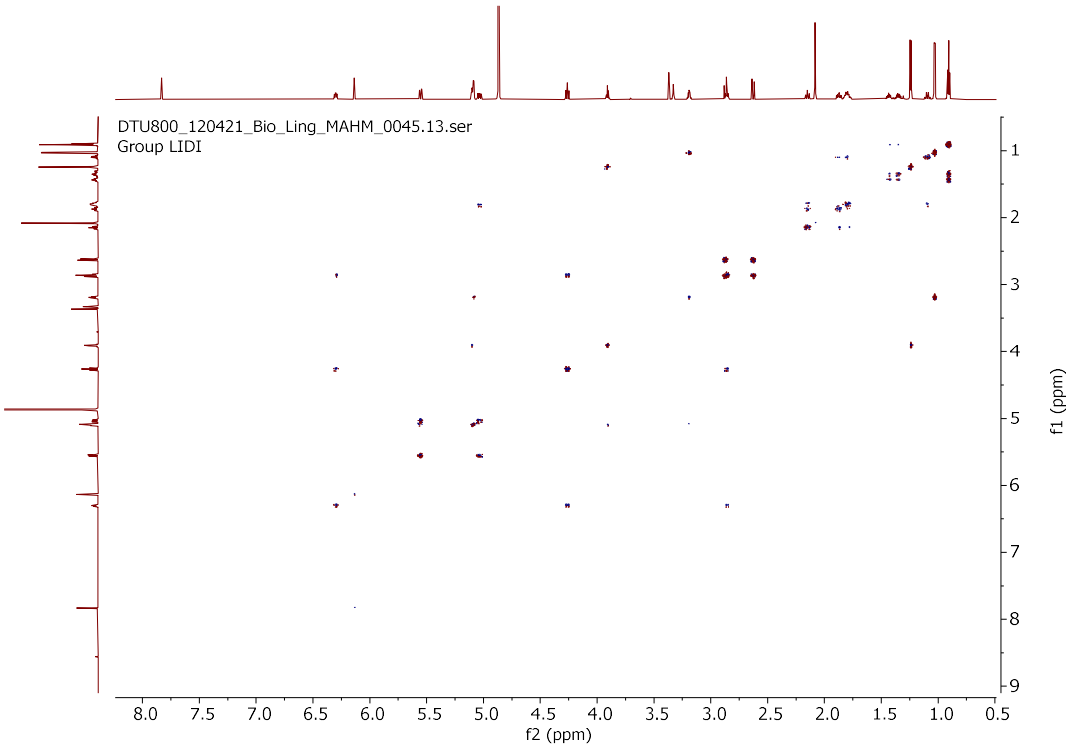

Figure S13. DQF-COSY spectrum of **1** in CD_3OD.

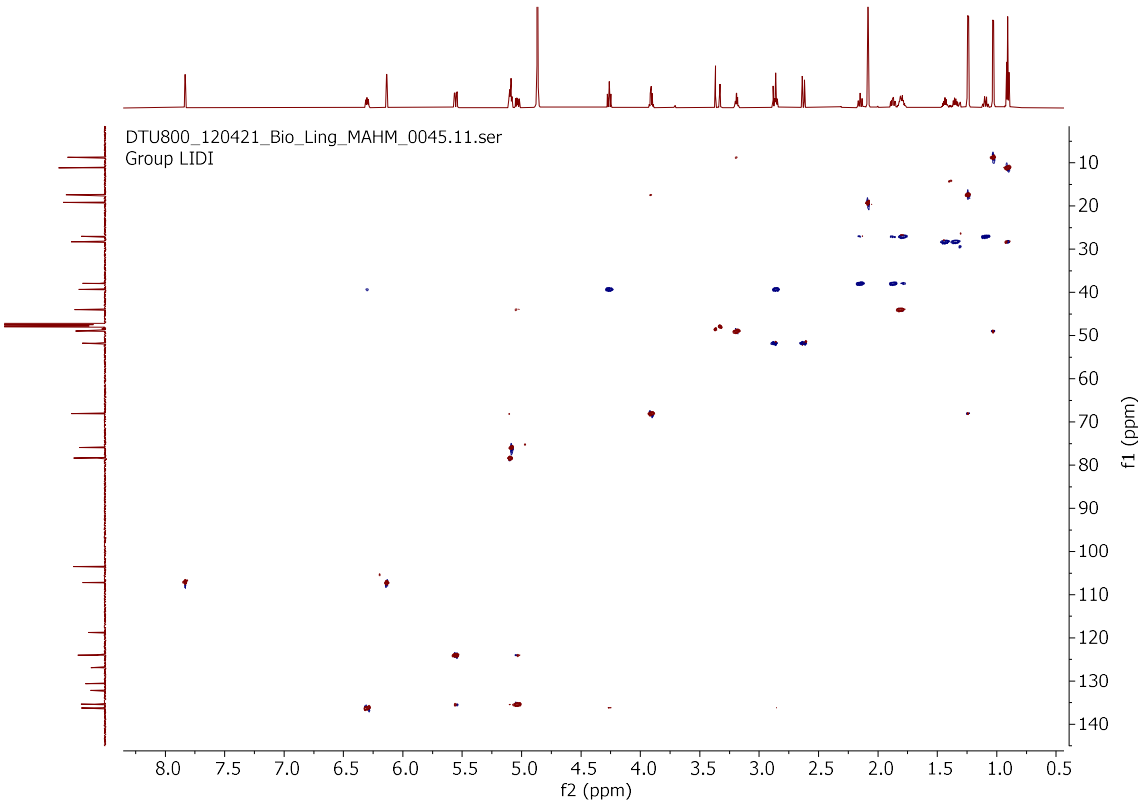

Figure S14. HSQC spectrum of **1** in CD_3OD.

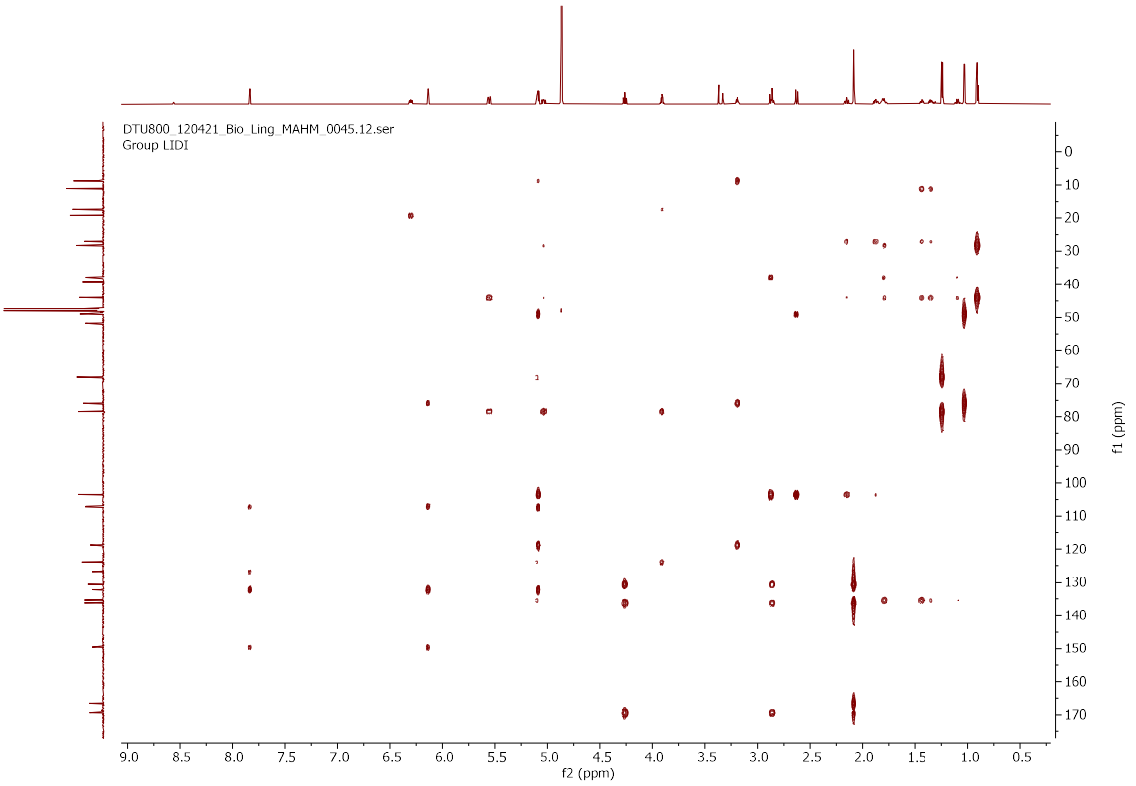

Figure S15. HMBC spectrum of **1** in CD_3OD.

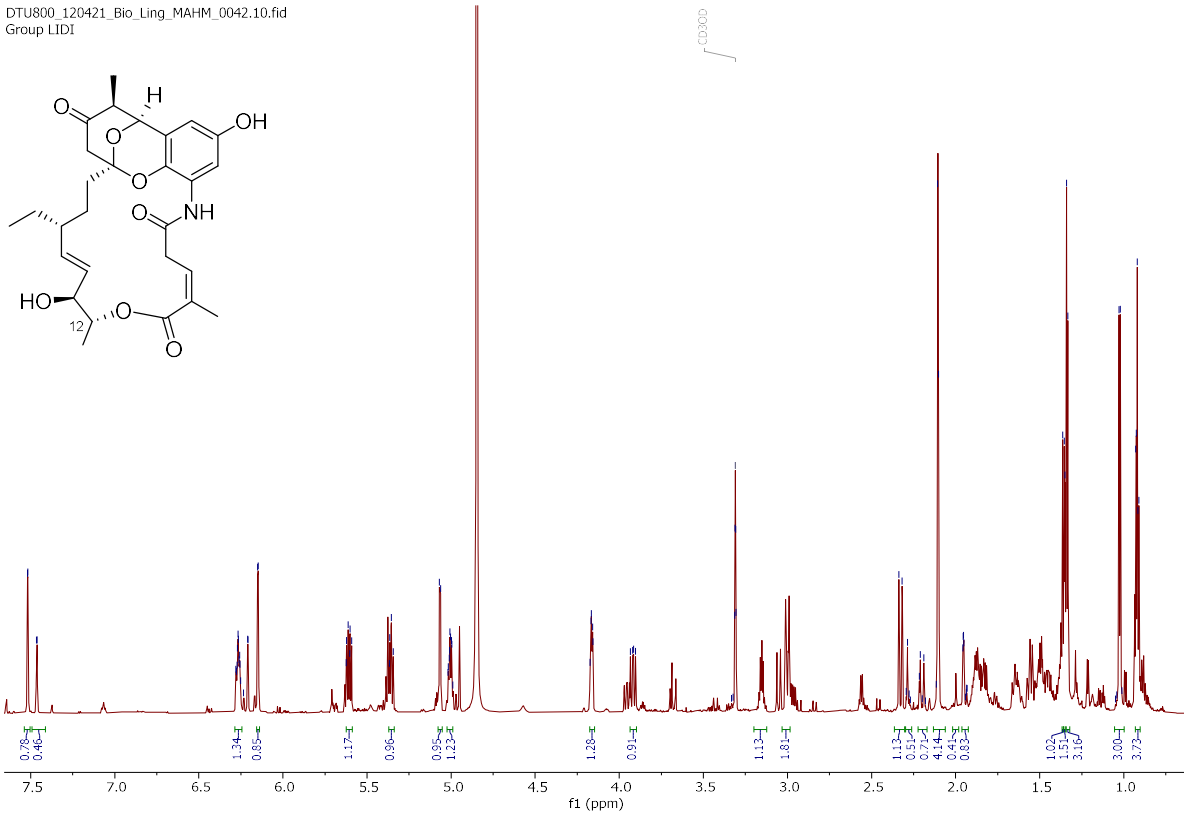

Figure S16. 1HNMR (800 MHz) spectrum of **2** in CD_3OD.

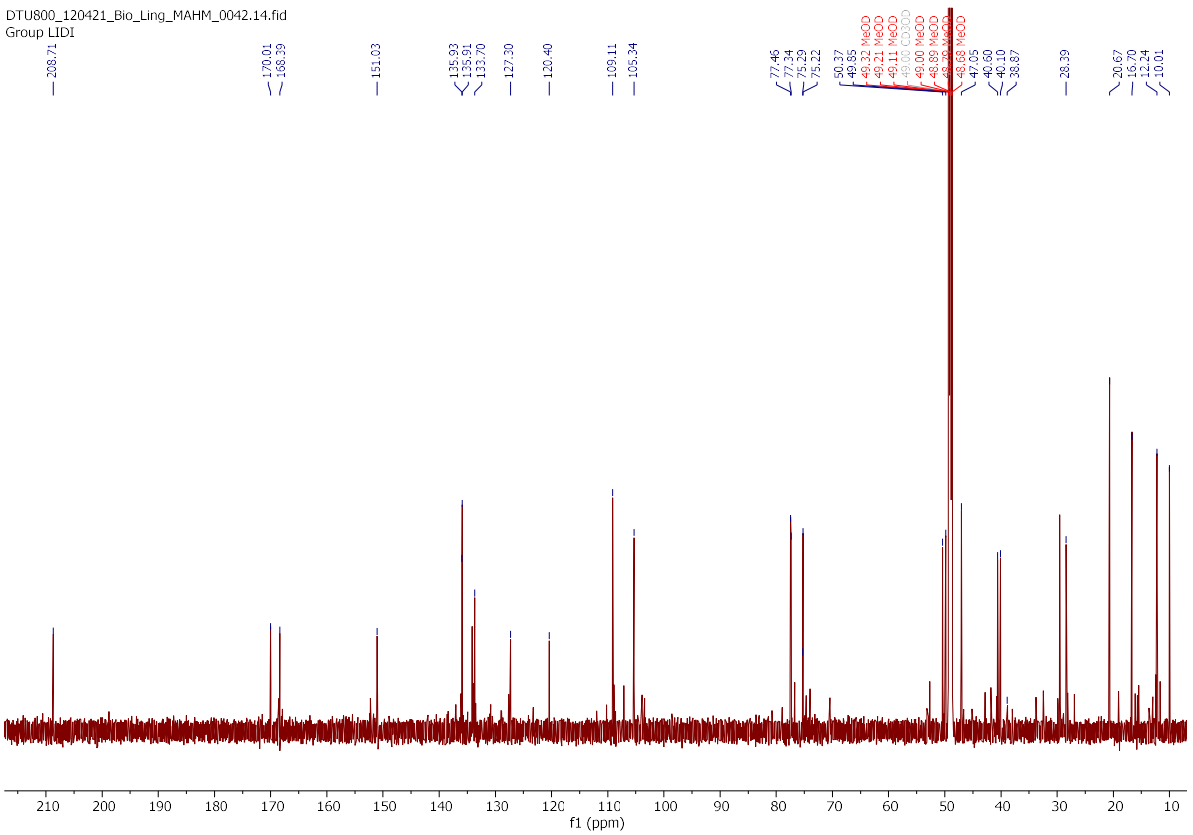

Figure S17. ^{13}C NMR (200 MHz) spectrum of **2** in CD_3OD.

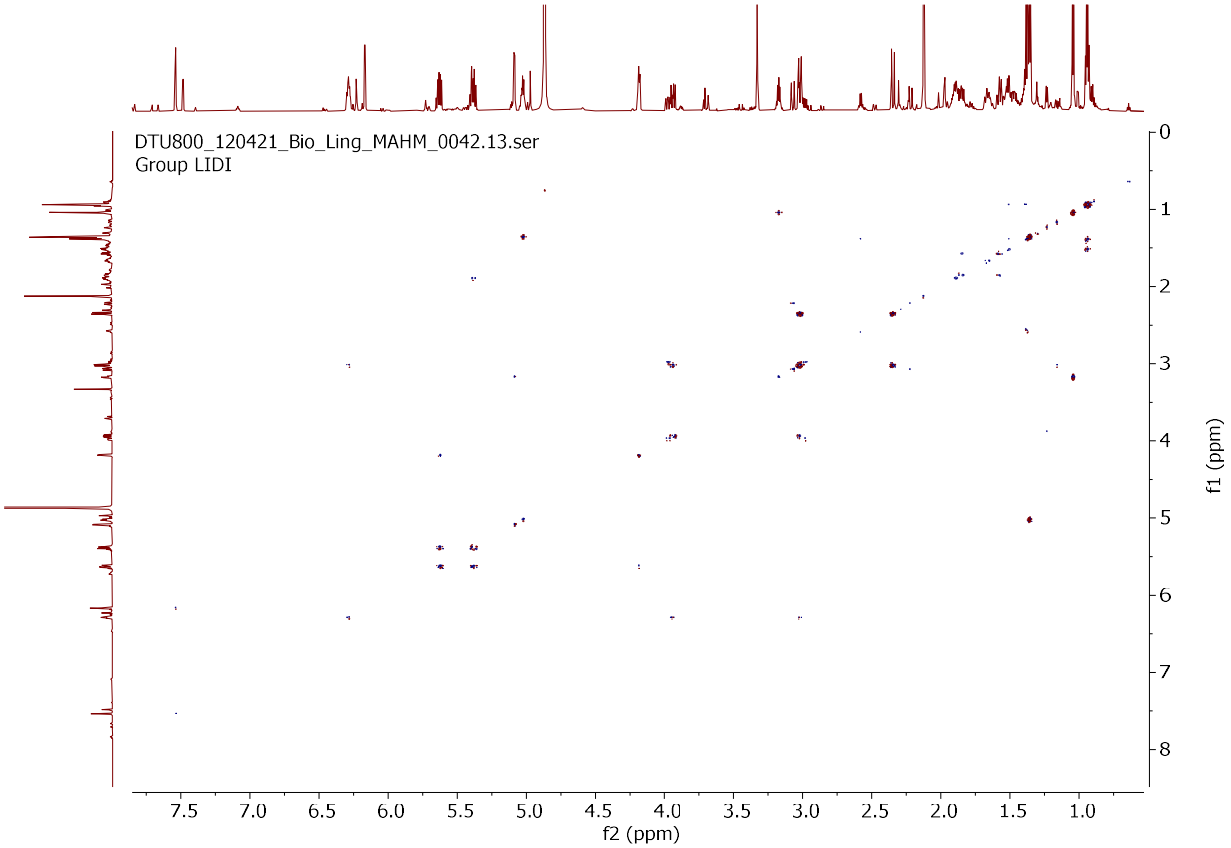

Figure S18. DQF-COSY spectrum of **2** in CD_3OD.

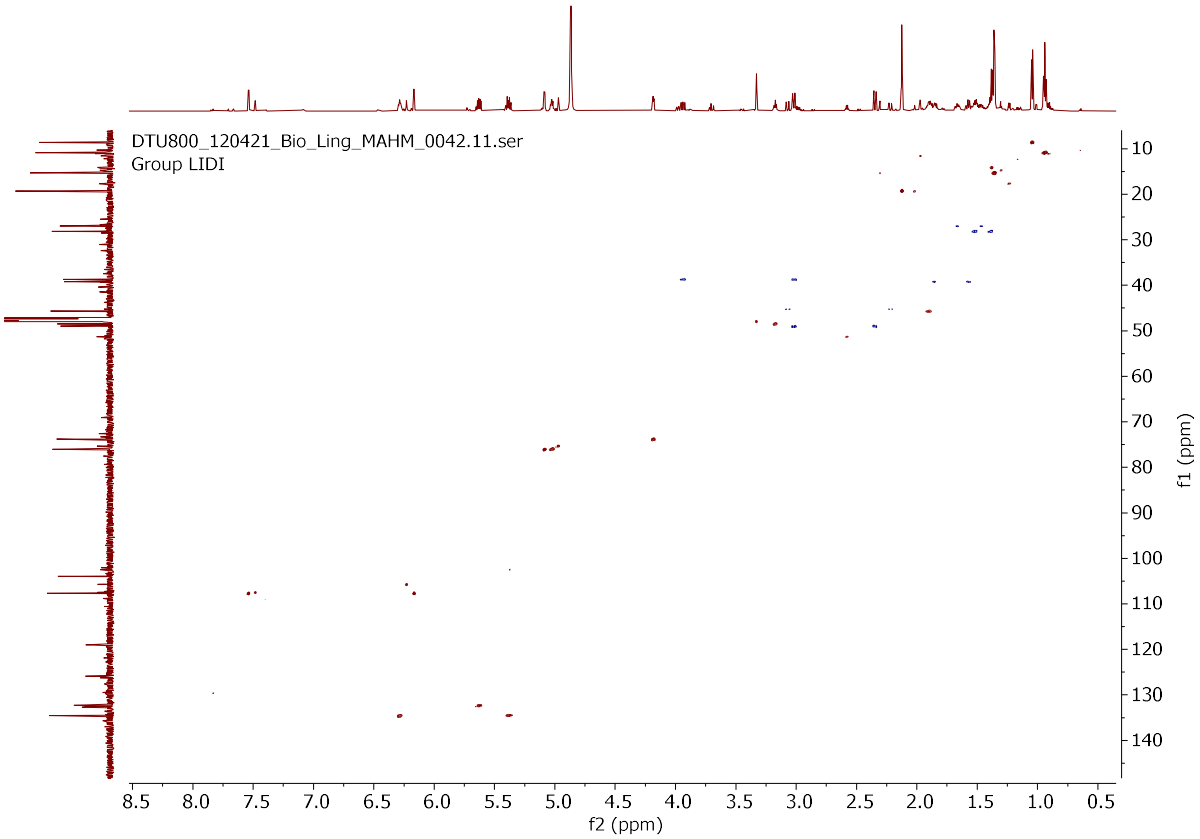

Figure S19. HSQC spectrum of **2** in CD_3OD.

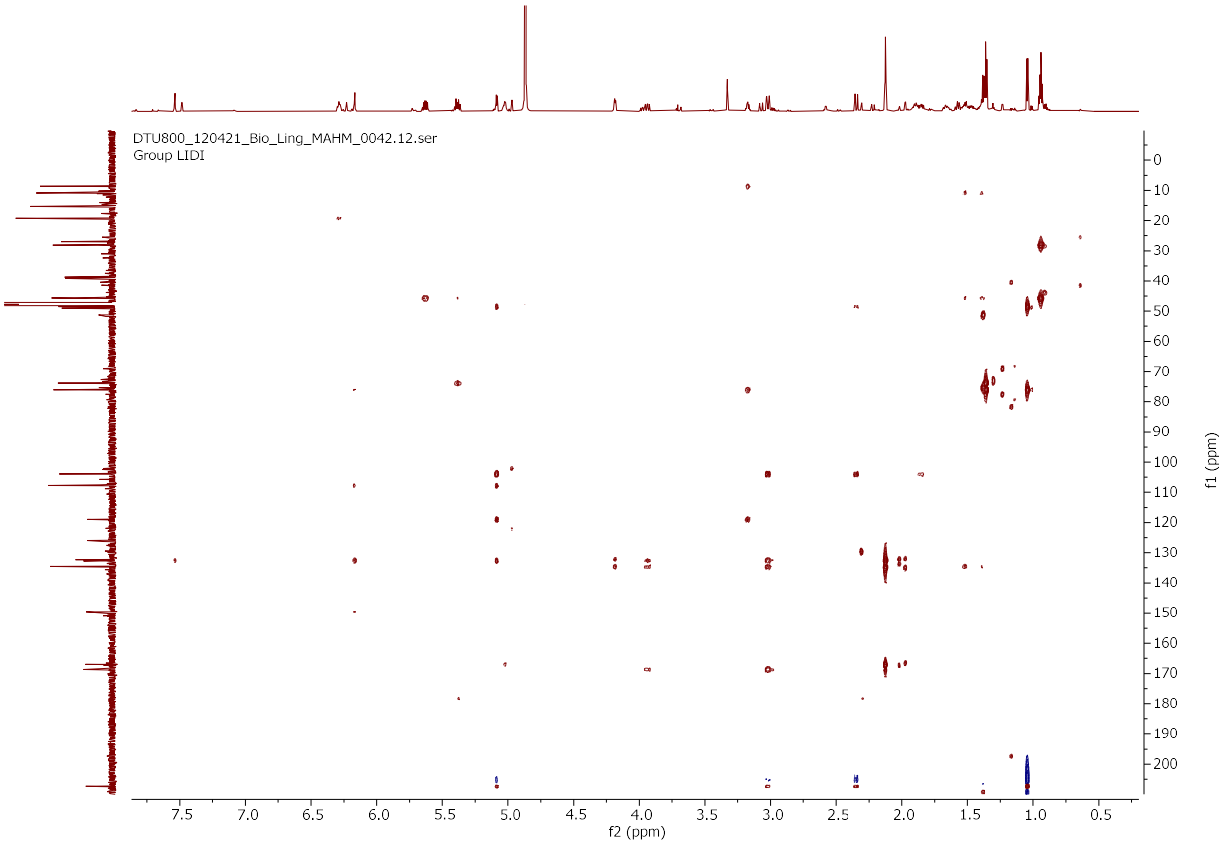

Figure S20. HMBC spectrum of **2** in CD_3OD.

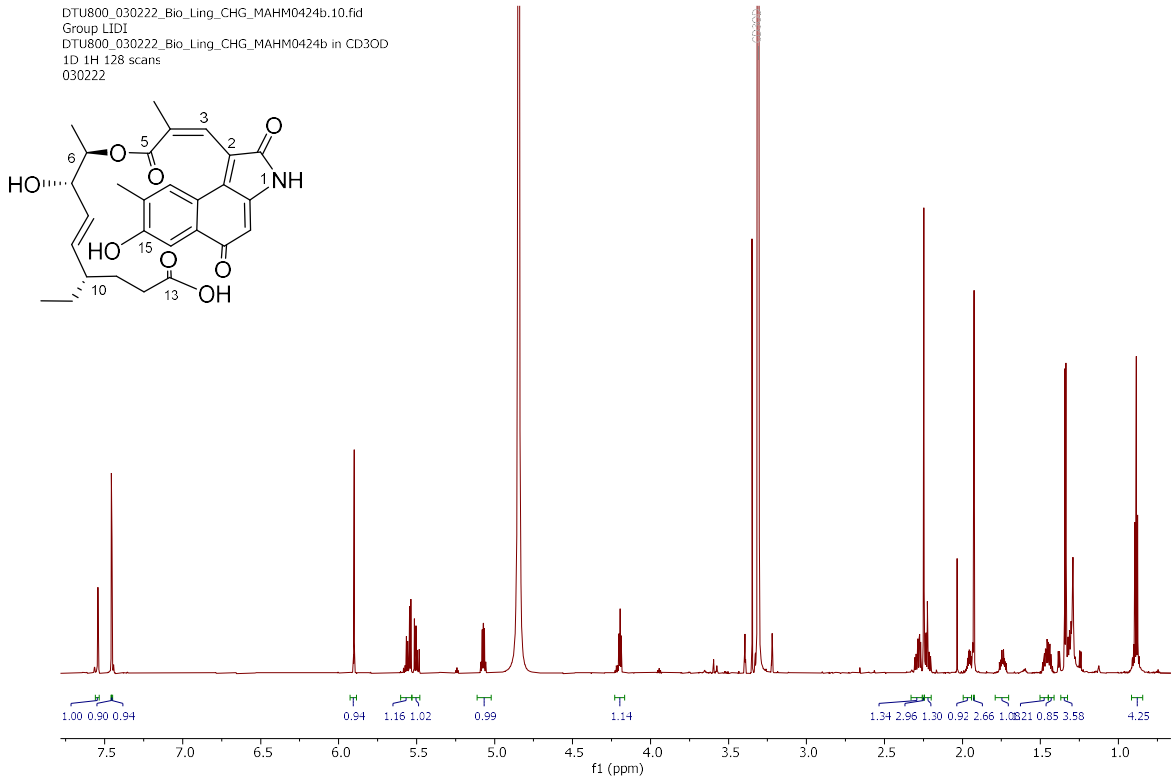

Figure S21. ^{1}H NMR (800 MHz) spectrum of **3** in CD_3OD.

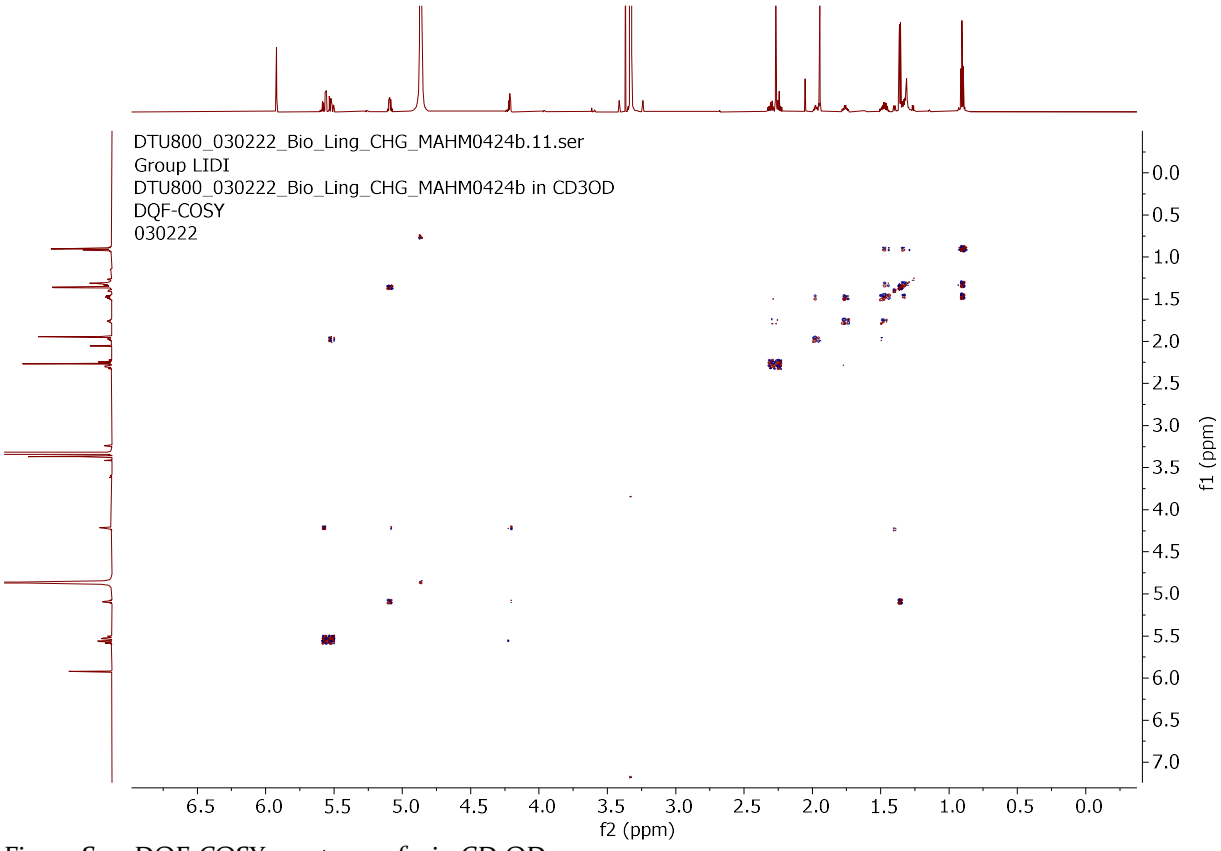

Figure S22. DQF-COSY spectrum of **3** in CD_3OD.

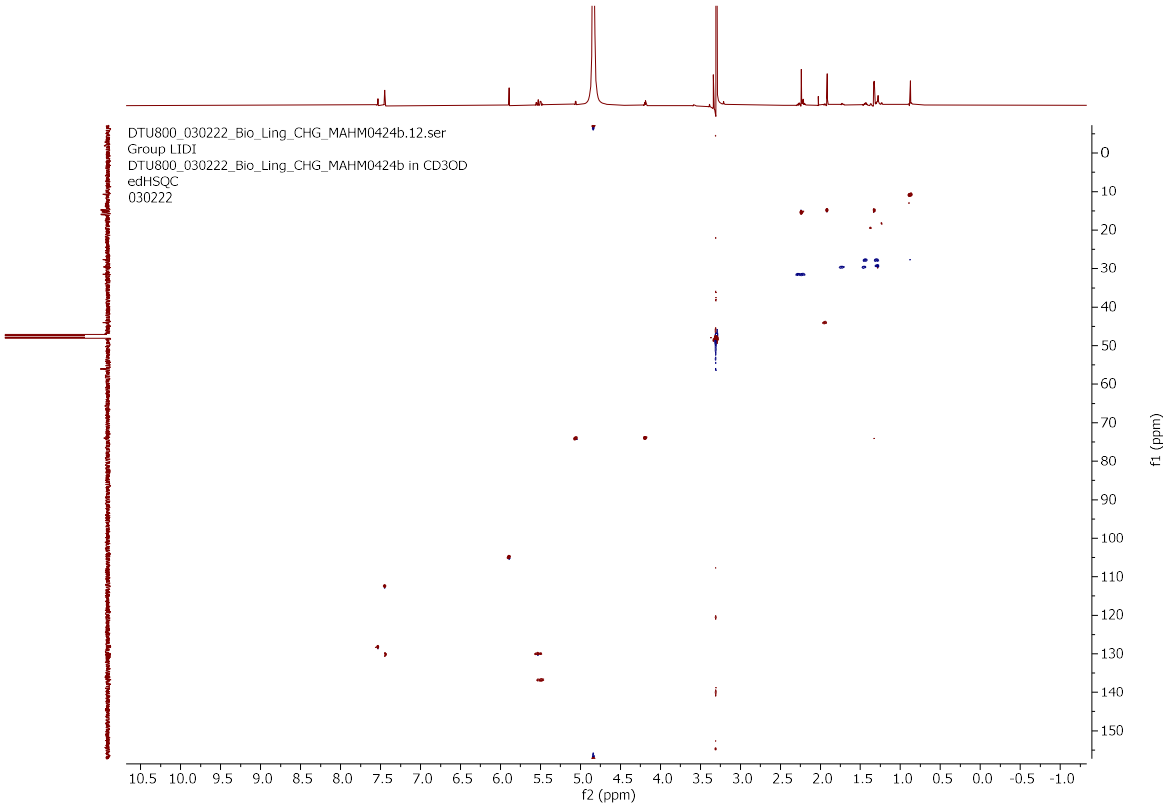

Figure S23. HSQC spectrum of **3** in CD_3OD.

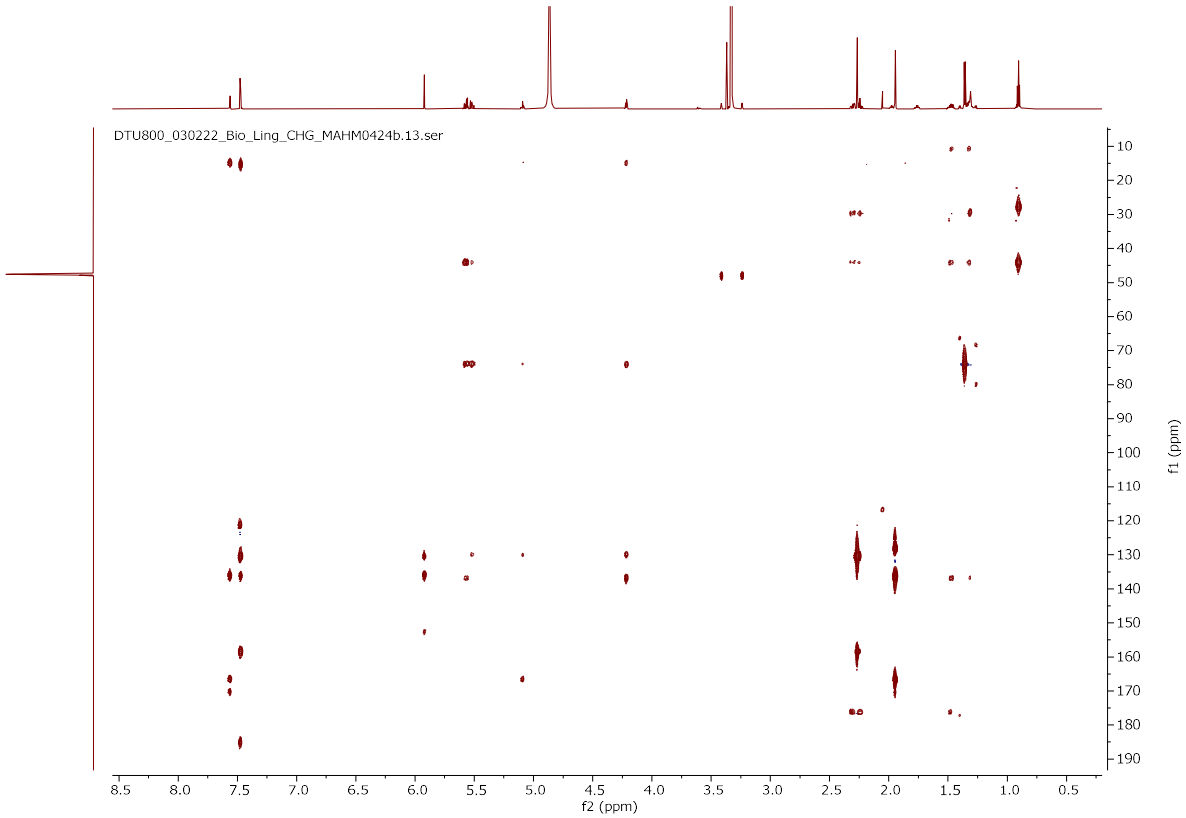

Figure S24. HMBC spectrum of **3** in CD_3OD.

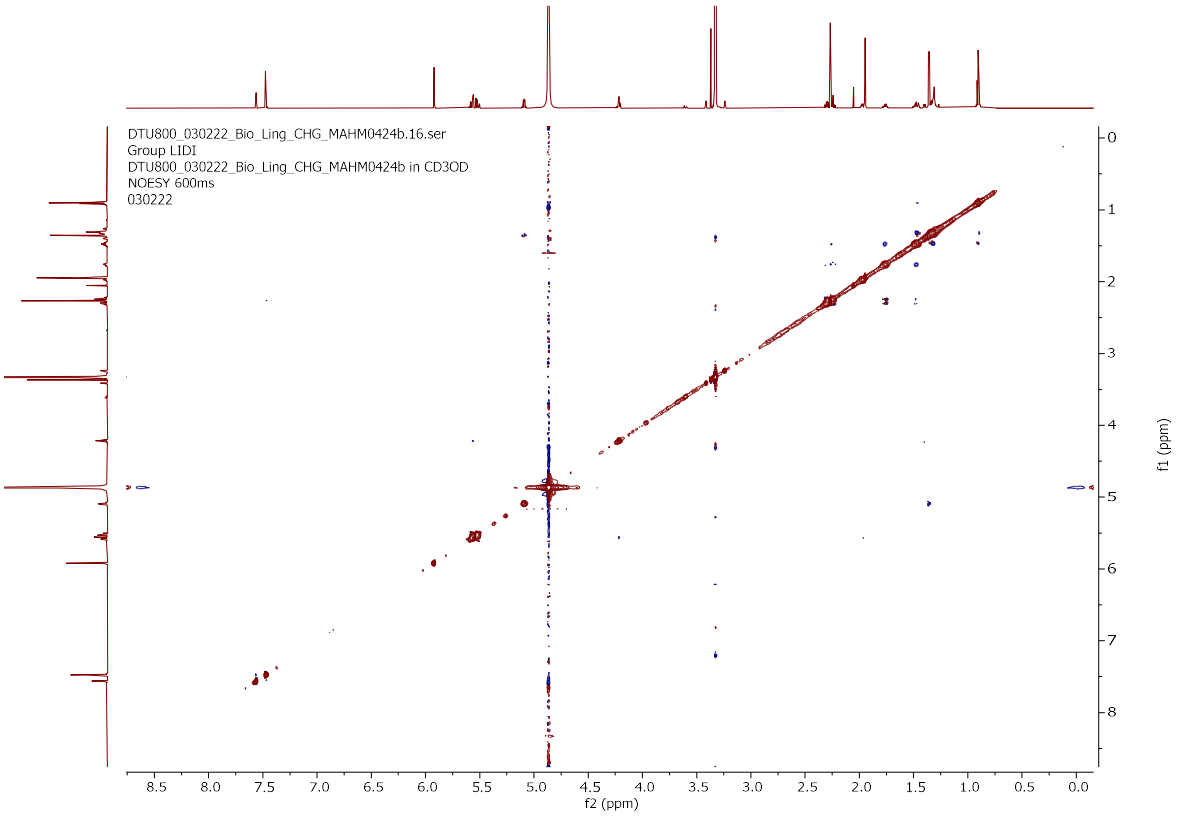

Figure S25. NOESY spectrum of **3** in CD_3OD.

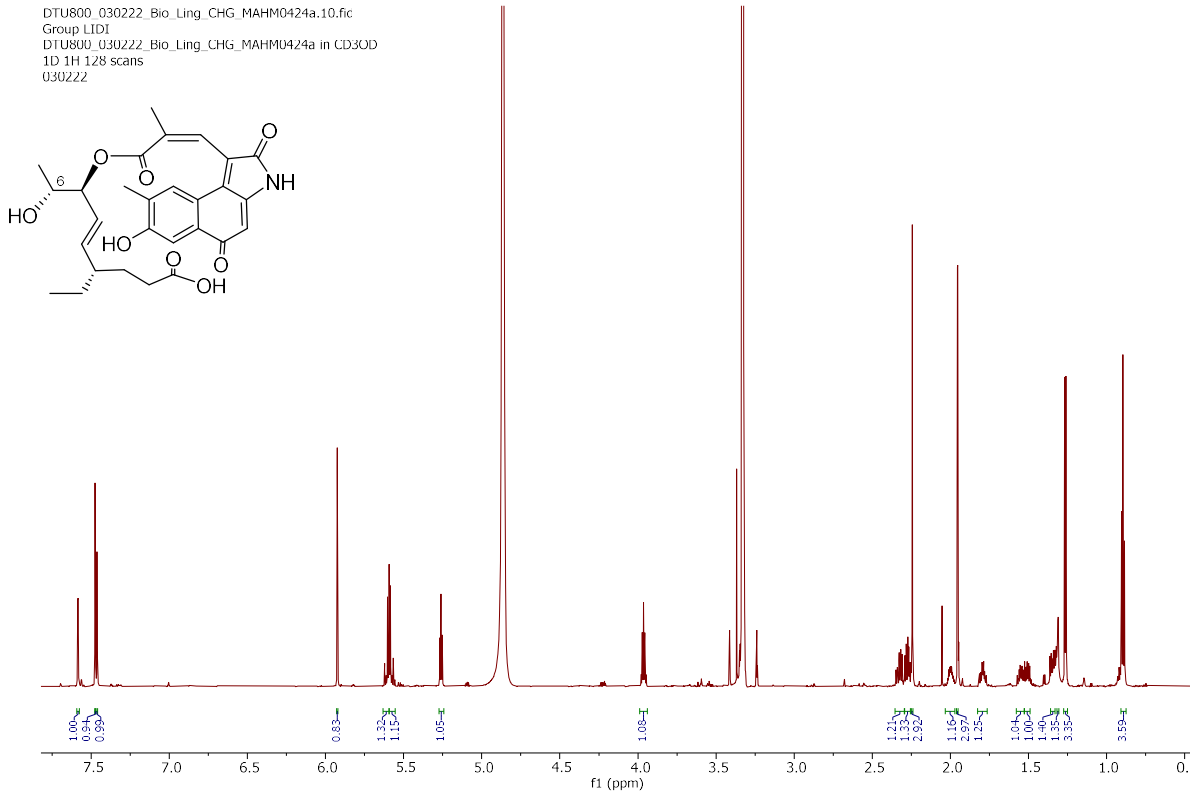

Figure S26. ^1H NMR (800 MHz) spectrum of **4** in CD_3OD.

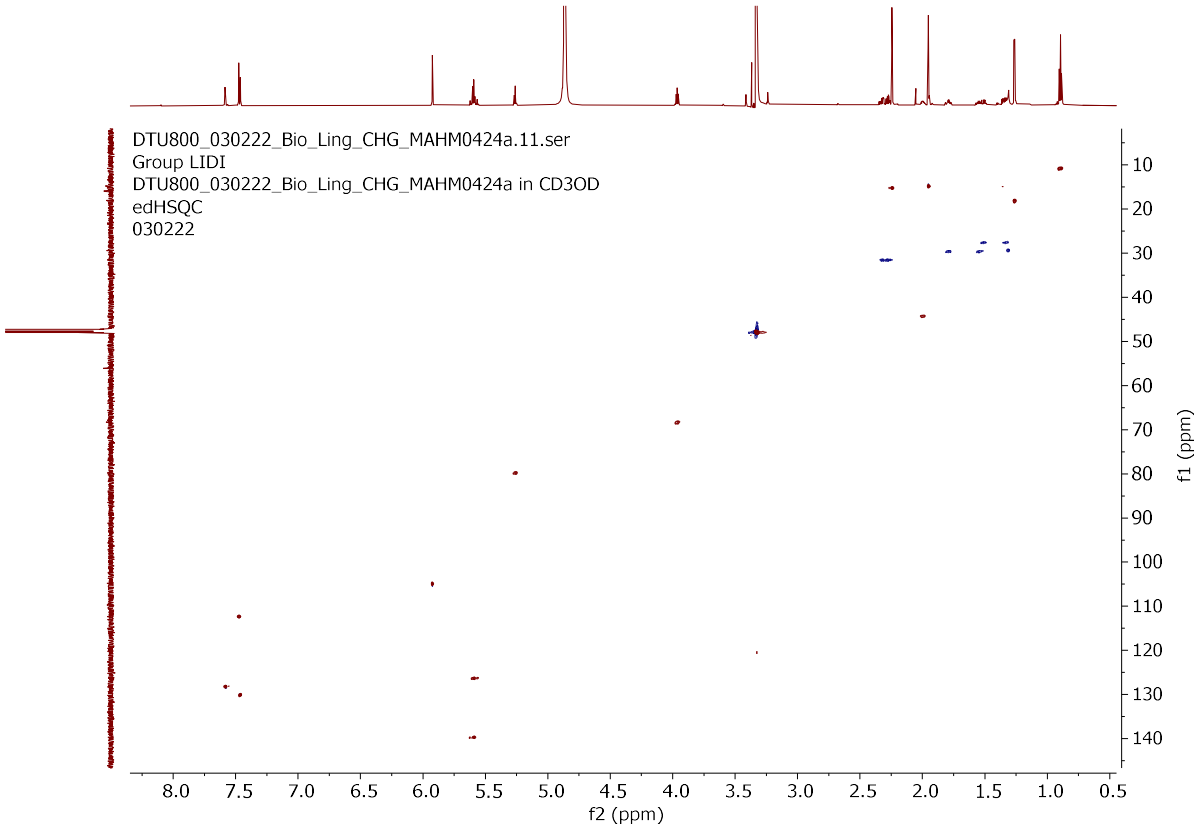

Figure S27. HSQC spectrum of **4** in CD_3OD.

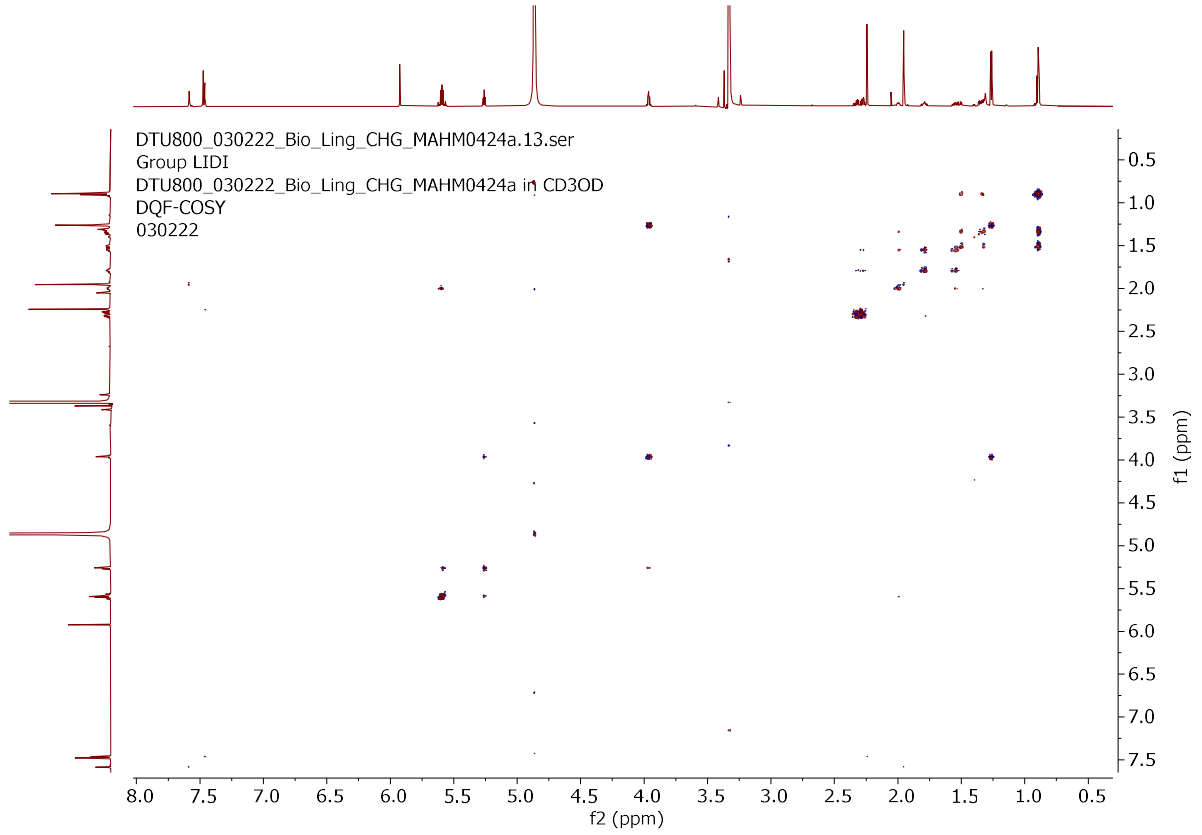

Figure S28. DQF-COSY spectrum of **4** in CD_3OD.

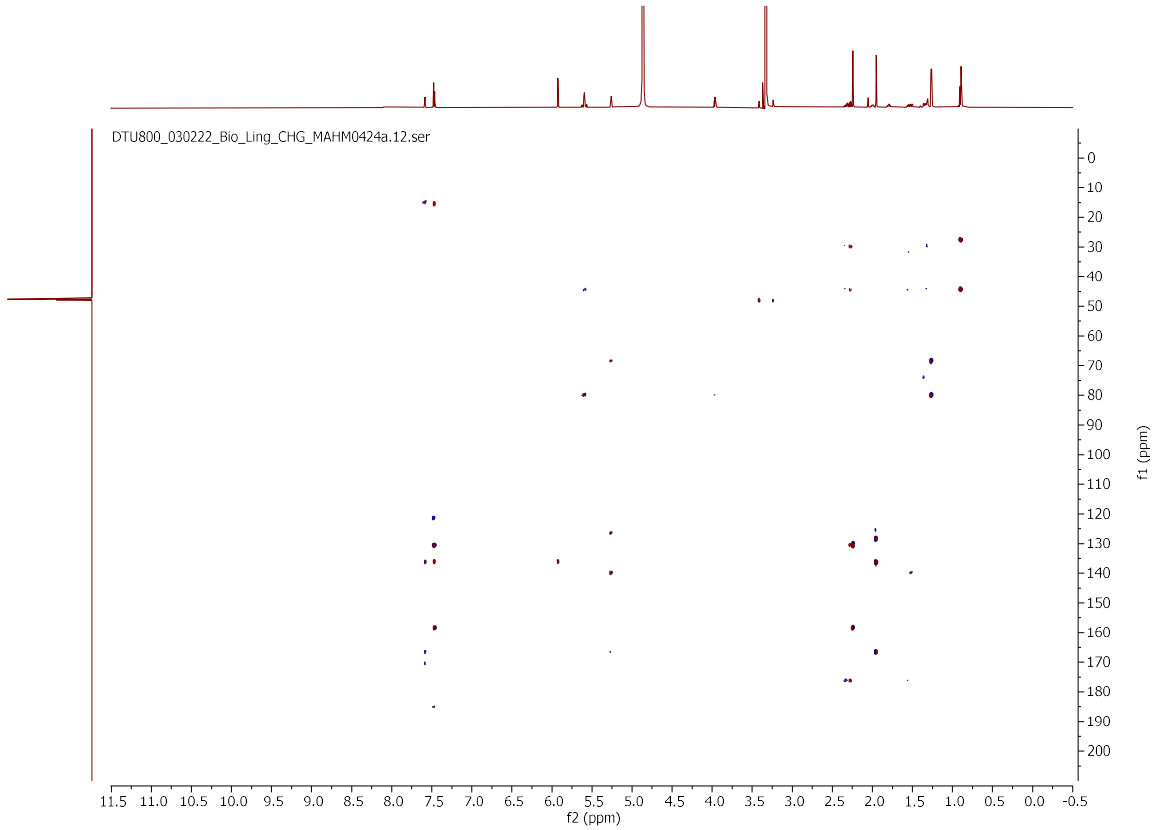

Figure S29. HMBC spectrum of **4** in CD_3OD.

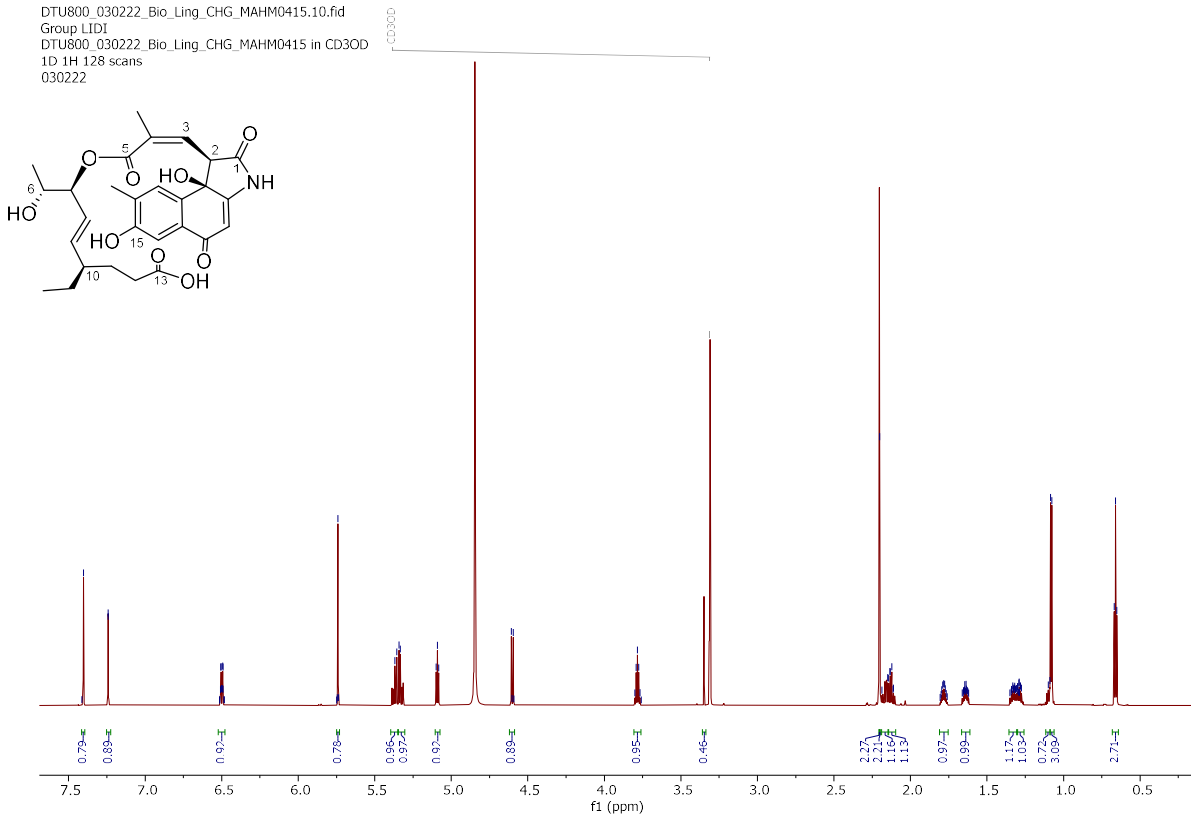

Figure S30. ^{1}H NMR (800 MHz) spectrum of **5** in CD_3OD.

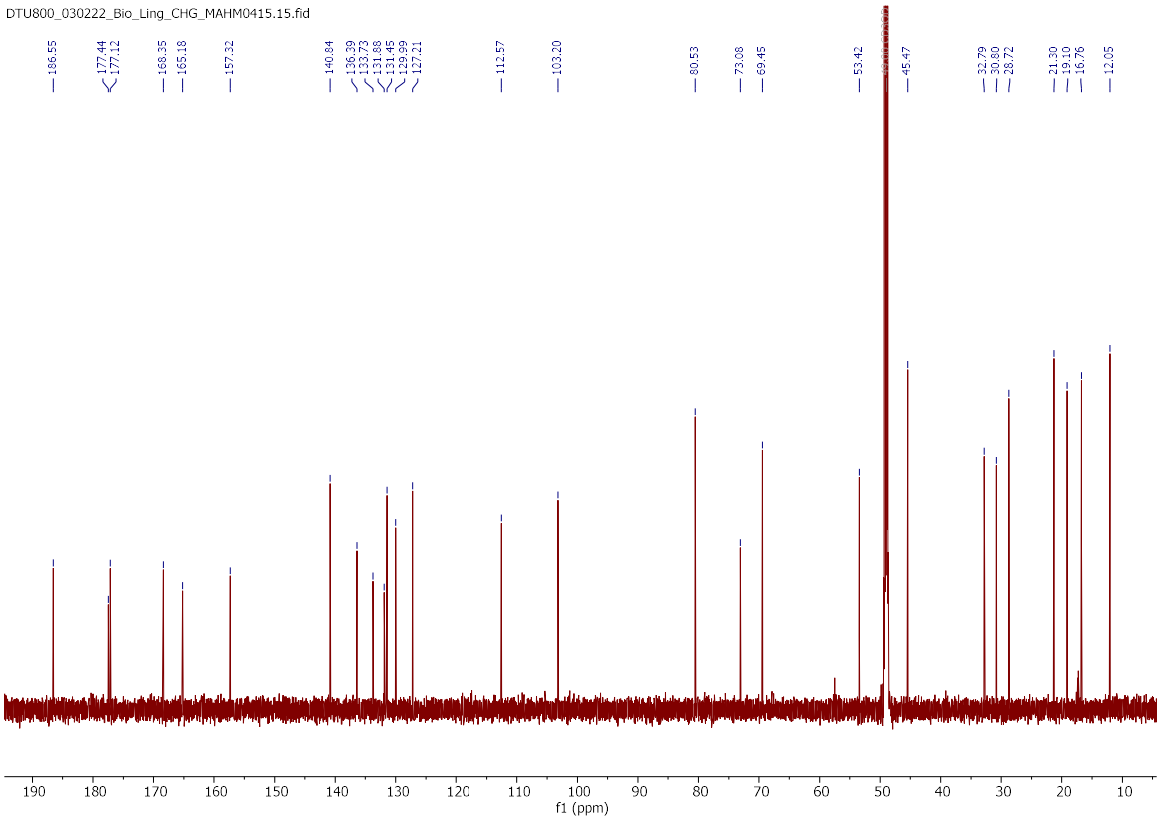

Figure S31. ^{13}C NMR (200 MHz) spectrum of **5** in CD_3OD.

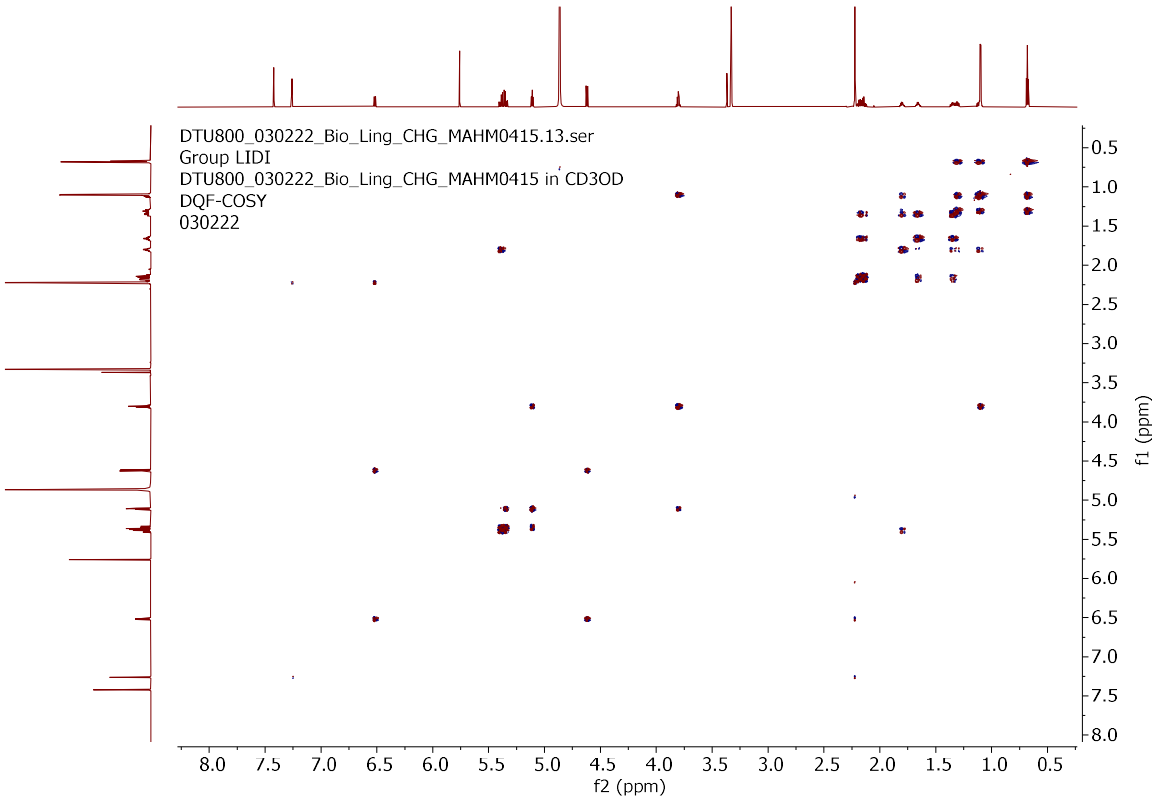

Figure S32. DQF-COSY spectrum of **5** in CD_3OD.

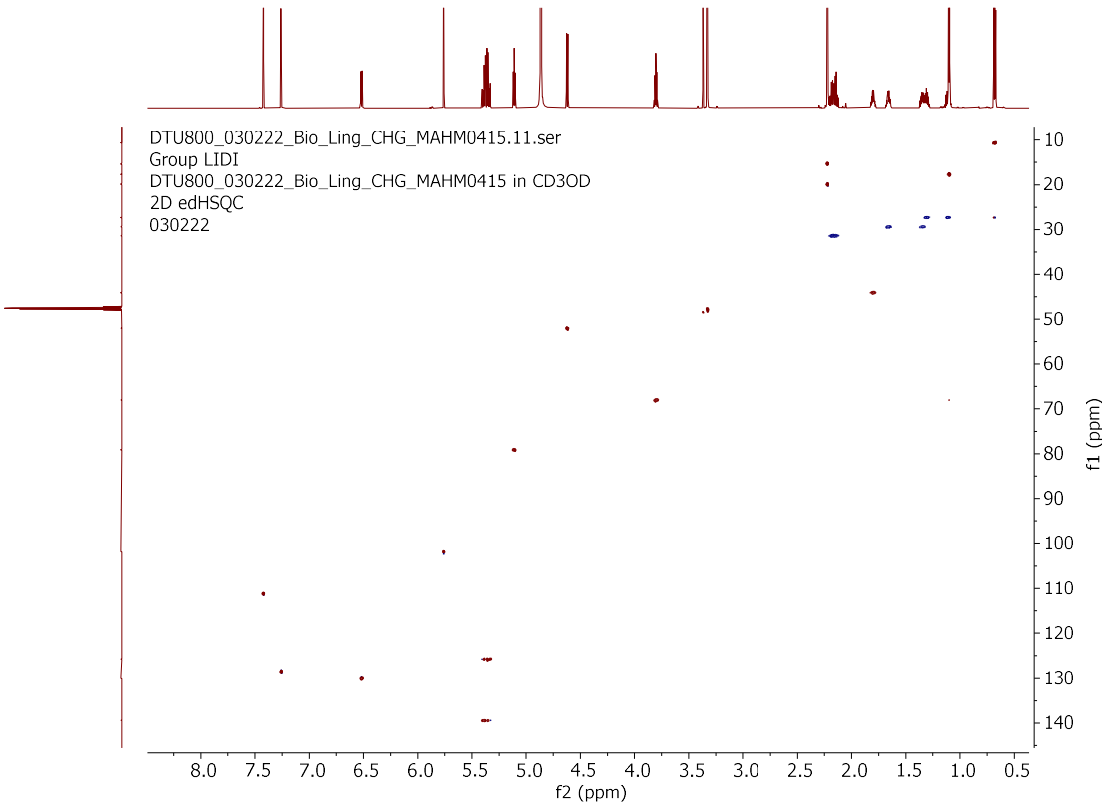

Figure S33. HSQC spectrum of **5** in CD_3OD.

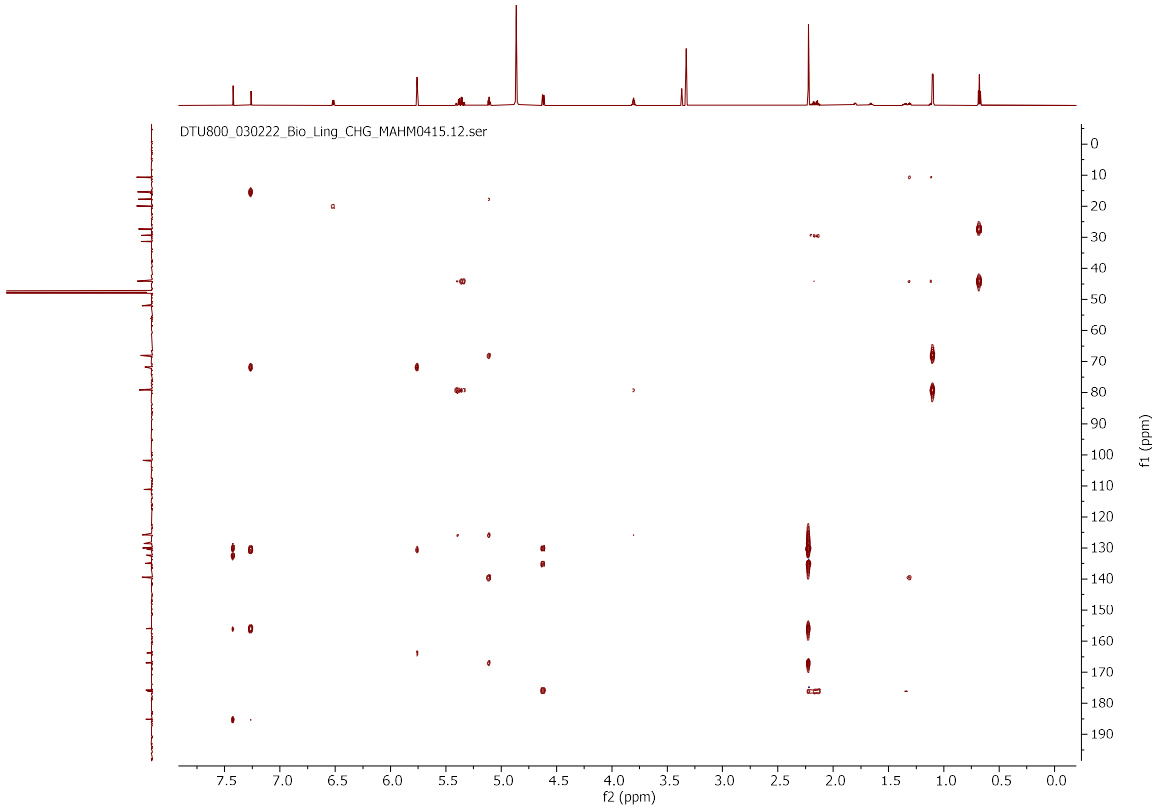

Figure S34. HMBC spectrum of **5** in CD_3OD.

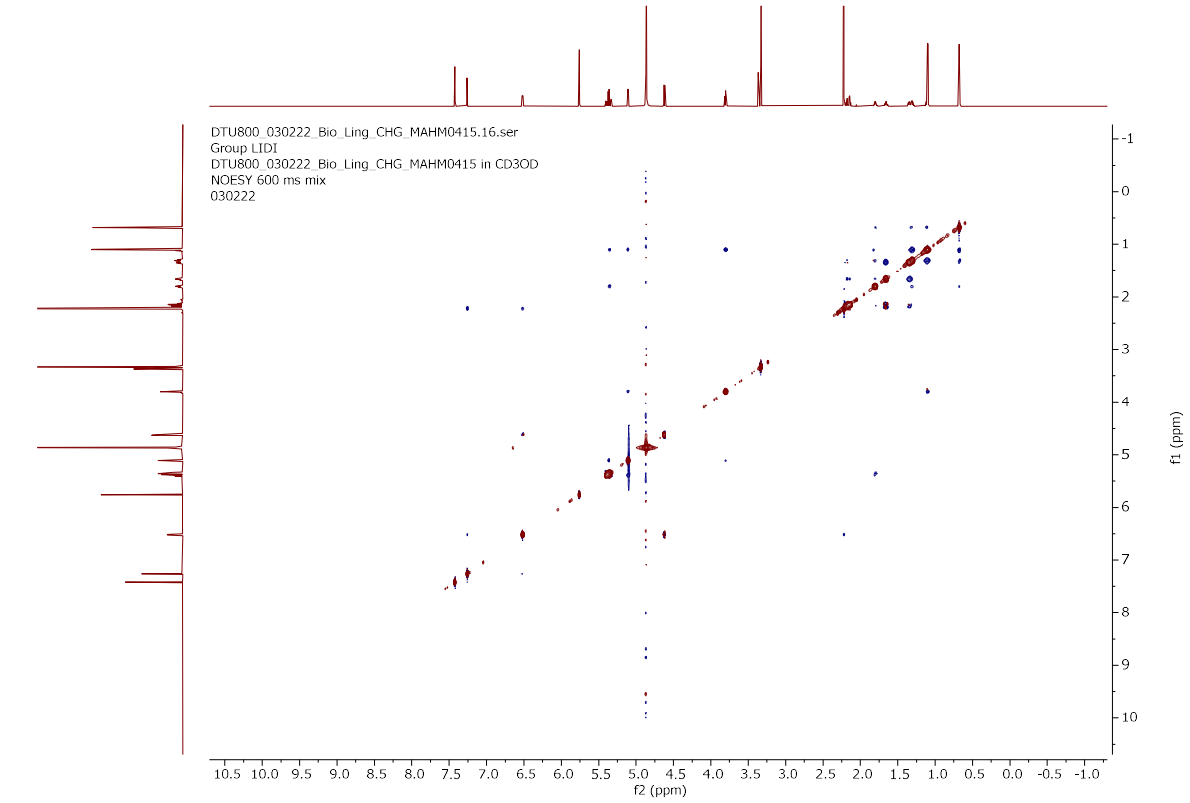

Figure S35. NOESY spectrum of **5** in CD_3OD.

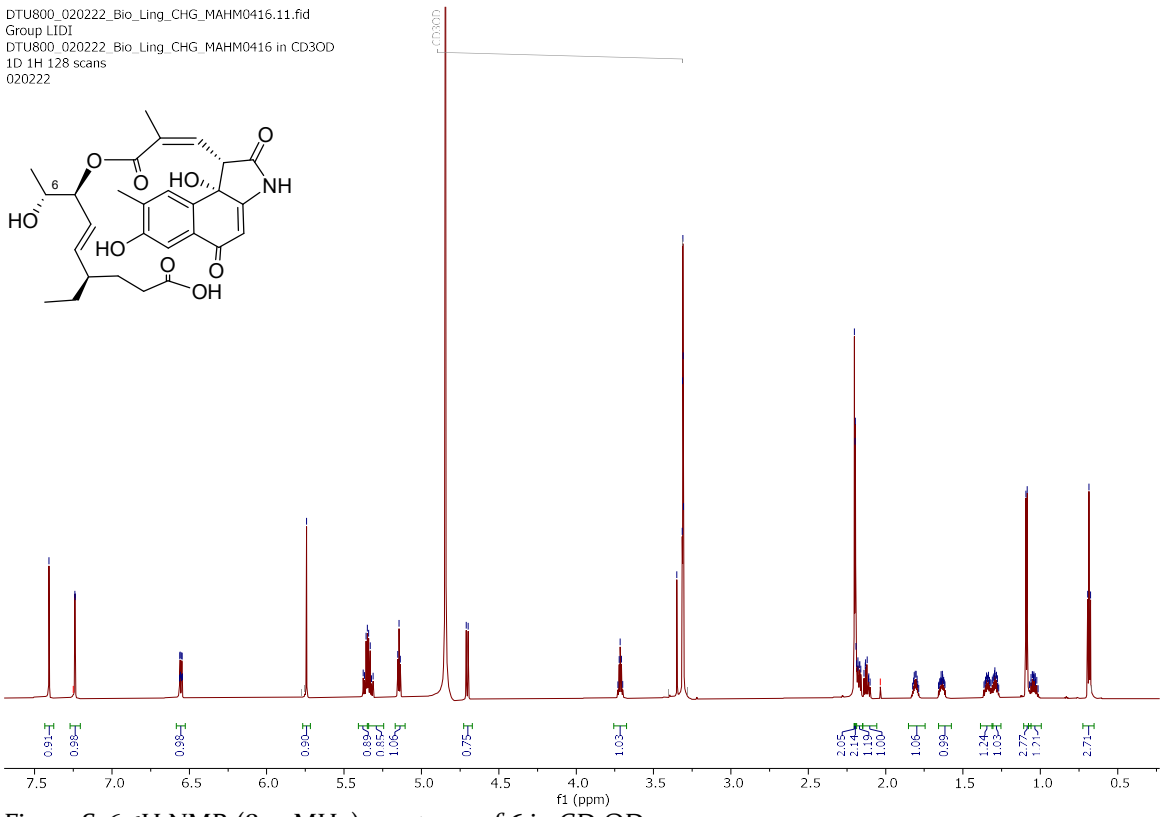

Figure S36. ^{1}H NMR (800 MHz) spectrum of **6** in CD_3OD.

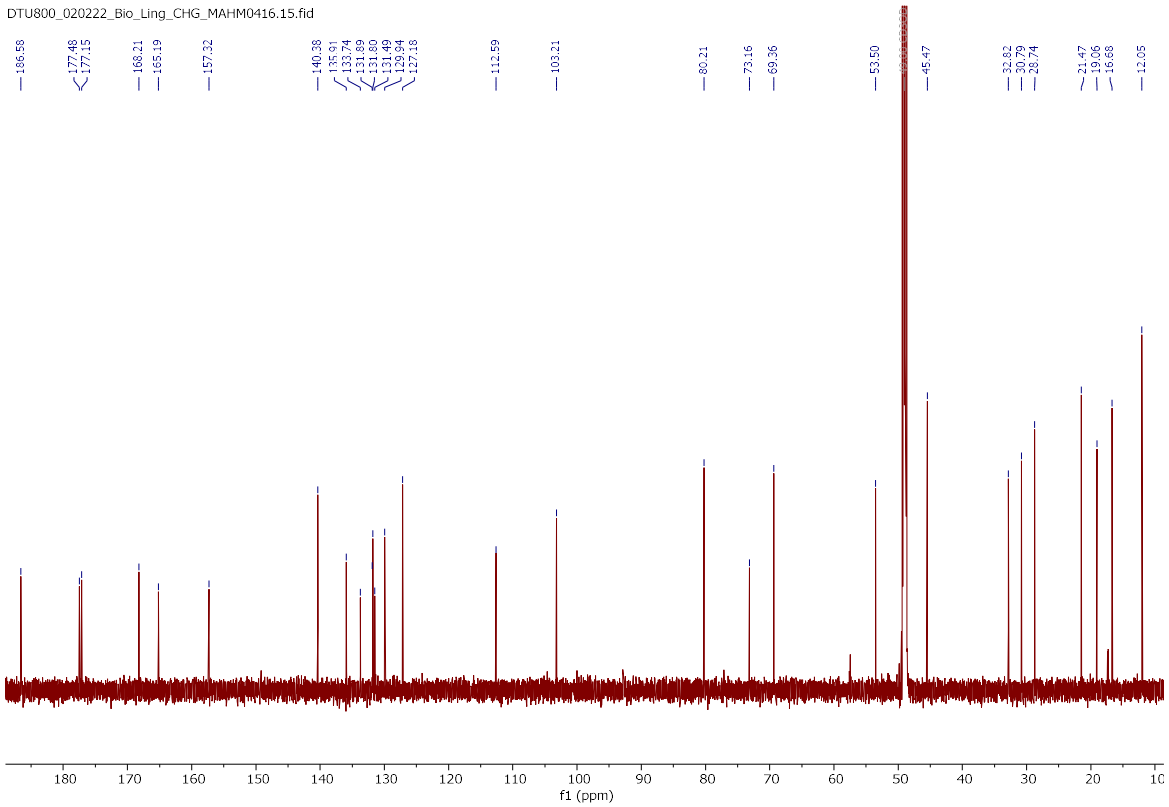

Figure S37. ^{13}C NMR (200 MHz) spectrum of **6** in CD_3OD.

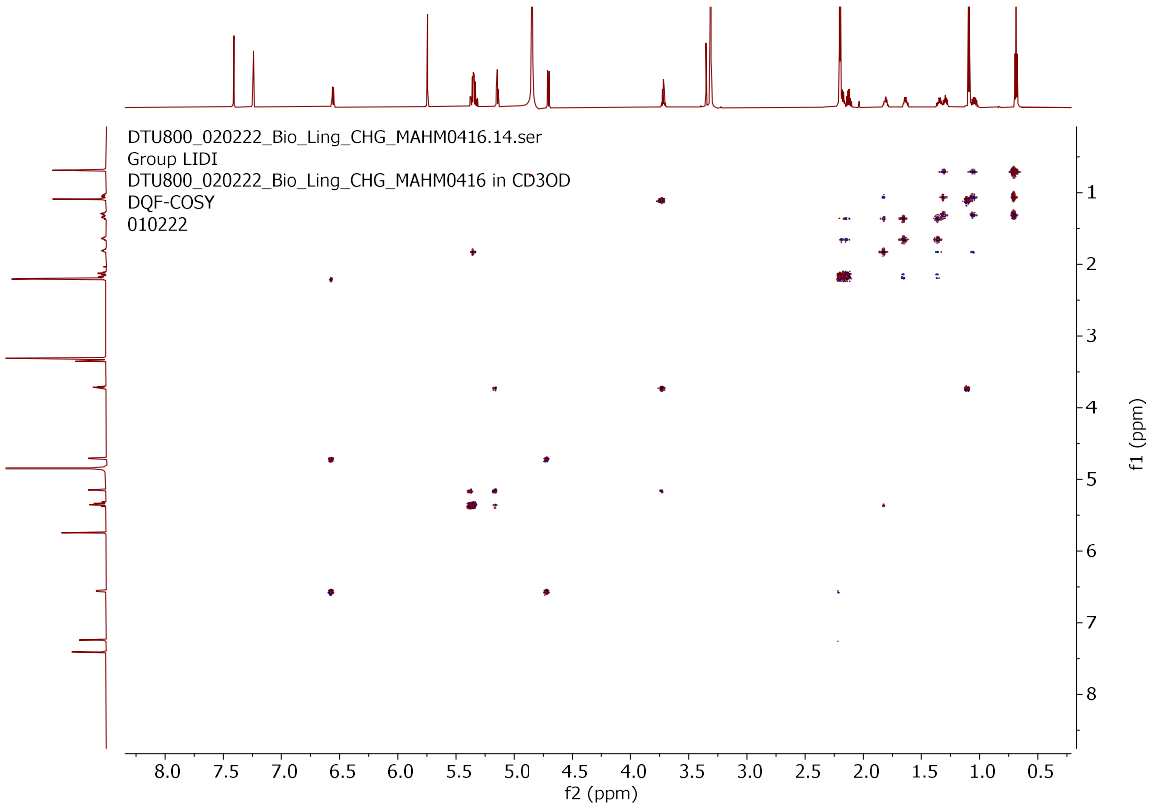

Figure S38. DQF-COSY spectrum of **6** in CD_3OD.

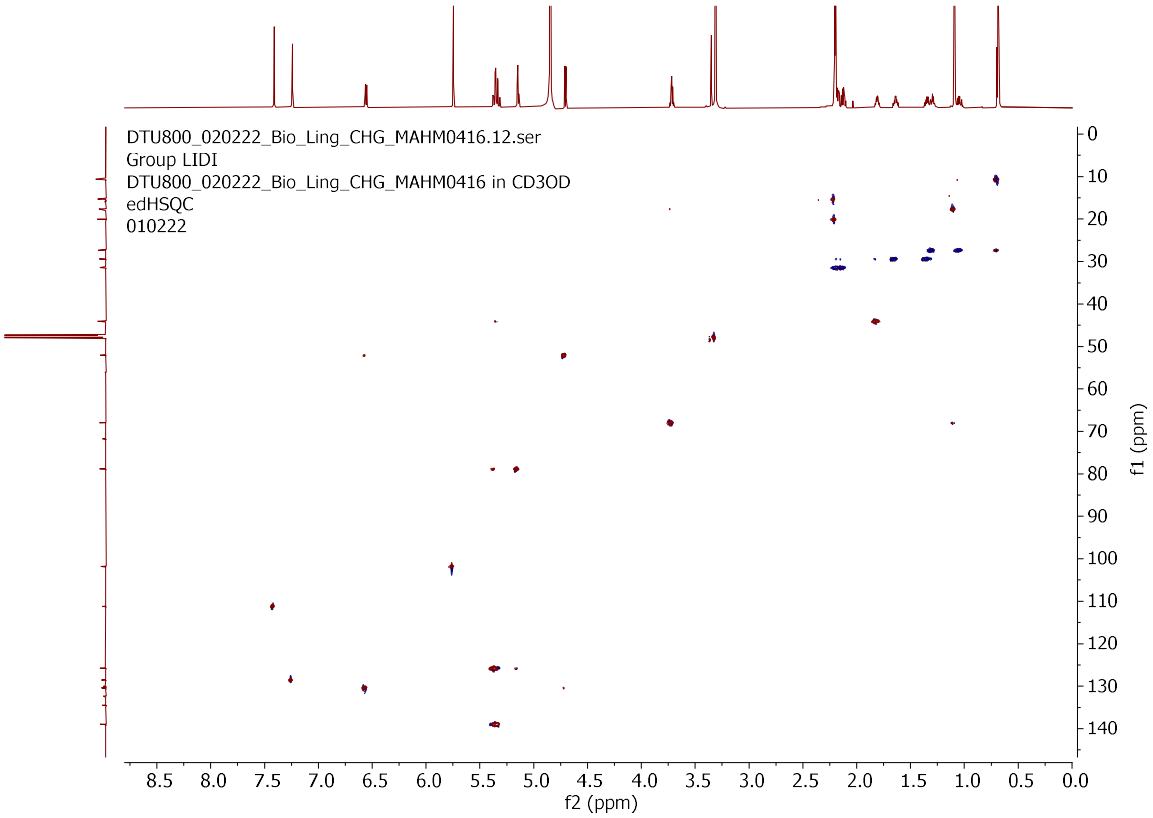

Figure S39. HSQC spectrum of **6** in CD_3OD.

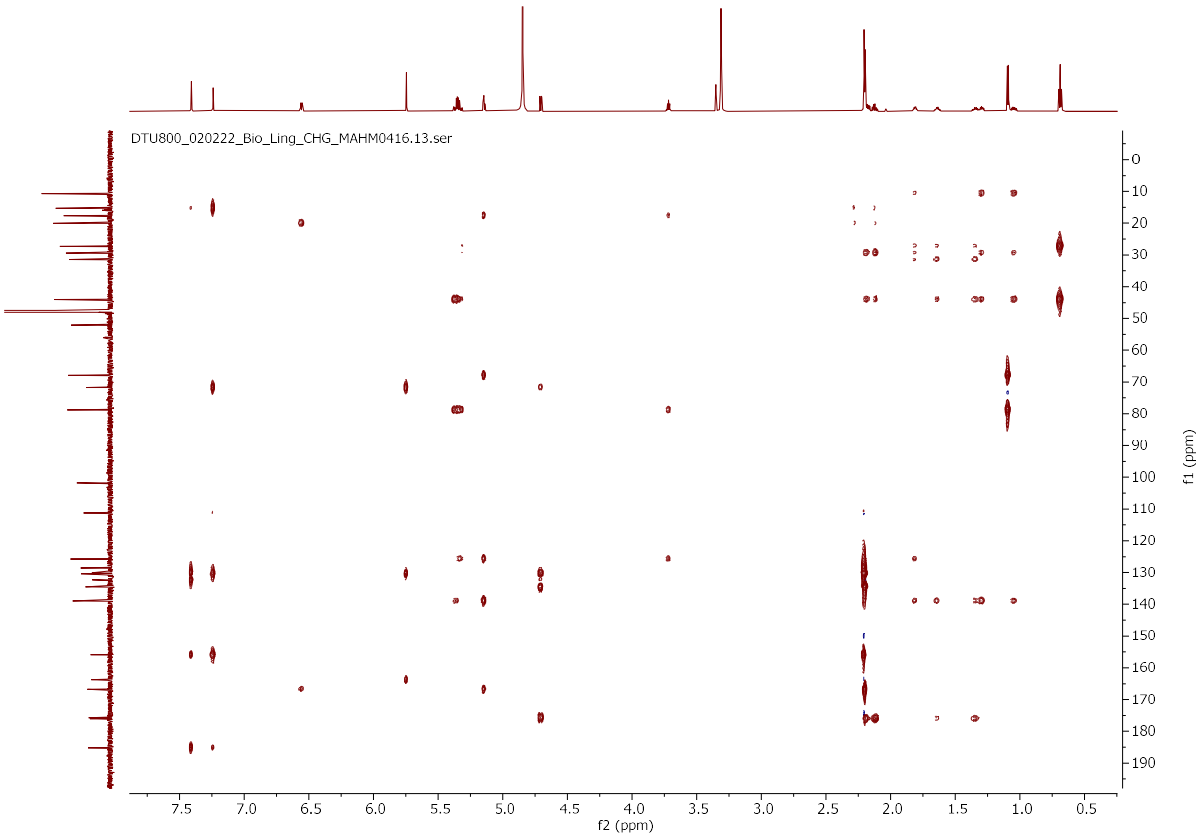

Figure S40. HMBC spectrum of **6** in CD_3OD.

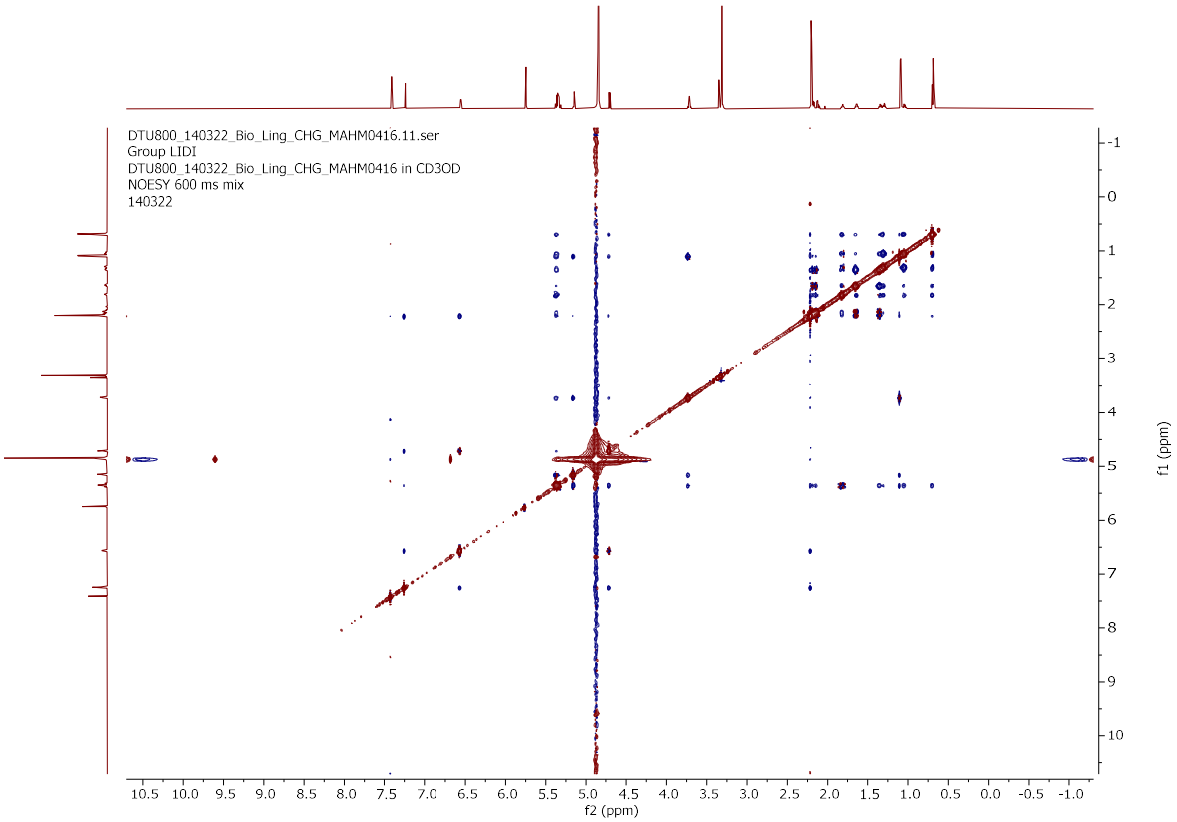

Figure S41. NOESY spectrum of **6** in CD_3OD.

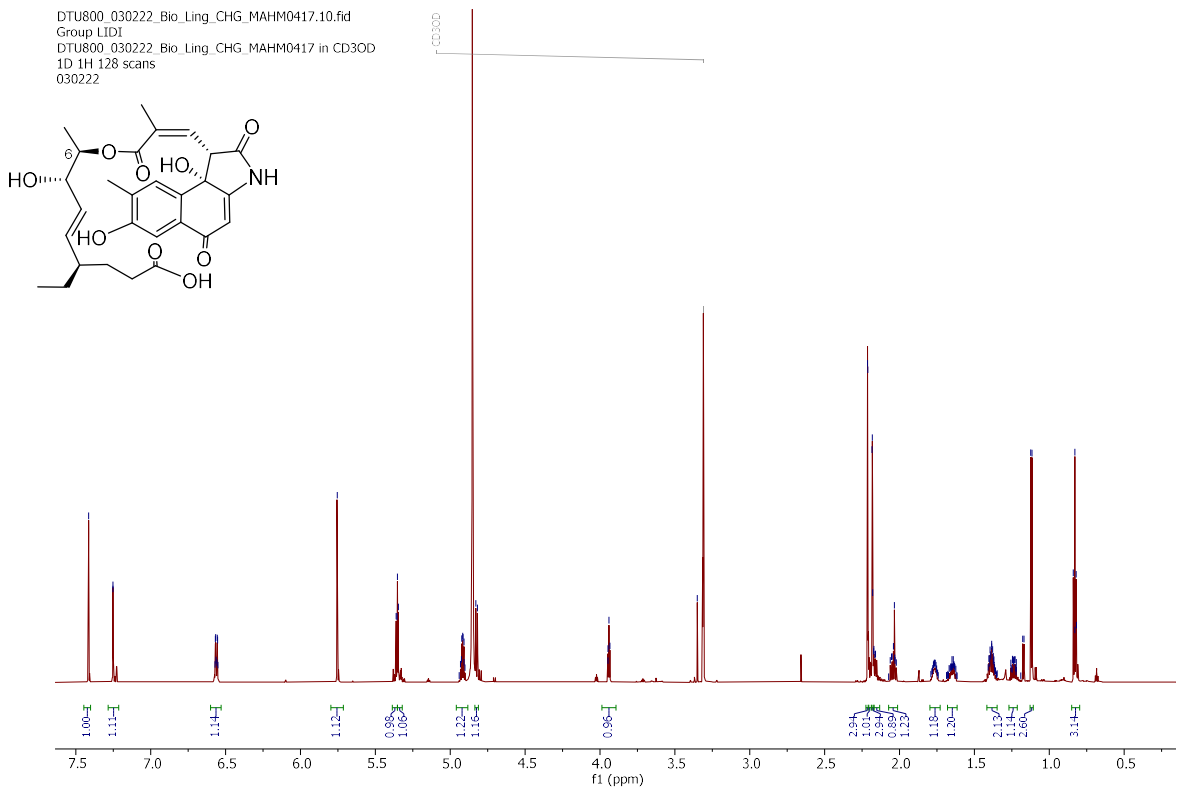

Figure S42. ^{1}H NMR (800 MHz) spectrum of **7** in CD_3OD.

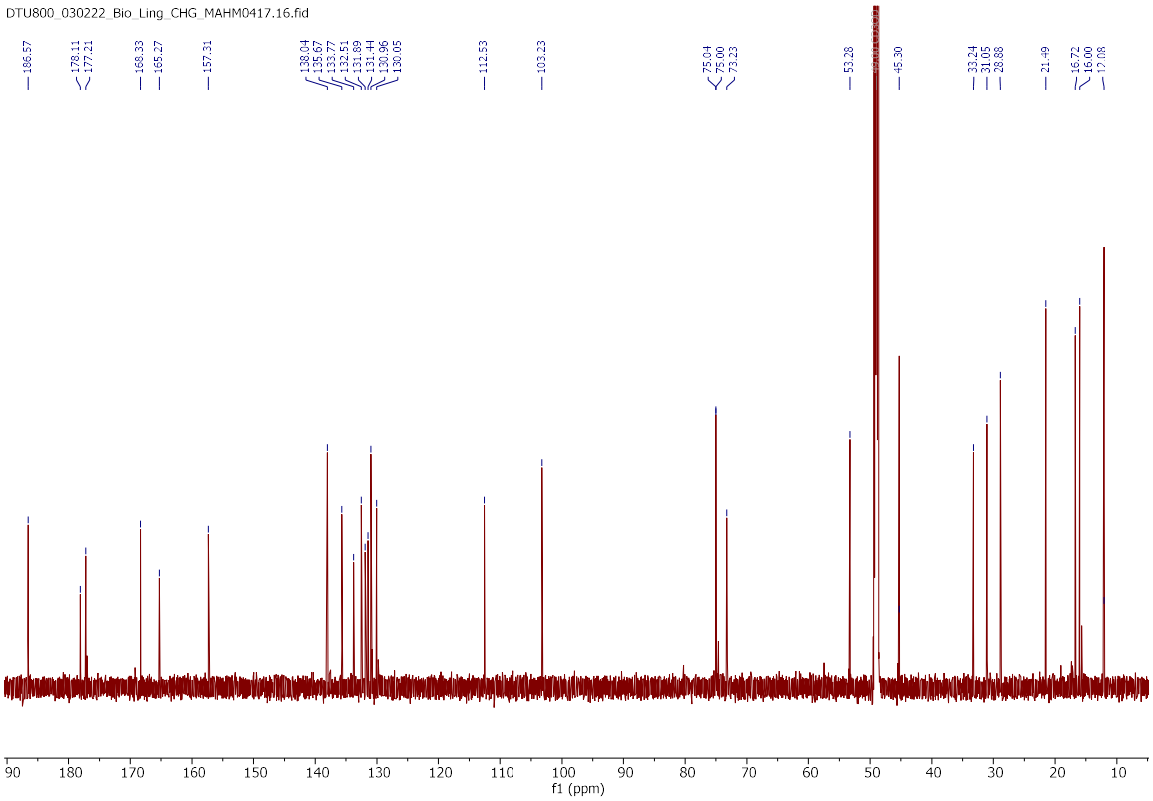

Figure S43. ^{13}C NMR (200 MHz) spectrum of **7** in CD_3OD.

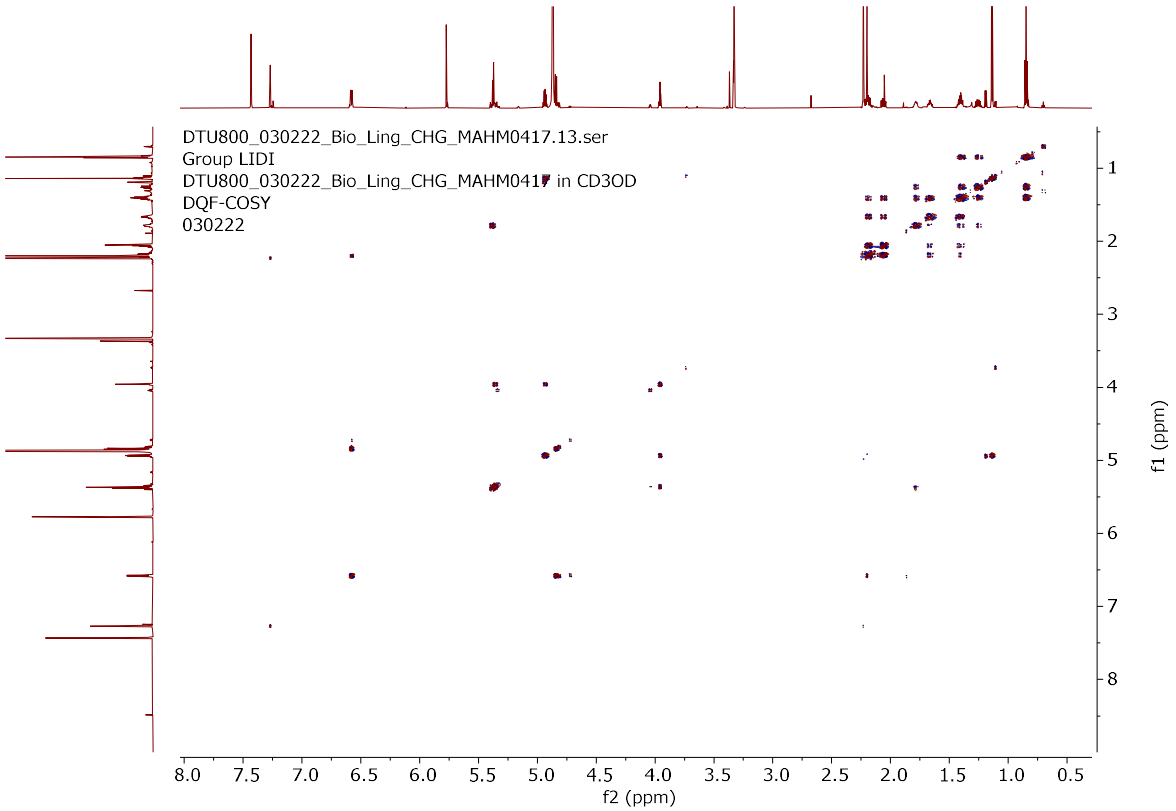

Figure S44. DQF-COSY spectrum of **7** in CD_3OD.

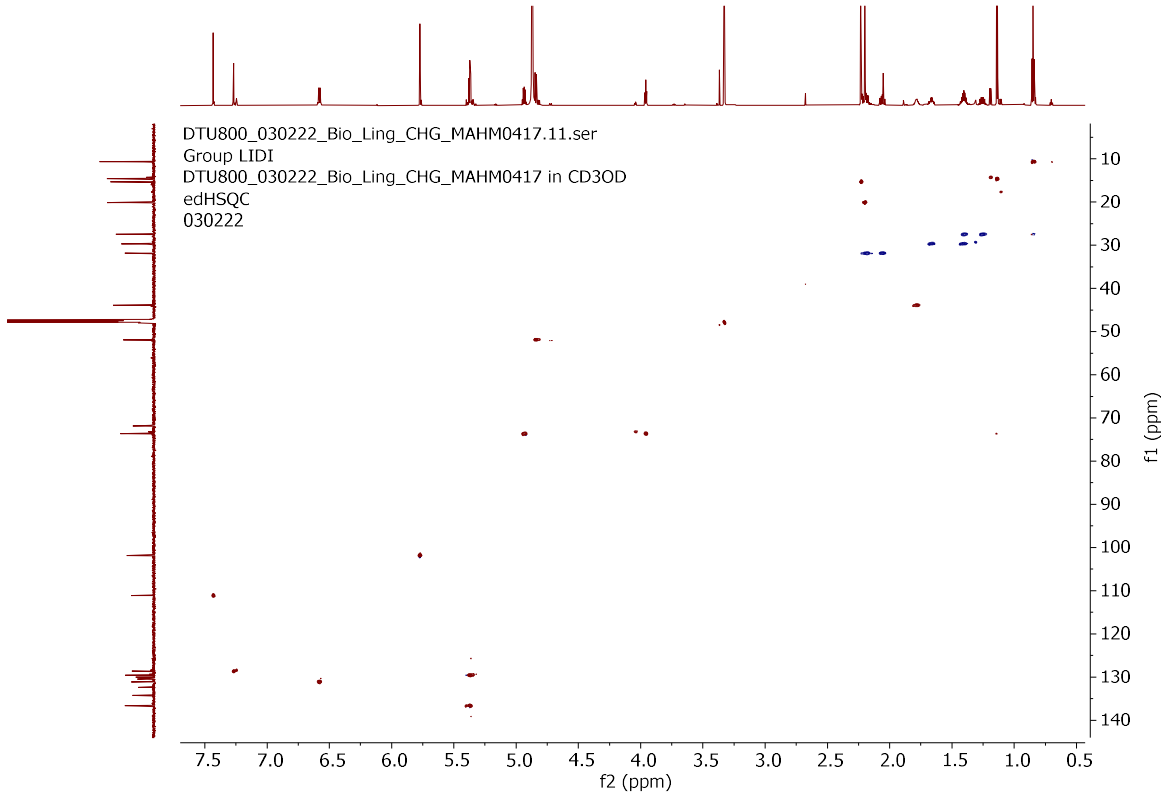

Figure S45. ^{13}HSQC spectrum of **7** in CD_3OD.

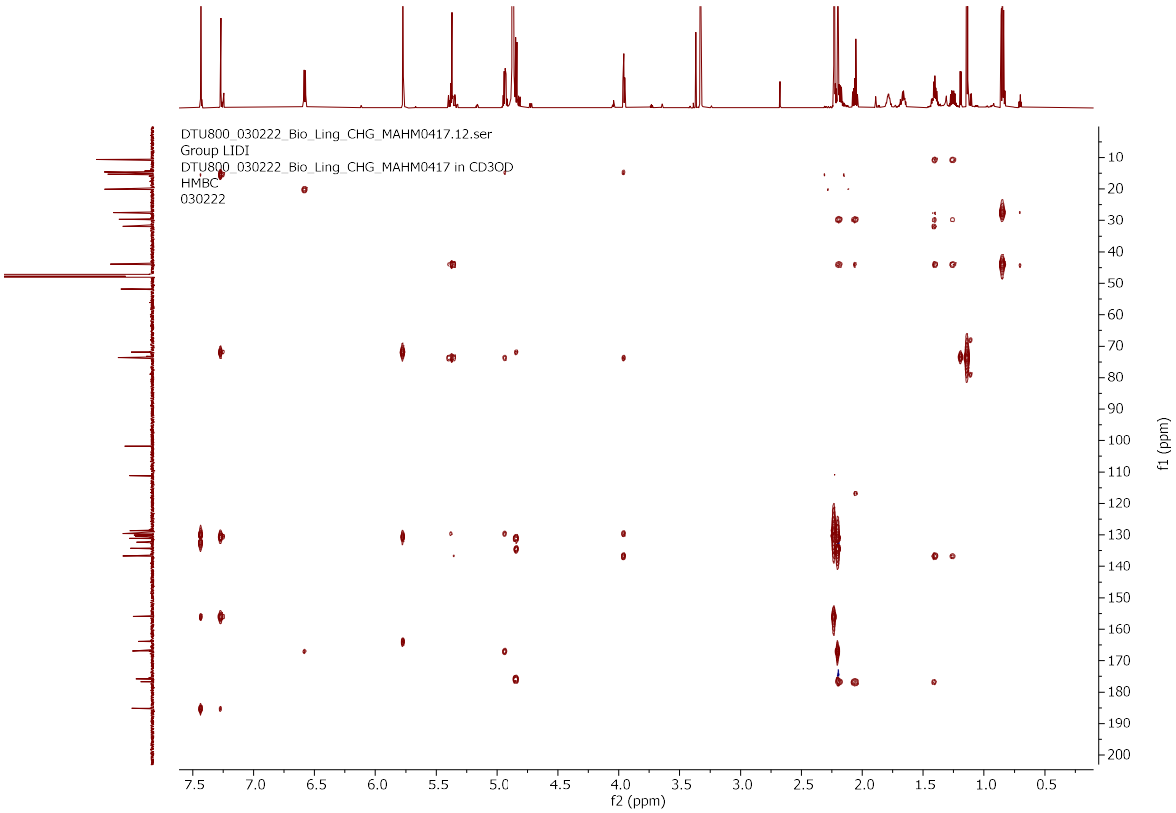

Figure S46. HMBC spectrum of **7** in CD_3OD.

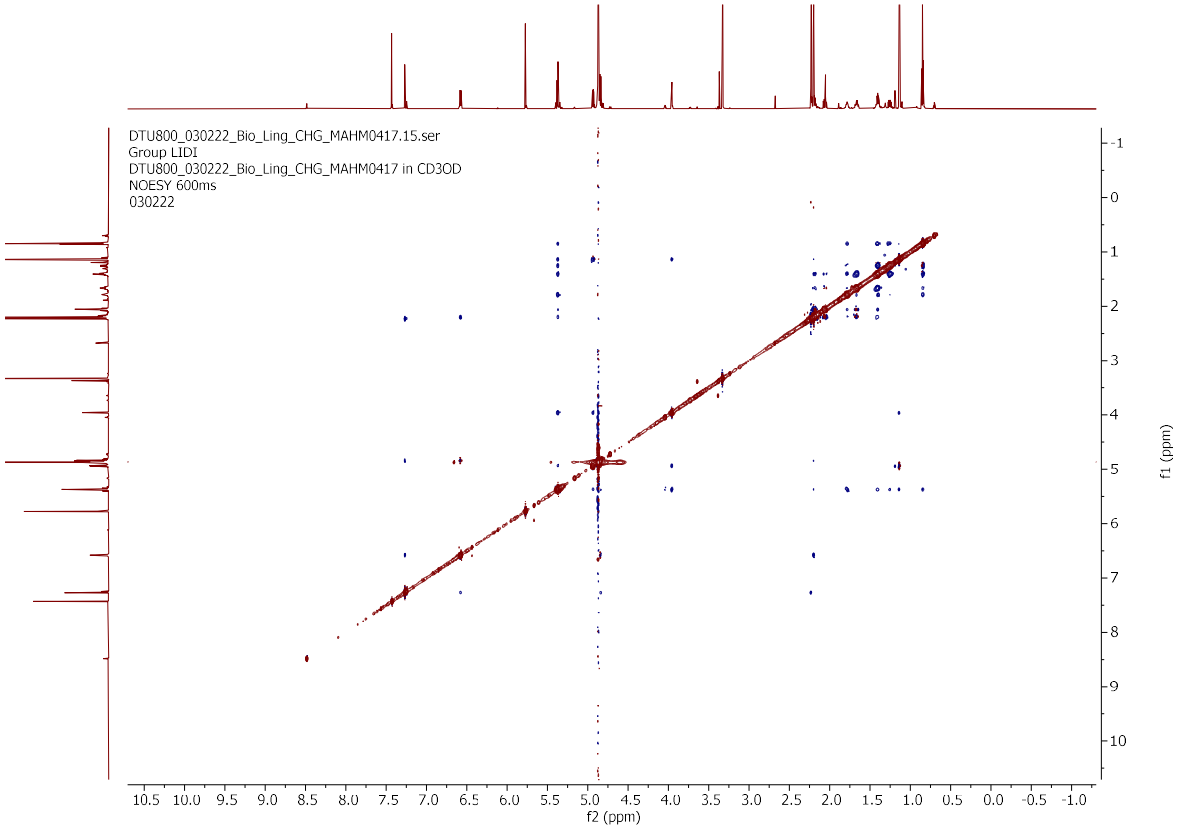

Figure S47. NOESY spectrum of **7** in CD_3OD.

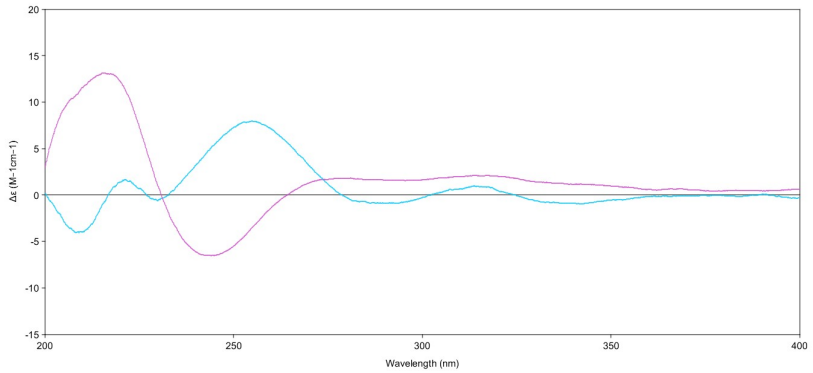

Figure S48. ECD curves of **1** and **2**.

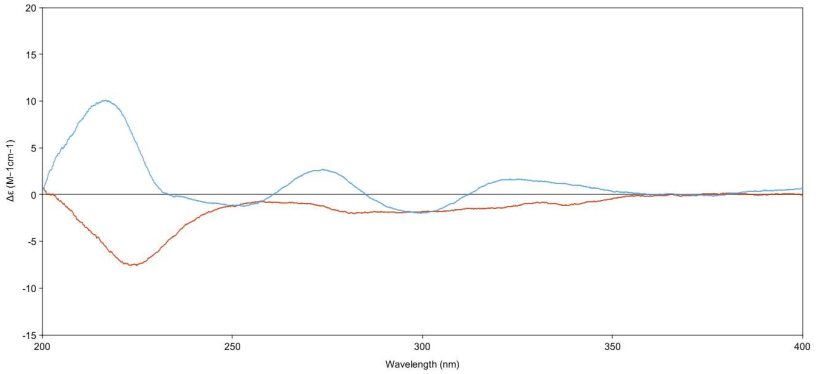

Figure S49. ECD curves of **3** and **4**.

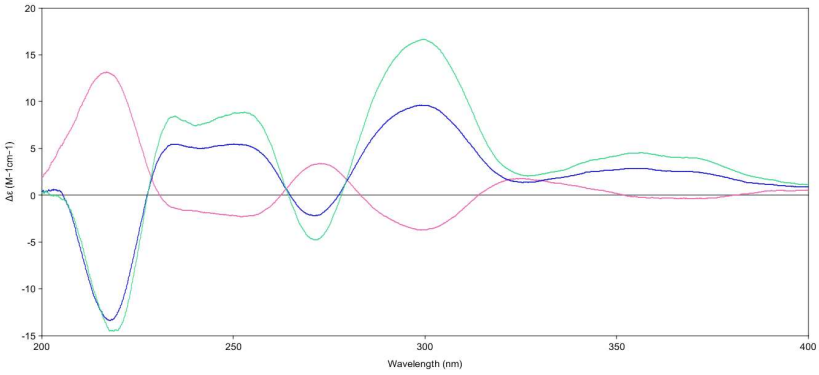

Figure S50. ECD curves of **5-7**.

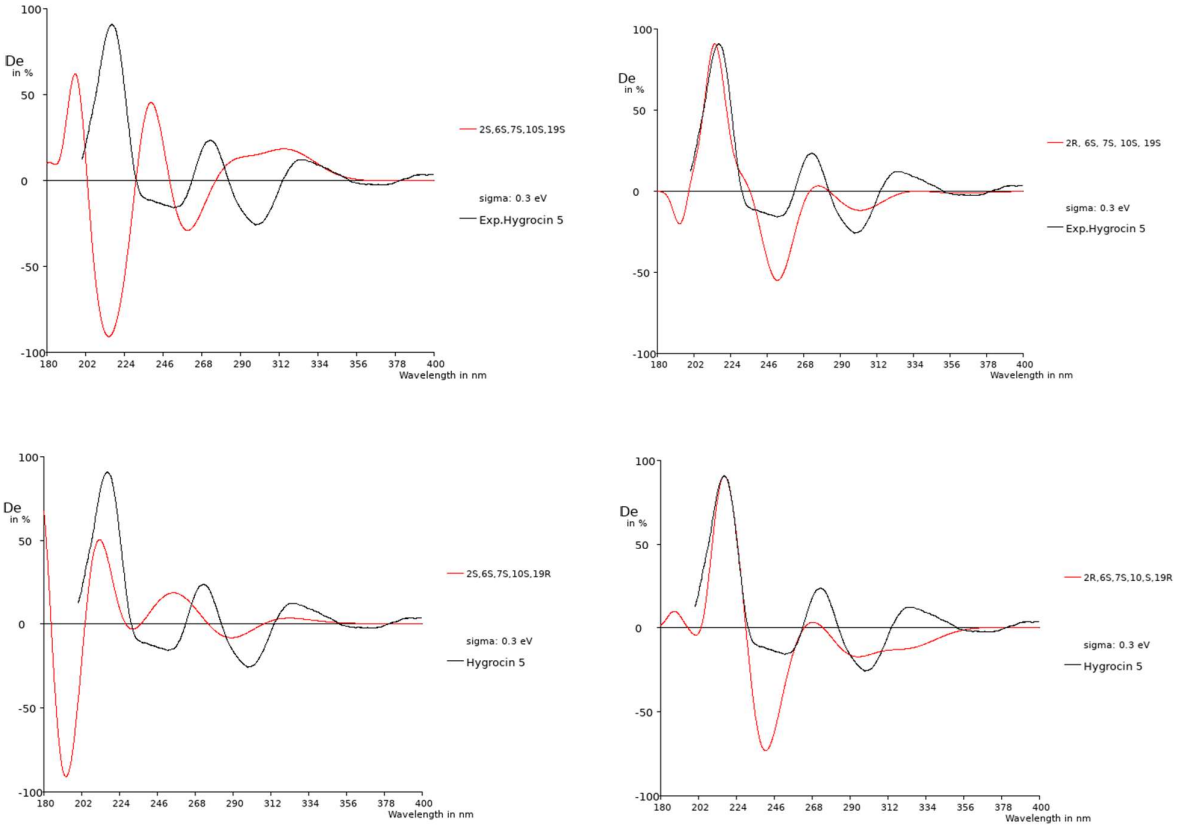

Figure S51. Comparison of the calculated and experimental ECD spectra of **5** in MeOH.

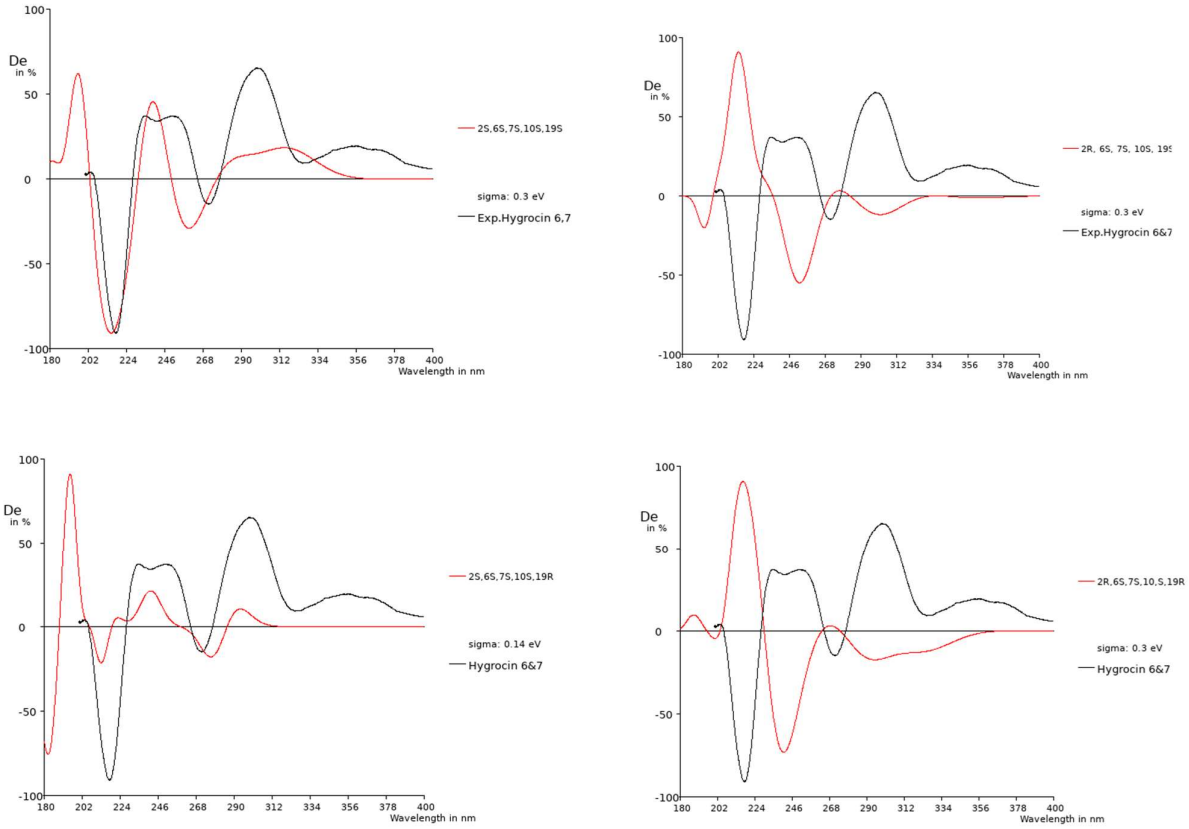

Figure S52. Comparison of the calculated and experimental ECD spectra of **6** & **7** in MeOH.